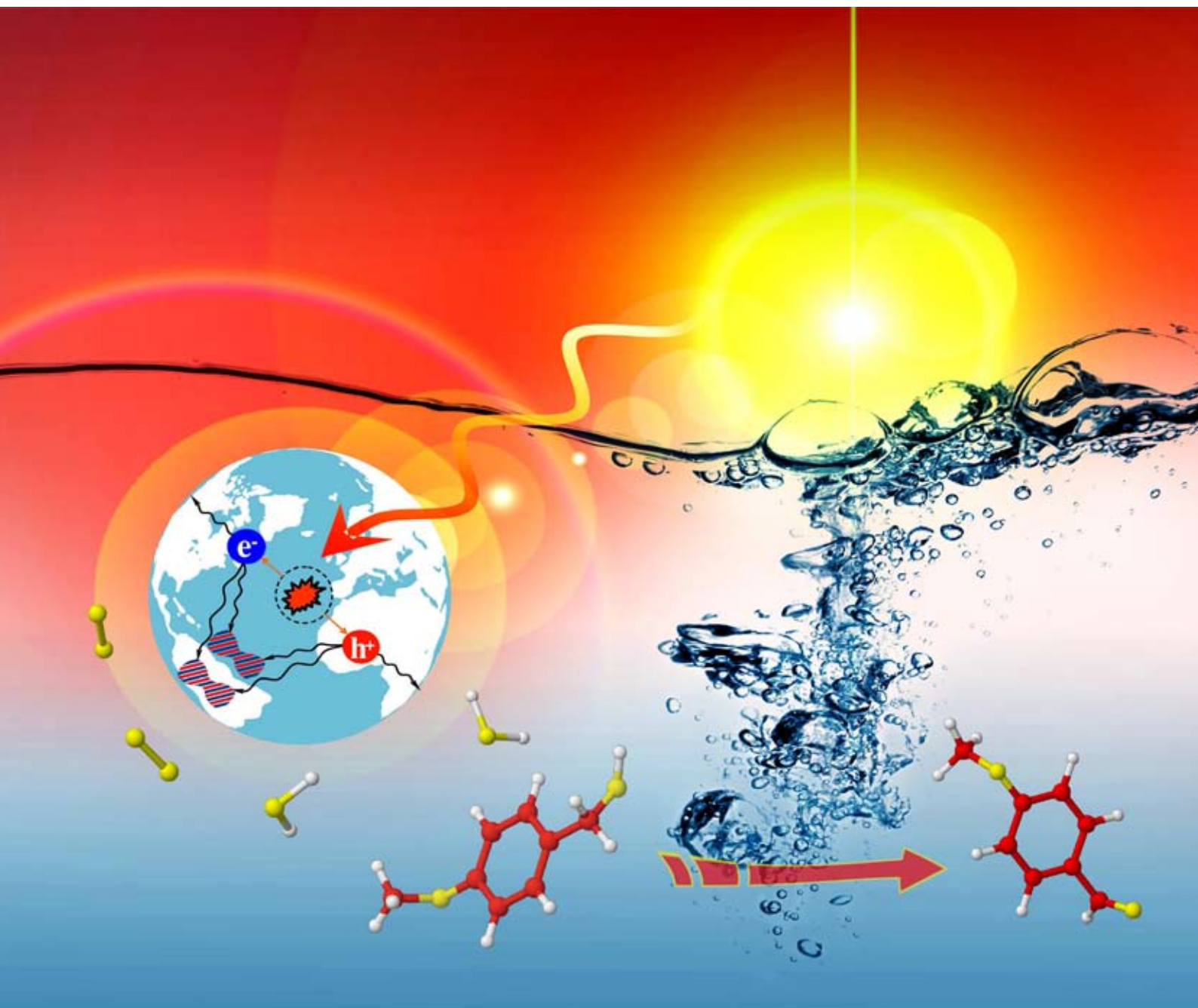


Green Chemistry

Cutting-edge research for a greener sustainable future

www.rsc.org/greenchem

Volume 11 | Number 4 | April 2009 | Pages 437–592



ISSN 1463-9262

Ravasio *et al.*
Selective hydrogenation of oils

Palmisano *et al.*
Photocatalytic oxidation of aromatic
alcohols in water

Clark *et al.*
Microwave-assisted preparation of amides

Pol *et al.*
Solvent free process for the generation
of conducting carbon spheres



1463-9262(2009)11:4;1-A

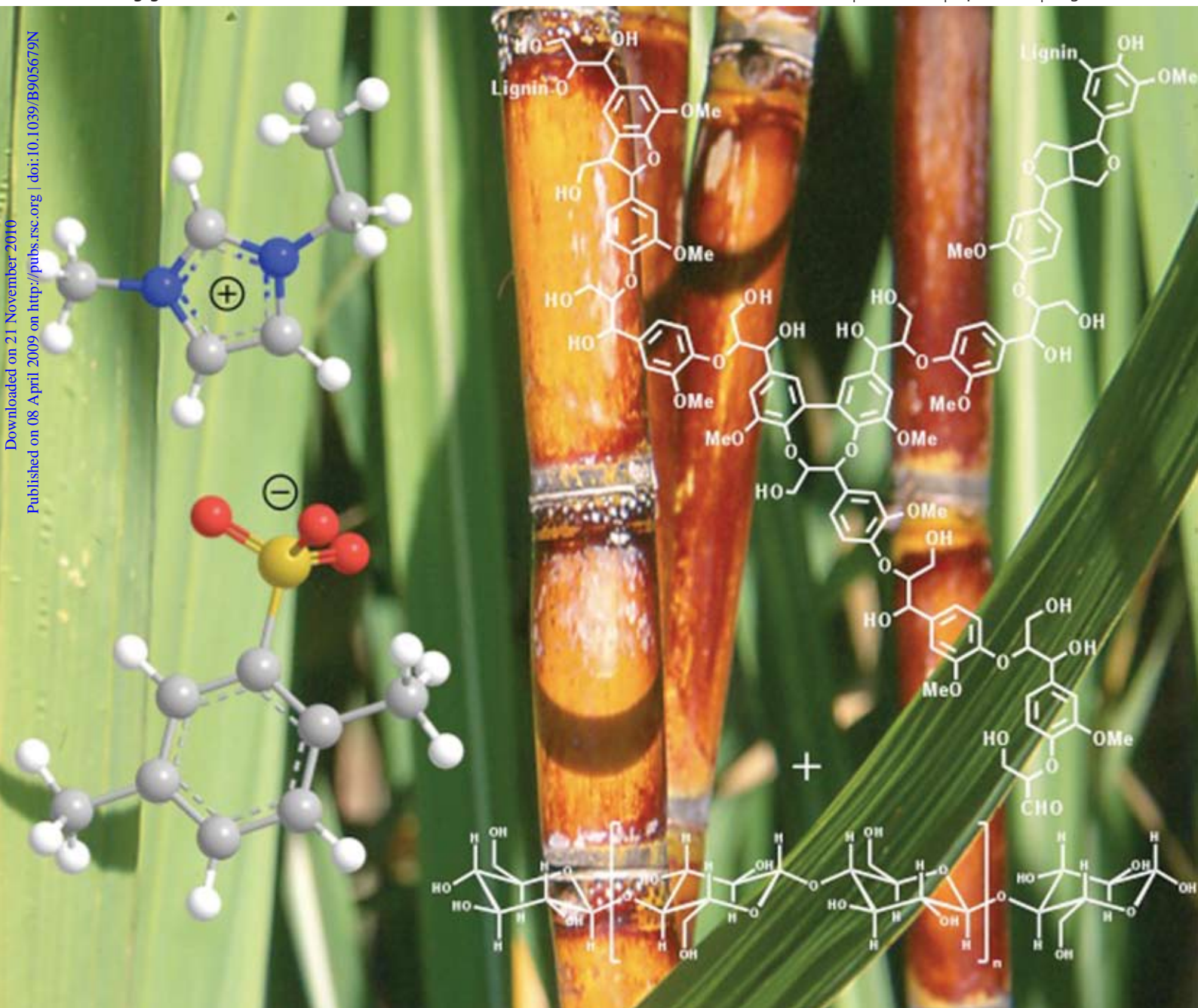
RSC Publishing

Green Chemistry

Cutting-edge research for a greener sustainable future

www.rsc.org/greenchem

Volume 11 | Number 4 | April 2009 | Pages 437–592



Downloaded on 21 November 2010
Published on 08 April 2009 on http://pubs.rsc.org | doi:10.1039/B905679N

ISSN 1463-9262

Tan *et al.*
Extraction of lignin from lignocellulose

Harmer *et al.*
Catalytic reactions using super acids in ionic liquids

Weinhold *et al.*
Improving the characterization of chitosan

Walsh *et al.*
Nanostructured membranes based on cellulose nanowhiskers

RSC Publishing

Green Chemistry

Cutting-edge research for a greener sustainable future

www.rsc.org/greenchem

RSC Publishing is a not-for-profit publisher and a division of the Royal Society of Chemistry. Any surplus made is used to support charitable activities aimed at advancing the chemical sciences. Full details are available from www.rsc.org

IN THIS ISSUE

ISSN 1463-9262 CODEN GRCHFJ 11(4) 437–592 (2009)



Cover

See Palmisano *et al.*, pp. 510–516. Selective photocatalytic oxidation of 4-substituted aromatic alcohols to aldehydes was performed in water by using rutile TiO₂ prepared at room temperature. The influence of the substituent group on oxidation rate and selectivity was studied. Authors thank Kadir Suat Yurdakal (www.italikajans.com) for cover production. Image reproduced with permission from Leonardo Palmisano from *Green Chem.*, 2009, **4**, 510.



Inside cover

See Tan *et al.*, pp. 339–345. Fractionation of lignocellulose: ionic liquid 1-ethyl-3-methylimidazolium xylenesulfonate, lignin, cellulose and sugarcane stalks. Photo courtesy of Canegrowers Australia. Image reproduced with permission from Suzie Tan from *Green Chem.*, 2009, **3**, 339.

CHEMICAL TECHNOLOGY

T25

Drawing together research highlights and news from all RSC publications, *Chemical Technology* provides a 'snapshot' of the latest applications and technological aspects of research across the chemical sciences, showcasing newsworthy articles and significant scientific advances.

Chemical Technology

April 2009/Volume 6/Issue 4

www.rsc.org/chemicaltechnology

EDITORIAL

447

Adoption of green chemistry—view from the Director of the ACS Green Chemistry Institute®

Robert Peoples, Director of the ACS Green Chemistry Institute®, discusses the adoption of green chemistry in a guest editorial for the journal.



ACS
Green
Chemistry
Institute®

EDITORIAL STAFF

Editor

Sarah Ruthven

Assistant editors

Sarah Dixon, Katie Dryden-Holt

Publishing assistant

Jessica-Jane Doherty

Team leader, Informatics

Stephen Wilkes

Technical editor

Edward Morgan

Production administration coordinator

Sonya Spring

Administration assistants

Aliya Anwar, Jane Orchard, Julie Thompson

Publisher

Emma Wilson

Green Chemistry (print: ISSN 1463-9262; electronic: ISSN 1463-9270) is published 12 times a year by the Royal Society of Chemistry, Thomas Graham House, Science Park, Milton Road, Cambridge, UK CB4 0WF.

All orders, with cheques made payable to the Royal Society of Chemistry, should be sent to RSC Distribution Services, c/o Portland Customer Services, Commerce Way, Colchester, Essex, UK CO2 8HP. Tel +44 (0) 1206 226050; E-mail sales@rscdistribution.org

2009 Annual (print + electronic) subscription price: £1027; US\$2013. 2009 Annual (electronic) subscription price: £924; US\$1811. Customers in Canada will be subject to a surcharge to cover GST. Customers in the EU subscribing to the electronic version only will be charged VAT.

If you take an institutional subscription to any RSC journal you are entitled to free, site-wide web access to that journal. You can arrange access via Internet Protocol (IP) address at www.rsc.org/ip. Customers should make payments by cheque in sterling payable on a UK clearing bank or in US dollars payable on a US clearing bank. Periodicals postage paid at Rahway, NJ, USA and at additional mailing offices. Airfreight and mailing in the USA by Mercury Airfreight International Ltd., 365 Blair Road, Avenel, NJ 07001, USA.

US Postmaster: send address changes to Green Chemistry, c/o Mercury Airfreight International Ltd., 365 Blair Road, Avenel, NJ 07001. All despatches outside the UK by Consolidated Airfreight.

PRINTED IN THE UK

Advertisement sales: Tel +44 (0) 1223 432246; Fax +44 (0) 1223 426017; E-mail advertising@rsc.org

For marketing opportunities relating to this journal, contact marketing@rsc.org

Green Chemistry

Cutting-edge research for a greener sustainable future

www.rsc.org/greenchem

Green Chemistry focuses on cutting-edge research that attempts to reduce the environmental impact of the chemical enterprise by developing a technology base that is inherently non-toxic to living things and the environment.

EDITORIAL BOARD

Chair

Professor Martyn Poliakoff
Nottingham, UK

Scientific Editor

Professor Walter Leitner
RWTH-Aachen, Germany

Associate Editors

Professor C. J. Li
McGill University, Canada

Members

Professor Paul Anastas
Yale University, USA
Professor Joan Brennecke
University of Notre Dame, USA
Professor Mike Green
Sasol, South Africa
Professor Buxing Han
Chinese Academy of Sciences,
China

Professor Shu Kobayashi,
University of Tokyo, Japan
Dr Alexei Lapkin
Bath University, UK
Professor Steven Ley
Cambridge, UK
Dr Janet Scott
Unilever, UK
Professor Tom Welton
Imperial College, UK

ADVISORY BOARD

James Clark, York, UK
Avelino Corma, Universidad
Politécnica de Valencia, Spain
Mark Harmer, DuPont Central
R&D, USA
Herbert Hugl, Lanxess Fine
Chemicals, Germany
Roshan Jachuck,
Clarkson University, USA
Makato Misono, nite,
Japan

Colin Raston,
University of Western Australia,
Australia
Robin D. Rogers, Centre for Green
Manufacturing, USA
Kenneth Seddon, Queen's
University, Belfast, UK
Roger Sheldon, Delft University of
Technology, The Netherlands
Gary Sheldrake, Queen's
University, Belfast, UK

Pietro Tundo, Università ca
Foscari di Venezia, Italy

INFORMATION FOR AUTHORS

Full details of how to submit material for publication in Green Chemistry are given in the Instructions for Authors (available from <http://www.rsc.org/authors>). Submissions should be sent via ReSource: <http://www.rsc.org/resource>.

Authors may reproduce/republish portions of their published contribution without seeking permission from the RSC, provided that any such republication is accompanied by an acknowledgement in the form: (Original citation) – Reproduced by permission of the Royal Society of Chemistry.

© The Royal Society of Chemistry 2009. Apart from fair dealing for the purposes of research or private study for non-commercial purposes, or criticism or review, as permitted under the Copyright, Designs and Patents Act 1988 and the Copyright and Related Rights Regulations 2003, this publication may only be reproduced, stored or transmitted, in any form or by any means, with the prior permission in writing of the Publishers or in the case of reprographic reproduction in accordance with the terms of licences issued by the Copyright Licensing Agency in the UK. US copyright law is applicable to users in the USA.

The Royal Society of Chemistry takes reasonable care in the preparation of this publication but does not accept liability for the consequences of any errors or omissions.

Ⓢ The paper used in this publication meets the requirements of ANSI/NISO Z39.48-1992 (Permanence of Paper).

Royal Society of Chemistry: Registered Charity No. 207890

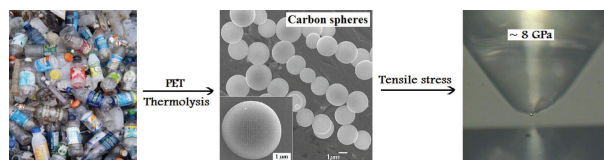
COMMUNICATIONS

448

A solvent free process for the generation of strong, conducting carbon spheres by the thermal degradation of waste polyethylene terephthalate

Swati V. Pol, Vilas G. Pol,* Dov Sherman and Aharon Gedanken

An efficient, solvent-free, catalyst-free process for the generation of strong, conducting, paramagnetic carbon spheres by the thermal degradation of waste polyethylene terephthalate polymer [PET] under autogenic pressure is demonstrated.

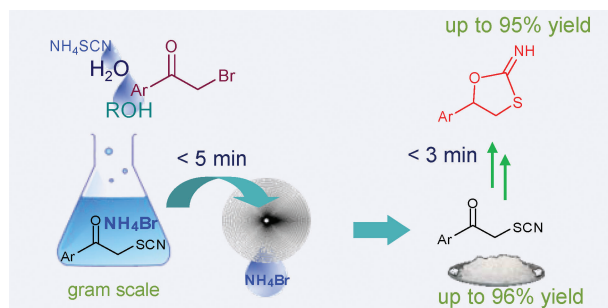


452

Simple and quick preparation of α -thiocyanate ketones in hydroalcoholic media. Access to 5-aryl-2-imino-1,3-oxathiolanes

Fabrizio R. Bisogno, Aníbal Cuetos, Iván Lavandera and Vicente Gotor*

A simple preparation of thiocyanate derivatives *via* nucleophilic substitution was accomplished in hydroalcoholic media in a few minutes and gave excellent yields. These compounds were employed for the efficient synthesis of valuable 2-imino-1,3-oxathiolane derivatives.

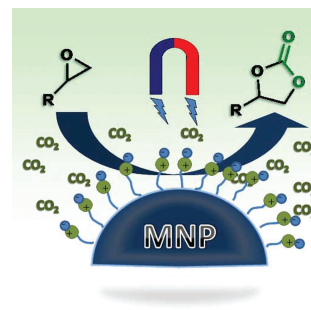


455

Magnetic nanoparticle supported ionic liquid catalysts for CO₂ cycloaddition reactions

Xiaoxi Zheng, Sanzhong Luo,* Long Zhang and Jin-Pei Cheng*

MNP-supported ionic liquid catalysts (MNP-ILs) were developed and evaluated in CO₂ cycloaddition reactions under a lower CO₂ pressure (1 MPa), showing essentially unchanged activity after 11 cycles.

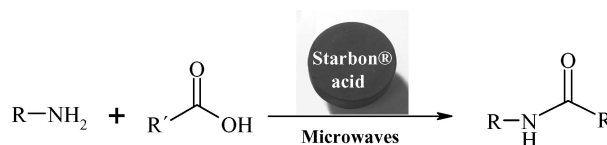


459

Microwave-assisted preparation of amides using a stable and reusable mesoporous carbonaceous solid acid

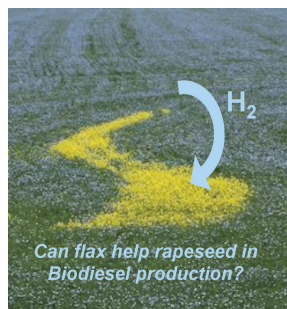
Rafael Luque,* Vitaly Budarin, James H. Clark* and Duncan J. Macquarrie

An efficient microwave assisted protocol provides quantitative yields of amides in short reaction times using Starbon® acids as catalysts.



COMMUNICATIONS

462

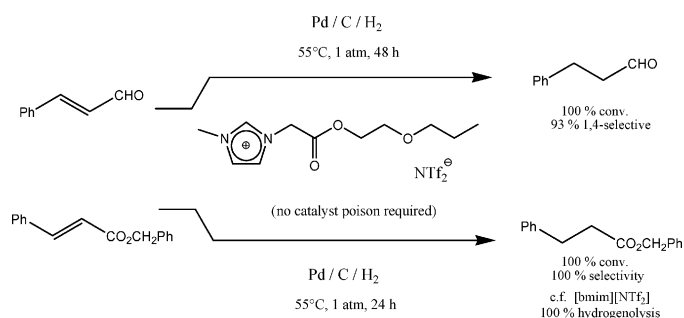


Selective hydrogenation of alternative oils: a useful tool for the production of biofuels

Federica Zaccheria, Rinaldo Psaro and Nicoletta Ravasio*

Highly selective hydrogenation of non-food oils like flax over non-toxic heterogeneous catalyst can be used to make them suitable for biodiesel formulation.

466



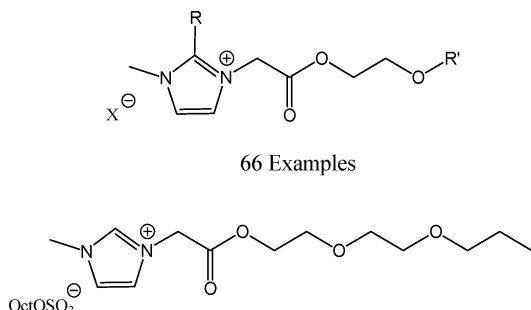
Selective hydrogenation of *trans*-cinnamaldehyde and hydrogenolysis-free hydrogenation of benzyl cinnamate in imidazolium ILs

Saibh Morrissey, Ian Beadham and Nicholas Gathergood*

The reductions of *trans*-cinnamaldehyde and benzyl cinnamate in 1-(alkoxycarbonylmethyl)alkyl-3-methylimidazolium bis(trifluoromethane)sulfonimides and alkylsulfates are presented and compared using conventional ionic liquids and VOCs. Notably selective 1,4-reductions are achieved without a traditional catalyst poison.

PAPERS

475

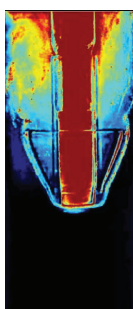


Biodegradable, non-bactericidal oxygen-functionalised imidazolium esters: A step towards 'greener' ionic liquids

Saibh Morrissey, Bruce Pegot, Deborah Coleman, M. Teresa Garcia, Damien Ferguson, Bríd Quilty and Nicholas Gathergood*

A series of imidazolium ionic liquids was prepared and screened against 7 bacterial strains.

484



The synthesis and fluorescent properties of nanoparticulate ZrO₂ doped with Eu using continuous hydrothermal synthesis

Helen Hobbs, Stephen Briddon and Ed Lester

A paper describing how fluorescent nanomaterials can be synthesised continuously using only water as the solvent.

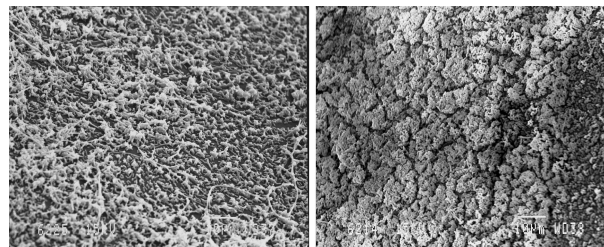
PAPERS

492


Antibiofilm activities of 1-alkyl-3-methylimidazolium chloride ionic liquids

Louise Carson, Peter K. W. Chau, Martyn J. Earle, Manuela A. Gilea, Brendan F. Gilmore,* Sean P. Gorman, Maureen T. McCann and Kenneth R. Seddon

A series of 1-alkyl-3-methylimidazolium chloride ionic liquids are active against biofilms of clinically significant microbial pathogens, including MRSA and *E. coli* (shown opposite).

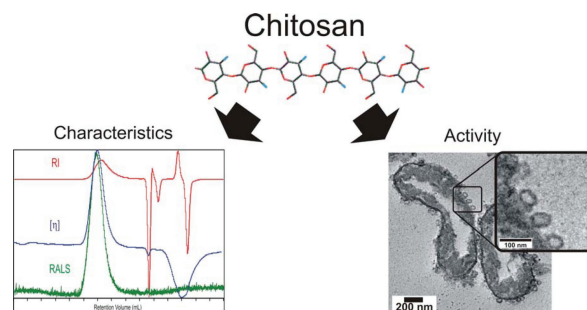


498


 **Strategy to improve the characterization of chitosan for sustainable biomedical applications: SAR guided multi-dimensional analysis**

Mirko X. Weinhold,* Janelle C. M. Sauvageau, Nadia Keddig, Marianne Matzke, Bernd Tartsch, Ingo Grunwald, Christian Kübel, Bernd Jastorff and Jorg Thöming

The biopolymer chitosan consists of a complex mixture of different chemical entities. Their specific effects on biological systems can only be understood on the basis of a thorough theoretical and experimental analysis, *i.e.* a multi-dimensional analysis.

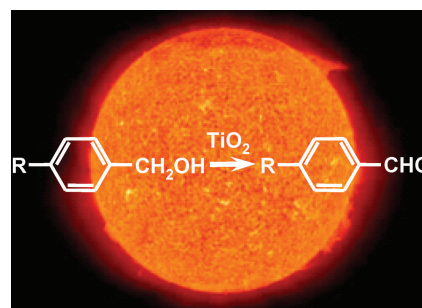


510


 **Selective photocatalytic oxidation of 4-substituted aromatic alcohols in water with rutile TiO₂ prepared at room temperature**

Sedat Yurdakal, Giovanni Palmisano, Vittorio Loddo, Oğuzhan Alagöz, Vincenzo Augugliaro* and Leonardo Palmisano*

Rutile TiO₂ catalysts were prepared at room temperature and used to perform the photocatalytic oxidation of 4-substituted aromatic alcohols to aldehydes in aqueous suspension, free of any organic co-solvent. The influence of the substituent group on the selectivity was studied.

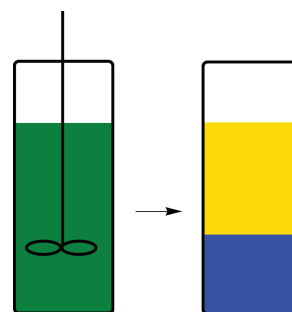


517

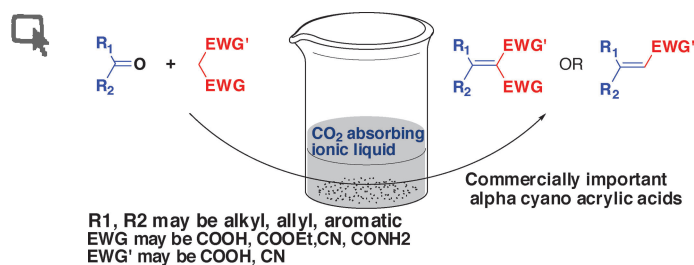
 **Catalytic reactions using superacids in new types of ionic liquids**

Mark A. Harmer,* Christopher P. Junk, Vsevolod V. Rostovtsev, William J. Marshall, Liane M. Grieco, Jemma Vickery, Robert Miller and Stella Work

We have used a combination of a superacid and a new type of superacid derived ionic liquid to catalyze reactions of industrial importance, leading to spontaneous phase separation aiding product separation.



526

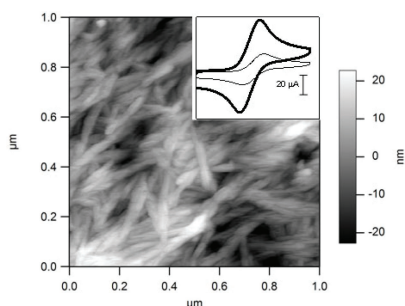


CO₂ absorbing cost-effective ionic liquid for synthesis of commercially important alpha cyanoacrylic acids: A safe process for activation of cyanoacetic acid

Yogesh O. Sharma and Mariam S. Degani*

Cost-effective and carbon dioxide absorbing ionic liquid, tri-(2-hydroxyethyl) ammonium acetate, was shown to perform multiple roles in Knoevenagel condensation. The reaction was scaled up for multi-gram synthesis of commercially important alpha cyanoacrylic acids.

531

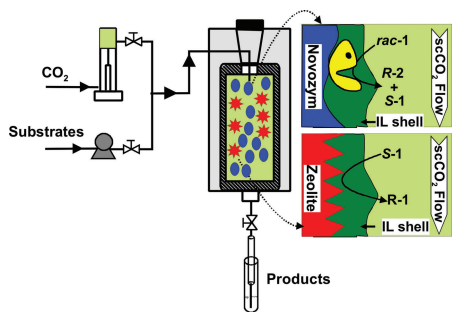


Permselective nanostructured membranes based on cellulose nanowhiskers

Wim Thielemans, Catherine R. Warbey and Darren A. Walsh*

Cellulose nanowhiskers can be extracted from cotton using an environmentally-benign process and can form stable films at solid surfaces. These films exhibit extremely promising molecular transport properties for the development of new separation and sensor technologies.

538

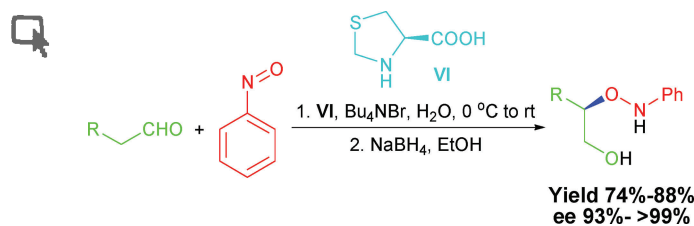


Long term continuous chemoenzymatic dynamic kinetic resolution of *rac*-1-phenylethanol using ionic liquids and supercritical carbon dioxide

Pedro Lozano,* Teresa De Diego, Corina Mira, Kimberley Montague, Michel Vaultier and José L. Iborra*

The long term continuous dynamic kinetic resolution of *rac*-phenylethanol in IL/scCO₂ biphasic systems was carried out by simultaneously using immobilized lipase (Novozym 435) and acidic zeolite catalysts.

543



Highly enantioselective L-thiaproline catalyzed α -aminoxylation of aldehydes in aqueous media

Pei Juan Chua, Bin Tan and Guofu Zhong*

Highly enantioselective L-thiaproline was used to catalyze α -aminoxylation of aldehydes in aqueous media followed by *in situ* reduction to afford the respective α -aminoxy alcohols in high yields (74–88%) and excellent enantioselectivities (93–>99%).

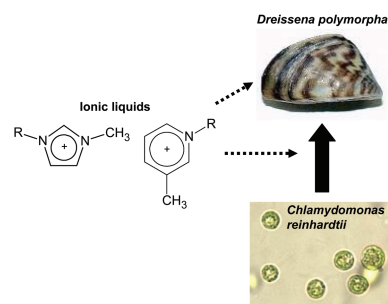
PAPERS

548

Acute toxic effects of ionic liquids on zebra mussel (*Dreissena polymorpha*) survival and feeding

David M. Costello,* Loretta M. Brown and Gary A. Lamberti

Pyridinium and imidazolium ionic liquids reduced zebra mussel survival and filtering rates. Zebra mussels exposed to long alkyl-chain ionic liquids exhibited reduced filtering at lower concentrations than predicted from mortality experiments.

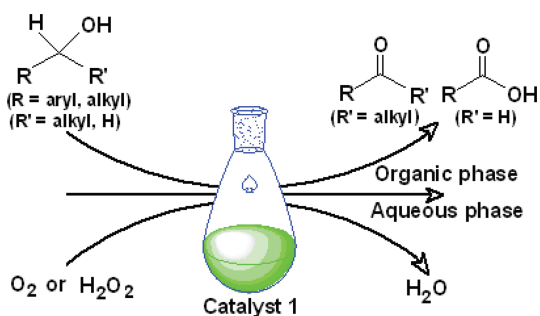


554

Applications of a high performance platinum nanocatalyst for the oxidation of alcohols in water

Prasenjit Maity, Chinnakonda S. Gopinath, Sumit Bhaduri* and Goutam Kumar Lahiri*

The water soluble, polymer supported, platinum carbonyl cluster derived nanocatalyst **1**, shows excellent activities towards the oxidations of a variety of primary and secondary alcohols by dioxygen or hydrogen peroxide in water.

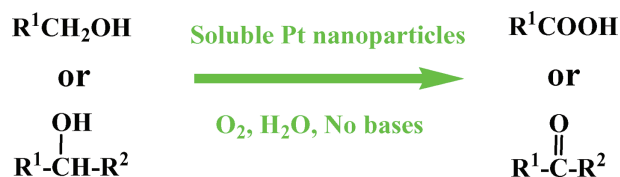


562

Base-free aqueous-phase oxidation of non-activated alcohols with molecular oxygen on soluble Pt nanoparticles

Tao Wang, Heng Shou, Yuan Kou* and Haichao Liu*

Soluble Pt nanoparticles, superior to other metal nanoparticles (e.g. Pd, Ru, Rh, Au), are efficient for aqueous-phase aerobic oxidation of nonactivated alcohols without base. Detailed mechanistic studies are reported for getting insights into these efficient catalysts.

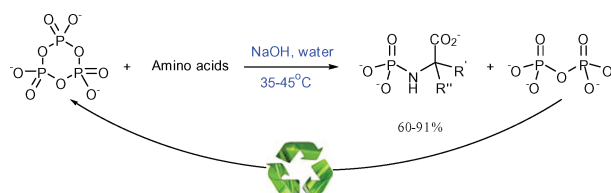


569

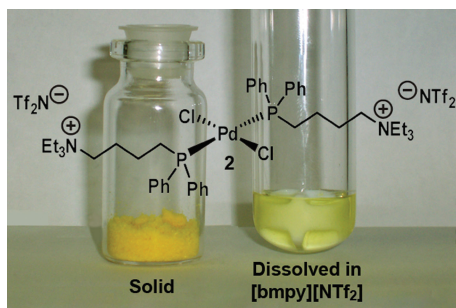
N-phosphorylation of amino acids by trimetaphosphate in aqueous solution—learning from prebiotic synthesis

Feng Ni, Shuting Sun, Chao Huang and Yufen Zhao*

A one-step synthesis of *N*-phosphono-amino acids (NPAA) in aqueous solution has been developed. Trimetaphosphate (P₃m) was used to convert amino acids into *N*-phosphono-amino acids with yields of 60~91%. The by-products, inorganic polyphosphates, was recycled to regenerate P₃m.



574

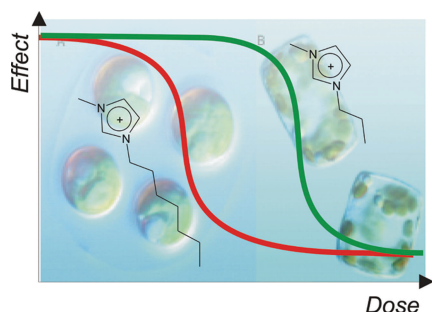


A recyclable triethylammonium ion-tagged diphenylphosphine palladium complex for the Suzuki–Miyaura reaction in ionic liquids

Marco Lombardo,* Michel Chiarucci and Claudio Trombini

The air stable palladium(II) complex **2** efficiently catalyzes the Suzuki–Miyaura reaction of aryl bromides and arylboronic acids in 1-butyl-3-methylimidazolium bis(trifluoromethylsulfonyl)imide ionic liquid ([bmpy][NTf₂]). After product extraction, the catalyst containing ionic liquid can be recycled and reused with no loss of catalytic activity.

580



Toxicity of imidazolium and pyridinium based ionic liquids towards algae. *Chlorella vulgaris*, *Oocystis submarina* (green algae) and *Cyclotella meneghiniana*, *Skeletonema marinoi* (diatoms)

Adam Latała, Marcin Nędzi and Piotr Stepnowski*

Diatoms are far more sensitive than green algae to ILs. A pronounced alkyl chain effect was also confirmed. The use of tetrafluoroborate and trifluoromethanesulfonate as counteranions gave rise to the toxic effects.

AUTHOR INDEX

- | | | | |
|--------------------------------|-------------------------------|-------------------------------|---------------------------|
| Alagöz, Oğuzhan, 510 | Gilea, Manuela A., 492 | Lozano, Pedro, 538 | Seddon, Kenneth R., 492 |
| Augugliaro, Vincenzo, 510 | Gilmore, Brendan F., 492 | Luo, Sanzhong, 455 | Sharma, Yogesh O., 526 |
| Beadham, Ian, 466 | Gopinath, Chinnakonda S., 554 | Luque, Rafael, 459 | Sherman, Dov, 448 |
| Bhaduri, Sumit, 554 | Gorman, Sean P., 492 | Macquarrie, Duncan J., 459 | Shou, Heng, 562 |
| Bisogno, Fabricio R., 452 | Gotor, Vicente, 452 | Maity, Prasenjit, 554 | Stepnowski, Piotr, 580 |
| Briddon, Stephen, 484 | Grieco, Liane M., 517 | Marshall, William J., 517 | Sun, Shuting, 569 |
| Brown, Loretta M., 548 | Grunwald, Ingo, 498 | Matzke, Marianne, 498 | Tan, Bin, 543 |
| Budarin, Vitaly, 459 | Harmer, Mark A., 517 | McCann, Maureen T., 492 | Tartsch, Bernd, 498 |
| Carson, Louise, 492 | Hobbs, Helen, 484 | Miller, Robert, 517 | Thielemans, Wim, 531 |
| Chau, Peter K. W., 492 | Huang, Chao, 569 | Mira, Corina, 538 | Thöming, Jorg, 498 |
| Cheng, Jin-Pei, 455 | Iborra, José L., 538 | Montague, Kimberley, 538 | Trombini, Claudio, 574 |
| Chiarucci, Michel, 574 | Jastorff, Bernd, 498 | Morrissey, Saibh, 466, 475 | Vaultier, Michel, 538 |
| Chua, Pei Juan, 543 | Junk, Christopher P., 517 | Nędzi, Marcin, 580 | Vickery, Jemma, 517 |
| Clark, James H., 459 | Keddig, Nadia, 498 | Ni, Feng, 569 | Walsh, Darren A., 531 |
| Coleman, Deborah, 475 | Kou, Yuan, 562 | Palmisano, Giovanni, 510 | Wang, Tao, 562 |
| Costello, David M., 548 | Kübel, Christian, 498 | Palmisano, Leonardo, 510 | Warbey, Catherine R., 531 |
| Cuetos, Anibal, 452 | Lahiri, Goutam Kumar, 554 | Pegot, Bruce, 475 | Weinhold, Mirko X., 498 |
| De Diego, Teresa, 538 | Lamberti, Gary A., 548 | Pol, Swati V., 448 | Work, Stella, 517 |
| Degani, Mariam S., 526 | Latała, Adam, 580 | Pol, Vilas G., 448 | Yurdakal, Sedat, 510 |
| Earle, Martyn J., 492 | Lavandera, Iván, 452 | Psaro, Rinaldo, 462 | Zaccheria, Federica, 462 |
| Ferguson, Damien, 475 | Lester, Ed, 484 | Quilty, Brid, 475 | Zhang, Long, 455 |
| Garcia, M. Teresa, 475 | Liu, Haichao, 562 | Ravasio, Nicoletta, 462 | Zhao, Yufen, 569 |
| Gathergood, Nicholas, 466, 475 | Loddo, Vittorio, 510 | Rostovtsev, Vsevolod V., 517 | Zheng, Xiaoxi, 455 |
| Gedanken, Aharon, 448 | Lombardo, Marco, 574 | Sauvageau, Janelle C. M., 498 | Zhong, Guofu, 543 |

FREE E-MAIL ALERTS AND RSS FEEDS

Contents lists in advance of publication are available on the web *via* www.rsc.org/greenchem – or take advantage of our free e-mail alerting service (www.rsc.org/ej_alert) to receive notification each time a new list becomes available.



Try our RSS feeds for up-to-the-minute news of the latest research. By setting up RSS feeds, preferably using feed reader software, you can be alerted to the latest Advance Articles published on the RSC web site. Visit www.rsc.org/publishing/technology/rss.asp for details.

ADVANCE ARTICLES AND ELECTRONIC JOURNAL

Free site-wide access to Advance Articles and the electronic form of this journal is provided with a full-rate institutional subscription. See www.rsc.org/ejs for more information.

* Indicates the author for correspondence: see article for details.



Electronic supplementary information (ESI) is available *via* the online article (see <http://www.rsc.org/esi> for general information about ESI).

Chemical Technology

UV indicators change colour before your skin does Sunburn detection is hot work

UK scientists have developed UV-sensitive indicators that change colour when there is a danger of sunburn.

Over 70 000 people in the UK are diagnosed with skin cancer each year and sunburn is a contributing factor. The signs of sunburn can take four to eight hours to develop, by which time the skin is already damaged. While there are several UV dosimeters on the market, most are unable to distinguish between different skin types. Also, they show a gradual colour change in response to sun exposure, which makes identifying the sunburn risk difficult. Andrew Mills and colleagues from the University of Strathclyde, Glasgow, have created what they claim is a 'simple, inexpensive, unambiguous sunburn indicator' that can be tuned to different skin types.

Mills' indicator uses a UV-driven acid-release agent coupled to a pH-indicating dye. Sunlight decomposes the acid-release agent leading to protonation of the dye, which causes a striking colour



change. The length of time before the colour changes can be altered by using different acid-release agents or dyes, explains Mills, meaning that the indicator could be varied for use on all skin types.

As an alternative to this indicator,

The striking colour change indicates the risk of sunburn

Mills has also made a blue indicator based on a tin oxide photocatalyst, which reduces a dye and becomes colourless on exposure to sunlight. 'The inorganic pigment materials match the way the skin absorbs UV radiation,' says Mills.

'It is the simplicity of the chemistry, and its ability to work on all skin types, that makes this research so effective,' comments Peter Robertson, an expert in photocatalysis at the Robert Gordon University, Aberdeen, UK. He adds how 'gratifying it is to see academic science coming up with a solution that is going to have an impact on society'.

Mills says he is optimistic that these indicators will become commercially available but adds that the greatest challenge will be getting our sun-loving society to accept them.

Nicola Wise

References

- A Mills *et al*, *Chem. Commun.*, 2009, DOI:10.1039/b900569b
A Mills and P Grosshans, *Analyst*, 2009, DOI:10.1039/b820288e

In this issue

Surfaces take a turn to do work

Rotating molecules anchored to a surface affect the surface properties

The medical power of attraction

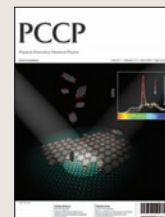
Magnetic microbeads remove pathogens from blood

Interview: Molecular logic

A Prasanna de Silva discusses sensors, supramolecular chemistry and Sri Lankan percussion's part in Irish music

Instant insight: Bone repair breakthrough

Thomas Webster and colleagues explain why today's bone implants are so much more than your grandparent's hip replacement



The latest applications and technological aspects of research across the chemical sciences

Application highlights

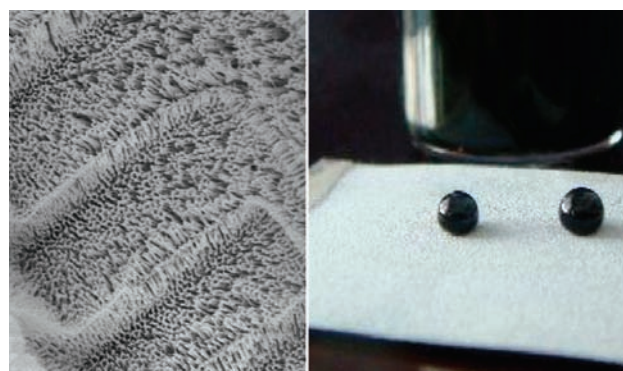
Oil-repelling surface could prevent leaks from oil pipelines

Nanowire forests repel liquids

Chinese researchers have made a surface that repels nearly all types of liquid. The surface could be used in a range of applications from kitchen equipment to oil pipelines, they claim.

Feng Zhou and colleagues at the Lanzhou Institute of Chemical Physics used electrochemistry to make a forest of aluminium oxide nanowires on the surface of aluminium foil. Using a process called anodisation, they formed nanoscale pores on the surface, which grew and merged, leaving nanowires behind. The team then modified the nanowires with perfluorosilanes, creating a surface that repelled a variety of liquids including water, alkanes and lubrication oils, such as ionic liquids.

'Super-oleophobic [extremely oil-repelling] surfaces are in high demand to seal in lubricating oils and prevent oil creep [where oil spreads across a device away from the component it is meant to be



lubricating],' explains Zhou. 'Creep may lead to lubrication failure or cause contamination of the surrounding environment. Surfaces that are non-adhesive and repellent to oils potentially have wide applications from kitchen facilities to oil transport pipelines.'

Other methods for making aluminium oxide nanowires involve etching porous aluminium oxide membranes using acids or bases, but they are time consuming, says

Modified aluminium oxide nanowires (left) can repel a wide range of liquids, including crude oil (right)

Reference

W Wu *et al*, *Chem. Commun.*, 2009, 1043 (DOI: 10.1039/b818633b)

Zhou. His electrochemical method is simple and quick, he adds.

'This work is important because it describes an elegant method to make aluminium surfaces repel a wide range of liquids, including water and various types of oil, which could be adopted on an industrial scale,' comments Steven Bell, an expert in super-repellent surfaces at Queen's University Belfast, UK. 'As with all approaches based on nano- and micro-structured surface features, the challenge will be to combine this impressive functionality with the long term durability which is needed for many practical applications.'

Zhou agrees that applying the method industrially will not be easy. 'Unlike the success in making various super-hydrophobic materials with different synthetic strategies, examples of super-oleophobicity are very rare,' he says. 'Extending the present idea to other materials, especially engineering coatings, will be a great challenge.'
Colin Batchelor

Rotating molecules anchored to a surface change the surface's properties

Surfaces take a turn to do work

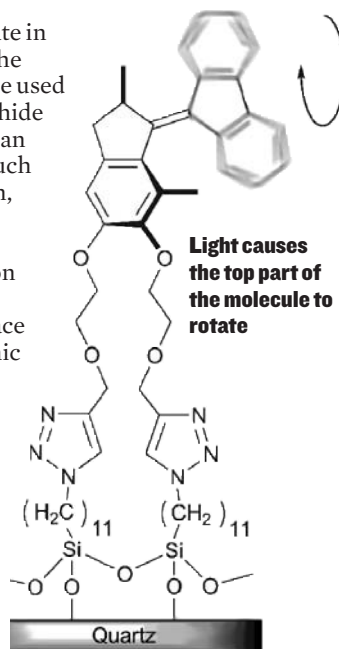
Light-driven molecular motors that rotate perpendicular to a surface can control the surface's properties, say scientists from the Netherlands and Canada.

Rotating molecules are widely used as molecular motors in biological systems, for tasks such as moving molecules away from cell nuclei. Ben Feringa, at the University of Groningen, the Netherlands, and colleagues have attempted to mimic biomolecular rotors by attaching photosensitive molecules to solid surfaces, which enables them to take control of the molecules' orientations.

The group anchored the molecules to quartz and silicon surfaces. When they shone light on the surfaces, the molecules underwent a photochemical isomerisation followed by a thermal inversion, which caused

the top part of them to rotate in concert perpendicular to the surface. The rotation can be used to alternately expose then hide functional groups, which can affect surface properties such as wettability and adhesion, explains Feringa.

'Our motivation was to employ the collective action of many nanomotors on a surface to change the surface properties in a fully dynamic fashion,' says Feringa. The motor is three orders of magnitude faster than previous surface-supported motors, which is a major step towards getting them to perform work, he adds. The team's next goal is to use the motors to control surface



hydrophobicity.

'The successful formation of fully functional surface-grafted molecular motors might be a first step towards the construction of more sophisticated and functional nanomolecular motors,' says Qing-Zheng Yang, an expert on photo-driven molecular motors at the University of Illinois, Urbana, US.

Feringa says he looks forward to attaching long polymer chains to the motors to amplify the motion. 'We would like to have motors that rotate in the microsecond time frame to see a propulsion effect on solvents, polymers or other nano-objects on top of the layer.'
Christina Hodkinson

Reference

B L Feringa *et al*, *Chem. Commun.*, 2009, DOI: 10.1039/b821755f

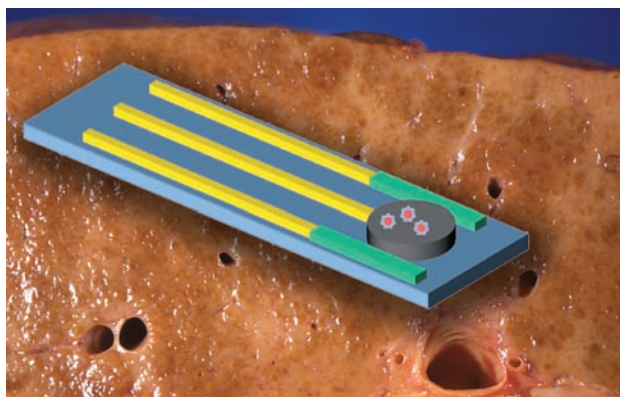
Enzyme's reaction with bile acids triggers current generation

Biosensor shows potential

US scientists have developed a simple electrochemical device that can be used to diagnose liver disease.

Liver disease affects more than 170 million people worldwide. One way to identify the disease is to look for increased bile acid concentration in the blood. Existing bile acid tests require expensive, non-portable equipment, which is a significant problem for the many sufferers who live far from medical facilities, says Brandon Bartling, at Case Western Reserve University, Cleveland.

Now Bartling and colleagues have made a cheap and portable bile acid sensor. It consists of an oxidising enzyme and its co-enzyme, nicotinamide adenine dinucleotide (NAD⁺), immobilised on an electrode's surface. When Bartling dropped a bile acid sample on to the sensor, the enzyme oxidised the acid, producing the reduced form of the co-enzyme, NADH, as the by-product. The sensor then oxidised the NADH, generating a current proportional to the bile acid concentration. Bartling showed that



the sensor could detect the total bile acid concentration in calf serum samples containing mixtures of the three principal human bile acids. He says this suggests that accurate diagnosis using human samples could be possible.

The sensor operates at a lower potential than similar biosensors, says Bartling, meaning that it oxidises only NADH and not any other species present in the sample. As a result, it doesn't need size-

The sensor is simpler and more sensitive than sensors with size-exclusion membranes

Reference
B Bartling, L Li and C-C Liu, *Analyst*, 2009, DOI: 10.1039/b900266a

exclusion membranes, which are used by other biosensors to filter out other oxidisable species that might interfere with current measurement.

Membranes' pores can get blocked with chemicals, explains Bartling. Product then builds up on the electrodes, reducing their sensitivity.

Chong Yuan, managing director of Diazyme Laboratories, La Jolla, US, which makes diagnostic tests, comments that the results may also have 'wide application potential for various clinically relevant biomarkers that can be involved in the enzymatic formation of NADH, such as homocysteine, a new emerging cardiovascular risk factor'. But he warns that 'further studies are needed to validate the test with human samples'.

Bartling is focusing on liver disease for the moment. He says he plans to develop a series of affordable, portable and user-friendly sensors to test for other biomarkers that can help to discriminate the type and severity of liver disease.

Frances Galvin

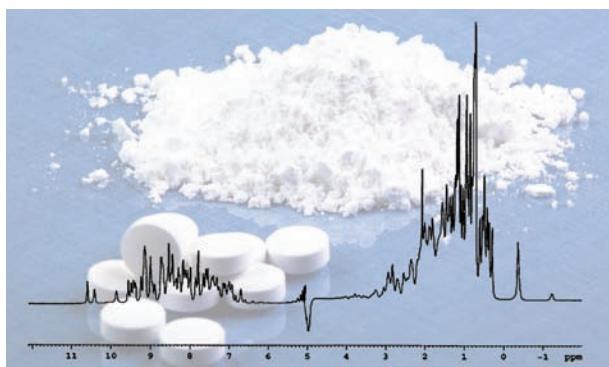
NMR and theory join forces to characterise drugs

Crystal clear method for identifying powders

Scientists in the UK and France have combined NMR and computational methods to determine the structures of powdered organic compounds. The protocol could be used by the pharmaceutical industry to identify if drugs contain different crystal structures (polymorphs) that could make them less effective.

Lyndon Emsley, at the University of Lyon, Villeurbanne, France, and colleagues tested their protocol, which is based on solid state NMR combined with density functional theory, on thymol, an antiseptic molecule found in thyme oil. They showed that the crystal structure they generated was the same as the single crystal X-ray structure determined previously.

Emsley says he was inspired by protein NMR, where proteins are isotopically labelled to make



them easier to characterise. 'We thought: can we adapt that to small molecules that can't be easily labelled?' he says. 'Ours is the only group working toward total structure determination of small organic molecules.'

Marc Baldus, a specialist in solid

The NMR-theory protocol can discriminate between drug polymorphs

Reference
E Salager et al, *Phys. Chem. Chem. Phys.*, 2009, DOI: 10.1039/b821018g

state protein NMR at Utrecht University, the Netherlands, hails the work as 'a landmark in establishing solid state NMR as a high resolution structural method in pharmaceutical chemistry and beyond'.

Emsley says the method performs as well as current powder X-ray diffraction methods but he believes that the integrated use of both techniques will result in a far more effective protocol.

'Our objective is to extend the technique to all drug-sized molecules and to apply it to discriminate between polymorphs,' says Emsley. He says he is confident that the method can be used to look at disordered, non-crystalline materials, such as those used in electronics and nanotechnology.

Philip Robinson

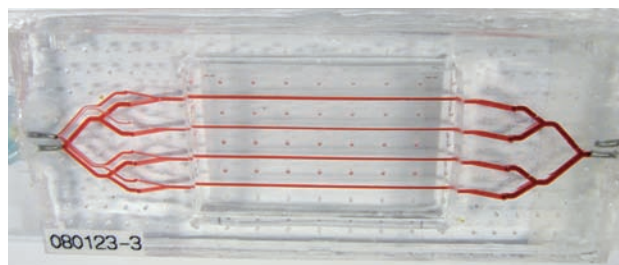
Magnetic microbeads remove pathogens from blood

The medical power of attraction

US scientists have made a microfluidic device that cleanses blood of toxic pathogens.

Sepsis is a lethal disease caused by a microbial infection that saturates the blood and overwhelms the body's defences. Commonly caused by the fungi *Candida albicans*, it kills over 200 000 people in the US each year. Antibiotics are the most effective treatment but sometimes they can't cope with the quickly-multiplying pathogens. Donald Ingber, at Children's Hospital Boston and Harvard Medical School, and colleagues say their device rapidly reduces the number of pathogens in the blood so the antibiotics have fewer pathogens to kill.

Ingber's device consists of four vertically stacked channels filled with flowing fungi-contaminated blood. He added magnetic microbeads coated with antibodies to the blood, which bound to the fungi. A magnetic field gradient generated across the channels continuously separated the fungi-bound beads from the blood. Ingber showed the



device can clear 80 per cent of the fungi, 1000 times faster than other blood cleansing prototypes.

'We have integrated proven microfluidics and micromagnetic technologies to engineer a potentially effective, low-cost and portable blood cleansing system that can be applied worldwide to save human lives,' says Ingber. He adds that the patient's blood would be diverted out of their body, through the device for cleansing before being returned to the circulation, with simultaneous antibiotic treatment.

'This is a refreshingly brilliant approach for treating patients with septicaemia. The proof-of-principle

A magnetic field across the channels separates the fungi-bound beads from blood

Reference
C W Yung *et al*, *Lab Chip*, 2009, DOI:10.1039/b816986a

is very convincing,' comments Tonse Raju, Medical Officer at the National Institutes of Health, Bethesda, US. 'However, major hurdles to be conquered are: effective cleansing when the blood flow rates are in the physiological range; removal of inflammatory products of sepsis that can perpetuate organ damage even in the absence of pathogens in the blood; and the problem of dealing with regions of the body where the organisms can reside without getting into circulation.'

Ingber says he is working on improving the device. 'We are currently developing a new process to increase the binding of magnetic beads to pathogens,' he explains. 'We are also developing new microfluidic designs that mimic the native architecture and function of the spleen, which is normally responsible for removing pathogens from the bloodstream. Prototypes demonstrate extremely high separation performance without the lost or dilution of circulating blood.'
Emma Shiells

Light-induced polymerisation in microchannels creates complex designs

Picture perfect particles

US scientists have developed a microfluidic method for making complex 3D microparticles they claim could be used in tissue engineering.

Patrick Doyle and colleagues at the Massachusetts Institute of Technology, Cambridge, call their method Lock Release Lithography (LRL). They shone UV light through transparent masks to polymerise monomers inside a microchannel into different shapes. Structures hanging down from the channel's ceiling then locked the particles in place and made indents in the particles' structures. By applying high pressure, the team released the dish-like structures and collected them. They also made particles with pillars on their surfaces using a channel with indents in its ceiling.

Doyle demonstrated that the

method can be used to make particles made of two different monomers. He polymerised the first monomer type and locked the structure in place. He then introduced the second monomer type into the channel and used light to polymerise it to the existing structure, making patterned particles with intricate shapes, interior features and borders by changing the masks.

'This is a very impressive approach towards truly complex particles. While a range of different asymmetric and multifunctional particles have been made in recent years, these particles are,



Intricate shapes are made by changing the masks and monomers

Reference
K W Bong, D C Pregibon and P S Doyle, *Lab Chip*, 2009, DOI: 10.1039/b821930c

without any doubt, outstanding,' says Joerg Lahann, a specialist in microparticles at the University of Michigan, Ann Arbor, US.

'We believe that LRL will provide a powerful means to mass-produce functional units in areas such as microfluidic operation, filtration and tissue engineering,' says Doyle. 'The length scales in LRL are ideally suited to generating tissue engineering mesoconstructs, each containing multiple cell lines that are precisely positioned within the particle.'

Currently, the particle size is limited to the micrometre range but Doyle says he plans to extend the technique to make other particle sizes.

Michael Brown

Interview

Molecular logic

A Prasanna de Silva tells Nicola Wise about sensors, supramolecular chemistry and how Sri Lankan percussion can play a part in Irish music



A Prasanna de Silva

A Prasanna de Silva is a professor at Queen's University Belfast, UK. His research interests include fluorescent sensors, molecule-based logic and molecular switches. He was awarded the RSC Award for Sensors in 2008 for his contribution towards 'switch and tell' sensor molecules and the invention of molecular logic.

What led you to specialise in supramolecular chemistry?

The philosophical breadth of supramolecular chemistry, especially in the hands of Jean-Marie Lehn and Seiji Shinkai, was clear to see during the early 1980s. Around this time, I had just completed my PhD research in organic photochemistry at Queen's University Belfast under Jim Grimshaw. Combining photochemistry with supramolecular chemistry permitted the fluorescence signalling of alkali metal ions—a virgin field at the time.

Your research helped develop blood diagnostic cassettes. How does this chemistry work?

Fluorescent molecular sensors can gather information about atomic or molecular behaviour from environments of nanometre dimensions. We developed sensors which contain a fluorescent unit and a receptor unit joined through a spacer module. This supermolecule loses its fluorescence capability owing to an inter-module photoinduced electron transfer (PET) quite similar to that seen in green plant photosynthesis. This PET process is stopped the moment the receptor module captures its target, for example a sodium ion, thereby switching the suppressed fluorescence back on. Thus the fluorescence signal measures the concentration level of the target species.

In collaboration with Roche Diagnostics (now Optomedical), we produced fluorescent PET sensors held inside small plastic cassettes. These sensors respond to various blood gases and electrolytes and are used in hospital critical care units, ambulances, general practice surgeries and even veterinary environments. The cassettes have had sales of over 55 million US dollars so far.

You have said in the past that you persuade molecules to perform arithmetic operations. What you mean by this?

Conventional silicon-based logic devices use electric voltages as the inputs and outputs. The first examples of molecular logic gates used chemical species such as protons and sodium ions as inputs along with fluorescence as the output. Nathan McClenaghan and I designed molecules which could perform the computation of adding one and one to get two. Though elementary, this computation is understandable to virtually everyone on the planet. So, persuading molecules to do arithmetic was an important early step on the journey of molecular logic and computation.

What is the next big thing that you would like to tackle in your lab?

Molecular logic and computation is a young field with a need to prove itself in different ways. Demonstrating real-life applications which conventional silicon-based computing cannot do would be one such avenue. We have already shown an application where a population of small micrometric objects are given identification tags made up of molecular logic gates. This is a bit like faces on people or number plates on cars except everything is a lot smaller. Such molecular computational identification (MCID) can address far smaller objects than those handled conveniently by the popular RFID (radiofrequency identification) technology. We now need to generalize this MCID technique and broaden its applicability.

What is hot at the moment in your research area?

Molecular computing or data processing in small spaces is the hot topic. These molecular devices will reach where silicon devices cannot easily go, whether it be inside living cells, on the surface of plastic beads or inside detergent micelles.

Which scientist, current or historic, do you most admire and why?

Thomas Andrews was the first professor of chemistry at the then Queen's College of Belfast 150 years ago. Every time water turns to vapour or ice, I am reminded of this man's work on the effects of temperature and pressure on materials. Also at that time, George Boole at University College Cork, Ireland laid the foundations of modern computing with his ideas on logic and algebra. These two giants in the north and the south of a small island changed the way the world worked.

If you weren't a scientist, what would you do?

I would have to be a percussionist. I have played all my life and, like many Sri Lankan kids, I got my grounding in rhythm at a young age. Northern Ireland, with its rich musical tradition, was a great place to put that rhythm to use. It was a just matter of time before I was introduced to a band where a Sri Lankan percussionist could blend with Irish fiddles, flutes, banjos, bodhrans and voices. We have enjoyed playing together for the last 13 years, even though I have been advised to hold onto my day job!

ISOLUTE® SLE+

Supported Liquid Extraction plates are now available in 200 mg and new 400 mg size.



IST
Biotage

ISOLUTE® SLE+
Part No. 820-0400-P01
Lot No. 6003501 HC



Replace traditional liquid-liquid extraction techniques with faster more efficient SLE+ Plates

- Easily transfer a current LLE method to SLE
- Improved productivity
- Improved drug recovery
- Reduced ion suppression

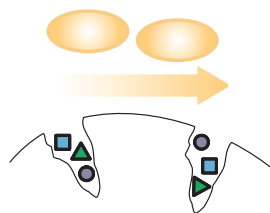
Effective
Sample
Preparation
without ACN

EVOLUTE®

An affordable next generation polymer-based SPE sorbent for cleaner samples.

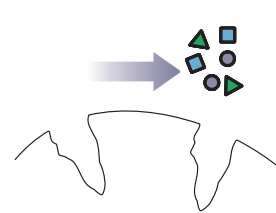
- **EVOLUTE ABN** extracts Acids, Bases and Neutrals
- **EVOLUTE CX** extracts Basic compounds and completely removes phospholipids from biological matrices

Sample Application



Drugs are retained while proteins pass straight to waste

Analyte Elution



Drugs are eluted

Go to www.biotage.com for more information, application notes, and to request a **FREE** sample.

Instant insight

Bone repair breakthrough

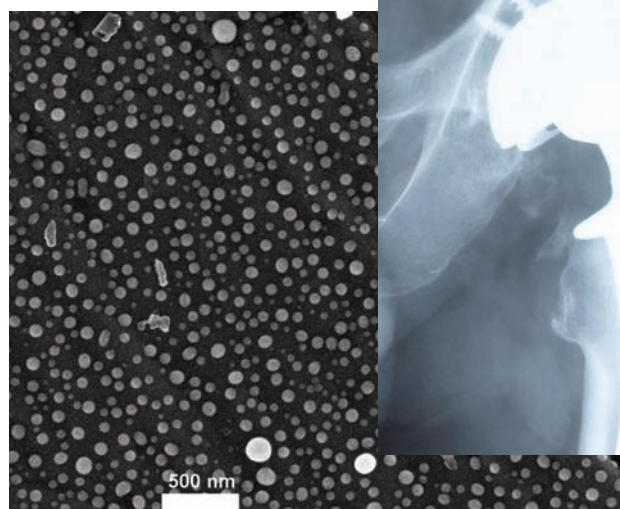
Thomas Webster and colleagues at Brown University, Providence, US, explain why today's bone implants are so much more than your grandparent's hip replacement thanks to nanotechnology

Bone fracture is very common among the elderly as bones become more brittle as we age. Active young people also have a high risk of bone fracture through every day life and sporting activities. If a fracture is small, it can be filled with bone cement, such as polymethylmethacrylate. However, if the fracture is large, more durable metal implants, such as titanium and titanium-based alloys, are used. The goal is to not only to fill the fracture space with a strong material that can support the body's weight, but also to promote new bone growth to fully restore the bone's functions.

In the past, bone implants were made of inert materials, chosen because they didn't severely influence bodily functions or generate scar tissue, which is a thick, insensitive tissue layer that can form around an implant. But this simple design principle causes implants to loosen from the surrounding bone after around 10 to 15 years. Loosening becomes worse with time and can cause significant pain. As a result, patients often undergo additional surgery (called revision surgery) to remove the loose implant and insert a new one. Revision surgery is clearly undesirable as it is costly, painful and requires therapy all over again for the patient.

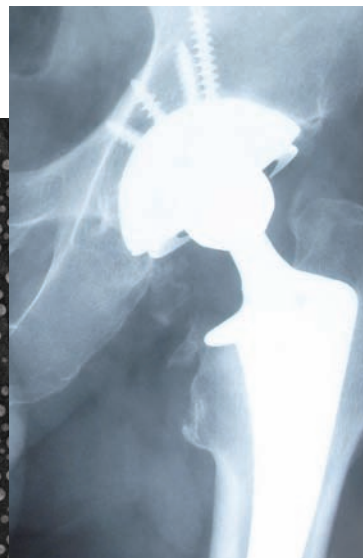
It is unsurprising that there has been an on-going effort to create implants that can integrate into the surrounding natural bone for the patient's lifetime. Using their understanding of bone composition and the bone-forming process, scientists have developed various methods to transform these once inert implants into implants that can promote bone growth.

One of the first approaches



to make more proactive bone implants uses surface chemistry to encourage the implant to interact with osteoblasts (bone-forming cells). This method has resulted in a number of implant materials, such as bioactive glass, that show good bone formation. However, scientists often need to resort to trial and error processes to find an implant material that not only increases bone growth but also has good mechanical properties for use in cementless implants, such as the hip implant. Such combinations are not always easy to find in one material or even a composite of materials.

Nanotechnology has taken a bold new step towards improving orthopedic implant devices. Orthopedic nanotechnology is based on understanding cell-implant interactions. Cells do not interact directly with an implant but instead interact through a layer of proteins that absorb almost instantaneously to the implant after insertion. Scientists have improved numerous implant materials,



including titanium and titanium alloys, porous polymers, bone cements and hydroxyapatite, by placing nanoscale features on their surfaces. The bulk materials' properties remain unchanged, maintaining their desirable mechanical properties, but the surface changes enhance the interactions with proteins. This causes bone-forming cells to adhere to the implant and activates them to grow more bone.

Scientists are also creating 'smarter' implants that can sense what type of tissue is growing on them, communicate the information to a hand-held device and release drugs on demand to promote tissue growth. These implants are designed to help avoid complications frequently observed after bone implantation, such as infection, inflammation (or scar tissue growth), implant loosening and, in the case of bone cancer, cancer recurrence. Scientists have been investigating implants that have inherent mechanisms to protect the body from infection (such as silver and zinc) or inhibit cancer growth (such as selenium).

Significant promise can be drawn from recent advances in biomaterials research, especially where nanotechnology is involved. But discovering the perfect biomaterial that can last the lifetime of a patient is still a challenge.

Read more in 'Opportunities for nanotechnology-enabled bioactive bone implants' in issue 18 of Journal of Materials Chemistry

Coating traditional implant materials, such as titanium, with selenium nanoclusters produces implants that can inhibit cancer

Reference
P A Tran *et al.*, *J. Mater. Chem.*, 2009, DOI: 10.1039/b814334j

Essential elements

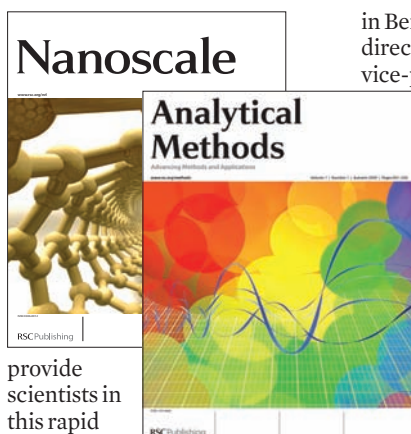
Announcing two new journals

The prestigious RSC Publishing journal portfolio is set for further expansion with the launch of two new monthly titles in autumn 2009.

Analytical Methods will highlight new and improved methods for the practical application of analytical science. The journal will complement the existing RSC journal portfolio of analytical science publications, and with its focus on fundamental and applied modern analytical science, will appeal to both academic and industrial scientists.

Analytical Methods was announced at Pittcon in Chicago, IL, US, on 8 March. Delegates had the opportunity to be the first to find out about this exciting new journal.

Nanoscale will publish experimental and theoretical work across the breadth of nanoscience and nanotechnology. Highly interdisciplinary, the journal will



provide scientists in this rapid growth field with a new platform characterised by the quality and innovation for which RSC Publishing products are renowned.

Nanoscale will be published in collaboration with leading nanoscience research centre, the National Center for Nanoscience and Technology (NCNST)

in Beijing, China. Chunli Bai, director of NCNST and executive vice-president of the Chinese Academy of Sciences, will be editor-in-chief of a new Asia-Pacific editorial office for *Nanoscale*. Markus Niederberger of ETH Zurich, Switzerland, and Francesco Stellacci from Massachusetts Institute of Technology, US, will head two further regional offices in Europe and North America.

From launch, the latest issue of *Analytical Methods* and *Nanoscale* will be freely available to all readers via the website. Free institutional online access to all 2009 and 2010 content will be available following a simple registration process.

Visit www.rsc.org/methods and www.rsc.org/nanoscale to find out more.

Better alerting

A programme to improve alerting services for RSC publications is underway. Subscribers to journal content E-Alerts can now view and amend their alerting preferences online via a secure link to a profile page provided on every alert they receive. With RSS feeds of latest articles published online (enhanced with structured subject and compound information where available)



and Google gadgets offering exciting new ways to discover RSC journal articles from your Google desktop, keeping up with the latest published research has never been easier.

For more information about alerting services and to subscribe visit www.rsc.org/Publishing/Technology/alerting.asp

Organic & Biomolecular Chemistry's 150th issue!

Issue 6, 2009 is the 150th issue of *OBC*. Since the first issue was published in January 2003, *OBC* has achieved tremendous success. With an impact factor of 3.167, can any other young journal boast such highly cited papers, published quickly after independent peer review?

Jeffrey Bode, University of Pennsylvania, US, comments, '*OBC* encourages and appreciates the development and application of innovative organic chemistry to a wide variety of contemporary problems. It is our choice for the

publication of new methods and concepts that reach beyond the traditional subdivisions of organic chemistry.'

Take a look at some of the high impact papers from leading scientists published in this 150th issue of *OBC*: a perspective on the design and synthesis of phosphole-based systems for novel organic materials by Yoshihiro Matano and Hiroshi Imahori; an emerging area article on metal-catalysed halogen exchange reactions of aryl halides by Tom Sheppard;

a communication on highly enantioselective asymmetric autocatalysis using chiral ruthenium complex-ion-exchanged synthetic hectorite as a chiral initiator by Kenso Soai and colleagues; and a full paper on ruthenium-based metallacrown complexes for the selective detection of lithium ions in water and in serum by fluorescence spectroscopy by Kay Severin *et al.* Don't miss these and the other articles in this celebratory issue. For more details visit www.rsc.org/obc

Chemical Technology (ISSN: 1744-1560) is published monthly by the Royal Society of Chemistry, Thomas Graham House, Science Park, Milton Road, Cambridge UK CB4 0WF. It is distributed free with *Chemical Communications*, *Journal of Materials Chemistry*, *The Analyst*, *Lab on a Chip*, *Journal of Atomic Absorption Spectrometry*, *Green Chemistry*, *CrysEngComm*, *Physical Chemistry Chemical Physics*, *Energy & Environmental Science* and *Analytical Abstracts*. *Chemical Technology* can also be purchased separately. 2009 annual subscription rate: £199; US \$396. All orders accompanied by payment should be sent to Sales and Customer Services, RSC (address above). Tel +44 (0) 1223 432360, Fax +44 (0) 1223 426017 Email: sales@rsc.org

Editor: Joanne Thomson
Deputy editor: Sarah Dixon
Associate editors: Celia Gitterman, Elinor Richards
Interviews editor: Ruth Doherty
Web editors: Nicola Convine, Michael Townsend, Debora Giovannelli
Essential elements: Christine Hartshorne, Rebecca Jeeves
Publishing assistant: Jackie Cockrill
Publisher: Graham McCann

Apart from fair dealing for the purposes of research or private study for non-commercial purposes, or criticism or review, as permitted under the Copyright, Designs and Patents Act 1988 and the copyright and Related Rights Regulations 2003, this publication may only be reproduced, stored or transmitted, in any form or by any means, with the prior permission of the Publisher or in the case of reprographic reproduction in accordance with the terms of licences issued by the Copyright Licensing Agency in the UK. US copyright law is applicable to users in the USA.

The Royal Society of Chemistry takes reasonable care in the preparation of this publication but does not accept liability for the consequences of any errors or omissions. The RSC is not responsible for individual opinions expressed in *Chemical Technology*. Content does not necessarily express the views or recommendations of the RSC.

Royal Society of Chemistry: Registered Charity No. 207890.

RSC Publishing

Adoption of green chemistry—view from the Director of the ACS Green Chemistry Institute®

DOI: 10.1039/b904513a

“There can be both real and perceived barriers to the greater adoption of green chemistry.”

That statement, written seven years ago by the Royal Society of Chemistry’s Environment, Health and Safety Committee, is just as valid in 2009 as it was in 2002. That does not mean, however, that we haven’t made progress. Just the opposite. We have made tremendous inroads in addressing and overcoming many of the barriers that were cited in the Committee’s “Note on Green Chemistry”.

For example, one of the listed barriers was insufficient guidance on best practices for green chemistry. Run a check today of the U.S. Environmental Protection Agency’s website and you will find a plethora of international programs and resources listed under the Agency’s “Gateway to International Best Practices & Innovations” (<http://www.epa.gov/ncei/international/chemicals.htm#programs>). There are links to numerous databases and case studies, programs and projects such as European Eco-Label and REMADE Scotland, and assorted newsletters, publications and reports.

Unfortunately, the current global economic downturn we are experiencing will adversely impact our efforts to promote and market the idea of introducing new green chemistry and engineering

processes. Companies are understandably pushing back on anything that might require additional monetary startup commitments. Of course, as I like to point out to executives, investors and lawmakers, green chemistry is a business and investment opportunity for our future. It can even be a competitive advantage.

I firmly believe that the monetary dol-drumms we are now experiencing are equivalent to a series of speed bumps we must pass over before we round the corner and get our green chemistry engines back up to highway speed. The speed bumps only temporarily slow down our journey to a sustainable world; they won’t stop us from getting there.

On the bright side, a major area of progress for green chemistry and the entire field of sustainability, in my opinion, has been a notable cultural movement toward not simply an acceptance of the need for sustainable products, but indeed a *demand* for eco-friendly products and practices. Entire industries have emerged and blossomed around this demand.

As heartening as this societal response has been, we must keep our commitment to green chemistry front and center in our minds and actions. We cannot let up. We must renew and reenergize, making our case to the public, to lawmakers, to industrial leaders, to educators and to

other chemists that green chemistry is the ultimate solution to a sustainable future. Communication is the key to advancing the green chemistry agenda and all of us have a responsibility in this area. When I say green chemistry what I really mean is green chemistry *and* green engineering are the keys to a sustainable world.

Sometimes, public and corporate memory can be short. Lessons learned and pledges made when times are lean are too often forgotten when things get better. As practitioners, teachers and staunch advocates for green chemistry, it is our individual and collective responsibility to tweak those fading memories. We must remind people that it is critically important not to lose sight of the fact that it is imperative that we find safer sustainable ways of conducting chemistry for the benefit of the citizens of our world without endangering or destroying the planet’s precious resources and environment.

There’s never been a better time to be a green chemist or engineer. If it sounds like I am beating the green chemistry drum a bit loudly, that’s because I am! I’m proud to be one of the drum majors in our march toward sustainability.

Robert Peoples

Director, ACS Green Chemistry Institute®, Washington DC, USA

A solvent free process for the generation of strong, conducting carbon spheres by the thermal degradation of waste polyethylene terephthalate

Swati V. Pol,^a Vilas G. Pol,^{*a} Dov Sherman^b and Aharon Gedanken^a

Received 3rd November 2008, Accepted 28th January 2009

First published as an Advance Article on the web 6th February 2009

DOI: 10.1039/b819494g

An efficient, solvent-free, catalyst-free approach is reported for the synthesis of strong, paramagnetic, conducting carbon microspheres from used polyethylene terephthalate (PET). The thermal decomposition of used PET polymer at 700 °C for 3 h in a closed reactor under autogenic [self generating] pressure yielded exceptionally hard spherical (2 to 10 μm diameters) solid carbon bodies, with the average tensile strength for a single [~6 μm diameter] carbon sphere calculated to be 8.30 ± 0.69 GPa.

The degradation of waste polymers¹ is a difficult task and a challenge for today's scientists due to their high volume and resistance to decomposition (often taking hundreds of years). This work is devoted to resolve the degradation challenge of used PET or waste² polymers, converting it in to technologically important very hard carbonaceous products. The scalable process is described for the remediation of polymer waste, and the obtained carbonaceous materials are characterized. Carbon materials are known to have a wide range of structural and textural properties, and thus extensive applications.³ Carbon spheres,⁴ beads,⁵ and onions⁶ have been synthesized by very different processes. Accordingly, various applications have been intensively developed, of which we highlight nanodevices,⁷ energy storage,⁸ separation technology,⁹ lubricants, *etc.*, which are attracting much interest from carbon scientists worldwide. Chemical vapor deposition,⁴ and pressure carbonization^{5,10} are a few convenient methods employed to synthesize spherical carbons. However, in the literature, most of the synthesis techniques to produce pure carbon spherules (CSs) are limited by several factors. In a few cases, the proportion and yield of the CSs is low, and the spheres cannot be easily separated from the remaining carbon soot. In some of the cases, the catalysts are trapped and remain as an additional impurities in the product that needs further processing. For practical applications, a high percentage of pure CSs are required.

To fabricate the high tensile strength carbon from the used PET, 1 g pieces of used PET are introduced into the stainless steel (SS) reactor having a 5 cc volume at room temperature. The closed SS reactor filled with used PET placed inside the center of the tube furnace, heated at 700 °C/3 h and gradually cooled. The reaction took place under the autogenic pressure of the decomposed PET, and produced 100% spherical carbon

bodies. Either used PET [washed Coca cola bottles] or PET bought from industrial sources produced similar CSs under analogous reaction conditions. The autogenic pressure during the course of the thermolysis of PET was measured as a function of temperature using a system consisting of a pressure transducer and pressure gauge, as described elsewhere.¹¹ The maximum pressure of 490 psi is recorded after the thermolysis of PET at 700 °C in a closed reactor. The autoclave, made of 'Haynes 230 alloy' (Parr instruments), could be repeatedly used for such incineration processes.

The SEM image (JEOL 6300F, Fig. 1a and its inset) shows the spherical morphology and the smooth surfaces of the formed CSs between 2 to 10 μm in diameter. The TEM (JEM-1200EX) of a single carbon sphere (CS) also showed a perfect spherical shape with a smooth surface (Fig. 1b). The 2D electron diffraction pattern of CS exhibits the typical 002 and 110 diffractions of the graphitic carbon (Fig. 1c). To probe whether the CSs are hollow or solid, microtome is performed according to Spurr's formulation. We broke one diamond knife and damaged a second during the horizontal cross section of the CSs. This reflects on the very hard nature of the CSs, which led us to further investigate the mechanical properties of the product. Fig. 1d clearly illustrates that the CSs are solid/full. Additionally, to check the strength, we applied 7000 psi pressure on these CSs for 20 min. TEM pictures revealed that under this pressure no changes in the size or shape of the CSs are observed. These results also indicated the solid and hard nature of the CSs. Such solid CSs might find application in lubricants. The lowering of reaction temperature below 700 °C fabricates 5–10 μm diameter carbon particles, which can have applications in printers, toners or filtration technology.

The C, H, N, S elemental chemical (Eager 200) analysis of the CSs showed the presence of ~97 wt% carbon and a very small presence of hydrogen (<0.4% wt%). Additional elemental analysis measurements, conducted by the energy dispersive X-ray technique (EDX) in the SEM mode, detected a huge peak of carbon (Fig. 2a) and additional elements such as ~1.4 wt% Si and 1 wt% of Ca.

Raman spectrum [Fig. 2b, Jobin Yvon Horiba] of CSs is characteristic of a mixture of disordered, D (1330 cm⁻¹), and nanosized graphitic, G (1590 cm⁻¹), crystals with an ID/IG ratio of 1.01. This ratio indicates a glass-like carbon structure, with some lattice edges within the analyzed CSs.¹² The XRD pattern [Fig. 2c] of as-prepared CSs shows a high relative intensity ratio of the 002 to 110 main diffraction peaks of the graphitic lattice. The interlayer spacing calculated from the 00l diffraction lines is roughly 0.346 nm. TGA measurement confirms that these as-formed solid CSs are stable or robust up to 600 °C either in air or

^aCenter for Advanced Materials and Nanotechnology, Bar-Ilan University, Ramat-Gan, 52900, Israel. E-mail: vilaspol@gmail.com

^bTechnion, Israel Institute of Technology, Department of Materials Engineering, 32000, Haifa, Israel

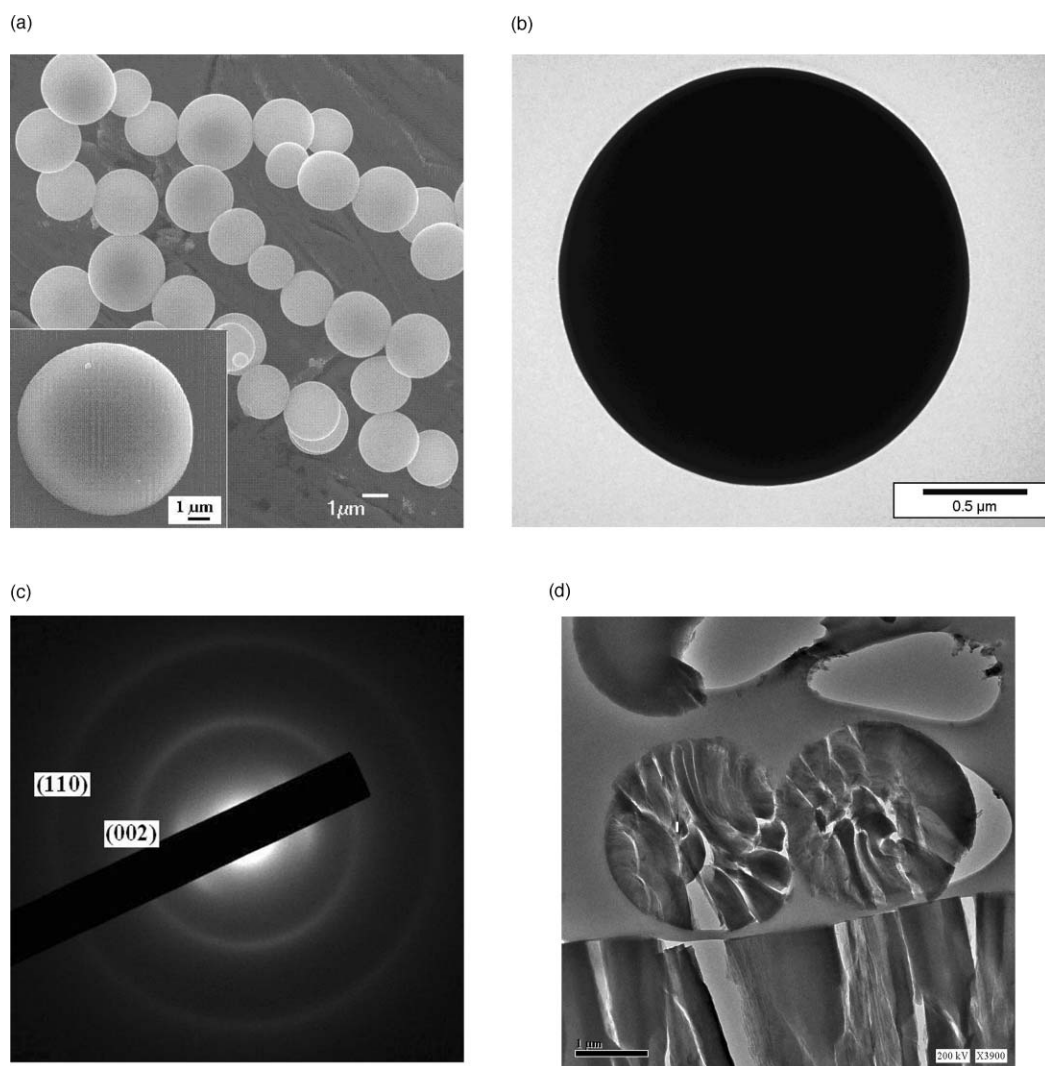


Fig. 1 HR-SE micrographs of (a) CSs, inset single CS, (b) TEM of CS, (c) ED pattern taken on CS, and (d) cross-section TE micrograph of CSs.

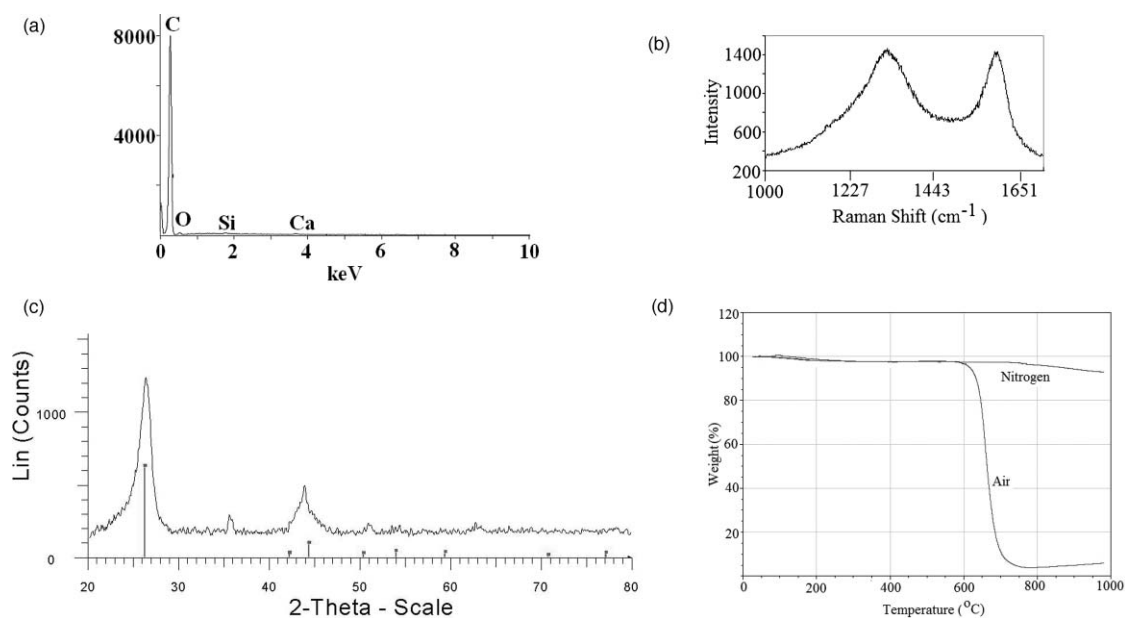


Fig. 2 (a) EDS of CSs, (b) Raman spectrum of CSs, (c) XRD pattern of CSs, (d) the TGA analysis of CSs in air and nitrogen atmosphere.

in an inert atmosphere (Fig. 2d). Above 600 °C, an additional 3% weight loss is noticed in nitrogen up to 980 °C, while the carbon starts burning in air atmosphere. The 3% remaining residue at 800 °C, under a flow of air, is due to the silica and Ca remains. The room temperature electron paramagnetic resonance (EPR, Bruker ER083 CS) spectrum is recorded at an X-band ($\nu = 9.77$ GHz) with a 100 kHz magnetic field modulation. The CSs showed a strong paramagnetic signal, peak-to-peak separation (ΔH_{pp}) of 40 G and a g -value of 2.00277, close to the g -factor for an unbound electron.¹³ The measured Brunauer-Emmett-Teller (BET) surface area (Micromeritics Gemini 2375) of CSs is 2.1 m²/g.

The impedance measurements were carried out using a battery test unit Model 1470 coupled with an FRA Model 1255 from Solartron, Inc. (driven by Corrware and ZPlot software from Scribner Assoc.). The alternating voltage amplitude in impedance measurements was 3 mV, and the alternating current frequency range used was 50 kHz to 100 Hz. The CSs sample pellet (geometric area around 3.1 cm²) was prepared at a pressure of 6000 psi. The impedance measurements of the CSs showed resistances of $R = 1.37 \Omega$ at RT and $R = 0.75 \Omega$ at 60 °C. When measured again at RT, the resistance is stabilized at around $R = 0.91 \Omega$. These numbers relate to the ac frequency of 50 kHz, and it should be mentioned that the resistance of the sample only slightly depends on the frequency (in the range of 50 kHz–100 Hz).¹² At the same time, the resistance of the “Pure-carbon–polyvinylidene fluoride” (PVDF is used as a binder) sample (3.1 cm² area) is around 16 Ω . From these preliminary results, we conclude that the carbon obtained from used PET possesses *ca.* 10 times higher conductivity ($1/R$) than that of the standard “Pure-carbon–PVDF” sample. The achieved higher conductivity could be due to the Si or Ca detected in EDX and TGA.

The tensile strength of the hard spheres was evaluated by direct measurement of the compressive load to fracture, conjugated with an analytical solution for CSs under compression. The moveable, flat diamond anvil was attached to a 2.5 N full capacity load cell (Fig. 3a), and both were attached to a step motor driven stage with displacement rate of minimum of $\dot{u} = 50$ nm per second. The CS on the moveable anvil (Fig. 3a and Fig. 3b) until full contact occurred. Thereafter, it was loaded to fracture while the load was directly recorded using Lab View software. The load showed linear behavior with time until fracture. The CS was broken at its center and divided into two major pieces, with dense solid carbonaceous debris (Fig. 3c and 3d). The well-shaped CSs are glass-like [Raman measurement] and hard enough due to their similar structure to Brooks–Taylor type mesophase hydrocarbons,¹⁴ which are the origin of the stripping pattern observed in the spherules cross sections. Brook and Taylor began a systematic study of carbonaceous¹³ mesophases, which generally lead to the formation of spherical carbon bodies with basal planes perpendicular to the spherule interface that formed under their autogenic pressure.¹⁵ Hishiyama *et al.* has been also proposed a detailed structural model based on the HR-TEM analysis on similar carbon spheres.¹⁶ Kulikovskiy studied the structure of hard graphite-like amorphous carbon films by electron diffraction and confirmed that under considerable compressive stress¹⁷ the interplane distance d_{002} could be shortened

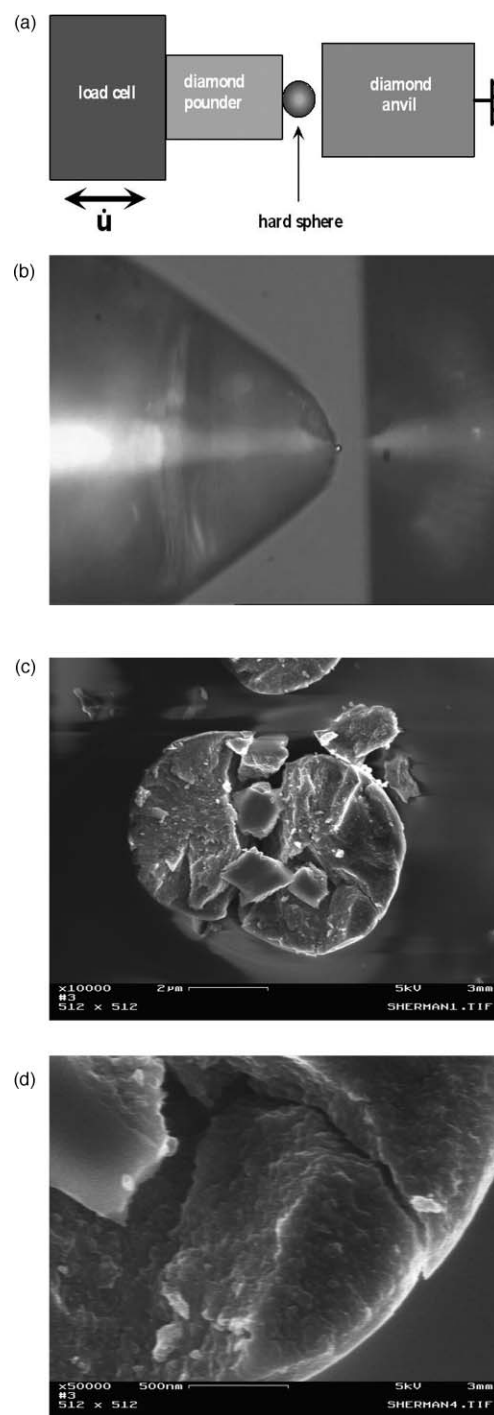


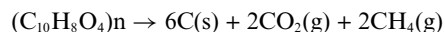
Fig. 3 (a) Compressive load apparatus, (b) the isolated single hard sphere moved by a micrometre size pin, (c) SEM images of a broken CS, and (d) densely packed carbon material shown at high resolution.

down to approximately 0.300 nm. Amaratunga *et al.* reported on hard elastic carbon thin films based on electron-energy-loss spectra, which revealed a reduction in Π (sp^2) bonding in the intersecting regions of the nanoparticles that are covalently¹⁸ linked by tetrahedral sp^3 bonds.

The tensile strength of the hard CSs is estimated by calculating the nominal (average) compressive stress, $\bar{\sigma}_{nom}$, using: $\bar{\sigma}_{nom} = P_{cr}/\pi r^2$, where P_{cr} is the load to fracture and r is the radius of the sphere. The diameter of the spheres was measured by an optical

microscope with a resolution of $\pm 0.2 \mu\text{m}$ ($\pm 3.3\%$ in our range of diameters) and the resolution of the load measurements was $\pm 5\%$, hence our results for a single measurement have a resolution of $\pm 8.3\%$. We performed 5 fracture tests. The average compressive stress at failure was, $\bar{\sigma}_{\text{nom}} = 830 \pm 69 \text{ MPa}$, with SD of 62 MPa, which is within the resolution of the results. $\bar{\sigma}_{\text{nom}}$ sets a common normalized load to fracture when hard carbon spheres under compression is concern. Analytical solutions for the stress distribution in hard spheres loaded between two hard plates exist in the literature.^{19–20} The recent analysis of Chau and Wei gives¹⁸ the most advanced analysis. We assume that in our experiments, when the hard sphere is in contact with the diamond plates, the contact is over a small contact zone ($\theta_0 \sim 2^\circ$). The Poisson's ratio of the hard sphere is assumed as 0.2. Using linear interpolation of the data given,²¹ we estimate that the maximum tensile stresses in the hard sphere before failure is $10\bar{\sigma}_{\text{nom}}$, namely, the maximum tensile stresses are $8.3 \pm 0.69 \text{ GPa}$. Lacerda *et al.* described the structure of argon assisted tetrahedral amorphous carbon films with highest stress²² ($>10 \text{ GPa}$) and plasmon energy (29.5 eV). In our study, the CS was broken in the middle based on the place of maximum tensile stresses, confirmed by SEM micrograph.

The TGA-MS measurements confirmed that used PET turns into CO_2 , CH_3 and oxygen at $-450 \text{ }^\circ\text{C}$, further dissociation of these molecules at $700 \text{ }^\circ\text{C}$ yielded CSs [35 wt%] under an autogenic pressure.



In conclusion, an efficient, solvent-free, catalyst-free, scalable approach for the synthesis of ultra strong (average tensile strength, $8.30 \pm 0.69 \text{ GPa}$), paramagnetic, conducting carbon microspheres (2 to $10 \mu\text{m}$) from used PET is demonstrated. This

report explains how the waste polymer can be turned into useful carbonaceous material with a simple, effective decomposition approach.

Notes and references

- 1 A. Salmiaton and A. Garforth, *Waste Management*, 2007, **27**, 1891.
- 2 M. Lu and S. Kim, *J. Appl. Polym. Sci.*, 2001, **80**, 1052.
- 3 M. Inagaki, *Solid State Ionics*, 1996, **86**, 833.
- 4 P. Serp, *Carbon*, 2001, **39**, 621.
- 5 M. Inagaki, M. Washiyama and M. Sakai, *Carbon*, 1988, **26**, 162.
- 6 S. Tomita, T. Sakurai, H. Ohta, M. Fujii and S. Hayashi, *J. Chem. Phys.*, 2001, **114**, 7477.
- 7 P. G. Collins, A. Zettl, H. Bando, A. Thess and R. E. Smalley, *Science*, 1997, **278**, 100.
- 8 G. L. Che, B. B. Lakshmi, E. R. Fisher and C. R. Martin, *Nature*, 1998, **93**, 346.
- 9 M. B. Shiflett and H. C. Foley, *Science*, 1999, **285**, 1902.
- 10 M. Inagaki, K. Kuroda and M. Sakai, *Carbon*, 1983, **21**, 231.
- 11 V. G. Pol and P. Thiyagarajan, *Ind. Eng. Chem. Res.*, 2009, **14**, 1484.
- 12 V. G. Pol, S. V. Pol, B. Markovsky, J. M. Calderon-Moreno and A. Gedanken, *Chem Mater.*, 2006, **18**, 1512.
- 13 H. B. Willard, L. L. Merritt and J. A. Dean, *Instrumental methods of analysis*, 5th edn, D. Van Nostrand Comp., New York, 1974, 189–202.
- 14 J. D. Brooks and G. H. Taylor, *Nature*, 1965, **206**, 697.
- 15 V. G. Pol, M. Motiei, J. M. Calderon-Moreno, M. Yoshimura and A. Gedanken, *Carbon*, 2004, **42**, 111.
- 16 Y. Hishiyama, A. Yoshida and M. Inagaki, *Carbon*, 1982, **20**, 79.
- 17 V. Kulikovskiy, K. Metlov, A. Kurdyumov, P. Bohac and L. Jastrabik, *Diamond Rel. Mater.*, 2002, **11**, 1467.
- 18 J. Amaratunga, M. Chhowalla, C. J. Kiely, I. Alexandrou, R. Aharonov and R. M. Devenish, *Nature*, 1996, **383**, 321.
- 19 S. Z. Wu and K. T. Chau, *Mech. Mater.*, 2006, **38**, 1039.
- 20 Y. Hiramoto and Y. Oka, *Inter. J. Rock Mech. Mining Sci.*, 1966, **3**, 89.
- 21 K. T. Chau and X. X. Wei, *Int. J. Solids Struct.*, 1999, **36**, 4473.
- 22 R. G. Lacerda, P. Hammer, F. L. Freire, Jr., F. Alvarez and F. C. Marques, *Diamond Relat. Mater.*, 2000, **9**, 796.

Simple and quick preparation of α -thiocyanate ketones in hydroalcoholic media. Access to 5-aryl-2-imino-1,3-oxathiolanes†‡

Fabrizio R. Bisogno, Anibal Cuetos, Iván Lavandera and Vicente Gotor*

Received 6th January 2009, Accepted 17th February 2009

First published as an Advance Article on the web 26th February 2009

DOI: 10.1039/b900137a

A simple preparation on gram-scale of thiocyanate derivatives *via* nucleophilic substitution of halogenated compounds with SCN salts at high substrate concentrations in a few minutes and excellent yields was successfully accomplished in hydroalcoholic media. The obtained compounds were employed for the efficient synthesis of valuable 5-aryl-2-imino-1,3-oxathiolane derivatives (a one-pot approach is also presented).

In the last few years, sustainable processes are highly demanded in the chemical industry.¹ The “process efficiency” concept is not only related to a high chemical yield, but also to the minimised use of large amounts of harmful organic solvents and production of chemical waste.² The choice of an appropriate solvent is not a simple issue.^{3–5} From an environmental point of view, aqueous solvents are often an attractive option.^{6,7} Consequently a number of organic processes are designed to be carried out either in pure water or in aqueous mixtures.^{8,9}

Thiocyanate compounds have attracted great attention as interesting intermediates due to its easy transformation into highly valuable molecules applied to both organosulfur and heterocyclic chemistry. These compounds possess a broad range of bioactivities and applications as anticancer agents, insecticides, antiasthmatic drugs, DNA topoisomerase inhibitors, *etc.*^{10–13} Several routes to prepare alkyl thiocyanate derivatives have been reported including the oxidative thiocyanation of silyl enol ethers with hypervalent iodine-lead(II) thiocyanate reagents¹⁰ and S_N2 reactions using task-specific ionic liquids containing SCN as a counterion^{11,12} or in organic solvents employing KSCN^{14,15} or TMSNCS.¹⁶ Also the α -thiocyanation of ketones using I₂¹⁷ or FeCl₃¹⁸ with NH₄SCN or the transformation of thiols employing a Ph₃P/Br₂/NH₄SCN mixture¹⁹ or alkenes with CAN/NH₄SCN²⁰ have been shown. Finally, the formation of β -hydroxy thiocyanates *via* oxirane ring-opening with NH₄SCN has been described.²¹ In most cases, several reagents, organic solvents and high temperatures were employed, and therefore purification by chromatography was necessary. This

is in contrast with the optimum conditions to synthesise these compounds since the isomerisation thiocyanate-isothiocyanate can occur in solution at temperatures above 50 °C and/or acidic conditions.^{10,16,22} For these reasons, the development of new procedures for the easy and rapid synthesis of thiocyanate derivatives in high yields is required.

Herein we report our efforts in the preparation of versatile thiocyanate compounds in aqueous mixtures at high substrate concentrations and further conversion into the interesting heterocyclic 2-imino-1,3-oxathiolane system employing mild reaction conditions and cheap reagents.

In a first set of experiments, we carried out the reactions using α -bromoacetophenone (**1a**) as the model substrate at a very high substrate concentration and room temperature (Table 1). MeCN and MeOH were chosen as solvents for the first approach since they could solubilise the SCN salt (entries 1 and 2). The reactions took place homogeneously and were accomplished very quickly but a tedious and inconvenient work-up was necessary: evaporation of the water-miscible solvent at low temperature to avoid the isomerisation of the thiocyanate group, redissolution of the crude reaction in a suitable solvent (for instance, CH₂Cl₂), wash with water several times to eliminate the remaining salts, and reevaporation of the organic solvent at low temperature. Bearing this in mind, we speculated that whether the reaction took place heterogeneously in an aqueous mixture and the desired product would precipitate, a simpler and more effective work-up could be applied. In this way, when a MeOH/H₂O 1 : 1 (v/v) mixture was employed (entry 3), a solid was quickly formed, then filtered off and washed with water, obtaining to our delight an excellent

Table 1 Optimisation of the model reaction^a

Entry	Solvent	Time/min	SCN source	Yield (%) ^b
1	MeCN	4	NH ₄ SCN	95
2	MeOH	4	NH ₄ SCN	90
3	MeOH/H ₂ O 1 : 1	10	NH ₄ SCN	94
4	MeOH	25	KSCN	87
5	MeOH/H ₂ O 1 : 1	20	KSCN	68
6	EtOH	3	NH ₄ SCN	93
7	EtOH/H ₂ O 1 : 1	8	NH ₄ SCN	96
8	^t PrOH	3	NH ₄ SCN	96
9	^t PrOH/H ₂ O 1 : 1	3	NH ₄ SCN	96

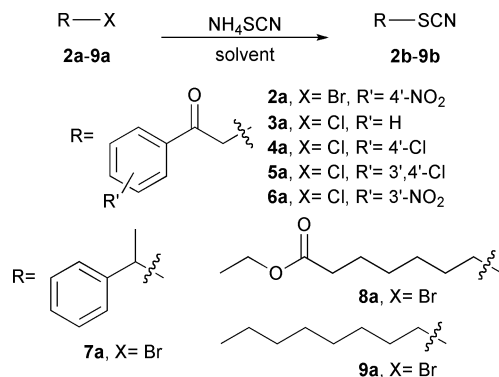
^a Substrate concentration: 1.25 M. For reaction conditions, see ESI†.

^b Isolated yields.

Departamento de Química Orgánica e Inorgánica, Instituto Universitario de Biotecnología de Asturias, University of Oviedo, 33006, Oviedo, Spain. E-mail: vgs@fq.uniovi.es; Fax: +34 985 103448; Tel: +34 985 103448

† Electronic supplementary information (ESI) available: General experimental procedures as well as compound characterisation of **1c**, **2c**, **4c**, **5c**, and **6c**. See DOI: 10.1039/b900137a

‡ Compounds **1b**,^{10,18} **2b**,^{13,29} **4b**,^{20,29} **5b**,²⁹ **6b**,^{30,31} **7b**,^{16,32} **8b**³³ and **9b**³⁴ have previously been described and their physical properties were in agreement with those reported.

Table 2 S_N2 reaction with different types of alkyl halides (**2a–9a**)^a

Entry ^a	Substrate	Product	Time	T/°C	Solvent	Yield (% ^b conv.) ^c
1	2a	2b	4 min	rt	^t PrOH/H ₂ O 1 : 1	97
2	3a	1b	24 h	rt	^t PrOH/H ₂ O 1 : 1	82
3	4a	4b	27 h	rt	^t PrOH/H ₂ O 1 : 1	96
4	5a	5b	27 h	rt	^t PrOH/H ₂ O 1 : 1	95
5	6a	6b	25 h	rt	^t PrOH/H ₂ O 1 : 1	94
6	7a	7b	5 h	rt	^t PrOH	16 ^d (65)
7	8a	8b	3.3 h	50	EtOH	95
8 ^e	9a	9b	3 h	50	^t PrOH/H ₂ O 1 : 1	30 ^d (88)

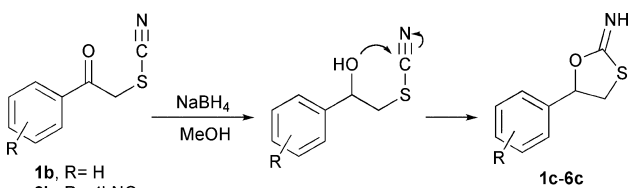
^a Substrate concentration: 1.25 M. For reaction conditions, see ESI†. ^b Isolated yields. ^c Conversions calculated by ¹H-NMR. ^d After *flash* chromatography on silica gel. ^e Substrate concentration: 0.26 M.

yield of the pure desired product **1b**. Regarding to the SCN source, the ammonium salt provided shorter reaction times as compared with the potassium one (entries 4 and 5), and therefore was chosen for the subsequent experiments. We extended this procedure to other alcohols such as EtOH and 2-propanol, these reactions were either homogeneous (entries 6 and 8) or heterogeneous (entries 7 and 9). For the homogenous one, we modified the work-up of the reactions. Once the process was complete, water (five-fold volume) was added to the crude, precipitating the final compound with very high yields. As can be noticed, water/organic solvent combinations also afforded excellent yields in a very short time.

Due to the simplicity of the reaction conditions and the excellent yields obtained when using the mixture ^tPrOH/H₂O, we tested it as a medium with different alkyl halides **2a–9a** (Table 2). From the results obtained, several interesting features can be highlighted. An important reactivity difference was noticed depending on the halide (compare Table 1, entry 9 with Table 2, entries 1–5) since the reaction with α -bromo ketones **1a–2a** took a few minutes while several hours for α -chloro derivatives **3a–6a** although excellent yields were also obtained. This fact can be explained due to the better ability of Br over Cl as leaving group. Such a big difference makes this method suitable to chemoselectively substitute bromide rather than chloride by careful control of the SCN equivalents and the reaction time. It is important to remark that these reactions were performed on gram-scale, showing the robustness of this methodology. On the other hand, it was noteworthy the different reactivity of activated substrates such α -carbonyl or benzylic halides (**2a–7a**, entries 1–6) in contrast to the non-activated ones (**8a–9a**, entries 7 and 8). In the case of compound **7a**, the solvent used was ^tPrOH due to the fact that in the aqueous solution a complex

mixture of products was obtained. For bromides **8a** and **9a**, no conversions were detected even after long reaction time when reactions were performed at room temperature, but good to excellent conversions were reached at 50 °C. To synthesise **8b**, ethanol was employed as solvent to avoid the transesterification reaction. The final product appeared as a second phase which could easily be separated as the pure derivative. When *flash* chromatography was used to isolate the final compounds **7b** and **9b** (entries 6 and 8), yields substantially dropped emphasising the relevance of avoiding this separation technique.

With the aim of demonstrating the applicability of this class of compounds we envisaged the possibility of synthesising several 2-imino-1,3-oxathiolane derivatives starting from α -thiocyanate ketones **1b–6b**. There are only a few reports concerning the synthesis of this valuable motif, either by [4 + 1] cycloaddition reactions employing harsh conditions (100 °C, sealed tube) in argon atmosphere²³ or by Cu(I)-catalysed coupling of *o*-iodophenols and aryl isothiocyanates under nitrogen atmosphere at 80 °C.²⁴ The 2-imino-1,3-oxathiolane core is present in compounds with potential bioactivities.^{23,25} With this in mind, we designed a strategy whereby simple reduction of the carbonyl moiety plus further addition of a suitable base and/or adjuvant such as a crown ether or phase transfer catalyst,²¹ it would be possible to obtain the desired heterocycle. Thus, the standard reduction of **1b** with NaBH₄ in MeOH was assayed (Table 3, entry 1). After three min, we were pleased to find out that the formed product was not the expected hydroxy thiocyanate intermediate but the 2-imino-1,3-oxathiolane derivative **1c**. This finding may be rationalised by considering the high pH (~9, see ESI†) due to the presence of hydride and methoxide species which deprotonate the OH group of the hydroxy thiocyanate intermediate. Those deprotonated species could act as suitable

Table 3 Preparation of 5-aryl-2-imino-1,3-oxathiolanes **1c–6c**^a


1b, R = H
2b, R = 4'-NO₂
4b, R = 4'-Cl
5b, R = 3',4'-Cl
6b, R = 3'-NO₂

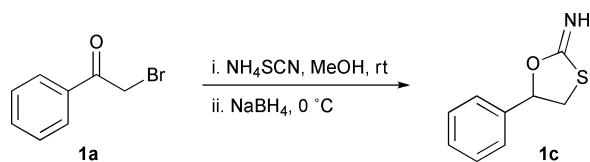
Entry	Substrate	Product	Time/min	Yield (%) ^b
1	1b	1c	3	95
2	2b	2c	3	71
3	4b	4c	3	84
4	5b	5c	3	90
5	6b	6c	3	95

^a For reaction conditions, see ESI†. ^b Isolated yields.

bases to catalyse the cyclisation step. Likewise, this procedure was successfully extended to other similar substrates obtaining the desired products **2c–6c** with high isolated yields in three min (entries 2–5).

In order to corroborate the proposed reaction pathway, we followed the formation of the desired heterocycle **1c** through ¹H-NMR. Thus, the α -thiocyanate ketone **1b** was dissolved in *d*₄-MeOH and the corresponding amount of NaBH₄ was added in the NMR tube, but unfortunately we were not able to detect any intermediate since the reaction proceeded extremely fast. We employed instead a mixture of *d*₈-THF : *d*₄-MeOH 90 : 10% v/v to decelerate the process, thus detecting the hydroxy thiocyanate derivative. These results are in agreement with the accepted mechanism for the epoxide–thiirane conversion.^{21,26–28}

Encouraged by these results and since the S_N2 reaction and the subsequent reduction/cyclisation process occurred under similar conditions, a one-pot three-step procedure starting from the α -bromo ketone **1a** to obtain 2-imino-5-phenyl-1,3-oxathiolane **1c** on gram-scale was carried out as depicted in Scheme 1. We were satisfied to find out that this process smoothly proceeded, furnishing the desired product in 88% overall yield in a few minutes.



Scheme 1 One-pot synthesis of 2-imino-5-phenyl-1,3-oxathiolane from α -bromoacetophenone.

In summary, an efficient protocol to easily obtain, in hydroalcoholic media, valuable α -thiocyanate ketones on gram-scale with excellent yields, at high substrate concentrations and very short reaction times has been developed. On the other hand, it has been demonstrated that a one-pot, three-step procedure was possible to efficiently access the promising 2-imino-1,3-oxathiolane core using readily available starting materials and

inexpensive reagents (NH₄SCN, NaBH₄) producing a minimal amount of waste with high atom economy.

Acknowledgements

F. R. B. is supported by the Programme Alβan, the European Union Program of High Level Scholarships for Latin America (scholarship no. E07D402519AR). I. L. thanks Principado de Asturias for personal funding (Clarín Program). Financial support from the Spanish Ministerio de Ciencia e Innovación (MICINN, Project CTQ2007–61126/PPQ) is gratefully acknowledged.

Notes and references

- R. A. Sheldon, *Green Chem.*, 2007, **9**, 1273.
- B. M. Trost, *Science*, 1991, **254**, 1471.
- C. Capello, U. Fischer and K. Hungerbuehler, *Green Chem.*, 2007, **9**, 927.
- V. Polshettiwar and R. S. Varma, *Curr. Opin. Drug Dis. Dev.*, 2007, **10**, 723.
- R. A. Sheldon, *Green Chem.*, 2005, **7**, 267.
- H. C. Hailes, *Org. Process Res. Dev.*, 2007, **11**, 114.
- C. J. Li and C. Liang, *Chem. Soc. Rev.*, 2006, **35**, 68.
- S. Shi and Y. Zhang, *Green Chem.*, 2008, **10**, 868.
- K. Ahlford, J. Lind, L. Maeler and H. Adolfsson, *Green Chem.*, 2008, **10**, 1055.
- O. Prakash, H. Kaur, H. Batra, N. Rani, S. P. Singh and R. M. Moriarty, *J. Org. Chem.*, 2001, **66**, 2019.
- A. Kamal and G. Choudan, *Tetrahedron Lett.*, 2005, **46**, 1489.
- F. Mohanazadeh and M. Aghvami, *Tetrahedron Lett.*, 2007, **48**, 7240.
- J. Rudolph, H. Theis, R. Hanke, R. Endermann, L. Johannsen and F.-U. Geschke, *J. Med. Chem.*, 2001, **44**, 619.
- R. J. Capon, C. Skene, E. H.-T. Liu, E. Lacey, J. H. Gill, K. Heiland and T. Friedel, *J. Org. Chem.*, 2001, **66**, 7765.
- R. B. N. Baig, V. S. Sudhir and S. Chandrasekaran, *Tetrahedron: Asymmetry*, 2008, **19**, 1425.
- P.-Y. Renard, H. Schwebel, P. Vayron, E. Leclerc, S. Dias and C. Mioskowski, *Tetrahedron Lett.*, 2001, **42**, 8479.
- J. S. Yadav, B. V. S. Reddy, U. V. S. Reddy and A. D. Krishna, *Tetrahedron Lett.*, 2007, **48**, 5243.
- J. S. Yadav, B. V. S. Reddy, U. V. S. Reddy and D. N. Chary, *Synthesis*, 2008, **8**, 1283.
- N. Iranpoor, H. Firouzabadi and H. R. Shaterian, *Tetrahedron Lett.*, 2002, **43**, 3439.
- V. Nair, L. G. Nair, T. G. George and A. Augustine, *Tetrahedron*, 2000, **56**, 7607.
- A. Bellomo and D. Gonzalez, *Tetrahedron Lett.*, 2007, **48**, 3047.
- P. A. S. Smith and D. W. Emerson, *J. Am. Chem. Soc.*, 1960, **82**, 3076.
- V. Nair, B. Mathew, A. U. Vinod, J. S. Mathen, S. Ros, R. S. Menon, R. L. Varma and R. Srinivas, *Synthesis*, 2003, **5**, 662.
- X. Lv, Y. Liu, W. Qian and W. Bao, *Adv. Synth. Catal.*, 2008, **350**, 2507.
- Y. Aizawa, T. Kanai, K. Hasegawa, T. Yamaguchi, Y. Iizuka, T. Iwaoka and T. Yoshioka, *J. Med. Chem.*, 1990, **33**, 1491.
- E. E. van Tamelen, *J. Am. Chem. Soc.*, 1951, **73**, 3444.
- C. C. Price and P. F. Kirk, *J. Am. Chem. Soc.*, 1953, **75**, 2396.
- M. Sander, *Chem. Rev.*, 1966, **66**, 297.
- H. Boehland, I. Berg, K. Heutzenroeder, H. Dehne and J. Teller, Germany (East), DD 284223, A5 19901107, CAN 1991, 115:40790.
- G. E. Lukes and G. P. Wilsey, Jr., USA, US 3222248, 19651207, CAN 1966, 64:35662.
- M. H. Elnagdi, A. H. H. Elghandour and K. U. Sadek, *Spectrochim. Acta A*, 1990, **46A**, 51.
- T. Ando, J. H. Clark, D. G. Cork, M. Fujita and T. Kimura, *J. Org. Chem.*, 1987, **52**, 681.
- I. Norihito, I. Tatsue, Y. Masae and N. Akira, Earth Chemical CO, Japan, JP 56086109, 19810713, CAN 1981, 95:145287.
- Y. Ju, D. Kumar and R. S. Varma, *J. Org. Chem.*, 2006, **71**, 6697.

Magnetic nanoparticle supported ionic liquid catalysts for CO₂ cycloaddition reactions†

Xiaoxi Zheng,^a Sanzhong Luo,^{*a} Long Zhang^b and Jin-Pei Cheng^{*b}

Received 5th January 2009, Accepted 20th February 2009

First published as an Advance Article on the web 27th February 2009

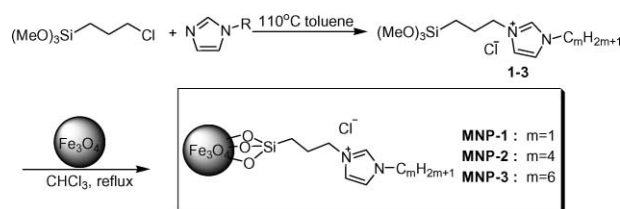
DOI: 10.1039/b823123k

MNP-supported ionic liquid catalysts (MNP-ILs) were developed and evaluated in CO₂ cycloaddition reactions under a lower CO₂ pressure (1 MPa), showing essentially unchanged activity after 11 reuses.

Beyond their simple use as alternative reaction media,¹ ionic liquids are increasingly being explored for targeted chemical tasks due to their modular and tunable structures and properties. Among various functional applications of ionic liquids, ionic liquid-type catalysts represent one of the most prominent advancements.² In this context, immobilization of ionic liquids has been proven to be an effective approach to improve their catalytic efficiency by facile catalyst recycling and reuse; and both organic polymers, such as polystyrene, and inorganic matrices, such as silica, have been frequently employed as the solid supports.³ Though good recyclability and reusability have been achieved in many of these cases, reduced activities are often observed because of poor dispersion of supported ionic liquids in the reaction system. New supports that ensure both good recyclability and activity are still highly desirable to develop supported ionic liquid catalysts.

Magnetic nanoparticles (MNPs) have recently appeared as a new type of catalyst support because of their good stability, easy synthesis and functionalization, high surface area and facile separation by magnetic forces, as well as low toxicity and price.⁴ These attractive features have made MNPs a promising alternative to porous/mesoporous catalyst supports. Recently, MNPs have been successfully utilized to immobilize enzymes,^{4c} transition metal catalysts⁵ and organocatalysts.⁶ Herein, we reported MNP-supported ionic liquids and their application as highly effective and recoverable catalysts for CO₂ cycloaddition reaction.⁷

The magnetic nanoparticle supported IL catalyst **MNP-1** was prepared following the procedure shown in Scheme 1. The ionic liquid precursors **1–3** were prepared by quaternization of *N*-alkyl imidazole with 3-chloropropyl-trimethoxysilane. Magnetite nanoparticles (Fe₃O₄), easily prepared *via* a co-precipitation method,⁸ were chosen as the support. The MNPs were first protected with a layer of silica to prevent aggregation,⁹



Scheme 1 Preparation of MNP-ILs catalysts.

and the obtained SiO₂-MNP was treated with precursor **1** in refluxing CHCl₃ to afford the catalyst **MNP-1** with 0.60 mmol g⁻¹ loading of ILs. Other MNP supported ionic liquids were prepared following the similar procedure with different *N*-alkylimidazole (Scheme 1, **MNP-2** and **MNP-3**).

A TEM image of **MNP-1** confirmed the nanometre size (8–10 nm) of the spherical-shaped catalyst as well as the existence of a silica coating (1–2 nm coating, Fig. 1a). Magnetization curves measured at room temperature showed that **MNP-1** is superparamagnetic (ESI, Figure S2).† The observation of a strong vibration peak at $\nu_{C=N}$ 1632 cm⁻¹ in the IR spectra proved the existence of the imidazolium moiety. The MNP catalysts were well dispersed in a range of solvents, such as H₂O, alcohol, THF and CH₂Cl₂.

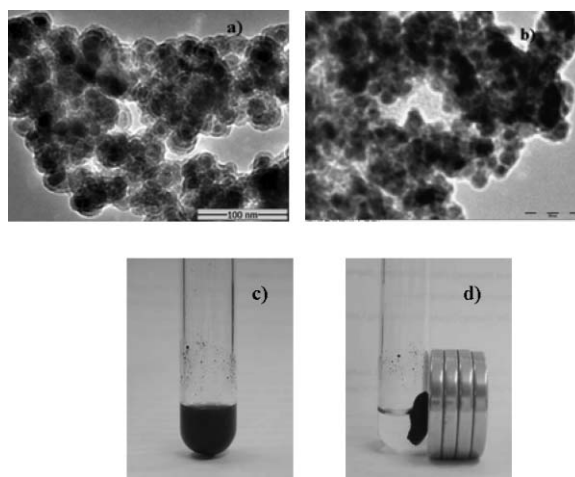


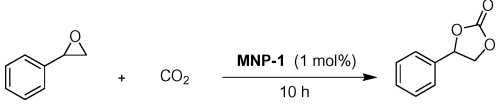
Fig. 1 (a) The TEM image of freshly prepared **MNP-1**; (b) **MNP-1** after 11 reaction cycles; (c) **MNP-1** dispersion in styrene oxide; (d) Catalyst separation with a small magnet.

The MNP-supported ILs were next evaluated in the reaction of CO₂ and epoxide, an important and atom-economic transformation that generates valuable cyclic carbonates from CO₂.

^aBeijing National Laboratory for Molecular Sciences (BNLMS), CAS Key Laboratory of Molecular Recognition and Function, Institute of Chemistry, Chinese Academy of Science, Beijing, 100190, China. E-mail: luosz@iccas.ac.cn; Fax: +86-10-62554449; Tel: +86-1062554446

^bDepartment of Chemistry and State-key Laboratory of Elemento-organic Chemistry, Nankai University, Tianjin, 300071, China. E-mail: chengjp@mail.most.gov.cn

† Electronic supplementary information (ESI) available: Experimental details and characterization of catalysts. See DOI: 10.1039/b823123k

Table 1 Influence of temperature and CO₂ pressure on the yield of styrene carbonate catalyzed by **MNP-1**^a


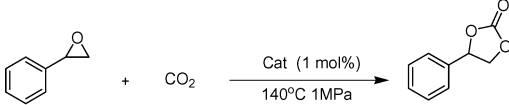
Entry	Temperature/°C	CO ₂ pressure/MPa	GC yield (%) ^b
1	140	0.1	— ^c
2	140	0.2	14
3	140	0.5	49
4	140	1.0	87
5	110	1.0	53
6	80	1.0	— ^c
7	25	1.0	— ^c

^a Reaction conditions: styrene oxide (10 mmol), **MNP-1** (1 mol%), 10 h.
^b Determined by GC. ^c No reaction.

Great efforts have been made to develop efficient catalysts for the cycloaddition of CO₂ to epoxide¹⁰ and ILs were recently found as a new type of catalyst for this reaction.¹¹ Supported ILs have also been examined as catalysts in the reaction and reasonably good activity and reusability have been achieved. For example, He *et al.*¹² reported that silica supported ILs could promote the reaction under high pressure (8 MPa) of CO₂ and the supported catalyst could be recycled 4 times. Han *et al.*¹³ grafted ILs onto a highly cross-linked polymer matrix, and the obtained catalyst could be reused for 4–5 cycles. In spite of those advances, the development of highly active heterogeneous IL catalysts for this important reaction is still highly desirable.

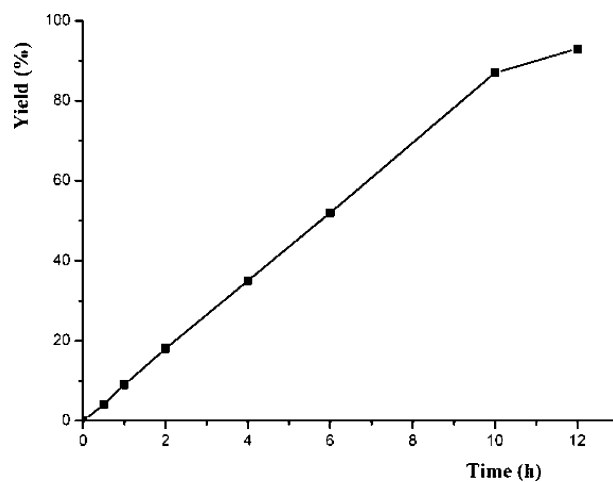
To our delight, the MNP-IL, *e.g.* **MNP-1**, was found to be an effective catalyst (with 1 mol% loading based on the imidazolium moiety) for the model reaction of styrene oxide (Table 1). The optimal conditions were determined to be 140 °C and 1 MPa CO₂. As shown in Table 1, the reaction under either lower temperature or lower pressure gave inferior results. It is noted the CO₂ pressure is significantly reduced over other supported IL catalysis wherein 6–8 MPa CO₂ was normally required to achieve equal activity.^{12,13} Under the optimal conditions, the reaction progress in the presence of 1 mol% of **MNP-1** was monitored by GC (Fig. 2). The conversion of styrene oxide increased gradually with the reaction time and nearly all the styrene oxide was converted to the desired cyclic carbonate in 12 h. No apparent by-products were observed by GC in all the experiments and the cyclic carbonate was obtained cleanly in 93% yield.

Other MNP-ILs have also been tested in the model reaction under the optimized conditions (Table 2). MNP-ILs with longer alkyl side chains on the imidazolium ring, **MNP-2** and **MNP-3** demonstrated lower activity (Table 2, entries 2 and 3). In control reactions, neither MNP nor silica-coated MNP showed any activity, proving the observed activity arose from the immobilized ionic liquid parts (Table 2, entries 4–6). The unsupported ionic liquid catalyst, [BMIM]Br, was also tested in the current reaction (Table 2, entry 7). The activity of our supported **MNP-1** was comparable to that of [BMIM]Br, highlighting the advantage of MNP supports for ionic liquid catalysis.

Table 2 The cycloaddition reaction of styrene oxide catalyzed by MNP-ILs^a


Entry	Cat.	GC yield (%) ^b
1	MNP-1	87
2	MNP-2	21
3	MNP-3	69
4	— ^c	— ^d
5	MNP	— ^d
6	SiO ₂ -MNP	— ^d
7	[BMIM]Br	94

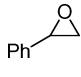
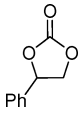
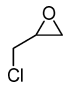
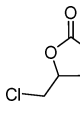

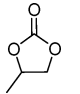
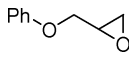
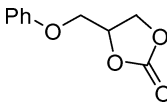
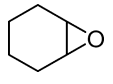
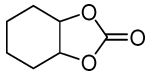
^a Reaction conditions: styrene oxide (10 mmol), cat. (1 mol%), at 140 °C, 10 h, 1 MPa CO₂ pressure. ^b Determined by GC. ^c No catalyst added. ^d No reaction.

**Fig. 2** Reaction progress monitored by GC. Reaction conditions: styrene oxide (10 mmol), **MNP-1** (1 mol%), at 140 °C, 1 MPa CO₂ pressure.

In the presence of **MNP-1** (1 mol%), the substrate scope was next inspected at 140 °C and 1 MPa CO₂ pressure. The results are summarized in Table 3. Pure carbonates from propylene oxide, epichlorohydrin and glycidyl phenyl ether were obtained quantitatively in 4 hours (Table 3, entries 2–4). The reaction also worked well with the sluggish cyclohexene oxide to afford high yield of the desired cyclic carbonate (Table 3, entry 5).

The recyclability of **MNP-1** was next evaluated using epichlorohydrin as the substrate. After each run, the catalyst can be easily collected by a magnet (Fig. 1c and d). The recovered catalyst was used directly for the next run after simply washing with CH₂Cl₂ and removing the residue solvent under vacuum. The recovered **MNP-1** still maintained similar activity after 11 cycles (ESI, Figure S4).† The TEM image confirmed that the reused catalyst was virtually unchanged after 11 runs (Fig. 1b). Elemental analysis indicated only a slight decrease of ionic liquid loading from 0.60 to 0.58 mmol g⁻¹. Altogether, these results suggest **MNP-1** is quite stable under the reaction conditions.

Table 3 Substrate scope of CO₂ cycloaddition reaction^a

Entry	Epoxide	Carbonate	Time/h	GC yield (%) ^b
1			12	93
2			4	99
3			4	99
4			4	95 ^c
5			72	98

^a Reaction conditions: Epoxide (10 mmol), MNP-1 (1 mol%) at 140 °C, 1 MPa CO₂ pressure. ^b Determined by GC. ^c Isolated yield.

In conclusion, we have developed the first example of MNP-supported ionic liquid catalysts. The MNP-supported catalyst MNP-1 demonstrated high activity in CO₂ cycloaddition reactions at a lower CO₂ pressure. The activity of the supported catalyst is comparable with that of the free ILs catalysts for this reaction. The catalysts could be easily recycled using a magnetic force and reused for up to 11 times with essentially no loss of activity. Further development of MNP-supported catalysts is currently under way in our laboratory.

General experimental procedure

The cycloaddition reactions were carried out in a 10 mL stainless steel reactor with magnetic stirrer. The reactor was first charged with the epoxide (10 mmol) and the catalyst (1 mol%). The reactor was then heated to the desired temperature, and CO₂ was loaded to a suitable pressure under stirring. The mixture was kept at this pressure during the reaction. After the reaction, the reactor was cooled to 0 °C by using iced water and CO₂ was released. The catalyst was easily separated by a magnet and the product was analyzed by GC (Varian CP-3800) with acetophenone as the internal standard. The retention time of the products were compared with available authentic standards. The products were analyzed at room temperature on a Bruker 300 MHz NMR spectrometer using CDCl₃ as solvent.

Notes and references

- 1 For examples, see: (a) H. Zhao and S. V. Malhotra, *Aldrichim. Acta*, 2002, **35**, 75; (b) R. Sheldon, *Chem. Commun.*, 2001, 2399; (c) P. Wasserscheid and W. Keim, *Angew. Chem., Int. Ed.*, 2000, **39**, 3772; (d) T. Welton, *Chem. Rev.*, 1999, **99**, 2071; (e) C. C. Tzschucke, C.

Markert, W. Bannwarth, S. Roller, A. Hebel and R. Haag, *Angew. Chem., Int. Ed.*, 2002, **41**, 3964; (f) J. Dupont, R. F. de Souza and P. A. Z. Suarez, *Chem. Rev.*, 2002, **102**, 3667; (g) P. Wasserscheid and T. Welton, *Ionic Liquids in Synthesis*, Wiley-VCH, Weinheim, 2003; (h) *Ionic Liquids: Industrial Applications to Green Chemistry*, ed R. D. Rogers and K. R. Seddon, American Chemical Society, Washington, DC, 2002, (ACS Symposium Series 818).

- 2 For examples, see: (a) J. A. Boon, J. A. Levinsky, J. L. Pflug and J. S. Wilkes, *J. Org. Chem.*, 1986, **51**, 480; (b) V. V. Namboodiri and R. S. Varma, *Chem. Commun.*, 2002, 342; (c) T. Welton and Coord, *Chem. Rev.*, 2004, **248**, 2459; (d) J. M. Xu, B. K. Liu, W. B. Wu, C. Qian, Q. Wu and X. F. Lin, *J. Org. Chem.*, 2006, **71**, 3991; (e) S. Z. Luo, X. L. Mi, L. Zhang, S. Liu, H. Xu and J.-P. Cheng, *Angew. Chem., Int. Ed.*, 2006, **45**, 3093.
- 3 For example, see: (a) R. T. Carlin and J. Fuller, *Chem. Commun.*, 1997, 1345; (b) T. H. Cho, J. Fuller and R. T. Carlin, *High Temp. Mater. Proc.*, 1998, **2**, 543; (c) M. H. Valkenburg, C. DeCastro and W. F. Hölderich, *Green Chem.*, 2002, **4**, 88; (d) M. H. Valkenburg, C. DeCastro and W. F. Hölderich, *Appl. Catal., A*, 2001, **215**, 185; (e) C. DeCastro, E. Sauvage, M. H. Valkenburg and W. F. Hölderich, *J. Catal.*, 2000, **196**, 86; (f) C. P. Mehnert, E. J. Mozeleski and R. A. Cook, *Chem. Commun.*, 2002, 3010; (g) A. Riisager, K. M. Eriksen, P. Wasserscheid and R. Fehrmann, *Catal. Lett.*, 2003, **90**, 149; (h) C. P. Mehnert, R. A. Cook, N. C. Dispenziere and M. Afeworki, *J. Am. Chem. Soc.*, 2002, **124**, 12932; (i) T. Welton, *Coord. Chem. Rev.*, 2004, **248**, 2459; (j) R. Sebesta, I. Kmentova and S. Toma, *Green Chem.*, 2008, **10**, 484; (k) D. Q. Xu, S. P. Luo, Y. F. Wang, A. B. Xia, H. D. Yue, L. P. Wang and Z. Y. Xu, *Chem. Commun.*, 2007, 4393–4395; (l) D.-Q. Xu, L.-P. Wang, S.-P. Luo, Y.-F. Wang, S. Zhang and Z.-Y. Xu, *Eur. J. Org. Chem.*, 2008, 1049–1053; (m) P. Li, L. Wang, Y. Zhang and G. Wang, *Tetrahedron*, 2008, **64**, 7633; (n) P. Li, L. Wang and Y. C. Zhang, *Eur. J. Org. Chem.*, 2008, 1157; (o) H.-L. Shim, M.-K. Lee, K.-H. Kim, D.-W. Park and S.-W. Park, *Polym. Adv. Technol.*, 2008, **19**, 1436.
- 4 For examples, see: (a) T.-J. Yoon, W. Lee, Y.-S. Oh and J.-K. Lee, *New J. Chem.*, 2003, **27**, 227; (b) A.-H. Lu, W. Schmidt, N. Matoussevitch, H. Bönemann, B. Spliethoff, B. Tesche, E. Bill, W. Kiefer and F. Schüth, *Angew. Chem., Int. Ed.*, 2004, **43**, 4303; (c) H. M. R. Gardimalla, D. Mandal, P. D. Stevens, M. Yen and Y. Gao, *Chem. Commun.*, 2005, 4432; (d) P. D. Stevens, J. Fan, H. M. R. Gardimalla, M. Yen and Y. Gao, *Org. Lett.*, 2005, **7**, 2085; (e) Y. Zheng, P. D. Stevens and Y. Gao, *J. Org. Chem.*, 2006, **71**, 537; (f) D. Lee, J. Lee, H. Lee, S. Jin, T. Hyeon and B. M. Kim, *Adv. Synth. Catal.*, 2006, **348**, 41; (g) R. Abu-Reziq, H. Alper, D. Wang and M. L. Post, *J. Am. Chem. Soc.*, 2006, **128**, 5279; (h) N. T. S. Phan, C. S. Gill, J. V. Nguyen, Z. J. Zhang and C. W. Jones, *Angew. Chem., Int. Ed.*, 2006, **45**, 2209–2212; (i) N. T. S. Phan and C. W. Jones, *J. Mol. Catal. A: Chem.*, 2006, **253**, 123–131.
- 5 A. Hu, G. T. Yee and W. Lin, *J. Am. Chem. Soc.*, 2005, **127**, 12486.
- 6 (a) M. Kawamura and K. Sato, *Chem. Commun.*, 2006, 4718; (b) C. O. Dálaigh, S. A. Corr, Y. Gun'ko and S. J. Connon, *Angew. Chem. Int. Ed.*, 2007, **46**, 4329; (c) M. Kawamura and K. Sato, *Chem. Commun.*, 2007, 3404; (d) S. Z. Luo, X. X. Zheng, H. Xu, X. L. Mi, L. Zhang and J.-P. Cheng, *Adv. Synth. Catal.*, 2007, **349**, 2431; (e) S. Z. Luo, X. X. Zheng and J.-P. Cheng, *Chem. Commun.*, 2008, 5719.
- 7 For magnetic ionic liquids, see: (a) J.-Y. Kim, J.-T. Kim, E.-A. Song, Y.-K. Min and H. Hamaguchi, *Macromolecules*, 2008, **41**, 2886–2889; (b) K. Naka, A. Narita, H. Tanaka, Y. Chujo, M. Morita, T. Inubushi, I. Nishimura, J. Hiruta, H. Shibayama, M. Koga, S. Ishibashi, J. Seki, S. Kizaka-Kondoh and M. Hiraoka, *Polym. Adv. Technol.*, 2008, **19**, 1421–1429.
- 8 T.-J. Yoon, J. S. K., B. G. Kim, K. N. Yu, M.-H. Cho and J.-K. Lee, *Angew. Chem., Int. Ed.*, 2005, **44**, 1068.
- 9 M. Shokouhimehr, Y. Piao, J. Kim, Y. Jang and T. Hyeon, *Angew. Chem., Int. Ed.*, 2007, **46**, 7039.
- 10 For recent examples, see: (a) N. Kihara, N. Hara and T. Endo, *J. Org. Chem.*, 1993, **58**, 6198; (b) H. Kawanami and Y. Ikushima, *Chem. Commun.*, 2000, 2089; (c) H. Yasuda, L. N. He and T. Sakakura, *J. Catal.*, 2002, **209**, 547; (d) M. Tu and R. J. Davis, *J. Catal.*, 2001, **199**, 85; (e) R. Srivastava, D. Srinivas and P. Ratnasamy, *Catal. Lett.*, 2003, **91**, 133; (f) B. M. Bhanage, S. Fujita, Y. Ikushima, K. Torii and M. Arai, *Green Chem.*, 2003, **5**, 71; (g) R. L. Paddock and S. T. Nguyen, *J. Am. Chem. Soc.*, 2001, **123**, 11498; (h) H. S. Kim, J. J. Kim, B. G. Lee, O. S. Jung, H. G. Jang and S. O. Kang, *Angew. Chem., Int. Ed.*, 2000, **39**, 4096; (i) A. G. Shaikh, *Chem. Rev.*,

- 1996, **96**, 951; (j) J. H. Clements, *Ind. Eng. Chem. Res.*, 2000, **25**, 663.
- 11 (a) For recent examples, see: J. J. Peng and Y. Q. Deng, *New J. Chem.*, 2001, **25**, 639; (b) H. Yang, Y. Gu, Y. Deng and F. Shi, *Chem. Commun.*, 2002, 274–275; (c) Y. J. Kim and R. S. Varma, *J. Org. Chem.*, 2005, **70**, 7882; (d) V. Calo, A. Nacci, A. Monopoli and A. Fanizzi, *Org. Lett.*, 2002, **4**, 2561; (e) H. Kawanami, A. Sasaki, K. Matsui and Y. Ikushima, *Chem. Commun.*, 2003, 896; (f) N. Eghbali and C. J. Li, *Green Chem.*, 2007, **9**, 213; (g) J. Sun, S. Fujita and M. Arai, *J. Organomet. Chem.*, 2005, **690**, 3490.
- 12 J. Q. Wang, X. D. Yue, F. Cai and L. N. He, *Catal. Commun.*, 2007, **8**, 167.
- 13 Y. Xie, Z. Zhang, T. Jiang, J. He, B. Han, T. Wu and K. Ding, *Angew. Chem., Int. Ed.*, 2007, **46**, 7255.

Microwave-assisted preparation of amides using a stable and reusable mesoporous carbonaceous solid acid

Rafael Luque,* Vitaly Budarin, James H. Clark* and Duncan J. Macquarrie

Received 28th November 2008, Accepted 13th January 2009

First published as an Advance Article on the web 29th January 2009

DOI: 10.1039/b821392p

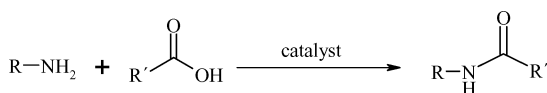
An efficient and green microwave assisted protocol to prepare amides from amines via *N*-acylation using acidic polysaccharide derived mesoporous materials provides quantitative yields of amides in short reaction times.

Introduction

Amide bond formations are one of the most important transformations carried out in pharmaceutical synthesis,¹ accounting for 65% of all preliminary screening reactions in industrial medicinal chemistry laboratories as recently reported.² Amides also represent a very important family of intermediates widely employed in the preparation of fine chemicals, cosmetics and food additives.^{1–3} However, the majority of the current employed protocols to form amides involve the use of stoichiometric activated toxic and corrosive reagents (e.g. acid anhydrides and/or acyl chlorides) with poor atom economy that generate considerable waste.^{4,5} Furthermore, an excess of these reagents is normally needed to achieve optimum amide yields and the reaction is water-sensitive with the efficient removal of water being a critical factor in the systems.^{5,6}

The development of cleaner syntheses are key to reducing the environmental impact of amide formations.² In this regard, the direct reaction of amines with carboxylic acids remains the most attractive approach.^{2,6,7} These types of reactions are arguably best carried out without catalysis where possible, however, reaction conditions remain harsh in order to accomplish direct amide formation.⁸

A range of greener catalytic methodologies have been reported for the preparation of amides. These include the *N*-acylation of amines with organic acids^{7,9} (Scheme 1), the use of solid supported reagents (e.g. polymer-bound acylating agents),¹⁰ arylboronic or boronic acid derivatives,^{6,11} and the use of microwave irradiation.^{5,10,12,13} Many different catalysts have been reported for the acylation of amines including transition metal salts,¹⁴ immobilised ionic liquids on mesoporous materials,^{7c} and solid acid catalysts.⁷



Scheme 1 Catalysed *N*-acylation of amines using organic acids.

We have previously reported the preparation of acidic polysaccharide-derived mesoporous materials (Starbon[®] acids) and their activity in a range of acid catalysed reactions including esterifications,^{15–17} etherifications,¹⁶ alkylations,¹⁵ and acylations¹⁵ under microwave irradiation.

Inspired by the reported results of Narender *et al.*^{7a} and Choudary *et al.*^{7b} that employed solid acids in the acylation of amines under conventional heating, we aimed to bring together the advantages of using a highly active and reusable water tolerant solid acid (Starbon[®] acid) as well as a microwave assisted protocol that is believed to enhance the rates of reactions as well as improving yields and potentially influencing selectivities in organic synthesis.^{18,19} Herein, we report the efficient and atom economic preparation of amides via *N*-acylation of primary and secondary amines under microwave irradiation using a Starbon[®] acid as catalyst and acetic acid as the acylation reagent.

Experimental

Starbons[®] acids were synthesized as recently reported in the literature.^{15–17} The material carbonised at 400 °C (herein after referred to as Starbon[®]-400) was chosen for its ideal hydrophilicity/hydrophobicity ratio and subsequently functionalised by suspending in H₂SO₄ (10 mL acid/g material) and heated for 4 h at 80 °C. After sulfonation, the solid acid was washed with distilled water until the washings were neutral, conditioned in boiling toluene (150 °C, 4 h) and water (100 °C, 3 h) and finally oven dried overnight (100 °C) before being tested in the catalytic reaction. Sulfonated materials are denoted as Starbon[®]-400-SO₃H.

A typical *N*-acylation was carried out by reacting 2 mmol of the amine with 2 mmol acetic acid and 0.1 g catalyst in a tube using microwave radiation at 300 W (120–130 °C maximum temperature reached) for 1–10 minutes. A general procedure to isolate the formed amides was performed as follows: the residue was then redissolved in DCM (5 mL), washed with brine (5 mL), diluted HCl (5 mL), brine (5 mL), diluted NaOH (5 mL), brine (5 mL), dried over MgSO₄, and the solvent evaporated under vacuum to yield the corresponding amide. Starbon[®] acids were reused after every reaction run. For this, the solid acids were filtered off from the mixture after reaction completion, washed with methanol and acetone and dried at 100 °C prior to their reuse in the reaction.

Microwave experiments were carried out in a CEM-DISCOVER model with PC control and monitored by sampling aliquots of reaction mixture that were subsequently analysed by GC/GC-MS using an Agilent 6890 N GC model equipped, with

Green Chemistry Centre of Excellence, The University of York, Heslington, YO10 5DD, York, UK. E-mail: jhc1@york.ac.uk, q62alsor@uco.es; Fax: +44 1904 432705; Tel: +44 1904 432865

a 7683B series autosampler, fitted with a DB-5 capillary column and an FID detector. Experiments were conducted in a closed vessel (pressure controlled) under continuous stirring.

Results and discussion

The use of acetic acid in the *N*-acylation reaction instead of the corrosive acetyl chloride and the lachrymator acetic anhydride provides many advantages from both economical and environmental standpoints, and water is the only by-product. The *N*-acylation of aniline (primary amine) was chosen as reaction test to compare the activity of a range of solid acid catalysts including acidic clays, zeolites and Al-MCM-1 materials. The results are shown in Fig. 1. Initially, a 1:1 ratio amine:acetic acid, 0.1 g catalyst, maximum microwave power output (300 W) and 15 min irradiation were selected as reaction conditions, in a similar way to previously reported results.¹⁵

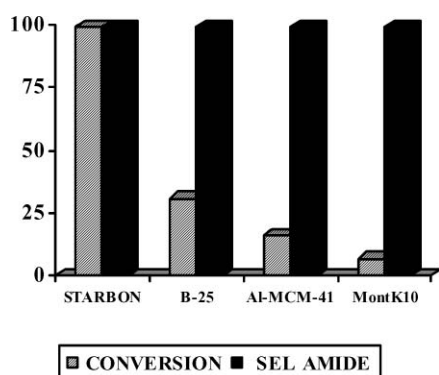


Fig. 1 Conversion and selectivity to amide (Sel Amide) of various solid acids in the *N*-acylation of aniline with acetic acid [Reaction conditions: 2 mmol aniline, 2 mmol AcOH, 0.1 g cat., microwave, 300 W (maximum power), 130 °C (maximum temperature reached), 15 min].

Blank runs in the absence of catalyst provided almost no conversion of starting material after microwaving for 15 min (Table 1, Blank).

Quantitative conversion of the starting material was found in less than 15 min reaction under microwave irradiation using Starbon®-400-SO₃H. Comparatively, the reaction rates using other solid acids were found to be between 5 to 10 times slower than that of the Starbon® acid. With Starbon® acid being the optimum catalyst for the reaction, the next step was to optimise the reaction parameters. As expected, a decrease in the microwave power and/or catalyst loading had a detrimental effect on the amide yield. Interestingly, the selectivity to amide was not significantly altered by changing these parameters and in general all solid acids were extremely selective to amide formation. The time of microwave irradiation and the catalyst loading were probably the most important parameters in the reaction. For most of the solid acids (excluding Starbon®), reasonable conversions (>50%) were only achieved at significantly longer times of irradiation (45 min and over) and/or doubling the quantities of catalyst (from 0.1 to 0.2 g).

In an attempt to broaden the scope of the methodology, a range of amines were employed as starting materials in the acylation reaction. The results are summarised in Table 1.

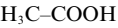
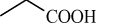
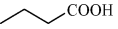
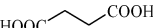
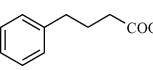
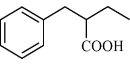
Table 1 *N*-Acylation of a range of amines with acetic acid using Starbon®-400-SO₃H as catalyst and acetic acid as acylating agent under microwave irradiation^a

Entry	Amine	Product	Time/min	Conversion ^c (mol%)	S _{amide} (mol%)
Blank ^b			15	<10	>98
1			10	90 (87)	>99
2			2	>99 (92)	>98
3			2	>99 (95)	>99
4			3	>95 (89)	>99
5			3	89 (83)	>99
6			5	87 (79)	>99
7			0.6	>99 (94)	>98
8			3	>99 (94)	>99
9			1	>99 (92)	>99
10			15	77	>99
11			15	68	>99
12			15	82	>95

^a 2 mmol amine, 2 mmol AcOH, 0.1 g Starbon-400-SO₃H, microwave, 300 W (maximum power output), 130 °C (maximum temperature reached). ^b Blank reaction in the absence of catalyst. ^c Isolated yields, where appropriate, are given in brackets.

A wide variety of primary and secondary aromatic, aliphatic and cyclic hindered and unhindered amines were effectively and selectively converted into their corresponding amides under mild conditions and with short times of reaction (0.5 to 15 min). Of note was also the remarkable tolerance of the reaction to substituents (from electron withdrawing to electron donating groups) and functionalities in the amines. The water-tolerant partially hydrophilic Starbon® acid is believed to push the equilibrium forward to the formation of amides without the need to remove the water generated in the acylation (which normally reverses the equilibrium and destroys the amide). This property may be due to the Starbons unusual starch-like structure which is still present at low temperatures of carbonisation (<400 °C);²⁰ this is consistent with our previous observation of Starbon® catalytic activity in water.²¹ In order to demonstrate the true scope of the proposed methodology,

Table 2 *N*-Acylation of benzylamine with a range of acids using Starbon®-400-SO₃H as catalyst under microwave irradiation^a

Entry	Acid	Time/min	Conversion ^b (mol%)	S _{amide} (mol%)
1		0.6	>99 (94)	>98
2		5	94 (89)	>99
3		5	90 (86)	>98
4		15	>99	75 ^c
5		10	>99 (92)	>99
6		10	88 (84)	>99

^a 2 mmol benzylamine, 2 mmol acid, 0.1 g Starbon-400-SO₃H, microwave, 300 W (maximum power output), 130 °C (maximum temperature reached). ^b Isolated yields, where appropriate, are given in brackets. ^c Selectivity to diamide.

a range of carboxylic acids were employed as reagents in the *N*-acylation of benzylamine (Amine Entry 7, Table 1). Results included in Table 2 proved the applicability of the protocol, as the Starbon® acid afforded quantitative yields of amides in less than 15 min of microwave irradiation. Of note were results obtained using succinic acid (1,4, butanedioic acid) in the reaction (Table 2, entry 4). Quantitative yield of diamide could be obtained in less than 30 min reaction under microwave irradiation.

The highly active sulfonated starbon was easily recovered from the reaction mixture whereupon the reaction rates returned to the background values. The recovered Starbon could be added to fresh substrate solutions giving almost identical activity and selectivity to the amides after 3 reuses to that observed in the first run (e.g. 3rd Starbon® acid reuse, aniline + acetic acid, 87% conversion, 99% selectivity to the amide compared to the 90% conversion, 99% selectivity obtained for fresh Starbon® acid). The catalyst is very stable under the reaction conditions, in good agreement with previously reported results that already proved the outstanding properties of this acidic polysaccharide-derived mesoporous material.^{15–17,20,21}

Conclusions

In conclusion, our efficient, atom economic and environmentally friendly protocol allowed the preparation of a wide range of intermediates for pharmaceuticals (e.g. acetanilide and *N*-acetyl-*p*-aminophenol) and fine chemicals. A variety of amides were successfully prepared from a range of amines and acids used as reagents in a 1:1 ratio, in a protocol that was demonstrated to be independent of the substrate combination and, most importantly, of the efficient removal of water that has been reported to be critical in order to achieve high amide yields.²² The Starbon® acid is a renewable and environmentally compatible catalyst that can easily be obtained from biomass, and has proven to be highly active, selective and reusable in the *N*-acylation of amines with acetic acid under microwave irradiation. Our

solid acid exhibited remarkably improved activities compared to commercially available alternatives.

Notes and references

- (a) T. W. Greene and P. G. M. Wuts, *Protective Groups in Organic Synthesis*, 2nd Ed., John Wiley and Sons Inc., New York, 1999; (b) R. C. Larock, *Comprehensive Organic Transformations*, Wiley-VCH, New York, 1999.
- D. J. Constable, P. J. Dunne, J. D. Haysler, G. R. Humphrey, J. L. Leazer, Jr., R. J. Linderman, K. Lorenz, J. Mansley, B. A. Pearlman, A. Wells, A. Zaks and T. Y. Zhang, *Green Chem.*, 2007, **9**, 411–420.
- (a) P. J. Dunn, S. Galvin and K. Hettenbach, *Green Chem.*, 2004, **6**, 43–48; (b) R. Vaidyanathan, V. G. Kalthod, D. P. Ngo, J. M. Manley and S. P. Lapekas, *J. Org. Chem.*, 2004, **69**, 2565–2568.
- (a) J. Mc Nulty, V. Krishnamoorthy and A. Robertson, *Tetrahedron Lett.*, 2008, **49**, 6344–6347; (b) S. Naik, G. Bhattacharjya, B. Talukdar and B. K. Patel, *Eur. J. Org. Chem.*, 2004, 1254–1260.
- C. A. G. N. Montalbetti and V. Falque, *Tetrahedron*, 2005, **61**, 10827–10852.
- K. Arnold, A. S. Batsanov, B. Davies and A. Whiting, *Green Chem.*, 2008, **10**, 124–134.
- (a) N. Narendar, P. Srinivasu, S. J. Kulkarni and K. V. Raghavan, *Green Chem.*, 2000, **2**, 104–105; (b) B. M. Choudary, V. Bhaskar, M. Lakshmi Kantam, K. Koteswara Rao and K. V. Raghavan, *Catal. Lett.*, 2001, **74**, 207–211; (c) S. M. Coman, M. Florea, V. I. Parvulescu, V. David, A. Medvedovici, D. De Vos, P. A. Jacobs, G. Poncelet and P. Grange, *J. Catal.*, 2007, **249**, 359–369.
- (a) D. Davidson and P. Newman, *J. Am. Chem. Soc.*, 1952, **74**, 1515–1516; (b) B. S. Jursic and Z. Zdravkovski, *Synth. Commun.*, 1993, **23**, 2761–2770.
- M. Basanagouda, M. V. Kulkarni, R. G. Kalkhambkar and G. M. Kulkarni, *Synth. Commun.*, 2008, **38**, 2929–2940.
- (a) E. Petricci, C. Mugnaini, M. Radi, F. Corelli and M. Botta, *J. Org. Chem.*, 2004, **69**, 7880–7887; (b) D. R. Sauer, D. Kalvin and K. M. Phelan, *Org. Lett.*, 2003, **5**, 4721–4724; (c) E. Petricci, M. Botta, F. Corelli and C. Mugnaini, *Tetrahedron Lett.*, 2002, **43**, 6507–6509.
- (a) K. Arnold, B. Davies, R. L. Giles, C. Grosjean, G. E. Smith and A. Whiting, *Adv. Synth. Catal.*, 2006, **348**, 813–820; (b) S. W. Coghlan, R. L. Giles, J. A. K. Howard, M. R. Probert, G. E. Smith and A. Whiting, *J. Organomet. Chem.*, 2005, **690**, 4784–4793; (c) K. Ishihara, S. Kondo and H. Yamamoto, *Org. Synth.*, 2002, **79**, 176–185.
- X. J. Wang, Q. Yang, F. Liu and Q. D. You, *Synth. Commun.*, 2008, **38**, 1028–1035.
- (a) C. Goretzki, A. Krlej, C. Steffens and H. Ritter, *Macromol. Rapid Commun.*, 2004, **25**, 513–516; (b) A. R. Hajipour and M. Ghasemi, *Indian J. Chem. B: Org. Chem. Incl. Med. Chem.*, 2001, **40**, 504–507; (c) A. Loupy and F. Volatron, *Tetrahedron*, 2002, **58**, 2155–2162; (d) F. Massicot, R. Plantier-Royon, C. Portella, D. Saleur and A. Sudha, *Synthesis*, 2001, 2441–2444; (e) M. P. Vazquez-Tato, *Synlett*, 1993, 506.
- A. K. Chakraborti and R. Gulhane, *Tetrahedron Lett.*, 2003, **44**, 6749–6753.
- V. Budarin, R. Luque, J. H. Clark and D. J. Macquarrie, *Chem. Commun.*, 2007, 634–636.
- R. Luque, V. Budarin, J. H. Clark and D. J. Macquarrie, *Appl. Catal., B*, 2008, **82**, 157–162.
- V. Budarin, J. H. Clark, R. Luque, D. J. Macquarrie, A. Koutinas and C. Webb, *Green Chem.*, 2007, **9**, 992–995.
- (a) C. O. Kappe, *Chem. Soc. Rev.*, 2008, **37**, 1127–1139; (b) C. O. Kappe, A. Stadler, *Microwaves in Organic and Medicinal Chemistry*, Wiley-VCH, Weinheim, 2005; (c) C. O. Kappe, *Angew. Chem., Int. Ed.*, 2004, **43**, 6250–6284.
- (a) *Microwaves in Organic Synthesis*, ed. A. Loupy, 2nd, Wiley-VCH, 2006; (b) *Microwave-assisted Organic Synthesis*, ed. P. Lidström and J. P. Tierney, Blackwell Scientific, 2004.
- V. Budarin, J. H. Clark, J. J. E. Hardy, R. Luque, K. Milkowski, S. J. Tavener and A. J. Wilson, *Angew. Chem., Int. Ed.*, 2006, **45**, 3782–3786.
- R. Luque, C. S. K. Lin, C. Du, D. J. Macquarrie, A. Koutinas, R. Wang, C. Webb and J. H. Clark, *Green Chem.*, 2009, DOI: 10.1039/b813409j.
- L. C. Chan and B. G. Cox, *J. Org. Chem.*, 2007, **72**, 8863–8869.

Selective hydrogenation of alternative oils: a useful tool for the production of biofuels

Federica Zaccheria,^{a,b} Rinaldo Psaro^a and Nicoletta Ravasio^{*a}

Received 7th October 2008, Accepted 5th February 2009

First published as an Advance Article on the web 13th February 2009

DOI: 10.1039/b817625f

Selective hydrogenation over 8% Cu/SiO₂ catalysts has been carried out on a series of non-food oils methylesters, allowing their transformation into materials suitable for biodiesel formulation.

The production of biodiesel (fatty acid alkyl esters) has been growing continuously during the last few years, particularly in Europe where it reached 5.7 millions tons in 2007.¹ It is also supposed to increase further to fulfil the decisions of the European Parliament.

While the use of vegetable oils as raw materials for the production of chemicals is a long established practice, an increase in the production of biodiesel will only be possible by making available new feedstocks apart from rapeseed, soybean and palm oil, for both economic and ethical reasons.² However, the use of alternative feedstocks may require modification of the production technology.

One way is represented by hydrotreating in a petroleum refinery, but this process gives straight-chain alkanes, thus losing lubricity, biodegradability and high flash point properties that are related to the presence of the ester moiety. Moreover, the reaction conditions are quite demanding (300–450 °C, 50 atm H₂, 6 h).³ Another way is to use raw materials that are not compatible with the actual transesterification technology, such as highly acidic oils, or unsuitable to obtain biodiesel, such as highly unsaturated oils and fats. Here, we wish to report that a selective hydrogenation process allows production of biodiesel starting from highly unsaturated fats and oils not belonging to the food production chain.

The degree of unsaturation of fatty acids is normally expressed as the iodine value (IV), *i.e.* the number of grams of iodine that have reacted with 100 g of product analysed, under controlled experimental conditions. The higher the index, the greater the degree of unsaturation. For biodiesel intended for transport use, the most remunerative one, a maximum iodine number limit is envisaged as 120 gI₂ per 100 g. Actually, biodiesel is usually produced by starting from vegetable oils having a iodine number lower or equal to 130, such as rapeseed oil (IV = 110–115), sunflower oil (IV = 120–130), soybean oil (IV = 125–135). The parent oil composition has a significant influence on the properties of the fuel obtained. In particular, the presence of

polyunsaturated fatty esters is the cause of oxidative stability concerns, while the presence of saturated ones is the cause of cold flow problems.

Oxidative processes bring about increased viscosity and lead to the formation of insolubles, which can potentially plug fuel filters and injection systems. Increased acidity and increased peroxide values resulting from oxidation reactions can also cause the corrosion of fuel system parts, hardening of rubber components and fusion of moving ones.⁴

The major unsaturated acids present in plant derived fatty substances are oleic acid (9-octadecenoic, C18:1), linoleic acid (9,12-octadecadienoic, C18:2) and linolenic acid (9,12,15-octadecatrienoic, C 18:3). Their relative rates of oxidation are 1:40:100, respectively,⁵ hence partial hydrogenation would lead to a significant increase in oxidative stability, particularly when C18:3 is reduced. Also the Cetane Number (CN \geq 51 according to European regulation), increases in the same way as oxidative stability, while NO_x emissions decrease with decreasing unsaturation.⁶

On the other hand, a high content of fully saturated compounds (stearic acid, C18:0 and palmitic acid, C16:0) has a very negative impact on the cold properties of the fuel (cloud point, pour point and low temperature filterability). It is well known that palm oil methyl esters suffer from very bad cold properties due to the presence of high amount of C16:0.⁷

For all these reasons the monounsaturated methyl oleate (C18:1) and methyl palmitoleate (C16:1) have been identified as the ideal components of biodiesel.⁸

Only recently, partial hydrogenation has been recognized as a valuable tool to increase the oxidative stability of soybean, linseed and sunflower oil.^{9,10} However, in order to maintain good cold properties it is mandatory not to increase the content of stearic acid and to limit the extent of *cis/trans* and positional isomerization. Thus, the methylester of natural C18:1 with the double bond at C9 and *cis* configuration has mp = –19.8 °C whereas its *trans* isomer has mp = +9 °C and the methylester of stearic acid has mp = +39 °C.

Fat and oil hydrogenation is one of the oldest catalytic reactions, and its use for the hardening of linseed and fish oil date back to 1903.¹¹ Ni catalysts, operating at 160–230 °C and 2–5 bar H₂, are by far the most commonly used ones in margarine production,¹² although Pd based catalysts have often been proposed due to their activity at lower temperature (120–140 °C) and lower *cis/trans* isomerization activity.^{13–15} However, both Ni and Pd catalysts show rather low diene:monoene selectivity, thus giving early formation of saturated compounds; thus the problem of achieving selective hydrogenation in unsaturated fatty

^aISTM-CNR, Via Golgi 19, 20133, Milano, Italy.
E-mail: n.ravasio@istm.cnr.it; Fax: +39 02 50314405; Tel: +39 02 50314382

^bDipartimento CIMA "Lamberto Malatesta", Via Venezian 21, 20133, Milano, Italy

Table 1 Selective hydrogenation of different methylester mixtures with Cu/SiO₂

	<i>t</i> /min	C18:3 (%mol)	C18:2 (%mol)	C18:1 (%mol)	C18:0 (%mol)	C16:0 (%mol)	CN ^a	IV ^b	Pp/ ^o C	Oxidation stability ^c /h
<i>Linseed oil methylesters</i>										
Before hydrogenation	30	58.2	16.7	16.3	3.4	5.4	36	186	-23	1.2
After hydrogenation		—	27	63	4.2	5.3	53	112	-11	5.3
<i>Plukenetia volubilis oil methylesters</i>										
Before hydrogenation	30	50.4	33.9	9.3	2.7	3.7	35	202	-25	n.d.
After hydrogenation		—	36.1	56.5	3.0	3.8	52	115	-13	n.d.
<i>Hempseed oil methylesters</i>										
Before hydrogenation	100	17.3	57	14.2	2.8	6.4	43	164	-20	n.d.
After hydrogenation		—	39.5	48.5	2.9	6.3	51	118	-13	n.d.
<i>Tobaccoseed oil methylesters</i>										
Before hydrogenation	120	0	79.2	11.6	2.4	6.7	46	145	-17	n.d.
After hydrogenation		0	33	57	3.0	6.5	52	111	-10	n.d.
<i>Grapeseed oil methylesters</i>										
Before hydrogenation	60	0	72.5	16.7	3.9	6.9	48	145	-18	n.d.
After hydrogenation		0	39	50	3.6	6.9	52	108	-12	n.d.
<i>Tall oil methylesters</i>										
Before hydrogenation	80	0	55 ^d	37	0.4	0.3	44	145	n.d.	<1
After hydrogenation		0	24	68	0.5	0.3	48	117	-18	4

^a Cetane numbers were calculated by using reported coefficient for each component.²² ^b Iodine Values were calculated by using the European Standard procedure CEN TC 307. ^c Expressed as Rancimat Induction Period. ^d 11% conjugated dienes.

acids with several double bonds without unwanted positional or *cis/trans* isomerization occurring at the same time has so far only been partly solved.

On the contrary, the use of copper hydrogenation catalysts in the fat and oils industry mainly relies on copper chromites for the production of fatty acid alcohols from esters.¹⁶ However, copper-based systems have long been known in edible oils hydrogenation as the most selective ones for the reduction of linolenate C18:3 to oleate C18:1 without affecting linoleate, the valuable component from the nutritional point of view. Monoenes are not reduced, therefore the percentage of saturation is scarcely changed during the hydrogenation process.^{17,18} Moreover, we already showed that Cu/SiO₂ catalysts prepared by chemisorption hydrolysis and pre-reduced *ex situ* are effective and very selective in the hydrogenation of rapeseed oil methylesters, obtaining up to 88% of C18:1 derivative without modifying the amount of C18:0 and with a *trans* content of about 20%.¹⁹

We also reported²⁰ that a selective hydrogenation process can be used to improve the stability of tall oil methylesters obtained from tall oil, a byproduct of pulp and paper industry, while keeping good cold properties (Table 1).

Here, we will focus both on different oils from plants that are being considered for biodiesel production but give poor quality fuel, and on oils that are not even supposed to be suitable for biofuels production due to their high content of polyunsaturated compounds. Hempseed, grapeseed and tobaccoseed oils have a very high linoleic C18:2 acid content, whereas linseed and *Plukenetia volubilis* oil have a high content of C18:3.

Table 1 sums up our results obtained in the selective hydrogenation of these sources by using low loading heterogeneous copper catalysts supported over silica. Such catalysts were prepared by means of a particular technique able to give systems with very high metal dispersion, which leads to an excellent activity in hydrogenation reactions under mild conditions.²¹

Both the oils rich in C18:2 and the oils rich in C18:3 can be easily reduced to produce biodiesel with fairly high monounsatu-

rated methyl ester content, thus meeting the European regulation as far as both IV and CN are concerned.

Oxidation stability for linseed oil jumps from a very low 1.2 hours to 5.3 hours, which is near to the limit required by the European legislation. In the case of tall oil methylesters, which are very unstable before the treatment due to the presence of conjugated dienes, we also observe a very significant improvement.

On the other hand, the stearic acid content remains almost unchanged during the hydrogenation process and *cis/trans* and positional isomerization are limited. This allows the oil to preserve good cold properties, represented here by the pour point that reaches values close to that of rapeseed oil methylesters (-9 °C), usually accepted as the optimum one.

On the contrary, the comparison with a commercial Nickel catalyst shows a dramatic difference in terms of cold properties. In fact, the sample reduced with this catalyst just after filtration appears cloudy (Fig. 1), and even at room temperature shows some precipitation due to saturated compounds and positional isomers.

Pre-reduction of these materials to catalysts exposing high metallic surface area allows hydrogenation under mild conditions of the dienic components without reducing C18:1 and thus producing oils with a very high content in oleic acid (but without rising the stearic acid content). According to the mechanism proposed by Dijkstra,²³ this may be due to the much higher activity of reduced Cu in hydrogen abstraction, as also shown in dehydrogenation reactions.²⁴ Thus, the hydrogenation of polyunsaturated oils proceeds through conjugation of the methylene interrupted double bonds, that are in turn caused by hydrogen abstraction. The faster hydrogenation observed for oils with high linolenic content (linseed and *Plukenetis volubilis* oils derived) with respect to the ones with high linoleic content also supports the hypothesis of the hydrogen abstraction. Actually, the doubly activated allylic hydrogens of a methylene group separating two double bonds have a higher probability of being

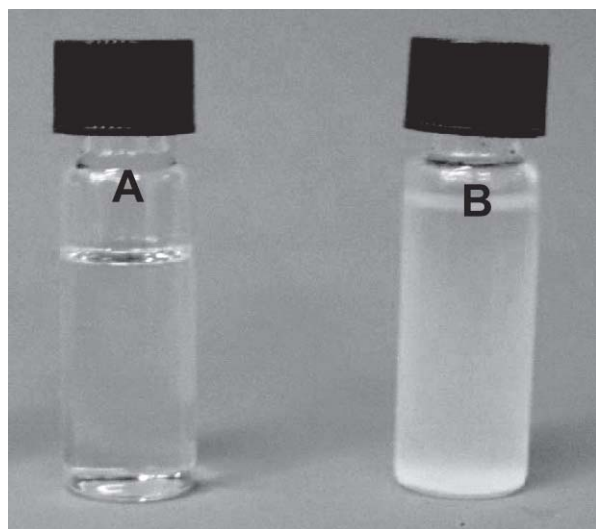


Fig. 1 Samples of linseed oil methylesters after hydrogenation with Cu/SiO₂ (A) and Ni Calsicat (B) and filtration (room T).

abstracted than allylic hydrogens of a methylene group adjacent to only one double bond.²³

Results are particularly relevant for tobaccoseed oil as this tobacco variety, selected for seed production, gives twice the yield of oil per ha with respect to rape, and moreover it can be grown in marginal lands without competing for food and with a low water consumption, thus making this source a good candidate as industrial crop. Nevertheless, crops like hemp give the opportunity for integration into biorefineries. In fact, besides oil, it provides high biomass content suitable for the production of biomaterials for building purposes and paper products.²⁵

Preliminary results show that the catalyst can be reused by just recharging the reactor with fresh methylesters after filtration, without the need of any catalyst reactivation. It is worth underlining that the catalyst shows good activity even if used with non-refined oil derived methylesters, as in the case of the tobaccoseed and linseed oil samples used in the present work.

The same stabilization process can be also applied to methylesters derived from fish oil. The peculiarity of fish oil with respect to vegetable ones is the presence of significant amounts of polyunsaturated compounds, such as C20:4, C20:5, C22:5 and C22:6, usually known as ω -3 and ω -6. With our catalyst, a simple hydrogen brushing with Cu/SiO₂ allows one to completely reduce the 23% portion of polyunsaturated compounds present in a sample derived from cod-liver oil, after just 10 minutes reaction, thus lowering the Iodine Value from 154 to 112. The initial Iodine Value could appear low if compared, for example, with linseed oil methylesters, but it does not reflect the very low oxidation stability of this kind of material. The presence of highly unsaturated acids, even in small amounts, actually has a disproportionately strong effect on oxidation stability, due to the fact that bis-allylic positions within polyunsaturated ester molecules are particularly prone to oxidative attack.²⁶ This is a common feature of all the marine-derived oils, and the hydrogenation reaction could also become interesting in order to obtain high quality biodiesel from algae extracted oils.

Conclusions

Selective hydrogenation carried out with low loading copper catalysts under mild conditions could represent a valuable and efficient tool for feedstock equalization.

Actually, starting from methylesters with a very different acidic distribution, it is possible to obtain mixtures with quite homogeneous composition in terms of unsaturation, thus giving materials suitable for biodiesel formulation. The high activity of the catalytic system and the almost complete selectivity, in principle give the opportunity to tune and shut off the hydrogenation process depending on the specifications requested for the product, just by following the hydrogen consumption. Moreover the catalyst is neither toxic nor pyrogenic, unlike Ni and Pd based ones.

This process gives the opportunity to plan a versatile protocol for the production of biofuels, able to face not only the price variations but also the different supply needs, depending on climatic and seasonal availability, thus making a wide portfolio of raw materials available without interfering with the food market.

Experimental

Methylesters were obtained by traditional transesterification starting from the parent vegetable oil by using MeOH and KOH or NaOMe depending on the starting acidity of the sample. In the case of tall oil, methylesters were obtained using 100 parts by weight of tall oil fatty acids and 100 parts by weight of methyl alcohol, in the presence of 0.5 g (approx. 0.3 ml) of concentrated sulfuric acid or 1 g of *para*-toluenesulfonic acid monohydrate. After drying, the ester fraction was distilled under reduced pressure (1 mbar at 180 °C) in order to obtain a distilled fraction purified from rosin acids to be used for hydrogenation experiments.

Catalysts were prepared by adding the support to a solution containing [Cu(NH₃)₄]²⁺ and slowly diluting the slurry with water. The solid was separated by filtration, washed with water, dried overnight at 120 °C and calcined in air at 350 °C for 4 h. Before reaction the catalyst was pre-reduced in H₂ (1 atm) at 270 °C.

Hydrogenation reactions were carried out in a stainless steel autoclave at 160 °C, under 4 atm H₂ (180 °C and 6 atm for tall oil methylesters), in the presence of powdered supported Cu catalysts (2% wt) with a 8% copper loading. SiO₂ (Davicat BET = 313 m² g⁻¹, PV = 1.79 ml g⁻¹) was used as the catalyst support. Reaction mixtures, separated by simple filtration, were analyzed by GC (HP-6890) using a non-bonded, bis-cyanopropylpolysiloxane (100 m) capillary column. Control tests done by ICP-AES did not show any catalyst contamination on the final product.

Acknowledgements

Prof. C. Fogher (Università Cattolica di Piacenza) is gratefully acknowledged for a sample of tobaccoseed oil. Dr P. Bondioli (Stazione Sperimentale Oli e Grassi, Milano) is acknowledged for a sample of *Plukenetia volubilis* oil and helpful discussion. The authors also thank the European Commission for financing

the Network of Excellence IDECAT (contract no. NMP3-CT-2005-011730).

Notes and references

- 1 2007 production by country, 2008, available at <http://www.ebb-eu.org/stats.php>.
- 2 Sustainable Bioenergy: a Framework for Decision Makers, 2007. Available at <http://esa.un.org/un-energy/pdf/susdev.Biofuels.FAO.pdf>.
- 3 A. Huber, P. O'Connor and A. Corma, *Appl. Catal. A: Gen.*, 2007, **329**, 120.
- 4 A. Monyem and J. van Gerpen, *Biomass Bioenergy*, 2001, **20**, 317.
- 5 *Lipid Oxidation*, ed. E. N. Frankel, The Oily Press, Bridgewater, UK, 2nd edn, 2005.
- 6 R. L. McCormick, M. S. Graboski, T. L. Alleman and A. M. Herring, *Environ. Sci. Technol.*, 2001, **35**, 1742.
- 7 T. C. Ming, N. Ramli, O. T. Lye, M. Said and Z. Kasim, *Eur. J. Lipid Sci. Technol.*, 2005, **107**, 505.
- 8 G. Knothe, *Energy Fuels*, 2008, **22**, 1358.
- 9 B. R. Moser, M. J. Haas, J. K. Winkler, M. A. Jackson, S. Z. Erhan and G. R. List, *Eur. J. Lipid Sci. Technol.*, 2007, **109**, 17.
- 10 A. Bouriazos, K. Mouraditis, N. Psaroudakis and G. Papadogianakis, *Catal. Lett.*, 2008, **121**, 158.
- 11 W. Normann, *DE Patent* 141029, 1903.
- 12 J. W. Veldsink, M. J. Bouma, N. H. Schöön and A. A. C. M. Beenackers, *Catal. Rev.*, 1997, **39**, 253.
- 13 V. Savchenko and I. Makaryan, *Platinum Met. Rev.*, 1999, **43**, 74.
- 14 K. Belkacemi, A. Boulmerka, J. Arul and S. Hamoudi, *Top. Catal.*, 2006, **37**, 113.
- 15 I. L. Simakova, O. A. Simakova, A. V. Romanenko and D. Yu. Murzin, *Ind. Eng. Chem. Res.*, 2008, **47**, 7219.
- 16 K. Noweck and H. Ridder, in *Ullmann's Encyclopaedia of Industrial Chemistry*, ed. W. Gerhartz, VCH, Weinheim, 5th edn, 1987, vol. A10, p. 277.
- 17 A. de Jonge, J. W. E. Coenen and C. Okkerse, *Nature*, 1965, **206**, 573.
- 18 S. Koritala and H. J. Dutton, *J. Am. Oil. Chem. Soc.*, 1969, **46**, 265.
- 19 N. Ravasio, F. Zaccheria, M. Gargano, S. Recchia, A. Fusi, N. Poli and R. Psaro, *Appl. Catal. A: General*, 2002, **233**, 1–6.
- 20 P. Bondioli, M. N. Ravasio, F. Zaccheria, PCT/IT2006/000258; WO2006/111997 A1.
- 21 F. Boccuzzi, A. Chiorino, M. Gargano and N. Ravasio, *J. Catal.*, 1997, **165**, 140.
- 22 M. Mittelbach and C. Remschmidt, *Biodiesel*, Boersedruck Ges.m.b.H., Vienna, Austria, 2004, pp. 141–144.
- 23 A. J. Dijkstra, *Eur. J. Lipid Sci. Technol.*, 2002, **104**, 29.
- 24 F. Zaccheria, N. Ravasio, R. Psaro and A. Fusi, *Chem.–Eur. J.*, 2006, **24**, 6426.
- 25 Sounding Circle: Building Straw Houses from flax to hemp, 2007. Available at http://soundingcircle.com/newslog2.php/_show_article/_a000195-001089.htm.
- 26 S. Schober and M. Mittelbach, *Lipid Technol.*, 2007, **19**, 281–284.

Selective hydrogenation of *trans*-cinnamaldehyde and hydrogenolysis-free hydrogenation of benzyl cinnamate in imidazolium ILs

Saibh Morrissey, Ian Beadham and Nicholas Gathergood*

Received 5th September 2008, Accepted 14th October 2008

First published as an Advance Article on the web 3rd November 2008

DOI: 10.1039/b815566f

trans-Cinnamaldehyde is selectively hydrogenated to hydrocinnamaldehyde using a commercially available palladium catalyst in novel imidazolium ILs. The selective hydrogenation extends to benzyl cinnamate, in which the ester is protected from hydrogenolysis under similar conditions.

Introduction

One of the principal present day problems facing the field of transition metal catalysis is inefficient recycling and reuse of costly catalysts. Even with cost-effective catalysts, selectivity can be poor and elaborate poisons or conditions may be needed to improve the results.¹ ILs have been shown to extend catalyst lifetime in heterogeneous hydrogenations² and facilitate product isolation by simple extraction with non-polar solvents or facile distillation. Many common ILs have been investigated as alternative solvents for catalytic hydrogenations. Of these studies, the greater part focus on the commercially available ILs of the form Rmim⁺ (R = alkyl chain) X⁻.³

While it is easy to achieve selective olefin reduction in α,β -unsaturated ketones using simple Pd/C reduction, with α,β -unsaturated aldehydes the situation is more challenging and product mixtures often arise.^{4,5} *trans*-Cinnamaldehyde is widely used as a model substrate because the products of its hydrogenation are extensively used in the fine chemical industry.^{4,6,7} The selectivity varies due to the possibility of reduction of either the olefin moiety, to give hydrocinnamaldehyde, or the aldehydic moiety, to give cinnamyl alcohol. Owing to the thermodynamically favoured reduction of the C=C bond over the C=O bond,^{4,8} the selectivity towards cinnamyl alcohol is generally poor. This can be frustrating as cinnamyl alcohol is used widely in the flavouring and perfume industries. Hydrocinnamaldehyde is also an important chemical and has uses in the perfumery industry and in the synthesis of anti-HIV compounds.⁹ In the field of metal catalysed hydrogenation ruthenium complexes generally lead to hydrogenation of the carbonyl moiety,¹⁰ whereas rhodium complexes lead to hydrogenation of the olefin moiety but typically high pressures of hydrogen are required.^{11–13}

Herein we present the results obtained for the hydrogenation of *trans*-cinnamaldehyde and benzyl cinnamate using the commercially available Pd/C catalyst at 1 atmosphere hydrogen pressure with the use of alternative green solvents (1–10). Palladium on carbon is well known as a universal catalyst

for olefin hydrogenation. However its efficient catalytic activity may lead to poor selectivity. Furthermore, the product ratio of unsaturated alcohol to saturated aldehyde depends on many factors, including the nanostructure of the metal catalyst,^{14,15} the degree of polarisation of the carbonyl group¹² and the phase-distribution of reagent, substrate and catalyst.^{13,16} The Pd-H bond is also amphipolar and can transfer hydrogen as either Pd^{δ-}-H^{δ+} or Pd^{δ+}-H^{δ-}, the latter being favoured by catalyst poisons, such as quinoline, and the Lindlar catalyst.¹⁷ With so many factors influencing selectivity it is not surprising that some of the solutions to the problem have been elaborate. Tessonier *et al.*,¹⁴ for instance, calcined hydrated palladium(I) nitrate at 350 °C (which had previously been added to carbon nanotubes and distilled water) for 2 hours to generate Pd nanoparticles. 100% conversion was achieved, resulting in 90% hydrocinnamaldehyde and 10% undesired 3-phenylpropanol. This compares very favourably with a commercial Pd-C catalyst that gave a 1:1 ratio of hydrocinnamaldehyde to 3-phenyl-1-propanol.¹⁴ Tessonier suggested that the improvement in selectivity with carbon nanotubes stemmed from the absence of either an oxygenated surface, or the micropores typically present on a conventional activated carbon support. Additionally an 'electronic modification through electron transfer between the metal and the support, which in turn modifies the absorption and selectivity of the products'^{18,19} was hypothesized to explain the simultaneous hydrogenation of C=C and C=O bonds on activated carbon, compared with the rapid desorption of C=C reduced product from the nanotubes. Notably, in neither case is reduction observed if hydrocinnamaldehyde is the substrate, indicating that it is not an intermediate in the reaction.

A more selective process, also involving a palladium catalyst, was developed by Ledoux *et al.*¹⁵ After first impregnating a carbon nanofibre support with the palladium salt, palladium(I) nitrate was dried overnight at 110 °C and reduced under a flow of hydrogen for 2 hours. This support was the major difference from Tessonier's procedure, with the nanofibres, prepared by a gas phase deposition using ethane and hydrogen over a nickel catalyst (from Al₂O₃, Ni(NO₃)₂/glycerol), followed by sonication of the fibres and cleaning with acid at 650 °C. In this case the hydrogenation was 98% selective for the C=C double bond of cinnamaldehyde, compared with a commercial Pd-C catalyst that gave mixtures of C=C hydrogenation, C=O hydrogenation, and complete reduction to 3-phenyl-1-propanol. Ledoux suggested that presence of residual acid on the charcoal, as well as the property that commercial Pd-C is covered with micropores to the extent of 60%, could explain the poor selectivity of palladium on ordinary activated carbon.

School of Chemical Sciences, National Institute for Cellular Biotechnology, Dublin City University, Glasnevin, Dublin 9, Ireland.
E-mail: Nick.Gathergood@dcu.ie; Fax: +353 1 700 5503; Tel: +353 1 700 7860

Our research effort is directed by the development of biodegradable, low toxicity solvents which can also offer performance advantages over established methods. This work began with Gathergood and Scammells in 2002²⁰ where the same principles that are used in the synthesis of biodegradable surfactants, were applied to the design of environmentally friendly ILs. Subsequent studies showed the presence of an ester linkage in the side chain of the IL cation (**1**) promoted biodegradation.²¹ The counterion was also a significant factor, with the octyl sulfate present in examples (**3**) which were readily biodegradable. We recently reported that key features which improve biodegradation and reduce antimicrobial toxicity were also required for improved catalyst performance in the selective hydrogenation of phenoxyocta-2,7-diene.²² Herein, we present our work studying the changes in conversion and selectivity in the hydrogenation reactions of cinnamaldehydes and benzyl cinnamate using novel biodegradable and/or low toxicity ILs and comparison with conventional ILs and common organic solvents. (Fig. 1). Recycling of the catalyst/IL media is also investigated.

Results

Synthesis of designer ILs for selective catalytic hydrogenation

Novel ILs (**2,4-10**) have been prepared containing ester and ether moieties in the side chain (Fig. 2).^{20,21} The ILs were readily synthesised from inexpensive alcohols and glycols, thus leading to imidazolium ILs with oxygen in the side chain of the cation.

trans-Cinnamaldehyde

The selective formation of hydrocinnamaldehyde is of both academic interest and of interest to the fine chemical industry (Fig. 3).²³

Using the pentyl derivative of imidazolium ILs **1** and **5**, selectivity towards hydrocinnamaldehyde generally ranged from 90 to 100%. The most impressive results obtained were achieved using the dimethyl derivative of the ILs, where under 1 atm. H₂ pressure 100% conversion and selectivity were reached at 24 h upon the 1st recycle (Table 1). Although slight variations in conversion and selectivity occurred during the recycling procedure, almost the same reaction efficiency can be seen upon the fourth recycle (conversion 97%, selectivity 100%) (Table 1).

When the side chain length is increased, and also contains an oxygen atom (**2**), the result obtained does not vary significantly; the conversion remains consistent at 100% and the selectivity still does not decrease below 90%. Thus, the method is shown

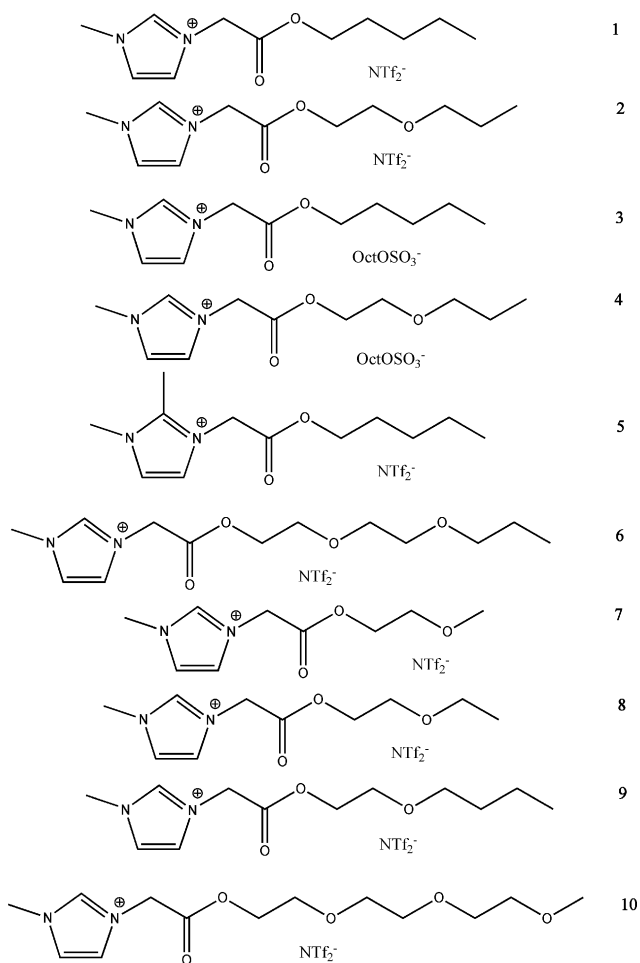


Fig. 1 Ionic liquids used as reaction solvents.

to be still applicable when an oxygen atom is present in the side chain of the IL (Table 2).

Upon increasing the number of oxygen atoms in the side chain from one to two, the selectivity is only slightly negatively affected. There is however a significant drop in conversion by the 3rd recycle (to 64%) (Table 3).

In order to compare the novel ILs with commercially available solvents, *trans*-cinnamaldehyde was hydrogenated using [Bmim][NTf₂] as well as [Bmim][OctOSO₃] and the results can be seen in Table 4. The results show that under 1 atm. H₂ pressure [Bmim][OctOSO₃] exhibits essentially the same selectivity as toluene, while [Bmim][NTf₂] gives a higher selectivity of 87%,

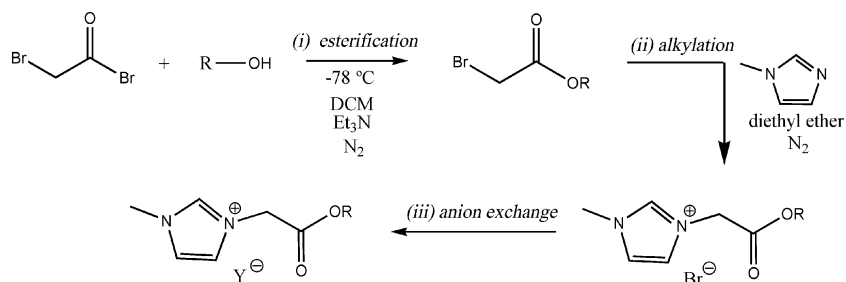


Fig. 2 Synthesis of novel ILs.

Table 1 Results from reactions using solvent 5 and 1

Solvent	Experiment (E)/Recycle (R)	Time (h)	% conversion	% selectivity 8
5	E1	24	8	100
		48	36	100
	R1	24	100	100
		48	100	93
	R2	24	48	73
		48	97	98
	R3	24	79	99
		48	100	96
	R4	24	89	100
		48	97	100
1	E1	48	98	94
	R1	48	100	93

Table 2 Results from reactions using solvent 2

Solvent	Experiment (E)/Recycle (R)	Time (h)	% conversion	% selectivity 8
2	E1	48	100	93 ^a

^a Isolated yield = 87%.

Table 3 Results from reactions using solvent 6

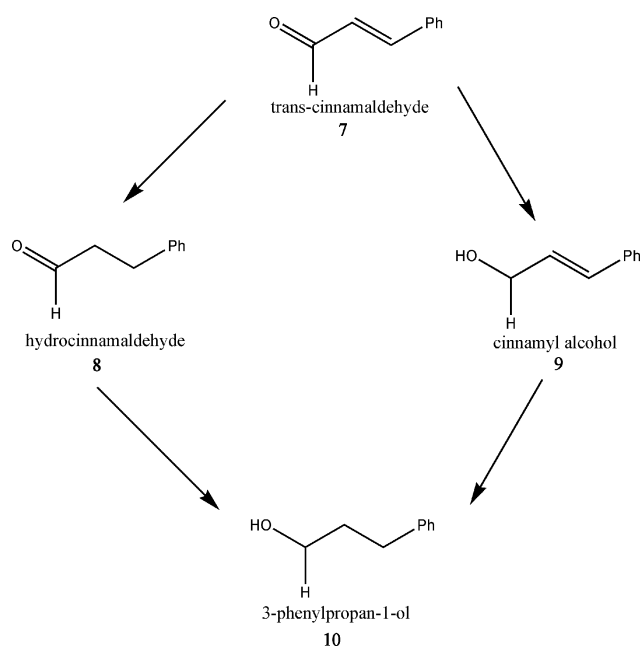
Solvent	Experiment (E)/Recycle (R)	Time (h)	% conversion	% selectivity 8
6	E1	24	32	100
		48	97	88 ^a
	R1	24	100	100
		48	100	88
	R2	24	31	100
		48	85	91
R3	24	34	90	
	48	64	93	

^a Isolated yield = 77%.

of a rhodium (I) complex (chlorotris(*meta*-trisulfonato triphenylphosphine). The reactions were carried out in a batch reactor (10–40 atm. H₂, 50–90 °C) and up to 99.9% selectivity towards the saturated aldehyde was observed using a biphasic system (water/toluene). Reductions of cinnamaldehyde based on ruthenium catalysts were carried out by Hajek *et al.*²⁵ and Qiu *et al.*²⁶ At 50 atm. H₂ using a 5% Ru/Y catalyst (Y: aluminosilicate zeolite used in petrochemistry), Hajek *et al.*²⁵ achieved selectivity up to 70% towards the unsaturated alcohol. Qiu *et al.*²⁶ achieved similar selectivity (79.1%), also towards the reduction of the carbonyl moiety, using a carbon nanotubes-supported Pd-Ru catalyst at 120 °C and 50 atm. H₂ pressure. Better results were obtained using the combined metal system than with each metal alone, speculated by the group to be due to a synergic effect or a promoting effect exerted by ruthenium. Our investigations using recyclable Pd/C catalysts in ILs at 1 atm. H₂ pressure to give selective reduction of the double bond in cinnamaldehyde represent a significant result.

Factors influencing selectivity

Selective reductions using imidazolium ILs have been rationalised on the basis of three parameters of the IL cation: 1) the presence or absence of a methyl group on the C₂ position of the imidazolium moiety, 2) the terminal alkyl chain length and, 3) the presence of oxygen atoms in the side chain. During their investigation into asymmetric hydrogenation in ILs, Jessop *et al.*²⁷ demonstrated that side chain length and substitution at the C₂ position of the imidazolium cation influenced enantioselectivity. Among their results, a comparison between ILs [emim][NTf₂] and [dmpim][NTf₂] ([dmpim]: 1,2-dimethyl-3-propylimidazolium) displayed differences in %ee obtained for the hydrogenation of tiglic and atropic acids. The %ee obtained when using ILs as reaction solvents was shown to be solvent-dependent. Chandrasekhar *et al.*²⁸ compared hydrogenation reactions using Adams' catalyst in poly(ethylene glycol) (400) and [emim][BF₄] and found that the yield dropped

**Fig. 3** Reduction pathway of cinnamaldehyde.

which is still lower than the selectivities of 93% achieved with ILs 1 and 2, or 100% obtained with ILs 5 and 6.

Nuithitikul and Winterbottom²⁴ selectively reduced the olefin moiety of cinnamaldehyde using an aqueous solution

Table 4 Hydrogenation of *trans*-cinnamaldehyde with commercially available solvents

Solvent	Experiment (E)/Recycle (R)	Time (h)	% conversion	% selectivity 8
[Bmim][NTf ₂]	E1	24	100	87
[Bmim][OctOSO ₃]	E1	24	100	69
Toluene	E1	24	100	67

by as much as 78% when [emim][BF₄] was used in place of PEG 400. An investigation of the quantitative adsorption of hydrogen on the catalyst in both solvents showed PEG 400 to allow superior adsorption, compared to the IL. The presence of repeated oxygen atoms in the PEG solvent was shown to affect the results obtained. Berger *et al.*²⁹ found the anion also had a significant effect on hydrogen solubility in ILs. [Bmim][BF₄] was found to solubilise hydrogen four times more effectively than [bmim][PF₆]. Our results also demonstrated that it was only possible to achieve highly selective hydrogenation of *trans*-cinnamaldehyde in the presence of the NTf₂ anion. We tentatively propose that steric effects around the cation (substitution at the C₂ position and the presence of ether oxygens in the cation side-chain) together with a subtle alteration in the uptake of hydrogen (influenced by the choice of anion) either in solution or at the catalyst surface, may be contributing to the superior selectivity exhibited by our novel ILs.

Benzyl cinnamate

In order to achieve the selective hydrogenation of the olefin moiety of benzyl cinnamate without hydrogenolysis of the benzyl ester (Fig. 4), elaborate conditions are often required.³⁰

The effect of catalyst loading, as well as the solvent effect was investigated during hydrogenations of benzyl cinnamate (Table 5).

The least amount of catalyst effective in inducing 100% conversion under 1 atm. H₂ pressure was 0.005g. Using half this value, only 32% conversion was achieved after 24h with IL **2**. The octylsulfate ILs (**3** and **4**) gave promising results in terms of selectivity; however this was only achieved when conversion was low for IL **3**, but with optimal conversion for IL **4**. The most compelling results from this data set are obtained using ILs **2** and **4**. Using 0.005 g catalyst, after 24 h, 100% conversion and selectivity were obtained under 1 atm. H₂ pressure. More surprising is that the selectivity was retained up to 48h, thus suggesting that hydrogenolysis of this compound in this IL system only occurs with the unsaturated ester. More evidence of this is observed when the non-hydrogenolysed reduced product **12** is further subjected to hydrogenation conditions using an increased amount of catalyst, under 1 atm. H₂ pressure, no hydrogenolysis is observed (Table 6). The significance of this result is that IL **2** completely prevents hydrogenolysis of the benzyl ester.

The system used to obtain 100% selectivity using IL **2** was recycled 4 times with no loss in activity (Table 7). After the fourth recycle, the selectivity remains constant, but the conversion decreases slightly to 91% on recycle 7. Only on recycle 8 was

Table 5 Effect of catalyst loading on hydrogenation

Solvent	Catalyst loading (g)	Time (h)	% conversion	% selectivity 12
1	0.01	24	100	0
	0.005	24	100	0
2	0.01	24	100	0
	0.005	24	100	100
	0.005	24	100	100
	0.005	48	100	100
	0.0025	24	32	100
3	0.01	24	100	53
	0.0025	24	5	100
	0.005	24	10	100
	0.005	48	19	100
	0.0025	48	0	0
4	0.005	24	11	100
	0.01	48	100	56
	0.005	48	100	100
	0.0025	48	0	0
	[Bmim][NTf ₂]	0.005	24	100
[Bmim][OctOSO ₃]	0.005	24	100	0
THF	0.005	24	100	0
Ethyl acetate	0.005	24	100	0
Methanol	0.005	24	100	0

Table 6 Hydrogenation of benzyl 3-phenylpropanoate (**12**)

Solvent	Catalyst loading (g)	Time (h)	No reaction
2	0.01	24	

Table 7 Recycling of IL **2** system

Solvent	Experiment (E)/Recycle (R)	% conversion	% selectivity 12
2	E1	100	100
	R1	100	100
	R2	100	100
	R3	100	100
	R4	100	100
	R5	97	100
	R6	91	100
	R7	91	100
	R8	81	100

a small drop in conversion observed (81%). This represents an improvement on previous recycling experiments using Pd(acac)₂ in IL **3** to selectively reduce phenoxyocta-2,7-diene, where a decrease in yield from 85 to 55% was observed on the first recycle.²²

Varying catalytic amounts were tested for the hydrogenation of benzyl cinnamate using IL **4**. As can be seen from the results displayed in Table 8, the increasing amount of catalyst favours

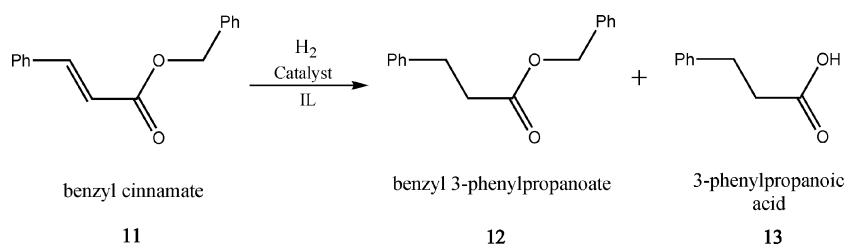


Fig. 4 Reduction of benzyl cinnamate.

Table 8 Varying catalytic amount for the hydrogenation of benzyl cinnamate in IL **4**

Solvent	Catalyst loading (g)	Time (h)	% conversion	% selectivity 12
4	0.005	24	100	100
	0.006		100	68
	0.007		100	55
	0.008		100	26
	0.009		100	25

Table 9 Effect of ILs of differing cation on the selective reduction of benzyl cinnamate

Solvent	Catalyst loading (g)	Time (h)	% conversion	% selectivity 12
6	0.005	24	100	44
7	0.005	24	100	7
8	0.005	24	100	0
9	0.005	24	100	34
10	0.005	24	100	0

hydrogenolysis, optimum conditions being observed with 0.005 g catalyst.

The effect of cation chain length and the number of oxygens in the side chain was investigated to determine whether only the cation from ILs **2** and **4** gave the best selectivity (Table 9).

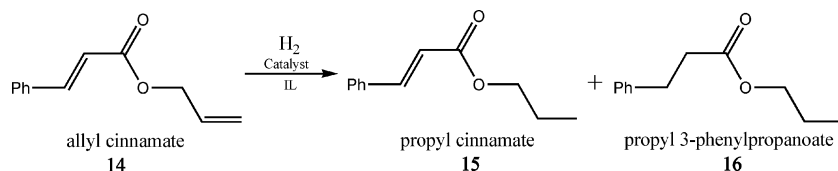
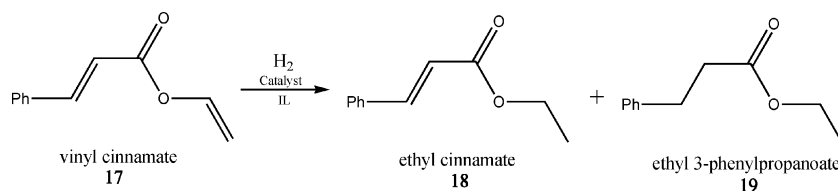
It is evident from the results obtained that any difference in the length of the side chain or the number of oxygen atoms contained within, negatively affects the selectivity of the reaction. This reaction is therefore sensitive to many changes in IL composition concerning the IL cation.

Based on the conditions from the result obtained using ILs **2** and **4** and 0.005 g catalyst, this system was used to test other compounds comprising hydrogenolysable functionalities.

Allyl cinnamate

The hydrogenation of allyl cinnamate can lead to the reduction either of the olefinic bonds, or even hydrogenolysis of the allyl functionality may be observed (Fig. 5).

Using both ILs **2** and **4** under 1 atm. H₂ pressure, impressive selectivities were reached in comparison with common organic solvents and classic ILs displaying no selectivity (Table 10).

**Fig. 5** Reduction of allyl cinnamate.**Fig. 6** Reduction of vinyl cinnamate.**Table 10** Hydrogenation of allyl cinnamate

IL	% conversion	% selectivity 15
2	100	84
4	100	71
[Bmim][NTf ₂]	100	0
[Bmim][OctOSO ₃]	100	0
Ethyl acetate	100	0

Table 11 Hydrogenation of vinyl cinnamate

IL	% conversion	% selectivity
2	100	0
4	100	49
Ethyl acetate	100	0

Vinyl cinnamate

Vinyl cinnamate was also used as a test-substrate in order to evaluate the selectivity obtained using the novel ILs in comparison with other more frequently used solvents (Fig. 6).

Only 49% selectivity was obtained using the octylsulfate IL, **4**, in comparison with no selectivity for IL **2** and ethyl acetate (Table 11).

Conclusion

We have demonstrated that novel imidazolium ILs display superior selectivity in olefin hydrogenation compared with conventional organic solvents and classic ILs. Hydrogenolysis-free hydrogenation of benzyl cinnamate was achieved using novel ILs without the need for a catalyst poison, under 1 atm. H₂ pressure. Furthermore *trans*-cinnamaldehyde was selectively reduced to hydrocinnamaldehyde with little or no over-reduction of the aldehydic moiety. The reactions were performed with only the use of the IL, substrate, a simple heterogeneous catalyst and under H₂ at 1 atm. pressure. Successful recycling of the systems was achieved without significant loss of activity. Overall, the novel ILs were found to be robust media for hydrogenation reactions as a replacement for harmful VOCs.

Experimental

Hydrogenation

Typical procedure. 10% Pd/C (5.0 mg unless otherwise stated) was weighed into a dry 2-neck round bottom flask. The pre-dried IL (2.0 mL) was then added to the flask, followed by the desired substrate (4 mmol) and 3 N₂/vacuum cycles were performed. The reaction mixture was allowed to stir for 10 minutes or until reaching the desired reaction temperature, or until all the substrate had dissolved in the IL. Hydrogen was then introduced to the reaction *via* a balloon, and the progress of the reaction was monitored by ¹H NMR at 24 and 48 hour intervals. Quantitative analysis of the reaction products was carried out by measuring the integration ratio of the peaks from the crude NMR spectrum. These values were then verified by purification of the product by column chromatography and thus the calculation of isolated yields. Upon termination of the reaction, the products were extracted using hexane (10 × 3 mL). The mass recovery after extraction from the IL was always > 98%. In the case of reactions carried out in octylsulfate ILs, the product was either distilled from the IL using high vacuum or a brief column was prepared to separate product from IL. These procedures generally led to a lower mass recovery (> 80%), due to product being lost on the column or lost during the distillation procedure. All reactions carried out in the NTF₂ ILs were carried out at 55 °C and 65 °C in the octylsulfate ILs.

Recycle procedure. Following extraction of the products from the IL, the IL (containing the catalyst) was dried and analysed by ¹H NMR. Following confirmation that the IL was substrate/product-free and had not degraded, fresh substrate was then added to the system and the reactions recommenced as described.

Benzyl 3-phenylpropanoate. ¹H NMR (400 MHz, CDCl₃) δ ppm 7.29–7.09 (m, 10H), 5.03 (s, 2H), 2.91 (t, *J* = 7.8 Hz, 2H), 2.62 (t, *J* = 7.8 Hz, 2H).

¹³C NMR (100 MHz, CDCl₃) δ ppm 172.80, 140.44, 135.94, 128.60, 128.56, 128.46, 128.36, 128.27, 126.33, 66.34, 35.21, 30.74.

Data consistent with literature.³¹

3-Phenylpropanoic acid. ¹H NMR (400 MHz, CDCl₃) δ ppm 11.00 (br s, 1H), 7.23–7.19 (m, 2H), 7.14–7.11 (m, 3H), 2.89 (t, *J* = 7.8 Hz, 2H), 2.69 (t, *J* = 7.8 Hz, 2H).

¹³C NMR (100 MHz, CDCl₃) δ ppm 178.97, 140.16, 128.59, 128.29, 126.40, 35.59, 30.58.

Data consistent with literature.³²

Hydrocinnamaldehyde. ¹H NMR (400 MHz, CDCl₃) δ ppm 9.85 (t, *J* = 1.4 Hz, 1H), 7.35–7.31 (m, 2H), 7.26–7.22 (m, 3H), 2.99 (t, *J* = 7.4 Hz, 2H), 2.83–2.79 (m, 2H).

¹³C NMR (100 MHz, CDCl₃) δ ppm 203.49, 141.32, 128.01, 127.99, 127.89, 40.33, 29.63.

Data consistent with literature.³³

3-Phenylpropan-1-ol. ¹H NMR (400 MHz, CDCl₃) δ ppm 7.23–7.18 (m, 2H), 7.14–7.10 (m, 3H), 3.62 (t, *J* = 6.6 Hz, 2H), 2.62 (t, *J* = 7.4 Hz, 2H), 1.82 (tt, *J* = 6.6, 7.4 Hz, 2H), 1.55 (br s, 1H).

¹³C NMR (100 MHz, CDCl₃) δ ppm 141.20, 129.01, 128.93, 126.50, 62.33, 34.30, 33.67.

Data consistent with literature.³⁴

Propyl cinnamate. ¹H NMR (400 MHz, CDCl₃) δ ppm 7.74 (d, *J* = 16 Hz, 1H), 7.56–7.54 (m, 2H), 7.42–7.38 (m, 3H), 6.50 (d, *J* = 16 Hz, 1H), 4.21 (t, *J* = 6.7 Hz, 2H), 1.79 (tq, *J* = 6.7, 7.8 Hz, 2H), 1.04 (t, *J* = 7.8 Hz, 3H).

¹³C NMR (100 MHz, CDCl₃) δ ppm 166.25, 143.20, 131.70, 129.29, 129.26, 129.00, 118.03, 61.52, 22.83, 17.01.

Data consistent with literature.³⁵

Propyl 3-phenylpropanoate. ¹H NMR (400 MHz, CDCl₃) δ ppm 7.34–7.30 (m, 2H), 7.25–7.22 (m, 3H), 4.09 (t, *J* = 7.0 Hz, 2H), 3.02 (t, *J* = 7.8 Hz, 2H), 2.69 (t, *J* = 7.8 Hz, 2H), 1.71 (tq, *J* = 7.0, 7.3 Hz, 2H), 0.97 (t, *J* = 7.3 Hz, 3H).

¹³C NMR (100 MHz, CDCl₃) δ ppm 173.06, 140.60, 128.50, 128.32, 126.25, 66.29, 37.43, 31.03, 21.98, 10.40.

Data consistent with literature.³⁶

Ethyl cinnamate. ¹H NMR (400 MHz, CDCl₃) δ ppm 7.73 (d, *J* = 16 Hz, 1H), 7.55–7.52 (m, 2H), 7.42–7.38 (m, 3H), 6.48 (d, *J* = 16 Hz, 1H), 4.31 (q, *J* = 7.1 Hz, 2H), 1.38 (t, *J* = 7.1 Hz, 3H).

¹³C NMR (100 MHz, CDCl₃) δ ppm 166.99, 144.93, 134.74, 130.55, 128.58, 128.06, 118.64, 60.50, 14.53.

Data consistent with literature.³⁵

Ethyl 3-phenylpropanoate. ¹H NMR (400 MHz, CDCl₃) δ ppm 7.34–7.30 (m, 2H), 7.25–7.23 (m, 3H), 4.19 (q, *J* = 7.2 Hz, 2H), 3.01 (t, *J* = 7.8 Hz, 2H), 2.67 (t, *J* = 7.8 Hz, 2H), 1.29 (t, *J* = 7.2 Hz, 3H).

¹³C NMR (100 MHz, CDCl₃) δ ppm 172.92, 140.62, 128.51, 128.34, 126.26, 60.43, 35.98, 31.01, 14.24.

Data consistent with literature.³⁷

IL preparation

ILs **1** and **3** were synthesised in accordance with the literature.²¹

Representative procedure for the preparation of α-bromoesters (2-propoxyethyl 2-bromoacetate). To a stirred solution of dichloromethane (350 mL), propoxyethanol (47.84 mL, 460 mmol), and triethylamine (69.3 mL, 500 mmol), under a nitrogen atmosphere at –78 °C was added dropwise bromoacetyl bromide (92.92 g, 460 mmol). After stirring at –78 °C for 3 h, the reaction mixture was allowed warm up to –20 °C and quenched by addition of water (50 mL). The organic phase was washed with distilled water (3 × 25 mL), saturated ammonium chloride (3 × 25 mL), saturated sodium bicarbonate (3 × 25 mL) and brine (2 × 25 mL). The organic phase was then dried over magnesium sulfate, filtered and solvents removed *via* rotary evaporation. The crude product was distilled (bp 100–102 °C) to give a pale yellow liquid in 83% yield (85.91 g, 382 mmol).

¹H NMR (400 MHz, CDCl₃) δ (ppm) 4.34 (t, *J* = 4.6 Hz, 2H), 3.88 (s, 2H), 3.67 (t, *J* = 4.6 Hz, 2H), 3.47 (t, *J* = 6.9 Hz, 2H), 1.66 (tq, *J* = 6.9, 7.3 Hz, 2H), 0.94 (t, *J* = 7.3 Hz, 3H).

¹³C NMR (100 MHz, CDCl₃) δ (ppm) 167.31, 73.07, 68.10, 65.42, 25.90, 22.81, 10.52.

Representative method for the preparation of bromide salts (3-Methyl-1-(propoxyethoxycarbonylmethyl)imidazolium bromide).

To a stirred solution of 1-methylimidazole (65.0 mmol, 5.33 g) in diethyl ether (60 mL) at $-15\text{ }^{\circ}\text{C}$ under a nitrogen atmosphere was added dropwise propoxyethyl 2-bromoacetate (78.0 mmol, 17.55 g). The reaction mixture was stirred vigorously at $-15\text{ }^{\circ}\text{C}$ for 1 h, then at RT for 24 h. The diethyl ether top phase was decanted and the IL washed with diethyl ether ($2 \times 20\text{ mL}$), then residual solvent removed on the rotary evaporator. The product was dried under high vacuum for 8 h yielding a pale yellow solid in 88% yield (17.59 g, 57.3 mmol).

$^1\text{H NMR}$ (400 MHz, CDCl_3) δ (ppm) 10.25 (s, 1H), 7.48 (t, $J = 1.8\text{ Hz}$, 1H), 7.35 (t, $J = 1.8\text{ Hz}$, 1H), 5.46 (s, 2H), 4.30 (t, $J = 4.8\text{ Hz}$, 2H), 4.02 (s, 3H), 3.61 (t, $J = 4.8\text{ Hz}$, 2H), 3.37 (t, $J = 6.8\text{ Hz}$, 2H), 1.54 (tq, $J = 6.8, 7.5\text{ Hz}$, 2H), 0.85 (t, $J = 7.5\text{ Hz}$, 3H).

$^{13}\text{C NMR}$ (100 MHz, CDCl_3) δ (ppm) 166.12, 138.74, 123.68, 122.77, 73.08, 67.89, 65.87, 50.28, 36.93, 22.75, 10.50.

M ($^{\circ}\text{C}$) 25–27 $^{\circ}\text{C}$.

IR (cm^{-1}) 3099, 2967, 2927, 1751, 1578, 1568, 1558, 1539, 1495, 1452, 1216, 1176.

MS m/z , Found 227.1410 $[\text{M}-\text{Br}]^+$, Calcd. $\text{C}_{11}\text{H}_{19}\text{N}_2\text{O}_3$ 227.1396.

Representative method for the preparation of NTf₂ salts (3-Methyl-1-(propoxyethoxycarbonylmethyl)imidazolium NTf₂) (2).

A flask was charged with 3-Methyl-1-(propoxyethoxycarbonylmethyl)imidazolium bromide (3.55 g, 7.00 mmol) and distilled water (20 mL). LiNTf_2 (2.15 g, 7.50 mmol) in distilled water (3 mL) was added in one portion and the suspension was stirred vigorously for 6 h at RT. The top aqueous layer was removed and the IL was washed with distilled water ($3 \times 10\text{ mL}$). The solvent was then removed on the rotary evaporator and the product was dried under high vacuum for 3 h to give a yellow viscous oil in 68% yield (2.43 g, 4.79 mmol).

$^1\text{H NMR}$ (400 MHz, CDCl_3) δ (ppm) 8.78 (s, 1H), 7.39 (t, $J = 1.8\text{ Hz}$, 1H), 7.36 (t, $J = 1.8\text{ Hz}$, 1H), 5.04 (s, 2H), 4.37 (t, $J = 4.8\text{ Hz}$, 2H), 3.95 (s, 3H), 3.67 (t, $J = 4.8\text{ Hz}$, 2H), 3.43 (t, $J = 6.7\text{ Hz}$, 2H), 1.61 (tq, $J = 6.7, 7.3\text{ Hz}$, 2H), 0.92 (t, $J = 7.3\text{ Hz}$, 3H).

$^{13}\text{C NMR}$ (100 MHz, CDCl_3) δ (ppm) 165.76, 137.50, 123.82, 123.34, 119.60 (q, $J = 319\text{ Hz}$), 72.99, 67.79, 65.91, 49.87, 56.49, 22.68, 10.37.

IR (cm^{-1}) 3164, 3117, 2968, 2927, 2862, 1751, 1569, 1558, 1539, 1495, 1452, 1353, 1198, 1135.

MS m/z , 227.2 $[\text{M}-\text{NTf}_2]^+$; MS: m/z , 280.0 $[\text{NTf}_2^-]$.

2,3 Dimethyl-1-(pentoxycarbonylmethyl)imidazolium NTf₂ (5).

The title compound was prepared from 2,3-dimethyl-1-(pentoxycarbonylmethyl)imidazolium bromide²¹ (3.36 g, 11.0 mmol) and LiNTf_2 (4.59 g, 16.0 mmol) according to the general procedure in 95% yield (5.30 g, 10.5 mmol).

$^1\text{H NMR}$ (400 MHz, CDCl_3) δ (ppm) 7.28 (d, $J = 2.2\text{ Hz}$, 1H), 7.26 (d, $J = 2.2\text{ Hz}$, 1H), 4.93 (s, 2H), 4.21 (t, $J = 6.8\text{ Hz}$, 2H), 3.82 (s, 3H), 2.56 (s, 3H), 1.68–1.60 (m, 2H), 1.34–1.27 (m, 4H), 0.92 (t, $J = 7.0\text{ Hz}$, 3H).

$^{13}\text{C NMR}$ (100 MHz, CDCl_3) δ (ppm) 165.78, 145.45, 122.38, 122.37, 119.70 (q, $J = 319\text{ Hz}$), 67.21, 49.17, 35.48, 27.93, 27.75, 22.18, 13.85, 9.75.

IR (cm^{-1}) 3154, 2962, 2930, 2862, 1751, 1595, 1558, 1546, 1539, 1495, 1452, 1354, 1197, 1137.

MS m/z , 225.2 $[\text{M}-\text{NTf}_2]^+$; MS: m/z , 280.0 $[\text{NTf}_2^-]$.

3-Methyl-1-(methoxyethoxycarbonylmethyl)imidazolium NTf₂ (7).

The title compound was prepared from 3-methyl-1-(methoxyethoxyoxycarbonylmethyl)imidazolium bromide (1.74 g, 6.26 mmol) and LiNTf_2 (2.16 g, 7.51 mmol) according to the general procedure in 91% yield (2.73 g, 5.70 mmol).

$^1\text{H NMR}$ (400 MHz, CDCl_3) δ (ppm) 8.85 (s, 1H), 7.39 (t, $J = 1.8\text{ Hz}$, 1H), 7.33 (t, $J = 1.8\text{ Hz}$, 1H), 5.07 (s, 2H), 4.40 (t, $J = 4.6\text{ Hz}$, 2H), 3.98 (s, 3H), 3.66 (t, $J = 4.6\text{ Hz}$, 2H), 3.40 (s, 3H).

$^{13}\text{C NMR}$ (100 MHz, CDCl_3) δ (ppm) 165.73, 137.75, 123.78, 123.18, 119.70 (q, $J = 319\text{ Hz}$), 69.75, 65.72, 63.24, 58.89, 49.93.

IR (cm^{-1}) 2926, 2855, 1750, 1636, 1558, 1539, 1495, 1452, 1365, 1204, 1129.

MS m/z , 199.1 $[\text{M}-\text{NTf}_2]^+$; MS: m/z , 280.0 $[\text{NTf}_2^-]$.

3-Methyl-1-(ethoxyethoxycarbonylmethyl)imidazolium NTf₂ (8).

The title compound was prepared from 3-methyl-1-(ethoxyethoxycarbonylmethyl)imidazolium bromide (2.93 g, 10.0 mmol) and LiNTf_2 (4.59 g, 16.0 mmol) according to the general procedure in 90% yield (4.42 g, 8.97 mmol).

$^1\text{H NMR}$ (400 MHz, CDCl_3) δ (ppm) 8.82 (s, 1H), 7.39 (t, $J = 1.8\text{ Hz}$, 1H), 7.34 (t, $J = 1.8\text{ Hz}$, 1H), 5.06 (s, 2H), 4.38 (t, $J = 4.6\text{ Hz}$, 2H), 3.97 (s, 3H), 3.68 (t, $J = 4.6\text{ Hz}$, 2H), 3.56 (q, $J = 7.1\text{ Hz}$, 2H), 1.22 (t, $J = 7.1\text{ Hz}$, 3H).

$^{13}\text{C NMR}$ (100 MHz, CDCl_3) δ (ppm) 165.76, 137.63, 123.80, 123.25, 119.70 (q, $J = 319\text{ Hz}$), 67.62, 66.67, 65.97, 49.92, 36.56, 15.01.

IR (cm^{-1}) 3169, 3116, 2967, 2927, 2859, 1751, 1581, 1569, 1558, 1495, 1452, 1352, 1196, 1135.

MS m/z , 213.1 $[\text{M}-\text{NTf}_2]^+$; MS: m/z , 280.0 $[\text{NTf}_2^-]$.

3-Methyl-1-(butoxyethoxycarbonylmethyl)imidazolium NTf₂ (9).

The title compound was prepared from 3-methyl-1-(butoxyethoxycarbonylmethyl)imidazolium bromide (1.85 g, 5.77 mmol) and LiNTf_2 (1.99 g, 6.92 mmol) according to the general procedure in 84% yield (2.73 g, 4.82 mmol).

$^1\text{H NMR}$ (400 MHz, CDCl_3) δ (ppm) 8.71 (s, 1H), 7.38 (t, $J = 1.8\text{ Hz}$, 1H), 7.36 (t, $J = 1.8\text{ Hz}$, 1H), 5.00 (s, 2H), 4.32 (t, $J = 4.8\text{ Hz}$, 2H), 3.91 (s, 3H), 3.64 (t, $J = 4.8\text{ Hz}$, 2H), 3.44 (t, $J = 6.7\text{ Hz}$, 2H), 1.54 (tt, $J = 6.7, 7.2\text{ Hz}$, 2H), 1.34 (tq, $J = 7.2, 7.5\text{ Hz}$, 2H), 0.89 (t, $J = 7.5\text{ Hz}$, 3H).

$^{13}\text{C NMR}$ (100 MHz, CDCl_3) δ (ppm) 165.78, 137.32, 123.83, 123.40, 122.33 (q, $J = 319\text{ Hz}$), 71.09, 67.78, 65.81, 49.78, 36.37, 31.50, 19.11, 13.78.

IR (cm^{-1}) 3164, 3123, 2959, 2934, 2864, 1756, 1582, 1569, 1558, 1495, 1453, 1354, 1197, 1135.

MS m/z , 241.2 $[\text{M}-\text{NTf}_2]^+$; MS: m/z , 280.0 $[\text{NTf}_2^-]$.

3-Methyl-1-(propoxyethoxyethoxycarbonylmethyl)imidazolium NTf₂ (6).

The title compound was prepared from 3-methyl-1-(methoxyethoxyethoxycarbonylmethyl)imidazolium bromide (1.91 g, 5.45 mmol) and LiNTf_2 (1.88 g, 6.54 mmol) according to the general procedure in 82% yield (2.46 g, 4.46 mmol).

$^1\text{H NMR}$ (400 MHz, CDCl_3) δ (ppm) 8.92 (s, 1H), 7.40 (t, $J = 1.7\text{ Hz}$, 1H), 7.31 (t, $J = 1.7\text{ Hz}$, 1H), 5.08 (s, 2H), 4.41 (t, $J = 4.8\text{ Hz}$, 2H), 4.00 (s, 3H), 3.77 (t, $J = 4.8\text{ Hz}$, 2H), 3.67

(t, $J = 4.8$, 2H), 3.61 (t, $J = 4.8$ Hz, 2H), 3.44 (t, $J = 6.8$ Hz, 2H), 1.61 (tq, $J = 6.8$, 7.2 Hz, 2H), 0.93 (t, $J = 7.2$ Hz, 3H).

^{13}C NMR (100 MHz, CDCl_3) δ (ppm) 165.71, 137.92, 123.80, 123.07, 122.00 (q, $J = 319$ Hz), 73.09, 70.58, 69.89, 68.42, 65.86, 50.02, 36.66, 22.76, 10.47.

IR (cm^{-1}) 3164, 3119, 2966, 2927, 2865, 1751, 1568, 1558, 1495, 1452, 1353, 1198, 1135.

MS m/z , 271.3 $[\text{M}-\text{NTf}_2]^-$; MS: m/z , 280.0 $[\text{NTf}_2]^-$.

3-Methyl-1-(methoxyethoxyethoxyethoxycarbonylmethyl)imidazolium NTf_2 (10). The title compound was prepared from 3-methyl-1-(methoxyethoxyethoxyethoxycarbonylmethyl)imidazolium bromide (2.20 g, 6.00 mmol) and LiNTf_2 (2.01 g, 7.00 mmol) according to the general procedure in 93% yield (3.17 g, 5.60 mmol).

^1H NMR (400 MHz, CDCl_3) δ (ppm) 8.78 (s, 1H), 7.37 (t, $J = 1.6$ Hz, 1H), 7.26 (t, $J = 1.6$ Hz, 1H), 4.99 (s, 2H), 4.31 (t, $J = 4.6$ Hz, 2H), 3.89 (s, 3H), 3.66 (t, $J = 4.6$ Hz, 2H), 3.57-3.54 (m, 6H), 3.49-3.47 (m, 2H), 3.28 (s, 3H).

^{13}C NMR (100 MHz, CDCl_3) δ (ppm) 165.78, 137.75, 123.96, 123.18, 119.70 (q, $J = 319$ Hz), 71.79, 70.42, 70.38, 70.32, 68.35, 65.57, 58.82, 49.92, 36.53.

IR (cm^{-1}) 3161, 3116, 2925, 2859, 1751, 1569, 1558, 1539, 1495, 1452, 1354, 1198, 1135.

MS m/z , 287.2 $[\text{M}-\text{NTf}_2]^-$; MS: m/z , 280.0 $[\text{NTf}_2]^-$.

Representative method for the preparation of OctOSO₃ salts (3-Methyl-1-(propoxyethoxycarbonylmethyl)imidazolium OctOSO₃) (4). To a solution of 3-Methyl-1-(propoxyethoxycarbonylmethyl)imidazolium bromide (3.68 g, 12.0 mmol) in distilled water (20 mL) was added in one portion sodium octyl sulfate (2.09 g, 9.00 mmol) and stirred at 60 °C for 2 h. The water was then slowly removed under vacuum. The precipitate was dissolved in DCM (5 mL) and washed with distilled water (2 × 3 mL). The product remaining was dried on the rotary evaporator and then under high vacuum for 8 h to give a pale yellow grease in 85% yield (3.33 g, 7.62 mmol).

^1H NMR (400 MHz, CDCl_3) δ (ppm) 9.45 (s, 1H), 7.48 (t, $J = 1.6$ Hz, 1H), 7.41 (t, $J = 1.6$ Hz, 1H), 5.25 (s, 2H), 4.36 (t, $J = 4.7$ Hz, 2H), 4.01 (m, 5H), 3.67 (t, $J = 4.7$ Hz, 2H), 3.43 (t, $J = 6.8$ Hz, 2H), 1.63-1.58 (m, 4H), 1.56-1.29 (m, 10H), 0.92-0.86 (m, 6H).

^{13}C NMR (100 MHz, CDCl_3) δ (ppm) 166.45, 138.89, 123.71, 123.06, 73.04, 67.92, 67.89, 65.67, 49.91, 36.58, 31.83, 29.50, 29.36, 29.26, 25.87, 22.73, 22.66, 14.13, 10.47.

IR (cm^{-1}) 3118, 2958, 2927, 2855, 1750, 1569, 1558, 1539, 1495, 1455, 1217, 1178, 1108.

MS m/z , 227.1 $[\text{M}-\text{OctSO}_4]^-$; MS: m/z , 209.0 $[\text{OctSO}_4]^-$.

References

- (a) Y. Kume, K. Qiao, D. Tomida and C. Yokoyama, *Catalysis Communications*, 2008, **9**, 369; (b) Y. Kanazawa and H. Nishiyama, *Synlett*, 2006, **19**, 3343; (c) F. Lopez-Linares, G. Agrifoglio, A. Labrador and A. Karam, *Journal of Molecular Catalysis A*, 2004, **207**, 115; (d) A. Mori, T. Mizusaki, Y. Miyakawa, E. Ohashi, T. Haga, T. Maegawa, Y. Monguchi and H. Sajiki, *Tetrahedron*, 2006, **62**, 11925; (e) T. Ikawa, H. Sajiki and K. Hirota, *Tetrahedron*, 2005, **61**, 2217.
- (a) Boxwell, P. Dyson, D. Ellis and T. Welton, *J. Am. Chem. Soc.*, 2002, **124**, 9334; (b) Dupont, G. Fonseca, A. Umpierre, P. Fichtner and S. Teixeira, *J. Am. Chem. Soc.*, 2002, **124**, 4228.
- (a) P. Dyson, D. Ellis, W. Henderson and G. Laurenczy, *Adv. Synth. Catal.*, 2003, 345; (b) P. Dyson, G. Laurenczy, C. Andre Ohlin, J. Vallance and T. Welton, *Chem. Commun.*, 2003, 2418; (c) L. Rossi, G. Machado, P. Fichtner, S. Teixeira and J. Dupont, *Catalysis Letters*, 2004, **92**(3-4), 149-255; (d) M. Steffan, M. Lucas, A. Brandner, M. Wollny, N. Oldenburg and P. Claus, *Chem. Eng. Technol.*, 2007, **30**, 481; (e) K. Anderson, P. Goodrich, C. Hardacre and D. Rooney, *Green Chemistry*, 2003, **5**, 448.
- P. Gallezot and D. Richard, *Catal. Rev.-Sci. Eng.*, 1998, **40**, 81.
- H. Miura, *Shokubai*, 2007, **49**, 232.
- X. Cheng, L. Hexing, D. Weilin, W. Jie, R. Yong and Q. Minghua, *Applied Catalysis A: General*, 2003, **253**, 359.
- P. Maki-Arvela, J. Haje, T. Salmi and D. Murzin, *Applied Catalysis A: General*, 2005, **292**, 1.
- U. Singh and M. Vannice, *Applied Catalysis A: General*, 2001, **213**, 1.
- (a) A. Muller, J. Bowers, J. Eubanks, C. Geiger, J. Santobianco, 1999, *WO/1999/008989*; (b) F. Bennett, A. Ganguly, V. Girijavallabhan, N. Patel, 1993, *EP0533342*; (c) P. Jadhav and H.-W. Man, *Tetrahedron Lett.*, 1996, **37**, 1153.
- P. Kluson and L. Cerveny, *Applied Catalysis A: General*, 1995, **128**, 13.
- I. Kostas, *Journal of Organometallic Chemistry*, 2001, **634**, 90.
- K. Nuithitkul and M. Winterbottom, *Catalysis Today*, 2007, **128**, 74.
- K. Nuithitkul and M. Winterbottom, *Chemical Engineering Science*, 2006, **61**, 5944.
- J. P. Tessonnier, L. Pesant, G. Ehret, M. Ledoux and C. Pham-Huu, *Applied Catalysis A: General*, 2005, **288**, 203.
- C. Pham-Huu, N. Keller, L. Charbonniere, R. Ziessel and M. Ledoux, *Chem. Commun.*, 2000, 1871.
- M. Bhor, A. Panda, S. Jagtap and B. Bhanage, *Catal. Lett.*, 2008, **124**, 157.
- T. Mallet and A. Baiker, *Applied Catalysis A: General*, 2000, **200**, 3.
- R. Schlögl, Surface composition and structure of active carbon, in: F. Schuth, K. S. W. Sing and J. Weitkamp, (Eds.), *Handbook of Porous Solids*, Wiley-VCH, 2002, 1863.
- C. Pham-Huu, N. Keller, G. Ehret and M. Ledoux, *J. Catal.*, 2001, **200**, 400.
- N. Gathergood and P. J. Scammells, *Aust. J. Chem.*, 2002, **55**, 557.
- (a) N. Gathergood, M. T. Garcia and P. J. Scammells, *Green Chemistry*, 2004, **6**, 166; (b) M. T. Garcia, N. Gathergood and P. J. Scammells, *Green Chemistry*, 2004, **7**, 9; (c) N. Gathergood, P. J. Scammells and M. T. Garcia, *Green Chemistry*, 2006, **8**, 156.
- S. Bouquillon, T. Courant, D. Dean, N. Gathergood, S. Morrissey, B. Pegot, P. J. Scammells and R. Singer, *Aust. J. Chem.*, 2007, **60**, 843.
- (a) F. Benvenuti, C. Carlini, M. Marchionna, A. M. Galletti and G. Sbrana, *Journal of Molecular Catalysis A*, 1999, **145**, 221; (b) Y. Kume, K. Qiao, D. Tomida and C. Yokoyama, *Catalysis Communications*, 2008, **9**, 369; (c) Y. Kanazawa and H. Nishiyama, *Synlett*, 2006, **19**, 3343; (d) F. Lopez-Linares, G. Agrifoglio, A. Labrador and A. Karam, *Journal of Molecular Catalysis A*, 2004, **207**, 115; (e) Y. Zhang, S. Liao, Y. Xu and D. Yu, *Applied Catalysis A*, 2000, **192**, 247.
- K. Nuithitkul and M. Winterbottom, *Chem. Eng. Sci.*, 2004, **59**, 5439.
- J. Hajek, N. Kumar, P. Maki-Arvela, T. Salmi and D. Murzin, *Journal of Molecular Catalysis A: Chemical*, 2004, **217**, 145.
- J. Qui, H. Zhang, X. Wang, H. Han, C. Liang and C. Li, *React. Kinet. Catal. Lett.*, 2006, **88**, 269.
- P. Jessop, R. Stanley, R. Brown, C. Eckert, C. Liotta and T. P. Ngo, Pollet, *Green Chem.*, 2003, **5**, 123.
- S. Chandrasekhar, S. Prakash and C. Rao, *J. Org. Chem.*, 2006, **71**, 2196.
- A. Berger, R. de Souza, M. Delgado and J. Dupont, *Tetrahedron: Asymmetry*, 2001, **12**, 1825.
- (a) A. Mori, T. Mizusaki, Y. Miyakawa, E. Ohashi, T. Haga, T. Maegawa, Y. Monguchi and H. Sajiki, *Tetrahedron*, 2006, **62**, 11925; (b) J. Le Bras, D. K. Mukherjee, S. Gonzalez, M. Tristany, B. Ganchegui, M. Moreno-Manas, R. Pleixats, F. Henin and J. Muzart, *New J. Chem.*, 2004, **28**, 1550; (c) H. Sajiki, T. Ikawa and K. Hirota, *Tetrahedron Lett.*, 2003, **44**, 8437; (d) T. Ikawa, H. Sajiki and

- K. Hirota, *Tetrahedron*, 2005, **61**, 2217; (e) D. Belotti, G. Cantagrel, C. Combellas, J. Cossy, F. Kanoufi and S. Nunige, *New J. Chem.*, 2005, **29**, 761.
- 31 P. Black, G. Cami-Kobeci, M. Edward, P. Slatford, M. Whittlesey and J. Williams, *Org. Biomol. Chem.*, 2006, **4**, 116.
- 32 (a) Sigma Aldrich, NMR W288918; (b) Beil., **9**, III, 2382.
- 33 (a) Sigma Aldrich, NMR 56660; (b) Beil., **7**, IV, 692.
- 34 (a) Sigma Aldrich, NMR 140856; (b) Beil., **6**, IV, 3198.
- 35 S. Yan-mei, L. Jing, Z. Ping, S. Zhi-guang, L. Ye-zhi and H. Hua-min, *Chem. Res. Chinese U.*, 2007, **23**, 669.
- 36 S. Kiyooka, Y. Wada, M. Ueno, T. Yokoyama and R. Yokoyama, *Tetrahedron*, 2007, **63**, 12695.
- 37 S. Chandrasekhar, G. Reddy, C. Nagesh and C. Reddy, *Tetrahedron Lett.*, 2007, **48**, 1269.

Biodegradable, non-bactericidal oxygen-functionalised imidazolium esters: A step towards 'greener' ionic liquids†

Saibh Morrissey,^a Bruce Pegot,^a Deborah Coleman,^a M. Teresa Garcia,^b Damien Ferguson,^c Bríd Quilty^c and Nicholas Gathergood^{*a}

Received 25th July 2008, Accepted 18th February 2009

First published as an Advance Article on the web 18th March 2009

DOI: 10.1039/b812809j

A series of imidazolium ionic liquids was prepared and screened against 7 bacterial strains. The incorporation of ether groups into the ester side-chain significantly reduced the toxicity compared with alkyl ester derivatives. Biodegradation data are also presented for 15 of the ionic liquids—including 6 examples which can be classed as readily biodegradable.

Introduction

Ionic liquids (ILs) have been under study as a replacement for volatile organic compounds (VOCs) and are now used as media for a variety of organic and inorganic reactions, ranging from catalytic hydrogenation^{1,2} and hydroformylation³ to the Friedel–Crafts⁴ and Diels–Alder⁵ reactions. ILs have also proved useful in the physical sciences, with applications emerging in analytical separations,⁶ near-infrared luminescence⁷ and photo-magnetism.⁸

A significant research effort ensued when ILs emerged as a possible 'green' alternative to common organic solvents.⁹ Although their negligible vapour pressures¹⁰ render ILs attractive alternatives to VOCs, other release routes aside from evaporation to the environment must be addressed before ILs can officially be categorised as 'green'.

In recent years investigations have commenced into the biological impact of ILs on the environment. With the field of ILs continuing to shift from the research laboratory to an industrial setting,^{11–13} toxicity and biodegradability have become additional factors to be considered before ILs gain acceptance as viable alternatives to VOCs.

Toxicological and ecotoxicological data for ILs have been collected using test systems based on different biological complexity levels. Toxicity and antimicrobial studies have been performed on a range of bacteria and fungi,^{14–17} acute toxicity studies have been carried out on fish,¹⁸ growth inhibition studies have been carried out on algae,^{19,20,21} and also on terrestrial plants.^{22,23} The variety of organisms studied now extends to higher classes such as the soil nematode²⁴ and the freshwater snail.²⁵

Most of the ionic liquids studied have been of the imidazolium and pyridinium classes, with alkyl or alkyloxy side-chains,

containing the anions, bromide (Br⁻), chloride (Cl⁻), hexafluorophosphate (PF₆⁻), and tetrafluoroborate (BF₄⁻). Preliminary experiments on the effects of ILs on rat cell lines and also human Caco-2 cell lines have been conducted,^{26,27,28} as well as enzymatic studies.²⁹

Results from these investigations prove that the toxicity of ILs increases with increasing alkyl chain length. This could be explained by the increased lipophilic character of the IL with increasing alkyl chain length, which may lead to IL incorporation into biological membranes and disruption of membrane proteins (polar narcosis).³⁰ The resulting increase in cell membrane permeability may also adversely affect the ability of cells to resist or repair membrane disruption.²¹

The contribution of ILs to anthropogenic waste is a major factor hindering their valid classification as 'green solvents'. To date, limited research has been carried out to determine the biodegradability of ILs.^{31–39}

Although an extensive range of ILs have been synthesized and tested for environmental toxicity, little research has been conducted in which the design of the ILs is the chief factor in reducing their environmental impact.⁴⁰

The work of Gathergood and Scammells in the field of biodegradable ILs began in 2002³¹ when they applied the same principles that are used in the synthesis of biodegradable surfactants to the design of ILs. A modified Sturm test (ISO9439) was used to evaluate the biodegradability of imidazolium ILs that have ester-linked side-chains. In these studies the most readily degraded IL gave a biodegradation of 59%, close to the pass level for this test (60%).

Gathergood *et al.*³² proceeded to test ILs for biodegradability, using the 'Closed Bottle Test' (OECD 301D) together with a modified Sturm test (OECD 301B). The ILs that incorporated an ester linkage in the side-chain showed a significant increase in biodegradation (close to 40%) when compared with their commercially available counterparts, [bmim][BF₄] and [bmim][PF₆] that show negligible biodegradation.

After studies by Garcia *et al.*³³ confirmed that the presence of an ester linkage promoted biodegradation, a range of ILs both with and without ester groups, were examined. Garcia determined that in both classes of IL, the octylsulfate counter ion showed the highest biodegradation. However, none of the ILs synthesized could yet be described as readily biodegradable.

^aNational Institute for Cellular Biotechnology, School of Chemical Sciences, Dublin City University, Glasnevin, Dublin 9, Ireland. E-mail: Nick.Gathergood@dcu.ie; Fax: +353 1 700 5503; Tel: +353 1 700 7860

^bDepartment of Surfactant Technology, IIQAB-CSIC, Jordi Girona, Spain

^cNational Institute for Cellular Biotechnology and School of Biotechnology, Dublin City University, Glasnevin, Dublin 9, Ireland

† Electronic supplementary information (ESI) available: Further experimental procedures and biodegradation results. See DOI: 10.1039/b812809j

Ultimately, by combining the features of a propyl or pentyl ester side-chain with the octylsulfate counterion, Gathergood *et al.*³⁴ were able to synthesize the first 'readily biodegradable ILs'. Two complementary test methods were chosen to investigate the biodegradability of Scammells and Gathergood's ILs. Firstly, using the 'Closed Bottle Test' (OECD 301D), reference test compounds [bmim][Br] and [bmim][BF₄] showed the lowest biodegradation level (0–1%). Imidazolium bromide salts containing ester moieties showed improved biodegradation (23–33%), while the octylsulfate ILs containing esters gave a further improvement in biodegradation levels (49–56%). These results were corroborated using the CO₂ Headspace test (ISO 14593). It was with ISO 14593 that the most impressive biodegradation levels so far were obtained (60–66%), with ILs containing an ester moiety and also the octylsulfate counter anion. Monitoring the disappearance of substrates during biodegradation tests by a battery of analytical tests, including NMR and HPLC is highly desirable, but if methods that take account of respirometric parameters, such as O₂ depletion (OECD 301D) and CO₂ formation (*e.g.* ISO9439, OECD 301B, ISO 14593) are neglected then the analysis cannot be relied upon to reflect biodegradation of a test sample.⁴¹

Herein we disclose the synthesis of a library of imidazolium-based ILs that enables us to compare the toxicity and biodegradability of the reported butyl (**1a–f**) and pentyl (**2a–f**) imidazolium esters³⁴ with decyl imidazolium ester **12a**⁴² as well as novel esters derived from ethylene glycol, diethylene glycol and triethylene glycol, with oxygenated side-chains ranging from 4 to 10 atoms in length. (Fig. 1).

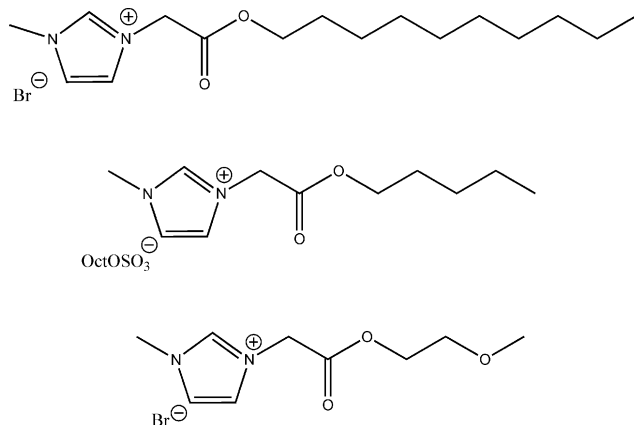


Fig. 1 Oxygen functionalized ILs.

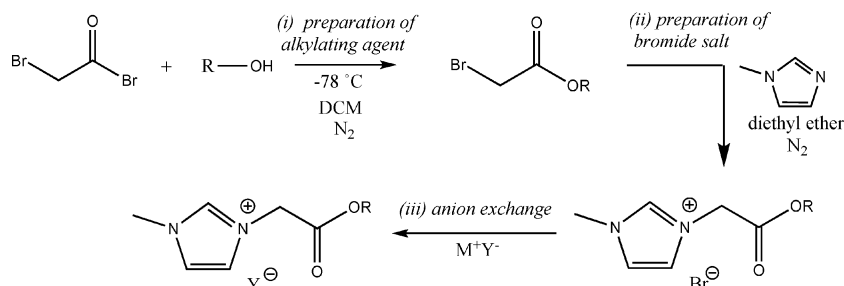


Fig. 2 2-Step synthesis of IL followed by anion exchange.

Results and discussion

Synthesis

Synthesis of the ILs described herein is carried out in two steps followed by anion exchange (Fig. 2).

The commercially available alcohols were reacted with bromoacetyl bromide to form the desired alkylating agents in good yields (62–88%). Pure 2-bromoesters were then obtained by distillation of the crude product under high vacuum to give colourless to pale yellow oils. This reaction was performed at scales up to 500 mmol with no compromise in yield or purity.

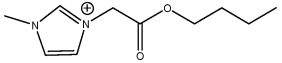
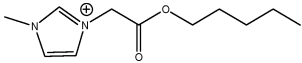
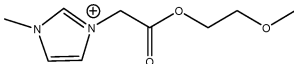
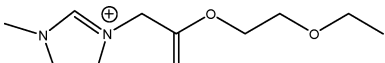
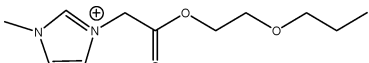
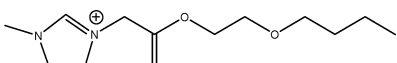
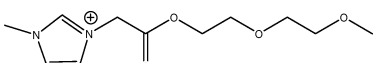
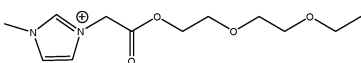
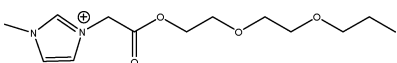
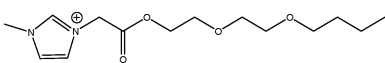
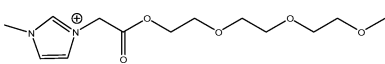
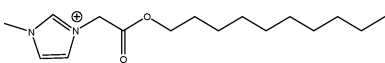
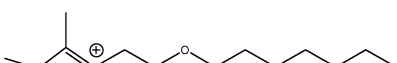
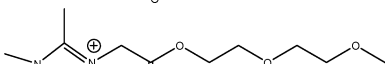
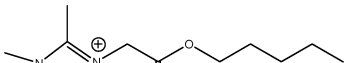
Subsequent alkylation of either 1-methylimidazole or 1,2-dimethylimidazole by the 2-bromoester at –15 °C for 3 hours, then at 20 °C for 18 hours resulted in precipitation of the desired bromide salt in good yields (82–98%). However, only moderate yields (55% and 51%, respectively) were recorded for two of the long-chain esters, **11a** and **12a**.

Although four of the bromide salts were viscous liquids (**1a**, **2a**, **13a**, **15a**) in most cases the bromides were solids at 20 °C. However, with only five exceptions (solids, **3d**, **10e**, **13f**, **15d** and **15f**) amongst the other counter-ions the remaining 66 esters were liquid at 20 °C, and even considering the solid examples, in no case did the melting point of the ester-functionalised ILs exceed 75 °C (significantly below the 100 °C limit for definition as ILs, Table 1).

The final counter-ion metathesis was carried out using potassium hexafluorophosphate, sodium tetrafluoroborate, sodium dicyanoamide, lithium trifluoromethanesulfonimide or sodium octylsulfate. This exchange is important as it results in changes to the bulk solvent properties of the corresponding IL. In most cases, the anion exchange reaction leads to ILs with decreased melting points, compared with their bromide salt analogues. This alteration in physical properties is especially marked in the case of the trifluoromethanesulfonimide (NTf₂⁻) salts, which were all liquids at 20 °C and appeared to be significantly less viscous than the other salts. The NTf₂⁻ salt was readily prepared by a simple reaction of the bromide IL with lithium trifluoromethanesulfonimide in water over 4–18 hours, which gave the desired IL as a separate phase, beneath the aqueous layer. The ion-exchange reactions proceeded in good yields (69–96%) and simply washing the hydrophobic IL with water proved to be an effective means of removing trace impurities.

In common with the trifluoromethanesulfonimide ILs, the PF₆⁻ salts formed a biphasic mixture with water. In most cases the hexafluorophosphate ILs exhibit slightly increased melting points, when compared with the NTf₂⁻ ILs (Table 1). A different

Table 1 IL data

IL Cation	Br ⁻	NTf ₂ ⁻	BF ₄ ⁻	PF ₆ ⁻	N(CN) ₂ ⁻	OctOSO ₃ ⁻
	1a 82 <i>liquid</i>	1b 86 <i>liquid</i>	1c 97 <i>liquid</i>	1d 93 <i>liquid</i>	1e 87 <i>liquid</i>	1f 61 <i>liquid</i>
	2a 97 <i>liquid</i>	2b 93 <i>liquid</i>	2c 95 <i>liquid</i>	2d 98 <i>liquid</i>	2e 98 <i>liquid</i>	2f 96 <i>liquid</i>
	3a 89 53–55 °C	3b 91 <i>liquid</i>	3c 95 <i>liquid</i>	3d 96 58–60 °C	3e 80 <i>liquid</i>	3f 95 <i>liquid</i>
	4a 93 24–26 °C	4b 90 <i>liquid</i>	4c 96 <i>liquid</i>	4d 98 <i>liquid</i>	4e 99 <i>liquid</i>	4f 96 <i>liquid</i>
	5a 88 25–27 °C	5b 68 <i>liquid</i>	5c 97 <i>liquid</i>	5d 97 <i>liquid</i>	5e 91 <i>liquid</i>	5f 85 <i>liquid</i>
	6a 89 28–30 °C	6b 84 <i>liquid</i>	6c 96 <i>liquid</i>	6d 95 <i>liquid</i>	6e 51 <i>liquid</i>	6f 93 <i>liquid</i>
	7a 97 52–54 °C	7b 91 <i>liquid</i>	7c 94 <i>liquid</i>	7d 91 <i>liquid</i>	7e 94 <i>liquid</i>	7f 82 <i>liquid</i>
	8a 92 28–30 °C	8b 87 <i>liquid</i>	8c 96 <i>liquid</i>	8d 96 <i>liquid</i>	8e 99 <i>liquid</i>	8f 93 <i>liquid</i>
	9a 98 32–34 °C	9b 82 <i>liquid</i>	9c 93 <i>liquid</i>	9d 91 <i>liquid</i>	9e 85 <i>liquid</i>	9f 98 <i>liquid</i>
	10a 94 48–50 °C	10b 86 <i>liquid</i>	10c 92 <i>liquid</i>	10d 79 <i>liquid</i>	10e 98 34–36 °C	10f 92 <i>liquid</i>
	11a 55 59–61 °C	11b 93 <i>liquid</i>	11c 94 <i>liquid</i>	11d 57 <i>liquid</i>	11e 75 <i>liquid</i>	11f 84 <i>liquid</i>
	12a 51 49–51 °C	12b 95 <i>liquid</i>	n/a	n/a	n/a	12f 79 <i>liquid</i>
	13a 92 <i>liquid</i>	13b 83 <i>liquid</i>	13c 95 <i>liquid</i>	13d 97 <i>liquid</i>	13e 78 <i>liquid</i>	13f 84 50–52 °C
	14a 88 74–75 °C	14b 96 <i>liquid</i>	14c 94 <i>liquid</i>	14d 95 <i>liquid</i>	14e 99 <i>liquid</i>	14f 94 <i>liquid</i>
	15a 81 <i>liquid</i>	15b 95 <i>liquid</i>	15c 93 <i>liquid</i>	15d 97 40–42 °C	15e 85 <i>liquid</i>	15f 86 63–65 °C

method of anion exchange was used to prepare the hexafluorophosphates, in which the 3-substituted 1-methylimidazolium bromide salt was refluxed in acetone for four days in the presence of potassium hexafluorophosphate to give the PF₆⁻ ILs in high yields (> 90%). The BF₄⁻ ILs were synthesized analogously to the PF₆⁻ salts using sodium tetrafluoroborate, giving ILs in equally good yields (> 90%). The corresponding N(CN)₂⁻ salts were again formed by reaction of the bromide IL with the sodium salt for four days, however the solvent was changed from acetone to acetonitrile and refluxing was unnecessary, with good yields (51–99%) of exchanged dicyanoamide IL obtained even at 20 °C. To obtain the IL octylsulfate, the bromide salt of the IL and sodium octylsulfate were stirred in water for 2 hours at 60 °C, according to the literature method.⁴³ The water was then slowly removed under vacuum. The resulting precipitate was subsequently dissolved in dichloromethane and washed with a small amount of distilled water. After evaporation of the solvent, the exchanged octylsulfate ILs were obtained in good yields, usually between 80 and 98%. Although two of the octylsulfate ILs (**13f** and **15f**) are solids at 20 °C, they still exhibit melting points significantly below 100 °C (Table 1). A study of hydrogenation vs. hydrogenolysis of benzyl cinnamate in ILs (**2b**, **3b**, **4b**, **5b**, **6b**, **9b**, **11b** and **15b**; **2f** and **5f**) prepared above has recently been reported by Gathergood *et al.*⁴⁴

Preparation of amide ILs

The method of preparation of the amide ILs is analogous to that for the ester derivatives. The only notable difference was that in the case of **19a** recrystallisation from diethyl ether was used to purify the intermediate bromoacetamide, rather than vacuum distillation. Good yields were obtained for the majority of the bromide and octylsulfate amide derivatives, with elevated melting points again recorded for the bromide salts (Table 2).

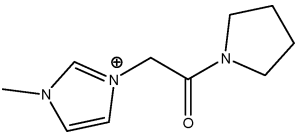
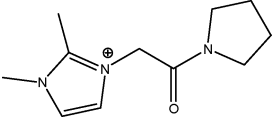
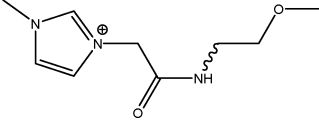
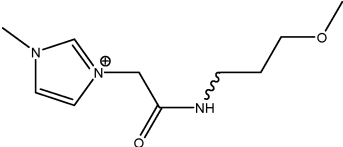
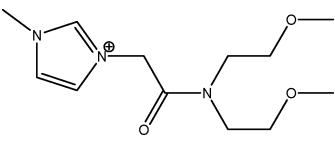
Although the 3-methoxypropylamide and bis(2-methoxyethyl)amide 3-methylimidazolium bromide salts (**19a** and **20a**, respectively) were solids at 20 °C, they both had melting points under 100 °C, technically qualifying them as ionic liquids. However, the pyrrolidine amide 3-methylimidazolium **16a** and 2,3-dimethylimidazolium bromide **17a** salts had melting points above 100 °C and hence were not classified as ionic liquids. In contrast, 2-methoxyethyl 3-methylimidazolium bromide was a liquid at 20 °C, as were octylsulfates **16f** and **20f**, derived from **16a** and **20a** by the previous anion-exchange process.

Toxicity

Seven strains of bacteria were used to assess the antimicrobial activity of the ILs: 4 Gram negative (*Pseudomonas aeruginosa*, *Escherichia coli*, *Klebsiella sp.*, *Salmonella sp.*) and three Gram positive (*Staphylococcus aureus*, *Enterococcus sp.*, *Bacillus subtilis*) organisms.

The minimum inhibitory concentrations were measured for those ILs that showed activity against any of the seven strains. A wide concentration range was tested (0–20 mg/mL). The MIC values for typical cationic antiseptic/antibacterial agents generally lie in the range of 8 µg/mL to 500 µg/mL.⁴⁵ The commercial disinfectants, BAC (benzalkonium chloride, a mixture of quaternary ammonium salts with hydrocarbon chains of 8, 10, 12, 14, 16 and 18 atoms length) and CPC

Table 2 Amide IL data

Amide (cation)	[Amide cat.]-[Br ⁻]	[Amide cat.]-[OctOSO ₃ ⁻]
<i>% yield</i>		
<i>Melting point</i>		
	16a 56 109–111 °C	16f 97 <i>liquid</i>
	17a 82 142–144 °C	17f 98 <i>liquid</i>
	18a 97 <i>liquid</i>	n/a
	19a 91 75–77 °C	n/a
	20a 91 68–70 °C	20f 92 <i>liquid</i>

(cetylpyridinium chloride, a pyridinium salt with a 16-carbon aliphatic chain) both have reported MIC values of 8 µg/mL for *S. aureus* 209, *S. aureus* R209 and *B. subtilis*. In the case of CPC, which is a discrete entity, having a molecular mass of 340 Da, this represents a MIC of 23.5 µM. Ionic liquids with long hydrocarbon chains also exhibit toxic properties, with the C-12-substituted 1-methyl-3-dodecylimidazolium bromide (MIC from 8 µg/mL to 32 µg/mL,⁴⁵ *i.e.* 24.2 to 96.7 µM) and especially C-14/C-16 showing pronounced biocidal properties (1-methyl-3-tetradecylimidazolium chloride/1-methyl-3-hexadecylimidazolium bromide – MICs from 4 µg/mL to 8 µg/mL,⁴⁵ (12.7 to 25.4 µM, C-14/10.3 to 20.7 µM, C-16) over a range of 10 bacteria and 2 fungi). The C-10 chain ionic liquid, 1-methyl-3-decylimidazolium chloride is also a good antiseptic, with MIC values of 8 µg/mL (30.9 µM) for *E. coli*, 16 µg/mL (61.8 µM) for *S. aureus* 209, and 32 µg/mL (123.6 µM) for *S. aureus* R209. Higher MICs were recorded for *S. typhimurium* and *B. subtilis* (both 125 µg/mL, *i.e.* 482.9 µM) and fungal strains *C. albicans* and *C. regularis* (both 250 µg/mL, 965.9 µM).⁴⁵ In fact imidazolium ionic liquids in which an ester linkage is used to attach a hydrocarbon chain (C-1 to 18) to the cationic core have recently been the subject of a patent application for anti-microbial compositions in the preservation of personal care products and cosmetics.⁴² In contrast, a number of our ILs containing ethereal side-chains linked *via* an ester to

the imidazole core exhibited no toxicity even at concentrations above 20 mg/mL, against any of 7 bacterial strains screened. Non-toxicity across a broad range of microorganisms has also been reported by Pernak, who synthesized 1-alkylimidazolium DL-lactates (5 examples, alkyl varying from methyl to pentyl) with MIC values >5.814 mM across a range of 5 Gram-negative rods, 5 Gram-positive cocci and 2 fungal strains.¹⁶ For our non-toxic ILs, MIC values greater than 20 mg/mL correspond to a lack of toxicity at concentrations from >27 mM to >75 mM, depending on the molecular mass of the IL. In most cases, all 7 bacterial strains showed no sensitivity towards each IL (MIC is quoted as > test concentration when no toxicity was shown at the concentration tested). These data are summarised in Table 3.

A toxicity study with the ester, 1-methyl-3-(decyloxy-carbonyl)methylimidazolium bromide (**12a**) which is known to exhibit toxicity due to its long alkyl chain, was completed as a reference. This experiment compares, for the same side chain length, the impact of the presence of the ether oxygens (in **11a**) on toxicity. As expected **12a** was toxic to all the different bacteria screened (Table 4), and in some cases even at low concentrations (Table 4 *E. coli*, *Enterococcus sp.* and *S. aureus*). A comparison of the results in Table 4 with those from Table 3, (**11a**), indicates that the presence of oxygen in the side chain is crucial to suppress the toxicity.

From the data collected it is apparent that all the bromide salts with an oxygenated side chain are non-toxic. At the forefront of

our results is the fact that IL series **1** and **2** (which lack ethereal side-chains) are the most toxic tested in this study (each showing toxicity with 3 different anions). These ILs, which have highly lipophilic cations, are the only ones to display toxicity with three different anions. The lipophilic octylsulfate salts (**1f**, **8f**, **10f**, **13f**, **14f**) together with the NTF₂⁻ (**1b**, **2b**, **3b**, **5b**, **7b**) salts were among the most toxic imidazolium salts studied, showing the highest number of ILs with MIC values in the range 2.5–10 mg/mL.

Results from the BF₄⁻ series provided further evidence for the toxicity of an alkyl chain, with the only toxic examples out of all the BF₄⁻ salts occurring in cases **2c** and **15c** (both containing pentyl ester side-chains without ether linkages). A similar trend was observed for the N(CN)₂⁻ salts in which only butyl (**1e**) and pentyl (**2e**) esters exhibited toxicity. However, a notable exception was observed when incorporation of a methyl group at C-2 of the imidazole ring in pentyl ester **15e** abolished the toxicity previously recorded for C-2 unsubstituted pentyl ester **2e**.

As previously mentioned, toxicity is frequently encountered with ionic liquids containing an extended hydrocarbon chain. Notably, Bodor *et al.*^{46–50} had shown that a long chain ester derivative of methyl imidazole (compound **21** in Fig. 3) shows effective antimicrobial activity at ppm concentrations.

The results in Table 3 show that all the ionic liquids prepared show significantly lower toxicity than derivatives without ester and ether or poly ether functional groups. ILs **17a**, **19a**, **20a** and **20f** demonstrate that the presence of oxygen atoms in the

Table 3 MIC^a values (low toxicities [high MIC] were recorded for all bacterial strains)

Strain	Counter Anion																			
(I–VII)	Bromide																			
	1a	2a	3a	4a	5a	6a	7a	8a	9a	10a	11a	13a	14a	15a	16a	17a	18a	19a	20a	
	>72	>69	>72	>68	>65	>62	>62	>59	>60	>55	>54	>60	>59	>66	>73	>69	>72	>68	>60	
(I–VII)	Trifluoromethanesulfonimide																			
	1b	2b	3b	4b	5b	6b	7b	8b	9b	10b	11b	13b	14b	15b	16b					
	21	20	21	>41	19	>38	19	>37	>36	>35	>35	>37	>37	>40	n/a					
(I–VII)	Tetrafluoroborate																			
	1c	2c	3c	4c	5c	6c	7c	8c	9c	10c	11c	13c	14c	15c	16c					
	>70	34	>70	>67	>64	>61	>61	>58	>56	>54	>53	>27	>27	7.2	n/a					
(I–VII)	Hexafluorophosphate																			
	1d	2d	3d	4d	5d	6d	7d	8d	9d	10d	11d	13d	14d	15d	16d					
	>58	>56	>58	>56	>54	>52	6.4	>50	>48	>47	>46	>50	>50	>54	n/a					
(I–VII)	Dicyanoamide																			
	1e	2e	3e	4e	5e	6e	7e	8e	9e	10e	11e	13e	14e	15e	16e					
	19	36	>75	>72	>68	>65	>65	>62	>59	>57	>57	>28	>28	>30	n/a					
(I–VII)	Octylsulfates																			
	1f	2f	3f	4f	5f	6f	7f	8f	9f	10f	11f	13f	14f	15f	16f	17f	18f	19f	20f	
	12	>48	>49	>47	>46	>44	>44	21	>42	20	>40	22	>21	>46	>50	>48	n/a	n/a	>42	

^a In mM, the number of microorganisms in 1 mL range from 10⁴ to 10⁵ n/a indicates compound was not synthesized.

Table 4 Percentage kill for seven strains of bacteria at various concentrations of **12a**

Strain (I–VII)	12a Concentration (µg/mL)								
	1000	500	250	125	63	31.5	15.75	7.88	3.94
	2.8 mM	1.4 mM	692.6 µM	346.3 µM	173.2 µM	86.6 µM	43.3 µM	21.6 µM	10.8 µM
(I) <i>E. coli</i>	91	82	92	92	37	28	17	9	10
(II) <i>Enterococcus sp.</i>	96	84	83	50	49	19	23	6	7
(III) <i>P. aeruginosa</i>	100	82	82	56	0	6	0	0	0
(IV) <i>Salmonella sp.</i>	86	88	74	58	10	0	0	0	0
(V) <i>Klebsiella sp.</i>	92	68	64	21	7	0	0	0	0
(VI) <i>S. aureus</i>	—	96	94	81	90	86	88	90	66
(VII) <i>B. subtilis</i>	100	83	82	80	0	0	0	0	0

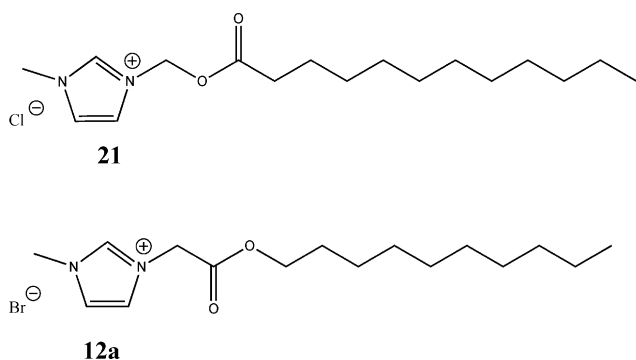


Fig. 3 Comparison of structures of **21** 1-[(*n*-undecylcarbonyloxy)-methyl]-3-methylimidazolium chloride and **12a** 3-methyl-1-(*n*-decylcarbonylmethyl)imidazolium bromide. Both are potent antibacterials.

side chain of amide derivatives also leads to low toxicity ILs, when compared with ILs containing hydrocarbon side-chains of similar length. (e.g. If **20a** is compared with dodecyl substituted imidazolium salts *vide supra*). These results have significant implications for the usefulness of the ILs, as the toxicity is exceptionally low.

Biodegradability

CO₂ Headspace test. To evaluate the biodegradability of the test ionic liquids, the “CO₂ Headspace” test (ISO 14593)⁵¹ was implemented. This method allows the evaluation of the ultimate aerobic biodegradability of an organic compound in an aqueous medium at a given concentration of microorganisms by analysis of inorganic carbon. The test ionic liquid, as the sole source of carbon and energy, was added at a concentration of 40 mg L⁻¹ to a mineral salt medium. These solutions were inoculated with activated sludge collected from an activated sludge treatment plant, washed and aerated prior to use and incubated in sealed vessels with a headspace of air. Biodegradation (mineralization to carbon dioxide) was determined by measuring the net increase in total organic carbon (TOC) levels over time.

Biodegradation data. Results for biodegradation of the octylsulfates at weekly intervals over 28 days are tabulated in the ESI† and represented graphically in Figs. 4–6.

ILs, **2f**, **5f**, **6f**, **9f**, **10f** and **13f** passed the CO₂ Headspace test (at least 60% over 28 days duration) and clearly are “readily biodegradable” according to this test (see Fig. 4 and Fig. 5). ILs **1f**, **3f**, **4f**, **7f**, and **8f** all show significant biodegradation (between 55–59% in CO₂ Headspace test) and represent a marked improvement over the negligible biodegradation result obtained for the imidazolium based ILs, [bmim][BF₄] and [bmim][PF₆].^{31,33,34} A decrease in biodegradation potential can be seen for the amide ILs, with none surpassing a threshold of 40% in the CO₂ Headspace test after 28 days (Fig. 6). This fact emphasises the importance of an ester linkage for successful biodegradation of these imidazolium ILs.

Conclusions

Several factors that are important in the development of green solvents for industry are melting point, toxicity and biodegradation. We have demonstrated that for a series of ionic liquids containing a wide range of ether and poly ether esters

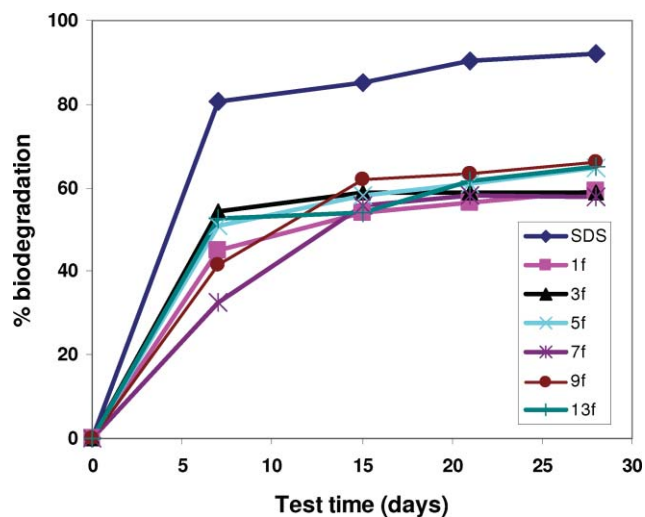


Fig. 4 Biodegradation of selected ILs.

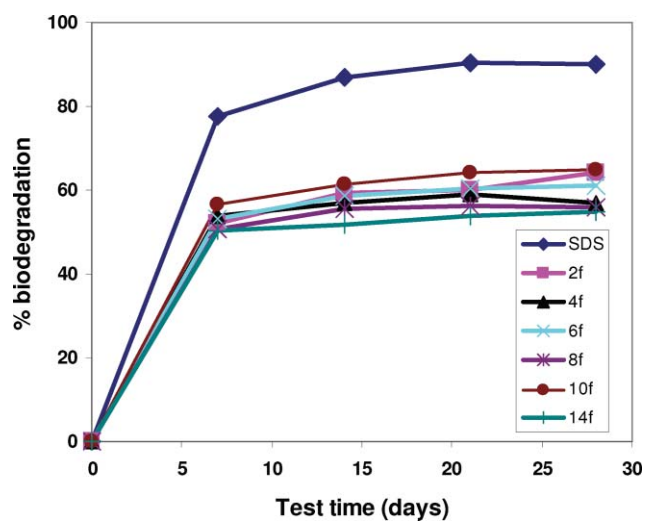


Fig. 5 Biodegradation of selected ILs.

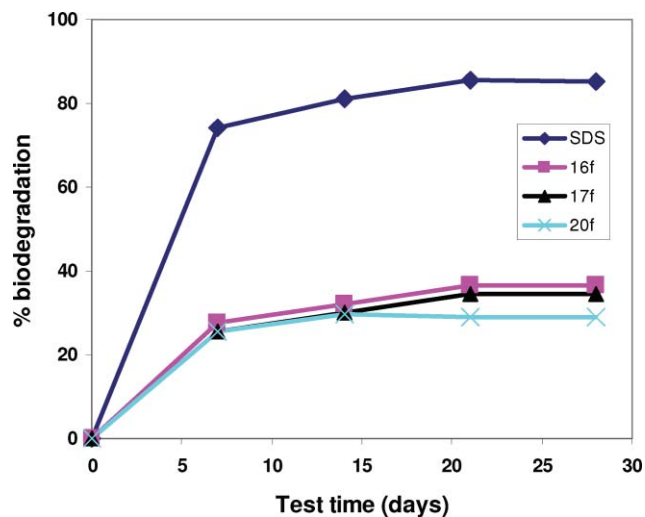


Fig. 6 Biodegradation of selected ILs.

many are liquid at room temperature and all have melting points below 100 °C. Examples containing extended poly ether side chains, *e.g.* **9b-f**, are liquid at room temperature. Toxicity studies show a clear trend that for all the ionic liquids prepared containing ether or poly ether side-chains a significant reduction in toxicity is observed, compared with the long chain alkyl substituted derivatives. **9a-f** and **10a-f** contain extended side-chains but nevertheless show no antimicrobial toxicity even at concentrations above 20 mg/mL (36–59 and 20–57 mM respectively, depending on molecular mass). Biodegradation results support previous studies demonstrating that an ester group is preferred over an amide. Whilst ILs with a butoxy- or propoxy- terminus are readily biodegradable, those with methoxy- or ethoxy- terminal substitution remained slightly below the 60% threshold for biodegradability.

Experimental

All chemicals were purchased from Aldrich, with the exception of lithium trifluoromethanesulfonimide, which was purchased from Solvionic. 1-Methylimidazole and bromoacetyl bromide were used without further purification. 1-Butanol, 1-pentanol, 2-(2-methoxyethoxy) ethanol, 2-(2-ethoxyethoxy) ethanol, 2-(2-propoxyethoxy) ethanol, 2-(2-butoxyethoxy) ethanol, 2-methoxyethanol, 2-ethoxyethanol, 2-propoxyethanol, 2-butoxyethanol, and 1-decanol were dried over 4 Å molecular sieves and used without further purification. 1,2-Dimethylimidazole was distilled before use. All organic solvents were dried and distilled before use. All NMR spectra of ILs were recorded in deuterated chloroform, acetonitrile or acetone on a Bruker 400 MHz spectrometer.

A representative synthetic method is given for each group of compounds prepared. All other information may be found in the ESI.†

CO₂ Headspace test

To evaluate the biodegradability of the test ionic liquids, the “CO₂ Headspace” test (ISO 14593) was also applied.⁵² This method allows the evaluation of the ultimate aerobic biodegradability of an organic compound in aqueous medium at a given concentration of microorganisms by analysis of inorganic carbon. The test ionic liquid, as the sole source of carbon and energy, was added at a concentration of 40 mg L⁻¹ to a mineral salt medium. These solutions were inoculated with activated sludge collected from an activated sludge treatment plant, washed and aerated prior to use and incubated in sealed vessels with a headspace of air. Biodegradation (mineralization to carbon dioxide) was determined by measuring the net increase in total organic carbon (TOC) levels over time compared with blanks. Sodium *n*-dodecyl sulfate (SDS) was used as a reference substance. The tests ran for 28 days and the extent of biodegradation was expressed as a percentage of the theoretical amount of inorganic carbon, based on the amount of test compound added at the start. CO₂ was estimated by GC according to the equation:

$$\% \text{CO}_2 (\text{headspace}) = \frac{(\text{GC peak height}_{\text{sample}} - \text{GC peak height}_{\text{air}})}{\text{GC peak height}_{\text{standard}}} \times \% \text{CO}_2 (\text{standard})$$

Toxicity studies

Minimum inhibitory concentrations (MICs) for the compounds were determined by serial two-fold dilutions in Mueller-Hinton broth using the broth microdilution method described by Amsterdam.⁵²

Strains were grown in Mueller-Hinton broth overnight. The compound solution and 96-well plates were ready before the cultures reached the desired growth phase. The compound to be tested was dissolved in sterile water and diluted in the test medium to twice the maximum concentration desired in the test, *i.e.*, the highest desired concentration was 20 mg/mL, so the ionic liquid was diluted to 40 mg/mL.

μL of Mueller-Hinton broth was dispensed into all wells of a microtitre plate. 100 μL of the 2× compound solution was pipetted into the wells in column 1 (far left of plate). The compound was mixed into the wells in column 1 by pipetting up and down 6–8 times. 100 μL was withdrawn from column 1 and added to column 2. This made column 2 a two-fold dilution of column 1. This was mixed up and down 6–8 times. 100 μL was transferred to column 3. This procedure was repeated down to column 10 only. 100 μL was discarded from column 10 rather than putting it in column 11. 5 μL of (2 × 10⁴ CFU/mL) the strain to be tested was dispensed into wells in the columns 11 to 1 in that order. Column 12 was used as a sterility control. The plates were incubated at 37 °C. Growth on the plates was noted and recorded after 18–36 hours. The MIC was the lowest concentration of the compound that completely inhibited growth of the organism in the microdilution wells as detected by the unaided eye.

Compounds that were water-insoluble were diluted in methanol. The MICs for these compounds were obtained using the same procedure described above. However, instead of diluting the compound directly in Mueller-Hinton broth, 20 μL of the solution (to give a final concentration of 20 mg/mL) was added to the first well in the row. The methanol was allowed to evaporate and then 200 μL of Mueller-Hinton broth was added, mixed and diluted using serial two-fold dilutions as described above.

Preparation of 2-propoxyethyl 2-bromoacetate

To a stirred solution of dichloromethane (350 mL), propoxyethanol (47.84 mL, 460 mmol), and triethylamine (69.3 mL, 500 mmol), under a nitrogen atmosphere at –78 °C was added dropwise bromoacetyl bromide (92.92 g, 460 mmol). After stirring at –78 °C for 3 h, the reaction mixture was allowed to warm up to –20 °C and quenched by addition of water (50 mL). The organic phase was washed with distilled water (3 × 25 mL), saturated ammonium chloride (3 × 25 mL), saturated sodium bicarbonate (3 × 25 mL) and brine (2 × 25 mL). The organic phase was then dried over magnesium sulfate, filtered and solvents removed *via* rotary evaporation. The crude product was distilled (bp 100–102 °C) to give a pale yellow liquid in 83% yield (85.91 g, 382 mmol).

¹H NMR (400 MHz, CDCl₃) δ (ppm) 4.34 (t, *J* = 4.6 Hz, 2H), 3.88 (s, 2H), 3.67 (t, *J* = 4.6 Hz, 2H), 3.47 (t, *J* = 6.9 Hz, 2H), 1.66 (tq, *J* = 6.9, 7.3 Hz, 2H), 0.94 (t, *J* = 7.3 Hz, 3H).

¹³C NMR (100 MHz, CDCl₃) δ (ppm) 167.31, 73.07, 68.10, 65.42, 25.90, 22.81, 10.52.

Preparation of 3-methyl-1-(2-(2-*n*-propoxyethoxy)-ethoxycarbonylmethyl) imidazolium bromide (9a)

To a stirred solution of 1-methylimidazole (50 mmol, 4.10 g) in diethyl ether (100 mL) at $-15\text{ }^{\circ}\text{C}$ under a nitrogen atmosphere was added dropwise 2-(2-propoxyethoxy)ethyl-2-bromoacetate (60 mmol, 16.14 g). The reaction mixture was stirred vigorously at $-15\text{ }^{\circ}\text{C}$ for 3 h, then at $20\text{ }^{\circ}\text{C}$ for 16 h. The diethyl ether phase was decanted and the IL washed with diethyl ether ($2 \times 30\text{ mL}$), then residual solvent removed on the rotary evaporator. The product was dried under high vacuum for 8 h yielding a white solid in 98% yield (17.16 g, 48.89 mmol).

$^1\text{H NMR}$ (400 MHz, CDCl_3) δ (ppm) 10.13 (s, 1H), 7.54 (t, $J = 1.8\text{ Hz}$, 1H), 7.34 (t, $J = 1.8\text{ Hz}$, 1H), 5.45 (s, 2H), 4.31 (t, $J = 4.6\text{ Hz}$, 2H), 4.02 (s, 3H), 3.68 (t, $J = 4.6\text{ Hz}$, 2H), 3.59–3.57 (m, 2H), 3.53–3.50 (m, 2H), 3.35 (t, $J = 6.9\text{ Hz}$, 2H), 1.53 (tq, $J = 6.9, 7.3\text{ Hz}$, 2H), 0.84 (t, $J = 7.3\text{ Hz}$, 3H).

$^{13}\text{C NMR}$ (100 MHz, CDCl_3) δ (ppm) 166.21, 138.54, 123.85, 122.84, 73.10, 70.62, 69.92, 68.55, 65.69, 50.29, 36.93, 22.76, 10.52.

MP ($^{\circ}\text{C}$) 32–34 $^{\circ}\text{C}$.

IR (KBr disc) (cm^{-1}) 2959, 2926, 2859, 1751, 1558, 1639, 1495, 1452.

MS m/z , Found 271.1648 $[\text{M}-\text{Br}]^+$, Calcd. $\text{C}_{13}\text{H}_{23}\text{N}_2\text{O}_4$ 271.1658.

MS m/z , 271.2 $[\text{M}-\text{Br}]^+$; MS: m/z , 79 and 81 $[\text{Br}^-]$.

Preparation of 3-methyl-1-(2-(ethoxy)ethoxycarbonylmethyl) imidazolium NTf_2^- (4b)

A flask was charged with 3-methyl-1-(2-(ethoxy)ethoxycarbonylmethyl) imidazolium bromide (2.93 g, 10.0 mmol) and distilled water (10 mL). LiNTf_2 (4.59 g, 16.0 mmol) in distilled water (3 mL) was added in one portion and the suspension was stirred vigorously for 4 h at $20\text{ }^{\circ}\text{C}$. The top aqueous layer was removed and the IL was washed with distilled water ($3 \times 10\text{ mL}$). The solvent was then removed on the rotary evaporator and under high vacuum for 8 h to give a liquid at $20\text{ }^{\circ}\text{C}$ in 90% yield (4.42 g, 8.97 mmol).

$^1\text{H NMR}$ (400 MHz, CDCl_3) δ (ppm) 8.82 (s, 1H), 7.39 (t, $J = 1.8\text{ Hz}$, 1H), 7.34 (t, $J = 1.8\text{ Hz}$, 1H), 5.06 (s, 2H), 4.38 (t, $J = 4.6\text{ Hz}$, 2H), 3.97 (s, 3H), 3.68 (t, $J = 4.6\text{ Hz}$, 2H), 3.56 (q, $J = 7.1\text{ Hz}$, 2H), 1.22 (t, $J = 7.1\text{ Hz}$, 3H).

$^{13}\text{C NMR}$ (100 MHz, CDCl_3) δ (ppm) 165.76, 137.63, 123.80, 123.25, 119.70 (q, $J = 319\text{ Hz}$, 2CF_3 's), 67.62, 66.67, 65.97, 49.92, 36.56, 15.01.

IR (thin film on salt plate) (cm^{-1}) 3169, 3116, 2967, 2927, 2859, 1751, 1581, 1569, 1558, 1495, 1452, 1352, 1196, 1135.

MS m/z , 213.1 $[\text{M}-\text{NTf}_2^-]^+$; MS: m/z , 280.0 $[\text{NTf}_2^-]$.

Preparation of 3-methyl-1-(2-(2-methoxyethoxy)-ethoxycarbonylmethyl) imidazolium PF_6^- (7d)

A flask was charged with 3-methyl-1-(2-(2-methoxyethoxy)-ethoxycarbonylmethyl) imidazolium bromide (3.55 g, 11.0 mmol) and acetone (10 mL). KPF_6 (3.31 g, 18.0 mmol) in acetone (5 mL) was added in one portion and the suspension was stirred vigorously for 4 days under reflux. The fine white precipitate was then filtered and washed with acetone ($2 \times 5\text{ mL}$). The solvent was removed from the product on the rotary evaporator. The product was then dried under high vacuum

for 4 h to give viscous liquid at $20\text{ }^{\circ}\text{C}$ in 91% yield (3.87 g, 9.97 mmol).

$^1\text{H NMR}$ (400 MHz, CDCl_3) δ (ppm) 8.60 (s, 1H), 7.53 (tt, $J = 1.8, 1.8\text{ Hz}$, 2H), 5.59 (s, 2H), 4.45 (t, $J = 4.6\text{ Hz}$, 2H), 4.00 (s, 3H), 3.82 (t, $J = 4.6\text{ Hz}$, 2H), 3.72 (t, $J = 4.6\text{ Hz}$, 2H), 3.62 (t, $J = 4.6\text{ Hz}$, 2H), 3.44 (s, 3H).

$^{13}\text{C NMR}$ (100 MHz, CDCl_3) δ (ppm) 165.98, 136.76, 123.33, 123.17, 71.16, 69.69, 67.85, 65.23, 57.54, 49.44, 35.84.

IR (thin film on salt plate) (cm^{-1}) 3172, 3124, 2926, 1751, 1580, 1569, 1559, 1495, 1457, 1218, 1181, 1106.

MS m/z , 243.2 $[\text{M}-\text{PF}_6^-]^+$; MS: m/z , 145.0 $[\text{PF}_6^-]$.

Preparation of 3-methyl-1-(2-(2-*n*-propoxyethoxy)-ethoxycarbonylmethyl) imidazolium BF_4^- (9c)

A dry flask was charged with 3-methyl-1-(2-(2-*n*-propoxyethoxy)ethoxycarbonylmethyl) imidazolium bromide (2.94 g, 8.38 mmol) and acetone (10 mL) under a nitrogen atmosphere. NaBF_4 (1.11 g, 10.1 mmol) was added in one portion and the suspension was stirred vigorously for 4 days under reflux. The fine white precipitate was filtered quickly in air and washed with dry acetone ($2 \times 3\text{ mL}$). The filtrate and washings were combined, solvent removed by rotary evaporation and then under high vacuum to give a slight viscous oil at $20\text{ }^{\circ}\text{C}$ in 93% yield (2.79 g, 7.79 mmol).

$^1\text{H NMR}$ (400 MHz, CDCl_3) δ (ppm) 8.95 (s, 1H), 7.45 (t, $J = 1.8\text{ Hz}$, 1H), 7.37 (t, $J = 1.8\text{ Hz}$, 1H), 5.12 (s, 2H), 4.38 (t, $J = 4.7\text{ Hz}$, 2H), 3.97 (s, 3H), 3.75 (t, $J = 4.7\text{ Hz}$, 2H), 3.67 (t, $J = 3.2\text{ Hz}$, 2H), 3.60 (t, $J = 3.2\text{ Hz}$, 2H), 3.44 (t, $J = 6.8\text{ Hz}$, 2H), 1.64 (tq, $J = 6.8, 7.6\text{ Hz}$, 2H), 0.94 (t, $J = 7.6\text{ Hz}$, 3H).

$^{13}\text{C NMR}$ (100 MHz, CDCl_3) δ (ppm) 166.23, 137.96, 123.79, 123.13, 73.06, 70.54, 69.89, 68.54, 65.66, 49.85, 36.52, 22.75, 10.49.

IR (thin film on salt plate) (cm^{-1}) 3166, 3121, 2964, 2927, 2866, 1750, 1581, 1574, 1569, 1558, 1495, 1452, 1220, 1181.

MS m/z , 271.3 $[\text{M}-\text{BF}_4^-]^+$; MS: m/z , 87.0 $[\text{BF}_4^-]$.

Preparation of 3-methyl-1-(*n*-butoxycarbonylmethyl) imidazolium $\text{N}(\text{CN})_2^-$ (1e)

A dry flask was charged with 3-methyl-1-(*n*-butoxycarbonylmethyl) imidazolium bromide (3.05 g, 11.0 mmol) and acetonitrile (10 mL) under a nitrogen atmosphere. $\text{NaN}(\text{CN})_2$ (1.42 g, 16.0 mmol) was added in one portion and the suspension was stirred vigorously for 4 days at $20\text{ }^{\circ}\text{C}$. The fine white precipitate was filtered quickly in air and washed with dry acetonitrile ($2 \times 1\text{ mL}$). The filtrate and washings were combined, solvent removed by rotary evaporation and then under high vacuum to give a light yellow oil at $20\text{ }^{\circ}\text{C}$ in 87% yield (2.51 g, 9.54 mmol).

$^1\text{H NMR}$ (400 MHz, CDCl_3) δ (ppm) 9.82 (s, 1H), 7.56 (t, $J = 1.8\text{ Hz}$, 1H), 7.46 (t, $J = 1.8\text{ Hz}$, 1H), 5.32 (s, 2H), 4.15 (t, $J = 6.8\text{ Hz}$, 2H), 4.02 (s, 3H), 1.61 (tt, $J = 6.8, 7.2\text{ Hz}$, 2H), 1.33 (tq, $J = 7.2, 7.5\text{ Hz}$, 2H), 0.87 (t, $J = 7.5\text{ Hz}$, 3H).

$^{13}\text{C NMR}$ (100 MHz, CDCl_3) δ (ppm) 164.10, 136.12, 121.89, 121.18, 64.85, 48.22, 34.87, 28.31, 16.96, 11.67 Note: C's from anion are not visible in $^{13}\text{C NMR}$.

IR (thin film on salt plate) (cm^{-1}) 2962, 2931, 2861, 2241, 2139, 1750, 1569, 1558, 1539, 1495, 1452, 1217, 1177.

MS m/z , 197.1 $[\text{M}-\text{N}(\text{CN})_2^-]^+$; MS: m/z , 66.0 $[\text{N}(\text{CN})_2^-]$.

Preparation of 3-methyl-1-(2-(*n*-propoxy)ethoxycarbonylmethyl)imidazolium octylsulfate (5f)

To a solution of 3-methyl-1-(2-(*n*-propoxy)ethoxycarbonylmethyl)imidazolium bromide (3.68 g, 12.0 mmol) in distilled water (20 mL) was added in one portion sodium octylsulfate (2.09 g, 9.00 mmol). The reaction was stirred at 60 °C for 2 h and then water was slowly removed under vacuum. The precipitate was dissolved in DCM (10 mL) and washed with distilled water (2 × 5 mL). The product remaining was dried on the rotary evaporator and then under high vacuum for 8 h to yield a yellow grease in 85% yield (3.33 g, 7.62 mmol).

¹H NMR (400 MHz, CDCl₃) δ (ppm) 9.45 (s, 1H), 7.48 (t, *J* = 1.6 Hz, 1H), 7.41 (t, *J* = 1.6 Hz, 1H), 5.25 (s, 2H), 4.36 (t, *J* = 4.7 Hz, 2H), 4.01 (m, 5H), 3.67 (t, *J* = 4.7 Hz, 2H), 3.43 (t, *J* = 6.8 Hz, 2H), 1.63–1.58 (m, 4H), 1.56–1.29 (m, 10H), 0.92–0.86 (m, 6H).

¹³C NMR (100 MHz, CDCl₃) δ (ppm) 166.45, 138.89, 123.71, 123.06, 73.04, 67.92, 67.89, 65.67, 49.91, 36.58, 31.83, 29.50, 29.36, 29.26, 25.87, 22.73, 22.66, 14.13, 10.47.

IR (thin film on salt plate) (cm⁻¹) 3118, 2958, 2927, 2855, 1750, 1569, 1558, 1539, 1495, 1455, 1217, 1178, 1108.

MS *m/z*, 227.1 [M-OctOSO₃⁻]⁺; MS: *m/z*, 209.0 [OctOSO₃⁻].

Acknowledgements

Enterprise Ireland (NG, SM, BP) and the EPA 2006-PHD-ET-7 studentship (NG, DC) are gratefully acknowledged for their financial support. We also thank Dr Orla Cahill for her assistance of DF.

References

- Anderson, P. Goodrich, C. Hardacre and D. Rooney, *Green Chem.*, 2003, **5**, 448–453.
- Steffan, M. Lucas, A. Brandner, M. Wollny, N. Oldenburg and P. Claus, *Chem. Eng. Technol.*, 2007, **30**, 481–486.
- Wasserscheid and H. Waffenschmidt, *J. Mol. Catal. A: Chem.*, 2000, **164**, 61–67.
- Wang and L. Wang, *Appl. Catal. A: Gen.*, 2004, **262**, 101–104.
- Meracz and T. Oh, *Tetrahedron Lett.*, 2003, **44**, 6465–6468.
- Liu, G. J. Liu and J. A. Jonsson, *Trends Anal. Chem.*, 2005, **24**, 20–27.
- Arenz, A. Babai, K. Binnemans, K. Driesen, R. Giernoth, A. Mudring and P. Nockemann, *Chem. Phys. Lett.*, 2005, **402**, 75–79.
- Heredia-Moya and K. Kirk, *J. Fluorine Chem.*, 2007, **128**, 674–678.
- M. J. Earle and K. R. Seddon, *Pure Appl. Chem.*, 2000, **72**, 1391–1398.
- M. J. Earle, J. Esperanca, M. A. Gilea, J. N. C. Lopes, L. P. N. Rebelo, J. W. Magee, K. R. Seddon and J. A. Widergren, *Nature*, 2006, **439**, 831–834.
- M. Volland, V. Seitz, Maase, M. Flores, M., R. Papp, K. Massonne, V. Stegmann, K. Halbritter, R. Noe, M. Bartsch, W. Siegel, and Becker, M. Huttenlock, O., *PCT Int. Appl. WO03/06225*, 2003.
- Weyershausen, K. Hell and U. Hesse, *Green Chem.*, 2005, **7**, 283–287.
- Weyershausen and K. Lehmann, *Green Chem.*, 2005, **7**, 15–19.
- K. M. Docherty and C. F. Kulpa Jr, *Green Chem.*, 2005, **7**, 185–189.
- M. Matsumoto, K. Mochiduki and K. Kondo, *J. Biosci. Bioeng.*, 2004, **98**, 344–347.
- J. Pernak, I. Goc and I. Mirska, *Green Chem.*, 2004, **6**, 323–329.
- J. Pernak, K. Sobaszkiwicz and I. Mirska, *Green Chem.*, 2002, **5**, 52–56.
- C. Pretti, C. Chiappe, D. Pieraccini, M. Gregori, F. Abramo, G. Monni and L. Intorre, *Green Chem.*, 2005, **8**, 238–240.
- A. Latala, P. Stepnowski, M. Nedzi and W. Mrozik, *Aquat. Tox.*, 2005, **73**, 91–98.
- C. Cho, T. P. Pham, Y. Jeon and Y. Yun, *Green Chem.*, 2008, **10**, 67–72.
- G. Lamberti and K. Kulacki, *Green Chem.*, 2008, **10**, 104–110.
- B. Jastorff, K. Molter, P. Behrend, U. Bottin-Weber, J. Filser, A. Heimers, B. Ondruschka, J. Ranke, M. Schaefer, H. Schroder, A. Stark, P. Stepnowski, F. Stock, R. Stormann, S. Stolte, U. Welz-Biermann, S. Ziegert and J. Thoming, *Green Chem.*, 2005, **7**, 362–372.
- P. Balczewski, B. Bachowska, T. Bialas, R. Biczak, W. Wieczorek and A. Balinska, *J. Agric. Food Chem.*, 2007, **55**, 1881–1892.
- R. P. Swatloski, J. D. Holbrey, S. B. Memon, G. A. Caldwell, K. A. Caldwell and R. D. Rogers, *Chem. Commun.*, 2004, 668–669.
- R. J. Bernot, E. E. Kennedy and G. A. Lamberti, *Environ. Toxicol. Chem.*, 2005, **24**, 1759–1765.
- J. Ranke, A. Muller, U. Bottin-Weber, F. Stock, S. Stolte, J. Arning, R. Stormann and B. Jastorff, *Ecotoxicol. Environ. Safety*, 2007, **67**, 430–438.
- S. Stolte, J. Arning, U. Bottin-Weber, A. Muller, W. Pitner, U. Welz-Biermann, B. Jastorff and J. Ranke, *Green Chem.*, 2007, **9**, 760–767.
- A. Garcia-Lorenzo, E. Tozo, J. Tojo, M. Teijera, F. J. Rodriguez-Berrolcal, M. P. González and V. S. Martinez-Zorzano, *Green Chem.*, 2008, **10**, 508–516.
- F. Stock, J. Hoffmann, J. Ranke, R. Stormann, B. Ondruschka and B. Jastorff, *Green Chem.*, 2004, **6**, 286–290.
- D. J. Couling, R. J. Bernot, K. M. Docherty, J. K. Dixon and E. J. Maginn, *Green Chem.*, 2006, **8**, 82–90.
- N. Gathergood and P. J. Scammells, *Aust. J. Chem.*, 2002, **55**, 557–560.
- N. Gathergood, M. T. Garcia and P. J. Scammells, *Green Chem.*, 2004, **6**, 166–175.
- M. T. Garcia, N. Gathergood and P. J. Scammells, *Green Chem.*, 2004, **7**, 9–14.
- N. Gathergood, P. J. Scammells and M. T. Garcia, *Green Chem.*, 2006, **8**, 156–160.
- K. Docherty, J. Dixon and C. Kulpa, *Biodegradation*, 2007, **18**, 481–493.
- A. Romero, A. Santos, J. Tojo and A. Rodriguez, *J. Hazard. Mater.*, 2008, **151**, 268–273.
- S. Stolte, S. Abdulkarim, J. Arning, A. K. Blomeyer-Nienstedt, U. Bottin-Weber, M. Matzke, J. Ranke, B. Jastorff and J. Thoming, *Green Chem.*, 2007, **10**, 214–224.
- A. Wells and V. Coombe, *Org. Process Res. Dev.*, 2006, **10**, 794–798.
- J. R. Harjani, R. D. Singer, M. T. Garcia and P. J. Scammells, *Green Chem.*, 2008, **10**, 436–438.
- P. Nockemann, B. Thijs, K. Driesen, C. Janssen, K. Van Hecke, L. Van Meervelt, S. Kossmann, B. Kirchener and K. Binnemans, *J. Phys. Chem. B*, 2007, **111**, 5254–5263.
- J. R. Harjani, R. Singer, M. T. Garcia and P. J. Scammells, *Green Chem.*, 2009, **11**, 83–90.
- S. T. Elder, A. Preuss, K.-U. Schoning and K. Muhlauer, Pub. No.: US 2008/0070966 A1.
- P. Wasserscheid, R. van Hal and A. Bosmann, *Green Chem.*, 2002, **4**, 400–404.
- S. Morrissey, I. Beadham and N. Gathergood, *Green Chem.*, 2009, **11**, DOI: 10.1039/b815566f.
- D. Demberelynamba, K.-S. Kim, S. Choi, S.-Y. Park, H. Lee, C.-J. Kim and I.-D. Yoo, *Bioorg. Med. Chem.*, 2004, **12**, 853–857.
- N. Bodor, R. Woods, C. Raper, P. Kearney and J. J. Kaminski, *J. Med. Chem.*, 1980, **23**, 474–480.
- N. Bodor, J. J. Kaminski and S. Selk, *J. Med. Chem.*, 1980, **23**, 469–474.
- N. Bodor and J. J. Kaminski, *J. Med. Chem.*, 1980, **23**, 566–569.
- N. Bodor, *Pat.*, US 39897111, 1976.
- N. Bodor, *Pat.*, US 4160099, 1979.
- ISO 14593: Water quality, *Evaluation of ultimate aerobic biodegradability of organic compounds in aqueous medium. Method by analysis of inorganic carbon in sealed vessels CO₂, headspace test*, 1999.
- D. Amsterdam, 1991. Susceptibility testing of antimicrobials in liquid media, 72–78. In *Antibiotics in Laboratory Medicine*, 3rd edition. Ed. V. Lorian, Williams and Wilkins, Baltimore.

The synthesis and fluorescent properties of nanoparticulate ZrO₂ doped with Eu using continuous hydrothermal synthesis

Helen Hobbs,^{a,b} Stephen Briddon^b and Ed Lester^a

Received 16th July 2008, Accepted 16th January 2009

First published as an Advance Article on the web 16th February 2009

DOI: 10.1039/b812149d

Fluorescent nanoparticles of zirconia doped with europium (ZrO₂:Eu³⁺) have been produced *via* the co-precipitation of simple metal salt precursors using continuous supercritical water hydrothermal synthesis. The effect of reaction temperature and residence time on both particle size and conversion were investigated. Increasing the reaction temperature from 200 to 400 °C increases the size of the particles: smaller diameters (<5 nm) were produced at lower temperatures and larger diameters (>20 nm) at higher temperatures. Varying residence time at constant temperatures (between 3.7 and 7 seconds) did not significantly affect the particle size. The structure of the nanoparticles synthesised at 400 °C was revealed to be cubic by X-ray diffraction. Conversion of the metal precursors to ZrO₂:Eu³⁺ was improved from 4 to 99% on increasing the temperature between 250 and 350 °C. The photoluminescent properties of the nanoparticles were also explored with respect to synthesis temperature. Fluorescence upon UV excitation at 255 nm, originating from Eu³⁺ doped in ZrO₂, was not significantly affected by the synthesis temperature. The emission spectra demonstrated characteristic f → f transitions of Eu³⁺ ions and can be explained through an effective dispersion of these ions within the ZrO₂ nanoparticles. Initial cell toxicity studies suggest that ZrO₂:Eu³⁺ nanoparticles do not cause any significant increase in cell death in Chinese hamster ovary cells following an 18 hour incubation at 37 °C. This paper describes a 'green' and controlled method for the continuous production of research scale quantities of nanomaterials.

Introduction

Zirconia-based materials are some of the most widely studied phosphors due to their many desirable properties and applications. For example, the corrosion resistance of zirconia is utilised in pumping components; strength, hardness, toughness and small grain size in blade edges; excellent surface finishes in optical fibre technologies; bio-inert properties and low wear rates in bioceramics and implant devices; high thermal stabilities and insulating properties in thermal barrier coatings; electrical properties in electrolytes; ability to resist oxidation in furnace elements *etc.*¹ The attainment of these specific properties is largely dependent on both the starting materials and the technique used to manufacture them. In particular, these nanoparticulate materials are of interest as they offer the potential for significant improvements in physical and mechanical properties resulting from reduced grain sizes.² Further to this, combining mechanically useful nanoparticles with the optical properties of rare earth ions offers enormous potential in the area of photonic applications such as solid state lasers, sensors, optical amplifiers, scintillators, phosphors and lamps.^{3–6}

It is important to note that the most established methods for producing nanoparticles involve the use of noxious chemicals,

have a complex and time-consuming sequence of stages, or may require expensive precursors. Such methods include the use of sol-gels (aerogels and xerogels),^{7–9} reduction of metal ions,¹⁰ zeolites,¹¹ reverse micelles,¹² hydrolytic processes,¹³ microwave irradiation,¹⁴ coprecipitation,¹⁵ and ageing of solutions.^{9,16} However, hydrothermal synthesis can use the tuneable properties of supercritical water (scW) in order to produce nanoparticles¹⁷ and provides a much more environmentally benign synthesis method. A supercritical fluid (SCF) is a substance heated above its critical temperature, T_c , and pressure, p_c .¹⁸ When water is heated towards its critical point (374 °C, 22 MPa), it exhibits excellent "tunability" in its chemical properties,¹⁹ changing from a polar liquid to a fluid with a low dielectric constant and low pH. The enhanced levels of OH⁻ ions have been shown to readily hydrolyse metal salts followed immediately by a dehydration step.^{17,20} The resultant nanoparticles produced after these two reactions can therefore exist as metal oxides or metals. The chemistry is relatively simple and thus hydrothermal synthesis has already been exploited by researchers for the batch production of ZrO₂ nanoparticles doped with Eu³⁺.²¹ However, the 'engineering' of these reactions for continuous operation is much more difficult. One of the key elements in the success of the flow reactor is how the scW mixes with the metal-salt solution. The control of the mixing zone where the particles form is particularly important, since poor mixing inevitably leads to reactor blockage.²² A continuous supercritical process has been designed²³ which does not block and exhibits several other advantages such as the continuous production of

^aSchool of Chemical, Environmental and Mining Engineering, University of Nottingham, University Park, Nottingham, NG7 2RD, UK

^bInstitute of Cell Signalling, School of Biomedical Sciences, Medical School, Queen's Medical Centre, Nottingham, NG7 2UH, UK

nanoparticles, the use of simple, biologically benign organic salts, such as acetates and formates, the ability to alter particle size and morphology by altering the operating parameters of temperature, residence time and metal salt concentration, and the ability to produce stable suspensions of nanoparticles in water or water-solvent mixtures.²⁴ Here, we report how continuous hydrothermal synthesis can be used to produce ZrO_2 nanoparticles doped with Eu^{3+} ions. Nanoparticle size can be controlled with correspondingly narrow polydispersities. The optical properties of these materials and their low toxicity to Chinese hamster ovary cells are also demonstrated.

Materials and methods

Hydrothermal synthesis of ZrO_2 nanoparticles doped with europium was conducted using the rig shown in Fig. 1, as previously described.²³ Briefly, a pipe-in-pipe concentric configuration was constructed using Swagelok® high pressure fittings; the outer tube consisted of a 3/8" tube (316 Stainless Steel, 0.065" wall thickness) and the inner tube was constructed from a 1/8" tube (316 Stainless Steel, 0.035" wall thickness). The supercritical water is fed downwards through the internal pipe; the aqueous metal salt stream is fed counter-currently upwards through the outer pipe. The reactor outlet is situated upwards through the outer pipe. De-ionised water (0.4 $\mu\Omega$ cm) with 0.25% v/v H_2O_2 (Fisher Scientific) was pumped through a pre-heating coil and heated to the desired temperature. It was brought into contact with a concurrently flowing solution of 0.02 M $\text{Zr}(\text{ac})_x(\text{OH})_y$ ($x + y \sim 4$) (Aldrich) with 5 mol% $\text{Eu}(\text{ac})_3 \cdot x\text{H}_2\text{O}$ (Aldrich). Control experiments were also performed with 0.02 M $\text{Zr}(\text{ac})_x(\text{OH})_y$ only and 0.001 M $\text{Eu}(\text{ac})_3 \cdot x\text{H}_2\text{O}$ only. The pressure was maintained at ca. 24 MPa by a Tescom back pressure regulator (Model 26-1762-24-043). The mixture was cooled immediately after the mixing point by a 14" counter current shell and tube water cooler and the products collected as aqueous suspensions. All collected samples were used as collected without further treatments.

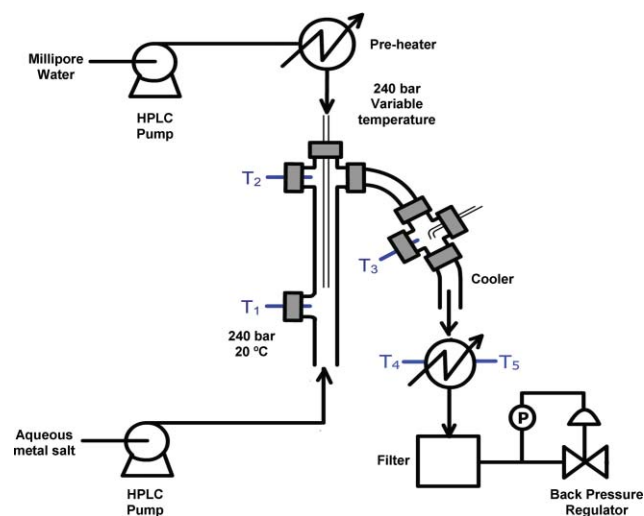


Fig. 1 A schematic of the supercritical water rig used for the hydrothermal synthesis of $\text{ZrO}_2:\text{Eu}^{3+}$.

Increasing temperature with a constant flow rate results in a decrease in residence time of the reaction mixture in the

reactor due to changes in density of the sub- or super-critical water. Therefore, for accurate comparisons between various temperatures (200–400 °C) a constant residence time was set (4 seconds) and flow rates calculated accordingly. The water stream was pumped at twice the speed of the metal salt stream.

Similarly, for accurate comparison of different residence times, the temperature of the system was set at a constant temperature (200, 250, 300, 350 or 400 °C) and flow rates adjusted accordingly to give residence times between 3.7 and 7 seconds.

Particle characterisation

Dry powders of $\text{ZrO}_2:\text{Eu}^{3+}$ nanoparticles, were obtained by freeze drying with liquid nitrogen and under low temperature vacuum (−80 °C) for more than 24 hours. Powder X-ray diffraction (XRD) data were collected using a Phillips XPERT θ -2 θ diffractometer with Cu-K α radiation (40 kV, 40 mA, 1.54056 Å). The sample was loaded onto an indented glass plate and scans were typically taken over a 2θ range of $20 \pm 80^\circ$ using a 0.02° step and 0.25 s per step. The PC IDENTIFY program was used to assess the purity of the $\text{ZrO}_2:\text{Eu}^{3+}$ powders by comparison to the JCPDS database. The APD program was used to estimate the size of the smallest particles in the sample by application of the Scherrer equation to the PXD line-widths (PC IDENTIFY and APD are part of the Phillips diffraction software package).

Sizing of the nanoparticles was carried out on a Zetasizer Nano S Dynamic Light Scattering (DLS) system using the aqueous solutions from the reactor. The instrument contains a 4 mW He–Ne laser operating at a wavelength of 633 nm. Measurements were made at a detection angle of 173° (*i.e.* backscatter) and 25 °C. Size data was obtained using three measurements and Auto:CONTIN²⁵ software using the following fixed parameters: refractive indices 1.33 (water) and 2.19 (ZrO_2) and viscosity of water 0.8872 cP.^{26,27}

TEM images were collected using a JEOL JEM-2000 FXII electron microscope operating at 200 keV. TEM samples were prepared by suspending in methanol, 4 drops were placed on a copper mesh (300 lines per inch mesh) and dried in air.

Nitrogen sorption isotherms and textural properties of the materials were determined in a conventional volumetric technique at 77K using nitrogen by a Micrometrics ASAP 2010 sorptometer. Before analysis, the samples were oven-dried at 60 °C and evacuated overnight under vacuum. The surface area was calculated using the Brunauer–Emmett–Teller (BET) method based on adsorption data in the partial pressure (P/P_0) range 0.05–0.35.

Conversion of the precursors to $\text{ZrO}_2:\text{Eu}^{3+}$ nanoparticles was calculated from Inductively Coupled Plasma Optical Emission Spectrometry (ICP-OES) measurements. Nitric acid (70%, Sigma–Aldrich, 2 mL) was added to solutions of the nanoparticles (18 mL) synthesised at 200, 250, 300, 350 and 400 °C. The resulting solutions were centrifuged at 4000 rpm for 30 min and the supernatants removed and analysed by ICP-OES (Perkin Elmer 3300 DV) for the presence of Zr^{4+} and Eu^{3+} ions. Since the starting concentrations were already known, the difference in values allows the concentration of Zr^{4+} and Eu^{3+} ions in the nanoparticle samples to be calculated and percentage conversion (during initial synthesis) to be deduced.

Excitation and emission spectra and emission lifetime data were obtained for each aqueous $\text{ZrO}_2:\text{Eu}^{3+}$ sample (200 μL) in a UV-transparent 96-well plate using a fluorimeter (Flexstation II) from Molecular Devices.

For cytotoxicity studies, Chinese hamster ovary (CHO) cells were grown to 70% confluency in 8-well glass bottomed plates (Nunc Labtek™) in Dulbecco's Modification of Eagle's Medium/Ham's F-12 (DMEM-F12) supplemented with 10% foetal calf serum and 2 mM glutamine in a humidified atmosphere of 5% CO_2 at 37 °C. On the day of assay, the medium was removed and replaced with 360 μL of serum free DMEM-F12, to which 40 μL of vehicle/particles at 10 \times final concentration were added. For the particles, final concentrations of either 20 or 80 $\mu\text{g mL}^{-1}$ of either $\text{ZrO}_2:\text{Eu}^{3+}$ and CdSe 520 quantum dots (Lumidots®, Sigma) were added. Parallel additions of the equivalent concentrations of toluene or water were also added as controls (2.5 and 10% v/v of each). Cells were then incubated for 2 or 18 h at 37 °C in a humidified atmosphere of 5% CO_2 . To assess cell death, trypan blue solution (0.002% w/v final concentration) was added to each cell sample. Images were recorded (3 per well) using a Zeiss Achroplan 20 \times NA0.6 LD objective lens and captured with a Zeiss AxioCam and Axiovision software.

Results and discussion

Continuous supercritical water hydrothermal synthesis was carried out using an aqueous solution of 0.02 M $\text{Zr}(\text{ac})_x(\text{OH})_y$ ($x + y \sim 4$) and 5 mol% $\text{Eu}(\text{ac})_3 \cdot x\text{H}_2\text{O}$ at various temperatures and flow rates. All solutions produced were colourless.

Fig. 2 shows the XRD trace for $\text{ZrO}_2:\text{Eu}^{3+}$ synthesized at 400 °C. The peaks best fit with pure phase, cubic ZrO_2 , (ICDD-PDF reference number 27-0997) with main peaks (in degrees 2 theta) at 30.5 (100%), 35.2 (30%), 50.7 (50%), 60.5 (20%), 63.3 (10%) and 74.8 (10%). Based on the Scherrer equation, this profile originates from particulates with a diameter of approximately 7 nm. The concentration of Eu^{3+} ions within the nanoparticles was too low to be detected by this method. BET measurements of $\text{ZrO}_2:\text{Eu}^{3+}$ nanoparticles synthesised at 400 °C revealed the surface area to be $180.1 \pm 1.3 \text{ m}^2 \text{ g}^{-1}$ and particle size was determined at 5.7 nm. (The equation: $d_{\text{BET}} = \frac{6}{\text{SSA} \times \rho}$

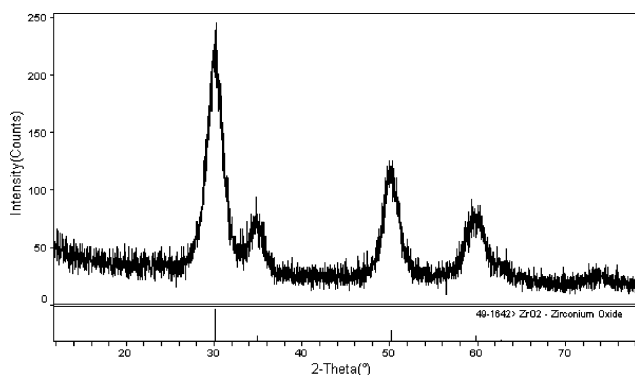


Fig. 2 XRD trace for $\text{ZrO}_2:\text{Eu}^{3+}$, the reference data for cubic ZrO_2 is also shown for comparison.

was used,²⁸ where SSA is specific surface area and ρ is density of $\text{ZrO}_2:\text{Eu}^{3+}$ —assumed to be the density of ZrO_2 5.89 g mL^{-1} .

The impact of increasing reaction temperature on particle size and morphology

To assess the effect of temperature on $\text{ZrO}_2:\text{Eu}^{3+}$ particle size, synthesis was performed between 200 and 400 °C and flow rates were adjusted accordingly to maintain a fixed residence time of 4 seconds at all temperatures investigated. Fig. 3 shows the change in particle size as analysed by DLS. The volume diameter (d_v) is used and is equivalent to the diameter of a regular, homogeneous sphere that has the same volume as the particle being measured.²⁹

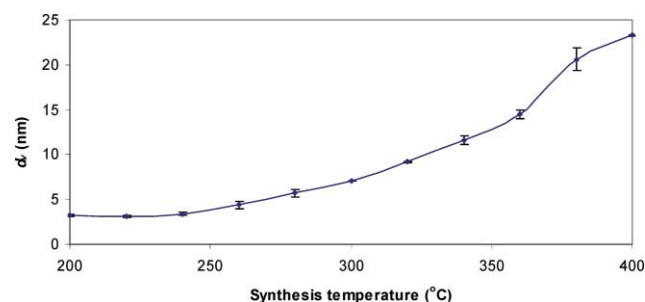


Fig. 3 Volume diameter (d_v) of $\text{ZrO}_2:\text{Eu}^{3+}$ nanoparticles synthesised at various temperatures (200–400 °C) and at constant residence time (4 seconds). An increase in synthesis temperature results in larger particle sizes.

Increasing the reaction temperature clearly increases the diameter of the $\text{ZrO}_2:\text{Eu}^{3+}$ nanoparticles (Fig. 3). This trend is also demonstrated by transmission electron microscopy (TEM) images shown in Fig. 4. The particles are approximately spherical in shape and increase in size on increasing temperature. As previously mentioned, the DLS measurements reported are the volume weighted average hydrodynamic size of the collection of particles being analysed and this value is influenced by hydration effects. In contrast, the TEM size is a number weighted average size of a dehydrated hard sphere. Hence, one would expect the DLS volume weighted diameter to always be slightly larger than the TEM measured diameter.³⁰ These discrepancies between TEM particle size and DLS particle size are observed on comparison of the data in Fig. 3 and 4. For example, at a synthesis temperature of 400 °C TEM particle size is approximately 5 nm whereas DLS particle size is 22.5 nm. The reason for this discrepancy may result from the larger hydrodynamic radius, or may simply be the result of agglomeration of particles in the dispersion. However, despite

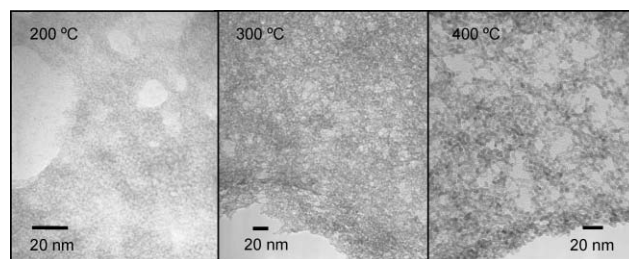


Fig. 4 TEM image for $\text{ZrO}_2:\text{Eu}^{3+}$ synthesised at 200, 300 and 400 °C. Particle size increases on increasing the synthesis temperature; particle shape is approximately spherical.

these discrepancies both techniques remain valuable for the analysis of nanoparticles. DLS measurements are rapid and can be made *in situ*, since hydrothermal synthesis produces an aqueous dispersion of particles, although the assumption is that the particles are spherical in shape. TEM on the other hand reveals important information, such as the particle shape, but requires sample preparation which can cause agglomeration of particles.

The impact of increasing residence time on particle size

The effect of increasing the residence time of the metal salt mixture in the reactor following contact with the hot pressurised water/hydrogen peroxide solution on particle size was also investigated. For each experiment, a constant temperature was set at 200, 250, 300, 350 or 400 °C and flow rates were altered accordingly to provide a range of residence times between 3.7 and 7 seconds. The particle sizes were analysed by DLS and the volume diameters *versus* residence times for each temperature studied are shown in Fig. 5.

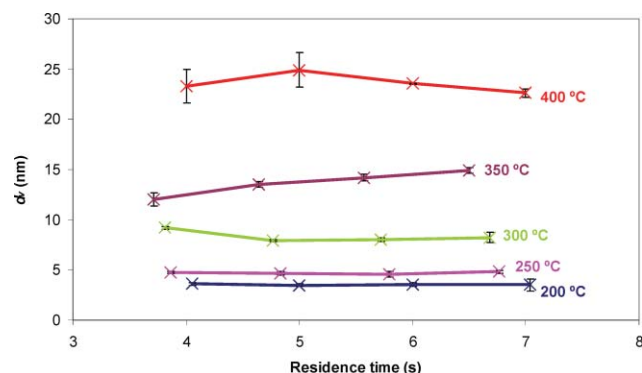


Fig. 5 Effect of residence time on DLS particle diameter of $\text{ZrO}_2:\text{Eu}^{3+}$ synthesised at various temperatures. Particle size increases on increasing temperature but is not significantly affected by residence time at any temperature investigated.

As previously discussed, particle size increases on increasing temperature and this is shown again in Fig. 5. Surprisingly, increasing the residence time does not dramatically affect the particle size and this suggests that the growth of particles is temperature dependent and not dependent on a reaction time between 3.7 and 7 seconds. A kinetic study below a 4 second reaction time is currently being investigated for different temperatures and its effect on nanoparticle size and conversion.

The impact of temperature on dopant concentration

Conversion of $\text{Zr}(\text{ac})_x(\text{OH})_y$ to $\text{ZrO}_2:\text{Eu}^{3+}$ nanoparticles was calculated from ICP-OES measurements and the results are shown in Fig. 6.

Low conversion (<10%) is observed at 200 and 250 °C, high conversion (>98%) at 350 and 400 °C and the mid-point is observed at around 300 °C (Fig. 6).

Similarly, conversion of $\text{Eu}(\text{ac})_3 \cdot x\text{H}_2\text{O}$ to Eu^{3+} ions within ZrO_2 was determined from ICP-OES measurements and the results can be seen in Table 1 alongside their mol% within ZrO_2 nanoparticles.

Table 1 Conversion of Zr^{4+} and uptake and mol% of Eu^{3+} in $\text{ZrO}_2:\text{Eu}^{3+}$ nanoparticles

Synthesis temp (°C)	200	250	300	350	400
% conversion of Zr^{4+} to ZrO_2	10	4	42	98	>99
% uptake of Eu^{3+} into ZrO_2	27	22	41	89	91
Eu^{3+} mol% within ZrO_2	12.9	28.3	4.9	4.5	4.6

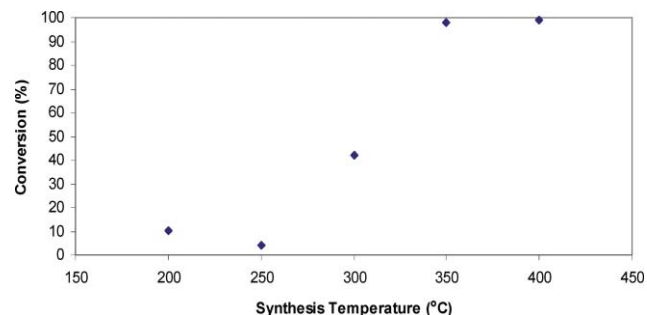


Fig. 6 Conversion of $\text{Zr}(\text{ac})_x(\text{OH})_y$ to ZrO_2 in $\text{ZrO}_2:\text{Eu}^{3+}$ nanoparticles. Increased synthesis temperature results in increased conversion between 250 and 350 °C.

As expected, conversion to $\text{ZrO}_2:\text{Eu}^{3+}$ increases on increasing temperature, specifically between 250 and 350 °C. This is likely due to the increased reaction energy which results in greater nucleation of nanoparticles. Interestingly, Eu^{3+} mol% taken up by the ZrO_2 nanoparticles is noticeably higher at 200 and 250 °C (13 and 28%, respectively) compared with those values at 300 °C and above (around 5%). This is because conversion of the europium precursor to Eu^{3+} ions is higher at these temperatures (27 and 22% respectively) in comparison with Zr^{4+} conversion (10 and 4% respectively). It is uncertain at present why the uptake of Eu^{3+} into ZrO_2 nanoparticles would be higher at the lower temperatures. Indeed it is also unclear whether ZrO_2 is doped with Eu^{3+} ions or if, in fact, nanoparticles of europium hydroxide or europium oxide are being formed alongside the ZrO_2 nanoparticles. To investigate this further, the experiment was repeated without the zirconia precursor *i.e.* only the europium precursor (0.001 M $\text{Eu}(\text{ac})_3 \cdot x\text{H}_2\text{O}$) in the metal salt feed. The TEM image of the product synthesised at 400 °C is shown in Fig. 7.

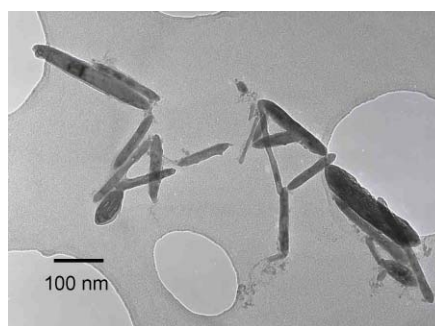


Fig. 7 TEM image of Eu-based nanorods.

The TEM image in Fig. 7 shows the rod-shaped particles resulting from the europium precursor only. No such rod shapes are seen in the samples of $\text{ZrO}_2:\text{Eu}^{3+}$ (Fig. 4) which suggests that the mixed metal salts do not form nanoparticles independently.

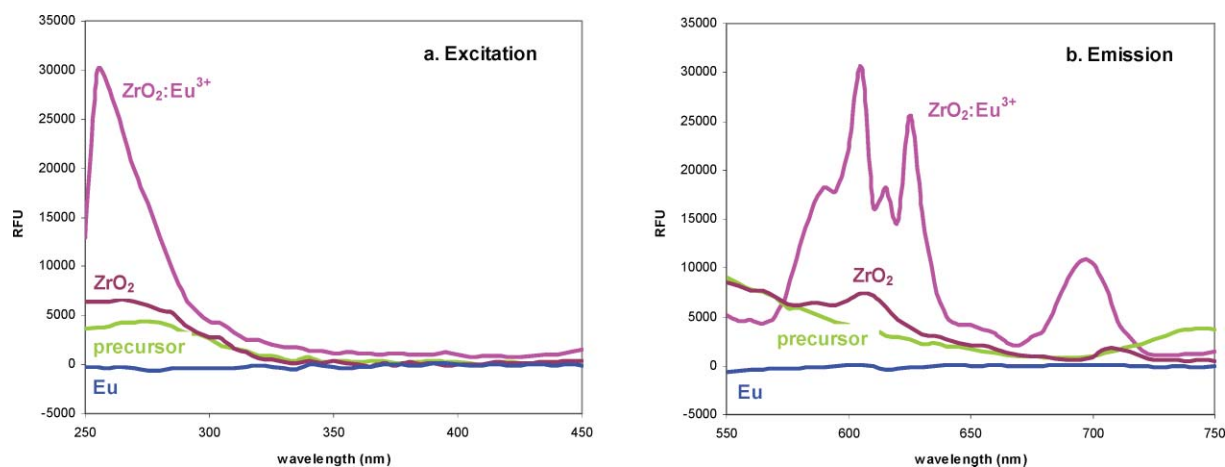


Fig. 8 (a) Excitation (λ_{em} 605 nm) and (b) emission (λ_{ex} 255 nm) scans for $ZrO_2:Eu^{3+}$ nanoparticles (synthesised at 300 °C), the starting precursor, undoped ZrO_2 nanoparticles and Eu-based nanorods (see Fig. 7). Only the $ZrO_2:Eu^{3+}$ nanoparticles show significant fluorescence typical of Eu^{3+} ions.

The europium is therefore most likely to be doped into the ZrO_2 nanoparticles forming a uniform mixture of metals rather than the simultaneous production of both ZrO_2 nanoparticles and Eu-based nanorods. To support this theory, fluorescence measurements were carried out and are described below.

The photoluminescence spectra of $ZrO_2:Eu^{3+}$ nanoparticles synthesised at 300 °C were obtained at an excitation wavelength of 255 nm and is shown in Fig. 8, alongside fluorescence spectra for the starting precursor, undoped ZrO_2 nanoparticles and Eu-based nanorods synthesised from the europium precursor. No fluorescence was detected for the starting metal salt precursors or for undoped ZrO_2 in aqueous solution. $Eu(ac)_3 \cdot xH_2O$ in aqueous solution is not fluorescent since quenching of optical properties is known to occur in an external water environment. However, when a host matrix is employed, such as ZrO_2 in this case, the rare earth ions are shielded from this adverse effect and fluorescence in aqueous media within ZrO_2 nanoparticles can be maintained.³¹ This result suggests that Eu^{3+} ions are effectively dispersed throughout the ZrO_2 nanoparticles and not residing primarily on their surface where they could be easily accessible, and therefore quenched, by the surrounding aqueous media. In addition, the ZrO_2 host has been reported to have a very low frequency of phonons and therefore provides a much improved emission efficiency of the dopant.³² This is supported by the result obtained for the Eu-based nanoparticles synthesised from an equivalent amount of europium precursor but without the ZrO_2 precursor. These nanorods (Fig. 7) were also found to have little or no fluorescence in aqueous solution suggesting that the quenching effects of water are still predominant, hence a host matrix is essential for protecting Eu^{3+} from the water and also to enhance and stabilise its fluorescence.

Photoluminescence spectra for $ZrO_2:Eu^{3+}$ nanoparticles synthesised at all temperatures investigated were also obtained and a selection of these spectra can be seen in Fig. 9.

No significant change in the photoluminescence for each $ZrO_2:Eu^{3+}$ sample was observed (Fig. 9). This lack of size dependent quantization effect is likely due to the $f \rightarrow f$ transitions involving electrons localised in atomic orbitals of the ions.³² This is in contrast to the optical properties of quantum dots,

such as CdS, which are size dependent due to the delocalization of electrons that have their wave functions spread over a large distance.³³

The five emission bands observed for $ZrO_2:Eu^{3+}$, which lie between 590 and 700 nm, are due to $^5D_0 \rightarrow ^5F_1$, $^5D_0 \rightarrow ^5F_2$, $^5D_0 \rightarrow ^5F_3$ and $^5D_0 \rightarrow ^5F_4$ transitions. The peak at 590 nm is due to $^5D_0 \rightarrow ^5F_1$ transitions.³⁴ The peak at 615 nm is due to $^5D_0 \rightarrow ^5F_2$ transitions and this splits into three components at 605, 615 and 625 nm due to lowering of local site symmetry of Eu^{3+} ions.³⁵ These transitions are also highly sensitive to structural change and environmental effects.²¹ $^5D_0 \rightarrow ^5F_3$ transitions are observed at 650 nm and $^5D_0 \rightarrow ^5F_4$ transitions are seen at 695 nm.

The impact of nanoparticles on mammalian cells

Our results have shown that hydrothermal synthesis can provide a greener route for the synthesis of fluorescent nanomaterials. However, a second advantage, and perhaps an important comparison (alongside effective fluorescence) is the toxicology of the end product. Quantum dots (such as CdSe and CdS) contain elements such as Cd which are harmful to cells but also are formulated in organic solvents such as toluene. The doped ZrO_2 product is produced in water but can also be presented to the cells in aqueous suspension giving a second advantage over quantum dots.

As an initial test for the toxicity of $ZrO_2:Eu^{3+}$ nanoparticles on mammalian cells, Chinese hamster ovary (CHO) cells were incubated with the nanoparticles for short (2 h) or long (18 h) incubation periods, since these times are considered representative of those which may be used for live cell imaging applications. CHO cells have a low level of background expression of cell surface receptors and signalling proteins and are therefore used very widely in cell signalling and live cell imaging applications as a host cell line for expression of proteins of interest. Since our original intention was to use the nanoparticles in such applications, this seemed an appropriate cell line to choose for our initial tests. Cells were incubated with the dye trypan blue following exposure to particles to assess any resulting cell death due to particle toxicity. Live cells exclude trypan blue from the

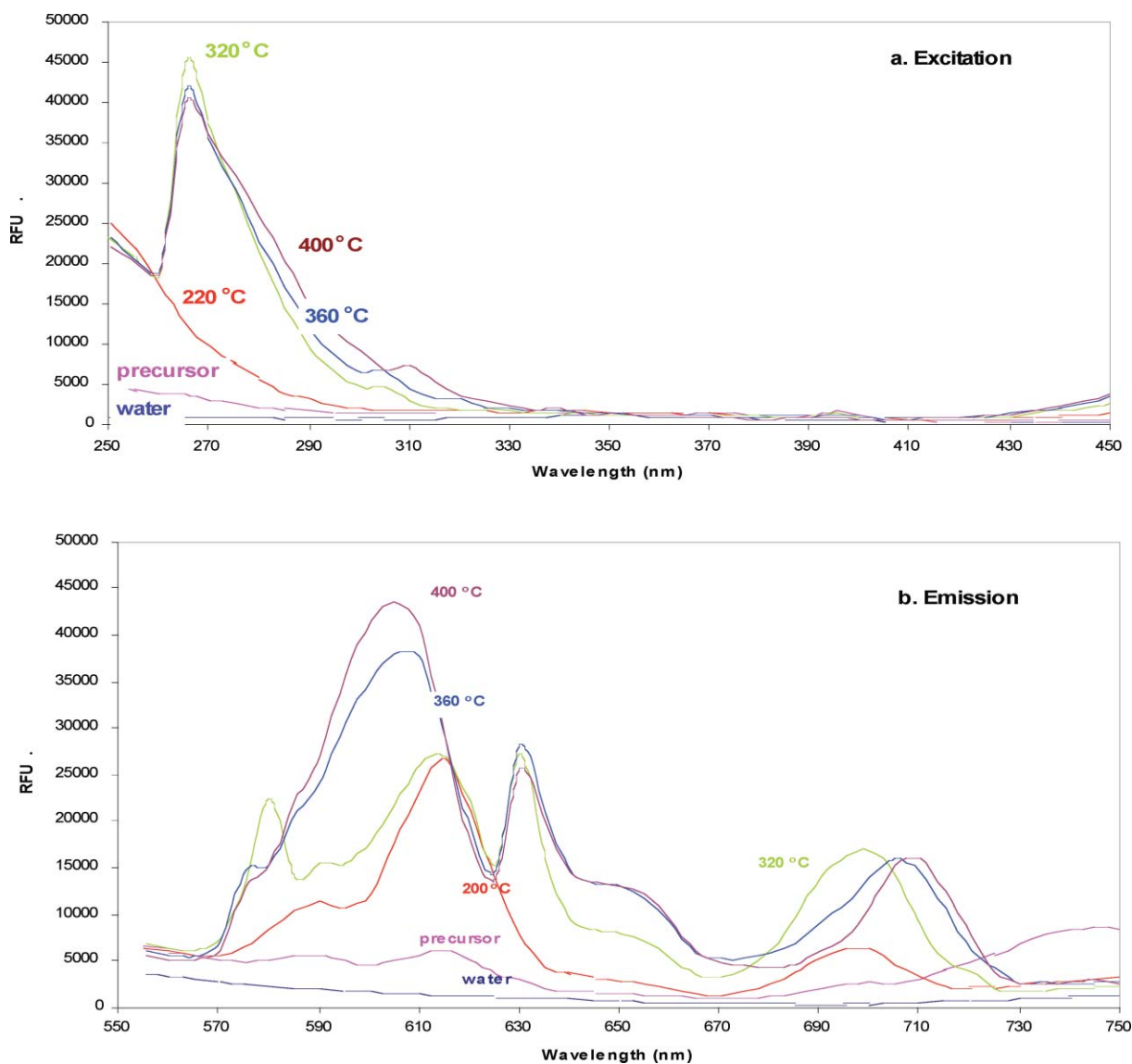


Fig. 9 Fluorescence spectra of $\text{ZrO}_2:\text{Eu}^{3+}$ nanoparticles synthesised at various temperatures. (a) Excitation scan ($\lambda_{\text{em}} 605 \text{ nm}$) and (b) emission scan ($\lambda_{\text{ex}} 255 \text{ nm}$). The spectra show characteristic $f \rightarrow f$ transitions for Eu^{3+} ions.

cytoplasm, but those cells which are dead have compromised membranes and therefore allow the dye to enter, appearing blue under the microscope. For comparison, cells were also incubated for the same times with a commercial CdSe quantum dot (CdSe 520 LumidotTM). The images can be seen in Fig. 10.

Following an 18 h incubation, it was apparent that even relatively high concentrations of $\text{ZrO}_2:\text{Eu}^{3+}$ particles ($80 \mu\text{g mL}^{-1}$) caused no significant increase in cell death compared to incubation with medium alone (Fig. 10d and 10a, respectively). In comparison, there was a large increase in the number of trypan blue positive cells following incubation with the same concentration of CdSe 520. This appeared to be mainly due to toxicity of the toluene vehicle (Fig. 10e), which was not the same for the aqueous vehicle of the ZrO_2 particles (Fig. 10b). Similar results were seen for the 2 h incubation period (not shown). Whilst trypan blue exclusion is a relatively crude method for assessing cell death, the initial result suggests that these $\text{ZrO}_2:\text{Eu}^{3+}$ nanoparticles could be suitable for use in future

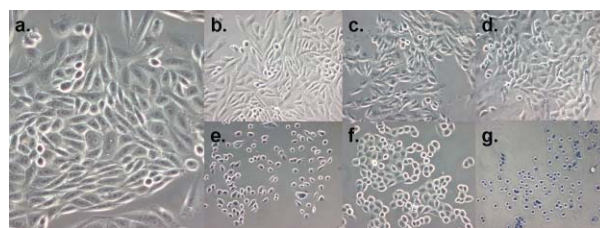


Fig. 10 Images of CHO cells following an 18 hour incubation at 37°C followed by trypan blue exclusion assay: a. medium (control), b. water, c. $\text{ZrO}_2:\text{Eu}^{3+}$ $20 \mu\text{g mL}^{-1}$, d. $\text{ZrO}_2:\text{Eu}^{3+}$ $80 \mu\text{g mL}^{-1}$, e. toluene, f. CdSe 520 $20 \mu\text{g mL}^{-1}$, g. CdSe 520 $80 \mu\text{g mL}^{-1}$. Each image shown is representative of the three taken in each of the four experiments performed.

biological applications. In particular these data suggest that the use of water soluble particles offers a significant advantage for these applications, as no further purification step from a toxic solvent is required.

Conclusions

Crystalline nanoparticles of ZrO₂ doped with Eu³⁺ have been successfully produced from simple metal salt precursors using continuous hydrothermal synthesis. Conversion of the metal salt precursors to nanoparticles increased with increasing the synthesis temperature. A temperature of 350 °C or above was required for >99% conversion. It was also shown that by simply adjusting the synthesis temperature, at constant residence time, the volume diameter of the nanoparticles could be controlled between 2 and 22.5 nm. However, only small changes in particle size were observed by increasing the residence time of the reaction at a constant temperature, suggesting that the growth of these particles is temperature dependent and independent of reaction time (between 3.7 and 7 seconds).

TEM images of the nanoparticles suggest that they are smaller in size (≤5 nm) than the experimental data given by DLS (2–23 nm). This is likely due to the fact that TEM is a number-weighted average size of a dehydrated hard sphere and DLS data is reported as the volume-weighted average hydrodynamic diameter. However, both techniques give important information regarding the characterisation of nanoparticles. XRD data showed that ZrO₂:Eu³⁺ is crystalline with a cubic structure and BET measurements demonstrated a large surface area of 180.1 ± 1.3 m² g⁻¹.

ZrO₂:Eu³⁺ nanoparticles synthesised at all temperatures were fluorescent upon UV-excitation at 255 nm giving rise to characteristic emission spectra (f → f transitions) for Eu³⁺ ions. Water is a known quencher of fluorescence, as indicated by the lack of fluorescence in the starting precursor. It is thought that the Eu³⁺ ions are uniformly distributed throughout the ZrO₂ matrix. If the Eu³⁺ ions were on the particle surface, it is likely that the aqueous medium would quench any fluorescence. Finally, initial cell toxicity studies suggest that ZrO₂:Eu³⁺ nanoparticles do not cause any significant increase in cell death in Chinese hamster ovary cells following incubation at 37 °C for 18 hours. Hence it is possible that these or similar nanoparticles would be suitable for use in future biological applications.

In conclusion, our nozzle design²³ allows efficient mixing of supercritical water and metal salt solution mixture for nucleation and growth of ZrO₂ nanoparticles doped with Eu³⁺. The continuous hydrothermal synthesis of nanoparticles is reproducible and reliable, using relatively benign metal salt precursors in a simple, one-step process. The produced stable aqueous nanoparticle suspensions do not require further formulation and the use of surfactants is eliminated. A larger scale-up reactor has also been built and so the continuous production of larger quantities of nano-materials is now possible on a kg per day scale.

Acknowledgements

We acknowledge the MRC for financial support. We thank Dr Hui Shang, Dr Jun Li and Mr Chris Somerfield for help with BET, XRD and ICP-OES experiments, respectively. We thank Prof. Marek Godlewski and Dr Sergiy Yatsunenka (Polish Academy of Sciences, Poland) for their help regarding fluorescence measurements.

References

- I. Birkby, R. Stevens, Applications of zirconia ceramics, in *Advanced Ceramic Materials*, Trans Tech Publications, Clausthal Zellerfe, 1996, Vol. 122, pp. 527–551.
- R. S. Lima and B. R. Marple, Thermal spray coatings engineered from nanostructured ceramic agglomerated powders for structural, thermal barrier and biomedical applications: A review, *J. Thermal Spray Technol.*, 2007, **16**(1), 40–63.
- T. Justel, H. Nikol and C. Ronda, New developments in the field of luminescent materials for lighting and displays, *Angew. Chem., Int. Ed.*, 1998, **37**(22), 3085–3103.
- B. Moine and G. Bizarri, Rare-earth doped phosphors: oldies or goldies?, *Mater. Sci. Eng., B*, 2003, **105**(1–3), 2–7.
- R. Reisfeld, Prospects of sol-gel technology towards luminescent materials, *Opt. Mater.*, 2001, **16**(1–2), 1–7.
- P. Yang, G. Wirnsberger, H. C. Huang, S. R. Cordero, M. D. McGehee, B. Scott, T. Deng, G. M. Whitesides, B. F. Chmelka, S. K. Buratto and G. D. Stucky, Mirrorless lasing from mesostructured waveguides patterned by soft lithography, *Science*, 2000, **287**, 465–467.
- S. Boujday, F. Wunsch, P. Portes, J. F. Bocquet and C. Colbeau-Justin, Photocatalytic and electronic properties of TiO₂ powders elaborated by sol-gel route and supercritical drying, *Sol. Energy Mater. Sol. Cells*, 2004, **83**(4), 421–433.
- R. Reisfeld, T. Saraidarov, M. Pietraszkiewicz and S. Lis, Luminescence of europium(III) compounds in zirconia xerogels, *Chem. Phys. Lett.*, 2001, **349**(3–4), 266–270.
- A. Speghini and M. Bettinelli, Preparation, structural characterization, and luminescence properties of Eu³⁺ doped nanocrystalline ZrO₂, *J. Mater. Res.*, 2005, **20**(10), 2780–2791.
- A. C. Curtis, D. G. Duff, D. G. Edwards, D. G. Jefferson, B. F. G. Johnson, A. I. Kirkland and A. S. Wallace, Preparation and Structural Characterization of an Unprotected Copper Sol, *J. Phys. Chem.*, 1988, **92**(8), 2270–2275.
- H. Zhang, C. L. Wang, M. J. Li, X. L. Ji, X. L. Zhang and B. Yang, Fluorescent nanocrystal-polymer composites from aqueous nanocrystals: Methods without ligand exchange, *Chem. Mater.*, 2005, **17**(19), 4783–4788.
- K. J. Klabunde and C. Mohs, *Chemistry of Advanced Materials*, Wiley, New York, 1998.
- C. Deng, C. Wang and Y. Li, *J. Am. Ceram. Soc.*, 2002, **85**(11), 2837.
- J. Liang, Z. Deng, X. Jiang, F. Li and Y. Li, Photoluminescence of tetragonal ZrO₂ nanoparticles synthesized by microwave irradiation, *Inorg. Chem.*, 2002, **41**(14), 3602–3604.
- S. Gutzov, M. Bredol and F. Wasgestian, Cathodoluminescence study of europium-doped zirconia and cassiterite powders, *J. Phys. Chem. Solids*, 1998, **59**, 69.
- G. K. Chuah, S. H. Liu, S. Jaenicke and J. Li, High surface area zirconia by digestion of zirconium propoxide at different pH, *Microporous Mesoporous Mater.*, 2000, **39**, 381.
- T. Adschiri, K. Kanazawa and K. Arai, Rapid and Continuous Hydrothermal Synthesis of Boehmite Particles in Subcritical and Supercritical Water, *J. Am. Ceram. Soc.*, 1992, **75**(9), 2615–2618.
- A. Cabanas, J. A. Darr, E. Lester and M. Poliakoff, Continuous hydrothermal synthesis of inorganic materials in a near-critical water flow reactor; the one-step synthesis of nano-particulate Ce_{1-x}Zr_xO₂ (x = 0–1) solid solutions, *J. Mater. Chem.*, 2001, **11**(2), 561–568.
- R. W. Shaw, T. B. Brill, A. A. Clifford, C. A. Eckert and E. U. Franck, Supercritical Water – a Medium for Chemistry, *Chem. Eng. News*, 1991, **69**(51), 26–39.
- T. Adschiri, K. Kanazawa and K. Arai, Rapid and Continuous Hydrothermal Crystallization of Metal-Oxide Particles in Supercritical Water, *J. Am. Ceram. Soc.*, 1992, **75**(4), 1019–1022.
- L. Chen, Y. Liu and Y. Li, Preparation and characterization of ZrO₂:Eu³⁺ phosphors, *J. Alloys Compd.*, 2004, **381**, 266–271.
- P. J. Blood, J. P. Denyer, B. J. Azzopardi, M. Poliakoff and E. Lester, A versatile flow visualisation technique for quantifying mixing in a binary system: application to continuous supercritical water hydrothermal synthesis (SWHS), *Chem. Eng. Sci.*, 2004, **59**(14), 2853–2861.
- E. Lester, P. Blood, J. Denyer, D. Giddings, B. Azzopardi and M. Poliakoff, Reaction engineering: The supercritical water hydrothermal synthesis of nano-particles, *J. Supercrit. Fluids*, 2006, **37**(2), 209–214.

- 24 A. Cabanas, J. Li, P. Blood, T. Chudoba, W. Lojkowski, M. Poliakoff and E. Lester, Synthesis of nanoparticulate yttrium aluminum garnet in supercritical water-ethanol mixtures, *J. Supercrit. Fluids*, 2007, **40**(2), 284–292.
- 25 S. W. Provencher, Eigenfunction Expansion Method for Analysis of Exponential Decay Curves, *J. Chem. Phys.*, 1976, **64**(7), 2773–2777.
- 26 *CRC handbook of chemistry and physics: a ready-reference book of chemical and physical data*. 83rd ed.; CRC Press, 2002–2003.
- 27 *Dispersion Technology Software (Nano series and HPPS)*. Malvern Instruments, Malvern, U.K., 2002–2003.
- 28 S. J. Gregg, K. S. Sing, *Adsorption, surface area and porosity*. 2nd ed.; Academic Press, London, 1982.
- 29 A. Jilavenkatesa, S. J. Dapkunas, L.-S. H. Lum, *Particle Size Characterization*, Materials Science and Engineering Laboratory, 2001.
- 30 *How different are the Z average and TEM sizes?*, Malvern Instruments, www.malvern.co.uk, 2007.
- 31 T. Saraidarov, R. Reisfeld and M. Pietraszkiewicz, Luminescent properties of silica and zirconia xerogels doped with europium(III) salts and europium(III) cryptate incorporating 3,3'-biisoquinoline-2,2'-dioxide, *Chem. Phys. Lett.*, 2000, **330**(5–6), 515–520.
- 32 P. N. Prasad, Nanocontrol of Excitation Dynamics. In *Nanophotonics*, John Wiley & Sons, Inc, 2004, pp. 153–175.
- 33 P. N. Prasad, Quantum-confined materials. In *Nanophotonics*, John Wiley & Sons, Inc, 2004, pp. 79–127.
- 34 K. Riwozki and M. Haase, Wet-chemical synthesis of doped colloidal nanoparticles: YVO₄ : Ln (Ln = Eu, Sm, Dy), *J. Phys. Chem. B*, 1998, **102**(50), 10129–10135.
- 35 B. N. Mahalley, R. B. Pode and P. K. Gupta, Synthesis of GdVO₄ : Bi,Eu red phosphor by combustion process, *Phys. Status Solidi A*, 2000, **177**(1), 293–302.

Antibiofilm activities of 1-alkyl-3-methylimidazolium chloride ionic liquids

Louise Carson,^a Peter K. W. Chau,^a Martyn J. Earle,^b Manuela A. Gilea,^b Brendan F. Gilmore,^{*a} Sean P. Gorman,^a Maureen T. McCann^a and Kenneth R. Seddon^b

Received 5th December 2008, Accepted 22nd January 2009

First published as an Advance Article on the web 18th February 2009

DOI: 10.1039/b821842k

Microbial biofilms are ubiquitous in nature and represent the predominant mode of growth of microorganisms. A general characteristic of biofilm communities is that they tend to exhibit significant tolerance to antimicrobial challenge compared with planktonic bacteria of the same species. The antibiofilm activity of a series of 1-alkyl-3-methylimidazolium chloride ionic liquids has been evaluated against a panel of clinically significant microbial pathogens, including MRSA. A comparison of antimicrobial activity against planktonic bacteria and established biofilms is presented. In general, these ionic liquids possess potent, broad spectrum antibiofilm activity.

Introduction

Ionic liquids are a novel class of low temperature molten salts, comprised of discrete cations and anions.^{1–3} Despite having been described almost a century ago,⁴ ionic liquids attracted a huge amount of interest in the past decade, not only as new alternatives to organic solvents in numerous industrial chemical processes,^{1,5} but also in a diverse array of applications ranging from synthetic and separation/extraction chemistry^{6,7} and, recently, to a number of biological processes^{8,9} and utilisation of ionic liquids as active pharmaceutical ingredients (APIs).¹⁰ Ionic liquids research has also been heavily concentrated towards ‘green’ applications and primarily the replacement of volatile organic compounds (VOCs) with safer alternatives^{11,12} in the chemical industry. Perhaps the most important and attractive property of ionic liquids, which has helped drive this phenomenal interest in the field, is the flexibility or ‘tunability’ in design of the physical, chemical and biological property sets by independent modification of the properties of the cation and anion.¹³

Biological properties of ionic liquids, such as toxicity, remain one of the least researched yet most highly debated topics in the field of ionic liquid research.^{12,14} Whilst much industry has been directed towards ‘green’ applications, the environmental impact (environmental accumulation, biodegradability, toxicity) of these compounds has recently attracted increased scrutiny.³ The most commonly encountered cations, the 1-alkyl-3-methylimidazolium ions,¹⁵ have been studied in a variety of systems to assess potential environmental impact. The ability of such ionic liquids to exert toxicological effects on aquatic organisms such as the bacterium *Vibrio fischeri*,¹⁶ *Daphnia magna* (crustacean),¹⁷ *Physa acuta* (freshwater snail),¹⁸ *Caenorhabditis elegans* (nematode),¹⁹ *Danio rerio* (zebra fish)²⁰ and the freshwater

green algae *Pseudokirchneriella subcapitata*²¹ has recently been investigated. These studies clearly demonstrate the potential negative environmental impacts of such compounds. However, toxicity may be exploited in a number of beneficial applications. Toxicity, itself an important tuneable characteristic, may prove to be one of the most desirable properties of ionic liquids,¹² in the design of new and improved antiseptics, disinfectants and anti-fouling reagents.

A number of recent publications have highlighted the antimicrobial activity of imidazolium, pyridinium and quaternary ammonium ionic liquids.^{16,22–26} Ionic liquids whose antimicrobial activities have been previously described are predominantly non-volatile, non-flammable, have low melting points and viscosities and broad thermal stability.¹² Indeed, such physical properties may, in theory at least, facilitate their use as surface biocides. Once the biological and toxicological properties of the ionic liquids have been suitably ‘tuned’, low viscosity and volatility may improve overall residence time and persistence of activity at the surface to be disinfected.

The antimicrobial activities of a series of 1-alkyl-3-methylimidazolium halides [C_nmim]X (where [C_nmim] = 1-alkyl-3-methylimidazolium; C_n = C_nH_(2n+1); n = 4, 6, 8, 10, 12, 14, 16, 18; and X = Cl, Br) were evaluated²⁴ against a panel of clinically significant bacterial and fungal pathogens (*Escherichia coli*, *Salmonella typhimurium*, *Staphylococcus aureus*, *Bacillus subtilis*, *Chlorella regularis* and *Candida albicans*). These compounds possessed good antimicrobial potency, which was dependant on alkyl chain length. Introduction of methyl and 2-hydroxyethyl substituents into the 2- and 3- positions respectively of the imidazolium ring improved the antimicrobial potency of these compounds.

Pernak and co-workers evaluated the antimicrobial activity of a series of 3-alkoxymethyl-1-methylimidazolium ionic liquids²² and 1,3-(dialkyloxymethyl)-substituted imidazolium ionic liquids²³ against clinically significant pathogens (rods, cocci and fungi). In each case, the antimicrobial activity was related to length of the substituent alkyl chain. Antimicrobial activity was lacking in ionic liquids with shorter alkyl or alkoxy substituents, whilst those ionic liquids bearing longer (>10)

^aSchool of Pharmacy, The Queens University of Belfast, Medical Biology Centre, 97 Lisburn Road, Belfast, UK BT9 7BL. E-mail: b.gilmore@qub.ac.uk; Fax: +44 (0) 28 90 247 794; Tel: +44 (0) 28 90 972 047

^bThe QUILL Research Centre, School of Chemistry, The Queen's University of Belfast, Belfast, UK BT9 5AG

carbon substituents displayed potent and broad spectrum antimicrobial activity. In these studies, the identity of the anion had no significant effect on antimicrobial activity. In a further study, Pernak *et al.* tested a range of protic ionic liquids containing a lactate anion.²⁵ A similar trend was observed, with antimicrobial activity increasing with chain length. Lactate anions with short substituents (up to pentyl or pentoxymethyl) exhibited no biological activity. Although different anions produced differing effects, no clear trend was observable. Importantly, these ionic liquids displayed ready decomposition by ozonation in aqueous solution. This may prove an important feature in the design of biodegradable antimicrobial ionic liquids which exhibit limited environmental impact.

In each case, the description of antimicrobial activity of ionic liquids has concentrated on the planktonic mode of microbial growth, with antimicrobial activity expressed in terms of minimum inhibitory concentrations (MIC) and minimum bactericidal concentrations (MBC), representing the standard assays for susceptibility testing. However, the predominant mode of growth of microorganisms, both pathogenic and environmental, is as highly-ordered surface-adhered communities encased within a self-produced protective extracellular polymeric matrix (glycocalyx), collectively known as a biofilm.^{27,28} It is now recognised that biofilms represent a major survival mechanism for microbial populations and are the cause of a host of industrially and clinically relevant complications; from chronic plant, animal and human infections, to failure of implanted medical devices and microbially-influenced biocorrosion.^{27–31} Therefore, knowledge of the antibiofilm activity of ionic liquids is both environmentally and clinically relevant. However, to date no study has addressed this important issue.

A general characteristic of biofilm communities is that they tend to exhibit significant tolerance/resistance to antibiotics and antimicrobial/biocidal challenge compared with planktonic bacteria of the same species.^{32–35} Bacterial colonisation of biotic or abiotic surfaces and production of extensive exopolysaccharide glycocalyxes provides a confluent protected biofilm.²⁹ The biofilm provides and maintains an advantageous, protected microenvironment where organic nutrients and ions may be sequestered from the environment, antimicrobial penetration is retarded,³⁶ and co-operative activities such as genetic exchange, resistance transfer and cross-feeding are facilitated.³⁷ Genetic and phenotypic diversity contributes to decreased susceptibility of the biofilm.^{30,38,39}

Therefore, significant limitations exist when attempting to extrapolate planktonic culture susceptibility data to environmental or clinical scenarios where the majority of microbial growth is as biofilms. This is illustrated by the NIH estimation that up to 80% of all chronic human infections are biofilm-mediated and that 99.9% of bacteria in aquatic ecosystems live as biofilm communities.^{40,41} Biofilms may persist in antimicrobial concentrations of up to 1000 times those required to eradicate planktonic cells.^{32,38,42}

In this report, we seek to present our findings on the *in vitro* antibiofilm activity of a range of 1-alkyl-3-methylimidazolium chloride ionic liquids against a panel of clinically relevant pathogenic bacteria (including MRSA) and fungi using the Calgary Biofilm Device (CBD), a high-throughput micro-titre plate-based technology for screening antimicrobial susceptibility

of microbial biofilms.³² This method permits the determination of minimum biofilm eradication concentration (MBEC), which is the concentration of an antimicrobial agent required to kill a microbial biofilm.⁴³ Early work by Pernak and co-workers has indicated that the antimicrobial activities of such imidazolium-based ionic liquids is independent of the type of anion,²² and so, we have restricted this study to an examination of the antibiofilm effects of 1-alkyl-3-methylimidazolium chlorides, being easily accessible by synthesis and relatively inexpensive.

Experimental

Synthesis of 1-alkyl-3-methylimidazolium chloride

1-Alkyl-3-methylimidazolium chlorides were prepared *via* the reaction of 1-methylimidazole with a slight excess of the corresponding 1-chloroalkane according to published protocols.^{44,45} The general structure $[C_n\text{mim}]\text{Cl}$ is shown in Fig. 1.

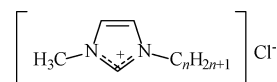


Fig. 1 General structure of 1-alkyl-3-methylimidazolium chlorides, $[C_n\text{mim}]\text{Cl}$, studied.

1-Alkyl-3-methylimidazolium chloride. A mixture of distilled (vacuum distilled from CaH_2 suspension) 1-methylimidazole (82.1 g, 1.00 mol) and 1-chloroalkane (1.05 mol, 1-chlorohexane = 126.7 g, 1-chlorooctane = 156.1 g, 1-chlorodecane = 185.6 g, 1-chlorododecane = 215.0 g, 1-chlorotetradecane = 244.5 g); (used as supplied from Aldrich) was heated with an oil bath at 100 °C in a one-neck round-bottom flask (500 cm³) equipped with a stirrer bar and reflux condenser, under an inert dinitrogen atmosphere. The end of the reaction was confirmed by testing for the presence of unreacted 1-methylimidazole, by adding a few drops of the reaction mixture to a solution of copper(II) sulfate in water. The development of a blue coloration indicates the reaction is not complete and should be heated for longer.⁴⁶ After three days and a negative 1-methylimidazole test, the reaction was connected to a high vacuum pump (at 1 mBar) and heated for 4 h at 100 °C (for $[C_{6-10}\text{mim}]\text{Cl}$) to distil out unreacted 1-chloroalkane, or recrystallised from boiling ethyl ethanoate (for $[C_{12-14}\text{mim}]\text{Cl}$). For each compound, purity was found to be 98–99% by ¹H NMR spectroscopy. Prior to use, water content was determined by Karl Fischer titration and found to be <0.1%. Solid to liquid crystal transitions (m.p.) and clearing point (c.p.) values for crystal forms were also determined by DSC; $[C_{12}\text{mim}]\text{Cl}$ m.p. = 51 °C, c.p. = 134 °C; $[C_{14}\text{mim}]\text{Cl}$ m.p. = 55 °C, c.p. = 195 °C; $[C_{16}\text{mim}]\text{Cl}$ = 66 °C, c.p. = 228 °C and $[C_{18}\text{mim}]\text{Cl}$ = 79 °C, c.p. = 235 °C.

Strains and growth media. The following strains were used in this study *Staphylococcus aureus* ATCC 29213, MRSA (clinical strain 201) and epidemic MRSA strain E-MRSA 15 (Kindly supplied by Dr Michael Tunney, QUB), *Staphylococcus epidermidis* ATCC 35984 (biofilm forming) and *Staphylococcus epidermidis* ATCC 12228 (non-biofilm forming), *Escherichia coli* NCTC 8196, *Pseudomonas aeruginosa* PA01, *Klebsiella aerogenes* NCTC 7427, *Burkholderia cenocepacia* J2315, *Proteus*

mirabilis NCTC 12442 and *Candida tropicalis* NCTC 7393. All microbial strains used in this study were stored at $-70\text{ }^{\circ}\text{C}$ in Microbank vials (Pro-Lab Diagnostics, Cheshire, UK) according to manufacturer's directions. All strains were subcultured to Müeller Hinton Agar (MHA; Oxoid, Basingstoke, UK) before testing.

MIC/MBC determination. Broth microdilution tests were performed according to NCCLS guidelines. Serial two-fold dilutions of each imidazolium salt (from an original working solution which had been $0.22\text{ }\mu\text{m}$ sterile filtered) in Müeller-Hinton Broth (MHB) ($100\text{ }\mu\text{l}$) were prepared in 96-well microtitre plates over the range $0.0000625\text{--}1\%$ w/v. The inoculum to be tested was prepared by adjusting the turbidity of an actively overnight growing broth culture in MHB to an optical density at 550 nm equivalent to $1 \times 10^8\text{ CFU/ml}$. The suspension was further diluted to provide a final inoculum density of $2 \times 10^5\text{ CFU/ml}$ in MHB as verified by total viable count. The inoculum to be tested ($100\text{ }\mu\text{l}$, $2 \times 10^5\text{ CFU/ml}$) was added to each well of the microdilution trays which were incubated aerobically for 24 h at $37\text{ }^{\circ}\text{C}$. Positive and negative growth controls were included in every assay (6 replicates). After determination of the MICs, minimum bactericidal concentrations (MBC) were determined by spreading $20\text{ }\mu\text{l}$ of suspension from wells showing no growth onto MHA plates, which were then incubated for 24 h and examined for 99.9% killing.

Biofilm susceptibility assay. Biofilms of each test organism were grown in the Calgary Biofilm Device (commercially available as the MBEC AssayTM for Physiology & Genetics (P & G), Innovotech Inc., Edmonton, Alberta, Canada).⁴⁷ The device, a micro-titre plated based assay, consists of two parts; a microtitre plate containing the inoculated test medium and a polystyrene lid with 96 identical pegs on which the microbial biofilm forms under gyrorotary incubation. The biofilm assay was conducted according to the MBECTM assay protocol as supplied by the manufacturer, with slight modifications.⁴⁷ Inocula of each test organism were prepared in MHB as described above and adjusted to provide a final inoculum density of $\sim 10^7\text{ CFU/ml}$ (as confirmed by viable count). Into each well of the 96-well microtitre plate packaged with the MBECTM P & G assay, $150\text{ }\mu\text{l}$ of the inoculated media was transferred to each of the test wells and the assay plate lid, bearing 96 pegs was placed into the microtitre plate. The MBEC assay plates were placed in a gyrorotary incubator ($37\text{ }^{\circ}\text{C}$, 95% relative humidity) for 24 h to permit growth and comparison of 24 h biofilms of each test strain. Positive and negative growth controls were included in each plate (6 replicates). Initial and 24 h planktonic viable counts were measured, as were 24 h biofilm, expressed as CFU peg^{-1} , according to manufacturers instructions. After 24 h , the peg lid of the MBEC assay plate was gently rinsed three times. After rinsing, the peg lid of the MBEC assay was transferred to a 'challenge' plate. Essentially, serial dilutions of each imidazolium salt were prepared in MHB and $200\text{ }\mu\text{l}$ of MHB containing various concentrations of ionic liquid was added to each well. Positive growth control and sterility control were included in each assay plate. After exposure of the biofilm to the antimicrobial challenge for $24 \pm 1\text{ h}$, the peg lid was removed from the challenge plate, rinsed three times in 0.9% saline as described and transferred to a 'recovery'

plate, each well contained MHB supplemented with neutralisers (final concentration in each well; 0.125% L-histidine, 0.125% L-cystiene, 0.25% reduced glutathione). Biofilms were dislodged into recovery media by sonication for 5 min and the peg lid discarded. The recovery plate was incubated overnight and visually checked after 24 h for turbidity. In addition, optical density measurements for each plate were recorded at 550 nm , clear wells were taken as evidence of biofilm eradication, and, an MBEC value assigned as the lowest concentration at which no growth was observed after 24 h incubation. Plates were incubated for a further 24 h to confirm biofilm eradication concentrations.

Results and discussion

All synthesised 1-alkyl-3-methylimidazolium salts [$C_n\text{mim}$]Cl ($n = 4, 6, 8, 10, 12, 14, 16$ or 18) were initially screened for antimicrobial activity by a simple zone of inhibition study against seeded *Staphylococcus aureus* and MRSA plates (data not shown). From these qualitative experiments, [$C_4\text{mim}$]Cl exhibited no measurable antimicrobial activity. It was therefore decided to evaluate the activity of [$C_n\text{mim}$]Cl compounds where $n = 6, 8, 10, 12$ and 14 carbon atoms. Both [$C_{16}\text{mim}$]Cl and [$C_{18}\text{mim}$]Cl dissolved extremely slowly and were not evaluated further. All imidazolium salts included in the study were tested for antimicrobial activity against a number of clinically relevant pathogens (cocci, rods and fungi). Minimum inhibitory concentration (MIC) values and minimum bactericidal concentration (or fungicidal concentration for *C. tropicalis*) (MBC) values were determined and are given in Table 1. These MIC and MBC values are in agreement with those published for 1-alkyl-3-methylimidazolium salts by Demberelnyamba *et al.*²⁴ and are comparable to those published by Pernak and coworkers for a range of 1-alkoxymethyl-3-methyl imidazolium chlorides²² against cocci, rods and fungi. In our experiments, the activity

Table 1 MIC and MBC (μM) values of 1-alkyl-3-methylimidazolium chlorides ([$C_n\text{mim}$]Cl)

Organism		n				
		6	8	10	12	14
<i>S. aureus</i> ATCC 29213	MIC	>1644	722	40	18	16
	MBC	>1644	>1444	643	36	66
<i>E-MRSA 15</i>	MIC	>1644	722	40	18	16
	MBC	>1644	>1444	321	73	66
MRSA	MIC	>1644	1444	160	36	16
	MBC	>1644	>1444	643	290	66
<i>S. epidermidis</i> ATCC 12228	MIC	>1644	361	40	36	7.75
	MBC	>1644	1444	644	145	33
<i>S. epidermidis</i> ATCC 35984	MIC	>1644	722	40	36	7.75
	MBC	>1644	1444	160	73	33
<i>E. coli</i> NCTC 8196	MIC	>1644	722	321	73	33
	MBC	>1644	1444	1287	73	33
<i>P. aeruginosa</i> PA01	MIC	>1644	>1444	>1287	580	264
	MBC	>1644	>1444	>1287	1161	264
<i>K. aerogenes</i> NCTC 7427	MIC	>1644	1444	643	73	33
	MBC	>1644	>1444	1287	145	66
<i>B. cenocepacia</i> J2315	MIC	>1644	>1444	1287	290	132
	MBC	>1644	>1444	1287	580	264
<i>P. mirabilis</i> NCTC 12442	MIC	>1644	1444	1287	580	264
	MBC	>1644	>1444	1287	1161	530
<i>C. tropicalis</i> NCTC 7393	MIC	>1644	1444	321	73	66
	MBC	>1644	>1444	321	73	132

of these compounds is dependent on the alkyl chain length, in keeping with observations made by numerous studies^{16,22–25} with compounds having alkyl chain lengths greater than 10 carbon atoms exhibiting potent, broad spectrum antimicrobial activity. The calculated average MIC values (for imidazolium salts with 8–14 carbon atoms in the alkyl chain) for Gram positive cocci, Gram negative rods and a representative fungi are plotted in Fig. 2 as the relationship between \log_{10} MIC (μM) and alkyl chain length. In general Gram positive organisms proved most sensitive to these compounds whilst Gram negative rods and representative fungi were less susceptible (Fig. 2), once again in keeping with the findings of Pernak *et al.*²²

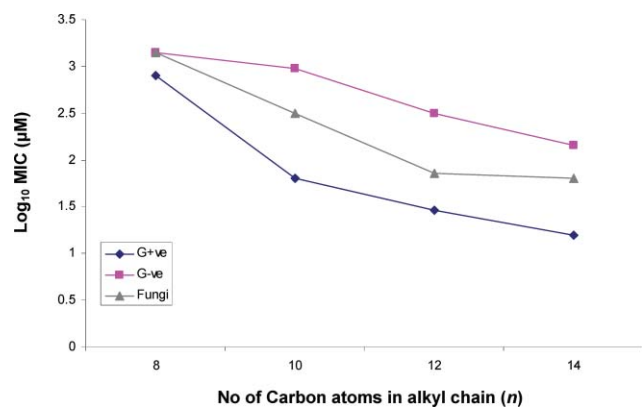


Fig. 2 Mean [C_nmim]Cl MIC values for Gram positive cocci, Gram negative rods and fungi.

In order to assess the antibiofilm activity of these compounds against a panel of clinically significant pathogens, biofilms of each strain (with the exception of *Staphylococcus epidermidis* ATCC 12228, a non-biofilm forming strain) were grown on polystyrene pegs of the Calgary Biofilm Device (CBD) as described by Ceri *et al.*³² This method was developed to permit reproducible, high throughput assaying of biofilm susceptibility to antimicrobial and biocidal agents. The CBD has also been validated as a suitable method for assessing the antimicrobial/antibiofilm efficacy of new agents.⁴⁸ Biofilms were grown for 24 h as described, and 24 h biofilm viable counts performed to determine average viable cell counts for each

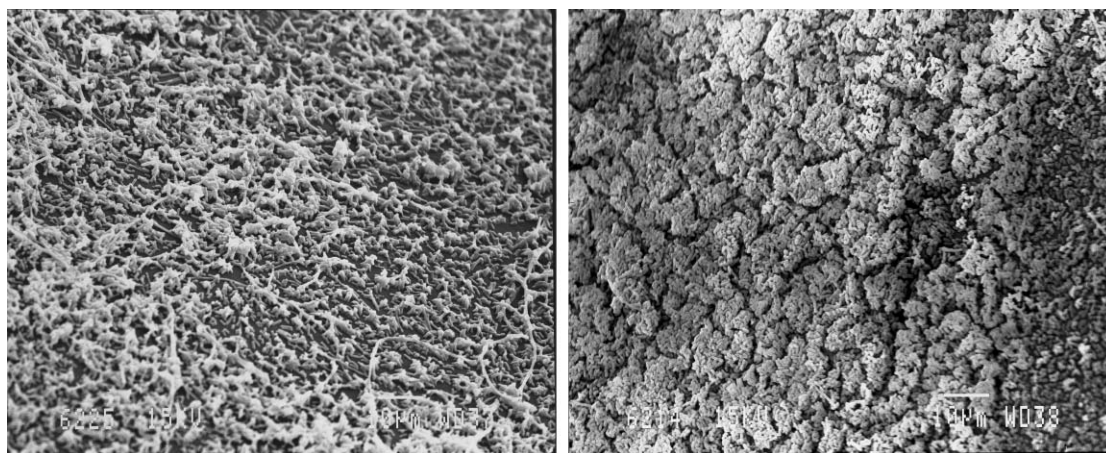


Fig. 3 Representative electron micrographs of 24 h. *E. coli* NCTC 8196 biofilms grown on polystyrene pegs of the Calgary Biofilm Device.

Table 2 MIC and MBEC (μM) values of 1-alkyl-3-methylimidazolium chlorides ([C_nmim]Cl)

Organism		n			
		8	10	12	14
<i>S. aureus</i>	MIC	722	40	18	16
ATCC 29213	MBEC	2708	2415	272	124
<i>E-MRSA 15</i>	MIC	722	40	18	16
	MBEC	2708	1207	272	248
<i>MRSA</i>	MIC	1444	160	36	16
	MBEC	21666	4829	545	124
<i>S. epidermidis</i>	MIC	722	40	36	7.75
ATCC 35984	MBEC	10833	4829	272	124
<i>E. coli</i>	MIC	722	321	73	33
NCTC 8196	MBEC	21666	9659	1089	124
<i>P. aeruginosa</i>	MIC	5416 ^a	2415 ^a	580	264
PA01	MBEC	21666	2415	1089	496
<i>K. aerogenes</i>	MIC	1444	643	73	33
NCTC 7427	MBEC	43331	19318	2179	248
<i>B. cenocepacia</i>	MIC	>1444	1287	290	132
J2315	MBEC	43331	19318	2179	496
<i>P. mirabilis</i>	MIC	1444	1287	580	264
NCTC 12442	MBEC	43331	9659	4357	1984
<i>C. tropicalis</i>	MIC	1444	321	73	66
NCTC 7393	MBEC	>43331	19318	8714	248

^a MIC values determined using the CBD method as per manufacturers protocol and defined as the lowest concentration of antibiotic in which a planktonic population could not be established by shedding of bacteria from a biofilm,⁴³ and not the NCCLS method. Included for clarification and comparison only.

of the test strain biofilms. Typical electron micrographs of a 24 h. *E. coli* biofilm, grown on pegs of the CBD, are shown in Fig. 3. Average 24 h biofilm viable counts are given in Fig. 4 and comparison of MIC and minimum biofilm eradication concentrations (MBEC) are given in Table 2. The minimum biofilm eradication concentrations of these compounds, displayed in Fig. 5, (as \log_{10} MBEC (μM)) was shown in these experiments to be dependent on alkyl chain length, similar to the observed effect of alkyl chain length on MIC in this and other studies. However, this effect may not necessarily be predicted since the observations of Smith *et al.* indicate that often no correlation exists between MIC and the efficacy of antimicrobial agents against microbial biofilms.⁴⁹ For each strain tested, the MBEC value decreased (increased antibiofilm potency)

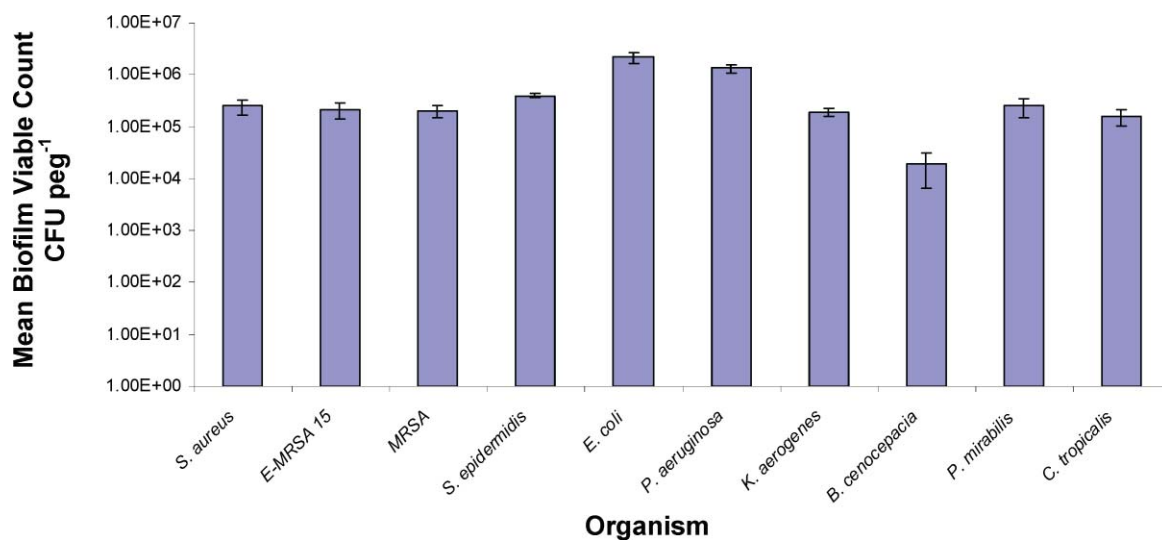


Fig. 4 Mean 24 h biofilm viable cell counts for each test organism grown on the Calgary Biofilm Device. Each value is expressed as the mean of six replicates.

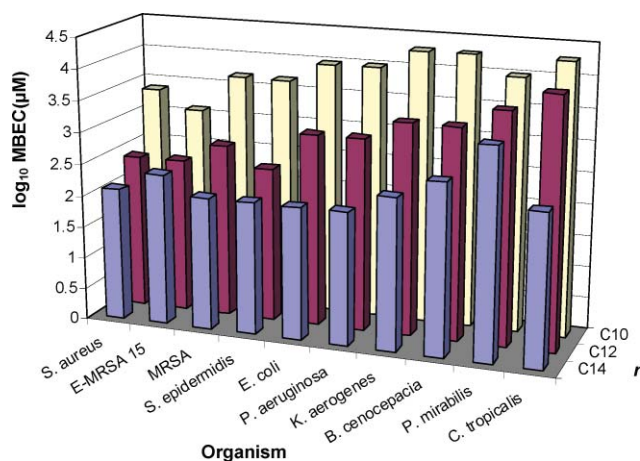


Fig. 5 Minimum biofilm eradication concentrations (MBEC) for $[C_n\text{mim}]\text{Cl}$ where $n = 10, 12,$ or 14 against a range of clinically significant pathogens. All MBEC values were repeated in quadruplicate.

with increasing alkyl chain length, with compounds $[C_n\text{mim}]\text{Cl}$ where $n \leq 10$ exhibiting potent, broad spectrum antimicrobial activity. With the exception of *Staphylococcus aureus* ATCC 29213 and E-MRSA 15, 1-octyl-3-methylimidazolium chloride exhibited essentially no antibiofilm activity. Similarly, 1-decyl-3-methylimidazolium chloride exhibited good antibiofilm activity against all Gram positive and most Gram negative strains, however, lacked potency against *K. aerogenes* and *B. cenocepacia* biofilms. In general, of the compounds tested in this series, $[C_n\text{mim}]\text{Cl}$ where $n = 14$, exhibited greatest antibiofilm activity against all microbial biofilms. The average MBEC values for Gram negative, Gram positive and the representative fungal strain, *C. tropicalis*, used in this study are shown in Fig. 6, (as \log_{10} MBEC (μM)). In summary, these data indicate that Gram positive microbial biofilms (in keeping with planktonic cultures) are generally more susceptible to 1-alkylmethylimidazolium ionic liquids than Gram positive microbial biofilms. The fungal strain tested, *Candida tropicalis*, exhibited a similar susceptibility

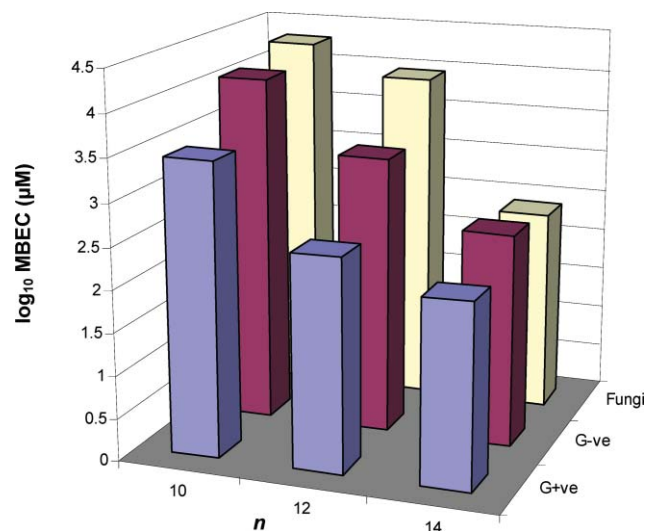


Fig. 6 Average minimum biofilm eradication concentrations (MBEC) for $[C_n\text{mim}]\text{Cl}$ where ($n = 10, 12,$ or 14) for Gram positive, Gram negative and fungi (*C. tropicalis*).

profile to these reagents as the representative Gram negative organisms tested in this study.

Conclusions

The principle aim of this study was to evaluate the antibiofilm activity of a range of 1-alkyl-3-methylimidazolium chlorides to test the general applicability of ionic liquids as biofilm eradication agents (for example in surface decontamination) and to assess the likely environmental impact of these compounds, given that the predominant mode of growth of microbes in the environment is as a surface adhered biofilm.^{26,27} To our knowledge this important aspect of their antimicrobial activity has not yet been discussed in the literature. Clinically, microbial biofilms are extremely problematic, and are implicated in implantable medical device-associated infections as well as many non-implant related chronic infections in humans,^{50,51} many of

which are recalcitrant to standard antimicrobial regimens. In this study we have shown that these compounds possess excellent, broad spectrum antimicrobial and antibiofilm activity against a panel of pathogen microorganisms, including clinical isolates of MRSA and other pathogens associated with hospital acquired, or nosocomial, infections. Therefore, the application of ionic liquids towards development of novel disinfectants/antiseptics for improved infection control within the hospital environment deserves further exploration. The employment of ionic liquid based antimicrobials may help address the significant patient cost (in terms of morbidity and mortality) and financial burden imposed by the ubiquitous spectre of hospital acquired infections (including those caused by multidrug resistant organisms such as MRSA), which is currently estimated to cost the NHS £1,000,000,000 annually.⁵² Industrially, microbial biofilms are responsible for billions of dollars in lost productivity every year, occurring in almost every water-based process causing pipe blockage corrosion and contamination.⁵³

This study highlights the potential of ionic liquids as antibiofilm agents which could have a range of clinical and industrial applications; however, the environmental impact of such reagents must be considered. The design of novel classes of ionic liquids with improved antibiofilm activities, reduced environmental impact, and improved toxicity profile should be possible through rational design, by improving the biodegradative properties of such reagents whilst retaining potent antimicrobial and antibiofilm activity.

Acknowledgements

We are grateful to the Industrial Advisory Board of QUILL and the EPSRC (Portfolio Partnership Scheme, grant number EP/D029538/1) for their continuing support.

Notes and references

- 1 K. R. Seddon, *J. Chem Technol. Biotechnol.*, 1997, **68**, 351–356.
- 2 A. Stark and K. R. Seddon, in *Kirk-Othmer Encyclopaedia of Chemical Technology*, ed. A. Seidel, John Wiley & Sons, Inc., Hoboken, New Jersey, 2007, vol. 26, pp. 836–920.
- 3 P. J. Scammells, J. L. Scott and R. D. Singer, *Aust. J. Chem.*, 2005, **58**, 155–169.
- 4 P. Walden, *Bull Acad Imper. Sci St. Petersburg.*, 1914, **8**, 405–422.
- 5 N. V. Plechkova and K. R. Seddon, *Chem. Soc. Rev.*, 2008, **37**, 123–150.
- 6 T. Welton, *Chem Rev.*, 1999, **99**, 2071–2083.
- 7 R. Rogers and K. R. Seddon, *Science*, 2003, **302**, 792–793.
- 8 S. Dreyer and U. Kragl, *Biotechnol Bioeng.*, 2008, **99**, 1416–1424.
- 9 N. Wehofskey, C. Wespe, V. Cerovsky, A. Pech, E. Hoess, R. Rudolph and F. Bordusa, *Chembiochem.*, 2008, **9**, 1493–1499.
- 10 W. L. Hough, M. Smiglak, H. Rodriguez, R. P. Swatloski, S. K. Spear, D. T. Daly, J. Pernak, J. E. Grisel, R. D. Carliss, M. D. Soutoullo, J. H. Davis, Jr. and R. D. Rogers, *New J. Chem.*, 2007, **31**, 1429–1436.
- 11 N. V. Plechkova and K. R. Seddon, in *Methods and Reagents for Green Chemistry: An Introduction*, ed. P. Tundo, A. Perosa and F. Zecchini, John Wiley & Sons, Inc., New York, 2007, pp. 105–130.
- 12 W. L. Hough and R. D. Rogers, *Bull. Chem. Soc. Jpn.*, 2007, **80**, 2262–2269.
- 13 M. Freemantle, *Chem Eng News.*, 1998, **76**, 32–37.
- 14 J. Ranke, S. Stolte, R. Stoermann, J. Arning and B. Jastorff, *Chem. Rev.*, 2007, **107**, 2183–2206.
- 15 R. P. Swatloski, J. D. Holbrey, S. B. Memon, G. A. Caldwell, K. A. Caldwell and R. D. Rogers, *Chem. Commun.*, 2004, 668–669.
- 16 K. M. Docherty and C. F. Kulpa, Jr., *Green Chem.*, 2005, **7**, 185–189.
- 17 R. J. Bernot, M. A. Brueseke, M. A. Evans-White and G. A. Lamberti, *Environ. Toxicol. Chem.*, 2005, **24**, 87–92.
- 18 R. J. Bernot, E. E. Kennedy and G. A. Lamberti, *Environ. Toxicol. Chem.*, 2005, **24**, 1759–1765.
- 19 R. P. Swatloski, J. D. Holbrey, S. B. Memon, G. A. Caldwell, K. A. Caldwell and R. D. Rogers, *Chem Commun.*, 2004, 668–669.
- 20 C. Pretti, C. Chiappe, D. Pieraccini, M. Gregori, F. Abramo, G. Monni and L. Intorre, *Green Chem.*, 2006, **8**, 238–240.
- 21 T. P. T. Pham, C. W. Cho, J. Min and Y. S. Yun, *J. Biosci. Bioeng.*, 2008, **105**, 425–428.
- 22 J. Pernak, K. Sobaszekiewicz and I. Mirska, *Green Chem.*, 2003, **5**, 52–56.
- 23 J. Pernak, K. Sobaszekiewicz and J. Foksowicz-Flaczyk, *Chem. Eur.*, 2004, **10**, 3479–3485.
- 24 D. Demberelynamba, K. S. Lim, S. Choi, S. Y. Park, H. Lee, C. J. Kim and I. D. Yoo, *Bioorg. Med. Chem.*, 2004, **12**, 853–857.
- 25 J. Pernak, I. Goc and I. Mirska, *Green Chem.*, 2004, **6**, 323–329.
- 26 J. Pernak and J. Feder-Kubis, *Chem. Eur. J.*, 2005, **11**, 4441–4449.
- 27 R. M. Donlan and J. W. Costerton, *Clin. Microbiol. Rev.*, 2002, **15**, 167–193.
- 28 L. Hall-Stoodley, J. W. Costerton and P. Stoodley, *Nat. Rev. Microbiol.*, 2004, **2**, 95–108.
- 29 M. M. Tunney, S. P. Gorman and S. Patrick, *Rev. Med. Microbiol.*, 1996, **74**, 195–205.
- 30 R. D. Wolcott and G. D. Ehrlich, *JAMA.*, 2008, **299**, 2682–2684.
- 31 I. B. Beech and J. Sunner, *Curr. Opin. Biotechnol.*, 2004, **15**, 181–186.
- 32 H. Ceri, M. E. Olson, C. Stremick, R. R. Read, D. Morck and A. Buret, *J Clin Microbiol.*, 1999, **37**, 1771–1776.
- 33 P. T. Gilbert, T. Maira-Litran, A. J. McBain, A. H. Rickard and F. Whyte, *Adv. Microbial. Phys.*, 2002, **46**, 203–256.
- 34 P. S. Stewart and J. W. Costerton, *Lancet.*, 2001, **358**, 135–138.
- 35 P. S. Stewart, *Int. J. Med. Microbiol.*, 2002, **292**, 107–113.
- 36 S. P. Gorman, J. G. McGovern, A. D. Woolfson, C. G. Adair and D. S. Jones, *Biomaterials.*, 2001, **22**, 2741–2747.
- 37 J. J. Harrison, R. T. Turner, L. L. R. Marques and H. Ceri, *Am. Sci.*, 2005, **80**, 1–5.
- 38 G. D. Ehrlich, F. Z. Hu, K. Shen, P. Stoodley and J. C. Post, *Clin. Orthop. Relat. Res.*, 2005, **437**, 20–24.
- 39 J. J. Harrison, H. Ceri and R. J. Turner, *Nat. Rev. Microbiol.*, 2007, **5**, 928–938.
- 40 K. Lewis, *Antimicrob. Agents Chemother.*, 2001, **45**, 999–1007.
- 41 J. W. Costerton and M. Wilson, *Biofilms.*, 2004, **1**, 1–4.
- 42 P. Gilbert, J. Das and I. Foley, *Adv. Dent. Res.*, 1997, **11**, 160–167.
- 43 M. E. Olson, H. Ceri, D. W. Morck, A. G. Buret and R. R. Read, *Can. J. Vet. Res.*, 2002, **66**, 86–92.
- 44 J. S. Wilkes, J. A. Levisky, R. A. Wilson and C. L. Hussey, *Inorg. Chem.*, 1982, **21**, 1263–1264.
- 45 C. J. Bowlas, D. W. Bruce and K. R. Seddon, *Chem. Commun.*, 1996, 1625–1626.
- 46 J. D. Holbrey, K. R. Seddon and R. Wareing, *Green Chemistry*, 2001, **3**, 33–36.
- 47 Innovotech Incorporated. [<http://www.innovotech.ca>] *Manufacturers Instructions: The MBEC Physiology & Genetics (P & G) Assay*.
- 48 L. Ali, F. Khambaty and G. Diachenko, *Bioresour. Technol.*, 2006, **97**, 1887–1893.
- 49 A. L. Smith, S. B. Fiel, N. Mayer-Hamblett, B. Ramsey and J. L. Burns, *Chest*, 2003, **123**, 1495–1502.
- 50 J. W. Costerton, P. S. Stewart and E. P. Greenberg, *Science*, 1999, **284**, 1318–1322.
- 51 S. P. Gorman and D. S. Jones, in: *Medical Implications of Biofilms* ed. M. Wilson, Cambridge University Press, Cambridge, 2003, pp. 136–170.
- 52 R. Plowman, *Euro. Surveill.*, 2000, **5**, 49–50.
- 53 BiofilmsONLINE.com: Primer: A Biofilm Primer. Montana State University, Centre for Biofilm Engineering. www.biofilmsonline.com/cgi-bin/biofilmsonline/ed_facts_primer.html (Accessed 04/09/2008).

Strategy to improve the characterization of chitosan for sustainable biomedical applications: SAR guided multi-dimensional analysis†

Mirko X. Weinhold,^{*a} Janelle C. M. Sauvageau,^a Nadia Keddig,^b Marianne Matzke,^c Bernd Tartsch,^d Ingo Grunwald,^e Christian Kübel,^{e,f} Bernd Jastorff^g and Jorg Thöming^a

Received 11th June 2008, Accepted 14th January 2009

First published as an Advance Article on the web 17th February 2009

DOI: 10.1039/b809941c

The biopolymer chitosan has shown great potential for a tremendous number of applications despite the fact that typical chitosan preparations are always mixtures of different chemical entities, natural impurities and process-induced impurities. However, chitosan preparations described in the literature or offered on the market are analytically highly undefined. Here we propose a T-SAR (thinking in terms of structure-activity-relationships) guided multi-dimensional analysis of distinct chitosan preparations with the aim a) to obtain the information needed for the production of reproducible chitosan preparations and b) to predict biological effects and technological properties of certain chitosan preparations. First, a physico-chemical description (molecular weight (M_w), polydispersity (M_w/M_n), fraction of acetylation (F_A), pattern of acetylation (P_A), hydrodynamic radius (R_h), intrinsic viscosity ($[\eta]$) of six selected samples was done. Furthermore chitosan properties like solubility, crystallinity, conformation (Mark-Houwink-plot) and impurities of all the chitosan preparations from different origins were determined and biological effects were also analyzed using test systems with two different bacteria (*Escherichia coli*, *Vibrio fischeri*). It was found that the presence of HCl enabled the water solubility of chitosan, while chloride-free chitosan was only soluble in acetic acid. The pattern of acetylation P_A showed no impact on this behavior. The analyzed biological effects revealed growth inhibition within 30 minutes for *E. coli* and a decreased bioluminescence for *V. fischeri* ($IC_{50} = 0.035$ w%). Thus, the strategy to check biological effects within a multi-dimensional analysis kit proved to be effective for detecting general structure-property-relationships of chitosan in relation to its biological effects.

I. Introduction

Chitin and chitosan are important biopolymers consisting of (1→4)-2-amino-2-deoxy-β-D-glucan (GlcN) and (1→4)-2-acetamido-2-deoxy-β-D-glucan (GlcNAc) units. Due to their interesting properties they take center stage for many different applications e.g. waste water treatment¹ (coagulant, heavy-metal binding,² protein binding), food industry (diet substance,³ cholesterol reducer⁴), biomedical (gene delivery,⁵ medical dressing,⁶ artificial tissue/skin,⁷ prosthesis coating,⁸ agriculture,⁹

animal food additive,¹⁰ seed/leaf coating¹¹), pharmaceutical (anti-adhesive,¹² drug delivery,¹³ wound-healing,¹⁴) and cosmetic uses (gelation agent, plaque inhibition,¹⁵ moisturizers,¹⁶ stabilizers¹⁶).

For any of these applications sustainable materials are required. In the light of chapter 19 of Agenda 21¹⁷ the following principles of green chemistry¹⁸ are of main relevance: “Chemical products should be designed to preserve efficacy of function while reducing toxicity” (4th principle). “A raw material or feedstock should be renewable rather than depleting whenever technically and economically practicable” (7th principle). “Chemical products should be designed so that at the end of their function they breakdown into innocuous degradation products and do not persist in the environment” (10th principle).

Chitosan has the potential to substitute conventional materials in many applications mentioned above. Typical synthetic materials, which are usually applied, may be toxic, not renewable and with unknown degradation pathway possibly resulting in (eco)toxic metabolites. As a consequence, the possibility of these negative impacts demands time and money-consuming tests to ensure the safety of synthetic materials for a broad application. In contrast, the application of chitosan, known as a non-toxic biopolymer, can avoid these problems. As a renewable resource it

^aUFT-Center for Environmental Research and Sustainable Technology, Department of Chemical Engineering-Recovery and Recycling, 28359, Bremen, Germany. E-mail: mirkoweinhold@gmx.de; Tel: +49 421 218-63389; Fax: +49 421 218-8297

^bUFT-Department of Applied Botany, Bremen, Germany

^cUFT-Department of General and Theoretical Ecology, Bremen, Germany

^dViscotek, a Malvern company, 68753, Waghäusel, Germany

^eFraunhofer Institute for Manufacturing Technology and Applied Materials Research (IFAM), 28359, Bremen, Germany

^fForschungszentrum Karlsruhe, Institute for Nanotechnology, 76344, Eggenstein-Leopoldshafen, Germany

^gUFT-Department of Bioorganic Chemistry, Bremen, Germany

† Electronic supplementary information (ESI) available: Further experimental details. See DOI: 10.1039/b809941c

has further outstanding properties such as biocompatibility^{19,20} as well as biodegradability.²¹ Nevertheless it has to be considered that those properties only account for pure chitosan. It is well known that chitosan processed from chitin may contain heavy metals, protein residues as well as acid/alkali residues. Those impurities of the polymer, caused by the production process and the source of the preparation, can have an impact on man and the environment and have to be considered within the hazard assessment. In general chitosan preparations are obtained from natural chitin sources as for example (crab shells, squid pen, fungi) by an alkaline deacetylation which leads to varying chitosan preparations depending on process parameters. These preparations consist of a mixture of different chitosan entities with different molecular weight and different fraction of acetylation, which can limit some specific applications. In contrast to this fact chitosan preparations described in the literature or offered on the market are analytically highly undefined. Mostly only a few parameters of the set of possible analytical data characterizing a type of a chitosan preparation are given. For most of the commercial chitosan preparations parameters like weight-averaged molecular weight M_w , polydispersity M_w/M_n , fraction of acetylation F_A , pattern of acetylation P_A and impurity content (protein, heavy metal) are usually not known. To make chitosan preparations sustainable, especially for pharmaceutical applications, it becomes inevitable to obtain a reproducibility of product batches and this requires a reliable characterization of chitosan. Even if this analysis, facing a broad variety of characteristics, remains highly challenging it is indispensable for the above demanded quality standards as well as for a sound hazard assessment analyzing the risks for man and the environment.

Historically, chitosan production is not accompanied by a detailed product analysis. Therefore scientists and applicants barely find well defined products on the market. Typically the obtained products are used as received. As a consequence scientific results are difficult to compare and structure-activity or structure property-relationships can hardly be analyzed. To overcome this deficiency we propose the following procedure to improve the output of chitosan related scientific tests. First, a multi-dimensional experimental investigation is performed that is based on a theoretical analysis of chemical and physical structure variety of chitosan. The analysis allows one to fully describe the sample mixture that depends strongly on origin of the raw precursor chitin and its preparation. Second, the given material is analyzed theoretically to allow for an identification of the variety of chitosan entities which can be all part of one single preparation. Third, drawn conclusions after combination of these steps are used to modify and improve existing production processes (if possible), interpret the effects on biological systems and yield strategies to get more defined products for detailed scientific tests in the future.

Throughout this work we use the nomenclature proposed by the European Chitin Society (EUCHIS).²² Chitin and chitosan will be classified on the basis of their solubility and insolubility in 0.1 M acetic acid. Insoluble material is named chitin, soluble material is defined as chitosan. The different types of acetylation will be expressed as the mole fraction of acetylation F_A . It is given in brackets after every distinct chitosan preparation e.g. a 10% acetylated chitosan A will be written as Chi A [0.1].

Theoretical analysis: T-SAR based analysis of distinct chitosan entities

A powerful tool for the understanding of properties and effects of chemicals is the approach of T-SAR (thinking in terms of structure-activity-relationships). However, T-SAR usually deals with distinct chemical entities which can be described by one or more chemical structural formulas. In contrast, T-SAR used on polymeric chitosan has to deal always with mixtures of different chitosan entities. These entities can differ with respect to their chain-length, the degree of branching, fraction of acetylation (F_A) and pattern of acetylation (P_A). Fig. 1a–f shows different types of chemical entities which all can be part of a distinct chitosan preparation. According to the systematic algorithm²³ to be used in T-SAR to determine physical and chemical properties of a distinct chemical entity the different structural elements of chitosan entities will now be theoretically analyzed.

Completely acetylated chitin [1.0] consists of only one monomer (acetylglucosamine) (Fig. 1a). Its structure is comparable with murein and cellulose, which are main structural polymers creating a part of the cell walls of bacteria (murein) and plants (cellulose). Natural chitin chains consist of several thousands monomers associated with one another by very strong hydrogen-bonds between the amide nitrogen and the amide carbonyl groups of adjacent chains. For deacetylation of the amino group function (chitin), relatively strong reactants (concentrated alkali solutions) have to be applied to remove this less reactive group. If, for instance, all chitin monomers are deacetylated this will yield “ideal” chitosan [0.0], which consists of only glucosamine units (Fig. 1b). Actually chitin and chitosan are both copolymers varying in chain length and F_A (Fig. 1c). Every chitin/chitosan chain possesses a reducing end group (aldehyde function) which is a typical characteristic for sugars (Fig. 1d). The ability of chitosan to dissolve in aqueous media is mainly derived from the protonation of the primary amino group function (Fig. 1e). Occurring charges are one of the main factors for the dissolution process. However, this is constrained by the pK_a of this group ($pK_a \approx 6$ to 6.5). At alkaline conditions the charge inducing protonation disappears which leads to precipitation. Chitin, in contrast, has only a low percentage of free primary amino groups and is therefore not able to establish enough charges for dissolution in aqueous media. In order to transform chitin into chitosan or vice versa a deacetylation or acetylation-process is necessary. Theoretically, this process can lead to different patterns of the remaining acetyl groups at the polymeric chain (Fig. 1f). For the same F_A acetyl groups possessing a well ordered pattern (e.g. deacetylated (D) and acetylated (A) units alternate), a random pattern (e.g. D and A are randomly distributed along the chain) or a blockwise pattern (e.g. all A units can be found in one or more blocks on the chain) is possible. The monomers in chitin and chitosan are connected *via* (1→4) β -glycosidic linkages (Fig. 1g). This β -linkage strongly restricts the chain-mobility in solution. The polymer chain is constrained in its flexibility and therefore chitosan possesses a relatively stiff chain resulting in huge intrinsic viscosity values in comparison to α -linked polysaccharides (e.g. amylose Fig. 1g). Being macromolecules, the appearance of chitin and chitosan can be classified as primary, secondary, tertiary and quaternary structures. The primary structure of chitin and chitosan

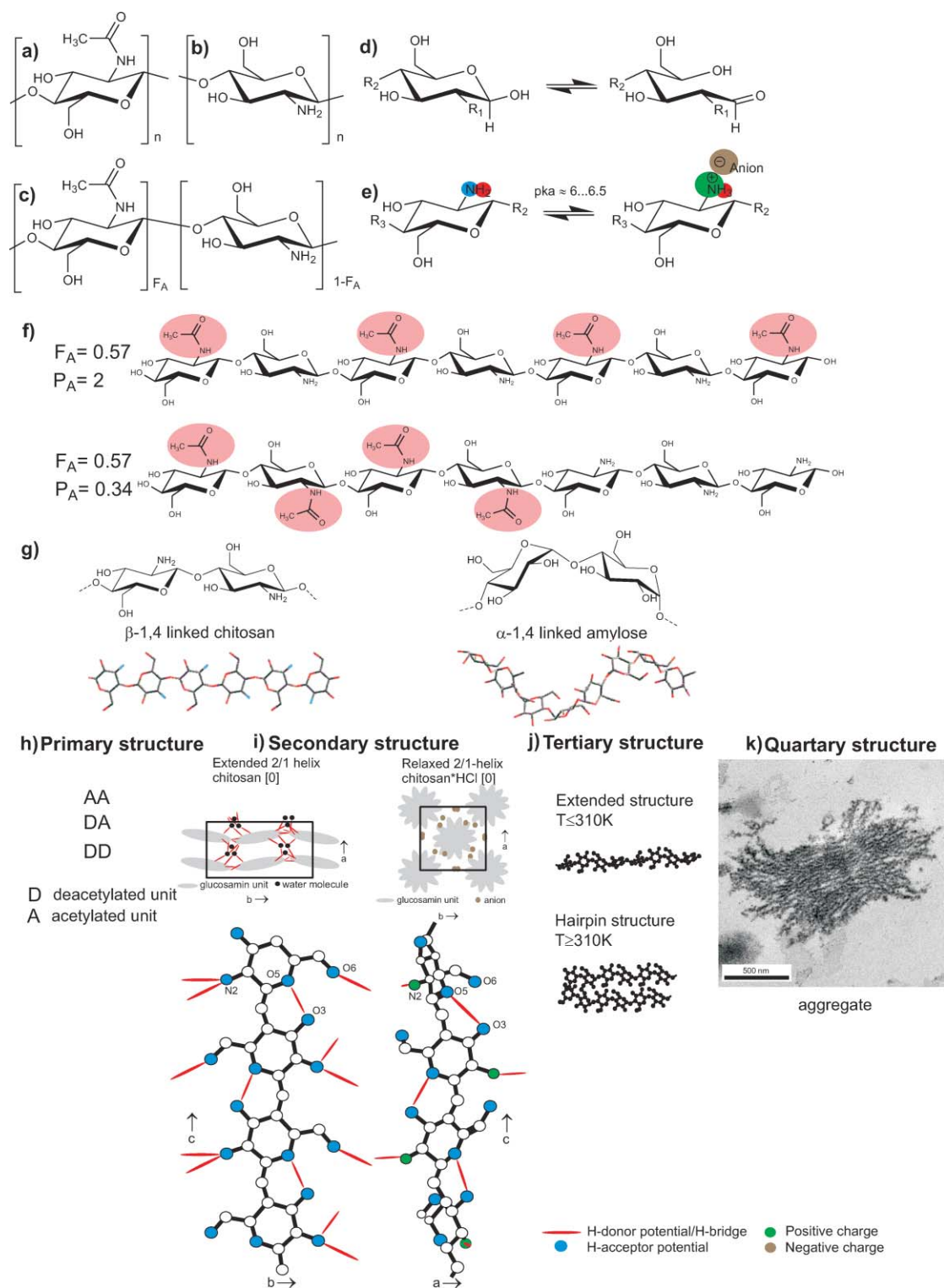


Fig. 1 Chemical structure of polymers chitin [1.0] (a) and chitosan [0.0] (b). Both polymers are partially acetylated and appear as copolymers (c) characterized by an average fraction of acetylation F_A . As sugar derivative chitin and chitosan possess a reducing end group function (aldehyde) (d). The amino group function of a deacetylated glucosamine unit shows a pH-dependent functionality (e). Chitin and chitosan can be distinguished by their pattern of acetylation P_A even at identical F_A (f). Remaining acetyl groups can be oriented in a blockwise, random or well-ordered pattern. Chitin and chitosan are connected *via* 1→4 β -glycosidic linkages which leads to a stiffer chain in comparison to 1→4 α -linked sugars (g). As a macromolecule, chitosan has a primary, secondary, tertiary and a quartary structure (h–k). The sequence of acetylated and deacetylated units determines the primary structure (h). The secondary structure depends on the presence of water, ions (acid) and the inter- and intramolecular hydrogen network (according to Okuyama *et al.*²⁴) (i). A temperature dependent tertiary structure of chitosan was theoretically calculated.²⁵ At 310 K the extended structure changes to a more stable hairpin structure (j). A TEM picture of a quartary structure of chitosan is shown in (k), which is better known as an aggregate.

depends only on the two variable monomers: acetylglucosamine and glucosamine (Fig. 1h). The sequence of these monomers will vary with respect to F_A and P_A . Different secondary structures (Fig. 1i) of solid chitosan crystallites were found by X-ray diffraction (XRD) and differing helical arrangement was revealed in the presence of different anions.²⁶ Chitosan shows an extended 2/1 helical structure, similar to chitin and cellulose. However, after crystallizing chitosan oligomer salts in the presence of different anions (e.g. nitrate, sulfate, chloride) the chain distorts and adopts a relaxed 2/1 helix (Fig. 1i right). This structure is believed to be similar to the structure appearing after dissolution. A calculated tertiary structure was found by Sakajiri *et al.*²⁵ (Fig. 1j). At higher temperatures ($T \geq 310$ K) the extended 2/1 structure changes to a hairpin structure which is still stable even though the temperature was decreased again. The association to an ensemble of many polymers (quartary structure) is forced by intermolecular interactions (Fig. 1k). Here a TEM image of a large chitosan aggregate is shown (Fig. 1k).

Every chitosan preparation shows several of these fundamental properties. Some of them can influence the experimental analysis (solubility, aggregation, polymeric character) and are important to interpret the experimental data in the right way. Other parameters (fraction of acetylation F_A , pattern of acetylation P_A , molecular weight M_w) may influence the effects on organisms more strongly and need to be analyzed before a detailed conclusion can be drawn. Within our approach we correlate physical and chemical properties of six selected chitosan preparations with the effects on two biological test systems. This correlation represents a starting point for a more detailed investigation about the impact of chitosan entities on organisms. Hence, we want to focus on the necessity of a combined theoretical and experimental analysis representing the basis for an improved insight into structure-property and structure-activity relationships of chitosan.

II. Experimental

Material

Chitosan C [0.06] and D [0.13] were purchased from Chipro (Bremen, Germany), chitosan H [0.02] was received from EU-TEC (Emden, Germany), chitosan P [0.03] from Sigma Aldrich (Germany) and chitosan AF [0.09] and AQ [0.11] from Heppe-Medical-Chitosan HMC (Halle, Germany). Sodium chloride, sodium acetate, ethanol, acetic acid anhydride, phosphoric acid (85%), ethylene glycol and acetic acid were obtained from Fluka (Germany). Ammonia (25%) was purchased from Merck KGaA (Germany) and bovine serum albumin [E.C. 9048-46-8] from Sigma Aldrich (Germany). Coomassie Brilliant Blue G-250 was purchased from Servia Biochemica (Heidelberg, Germany). All reagents used were of analytical grade.

Purification of chitosan

Received chitosan preparations did sometimes contain a few percentage of insoluble matter. To get rid of this impurity insoluble matter was removed the following way. Chitosan powder was dissolved in 0.5 M acetic acid (10 g/L) for 24 h. The clear solution was centrifuged for 10 min (3,577 g) with an ultracentrifuge (Heraeus Instruments, Germany) and the

supernatant was filtered through a 0.45 μm cellulose nitrate filter (Sartorius, Germany). The final products were then lyophilized.

Determination of the F_A

The F_A was determined by $^1\text{H-NMR}$ spectroscopy as reported in the past by several working groups. Fig. 2 shows the $^1\text{H-NMR}$ of a chitosan sample with assignments according to Vårum *et al.*²⁷ Chitosan samples were dissolved in $\text{D}_2\text{O}/\text{DCI}$ and the NMR-spectra were recorded on a Bruker AVANCE WB-360 (8.4 Tesla) spectrometer. The F_A values were received by integration of the signals and subsequent calculation. For signal integration two methods were used. The integration method proposed by Hirai *et al.*²⁸ was crosschecked with the method of Vårum *et al.*²⁷ After crosschecking both methods the deviation for the F_A values did not exceed the method inherent deviations of 2% (data not shown). For further F_A determination the more convenient method (measurements at room temperature are possible) according to Hirai *et al.* was chosen.

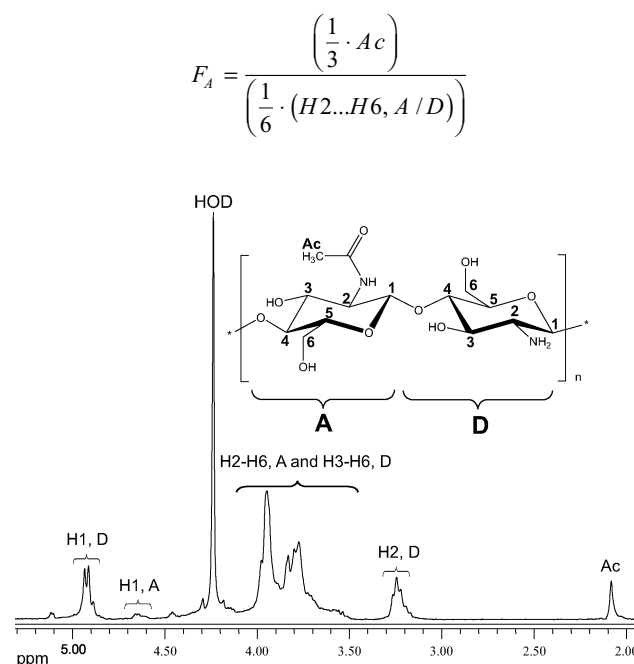


Fig. 2 $^1\text{H-NMR}$ spectrum of Chi D (80 °C). The signals show a chemical shift for a change in the acetylation at the amino group. The H1 of the deacetylated unit (H1,D) appears at 4.9 ppm while H1 in the acetylated glucosamin unit (H1,A) shows a shift to 4.6 ppm. Signals from H2 to H6 (H2–H6,A), (H3–H6,D) overlap between 3.5 and 4.1 ppm, however, H2 of the deacetylated unit (H2,D) can be found well separated at 3.2 ppm. Finally the acetyl protons (Ac) cause a signal at 2.1 ppm.

Determination of the P_A

Chitosan as a copolymer can be characterized by different sequences of the monomers along the chain. The possible patterns chitosan can adopt are alternating, random or block distribution. $^{13}\text{C-NMR}$ data were compared with sequences based on random statistics (Bernoullian model for trial propagation^{29,30}). Fitted $^{13}\text{C-NMR}$ data of degraded samples were used to determine the area of the diad frequencies (F_{AD} , F_{DD} , F_{AA}

and F_{DA}) as shown by Vårum *et al.*²⁷ The signal intensities were compared with a random Bernoullian statistic using the following equation:

$$P_A = \frac{F_{AD}}{(2 \cdot F_{AA}) + F_{AD}} + \frac{F_{AD}}{(2 \cdot F_{DD}) + F_{AD}}$$

The resulting pattern of acetylation P_A values of 0 refers to a completely blockwise, 1 to a completely random and 2 to a completely alternating distribution. Since the diad intensities are obtained by a peak fitting procedure and that the signal to noise ratio in ¹³C-NMR is rather high we set the standard deviation to 10% for this value.

Triple detection size exclusion chromatography (SEC³)

The biopolymer analysis was performed with a triple detection size exclusion chromatography system (SEC³, Viscotek, USA) consisting of an online two channel degasser, a high pressure pump, an autosampler (all parts integrated in the GPCmax, Viscotek, USA), a 0.5 µm stainless steel in-line filter with a nylon membrane, two serially connected ViscoGEL columns (PWXL mixed bed 6–13 µm methacrylate particles, 7.8 × 300 mm), a temperature controlled triple detector array (TDAmx 305, Viscotek, USA) with a differential refractometer at $\lambda = 660$ nm (RID 3580), a right angle (90 °) light scattering detector (RALS) with a semiconductor laser diode at $\lambda = 670$ nm and a four capillary, differential Wheatstone bridge viscometer. The SEC conditions were as follows: a degassed 0.3 M CH₃COOH/0.3 M CH₃COONa buffer (pH = 4.5) with 1% ethylene glycol was used as eluent, the sample concentration was 0.3–1 mg/mL and samples were dissolved for 24 h under shaking, injection volume varied from 10 to 100 µL, flow rate was maintained at 0.7 mL/min, and the column and detector temperature were kept at 30 °C. Before injection, the sample solutions were filtered through a 0.45 µm cellulose nitrate disposable membrane (Sartorius, Germany). To ensure a low light scattering noise level the eluent was filtrated through a 16–40 µm glass filter. A polyethyleneoxide standard ($M_w = 22,411$, $[\eta] = 0.384$ dL/g, $M_w/M_n = 1.03$) was used to normalize the viscometer and the light scattering detector. Data acquisition and processing were carried out by use of OmniSEC 4.1 software (Viscotek Corporation). A dn/dc of 0.163 was used for the M_w calculation³¹ (for more information the reader is referred to the ESI†). The combination of online viscometer and light scattering detector provides essential information on the hydrodynamic size R_h of polymers in solution after employing Einstein's viscosity equation:

$$[\eta] \cdot M_w = \frac{10}{3} \cdot \pi \cdot R_h^3$$

X-ray diffraction

An X'PERT PRO MPD multi purpose diffractometer from PANalytical (Almelo, Netherlands) was used for powder diffraction. A focussing reflexion technique (Bragg-Brentano-geometry) was used for the measuring procedure. Spectra were recorded with Cu K α radiation. A nickel filter, a fixed 0.25°

divergency-aperture and 10 mm broad mask were used in front of the sample. The sample shape was round with 16 mm diameter. Behind the sample a secondary graphite monochromator and a X'Celerator multi-channel-detector from PANalytical (Almelo, Netherlands) were located. The starting value for the diffraction angle was 3° 2 θ and the end value was 65° 2 θ (no signals could be detected after 65°). The step width (integration area) was 0.0167113° 2 θ . The measurement time was 283 sec per grade in continuous mode. Received crystallographic data were viewed and analyzed with brass 2.0.³²

Protein assay

Proteins were determined by the dye-binding assay of Bradford.³³ The dye concentrate was prepared from Coomassie Brilliant Blue G-250 by dissolving 30 mg in 255 mL water, 15 mL ethanol (99%) and 30 mL phosphoric acid (85%). For the micro-plate assay, 20 µg of chitosan solution (10 mg/mL) in 0.5 M HAC was pipetted in micro-plate wells as well as 20 µg bovine serum albumin (BSA) standard solutions (2 mg/mL to 2.5 µg/mL). Fresh prepared dye reagent (80 µg) was added, and the mixture was vigorously shaken immediately. After incubating for 10 min in darkness at room temperature, samples were readout against appropriate solvent-dye blanks at 570 nm. Spectra were evaluated by means of a recording micro-plate reader (Wallac 1420).

Electron microscopy

The transmission electron microscopy (TEM) was performed using a FEI Tecnai F20 STwin at 200 kV in BF-TEM mode offering a point resolution of 0.24 nm. Escherichia coli K12 (DSM 30083) solutions were used for the microscopy experiments. Bacteria cultures were grown in buffered LB media (yeast extract 0.5%, tryptone 1%, NaCl 1%, pH 5.5) over night at 37 °C. 1 mL of this cell suspension was added to 30 mL autoclaved LB media and incubated for 2.5 h. Furthermore, autoclaved Chi D [0.13] dissolved in LB media was added with a final concentration of 1 w%. After 30 min, 3 h and 21 h 1 mL samples were taken. The bacteria cells were conveyed into 4% paraformaldehyde. Additionally they were dehydrated, embedded in SPURRs resin and stained with heavy metal (uranyl and lead) before analysis.

Moisture determination

The moisture content of the samples was determined with a thermogravimetric moisture analyzer MA 45 (Sartorius, Germany). 0.2 up to 0.5 g per sample were used and dried with infrared radiation (5 min, 80 °C) until the weight was stable. The moisture content was calculated from the loss of weight during this treatment and the standard deviation was not higher than 0.5% for the values thus obtained.

ICP-MS analysis

The analyses were carried out by inductively coupled plasma-mass spectrometry (ICP-MS) using a 266 nm frequency-quadrupled Nd:YAG laser (Finnigan UV LaserProbe) coupled to a ThermoFinnigan Element2. Instrument tuning was

repeated daily using a 1 ppb multi-element-solution to obtain a highly stable signal, good peak shape and optimum resolution. Sample flow rate was maintained at 100–200 $\mu\text{L min}^{-1}$. Sample preparation was done in a clean room by microwave assisted decomposition in closed vessels. Used ultrapure grade water was prepared by a MilliQ-water system (more than 18 $\text{M}\Omega\text{ cm}^{-1}$). Ultrapure grade nitric acid was prepared by double distillation with a Cupola Distillation Device from PicoTrace (Bovenden, Germany). Samples were merged with 10 mL HNO_3 (65%) and heated for 15 minutes to 200 $^\circ\text{C}$ in the microwave and finally kept for 15 minutes. Afterwards samples were evaporated to dryness. Residues were dissolved in diluted nitric acid (2 mL HNO_3 + 8 mL ultrapure water) again through microwave-heating. The final solutions were replenished to 25 g with ultrapure water. All sample solutions were stored in acid-cleaned PP vessels. Used stock standard solutions of the measured elements were obtained from Merck (Darmstadt, Germany) and Alfa Aesar (Karlsruhe, Germany).

Chloride determination

Chloride content was measured with a dye producing kit (LCK311, Dr. Lange GmbH (Düsseldorf, Germany)). 1 mL of the chitosan solution (1 mg/mL in 0.5 M HAc) was added to the test tube and shaken. Existing chloride reacted quantitatively with $\text{Hg}(\text{SCN})_2$ to insoluble HgCl_2 , whereas the emerging thiocyanate ions reacted with iron ions to produce the red $\text{Fe}(\text{SCN})_3$ compound. After 3 min the resulting dye was detected with a CADAS200 UV-VIS spectrometer (Dr. Lange) at 468 nm. The chloride content could be determined by the linear relationship to the absorbance.

Luminescent bacteria acute toxicity test

The toxicity tests with the luminescent bacterium *V. fischeri* were conducted using the test kit LCK 482 from Dr. Lange. The 30 min standard bioluminescence inhibition assay was carried out according to a modified DIN EN ISO 11348–2 test protocol. Stock solutions of all samples were prepared (pH 7.0, including 2% NaCl). The pH values were checked, because the pH tolerance of *V. fischeri* covers a range from 6–8. Deviations from this range can lead to a pH related luminescence inhibition. All concentrated stock solutions were prepared in deionised water at least 12 hours before testing and stirred thoroughly. To cover a broad range of concentrations and to get complete concentration response curves we used dilution steps from 0.5 to 0.01 w%. The complete assay (including the preparation of the bacteria as well as the dilution of the test samples)

was performed at 15 $^\circ\text{C}$ using thermostats (LUMIStherm, Dr. Lange). The test kit contained liquid-dried bacteria which were rehydrated according to the test protocol with the corresponding reactivation solution for 15 min. In the next step 500 μL aliquots of this bacteria suspension were preincubated again for 15 min at 15 $^\circ\text{C}$. After measuring the initial luminescence with a luminometer (LUMIStox 300, Dr. Lange), 500 μL of the diluted samples were added to each 500 μL aliquot of the bacterial suspension. After an incubation period of 30 min at 15 $^\circ\text{C}$ the final bioluminescence was measured. The relative toxicity of the samples was expressed as percentage inhibition compared to a nontoxic control (bacterial suspension with 2% NaCl solution). Positive controls (7.5% NaCl solutions) were measured within every assay to ensure a constant quality of the test data. Tests were carried out at least twice.

III. Results and discussion

Physico-chemical characterization of chitosan preparations

First, the different chitosan preparations were analyzed to receive information about their physico-chemical characteristics (Table 1). Six samples were selected to represent the variety of chitosan preparations and were divided into two subgroups. The first three (Table 1) had a comparable F_A of about 0.05 but with different M_w . The M_w increased from 170 kg/mol (Chi C) to 310 (Chi P). The second group had a F_A of about 0.10 and molecular weights from 151 (Chi AF) to 611 (Chi AQ) (Table 1). Not only chitosan made from crab chitin (α -chitin) was used but also chitosan from squid pen (β -chitin) was investigated (Chi H). As expected, different commercial samples showed a big variety in M_w ranging from 151 kg/mol to 611 kg/mol. Rephrasing this description, the degree of polymerization (DP) of several hundreds of (acetyl)-glucosamine units (Chi C) increases to several thousand (Chi AQ). We must note that all samples showed a rather broad molecular weight distribution (M_w/M_N) of more than 2.2 (Table 1). Hence, in the smallest preparation one can also find molecules with a DP of up to 100 while the largest preparation includes a DP of up to 7,000.

The results for the pattern analysis P_A showed slight differences between different chitosan preparations. All values are found to be between 0.5 and 1, which indicates a random-dominated pattern of the acetyl groups. The lowest value of 0.57 ± 0.1 was found for preparation H, which is considered as random-dominated pattern but with increasing block character. Only when the value drops below 0.5 one can consider the pattern as block-dominated. A completely blockwise pattern is present if the value becomes zero. Although all chitosan

Table 1 Physico-chemical parameters of different chitosan preparations. M_w —weight averaged molecular weight, M_N —number averaged molecular weight, M_w/M_N —polydispersity, $[\eta]$ —intrinsic viscosity, R_h —hydrodynamic radius, DP_w —degree of polymerization, F_A —fraction of acetylation, P_A —pattern of acetylation

Chitosan preparation	Origin	M_w [kg/mol]	M_N [kg/mol]	M_w/M_N	$[\eta]$ [mL/g]	R_h [nm]	DP_w	F_A	P_A
Chitosan C	crab	170 \pm 2.3%	53	3.2	314	18.2	1018	0.06	0.81
Chitosan H	squid	286 \pm 8.3%	88	3.3	510	25.8	1723	0.02	0.57
Chitosan P	crab	310 \pm 0.9%	131	2.4	670	29.8	1879	0.03	0.78
Chitosan AF	crab	151 \pm 2.0%	56	2.7	334	18.3	935	0.09	0.60
Chitosan D	crab	159 \pm 3.3%	54	2.9	358	18.9	922	0.13	0.96
Chitosan AQ	crab	611 \pm 6.6%	288	2.2	1214	46.4	3546	0.11	0.87

preparations are made from different sources of chitin, no significant impact on the P_A could be found. It seems unimportant for the P_A whether the chitin crystallites are present as α - or β -chitin in the heterogeneous production process. Furthermore production processes accompanied by more or less hydrolysis also yield in a random pattern product. That means for deacetylation routes, which yield target F_A values of 0.13 or lower, the pattern seems to adopt a random-dominated pattern. However, we studied only samples with F_A values lower than 0.13. For a clear general prediction high acetylated chitosan preparations also need to be measured in the future.

The investigated samples were all produced by means of the heterogeneous deacetylation using solid chitin particles in strong hot alkali solutions. Alternatively, it is also possible to dissolve chitin in NaOH solution under certain conditions followed by subsequent heating for ambient time. This different route is known as the homogeneous deacetylation. On the one hand our results are in contrast to findings of Kurita and coworkers,³⁴ who claimed that chitosan prepared by a heterogenous deacetylation should give block-type copolymers while the homogeneous process should yield random-type copolymers. On the other hand we confirmed observations seen by Vårum as well as Sashiwa and coworkers.^{27,35,36} They also found only random pattern polymers for a limited pool of heterogeneously and homogeneously produced samples. In the past, different patterns were often used to explain water solubility and swelling behavior even if the existence of blockwise chitosan could not be proven. Whether this pattern explains these macroscopic effects and what else has to be taken into account will be shown in the section "Impurities of chitosan preparations".

Conformational analysis

The intrinsic viscosity $[\eta]$ measured in a specific solvent is related to M_w by the Mark-Houwink equation

$$[\eta] = K \cdot M^a$$

The so-called Mark-Houwink constants (K) and (a) depend upon the type of polymer, solvent and the temperature used during the viscosity measurement. The plot of $\log [\eta]$ vs. $\log M_w$ usually gives a straight line with slope (a) and intercept (K). The slope (a) can vary from 0 (compact sphere) over 0.65–0.85 (random coil) to 1.8 (very stiff chain) revealing information about the polymer conformation in solution. Conformational plots (Mark-Houwink-plot) were made for every chitosan preparation (Fig. 3). Molecular weight as well as $[\eta]$ were determined simultaneously during a chromatographic run for the polydisperse samples. As already shown by Weinhold *et al.*³⁷ the conformational plots revealed lines with a strong curvature and a decreasing slope for increasing molecular weight. Chitosan with a small molecular weight showed a greater slope (1.1 to 0.95) compared to medium sized chitosan (0.95 to 0.75), the smallest slope was found for large sized chitosan (0.75 to 0.4). However, the plots are not identical for different chitosan preparations. Up to a molecular weight of 170 kDa all plots show a similar behavior and a very high slope. For the higher molecular weight preparations Chi C, AF and D decrease in $[\eta]$ more strongly than Chi H, P and AQ. The preparation with the lowest decrease is Chi AQ and the one with the highest

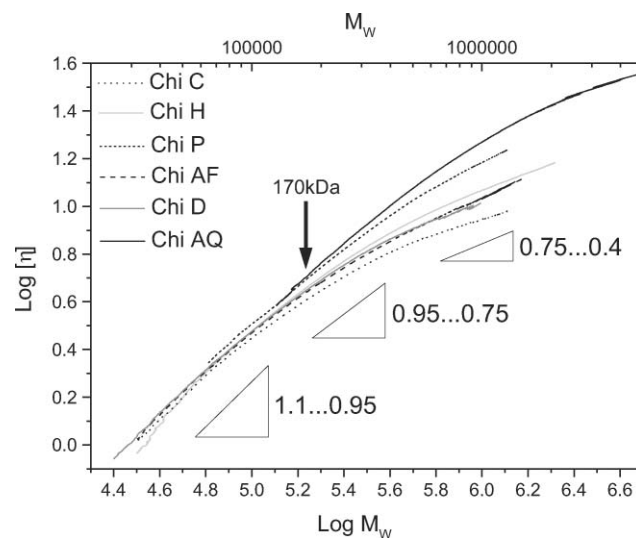


Fig. 3 Mark-Houwink-plot for all six different chitosan preparations. The plots of chitosan C (dotted black), H (light grey), P (small dashed black), AF (dashed black), D (grey) and AQ (black) show a similar behavior: decreasing slope with increasing M_w . This slight curvature leads to a more random coil behavior of high molecular weight chitosans (slope 0.4 to 0.75) while low molecular weight chitosans possess a relatively stiff chain (slope 0.75 to 1.1).

decrease is Chi C. The sagging of the curve shows a relation to the M_w of these polydisperse samples resulting in a stronger decrease for smaller M_w and a weaker decrease for high M_w . The analysis reveals that different chitosan entities coil in a different way in solution. This coiling of chitosan does not change stepwise or at a certain point, it is rather a continuous change over the whole molecular weight range. This means that large sized chitosan provides a more random-coiled/spherical structure while smaller sized chitosan possesses a stiffer chain and appears more wormlike. It is an expected behavior for semi-stiff polymer chains which derives from the non-Gaussian behavior of short wormlike chains and Gaussian behavior of large flexible chains in solution. These considerations explain quite well the continuous change of the slope in the M-H plot for chitosan when a wide range of molar masses is explored. Previous publications dealing with conformational analysis of chitosan used only a limited range of molar masses. Therefore only short extracts of the M-H plot were received with almost linear behavior. Published (K) and (a) values differ significantly in the literature depending on their explored molecular mass range. The observed non-linearity leads to a continuous change of (K) and (a) values and therefore to a loss of their "constant character". This means that the accepted procedure to determine the molecular weight of chitosan by using the M-H equation, published (K) and (a) values and viscosity data from experiments can not be applied if an accurate molecular weight determination is required. This is of even more importance when this conformational transition behaves different for different chitosan preparations as shown for the investigated samples. Without changes of the chemical environment it is not easy to understand the difference in the intrinsic viscosity for one distinct molecular weight fraction. Compact aggregates, which are known to have rather high molecular weights combined with a low viscosity, were not present during the analysis. Shoulders or double peaks

in the light scattering signals due to the presence of aggregates could not be observed. Another indication for the decrease of $[\eta]$ with increasing M_w can be the presence of a branched chain. Branching reduces the R_h of a polymer and therefore also the intrinsic viscosity without a decrease in the molecular weight. Although chitin is known to be a linear polymer, the reaction conditions used (strong alkali, high temperature) to get to chitosan are not very gentle. If, for instance, the reaction conditions are appropriate for a strong hydrolysis they may also be appropriate for cross-linking reactions. This will lead to an earlier decrease in the Mark-Houwink plot for a high molecular weight chitosan, as shown in Fig. 3. However, to prove this branching hypothesis, further investigations are required.

Impurities of chitosan preparations

Especially marine organisms can be contaminated by heavy metals depending of the area and the mechanism of accumulation in target species. To be sure about the purity of the preparation used in biological tests and for pharmaceutical uses in general, heavy metal contents were determined for every chitosan preparation. Along with cadmium and arsenic concentrations (which are typically tested) we also analyzed the most common heavy metals (see Fig. 4 for details). The overall heavy metal content revealed big differences for the analyzed preparation. While cadmium and arsenic, known as two of the most cytotoxic heavy metals, could only be found in trace amounts, noteworthy amounts of chromium, nickel and copper could be detected. The detected concentrations varied strongly between individual samples (Fig. 4). Significant amounts of chromium (Chi C 33.1 mg/kg, Chi P 16 mg/kg, Chi AF 11.7 mg/kg, Chi D 12.5 mg/kg), copper (Chi H 134.2 mg/kg, Chi AF 17.2 mg/kg), nickel (Chi C 11.9 mg/kg, Chi P 13.1 mg/kg) and zinc (Chi H 14.4 mg/kg, Chi AF 38 mg/kg) were found in the mentioned samples. Surprisingly, preparation H showed a very high value of copper which already manifested in the light green appearance of these grains. According to information of the manufacturer tap water in contrast to deionized water was used to remove alkali residues from the freshly deacetylated product. This treatment combined with the ability of chitosan to bind metal ions by complexation obviously may cause the accumulation of copper in the product. This indicates that not only the selection of natural sources can influence the heavy-metal content but also the steps of preparing a distinct chitosan type need to be considered.

Heavy metal impurity of chitosan is just one important parameter which limits its application for medical purposes. Other important impurities like protein and ash content were

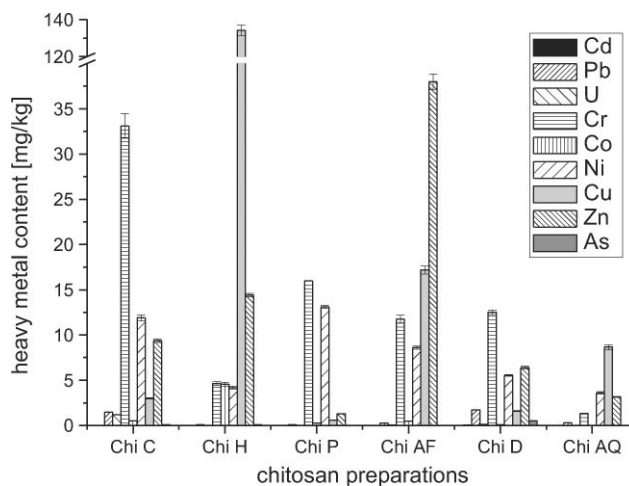


Fig. 4 Heavy metal content of different chitosan preparations. Cadmium and arsenic were only found in trace amounts. However, significant amounts of chromium (Chi C 33.1 mg/kg, Chi P 16 mg/kg, Chi AF 11.7 mg/kg, Chi D 12.5 mg/kg), copper (Chi H 134.2 mg/kg, Chi AF 17.2 mg/kg), nickel (Chi C 11.9 mg/kg, Chi P 13.1 mg/kg) and zinc (Chi H 14.4 mg/kg, Chi AF 38 mg/kg) were found in the samples.

also determined as well as moisture and chloride content (Table 2). Furthermore the solubility in water (pH = 7), as a necessary criterion for several biological and medical assays, and the solubility in diluted acetic acid (0.5 M) was checked (Table 2). Although the production process for chitosan uses strong alkali/acidic media residual protein was found in all samples ranging from 0.7 to 1.9% (Table 2). In general, the production processes applied for the preparations analyzed within this study were able to minimize the protein content of the product but were not able to remove protein traces completely. Ash contents ranged from 0.3 to 1% indicating a very low level of inorganic impurities/residuals in every preparation. A strong difference was found with respect to the chloride content of the samples. While the investigation of Chi C, H, P and AQ preparation revealed just trace amounts, a rather high value of chloride was found for Chi D. Furthermore Chi D was the only preparation which showed, against the usual theory, water solubility at a pH of 7. The fact that the pH of the water decreased after dissolution to 4.5 indicates the presence of acid residue in this specific sample. This is known for chitosan derivatives like the salt chitosan*HCl, which shows solubility in water, in contrast to chitosan. Combining the high chloride content and the acidic character of this chitosan preparation a clear evidence was found for the presence of chitosan*HCl. The solubility of the other samples was limited to acetic acid only (Table 2). No

Table 2 Impurity contents and solubility of different chitosan preparations. Water solubility was monitored in neutral water (pH = 7) merged with solid chitosan. After 24 h the pH was measured again. Chloride content is given in mg per gram chitosan

Chitosan preparation	Protein [%]	Ash [%]	Moisture [%]	Cl ⁻ [mg]	Solubility in H ₂ O (pH = 7)	Solubility in 0.5 M HAc (pH = 2)
Chitosan C	1.0	1.0	9.3	4.4	–	(pH = 7.8) +
Chitosan H	1.0	0.5	2.9	3.0	–	(pH = 8.3) +
Chitosan P	0.9	0.3	10.2	0.7	–	(pH = 7.6) +
Chitosan AF	1.8	n.d.	3.5	1.9	–	(pH = 7.9) +
Chitosan D	0.7	0.5	10.1	135.9	+	(pH = 4.5) +
Chitosan AQ	1.9	n.d.	9.5	9.0	–	(pH = 8.1) +

clear correlation could be found when comparing the solubility results with the P_A values (Table 1 and 2). All acid-soluble samples possess a random-dominated pattern also comprising the water-soluble preparation. Thus, a random pattern seems not to be the prerequisite for water solubility. However, in cases where this random-pattern polymer chain exists as a salt, water solubility is enabled. This conclusion becomes clear if the different crystalline structures of chitosan and chitosan*HCl are considered (Fig. 1h). The structure of chitosan*HCl is stabilized by less intramolecular hydrogen bonds due to the distortion of the chain. Together with occurring charges at the amino group and the presence of anions in the unit cell, intermolecular hydrogen bonds are also reduced. Combining this weaker crystalline form with the present negative and positive charges enhances the penetration by polar media like water. This is believed to be the explanation for the different solubility of different chitosan preparations.

Crystallinity

X-ray diffraction (XRD) measurements on different chitosan preparations revealed three major signals as expected from previous studies³⁸ (Fig. 5). Chitosan C, H, P and AF showed a very similar scattering behavior with more or less pronounced peaks at 11° , 20° and 22° and only slight changes in the overall scattering intensity between every preparation. In contrast, the scattering intensity of Chi D*HCl is greatly reduced and no clear reflection spots could be observed. Apparently, no influence of the F_A or the M_w on the scattering intensity or peak positions could be found. Although broad signals are already an indication for semi-crystalline material, Chi D contains even less crystalline domains than other samples according to the scattering intensity. However, we do not want to overestimate the decrease of scattering intensity since this can also be influenced by slight differences in the sample preparation.

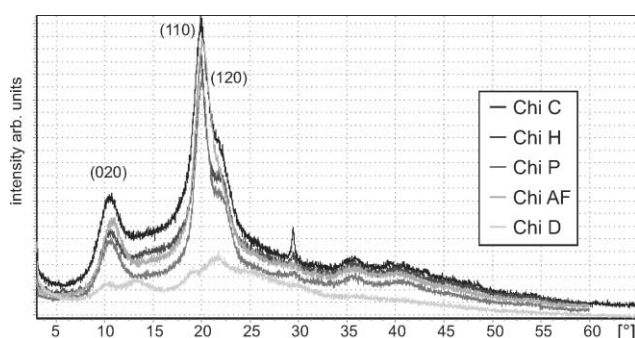


Fig. 5 Five different diffractograms of Chi C (black), H (dark grey), P (grey), AF (bright grey) and D (very bright grey). All samples are semi-crystalline with rather broad reflection spots. Chi C, H, P, AF show a very similar scattering behavior while the intensity of Chi D shows a strong decrease.

Similar XRD experiments were done by Kurita and Aiba and coworkers.^{34,39} They proposed that different scattering behaviors must be related to different patterns of acetylation for a pool of differently acetylated chitosan preparations (homogeneously and heterogeneously produced). In order to verify these results we measured the P_A by a separate method and compared it to our XRD results. Found P_A values could neither be correlated to any scattering intensity nor resulted in significant peak shifts. Samples with rather different P_A values (Chi C, H, AF) based on the NMR method showed very similar scattering behavior. That means the impact on diffraction behavior could in our case not be deduced from the pattern of acetylation.

Biological effects

Based on our analytical data, chitosan preparation D [0.13] was chosen for further biological tests mainly based on its good water solubility. Furthermore it had low contents of protein and heavy metals to avoid any possible impact on bacteria. Additionally, to fulfill sterile conditions the used chitosan preparation was autoclaved before testing in the growth assay of *E. coli*. After this treatment physico-chemical parameters were again analyzed and differences in comparison to an untreated sample are summed up in Table 3.

A culture of *E. coli* bacteria was incubated with a 1 w% solution of Chi D [0.13] and TEM photographs were taken after 30 min, 3 h and 21 h (see Fig. 6). The presence of Chi D [0.13] showed a change in cell morphology depending on incubation time. Firstly, up to 70 nm large blebs occurred upon the cell surface after 30 min (Fig. 6b-I). Secondly, blebs were still present accompanied with a loss of integrity in the bacteria cell membrane (Fig. 6c and c-I). The cells started to deform and some of the cytoplasm were missing due to membrane damage (Fig. 6c-II). After 21 h incubation time this effect increased and only a few cells could be found in the sample which had not been fragmented. In particular cell membranes were destroyed (Fig. 6d-I) and the cells lost their plasmatic content. The origin of this appearance can be deduced from two facts. It is possible that blebs are fragments of the cell membrane produced by the cell as a reaction on the chitosan treatment. The second possibility is that blebs themselves may consist of pure chitosan. In this case it is difficult to clear up this observation because membrane fragments as well as chitosan were both heavy metal labeled for the visualization in TEM. However, the chitosan preparation used has average hydrodynamic diameters of ca. 30 nm or even more if the polydispersity of this sample is considered. This size, which is in the order of magnitude of the bleb size, argues for chitosan consisting blebs. An aggregation (compare Fig. 1k) or association on the cell surface of several chitosan chains may produce such blebs if the incubation time is appropriate. The appearing blebs indicate a molecular interaction of chitosan at the cell surface which finally leads to

Table 3 Changes of the physico-chemical parameters before and after autoclaving of a chitosan solution

Chitosan preparation	Origin		M_w [kg/mol]	M_n [kg/mol]	M_w/M_n	$[\eta]$ [mL/g]	R_h [nm]	DP_w	F_A	P_A
Chitosan D	untreated	crab	$159 \pm 3.3\%$	54	2.9	358	18.9	922	0.13	0.96
Chitosan D	autoclaved	crab	$91 \pm 0.3\%$	35	2.6	210	12.9	525	0.13	0.96

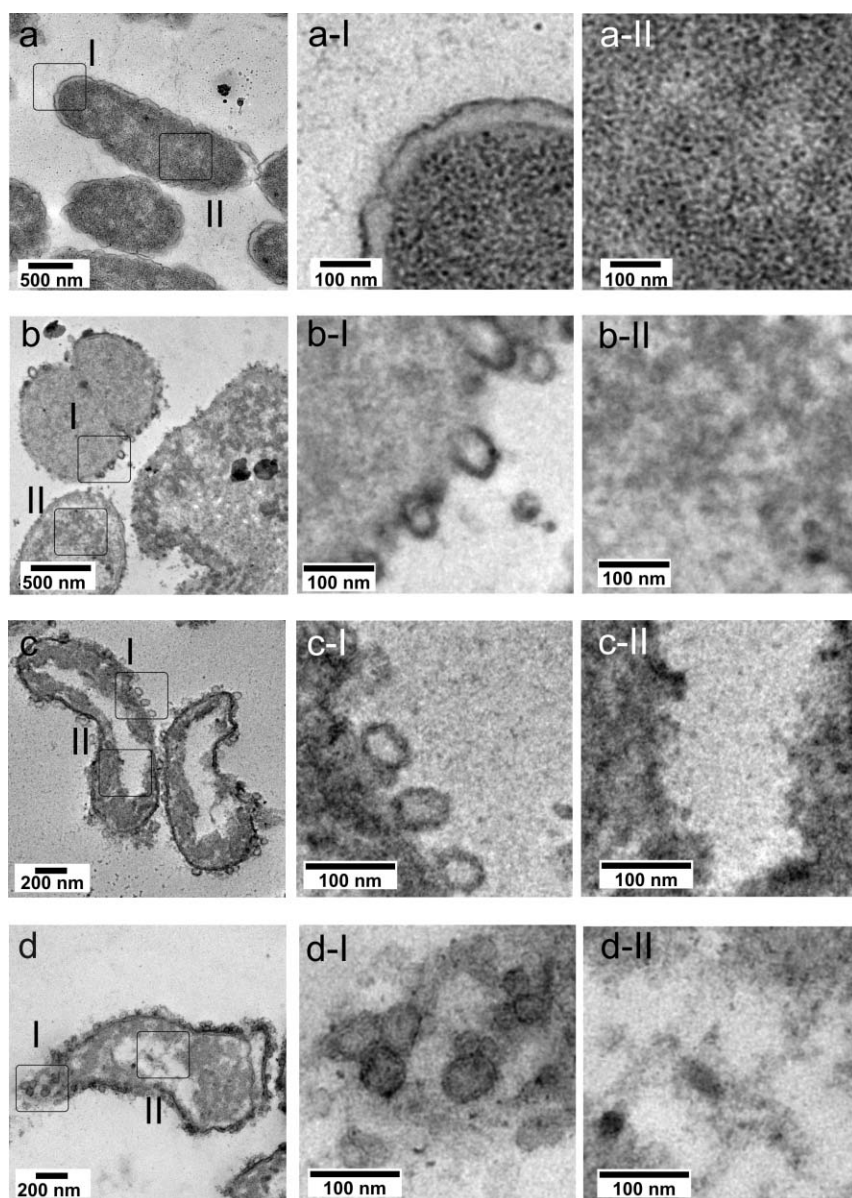


Fig. 6 TEM images of different bacteria cultures (*E. coli* K 12). The control sample (a) is compared to a sample treated for 30 min (b), 3 h (c) and 21 h (d) with 1 w% chitosan D. Already after 30 min blebs of up to 70 nm diameter are appearing on the cell membrane surface. The number of blebs multiplies drastically with time and disintegration of the cell membranes connected to death of the cells could be monitored for longer incubation times.

a destruction of the membrane structure and consequently to cell death. Therefore deformation and death of the cells can be directly correlated to the exposition to chitosan entities. Possible side-effects of chitosan by-products can be clearly excluded due to the examined purity of preparation D.

The bioluminescence inhibition assay of *Vibrio fischeri* exhibited a comparable effect. This result was similar to that one found in growth inhibition assays performed with *E. coli* cells (data not shown). The luminescence decreases with increasing concentration of Chi D [0.13] (Fig. 7). At a concentration of only 0.5 w% the luminescence was inhibited up to 80%. Already at a concentration of about 0.035 w% the inhibition reached the half maximal inhibitory concentration value (IC_{50}). While 1 w% of Chi D [0.13] resulted in a disintegration of cell wall

and membrane of *E. coli* cells the results obtained for *V. fischeri* showed that the effect on this bacteria started already at a 100 fold lower dose.

The shown bacteria tests revealed a large difference in the effective concentration. This can be a critical point with respect to ecotoxicological effects, if chitosan is used as “anti-microbial agent” for agricultural applications (e.g. soil additive, seed/leaf coating). Up to now it is unknown to what extent the ecosystem in the soil or on plants is unbalanced by the use of chitosan. As long as the molecular mechanisms of the toxic effects of chitosan entities are not analyzed and elucidated a general use of chitosan as anti-microbial agent is not recommended.

The tested preparation with a mean molecular weight of 91 kg/mol and F_A of 0.13 showed remarkable effects on these

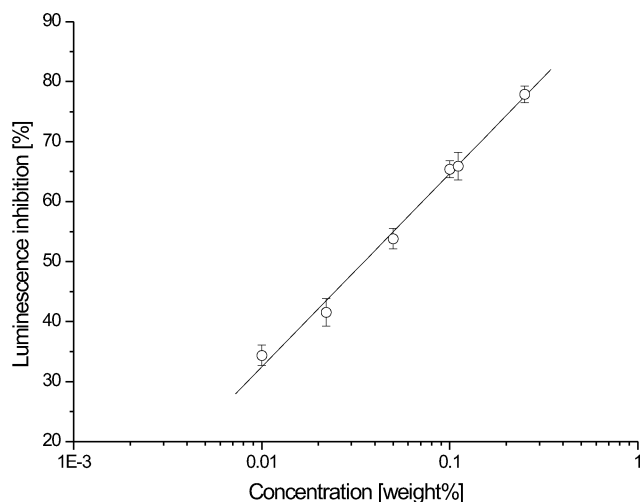


Fig. 7 Plot of luminescence inhibition of *Vibrio fischeri* in percent versus the concentration of chitosan in weight percent. The half maximal inhibitory concentration IC_{50} could be found at 0.035 w%.

two bacteria, however, this does not especially mean that this mean molecular weight is responsible for these effects. Due to the polydispersity of the sample it also contains *ca.* 2% of molecular weights higher than 600 kg/mol, *ca.* 7% higher than 300 kg/mol and *ca.* 15% with a smaller weight than 16 kg/mol. While small chitosan entities may show a different mode of action (*e.g.* uptake in the cell) large molecular weights may behave completely different (*e.g.* bleb formation). Although this sample was thoroughly analyzed the observed effects can not be ascribed to one specific structure. This means that typical commercial samples are not suitable for a detailed investigation without any refinement. In order to refine these samples a fractionation of this sample is necessary to obtain different molecular weight fractions with low polydispersity indexes, which we intend to show in the future. After this refinement, sample quality will reach the level at which structure-activity questions are feasible and can be answered precisely.

IV. Conclusion

An essential need for a systematic and standardized multi-dimensional analysis of chitosan was clearly demonstrated investigating six examples of different chitosan preparations. These preparations varied drastically in almost all characteristics determined, which may be exemplary for commercial chitosan preparations in general. Our findings reveal a variety of composition as well as properties of different chitosan preparations. It becomes obvious that it is difficult or even impossible to obtain identical chitosan preparations when different batches of raw materials are used or the parameters of production are not well known. Although the production has been known for decades, sample qualities do not fulfill the requirements for a structure-activity investigation without refinement. The application of a multi-dimensional analysis can avoid flaws during production and is a necessary approach to enable a structure-activity investigation in chitosan research. Our multi-dimensional analysis enabled interesting correlation between different physico-chemical parameters. Characteristics like M_w and F_A change with no relation to the source or the P_A . All

samples showed a random-pattern regardless of high or low molecular weight and F_A . All preparations showed a molecular-weight-dependent change in conformation from a stiff chain to a more compact structure, however, the transition to a more compact structure varied between different samples. As a consequence, the accepted procedure to determine the molecular weight of chitosan by using the M-H equation, published (K) and (a) values and viscosity data from experiments can not be applied if an accurate molecular weight determination is required. Solubility behavior of a chitosan preparation could be deduced and explained by combining different methods. It was found that the occurrence of chitosan*HCl enabled water solubility (pH = 7), while chitosan without HCl were only soluble in acetic acid. The P_A showed no impact on this behavior despite assumptions to the contrary. Even chloride-free random pattern chitosan preparations showed no water solubility. The biological effects on different bacteria revealed fast effects (30 min) on *E. coli* and also decreased the bioluminescence of *V. fischeri* (IC_{50} = 0.035 w%).

We want to point out that the use of chitosan is based on renewable alternative feedstock and its flexible field of applications can be build up to a portfolio of green and sustainable chemical products that can dominate future world markets. However, depending on the application or the expected effect of a chitosan preparation the used data basis should be as broad as possible. Only one analytical method is not enough for a full characterization of this challenging macromolecule. Nevertheless, without determining important parameters the future of chitosan to become a market-ready product will end before it could have started. By the application of the T-SAR guided multidimensional analysis it will be possible to modify several parameters in further research. An increase in more specific information about molecular characteristics in correlation with biological activity of chitosan can open up more fields for new applications and facilitates chemical-customizing for already existing applications. This analysis kit is considered to be a necessary approach on the way to biodegradable products made from environmentally benign chemicals.

Acknowledgements

We would like to acknowledge the following people for contributions to this paper: Heike Anders for heavy metal quantification, Dr. Johannes Birkenstock for XRD measurements, Dr. Wolfgang Lindenthal for the gift of chitosan and Johannes Stelten for his valuable advice concerning NMR.

References

- 1 R. Muzzarelli, M. Weckx, O. Filippini and F. Signon, *Carbohydrate Polymers*, 1989, **11**, 293–306.
- 2 R. Muzzarelli, *Carbohydrate Polymers*, 1985, **5**, 85–89.
- 3 R. Muzzarelli, *Carbohydrate Polymers*, 1996, **29**, 309–316.
- 4 M. Sugano, S. Watanabe, A. Kishi, M. Izume and A. Ohtakara, *Lipids*, 1988, **23**, 187.
- 5 V. Vijayanathan, T. Thomas and J. Thomas, *Biochemistry*, 2002, **41**, 14085–14094.
- 6 A. Niekraszewicz, *Fibres and Textiles in Eastern Europe*, 2005, **13**, 16–18.

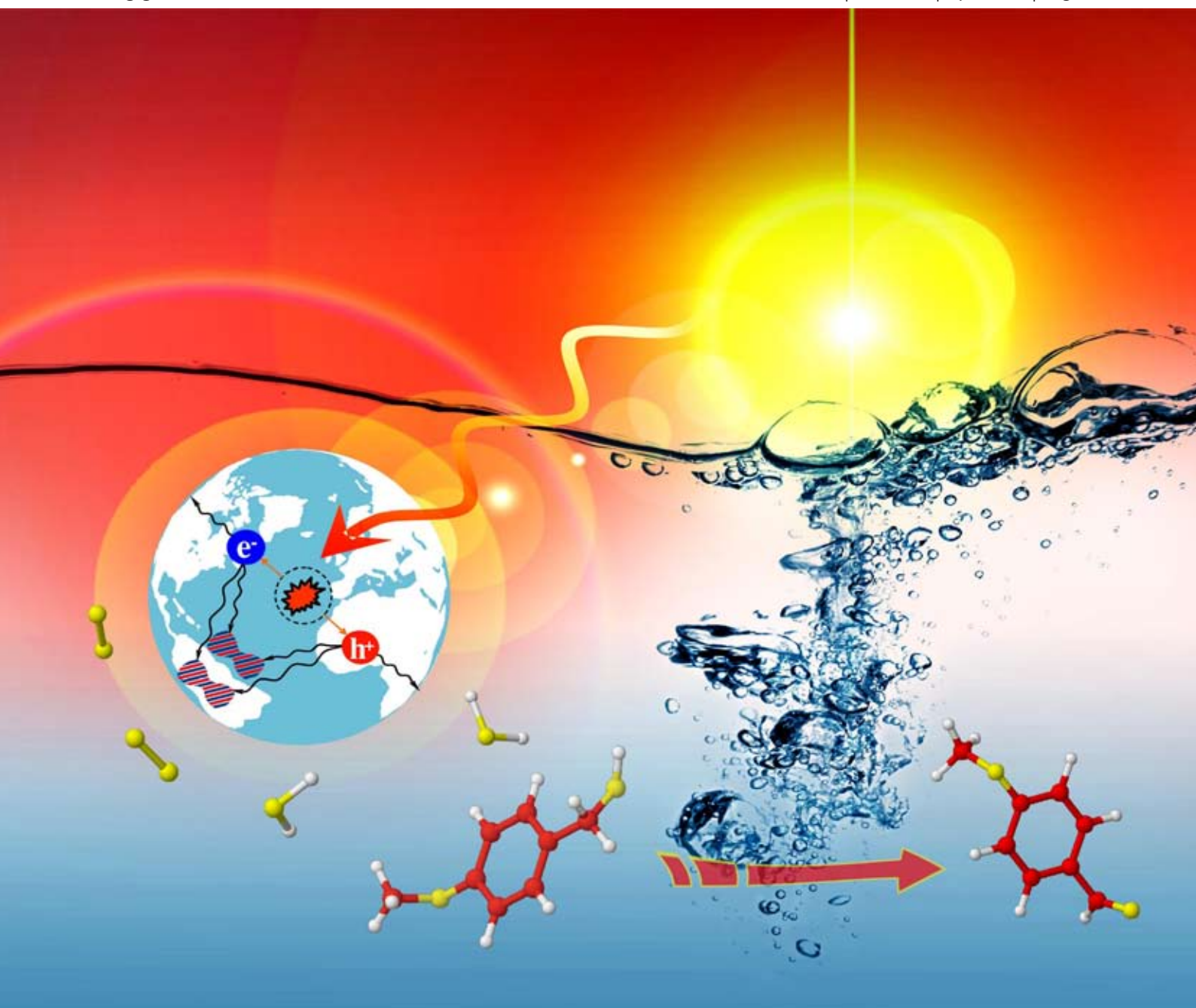
- 7 H. Liu, J. Mao, K. Yao, G. Yang, L. Cui and Y. Cao, *Journal of Biomaterials Science*, 2004, **15**, 25–40.
- 8 R. Muzzarelli, G. Biagini, A. DeBenedittis, P. Mengucci, G. Manjini and G. Tosi, *Carbohydrate Polymers*, 2001, **45**, 35–41.
- 9 P. Vander, K. Vårum, A. Domard, N. E. Gueddari and B. Moerschbacher, *Plant. Physiol.*, 1998, **118**, 1353.
- 10 S. Hirano, C. Itakura, H. Seino, Y. Akiyama, I. Nonaka, N. Kanbara and T. Kawakami, *J. Agric. Food Chem.*, 1990, **38**, 1214–1217.
- 11 K. Turnblad and Y. Chen, Patent 5876739, 1999.
- 12 E.-M. Decker, C. von Ohle, R. Weiger, I. Wiech and M. Brex, *Journal of Periodontal Research*, 2005, **40**, 373–377.
- 13 A. Vila, A. Sanchez, M. Tobio, P. Calvo and M. Alonso, *J. Controlled Release*, 2002, **78**, 15.
- 14 D. Kweon, S. Song and Y. Park, *Biomaterials*, 2003, **24**, 1595–1601.
- 15 R. Torsi, R. M. C. Guznian and C. Pruzzo, *J. Dent. Res.*, 1997, **76**, 665–672.
- 16 R. Kroepke, W. Lindemann and Beiersdorf AG, *EU Patent 1438954*, 2003.
- 17 <http://www.un.org/esa/sustdev/agenda21.htm>.
- 18 P. T. Anastas, and J. C. Warner, *Green Chemistry Theory and Practice*, Oxford University Press, New York, 1998.
- 19 A. Domard and M. Domard, *Polymeric Biomaterials*, Vol. 9, Basel, New York, 2002.
- 20 S. Hirano, H. Seino, Y. Akiyama and I. Nonaka, *Polym. Mater. Sci. Eng.*, 1988, **59**, 897.
- 21 K. Lee, W. Ha and W. Park, *Biomaterials*, 1995, **16**, 1211.
- 22 G. A. F. Roberts, *Advances in Chitin Science*, 2007, **10**, 3–10.
- 23 B. Jastorff, R. Störmann and U. Wölcke, *Struktur-Wirkungs-Denken in der Chemie-eine Chance für mehr Nachhaltigkeit*, Aschenbeck und Isensee Universitätsverlag Oldenburg, 2003.
- 24 K. Okuyama, K. Noguchi, M. Kanenari, T. Egawa, K. Osawa and K. Ogawa, *Carbohydrate Polymers*, 2000, **41**, 237–247.
- 25 T. Sakajiri, T. Kikuchi, I. Simon, K. Uchida, T. Yamamura, T. Ishii and H. Yajima, *Journal of Molecular Structure: THEOCHEM*, 2006, **764**, 133–140.
- 26 K. Ogawa, T. Yui and K. Okuyamac, *International Journal of Biological Macromolecules*, 2004, **34**, 1–8.
- 27 K. Vårum, M. Anthonsen, H. Grasdalen and D. Smidsrød, *Carbohydrate Research*, 1991, **211**, 17–23.
- 28 A. Hirai, H. Odani and A. Nakajima, *Polym. Bull.*, 1991, **26**, 87.
- 29 A. Mireau and P. Bovey, *NMR of Polymers*, Academic press, San Diego, 1996.
- 30 A. Mireau, *A practical guide to understanding the NMR of Polymers*, Academic press, New Jersey, 2005.
- 31 M. Rinaudo, M. Milas and P. Dung, *Int. J. Biol. Macromol.*, 1993, **15**, 281–285.
- 32 J. Birkenstock, R. Fischer and T. Messner, Brass 1.0 beta: The bremen rietveld analysis and structure suite, 2003.
- 33 M. M. Bradford, *Anal. Biochem.*, 1976, **72**, 248–354.
- 34 K. Kurita, T. Sannan and Y. Iwakura, *Makromol. Chem.*, 1977, **178**, 3197–3202.
- 35 H. Sashiwa, H. Saimoto, Y. Shigemasa, R. Ogawa and S. Tokura, *Carbohydrate Polymers*, 1991, **16**, 291–296.
- 36 H. Sashiwa, H. Saimoto, Y. Shigemasa and S. Tokura, *Carbohydrate Research*, 1993, **242**, 167–172.
- 37 M. Weinhold, J. Sauvageau, B. Tartsch, P. Clarke, B. Jastorff and J. Thöming, *Advances in Chitin Science*, 2007, **10**, 66–71.
- 38 M.-K. Jang, B.-G. Kong, Y.-I. Jeong, C. H. Lee and J.-W. Nah, *Journal of Polymer Science, Part A: Polymer Chemistry*, 2004, **42**, 34233432.
- 39 S. Aiba, *Int. J. Biol. Macromol.*, 1991, **13**, 40–44.

Green Chemistry

Cutting-edge research for a greener sustainable future

www.rsc.org/greenchem

Volume 11 | Number 4 | April 2009 | Pages 437–592



ISSN 1463-9262

Ravasio *et al.*
Selective hydrogenation of oils

Palmisano *et al.*
Photocatalytic oxidation of aromatic
alcohols in water

Clark *et al.*
Microwave-assisted preparation of amides

Pol *et al.*
Solvent free process for the generation
of conducting carbon spheres



1463-9262(2009)11:4;1-A

RSC Publishing

Selective photocatalytic oxidation of 4-substituted aromatic alcohols in water with rutile TiO₂ prepared at room temperature†

Sedat Yurdakal,^{a,b} Giovanni Palmisano,^a Vittorio Loddo,^a Oğuzhan Alagöz,^c Vincenzo Augugliaro^{*a} and Leonardo Palmisano^{*a}

Received 7th November 2008, Accepted 27th January 2009

First published as an Advance Article on the web 18th February 2009

DOI: 10.1039/b819862d

Home-prepared (HP) rutile TiO₂ catalysts were prepared at room temperature by using H₂O and TiCl₄ in different ratios and without addition of additives. The catalysts were used for carrying out the selective photocatalytic oxidation of 4-methoxybenzyl alcohol to 4-methoxybenzaldehyde in aqueous suspension, free from any organic co-solvent. The selectivities showed by the home prepared catalysts were in the 45–74% range, up to four times higher than that of a commercial rutile TiO₂ sample, the reaction rates being comparable. By using the most selective photocatalyst, the oxidation of benzyl, 4-methylbenzyl, and 4-nitrobenzyl alcohols was also carried out in order to investigate the influence of the substituent group on the oxidation rate and selectivity. The presence of an –OCH₃ group positively influenced the selectivity whereas a –NO₂ group showed to have a detrimental effect. The Hammett relationship effectively describes the influence of substituent group on the kinetic constant of partial oxidation of aromatic alcohols to aldehydes.

1. Introduction

Among the advanced oxidation processes investigated in the last decades, photocatalysis in the presence of an irradiated semiconductor has proven to be very effective in the field of environment remediation. The use of irradiation to initiate chemical reactions is the principle on which heterogeneous photocatalysis is based; in fact, when a semiconductor oxide is irradiated with suitable light, excited electron–hole pairs result that can be applied in chemical processes to modify specific compounds. The main advantage of heterogeneous photocatalysis, when compared with the chemical methods, is that in most cases it is possible to obtain a complete mineralization of the toxic substrate even in the absence of added reagents. The radical mechanism of photocatalytic reactions, which involve fast attacks of strongly oxidant hydroxyl radicals,¹ determines their unselective features. Additional advantages are: (i) its non-specificity; (ii) the possibility of treating effluents having very low concentrations of contaminants without lowering the reaction rate to negligible values; (iii) the possibility of operation at ambient temperature and pressure; (iv) the use of a cheap oxidant, *i.e.* molecular oxygen.

Various semiconductor materials have been tested as oxidation photocatalysts, but it is generally accepted that anatase TiO₂ is the most reliable material due to its low cost, high photostability and its ability to be activated by near UV-light and also by the solar radiation. Among the crystalline phases of TiO₂ (anatase, rutile and brookite), anatase, pure or in mixture with rutile, shows the highest activity. Rutile, which is the most thermodynamically stable phase, usually shows scarce photo-activity. Likely reasons invoked to explain the poor performance of rutile with respect to anatase phase are that it shows a very low hydroxyl group surface concentration and a high recombination rate of the photogenerated e[–]–h⁺ pairs.^{2–5} However, while rutile produced at very high temperature (*ca.* 1000 K) shows a poor photoreactivity,⁶ rutile home prepared at low temperature exhibits a certain photocatalytic activity.⁷ The preparation of photo-active rutile samples is generally carried out at room temperature in highly concentrated acidic solutions. Yin *et al.*,⁸ for instance, crystallized TiO₂ at room temperature in the presence of HCl, HNO₃ or H₂SO₄ by using titanium tetraisopropoxide as the precursor. It is worth noting that in the absence of acids they obtained amorphous TiO₂. Yang *et al.*⁹ used Ti(SO₄)₂ as the precursor but the crystallization occurred after a long time and in HNO₃ solution. Fei *et al.*¹⁰ prepared rutile nanorods photo-active for the degradation of harmful molecules, starting from titanium isopropoxide solution at room temperature in a concentrated HNO₃ solution.

The partial oxidation of –CH₂OH to –CHO group is a key reaction step throughout many organic syntheses; this reaction is commonly used in the preparation of many organic products, due to the wide use of aldehyde derivatives in the flavour, confectionary, and beverage industries.¹¹ Generally the conditions, in which the industrial synthetic processes are carried out, are environmentally harmful as they involve organic solvents at high temperature and pressure and stoichiometric oxygen donors that

^a“Schiavello-Grillone” Photocatalysis Group – Dipartimento di Ingegneria Chimica dei Processi e dei Materiali, Università degli Studi di Palermo, Viale delle Scienze, 90128, Palermo, Italy. E-mail: augugliaro@dicpm.unipa.it, palmisano@dicpm.unipa.it; Fax: +39 091 23863768; Tel: +39 091 23863746

^bKimya Bölümü, Fen Fakültesi, Anadolu Üniversitesi, Yunus Emre Kampüsü, 26470, Eskişehir, Turkey

^cKimya Bölümü, Fen Fakültesi, Ankara Üniversitesi, Tandoğan, 06100, Ankara, Turkey

† Electronic supplementary information (ESI) available: SEM images and NMR analysis. See DOI: 10.1039/b819862d

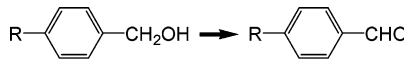
are not only expensive and toxic compounds but also produce high amounts of dangerous wastes.

Selective photocatalysed oxidation of diols to the corresponding hydroxy-carbonylic compounds was carried out in aqueous acetonitrile¹² or dichloromethane¹³ TiO₂ suspensions; decatungstate anion¹⁴ heterogenized on silica was also used in dichloromethane solvent. It was found that the adsorption of the diol is an important parameter able to affect efficiency and selectivity of the photocatalytic process. Photocatalytic oxidation of aromatic alcohol has been carried out either in acetonitrile medium¹⁵ or in air.¹⁶ However, recently partial oxidation of aromatic alcohol has been carried out in water suspensions. 4-Methoxybenzyl alcohol (MBA) has been partially oxidized to 4-methoxybenzaldehyde (MBAD): a 10% selectivity was found by using Degussa P25 whereas by using HP anatase-rutile samples obtained with different aging times¹⁷ at 373 K a higher selectivity was obtained (up to 41% with pure anatase). By using a similar preparation method pure brookite sample¹⁸ showed higher selectivity than pure rutile (39% and 32%, respectively). Later on, 60% of selectivity was attained with home prepared rutile synthesised at 333 K under similar experimental conditions.¹⁹ The investigation of the reaction pathway¹⁷⁻¹⁹ indicated that in all cases the MBA photocatalytic oxidation proceeds through two parallel reaction routes: the first one determines the MBA partial oxidation to MBAD while the second one eventually causes the direct mineralization of MBA to CO₂. This last pathway occurs through a series of reactions taking place over the catalyst surface and producing intermediates not desorbing to the bulk of solution. It was found that the increase of aging time increases both the rutile/anatase ratio, the crystallinity of catalysts and the activity for alcohol oxidation but it decreases the selectivity to aldehyde. In the competition between partial and complete oxidation, more crystalline catalysts favour the complete oxidation while less crystalline or amorphous catalysts, even if less reactive, favour the partial oxidation. The influence of calcination temperature on catalyst crystallinity, photoreactivity and selectivity was also investigated by using pure rutile samples. The crystallinity always increased while the reactivity showed a maximum at 673 K and then it decreased owing to the surface dehydroxylation. As expected the selectivity continuously decreased, the highest one being obtained with lesser crystalline sample. In order to find likely explanations for the different photo-activity shown by home prepared anatase and commercial catalysts, their textural, bulk and surface properties have been investigated.^{20,21} It was found that the textural and intrinsic electronic features of catalysts were almost the same; on the contrary ATR-FTIR studies indicated that the higher selectivity found for home-made catalysts with respect to commercial ones is related to their low crystallinity and to their high surface hydroxyl group density that induces an enhanced hydrophilicity of the TiO₂ surface. Both of these properties promote the desorption of the photo-produced aldehyde thus hindering its further oxidation.

In the present work, TiO₂ rutile catalysts have been obtained at room temperature with a preparation method in milder conditions than those previously reported. These catalysts have been used to investigate the selective photo-oxidation of MBA to MBAD in water. In order to investigate if the reaction selectivity towards the partial oxidation depends on the catalyst

Table 1 4-substituted alcohols and corresponding aldehydes

-R	Alcohol	Aldehyde
-H	BA	BAD
-OCH ₃	MBA	MBAD
-CH ₃	MeBA	MeBAD
-NO ₂	NBA	NBAD



or also on the chemical nature of aromatic alcohol used, the photocatalytic oxidation of some 4-substituted benzyl alcohols to the corresponding aldehydes (see Table 1), *i.e.* benzyl alcohol (BA) to benzaldehyde (BAD), 4-methylbenzyl alcohol (MeBA) to 4-methylbenzaldehyde (MeBAD) and 4-nitrobenzyl alcohol (NBA) to 4-nitrobenzaldehyde (NBAD), has been investigated by using the same HP rutile sample. For the sake of comparison a commercial rutile TiO₂ (Sigma Aldrich, SA) sample was also tested under the same experimental conditions used for all the HP samples.

2. Experimental

2.1 Catalyst Preparation and characterization

The precursor solutions were obtained by adding 20 mL of TiCl₄ (> 97%, Fluka) to 400, 700, 1000, 1500 or 2000 mL water contained in a volumetric flask; the addition was carried out very slowly without agitation in order to avoid the warming of the solution as the TiCl₄ hydrolysis is a highly exothermic reaction. At the end of the addition, the resulting solution was mixed for 2 min by a magnetic stirrer and then the flask was sealed and maintained at room temperature (*ca.* 298 K) for a total aging time ranging from 4 to 9 days. Just after *ca.* 12 h aging, the sol became a transparent solution and then, after waiting a few days, the precipitation process started. The solid powder that precipitated at the end of the whole treatment was separated by centrifugation (20 min at 5000 rpm) and dried at room temperature. The final home-prepared (HP) catalysts are hereafter indicated as HP1/20, HP1/35, HP1/50, HP1/75 and HP1/100 where the numbers indicate the TiCl₄/H₂O volumetric ratio.

XRD patterns of the powders were recorded by a Philips diffractometer using the Cu K α radiation and a 2 θ scan rate of 1.28° min⁻¹. SEM images were obtained using an ESEM microscope (Philips, XL30) operating at 25 kV. A thin layer of gold was evaporated on catalysts samples, previously sprayed on the stab and dried at room temperature. BET specific surface areas were measured by the single-point BET method using a Micromeritics Flow Sorb 2300 apparatus.

Before the analysis, the samples were dried for 1 h at 100 °C, for 2 h at 150 °C and degassed for 0.5 h at 150 °C.

2.2 Photoreactivity set up and procedure

A cylindrical Pyrex batch photoreactor with an immersed lamp, containing 0.5 L of aqueous suspension, was used to perform the reactivity experiments. The photoreactor was provided with ports in its upper section for the inlet and outlet of oxygen and for sampling. A magnetic stirrer guaranteed a satisfactory

suspension of the photocatalyst and the homogeneity of the reacting mixture. A 125 W medium pressure Hg lamp (Helios Italquartz, Italy), axially positioned within the photoreactor, was cooled by water circulating through a Pyrex thimble; the temperature of the suspension was about 300 K. The radiation energy impinging on the suspension had an average value of 10 mW cm⁻². It was measured at 360 nm by using a radiometer UVX Digital.

The initial concentration used for MBA, BA, MeBA and NBA was 1 mM. Since the surface area and the agglomerate size of the various photocatalysts were different, the photoreactivity runs were carried out at equal irradiation conditions of the suspension, *i.e.* at equal flow of photons absorbed by the suspensions. For each catalyst the amount chosen for the photocatalytic runs was that for which the resulting suspension was able to absorb 90% of the impinging radiation. This choice also guaranteed that all the catalyst particles were irradiated. Measurements of the transmitted light in the presence of the suspension were carried out by using the radiometer above described. An amount of 0.2 g L⁻¹ was used for HP1/20, HP1/75 and HP1/100 samples, 0.4 g L⁻¹ for the commercial SA catalyst, while an amount of 0.6 g L⁻¹ was required for HP1/35 and HP1/50 samples. A selected run of MBA photo-oxidation was carried out by using 0.2 g L⁻¹ of HP1/50. NaOH 1 M solution was used to adjust the initial pH to 7.

Before switching on the lamp, oxygen was bubbled into the suspension for 30 min at room temperature to reach the thermodynamic equilibrium. Adsorption of the alcohols under dark conditions was always quite low, *i.e.* less than 5%. During the run, samples of reacting suspension were withdrawn at fixed time intervals; they were immediately filtered through a 0.45 µm hydrophilic membrane (HA, Millipore) before being analysed.

The quantitative determination and identification of the species present in the reacting suspension was performed by means of a Beckman Coulter HPLC (System Gold 126 Solvent Module and 168 Diode Array Detector), equipped with a Luna 5 µ Phenyl-Hexyl column (250 mm long × 2 mm id), using Sigma Aldrich standards. Retention times and UV spectra of the compounds were compared with those of standards. The eluent consisted of: 17.5% acetonitrile, 17.5% methanol, 65% 40 mM KH₂PO₄ aqueous solution. TOC analyses were carried out by using a 5000 A Shimadzu TOC analyser. All the used chemicals were purchased from Sigma Aldrich with a purity > 99.0%.

A specific photocatalytic run was performed in order to characterize the aldehyde produced by MBA partial oxidation. For this run 500 mL of 10 mM MBA solution and 0.6 g L⁻¹ of HP1/50 catalyst were used; the run lasted 12 h and a 75%

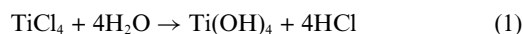
conversion of MBA was reached. In the course of this run no samples were withdrawn from the photoreactor. At the end of the run the whole suspension was filtered by using a paper filter (Whatman) and the catalyst was separated. Then the organic products present in the aqueous phase were extracted with CHCl₃ and concentrated by a rotovapor apparatus (model Buchi Rotovapor M). MBAD was separated by column chromatography by using a silica support (Silicagel 60, Merck) and a mixture of hexane and ethyl acetate (8 : 1 v/v) as the mobile phase. The recovered catalyst was used for performing another run at the same experimental conditions in order to check the occurrence of deactivation phenomena. The same results were obtained thus confirming, as expected, that in aqueous medium the TiO₂ catalyst shows a stable activity.

¹H-, ¹³C-NMR spectra were obtained by using a Bruker DPX FT NMR (500 MHz) spectrometer. The spectrometer was equipped with a 5 mm PABBO BB-inverse gradient probe. CDCl₃ was used as a solvent. Standard Bruker pulse programs (Bruker program 1D WIN-NMR, release 6.0) was used throughout the experiments.

3. Results and discussion

3.1 Characterization of photocatalysts

Both the hydrolysis of TiCl₄ and subsequent condensation steps were carried out at room temperature, producing the photocatalysts with the following stoichiometric reactions:



The preparation conditions and some physical features of photocatalysts are summarized in Table 2. In agreement with the literature,^{8,9} only nuclei of the thermodynamically stable rutile phase are formed in strongly acidic solution, even if at a very low precipitation rate. It has been found by us that only aging of the sol produces rutile crystals and that a decrease of the TiCl₄/H₂O v/v ratio lowers the time needed for crystal precipitation. For instance a catalyst was prepared with a TiCl₄/H₂O ratio of 0.1 for which the crystal precipitation started after only 50 days of aging. For this reason ratios higher than 0.05 (that of HP1/20) have not been used in the present investigation.

XRD patterns of HP and commercial samples are reported in Fig. 1. The peaks assignable to rutile are those at 2θ = 27.5°, 36.5°, 41°, 54.1° and 56.5°; it may be noted that the peaks of commercial rutile are well defined while those of all of the HP samples are broad, indicating that their crystallinity is low.

Table 2 BET specific surface area (SSA), particle size and crystallite size of the photocatalysts

Catalyst	TiCl ₄ /H ₂ O v/v ratio	SSA/m ² g ⁻¹	Aging time/days	Time for precipitation starting/days	Agglomerates size/nm	Crystallite size/nm
HP1/20	0.05	129	9	8	286	5.5
HP1/35	0.029	116	6	3	1050	5.6
HP1/50	0.02	118	6	3	719	6.8
HP1/75	0.013	125	4	2	304	7.1
HP1/100	0.01	135	4	2	244	6.1
SA	—	2.5	—	—	240	52

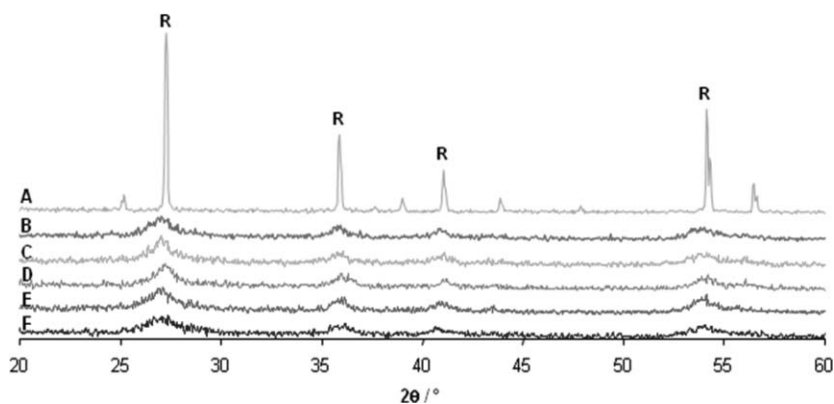


Fig. 1 XRD patterns of HP and commercial TiO₂ samples; (A) SA, (B) HP1/100, (C) HP1/75, (D) HP1/50, (E) HP1/35, (F) HP1/20. “R” = rutile peaks.

Size values of primary crystallites (calculated using the Scherrer equation) were quite low (5.5–7.1 nm), and very similar to each other. The sizes of the crystallite aggregates were much higher (see Table 2), as estimated from SEM observations, and they increased with the increase of the TiCl₄/H₂O ratio, *i.e.* acidity, and the time needed for the starting of precipitation. The size values of agglomerates decreased from HP1/35 to HP1/100, but the situation for HP1/20 was quite different. Due to the high Ti/H₂O ratio, the precipitation started only at the end of 8th day, so that the time allowed for particle aggregation (1 day) was much lower than that of all the other preparations. This fact should justify the low value of agglomerate size reported in Table 2 for HP1/20 sample.

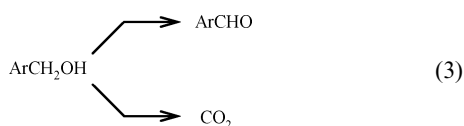
BET specific surface areas of HP samples are significantly higher than that of SA. The former ones, except that of HP1/20, increase with the decrease of agglomerate size.

3.2 Photoreactivity

In the initial part of this investigation, the photocatalytic oxidation of MBA was carried out by testing all the HP rutile catalysts together with the commercial one at equal reaction conditions.

No oxidation of MBA was observed in the absence of irradiation and/or catalyst and/or oxygen under the same experimental conditions used for the photoreactivity runs. Irradiation, catalyst and oxygen were all needed for the occurrence of the process.

All the photoreactivity runs indicated that the rates of formation of MBAD and CO₂ had values different from zero once the irradiation was turned on. These experiments confirmed that the MBA degradation^{17,19} proceeds through two parallel pathways, both effective since the start of irradiation: (i) partial oxidation of MBA to the corresponding aldehyde, MBAD, which is released to the liquid phase and may compete with MBA for mineralization; and (ii) complete oxidation of MBA to CO₂ and H₂O through intermediates which do not desorb from the catalyst surface. Eqn 3 describes the MBA degradation process:



Selectivity values depend on the competition between the two pathways; surface physico-chemical and structural properties of the photocatalysts are the most important factors influencing that competition, although other parameters like the structure of the starting aromatic molecule and its initial concentration cannot be neglected.

A run was carried out with a catalyst amount smaller than the optimal one in order to check if the absorbed photon flow affects the selectivity towards aldehyde. For this run performed by using 0.2 g L⁻¹ of the HP1/50 sample, Fig. 2 reports the MBA, MBAD and CO₂ concentration values and the carbon balance *versus* irradiation time. Overall conversion of MBA and selectivity to aldehyde are also reported (they are quoted to the right ordinate axis). The carbon balance has been performed by summing the MBA and MBAD concentrations to that of CO₂ concentration, by dividing by 8 the value obtained by TOC determination.

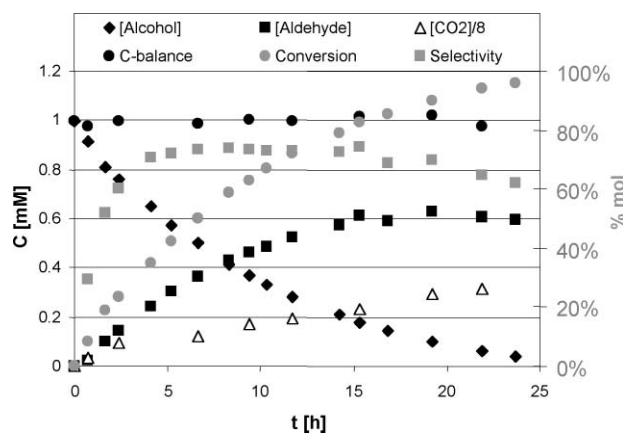


Fig. 2 Experimental results of photocatalytic oxidation of MBA using the HP1/50 (0.2 g L⁻¹) sample. Conversion and selectivity are scaled on the right side. The CO₂ concentration values were divided by 8 for normalization purposes.

It is worth noting that the slope of CO₂ concentration data is different from zero at zero time thus indicating that this CO₂ is not produced through subsequent oxidation of the initially produced MABD released to the liquid phase. The selectivity values plateaued at their highest value in the conversion range of 20–80%. From 0 to 20% conversion, the selectivity increases

probably because of the occurrence of transient phenomena on the catalyst surface;²² it must be underlined that the TOC and MBAD quantitative determinations at low MBA conversion may be strongly affected by experimental errors. For conversions higher than 80% the selectivity decreases along with the MBAD concentration in the liquid phase (see Fig. 2). In this condition the produced aldehyde molecules favourably compete with remaining alcohol molecules for adsorption and (photo)oxidation onto the surface sites. On the basis of this finding the comparison of catalyst performances has been done by determining the selectivity and the time needed for achieving a MBA conversion of 50%.

The photoreactivity results obtained with the HP and commercial (SA) catalysts are summarized in Table 3. This Table reports the reaction time needed for 50% MBA conversion, $t_{1/2}$, the corresponding selectivity to MBAD and the carbon balance percentage. It can be noticed that all the HP catalysts results are much more selective (*ca.* 2–4 fold) than SA, but the HP1/50 sample showed the highest selectivity (74%) towards MBAD production. To the best of our knowledge this value is the highest one ever reported in the literature for heterogeneous photocatalytic oxidation of alcohol to aldehyde in water. The HP1/35, HP1/75 and HP1/100 samples showed a similar selectivity, *i.e.* *ca.* 60%, while the HP1/20 sample the lowest one, *i.e.* 45%. The commercial catalyst, SA, which exhibits a selectivity far lower than those of HP samples, however gives rise to a similar reactivity, *i.e.* $t_{1/2}$.

The carbon balance, verified by taking into account only the unreacted alcohol, the produced aldehyde and CO₂, was quite satisfied by the HP samples with higher selectivity (HP1/35 and HP1/50). It may be noted from the data in Table 3 that the failure on carbon balance increases with the decrease of the sample selectivity, being the highest one for the commercial sample (*i.e.* the one with the lowest selectivity). In the course of the photocatalytic runs, in addition to the main products of MBA oxidation, *i.e.* aldehyde and CO₂ (see eqn 3), hydroxylated aromatics, benzoic acids and open-ring products were also found. The amounts of these last products depended on the used photocatalyst; for the most selective HP samples only traces of them were found while for the others HP and the commercial sample the amounts were higher. It is likely that these products arise from the subsequent oxidation of produced aldehyde, being this pathway more relevant for the less selective, and therefore more oxidizing, samples.

Table 3 Photocatalysts performance for MBA photo-oxidation to MBAD for 50% conversion

Catalyst	Catalyst amount/g L ⁻¹	$t_{1/2}$ /h	Selectivity (% mol)	C balance (%) ^a
HP1/20	0.2	2.3	45	91
HP1/35	0.6	3.6	60	96
HP1/50	0.2	6.65	74	99
HP1/50	0.6	2.6	72	98
HP1/75	0.2	2.95	55	94
HP1/100	0.2	3.3	61	96
SA	0.4	2.15	21	70

^a C-balance was obtained as sum of MBA, MBAD and CO₂ concentration.

By comparing the results obtained from runs carried out with different amounts of HP1/50 (see Table 3), it may be noted that the use of lower amounts of photocatalyst (0.2 instead of 0.6 g L⁻¹, three times less) gives rise to a small increase of the selectivity while the $t_{1/2}$ increases about three times. By considering that the suspension with 0.2 g of catalyst absorbs about half of the photons absorbed with 0.6 g but that the photons absorbed per unit mass of catalyst increase about 150%, it can be concluded that the photoprocess is quite insensitive to the irradiation conditions, at least under the used experimental conditions.

In order to check the potentiality of this process as a green synthetic one, produced MBAD and residual MBA were separated, analysed and purified according to the procedure described in the experimental section. MBAD was isolated with a yield of *ca.* 48%. ¹H-NMR and ¹³C-NMR analyses (see ESI†) confirmed that the obtained MBAD has a high purity (>99%).

In the last part of this study the effect of different substituent groups on the photoprocess performance was investigated with the aim of checking if the selectivity to the corresponding aldehyde is a feature of the photocatalyst or it is affected by the chemical nature of aromatic alcohol. The most selective sample, HP1/50, and the commercial one, SA, were used to carry out the photo-oxidation of benzyl alcohol (BA), 4-methylbenzyl alcohol (MeBA) and 4-nitrobenzyl alcohol (NBA). The photoreactivity results obtained with the 4-substituted alcohols are summarized in Table 4; the figures in Table 4 are the averages of three independent experiments.

A thorough investigation of the intermediates produced in the course of photocatalytic degradation was not the aim of this paper. As found with MBA, the oxidation of MeBA, BA, and NBA mainly produced the corresponding aldehydes and CO₂, this finding suggesting that the mineralization of adsorbed alcohol molecules occurs by means of subsequent oxidative steps producing species which do not desorb from the photocatalyst surface to the solution. Small amounts of hydroxylated derivatives and open ring products were detected for NBA tested with HP1/50; their amounts were much higher when SA was used.

By taking as reference the unsubstituted benzyl alcohol, the data of Table 4 indicate that the presence of electron donor groups (–OCH₃ and –CH₃) positively affects the selectivity for both photocatalysts, although the commercial sample (SA) shows in all cases the worst performance. On the contrary the electron withdrawing group (–NO₂) was detrimental and a very scarce selectivity was observed. It can hence be stated that the presence of an electron withdrawing group such as –NO₂ favours the reaction pathway leading to the breakage of the aromatic ring with formation of over oxidised species and eventually CO₂. The same behaviour was observed in the hydroxylation of various aromatic species.^{23a} In that case it has been reported²³ that the presence of an electron donor group, due to its inductive and delocalization effects, hinders oxidant attacks towards the aromatic ring.

In reference to the oxidation rate, the data of Table 4 indicate that reaction times needed to achieve 50% conversion of alcohol decrease in the order: BA > MeBA > MBA while time was longer from BA to NBA. This order indicates that the reaction rate is enhanced by electron-donating substituents and retarded

Table 4 Results of photocatalytic oxidation of BA, MBA, MeBA, NBA, using HP1/50 (0.6 g L⁻¹) and SA samples (0.4 g L⁻¹). The selectivity to aldehyde was determined for 50% conversion of alcohol

Catalyst	MBA		MeBA		BA		NBA	
	HP1/50	SA	HP1/50	SA	HP1/50	SA	HP1/50	SA
$t_{1/2}/h$	2.6	2.15	4.2	4.2	6.5	3.8	9.8	6.7
Selectivity (% mol)	72	21	47	9.5	42	9.2	5.3	3.3
C Balance (% mol)	98	70	96	68	95	66	90	65
k_0/h^{-1}	0.267	0.266	0.165	0.265	0.107	0.182	0.07	0.073

by electron-withdrawing substituents. By considering that no correlation was found between reactivity and the water–octanol partition coefficients of aromatic alcohols (or aldehydes), it may be assumed that the electronic properties of substituent groups play a more significant role than the relative solubility in water of reagents and products. On this ground the influence of the substituent group on the rate of partial oxidation of aromatic alcohols can be interpreted in terms of Hammett's relationship.²⁴

The basic Hammett equation is:

$$\log \left(\frac{k_{PO}}{k_{PO}^0} \right) = \rho \sigma \quad (4)$$

in which k_{PO} is the kinetic constant of the partial oxidation reaction of the substituted reactant, k_{PO}^0 that of the unsubstituted reactant, σ the substituent constant which is related to the electron orientation effect of the specific substituent R and ρ the reaction constant which depends only on the type of reaction but not on the substituent used. The reaction constant, or sensitivity constant, ρ , describes the susceptibility of the reaction to substituents. A plot of ($\log k_{PO}$) versus σ for a given reaction with many differently substituted reactants gives a straight line with slope equal to ρ .

In the present case the rates of overall oxidation of alcohol and of partial oxidation to aldehyde are well described by first order kinetics with respect to alcohol concentration:

$$-\frac{dC_{ArOH}}{dt} = k_0 C_{ArOH} = (k_{min} + k_{PO}) C_{ArOH} \quad (5)$$

$$\frac{dC_{ArO}}{dt} = k_{PO} C_{ArOH} \quad (6)$$

in which C_{ArOH} and C_{ArO} are the concentration of aromatic alcohol and aldehyde, respectively, t the irradiation time, k_0 the first order kinetic constant of overall oxidation reaction and k_{min} that of mineralization reaction. Dividing eqn 6 for eqn 5 produces:

$$\frac{dC_{ArO}}{dC_{ArOH}} = \frac{k_{PO}}{k_{min} + k_{PO}} \quad (7)$$

Integration of eqn 7 with the condition that at the start of irradiation, *i.e.* for $C_{ArOH} = C_{ArOH,0}$, $C_{ArO} = 0$ gives:

$$\frac{C_{ArO}}{C_{ArOH,0} - C_{ArOH}} = \frac{k_{PO}}{k_{min} + k_{PO}} \quad (8)$$

The left hand side term of eqn 8 represents the reaction selectivity towards aldehyde, S , and the $(k_{min} + k_{PO})$ term is equal to k_0 . The values of k_0 may be determined by a best

fitting procedure applied to the experimental data of alcohol concentration versus time once integration of eqn 5 is performed. In this way the k_{PO} values can be calculated as:

$$k_{PO} = S k_0 \quad (9)$$

Table 4 reports the values of k_0 obtained by a least-squares best fitting procedure applied to all the photoreactivity runs; the reported figure is the average of three independent experiments. By using eqn 9 the values of k_{PO} have been calculated. Fig. 3 reports in a semilogarithmic plot the values of k_{PO} versus the Hammett constant of each substituent group of the aromatic alcohol for both used catalysts. The solid straight lines through the data represent the Hammett relationship (eqn 4) best fitted to HP1/50 data ($R^2 > 0.99$) and SA ones ($R^2 > 0.94$). The ρ values obtained by the best fitting procedure are -3.32 and -2.75 for HP1/50 and SA, respectively. The very good proportional relationship shown in Fig. 3 confirms the influence of the electrophilic nature of the substituent on the photocatalytic partial oxidation of aromatic alcohols to aldehydes.

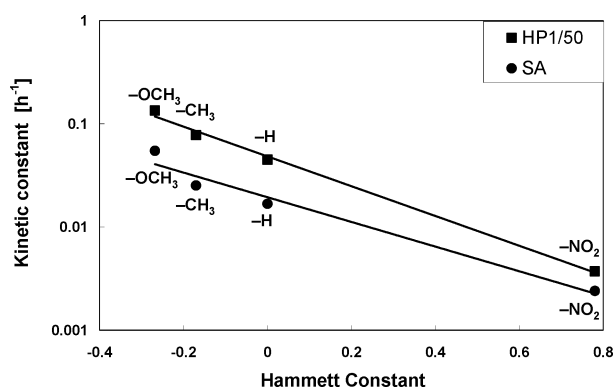


Fig. 3 Correlation between the kinetic constant of partial oxidation reaction, k_{PO} , and the Hammett constant.

Conclusions

In conclusion the reported results indicate that heterogeneous photocatalytic methods may be used for synthesis of valuable organic compounds with selectivities as high as 74%. The rate of the process is that typical of heterogeneous photocatalytic systems but it could be enhanced by increasing the photon flow absorbed by the suspension, *i.e.* by using lamps of higher power; in this way also the process efficiency should improve. The catalyst preparation method and the photoprocess conditions obey the principles of green chemistry as neither organic solvents nor heavy-metal catalysts have been used. The whole process does not use or generate hazardous substances but it minimizes the

associated environmental impacts; moreover it would be able to reduce the amount of energy used in the process if photocatalysts that are able to use cheap and clean solar energy are developed. The investigation of the effect of the aromatic alcohol substituent on the partial oxidation performance shows that this effect is well described by the Hammett's relationship, whose validity is widely confirmed for homogeneous reacting systems but for very few cases²⁵ in heterogeneous photocatalytic systems.

Acknowledgements

AA wish to thank Dr Güner Saka (Anadolu Üniversitesi-BİBAM Research Center, Eskişehir, Turkey) for NMR analyses.

References

- 1 M. Schiavello, *Heterogeneous Photocatalysis*, John Wiley & Sons, New York, 1995.
- 2 S. Yang, Y. Liu, Y. Guo, J. Zhao, H. Xu and Z. Wang, *Mater. Chem. Phys.*, 2002, **77**, 501.
- 3 H. Kawaguchi and T. Wejima, *Kagaku Kogaku Ronbunshu*, 1983, **9**, 107.
- 4 H. Kawaguchi, *Environ. Technol. Lett.*, 1984, **5**, 471.
- 5 V. Augugliaro, L. Palmisano, A. Sclafani, C. Minero and E. Pelizzetti, *Toxicol. Environ. Chem.*, 1988, **16**, 89.
- 6 A. Sclafani, L. Palmisano and M. Schiavello, *J. Phys. Chem.*, 1990, **94**, 829, and references therein.
- 7 (a) M. Nag, P. Basak and S. V. Manorama, *Mater. Res. Bull.*, 2007, **42**, 1691; (b) S. Yin, R. Li, Q. He and T. Sato, *Mater. Chem. Phys.*, 2002, **75**, 76; (c) L. Li, J. Liu and Z. Jia, *Mater. Lett.*, 2006, **60**, 1753.
- 8 S. Yin, R. Li, Q. He and T. Sato, *Mater. Chem. Phys.*, 2002, **75**, 7.
- 9 S. Yang, Y. Liu, Y. Guo, J. Zhao, H. Xu and Z. Wang, *Mater. Chem. Phys.*, 2002, **77**, 501.
- 10 B. Fei, Z. Deng, J. H. Xin, Y. Zhang and G. Pang, *Nanotechnology*, 2006, **17**, 1927.
- 11 (a) Y. Mao and A. Bakac, *Inorg. Chem.*, 1996, **35**, 3925; (b) U. R. Pillai and E. S. Demessie, *J. Catal.*, 2002, **211**, 434.
- 12 M. A. Fox, H. Ogawa and P. Pichat, *J. Org. Chem.*, 1989, **54**, 3847.
- 13 A. Molinari, M. Bruni and A. Maldotti, *J. Adv. Oxid. Technol.*, 2008, **11**, 143.
- 14 A. Maldotti, A. Molinari and F. Bigi, *J. Catal.*, 2008, **253**, 312.
- 15 O. S. Mohamed, A. E. M. Gaber and A. A. Abdel-Wahab, *J. Photochem. Photobiol., A*, 2002, **148**, 205.
- 16 U. R. Pillai and E. Sahle-Demessie, *J. Catal.*, 2002, **211**, 434.
- 17 G. Palmisano, S. Yurdakal, V. Augugliaro, V. Loddo and L. Palmisano, *Adv. Synth. Catal.*, 2007, **349**, 964.
- 18 M. Addamo, V. Augugliaro, M. Bellardita, A. Di Paola, V. Loddo, G. Palmisano, L. Palmisano and S. Yurdakal, *Catal. Lett.*, 2008, **126**, 58.
- 19 S. Yurdakal, G. Palmisano, V. Loddo, V. Augugliaro and L. Palmisano, *J. Am. Chem. Soc.*, 2008, **130**, 1568.
- 20 V. Augugliaro, H. Kisch, V. Loddo, M. J. López-Muñoz, C. Márquez-Álvarez, G. Palmisano, L. Palmisano, F. Parrino and S. Yurdakal, *Appl. Catal., A*, 2008, **349**, 182.
- 21 V. Augugliaro, H. Kisch, V. Loddo, M. J. López-Muñoz, C. Márquez-Álvarez, G. Palmisano, L. Palmisano, F. Parrino and S. Yurdakal, *Appl. Catal., A*, 2008, **349**, 189.
- 22 S. Yurdakal, V. Loddo, G. Palmisano, V. Augugliaro and L. Palmisano, *Catal. Today*, 2008, DOI: 10.1016/j.cattod.2008.06.032.
- 23 (a) G. Palmisano, M. Addamo, V. Augugliaro, T. Caronna, E. García-López, V. Loddo and L. Palmisano, *Chem. Commun.*, 2006, **9**, 1012; (b) V. Augugliaro, T. Caronna, V. Loddo, G. Marci, G. Palmisano, L. Palmisano and S. Yurdakal, *Chem.–Eur. J.*, 2008, **14**, 4640; (c) E. Baciocchi, M. Bietti, B. Chiavarino, M. E. Crestoni and S. Fornarini, *Chem.–Eur. J.*, 2002, **8**, 532.
- 24 L. P. Hammett, *J. Am. Chem. Soc.*, 1937, **59**, 96.
- 25 (a) B. Sangchakr, T. Hisanaga and K. Tanaka, *J. Photochem. Photobiol., A*, 1995, **85**, 187; (b) K. Tanaka and K. S. N. Reddy, *Appl. Catal., B*, 2002, **39**, 305.

Catalytic reactions using superacids in new types of ionic liquids†

Mark A. Harmer,^{*a} Christopher P. Junk,^a Vsevolod V. Rostovtsev,^a William J. Marshall,^a Liane M. Grieco,^a Jemma Vickery,^b Robert Miller^a and Stella Work^b

Received 23rd October 2008, Accepted 13th January 2009

First published as an Advance Article on the web 9th February 2009

DOI: 10.1039/b818788f

We will describe the use of superacids, in particular 1,1,2,2-tetrafluoroethanesulfonic acid (TFESA) and 1,1,2,3,3,3-hexafluoropropanesulfonic acid (HFPSA) in the presence of ionic liquids for improved chemical processing for a range of industrially important chemical reactions. In a number of cases the reaction mixture starts as a single phase, allowing for high reactivity, then separates into two phases upon completion of the reaction. This allows for ease of product separation. P. T. Anastas and T. C. Williamson, *Green Chemistry: Frontiers in Benign Chemical Syntheses and Processes*, Oxford University Press, 1998.¹

Introduction

In this paper, we will expand upon our earlier work, namely the use of new Brønsted superacidic catalysts for a number of acid catalyzed reactions of industrial importance.^{2,3} Traditional homogeneous acids, such as hydrofluoric (exceptionally hazardous) and sulfuric acids have a number of drawbacks in industrial processes including the generation of large amounts of waste associated with product separation. Replacement of these acids with highly active catalysts (such as superacids) that can be recycled and easily separated has the potential to reduce waste, reduce energy needs, cut down the process time, and make the overall process safer and more economical. For example, triflic acid is already employed in fine chemical synthesis, and ionic liquids (anions). Interest in these materials is growing.⁴⁻⁷

We have recently described the use of superacids of the form RCHFCF₂SO₃H (R = F, Cl, CF₃, or fluoroalkoxy).² Compared to triflic acid, these acids are safer to handle due to their higher boiling point/lower volatility. They also incorporate an easily identifiable proton that can be monitored by NMR.

Acid catalysts are employed in an extensive range of commercial reactions.⁸ Alkylations are common in the commercial production of ethyl benzene, trimethylpentane for high octane fuels, and cumene and linear alkyl benzenes for the surfactants industry. Traditionally, homogeneous acid catalyst such as AlCl₃, FeCl₃, H₂SO₄, HF and BF₃, are employed.^{9,10} Isomerization products are used in refining and preparation of lubricants¹¹ and acylation is important in a wide range of areas.^{12,13} The use of ethers and polyethers also have a wide range of applications.^{14,15}

Here, we describe the use of fluoroalkylsulfonic acids such as 1,1,2,2-tetrafluoroethanesulfonic acid (TFESA) and 1,1,2,3,3,3-hexafluoropropanesulfonic acid (HFPSA). As we have discussed before, these have acidities similar to triflic acid, a well known superacid.⁷ The present work utilizes the conjugate base of these acids to make a range of ionic liquids, and then uses the ionic liquid in combination with the conjugate acid as a catalyst system for a range of reactions.

The main aim of this work is to develop simplified chemical reactions where the catalyst can easily be removed and separated from the products. Effective catalyst separation, leading to minimum waste, is one of the underlying goals of green chemistry.¹ While catalysts are available for many kinds of reactions, it is often quite difficult to remove the catalyst from the products.¹⁶ Techniques such as distillation, liquid-liquid extraction, and absorption onto some kind of sacrificial absorbent are often employed. All of these approaches are energy intensive. In our studies we have developed a catalyst-ionic liquid system for two different reaction types. These are single phase at the beginning of the reaction, but become two phase at the end. This leads to easy separation of the catalyst from the products *via* simple decantation. In this paper we describe our preliminary findings.

Results and discussion

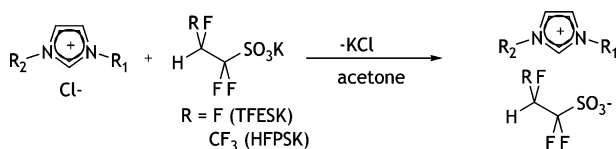
In this paper we describe a series of new ionic liquids where the anion is derived from the superacids 1,1,2,2-tetrafluoroethanesulfonic acid and 1,1,2,3,3,3-hexafluoropropanesulfonic acid. These ionic liquids are similar to the well known ionic liquids which have triflate as the anion. We also show how to use the ionic liquids in conjunction with the superacid to catalyze a variety of reactions, namely, alkylation, isomerization of olefins and etherifications. The ionic liquids can be conveniently prepared from the potassium salt of the anion and the corresponding imidazolium salt *via* a simple metathesis reaction (see Scheme 1 and Experimental Section).

For example, 1-ethyl-3-methylimidazolium 1,1,2,2-tetrafluoroethanesulfonate [EMIM-TFES] can be synthesized from EMIM-Cl and TFESK in acetone. Potassium chloride

^aDuPont Central Research and Development, Experimental Station, Wilmington, Delaware, 19880, USA. E-mail: Mark.A.Harmer@USA.DuPont.Com

^bSchool of Chemistry, University of Bristol, UK

† Electronic supplementary information (ESI) available: Crystal packing of EMIM-nonaflate. CCDC reference numbers 715667 and 715668. For ESI and crystallographic data in CIF or other electronic format see DOI: 10.1039/b818788f



precipitates out of the acetone solution and the ionic liquid is isolated as a pale yellow liquid, which crystallized upon standing. Compared to triflate-based ionic liquids, and indeed the vast majority of ionic liquids reported in the literature, one important feature of these ionic liquids is the ability to track both the cation and the anion *via* ^1H NMR. As we have discussed previously,² both 1,1,2,2-tetrafluoroethane- and 1,1,2,3,3,3-hexafluoropropanesulfonates have characteristic ^1H NMR signals around 5.6 and 6.1 ppm, respectively. Therefore, EMIM-TFES has well-defined ^1H signals from both the anion and cation allowing for a simple check on cation/anion ratio as well as any variations that may result as an effect of ion exchange due to impurities, Fig. 1. This allows for ease of monitoring of the ionic liquids during their use in chemical reactions.

Several ionic liquids have been synthesized based upon the above two superacids. These include BMIM-TFES, EMIM-TFES, BMIM-HFPS, B2MIM-HPFS and a phosphonium based ionic liquid TBP-TFES (TBP = tetrabutylphosphonium), and their physical properties are summarized in Table 1. All of the ionic liquids show high thermal stability (see a representative TGA on Fig. 2), allowing for a wide range of operating temperatures. Most of the ionic liquids were miscible with water and polar organic solvents such as acetone, ethanol, ether,

tetrahydrofuran and acetonitrile, and only slightly soluble in toluene and hexane. TBP-HFPS is less polar, as evidenced by its low solubility in water, but high solubility in toluene. In addition to the above ionic liquids, we also synthesized 1-dodecyl-3-methylimidazolium-TFES which is more hydrophobic. A number of these ionic liquids have been used with superacids as reaction medium for a range of transformations.^{17,18}

It is interesting to note that EMIM-TFES was liquid for several weeks at room temperature before undergoing a sudden exothermic crystallization. Suitable crystals for X-ray diffraction were grown for EMIM-TFES¹⁹ and EMIM-nonaflate^{20,21} and the single crystal structures were completed in order to compare the effects of the CHF_2 group *versus* the purely fluoroalkyl CF_3 on the crystal packing and close contacts. The packings are shown in Fig. 3 (see ESI for the packing of EMIM-nonaflate[†]). The overall packing of EMIM-nonaflate is layered along the crystallographic b-axis with the negative SO_3 and positive EMIM regions alternating with fluoroalkyl chain regions. The EMIM-TFES structure forms a much different non-layered packing motif. The TFES anions form in a head-to-tail arrangement with each other driven by the strong $\text{CH}\cdots\text{O}$ interaction of the CHF_2 group with a short $\text{CH}\cdots\text{O}$ distance of 2.27 Å. Not surprisingly, an examination of the environment around the SO_3 groups show close $\text{O}\cdots\text{H}$ contacts to neighboring sp^2 hydrogen on the cationic EMIM for both structures. It is the additional strong $\text{CH}\cdots\text{O}$ contacts from the CHF_2 group that differentiates the EMIM-TFES structure. The structure of EMIM-triflate²² found in the literature compares well with the layered EMIM-nonaflate structure in terms of overall packing and close contacts.

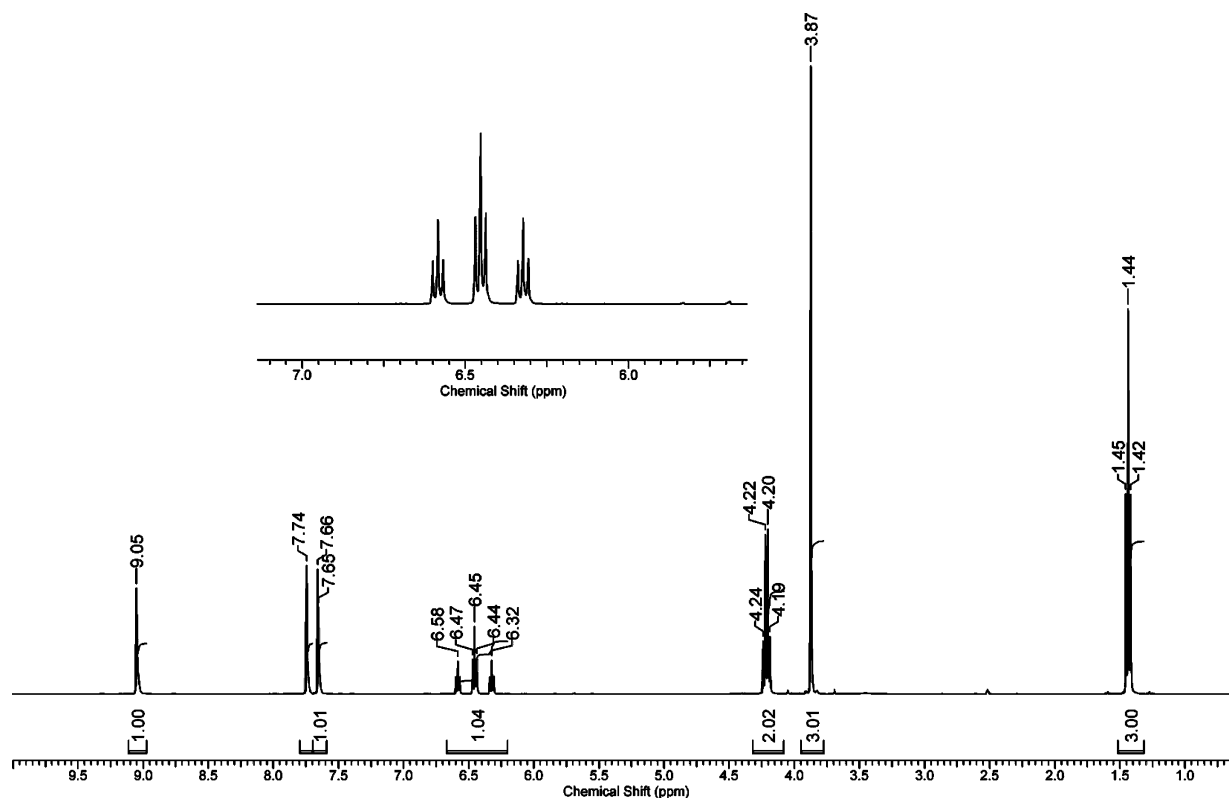
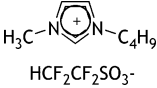
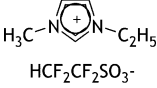
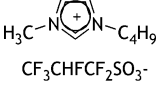
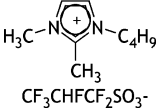
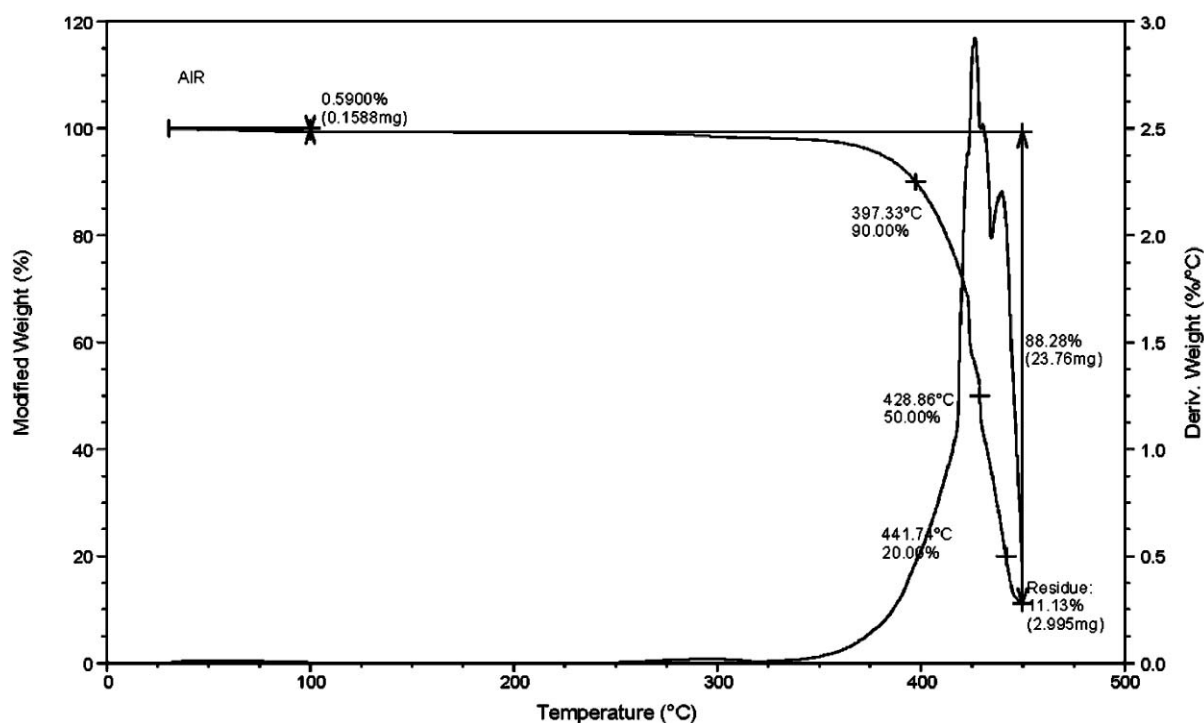


Fig. 1 ^1H NMR of EMIM-TFES, showing both the anion and cation peaks.

Table 1 Physical properties of ionic liquids

Name	Structure	mp, °C	T ₁₀ , 10% decomposition temperature, °C	Viscosity at 25 °C, cp
BMIM-TFES		<25	375	167
EMIM-TFES		45	397	84
BMIM-HFPS		<25	360	293
TBP-HFPS	(C ₄ H ₉)P ⁺ CF ₃ CHFCF ₂ SO ₃ ⁻	73	360	—
B2MIM-HFPS		<25	375	690

**Fig. 2** TGA of the ionic liquid EMIM-TFES.

The alkylation of aromatic compounds such as benzene and benzene derivatives with olefins is carried out on a large scale in the chemical industry.²³ Alkylbenzenes have many industrial uses. For example, ethyl benzene, formed by the reaction of ethylene with benzene, is an intermediate in styrene production. Alkylation of benzene with propylene yields cumene, an intermediate in phenol and acetone production. Linear alkyl benzenes are synthesized from the reaction of longer-chain olefins (*ca.* 10–18 carbon atoms) with benzene or benzene derivatives; the

linear alkyl benzenes are then sulfonated to produce surfactants. One disadvantage to these reactions is the cost associated with separating the catalyst from the reaction product(s). The main catalyst used is HF.²⁴ It is clearly advantageous to carry out the alkylation reaction in such a way that the catalyst could be easily separated from the reaction product(s).

Ionic liquids are liquids composed of only ions that are fluid around or below 100 °C.²⁵ Ionic liquids exhibit negligible vapor pressure.²⁶ Much research has been devoted to design and

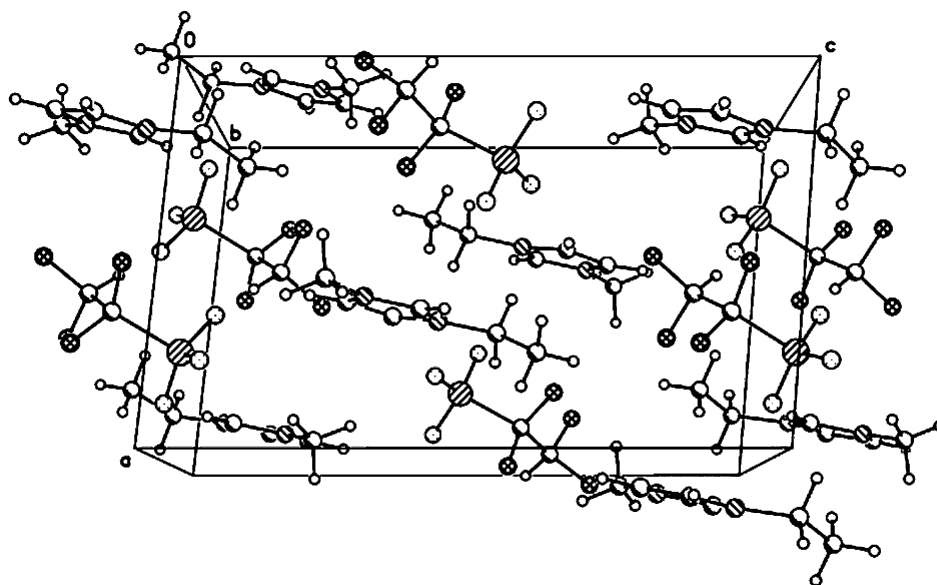
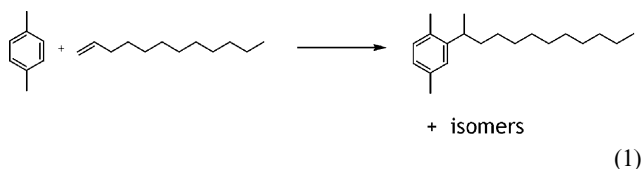


Fig. 3 Crystal packing of EMIM-TFES.

development of ionic liquids as replacements for conventional solvents in an effort to reduce the amount of volatile emissions and decrease the level of aquifer and drinking water contamination. We have found that aromatic alkylation reactions can be carried out in ionic liquids, and that the homogeneous acid catalyst can be easily removed as the reaction mixture separates into two phases after the product is formed.

The combination of ionic liquids and superacid catalysts including TFESA and HFPSA was investigated using the Friedel–Crafts alkylation reaction. This process currently uses homogenous acids (hydrofluoric and sulfuric) as catalysts of choice.²⁴ There is a drive in industry to replace these acids with more benign alternatives and the use of ionic liquids as reaction medium provides one potential solution to this problem.



The alkylation of *p*-xylene with 1-dodecene was studied for the majority of this work, however similar results were also obtained using benzene. Our preference for initially using xylene is simply the fact that it is less toxic and safer to use than benzene. Initial experiments investigated the activity of the acids in the absence of any ionic liquid. Complete conversion to alkylated products (>99%) was observed after 15 minutes, however the reaction product was deep red and the acid appeared to be dissolved in the alkylate product, making separation difficult (see Experimental Section). The product distribution has been previously described² in terms of the olefin isomers, with the 2-aryl-isomer being most preferred. There was no observed skeletal isomerization of the olefin prior to alkylation, which can lead to unwanted non-linear alkyl aromatics. With a single-phase solution formed at the end of the reaction, a purification step is required to separate the acid catalyst from

the alkylated products using either distillation or absorption of the catalyst on a basic support. Our initial idea was to use an ionic liquid that might yield a biphasic system, with the acid catalyst-IL system in one phase and the reactants in the second phase.

Two ionic liquids were investigated: 1-butyl-3-methylimidazolium 1,1,2,2-tetrafluoroethanesulfonate (BMIM-TFES) and 1-dodecyl-3-methylimidazolium 1,1,2,2-tetrafluorosulfonate (C₁₂MIM-TFES) with HFPSA as the catalyst (although similar results were found using TFESA). These ionic liquids were chosen to compare the effect of the imidazolium cation structure on the outcome of the reaction. We found that initially the system formed a single phase, but as the amount of product increased, the reaction mixture phase-separated into products in one phase and the acid and ionic liquid in the other phase (shown in Fig. 4). This phase separation enabled easy isolation of the products from the catalysts. Following alkylation, phase separation occurs with between 95–99% conversion of the 1-dodecene with excess xylene (see Experimental Section). The ionic liquid also serves as a ‘solvent’ that sequesters the acid at the end of the reaction. The separation time is between 30 and 60 min.

With excess xylene, the conversion to alkylated product (95–99%) is obtained after 1 hour reaction time (followed by GC), which is longer than when the acid is used by itself. There was no significant difference in activity between the two ionic liquids, BMIM-TFES and C₁₂MIM-TFES, with HFPSA. Note that the amount of ionic liquid is quite low (less than 10 vol%) which is preferable economically.

Interestingly, the ratio of the acid to ionic liquid had a very strong effect upon both the activity and conversion. The ratio was varied, allowing determination of the optimum acid to ionic liquid ratio. The results are shown in Table 1, which gives % conversion values for the formation of alkylated products from the starting reagents varying the ratio of acid-IL. The results show that the highest conversion rates are seen when there is an excess of acid (Table 2).

Table 2 Alkylation of xylene with 1-dodecene in the presence of the superacid HFPSA and C₁₂MIM-TFES, with different ratios of the superacid to the ionic liquid at 100 °C (see Experimental section for details)

Molar Ratio of Superacid to IL	% conversion after 15 mins	% conversion after 60 mins	% conversion after 120 mins
3:1	70.4	95	96
1:1	5.7	50	85.7
1:3	0	0	<1



Fig. 4 HFPSA-catalyzed alkylation of xylene in the absence (left) and presence (right) of an ionic liquid.

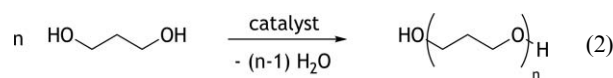
The data show that there is an optimum acid/ionic liquid ratio. High activity and conversion were obtained at the high superacid/IL ratio. Careful analysis of the alkylate phase, after exhaustive water extractions following separation from the ionic liquid/acid phase, reveals that less than about 1% of the acid is present in the product phase (with greater than 99% in the ionic liquid phase). We also estimate that there is less than 1% of the ionic liquid in the product phase. The ionic liquid/acid phase has also been recycled to yield 99% conversion upon one re-cycle, but with a lower conversion on the second recycle (60–70%).

Post-reaction phase separation is a simple and effective way to separate the products. We also note that a similar reaction using an ionic liquid with a Lewis acid, Sc(OTf)₃, has been reported.²⁷ Interestingly, alkylation is not observed when EMIM-triflate is used as the ionic liquid. The authors used an excess of EMIM-triflate and it is possible that reaction was prevented by the deactivation of catalyst by ionic liquid (acidity of superacids is lowered in ionic liquids^{17,28}). It is also possible that ionic liquid may improve the phase compatibility of the catalyst with the hydrophobic organic reactants, acting as a pseudo phase transfer catalyst. It would be interesting to see if lowering the amount

of IL (a high catalyst/IL ratio) gives rise to alkylation. From a practical point of view, it would be ideal to have both minimum acid and minimum IL, yielding a phase-separated system after reaction.

We also investigated the acid catalyzed polymerization of 1,3-propanediol in the presence of an ionic liquid and acid catalyst. 1,3-Propanediol can be prepared using a recently commercialized fermentation process based upon corn-derived glucose. The polyether made from the acid-catalyzed condensation of 1,3-propanediol, PO3G, is 100% renewably resourced and is now available under the trade name Cerenol®.²⁹ The desired polymer molecular weight M_n can be varied from 250 to 3000 depending upon the reaction conditions, giving a range of low viscosity liquids to highly viscous polymers. Other renewable polymers are polylactic acid and polyglycolide.³⁰ These polymers are starting to find a wide range of uses as lubricants, coatings, oils, clothing, and additives in other polymer systems. The interest in renewably resourced chemicals and polymers is an active area of interest.^{31–33}

Polymerization of 1,3-propanediol to polyol was performed using TFESA (bp 212 °C) and ionic liquids, such as EMIM-TFES (see Experimental section). Similar results were obtained using the ionic liquid BMIM-TFES. This reaction can also be carried out with a wide range of catalysts, including sulfuric acid, although superacids have the advantage of fewer by-products (sulfate esters are common in sulfuric acid based reactions).³⁴



The homogeneous solution of 1,3-propanediol and TFESA in EMIM-TFES was heated at 160 °C under a nitrogen atmosphere. Water slowly evolved as polymerization took place and was collected in a condenser, assisted by a slow nitrogen purge. As the polymer forms, the solution goes from a single-phase to a two-phase system. Upon cooling, two phases were clearly visible. The top phase was shown *via* ¹H NMR spectroscopy to be polymerized 1,3-propanediol (polyol) with molecular weight (M_n) of 2907, after a reaction time of 10.5 hours. Most of the acid and ionic liquid were found to be in the lower phase. The time it took for phase separation was between one and two hours, probably due to the higher viscosity of the polymer. The lower phase can be easily separated by decantation and recycled. In this case, EMIM-TFES is readily soluble in 1,3-propanediol and as the less polar polymer is formed, both the ionic liquid and acid form a separate phase. Between 1.5 and 2 wt% of the original acid is found in the polymer layer together with less than 1 wt% of the IL. At the same time, less than 1 wt% of the product is found in the lower acid/IL phase. Traces of the acid can be removed from that layer completely by treatment with CaCO₃. The catalyst/IL phase was recycled and the rate of evolution of water, which is related to the conversion rate, was about the same as during the first cycle. The resulting polymer showed M_n of 3000 after reaction time of 10.5 hours (Fig. 5).

We have also investigated etherification of *n*-pentanol. Di-*n*-pentylether has a wide range of industrial uses.¹⁵ The etherification of *n*-pentanol with a range of acid catalysts has

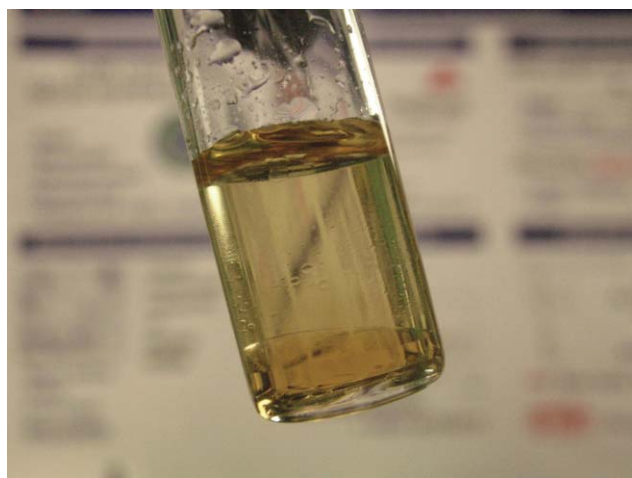
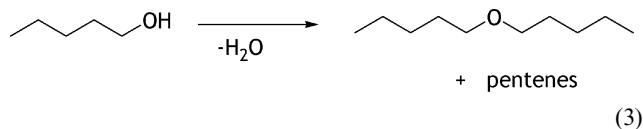


Fig. 5 Formation of the polyol product PO3G (M_n 2907, top layer), with the TFESA catalyst and ionic liquid in the lower phase.

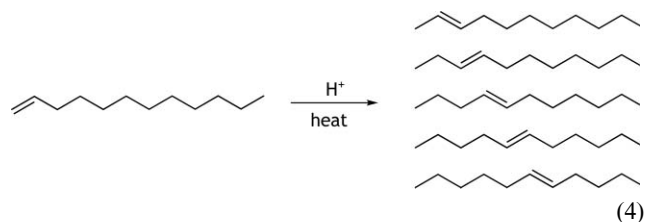
recently been described.¹⁵ We attempted this reaction using a mixture of TFESA and EMIM-TFES at 165 °C in a sealed pressure vessel (*ca.* 25 psi, 6–8 hours). Under these conditions an equilibrium mixture is formed between di-*n*-pentylether, water, and *n*-pentanol, including about 10% dehydration to the pentenes.



Typical conversions (around 70%) were obtained after heating for 6 hours. Thus the final mixture contained about 70% di-*n*-pentylether, 15% *n*-pentanol and 15% pentenes (measured *via* GC, pentene is hard to quantify as the reaction vessel was vented at atmospheric pressure). We found that fast phase separation occurs at the end of the reaction (after shaking the two phases are reformed within 1–2 minutes). However, the product distribution in the two phases is not as distinct as in the reactions described above (as determined by careful ¹H NMR analysis with comparisons to the pure individual species, *n*-pentanol, di-*n*-pentylether, TFESA and EMIM-TFES). At least 10% of the *n*-pentanol and di-*n*-pentylether mixture was found in the IL phase, along with some ionic liquid being found in the main product phase (about 5 wt% of the ionic liquid). The product of this reaction is more polar than alkyl benzenes or long chain polyols, leading to a greater degree of phase miscibility with the ionic liquid phase. More work is needed to find the optimum IL-catalyst-alcohol system for this reaction.

Various methods have been described in the past for the catalytic isomerization of hydrocarbons,³⁵ including the use of superacids. The products, a mixture of internal olefins, are subsequently used in a range of major industrial processes in the context of petrochemical oil-refining.³⁶ Olefin chemistry involving *cis-trans*-isomerization, or double bond migration, is widely known.^{36,37} The olefin isomer products are useful in the formulation of well fluids such as drilling mud for offshore drilling. Whereas TFESA showed virtually no catalytic activity in this reaction when used neat, when in C₁₂MIM-TFES,

the same catalyst showed conversion to the thermodynamic mixture of six isomers (see below), depending upon the reaction conditions and the nature of the ionic liquid. This reaction system differs from the ones described above in that it is essentially biphasic from the very start of the reaction. Thus, the reactivity will depend on the nature of the interface and the availability of the acid to the reagents (1-dodecene in this case). As discussed below, longer chain ILs appear to be more effective.



The isomerization was investigated by mixing the ionic liquid (for example 1 g of C₁₂MIM-TFES), TFESA (0.5 g) and 1-dodecene (30 ml). The stirred mixture was heated to 100 °C for 2 hours, and the reaction progress was followed by GC as described previously.² GC analysis confirmed the conversion of 1-dodecene to a thermodynamic mixture of isomers, with about 15% of the 1-dodecene remaining (85% conversion). A similar result was obtained in 1-hexadecyl-3-methylimidazolium TFES ionic liquid. A series of 1-alkyl-3-methylimidazolium TFES ionic liquids was investigated. The order of activity (measured as the time to reach equilibrium distribution of isomeric olefins), based on the length of the alkyl group, was found to be hexadecyl ≥ dodecyl > hexyl >> butyl ≈ ethyl. The conversion in EMIM-TFES was less than 10% after two hours, and a similar result was obtained for BMIM-TFES. The 1-Hexyl-3-methylimidazolium TFES/TFESA system gave 50% conversion after two hours. The ratio of the ionic liquid to TFESA did not appear to have a dramatic effect on the rate of this reaction. It is likely that the longer alkyl chain on the imidazolium cation gives rise to higher activity through better dispersion of the reagent in the IL/acid phase.

Summary

We have shown that superacids such as 1,1,2,2-tetrafluoroethanesulfonic acid can be used in conjunction with ionic liquids made from the anion of the same acid in the chemical processing of a number of chemically important reactions (alkylation, etherification and isomerization). Interesting phase change behavior occurs during alkylation and etherification reactions which facilitates easy separation of the products. We applied this biphasic catalytic system to the synthesis of a new kind of polymer based upon the acid-catalyzed polycondensation of 1,3-propanediol, which can be derived from a renewable resource. Olefin isomerization can also be catalyzed using superacid-ionic liquid mixtures, although the chemical structure of the ionic liquid has a very strong effect on conversion: the longer alkyl chains on the ionic liquid gave higher conversions, presumably due to an enhanced interfacial interaction of the olefin with the catalyst. These preliminary findings point to the potential use of carefully

selected ionic liquids and superacids in improved chemical processing.

Experimental section

The synthesis of TFESA and HFPSA has recently been described.² For TFESA: ¹⁹F NMR (CD₃OD) δ -125.2 (dt, ³J_{FH} = 6 Hz, ³J_{FF} = 8 Hz, 2F); -137.6 (dt, ²J_{FH} = 53 Hz, 2F). ¹H NMR (CD₃OD) δ 6.3 (tt, ³J_{FH} = 6 Hz, ²J_{FH} = 53 Hz, 1H). For HFPSA: ¹⁹F NMR (D₂O) δ -74.5 (m, 3F); -113.1, -120.4 (AB q, J = 264 Hz, 2F); -211.6 (m, 1F). ¹H NMR (D₂O) δ 5.8 (m, ²J_{FH} = 43 Hz, 1H).

The ionic liquids were synthesized from the respective halides of the cations and the corresponding potassium sulfonate salt of the acid. Examples of the syntheses of four ionic liquids are described below.

Synthesis of 1-butyl-3-methylimidazolium

1,1,2,2-tetrafluoroethanesulfonate (BMIM-TFES)

1-Butyl-3-methylimidazolium chloride (60.0 g) and high purity dry acetone (>99.5%, 300 ml) were combined in a one-liter flask and warmed to reflux with magnetic stirring until the solid completely dissolved. At room temperature in a separate one-liter flask, potassium-1,1,2,2-tetrafluoroethanesulfonate² (TFES-K, 75.6 g) was dissolved in high purity dry acetone (500 ml). These two solutions were combined at room temperature and allowed to stir magnetically for 2 hr under positive nitrogen pressure. The stirring was stopped and the KCl precipitate was allowed to settle, then removed by suction filtration through a fritted glass funnel with a celite pad. The acetone was removed *in vacuo* to give a yellow oil. The oil was further purified by diluting with high purity acetone (100 ml) and stirring with decolorizing carbon (5 g). The mixture was again suction filtered and the acetone removed *in vacuo* to give a colorless oil. This was further dried at 4 Pa and 25 °C for 6 hr to provide 83.6 g of product. ¹⁹F NMR (DMSO-d₆) δ -124.7 (dt, J = 6 Hz, J = 8 Hz, 2F); -136.8 (dt, J = 53 Hz, 2F). ¹H NMR (DMSO-d₆) δ 0.9 (t, J = 7.4 Hz, 3H); 1.3 (m, 2H); 1.8 (m, 2H); 3.9 (s, 3H); 4.2 (t, J = 7 Hz, 2H); 6.3 (dt, J = 53 Hz, J = 6 Hz, 1H); 7.4 (s, 1H); 7.5 (s, 1H); 8.7 (s, 1H).% Water by Karl-Fisher titration: 0.14%. Analytical calculation for C₉H₁₂F₆N₂O₃S: C, 37.6; H, 4.7; N, 8.8. Experimental Results: C, 37.6; H, 4.6; N, 8.7. TGA (air): 10% wt. loss @ 380 °C, 50% wt. loss @ 420 °C. TGA (N₂): 10% wt. loss @ 375 °C, 50% wt. loss @ 422 °C.

Synthesis of 1-ethyl-3-methylimidazolium

1,1,2,2-tetrafluoroethanesulfonate (EMIM-TFES)

To a one-liter round-bottom flask was added 1-ethyl-3-methylimidazolium chloride (EMIM-Cl, 98%, 61.0 g) and reagent grade acetone (500 ml). The mixture was gently warmed (50 degrees C) until almost all of the EMIM-Cl dissolved. To a separate 500 ml flask was added potassium 1,1,2,2-tetrafluoroethanesulfonate (TFES-K, 90.2 g) along with reagent grade acetone (350 ml). This second mixture was stirred magnetically at 24 °C until all of the TFES-K dissolved. These solutions were combined in a 1 liter flask producing a milky white suspension. The mixture was stirred at 24 °C for 24 hrs. The KCl precipitate was then allowed to settle leaving a clear green

solution above it. The reaction mixture was filtered once through a celite/acetone pad and again through a fritted glass funnel to remove the KCl. The acetone was removed *in vacuo* first on a rotovap and then on a high vacuum line (4 Pa, 25 °C) for 2 hr. The product was a viscous light yellow oil, which crystallized upon standing (76.0 g, 64% yield). ¹⁹F NMR (DMSO-d₆) δ -124.7 (dt, J_{FH} = 6 Hz, J_{FF} = 6 Hz, 2F); -138.4 (dt, J_{FH} = 53 Hz, 2F). ¹H NMR (DMSO-d₆) δ 1.3 (t, J = 7.3 Hz, 3H); 3.7 (s, 3H); 4.0 (q, J = 7.3 Hz, 2H); 6.1 (tt, J_{FH} = 53 Hz, J_{FH} = 6 Hz, 1H); 7.2 (s, 1H); 7.3 (s, 1H); 8.5 (s, 1H).% Water by Karl-Fisher titration: 0.18%. Analytical calculation for C₈H₁₂N₂O₃F₄S: C, 32.9; H, 4.1; N, 9.6 Found: C, 33.3; H, 3.7; N, 9.6. Mp 45–46 °C. TGA (air): 10% wt. loss @ 379 °C, 50% wt. loss @ 420 °C. TGA (N₂): 10% wt. loss @ 378 °C, 50% wt. loss @ 418 °C.

Synthesis of 1-ethyl-3-methylimidazolium

1,1,2,3,3,3-hexafluoropropanesulfonate (EMIM-HFPS)

To a one-liter round-bottom flask was added 1-ethyl-3-methylimidazolium chloride (EMIM-Cl, 98%, 50.5 g) and reagent grade acetone (400 ml). The mixture was gently warmed (50 °C) until almost all of the EMIM-Cl dissolved. To a separate 500 ml flask was added potassium 1,1,2,3,3,3-hexafluoropropanesulfonate (HFPS-K, 92.2 g) along with reagent grade acetone (300 ml). This second mixture was stirred magnetically at room temperature until all of the HFPS-K dissolved. These solutions were combined and stirred under positive N₂ pressure at 26 °C for 12 hr producing a milky white suspension. The KCl precipitate was allowed to settle overnight leaving a clear yellow solution above it. The reaction mixture was filtered once through a celite/acetone pad and again through a fritted glass funnel. The acetone was removed *in vacuo* first on a rotovap and then on a high vacuum line (4 Pa, 25 °C) for 2 hr. The product was a viscous light yellow oil (103.8 g, 89% yield). ¹⁹F NMR (DMSO-d₆) δ -73.8 (s, 3F); -114.5, -121.0 (ABq, J = 258 Hz, 2F); -210.6 (m, J_{HF} = 41.5 Hz, 1F). ¹H NMR (DMSO-d₆) δ 1.4 (t, J = 7.3 Hz, 3H); 3.9 (s, 3H); 4.2 (q, J = 7.3 Hz, 2H); 5.8 (m, J_{HF} = 41.5 Hz, 1H); 7.7 (s, 1H); 7.8 (s, 1H); 9.1 (s, 1H).% Water by Karl-Fisher titration: 0.12%. Analytical calculation for C₉H₁₂N₂O₃F₆S: C, 31.5; H, 3.5; N, 8.2. Experimental Results: C, 30.9; H, 3.3; N, 7.8. TGA (air): 10% wt. loss @ 342 °C, 50% wt. loss @ 373 °C. TGA (N₂): 10% wt. loss @ 341 °C, 50% wt. loss @ 374 °C.

Synthesis of tetradecyl(tri-*n*-butyl)phosphonium

1,1,2,3,3,3-hexafluoropropanesulfonate ([4.4.4.14]P-HFPS)

To a 4 l round-bottom flask was added the ionic liquid tetradecyl(tri-*n*-butyl)phosphonium chloride (Cyphos® IL 167, 345 g) and deionized water (1000 ml). The mixture was magnetically stirred until it was one phase. In a separate 2 liter flask, potassium 1,1,2,3,3,3-hexafluoropropanesulfonate (HFPS-K, 214.2 g) was dissolved in deionized water (1100 ml). These solutions were combined and stirred under positive N₂ pressure at 26 °C for 1 hr producing a milky white oil. The oil slowly solidified (439 g) and was removed by suction filtration and then dissolved in chloroform (300 ml). The remaining aqueous layer (pH = 2) was extracted once with chloroform (100 ml). The chloroform layers were combined and washed with an aqueous sodium carbonate solution (50 ml) to remove any

acidic impurity. They were then dried over magnesium sulfate, suction filtered, and reduced *in vacuo* first on a rotovap and then on a high vacuum line (4 Pa, 100 °C) for 16 hr to yield the final product as a white solid (380 g, 76% yield). ¹⁹F NMR (DMSO-*d*₆) δ -73.7 (s, 3F); -114.6, -120.9 (ABq, *J* = 258 Hz, 2F); -210.5 (m, *J*_{HF} = 41.5 Hz, 1F). ¹H NMR (DMSO-*d*₆) δ 0.8 (t, *J* = 7.0 Hz, 3H); 0.9 (t, *J* = 7.0 Hz, 9H); 1.3 (br s, 20H); 1.4 (m, 16H); 2.2 (m, 8H); 5.9 (m, *J*_{HF} = 42 Hz, 1H). % Water by Karl-Fisher titration: 895 ppm. Analytical calculation for C₂₉H₅₇F₆O₃PS: C, 55.2; H, 9.1; N, 0.0. Experimental Results: C, 55.1; H, 8.8; N, 0.0. TGA (air): 10% wt. loss @ 373 °C, 50% wt. loss @ 421 °C. TGA (N₂): 10% wt. loss @ 383 °C, 50% wt. loss @ 436 °C.

Catalyst testing

All reagents were reagent grade.

Akylation²

The ionic liquid 1-dodecyl-3-methylimidazolium 1,1,2,2-tetrafluoroethanesulfonate (0.19 g) was placed in a round bottomed flask and dried at 150 °C for 48 hours. 1,1,2,3,3,3-Hexafluoropropanesulfonic acid (0.5 g) was added, followed by the addition of 5 ml of 1-dodecene and 15 ml of *p*-xylene. The mixture was heated to 100 °C under a nitrogen atmosphere. After 2 hours reaction time, gas chromatographic analysis showed near complete reaction (>95%) of the 1-dodecene to give the alkylated product. The ionic liquid and acid formed a distinct second phase that separated out at the bottom of the flask. GC analysis was performed as follows. Samples were diluted 1 to 20 in ether for GC analysis. All of the samples were analyzed by a Hewlett Packard 5890 Series II GC equipped with FID detectors. Product identification was carried out with a GC-MS analysis and ¹H NMR. The products were identified by comparison of their spectra and retention time in GC with those of authentic samples. In the case of the alkylation reactions (carried out at 100 °C with conversion close to 99%), the products contain >95% linear alkylate and the remainder (<5%) are the 4% branched alkylates from the ~ 4% branched olefins (impurity in the feed), and dimers of 1-dodecene. Full details for these reactions has been reported previously.²

Polyol Formation (etherification)

1,3-Propanediol (20 g) was placed in a three-neck round-bottom flask. To this was added TFESA (0.16 g, 0.8 wt% in the final solution). BMIM-TFES (4 g) was also added and the solution and contents were purged with nitrogen for two hours. The homogeneous solution was heated using an oil bath at 160 °C under a nitrogen atmosphere. Water slowly evolved and was collected in a condenser. After approximately 9–10 hours the solution went from a single phase to a two-phase system. Upon cooling to 75 °C, two phases were clearly visible. The top phase was shown *via* ¹H NMR spectroscopy to be essentially polymerized propanediol (polyol). The molecular weight (*M*_n) was 2907, after a reaction time of 10.5 hours. The acid and ionic liquid were found to be essentially in the lower phase with polyol in the upper phase. The lower phase can easily be separated and recycled.

References

- P. T. Anastas and T. C. Williamson, *Green Chemistry: Frontiers in Benign Chemical Syntheses and Processes*, Oxford University Press, 1998.
- M. A. Harmer, C. Junk, V. Rostovtsev, L. G. Carcani, J. Vickery and Z. Schnepf, *Green Chem.*, 2007, **9**, 30–37.
- V. V. Rostovtsev, L. M. Bryman, C. P. Junk, M. A. Harmer and L. G. Carcani, *J. Org. Chem.*, 2008, **73**, 711–714.
- J.-P. Simonato, *Chem. Ind.*, 2005, 20–21.
- E. Marx, *Speciality Chemicals Magazine*, 2004, **24**, 24–25.
- Y. Katsuhara, M. Aramaki, A. Ishii, T. Kume, C. Kawashima and S. Mitsumoto, *J. Fluor. Chem.*, 2006, **127**, 8–17.
- G. A. Olah, G. K. Surya Prakash and J. Sommer, *Superacids*, Wiley, 1985.
- J. A. Horsley, *Chemtech*, 1997, **27**, 45–49.
- A. de Angelis, C. Flego, P. Ingallina, L. Montanari, M. G. Clerici, C. Carati and C. Perego, *Cat. Today*, 2001, **65**, 363–371.
- J. A. Kocal, B. V. Vora and T. Imai, *Appl. Cat. A: General*, 2001, **221**, 295–301.
- S. J. Miller, *Stud. Surf. Sci. Cat.*, 1994, **84**, 2319–2326.
- G. A. Olah, *Friedel–Crafts Chemistry*, Wiley, 1973.
- G. Sartori and R. Maggi, *Chem. Rev.*, 2006, **106**, 1077–1104.
- R. Bringle, J. Tejero, M. Iborra, J. F. Izquierdo, C. Fite and F. Cunill, *Ind. Eng. Chem. Res.*, 2007, **46**, 6865–6872.
- J. Tejero, F. Cunill, M. Iborra, J. F. Izquierdo and C. Fite, *J. Mol. Cat. A: Chem.*, 2002, **182–183**, 541–554.
- J. H. Clark, *Catalysis of Organic Reactions by Supported Inorganic Reagents*, John Wiley & Sons, 1994.
- K. E. Johnson, R. M. Pagni and J. Bartmess, *Monatsh. Chem.*, 2007, **138**, 1077–1101.
- V. I. Parvulescu and C. Hardacre, *Chem. Rev.*, 2007, **107**, 2615–2665.
- Crystal data for EMIM-TFES (04307): C₈H₁₂F₄N₂O₃S, FW = 292.26, monoclinic, space group P21/n, a = 8.770(8) Å, b = 9.766(9) Å, c = 14.282(12) Å, β = 95.363(12)°, U = 1217.9(18) Å³, T = -100.°C, Z = 4, D_{calcd} = 1.59g/cm³. Data were collected using a Bruker Apex-II CCD system equipped with MoKα radiation yielding 9216 total reflections, 2998 unique, R_{int} = 0.041. Structure solved and refined on F² using SHELXL94.³⁸ All non-hydrogen atoms were refined with anisotropic thermal parameters. Hydrogen atoms were idealized using a riding model. The final R values were wR₂ = 0.123 and R₁ = 0.049 using all data. Crystallographic data have been deposited at the Cambridge Crystallographic Data Centre with deposition number CCDC 715667.
- Crystal data for EMIM-nonaflate (05219): C₁₀H₁₁F₉N₂O₃S, FW = 410.27, monoclinic, space group P21/c, a = 9.178(4) Å, b = 34.444(13) Å, c = 10.022(4) Å, β = 91.711(7)°, U = 3167(2) Å³, T = -100.°C, Z = 8, D_{calcd} = 1.72g/cm³. Data were collected using a Bruker Apex-II CCD system equipped with MoKα radiation on a non-merohedrally twinned crystal. Cell_{now}, Saintplus and Twinabs used to integrate data on two domains yielding 11349 total reflections. Structure solved and refined on F² using SHELXL94.³⁸ All non-hydrogen atoms were refined with anisotropic thermal parameters. Hydrogen atoms were idealized using a riding model. The final R values were wR₂ = 0.258 and R₁ = 0.171 using all data. The high-r factors are attributed to some un-modeled overlap twinned crystal. Crystallographic data have been deposited at the Cambridge Crystallographic Data Centre with deposition number CCDC 715668.
- P. Bonhote, A.-P. Dias, N. Papageorgiou, K. Kalyanasundaram and M. Graetzel, *Inorg. Chem.*, 1996, **35**, 1168–1178.
- A. R. Choudhury, N. Winterton, A. Steiner, A. I. Cooper and K. A. Johnson, *CrystEngComm*, 2006, **8**, 742–745.
- C. Perego and P. Ingallina, *Cat. Today*, 2002, **73**, 3–22.
- K. Weissermel and H.-J. Arpe, *Industrial Organic Chemistry*, WILEY-VCH, Weinheim, 2003.
- N. V. Plechkova and K. R. Seddon, *Chem. Soc. Rev.*, 2008, **37**, 123–150.
- M. J. Earle, J. M. S. S. Esperanca, M. A. Gilea, J. N. Canongia Lopes, L. P. N. Rebelo, J. W. Magee, K. R. Seddon and J. A. Widegren, *Nature*, 2006, **439**, 831–834.
- C. E. Song, E. J. Roh, W. H. Shim and J. H. Choi, *Chem. Comm.*, 2000, 1695–1696.
- C. Thomazeau, H. Olivier-Bourbigou, L. Magna, S. Luts and B. Gilbert, *J. Am. Chem. Soc.*, 2003, **125**, 5264–5265.

- 29 N. Canter, *Tribology & Lubrication Technology*, 2007, October, 14–15.
- 30 B. Gupta, N. Revagade and J. Hilborn, *Prog. Polym. Sci.*, 2007, **32**, 455–482.
- 31 J. H. Clark, V. Budarin, F. E. I. Deswarte, J. J. E. Hardy, F. M. Kerton, A. J. Hunt, R. Luque, D. J. Macquarrie, K. Milkowski, A. Rodriguez, O. Samuel, S. J. Tavener, R. J. White and A. J. Wilson, *Green Chem.*, 2006, **8**, 853–860.
- 32 R. A. Sheldon, I. Arends and U. Hanefeld, *Green Chemistry and Catalysis*, Wiley-VCH, 2007.
- 33 S. Fernando, S. Adhikari, C. Chandrapal and N. Murali, *Energy & Fuels*, 2006, **20**, 1727–1737.
- 34 V. B. Kazansky, *Reac. Kinet. Cat. Lett.*, 1999, **68**, 35–43.
- 35 H. N. Dunning, *J. Ind. Eng. Chem.*, 1953, **45**, 551–564.
- 36 W. A. Herrmann and M. Prinz, *Applied Homogeneous Catalysis with Organometallic Compounds (2nd Edition)*, 2002, **3**, 1119–1130.
- 37 M. Mirza-Aghayan, R. Boukherroub, M. Bolourtchian, M. Hoseini and K. Tabar-Hydar, *J. Organomet. Chem.*, 2003, **678**, 1–4.
- 38 G. Sheldrick, *Shelxtl Software Suite*, 5.1 5.1, Bruker AXS Corp, Madison, Wisconsin, 1996.

CO₂ absorbing cost-effective ionic liquid for synthesis of commercially important alpha cyanoacrylic acids: A safe process for activation of cyanoacetic acid†‡

Yogesh O. Sharma and Mariam S. Degani*

Received 20th October 2008, Accepted 5th January 2009

First published as an Advance Article on the web 11th February 2009

DOI: 10.1039/b818540a

Cost-effective and carbon dioxide absorbing ionic liquid, tri-(2-hydroxyethyl) ammonium acetate, was shown to perform multiple roles in Knoevenagel condensation. It acted as an environmentally benign solvent, as an activating catalyst for the less reactive cyanoacetic acid and also as a risk reduction medium for the unevenly generated large amount of CO₂ gas for large scale reactions. The reaction was scaled up for multi-gram synthesis of commercially important alpha cyanoacrylic acids.

1. Introduction

Although the Knoevenagel reaction is simple when used on laboratory scale batches, it has some critical drawbacks when carried out on a large scale in industry. The vigorous and uneven generation of carbon dioxide gas, due to unreacted cyanoacetic acid or malonic acid and also during the subsequent decarboxylation of the product, is a critical problem. The presence of volatile organic solvents and bases such as pyridine and piperidine make the system even more unsafe. The sudden excess of gas along with volatile organic solvents at higher temperature and pressure can lead to bursting of equipment due to excess pressure.¹ Although some development has been reported in this regard previously,¹ the green chemistry aspect has not been covered extensively. Hence, it is desirable to develop an alternative technology to avoid potential hazards of sudden gas evolution associated with Knoevenagel condensation.

Another difficulty with this reaction is that the Knoevenagel condensation, although simple when carried out with malononitrile and cyanoacetate esters, does not proceed smoothly under standard conditions of mild acid or base when the less reactive cyanoacetic acid is used as the nucleophile and ketones are the electrophiles.² No significant development has been reported in recent years for the Knoevenagel condensation of cyanoacetic acid. Many of the earlier reports indicate that cyanoacetic acid condensation with aldehyde leads to decarboxylated products.^{3–5} To the best of our knowledge only few generalized methods are reported wherein diverse carbonyl compounds are used for condensation, and the subsequent decarboxylation does not occur.^{6–9} Use of environmentally unfriendly reagents and

solvents like piperidine, pyridine, benzene, potassium cyanide, sodium cyanide, chloroacetic acid and acetic acid makes all these methods less acceptable.^{3,4,6–10} Hence, a versatile, rapid, safe and environmentally friendly method for cyanoacetic acid condensation with carbonyl compounds which could lead to many important intermediates is relevant to explore.

Application of ionic liquids (ILs) has now become a topic of wide interest in many disciplines of science and technology. Ionic liquids are now being utilized effectively in industries and many such processes are currently in operation on industrial scales.^{11,12} However, use of ILs in industries is still limited mostly due to the expensive cations and anions used in their synthesis. It is therefore relevant to explore and utilize cheaper ionic liquids to make them economically viable. In this context, recently many cost-effective alkanolamine based ILs have been identified.¹³ We have recently reported the application and catalytic potential of alkanolamine based ionic liquids for environmentally friendly organic synthetic methodology.¹⁴ These alkanolamines and their salts are extensively being studied for their synthetic as well as engineering applications in industries including absorption of large amounts of CO₂ evolved in industries by combustion of coals. The gas absorption potential of these alkanolamines and their salts is very well established and its proposed mechanism has been studied in detail.^{13,15} Encouraged by these facts the possibility of these ionic liquids as risk reduction medium in large scale gas evolving reactions was studied in detail.

2. Results and discussion

Reactions of structurally diverse aldehydes and ketones with various active methylene compounds were carried out in tri-(2-hydroxyethyl) ammonium acetate. Reactions of aldehydes with cyanoacetic acid were carried out at 80 °C (Scheme 1). It was observed that aromatic aldehydes reacted smoothly with cyanoacetic acid leading to good yields of the alpha cyanoacrylic acids in all cases (Table 1, entries 1–10). Yields of the products improved when excess (1.5 molar equivalent) of cyanoacetic acid was used instead of using equimolar quantities.

Department of Pharmaceutical Sciences and Technology, Institute of Chemical Technology, N.Parekh Marg, Matunga, Mumbai, 400019, India. E-mail: msdegani@udct.org, m_degani@yahoo.com; Fax: +91 22 24145614; Tel: +91 22 24145616

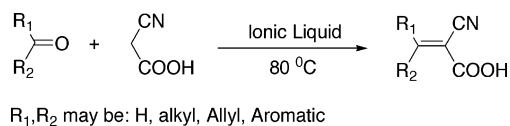
† Part of this work has been covered in Indian patent application no. 1649/MUM/2008.

‡ Electronic supplementary information (ESI) available: ¹H NMR, ¹³C NMR and FTIR spectra. See DOI: 10.1039/b818540a

Table 1 Knoevenagel condensation of carbonyl compounds in alkanolamine ionic liquid

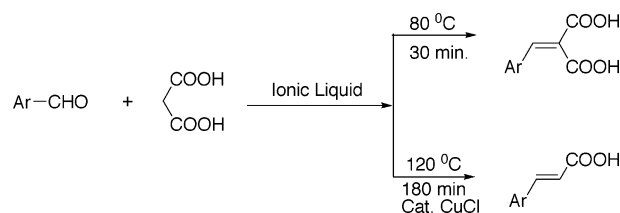
Sr. no.	Aldehyde/ketone	Active methylene compound ^a	Temp. (°C)	Time (min.)	Isolated ^b yield %	m.p. (m.p. ^{4,6,7,10}) °C
1	benzaldehyde	CAA	80	45	84	179 (178)
2	3-NO ₂ benzaldehyde	CAA	80	45	81	167 (167)
3	4-OH benzaldehyde	CAA	80	45	78	224 (223)
4	furfuraldehyde	CAA	80	45	82	215 (218)
5	2-Cl benzaldehyde	CAA	80	60	72	208 (209)
6	piperonal	CAA	80	60	78	230 (231)
7	4-OCH ₃ benzaldehyde	CAA	80	60	79	228 (227)
8	4-OH,3-OCH ₃ benzaldehyde	CAA	80	60	87	199 (199)
9	3-NO ₂ ,4-OH,5-OCH ₃ benzaldehyde	CAA	80	60	82	214
10	salicylaldehyde	CAA	80	45	87	228 (228)
11	cinnamaldehyde	CAA	80	45	83	206 (209)
12	acetophenone	CAA	80	240	NR ^c	—
13	acetone	CAA	reflux	240	55 ^c	131 (132)
14	benzophenone	CAA	80	240	NR ^c	—
15	benzaldehyde	MA	80	30	67 ^d	191(192)
16	furfuraldehyde	MA	80	30	62 ^d	195 (195)
17	benzaldehyde	MA	120	180	70 ^e	133 (133)
18	3,4-dimethoxy benzaldehyde	MA	120	180	60 ^e	181 (181)
19	benzaldehyde	ECA	80	45	82	49 (50)
20	4-OCH ₃ benzaldehyde	ECA	80	45	78	80 (80)
21	4-OH benzaldehyde	CAM	80	60	68	245 (246)
22	4-Cl benzaldehyde	CAM	80	60	72	209 (210)
23	4-OCH ₃ Benzaldehyde	MN	RT	5	87	115 (115)
24	cinnamaldehyde	MN	RT	10	77	127 (128)
25	cyclohexanone	MN	RT	240	78 ^d	Liq.
26	acetone	MN	RT	240	80	Liq.
27	acetophenone	MN	RT	300	72 ^d	92 (92)
28	benzophenone	MN	RT	300	62	138 (138)

^a 1.5 equivalent of cyanoacetic acid was used. ^b Evaluated by weight of isolated alkenes after purification (all products are known compounds and exhibit satisfactory spectroscopic data of ¹HNMR and IR). ^c Catalytic sodium methoxide was used. ^d Formation of impurities was observed. ^e 1 mol% CuCl was added, exclusive monocarboxylic acid obtained, NR: no reaction, CA: cyanoacetic acid, MA: malonic acid, ECA: ethyl cyanoacetate, MN: malononitrile, CAM: cyanoacetamide.

**Scheme 1** Knoevenagel condensation of carbonyl compounds with cyanoacetic acid.

The time required for completion of reaction was shorter in the case of aromatic aldehydes (45–60 minutes) (entries 1–10) compared to aliphatic ketones and allylic aldehyde (60–240 minutes) (entries 11–13). When reaction of acetone with cyanoacetic acid was carried out under similar conditions, the yield obtained initially was not satisfactory. Addition of sodium methoxide (20 mol%) enhanced the reaction rate considerably in this case and significant improvement in the yield was observed (entry 13). Under similar conditions, reaction of cyclohexanone leads to the formation of impurities. No product formation was observed when benzophenone and acetophenone were reacted with cyanoacetic acid even though the reactions were continued for longer periods and at higher temperatures with sodium methoxide as catalyst (entries 12, 14).

In the case of other active methylene compounds, for example malonic acid, reaction with aromatic aldehydes gave either malonic acid derivatives or cinnamic acid derivatives (Scheme 2) depending on the reaction parameters. Careful control of reaction time and temperature led to good yields of malonic acid

**Scheme 2** Selective Knoevenagel condensation of aromatic aldehyde with malonic acid in ionic liquid.

derivatives (entries 15–16). Increase in reaction temperature and time offered the cinnamic acid derivatives as major products, however addition of catalytic cuprous chloride (1 mol%) significantly increased the reaction rate to form exclusively monocarboxylic acid product (entries 17–18). Ethyl cyanoacetate reacted with aromatic aldehydes to give the respective products without any decarboxylation in good yields under similar conditions (entries 19–20). Similarly, cyanoacetamide reacted with aromatic aldehydes to give the respective products in reasonable yields (entries 21–22). Reactions of aldehydes and ketones were also carried out with malononitrile. Very fast reactions (5–30 min) of aromatic aldehydes with malononitrile in the presence of IL were observed at room temperature. The yields were excellent for both the aldehydes reacted (entries 23–24). Ketones (entries 25–28) reacted with malononitrile but the time required for optimum conversion was longer (240–300 min) as compared

to aldehydes. In reactions of ketones bearing alpha hydrogen atoms, impurities, which were identified as self condensation products of ketones were observed, in addition to the desired products (entries 25, 27). This was confirmed by carrying out the self condensation of ketones such as acetophenone and cyclohexanone under similar conditions with ionic liquid without the addition of nucleophile such as malononitrile. The formed impurity was identified by chromatographic comparison with the authentic sample.

Experiments for testing the recyclability of ionic liquid were performed using 4-methoxybenzaldehyde and cyanoacetic acid as reactants. The recovered ionic liquid was used successively three times showing no significant loss in its catalytic activity. No structural changes were observed in ionic liquid after recycling.

Studies on carbon dioxide absorption were performed on two 50 g batches using tri-(2-hydroxyethyl) ammonium acetate in a high pressure autoclave under conditions similar to those employed for Knoevenagel condensation. The study was performed at two different temperatures 50 °C and 80 °C and initial CO₂ pressure of 2.757 kPa (400 psi) and 3.447 kPa (500 psi) respectively. The drop in pressure due to ionic liquid absorption was recorded at regular intervals of 10 minutes. A considerable drop in pressure was observed in the reaction vessel at both the temperatures (Fig. 1).

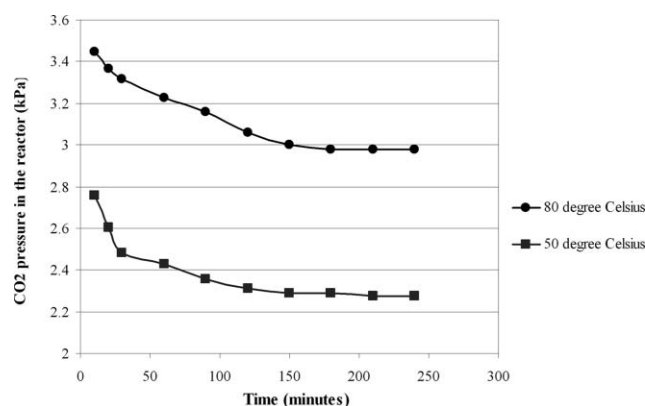


Fig. 1 CO₂ pressure drop due to absorption in ionic liquid at constant temperature.

The reaction mechanism for gas absorption by alkanolamine ionic liquids has been recently studied by Yuan and coworkers.¹³ Using a similar approach, FTIR spectra of tri-(2-hydroxyethyl) ammonium acetate before and after the gas absorption were compared for identification of changes due to carbon dioxide absorption (Fig. 2). The appearance of a prominent new band at 1652 cm⁻¹ was observed after the CO₂ absorption in the ionic liquid. This suggests the formation of an unstable carbamic acid intermediate in the zwitter-ionic form (Scheme 3). Persistent evolution of CO₂ gas from the ionic liquid was observed for several hours when the ionic liquid was kept at room temperature and atmospheric pressure after absorption. This indicated that tri-(2-hydroxyethyl) ammonium acetate absorbs carbon dioxide and slowly releases it under different experimental conditions.

The proposed mechanism for ionic liquid mediated Knoevenagel condensation could be explained by the formation of hydrogen bonding of ionic liquid with the reactants (Scheme 4). This facilitates the nucleophilic attack on carbonyl compounds,

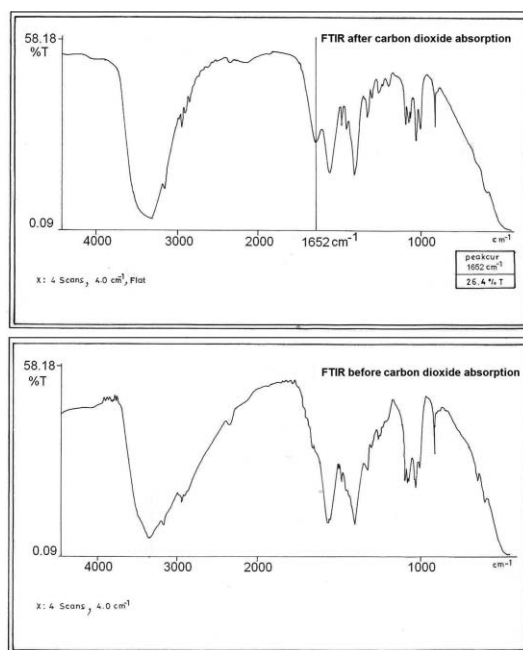
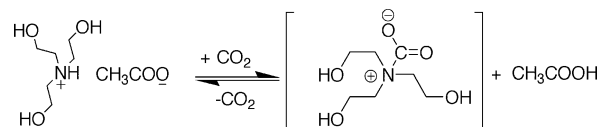


Fig. 2 FTIR spectra of the ionic liquid after and before CO₂ absorption.



Scheme 3 Proposed mechanism for CO₂ absorption by ionic liquid.

and subsequent dehydration leads to the product. Simultaneous removal of water during the reaction is not required presumably because the generated water molecules are involved in strong hydrogen bonding with the ionic liquid. Various intermediates of commercial importance were synthesized using the methodology (Table 2).

3. Experimental

3.1 General

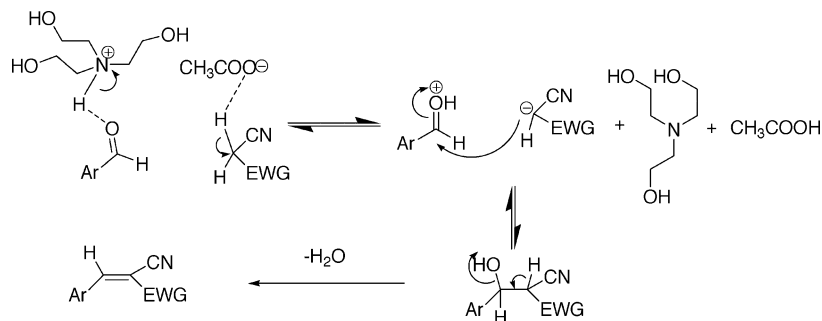
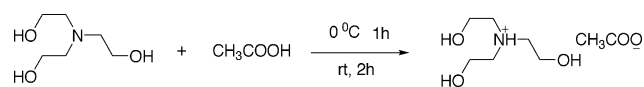
The ionic liquid was prepared by a previously reported method¹³ without any modifications (Scheme 5), and characterized by FTIR, ¹H NMR and ¹³C NMR spectroscopy. The reagents and solvents were commercially available. The products were purified using column chromatography wherever needed. All synthesized compounds are known, and identified by spectroscopic data, melting points and by comparison with available standards. FTIR spectra were obtained on a Perkin-Elmer infrared spectrometer with KBr discs and ¹H NMR spectra were recorded in CDCl₃ or DMSO-D₆ on a JEOL 300 MHz spectrometer with TMS as internal standard.

3.2 Typical experimental procedure (Table 1, entries 1–14)

Cyanoacetic acid (0.94 g, 0.011 mol) and 4-methoxy benzaldehyde (1.0 g, 0.0074 mol) were stirred with 2 g of ionic liquid in a round bottom flask and reaction mixture was heated to 80 °C. The reaction was monitored by TLC and after

Table 2 Commercial applications of selected alpha cyanoacrylic acids

Sr. no. (Table 1)	Compound	Commercial application
3	(E)-2-cyano-3-(4-hydroxyphenyl)acrylic acid	High value matrix substance in MALDI MS
8	(E)-2-cyano-3-(4-hydroxy-3-methoxyphenyl)acrylic acid	High value matrix substance in MALDI MS
9	(E)-2-cyano-3-(4-hydroxy-3-methoxy-5-nitrophenyl)acrylic acid	Possible entacapone intermediate
4	(E)-2-cyano-3-(furan-2-yl)acrylic acid	Intermediate for animals food-preservative
11	(2E,4E)-2-cyano-5-phenylpenta-2,4-dienoic acid	Intermediate for agrochemicals

**Scheme 4** Proposed mechanism for IL catalyzed Knoevenagel condensation.**Scheme 5** Synthesis of ionic liquid tri-(2-hydroxyethyl) ammonium acetate.

completion, (E)-2-cyano-3-(4-methoxyphenyl)acrylic acid, was isolated (1.33 g, 79%) by acidification with aqueous hydrochloric acid (pH=5) at 5 °C and subsequent filtration. Traces of aldehyde if any, were removed by washing the product with hexane.

3.3 Typical experimental procedure (Table 1, entries 23–28)

Malononitrile (0.4884 g, 0.0074 mol) and 4-methoxy benzaldehyde (1 g, 0.0074 mol) were stirred with 2 g of ionic liquid in a round bottom flask at room temperature. The reaction was monitored by TLC and after completion, 2-(4-methoxybenzylidene)malononitrile (1.177 g, 87%) was isolated by quenching the reaction mixture with water at 5 °C and subsequent filtration. Traces of aldehyde if any, were removed by washing the product with hexane.

3.4 Experimental procedure for a larger batch

To 200 g ionic liquid in a three neck round bottom flask with overhead stirrer, cyanoacetic acid (93.5 g, 1.1 mol) was added and the temperature was raised to 85 °C. To this, 4-methoxy benzaldehyde (100 g, 0.74 mol) was added portion wise over a period of 15 min. The reaction was monitored by TLC. After completion of the reaction (3 hours) (E)-2-cyano-3-(4-methoxyphenyl) acrylic acid was isolated (122 g, 82%) by quenching the reaction mixture in 2 liters of chilled water, acidification with aqueous hydrochloric acid (pH ~ 5–6) and subsequent filtration. Traces of aldehyde were removed by washing the product with hexane. The ionic liquid was recovered by evaporating the water under reduced pressure.

(A similar ratio of reactants and IL gave 80% yield from a 10 g batch of 4-methoxy benzaldehyde.)

3.5 Spectroscopic data for ionic liquid and selected compounds

Tri-(2-hydroxyethyl) ammonium acetate. IR (KBr, $\nu_{\max}/\text{cm}^{-1}$): 3310, 3154, 2936, 1560, 1482, 1456, 1404, 1326, 1295, 1092, 1077, 1062, 1025, 1000, 911; δ_{H} (300 MHz; DMSO- d_6): 1.792 (s, 3H, CH₃COO), 2.4 (t, 6H, $J = 6$ Hz, CH₂N), 3.32 (t, 6H, $J = 6$ Hz CH₂O), 5.4, (br s, 3H, OH); δ_{C} (300 MHz; DMSO- d_6): 21.16, 57.15, 59.13, 172.

(Table 1. Entry 7). Yellow crystals, melting point 228 °C.

IR (KBr, $\nu_{\max}/\text{cm}^{-1}$): 2824, 2550, 2230, 1697, 1602, 1587, 1492, 1430, 1290, 1213, 1094, 921, 833.

δ_{H} (300 MHz; DMSO- d_6): 3.85 (s, 3H, OCH₃), 7.11(d, 2H, $J = 9$ Hz, ArH), 8.03 (d, 2H, $J = 9$ Hz, ArH), 8.23 (s, 1H); δ_{C} (300 MHz; DMSO- d_6): 53, 104, 119, 121, 128, 137, 158, 167, 168.

(Table 1. Entry 13). White crystals, melting point 131 °C.

IR (KBr, $\nu_{\max}/\text{cm}^{-1}$): 3410, 2886, 2219, 1699, 1602, 1411, 1367, 1290, 1255, 1089, 917, 780, 759, 599; δ_{H} (300 MHz; CDCl₃; Me₄Si): 2.36 (s, 3H, CH₃), 2.44 (s, 3H, CH₃), 10 (s br, 1H, COOH).

δ_{C} (300 MHz; CDCl₃; Me₄Si): 23.27, 27.95, 104.5, 115.22, 166.7, 177.2.

(Table 1. Entry 20). Yellow crystals, melting point 80 °C.

IR (KBr, $\nu_{\max}/\text{cm}^{-1}$): 2990, 2916, 2215, 1710, 1584, 1561, 1513, 1431, 1262, 1211, 1184, 1127, 1089, 1017, 837; δ_{H} (300 MHz; CDCl₃; Me₄Si): 1.39 (t, $J = 7.1$ Hz, 3H, CH₃), 3.89 (s, 3H, OCH₃), 4.38 (q, $J = 7.1$ Hz, 2H, CH₂), 7.01 (d, $J = 9$ Hz, 2H, ArH), 8.02 (d, $J = 9$ Hz, 2H, ArH), 8.19 (s, 1H, CH); δ_{C} (300 MHz; CDCl₃; Me₄Si): 14.2, 55.6, 62, 99.36, 114.7, 116.2, 124.37, 133, 154.4, 163.13, 163.79.

(Table 1. Entry 23). Yellow crystals, melting point 115 °C.

IR (KBr, $\nu_{\max}/\text{cm}^{-1}$): 2921, 2211, 1603, 1571, 1512, 1406, 1369, 1319, 1277, 1183, 1155, 1093, 1021, 833; δ_{H} (300 MHz; CDCl₃;

Me₄Si): 3.92 (s, 3H, CH₃O), 7.01 (t, $J = 9$ Hz, 2H, ArH), 7.66 (s, 1H, CH), 7.90 (d, $J = 9$ Hz, 2H, ArH); δ_{C} (300 MHz; CDCl₃; Me₄Si): 55, 114, 124, 133, 158, 164.

4. Conclusion

Interestingly, the cost-effective and less explored ionic liquid, tri-(2-hydroxyethyl) ammonium acetate performed multiple roles in this methodology such as acting as an environmentally benign solvent, an activating catalyst for the less reactive cyanoacetic acid and also as a risk reduction medium for unevenly generated CO₂ gas during the reaction. Another important aspect of this methodology is that alpha cyanoacrylic acids, useful intermediates in pharmaceuticals and fine chemicals could easily be synthesized. Scale up of the reaction parameters were successfully carried out for multi-gram batch size. The ionic liquid was recycled three times without any significant loss in the catalytic activity.

Acknowledgements

Y.O.S. thanks CSIR New Delhi, Govt. of India for financial support.

References

- 1 M. Kaufhold, J. Metz, US Patent 5008429.
- 2 A. P. Davis and K. M. Bhattarai, *Tetrahedron*, 1995, **51**, 8033.
- 3 N. Ragoussis and V. Ragoussis, *J. Chem. Soc. Perkin Trans 1*, 1998, 3529.
- 4 A. Nohara, H. Kurki, T. Saijo, H. Sugihara, M. Kanno and Y. Sanno, *Korean J. Med. Chem.*, 1977, **20**, 141.
- 5 R. V. Hangarge, S. A. Sonwane, D. V. Jarikote and M. S. Shingare, *Green Chem.*, 2001, **3**, 310.
- 6 M. J. Astle and W. C. Gergel, *J. Org. Chem.*, 1956, **21**, 493.
- 7 F. S. Prout, *J. Org. Chem.*, 1953, **18**, 928.
- 8 A. Lapworth and J. Alexander McRae, *J. Chem. Soc. Trans.*, 1922, **121**, 1699.
- 9 A. Lapworth and J. Alexander McRae, *J. Chem. Soc. Trans.*, 1922, **121**, 2741.
- 10 W. M. Rodionow and A. M. Fedorowa, *Arch. Pharm.*, 1933, **271**, 292.
- 11 P. Wasserscheid and T. Welton, *Ionic Liquid in Synthesis*, Wiley-VCH, 2004.
- 12 N. V. Plechkova and K. R. Seddon, *Chem. Soc. Rev.*, 2008, **37**, 123.
- 13 X. L. Yuan, S. J. Zhang and X. M. Lu, *J. Chem. Eng. Data*, 2007, **52**, 596.
- 14 Y. O. Sharma and M. S. Degani, *J. Mol. Cat. A: Chemical*, 2007, **277**, 215.
- 15 X. Yuan, S. Zhang, J. Liu and X. Lu, *Fluid Phase Equilibria*, 2007, **257**, 195.

Permselective nanostructured membranes based on cellulose nanowhiskers

Wim Thielemans, Catherine R. Warbey and Darren A. Walsh*

Received 14th October 2008, Accepted 5th January 2009

First published as an Advance Article on the web 13th February 2009

DOI: 10.1039/b818056c

Nanostructured thin films of cellulose nanowhiskers derived from cotton were formed using a simple drop-coating procedure. The hydrogen-bonded cellulose films were stable in aqueous solutions and their permselective properties were probed using voltammetric techniques. The nanowhisker extraction procedure produces cellulose nanowhiskers with negatively-charged sulfate surface groups that inhibit the transfer of negatively-charged species through the nanowhisker membrane, while the diffusion of neutral species is only slightly hindered. Using rotating-disk electrode measurements, the diffusion of various species within the film was studied and it was shown that the positively-charged species, $\text{Ru}(\text{NH}_3)_6^{3+}$, was adsorbed by the film, whereas the negatively-charged species, IrCl_6^{3-} , was excluded by the film. The thermodynamics of adsorption of the positively-charged species by the cellulose nanoparticles were then studied using isotherm data. These observations open up new possibilities in electrochemical sensor development using renewable cellulosic materials as building blocks. Furthermore, charge-based permselective membranes can also be formed using free standing cellulose nanowhisker films, which offer the promise of renewable, selective membranes for separation technologies.

Introduction

The development and applications of nanostructured materials have been extremely active areas of research for a number of years. The unique magnetic,¹ optical,² catalytic,³ and structural properties⁴ of nanostructured materials means that the number of potential applications of these materials is vast, ranging from the development of new lightweight materials for the construction industry to the identification of the human immunodeficiency (HIV) virus.^{5,6} Given the current emphasis on green chemistry and chemical process, the application of the fundamental principles of green chemistry to nanotechnology may broaden the appeal of nanotechnology to consumers and open up new markets for “renewable nanomaterials.”

Cellulose is the most abundant macromolecule on earth, produced at the rate of 10^{11} – 10^{12} tons per year by nature.⁷ Applications of cellulose are diverse, including use as an emulsifier,^{8,9} a stabilizer,¹⁰ a gelling agent,¹¹ and a stationary phase for chiral-HPLC separations.¹² Natural cellulose consists of crystalline and amorphous regions. The amorphous regions are highly susceptible to hydrolysis and, under controlled conditions, may be removed leaving the crystalline regions intact. The extraction of crystalline cellulose regions, which are in the form of nanowhiskers, is a simple and environmentally-friendly process. The nanowhiskers can be subsequently used as biodegradable additives in nanocomposite materials.^{13,14} Nanocomposite materials based on cellulose nanowhiskers have attracted much attention recently due to their mechanical properties.^{15,16} Cel-

lulosic materials have also shown some promising applications in the development of alternative energy sources. For example, nanoporous regenerated cellulose membranes have been used in place of proton-exchange membranes in microbial fuel cells.¹⁷ Membranes formed from cellulose acetate and nitrate have also been used extensively in electroanalytical applications.^{18–20} However, investigations into the electrochemical properties of membranes formed from cellulose nanoparticles have not been widely reported. In one recent study, the formation of nanoporous, thin films of cellulose nanowhiskers incorporating “receptor” polymer molecules that could selectively accumulate and transport hydrophobic species such as triclosan and $\text{Fe}(\text{CN})_6^{3-}$ was reported.²¹

In this contribution, the transport properties of membranes, formed from cellulose nanowhiskers are fully explored. Extraction of the nanowhiskers from cotton using H_2SO_4 yields highly-stable aqueous suspensions of nanowhiskers with negatively-charged sulfate groups due to the esterification of surface hydroxyl groups.²² Thin, nanoporous films of these negatively-charged nanowhiskers can be formed easily at solid surfaces by simple drop-coating procedures. The stability of these films, due to interparticle hydrogen bonding, is such that these films remain stable in aqueous solutions, and can also be peeled from the surfaces and can be used as free standing membranes. The transport properties of these films were studied using classical voltammetric techniques. This revealed that anionic species were repelled by the film, while cationic species were selectively accumulated within the films. Using cyclic voltammetry and rotating-disk electrode (RDE) measurements, the partition of the various redox mediators into the films was studied. The negatively-charged cellulose films can retain cationic species, even when in contact with electrolyte solutions containing no redox-active species, indicating a high energy of interaction

School of Chemistry and Department of Chemical and Environmental Engineering, The University of Nottingham, Nottingham, UK NG7 2RD. E-mail: darren.walsh@nottingham.ac.uk; Fax: 0115 9513437; Tel: 0115 9513562

between the binding sites on the film and the cationic species. The thermodynamics of this interaction were examined using isotherm data and the potential of these naturally-occurring nanostructured materials in electrochemical sensor development and permselective membranes is briefly discussed. This work opens the door to a new technology combining simple stable membrane formation with biodegradability, biocompatibility, renewability and high effectiveness.

Experimental section

All reagents were from Sigma-Aldrich and were the highest grade available. Aqueous cellulose nanowhisker solutions were prepared from cotton using the method described by Revol.²³ Briefly, cotton wool was hydrolysed using 64 wt% sulfuric acid (8.75 mL acid per g of cotton) at 45 °C for 35 min. The resulting nanowhiskers were centrifuged, washed three times with distilled water and dialyzed to neutrality (of the effluent) against tap water. The suspension was then sonicated twice for 5 min each using a Branson Sonifier (Branson Ultrasonics Corp., Danbury, Connecticut), while ensuring the temperature did not rise above 35 °C. In between sonication steps, the nanowhisker suspension was ion-exchanged with a mixed bed resin (Amberlite MB6113) to replace surface cations with hydrogen. The stable dispersion was subsequently filtered over a No. 2 fritted filter to remove residual aggregates and concentrated to 1.5 wt% by water evaporation at 45 °C in a convection oven. The cellulose nanowhisker yield was approximately 30%.

Nanoporous cellulose films at electrode surfaces were prepared by dispensing a 10 μL aliquot of the homogeneous cellulose nanowhisker solution onto a glassy carbon electrode surface using a micropipette and drying at 40 °C for 45 minutes in a convection oven while maintaining the electrode upright. For cyclic voltammetry experiments, a 3 mm diameter glassy carbon electrode (CH Instruments, Austin, Texas) was used. RDE experiments were performed using a 5 mm diameter glassy carbon RDE and Modulated Speed Rotator from Pine Research Instrumentation (Raleigh, North Carolina). All measurements were performed using a computer-controlled Model 760 C potentiostat (CH Instruments Inc., Austin, Texas) and a conventional three-electrode cell containing a silver/silver chloride reference electrode and a 1 cm^2 platinum flag as counter electrode.

Characterization of the films was performed using a model MFP3D atomic force microscope (Asylum Research Atomic Force Microscopes, Santa Barbara, California) in tapping mode using a probe oscillation rate of 1 Hz. To determine the thickness of the drop-coated cellulose films, a cut was made in the middle of the film using a sharp blade. A tapping-mode AFM image was then recorded at an oscillation rate of 0.20 Hz to record the film thickness, calculated as the average height difference between the centre of the cut and a position on the film surface 80 μm across the film.

Results and discussion

Preparation of nanoporous cellulose films

Cellulose forms the structurally strong framework in plant cell walls. It comprises a linear polymer consisting of β -(1 \rightarrow 4)-D-glucopyranose units in ${}^4\text{C}_1$ conformation. The equatorial con-

formation of the glucopyranose residues stabilizes the structure, increasing its rigidity and extensive intra- and intermolecular hydrogen bonding also cause complete insolubility in water. Natural cellulose is composed of nanowhiskers (4–20 nm in width and 100–40,000 nm long), which can be produced using acid hydrolysis of the cellulose source. A solution of cellulose nanowhiskers (1.5% w/w) from cotton was used in the present study to form films at glassy carbon electrodes using a solvent-evaporation technique. Upon drying, hydrogen bonds are formed between adjacent nanowhiskers, resulting in an extremely stable thin film at the electrode surface.²¹ Reported literature values for the tensile modulus between 6 and 15 GPa are a clear sign of the strong interparticle interactions.¹⁶ Similar values have been measured by the authors. A typical atomic force microscope image of a cellulose nanowhisker film formed at a glassy carbon surface is shown in Fig. 1. The drop-coated cellulose nanowhiskers formed a porous deposit with 50–100 nm pores visible throughout the deposit. The thickness of the cellulose films, as determined using AFM, was $2.0 \pm 0.5 \mu\text{m}$.

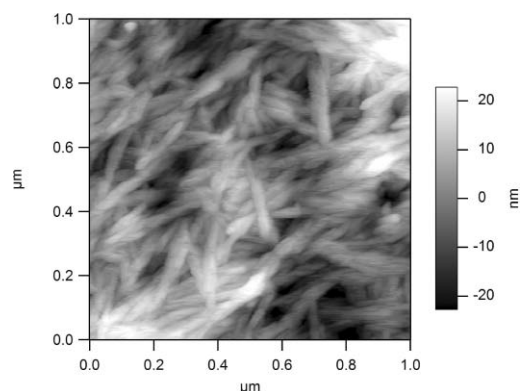


Fig. 1 Tapping-mode AFM image of cellulose nanowhiskers at a glassy carbon electrode prepared by drop coating the surface with 10 μL of 1.5% aqueous nanowhisker suspension and drying at 40 °C for 45 minutes.

Voltammetry of redox mediators at cellulose-modified electrodes

Typical cyclic voltammetric responses for 1 mM solutions of ferrocenemethanol (FcOH), potassium hexachloroiridate (IrCl_6^{3-}) and ruthenium hexamine ($\text{Ru}(\text{NH}_3)_6^{3+}$) at bare and cellulose-modified glassy carbon electrodes are shown in Fig. 2. At the bare electrode surfaces, the voltammetric currents were similar in magnitude due to the similar diffusion coefficients of each species in the electrolyte solution ($7.8 \times 10^6 \text{ cm}^2 \text{ s}^{-1}$, $7.5 \times 10^6 \text{ cm}^2 \text{ s}^{-1}$ and $6.0 \times 10^6 \text{ cm}^2 \text{ s}^{-1}$ for FcOH, IrCl_6^{3-} and $\text{Ru}(\text{NH}_3)_6^{3+}$, respectively).^{24–26} Upon modifying the electrode with the cellulose film, the difference between the anodic and cathodic peak potentials, ΔE_p , was $97 \pm 4 \text{ mV}$, $72 \pm 5 \text{ mV}$ and $83 \pm 5 \text{ mV}$ for IrCl_6^{3-} , FcOH and $\text{Ru}(\text{NH}_3)_6^{3+}$, respectively. These values are slightly higher than that expected for reversible, one-electron redox reactions and may be due to sluggish interfacial kinetics at the modified electrodes or some residual ohmic drop within the cell.

In each case, the anodic and cathodic peak currents, $i_{p,a}$ and $i_{p,c}$, increased with $v^{1/2}$, where v is the experimental sweep rate and the ratio $i_{p,a}:i_{p,c}$ was close to 1. Close inspection of Fig. 2 reveals that the formal potentials of the anionic and cationic mediators shift to slightly more positive and negative potentials, respectively,

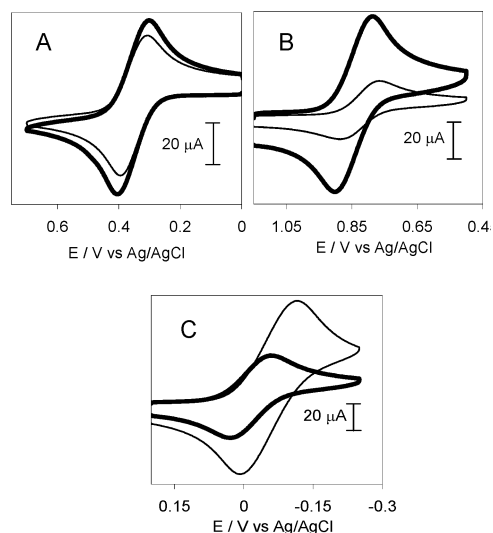


Fig. 2 CVs obtained in a solution of (A) 1 mM FcOH, (B) 1 mM IrCl_6^{3-} , and (C) 1 mM $\text{Ru}(\text{NH}_3)_6^{3+}$ in 0.1 M KCl at a bare glassy carbon electrode (heavy line) and a cellulose-modified electrode (light line) using a sweep rate of 0.3 V s^{-1} .

upon modification of the electrode with cellulose. However, the formal potential of FcOH at the cellulose-modified electrode was almost identical to that observed at the bare electrode. Therefore, the cationic and anionic mediators appeared to interact with the negatively-charged cellulose, while the oxidation of the neutral species appeared to be unaffected by the presence of the film. These observations suggest the presence of electrostatic interactions between the charged analytes and the negatively-charged membrane and this is explored in more detail in the following sections. Further evidence indicating the presence of electrostatic interactions between the solution-phase redox species and the cellulose membrane may be obtained by examining the magnitudes of the voltammetric currents obtained in each mediator solution. The current obtained using the IrCl_6^{3-} solution decreased significantly in the presence of the cellulose film compared to the bare electrode, while the voltammetric current measured in the $\text{Ru}(\text{NH}_3)_6^{3+}$ solution increased at the modified electrode. However, the current obtained in the neutral FcOH solution was only slightly reduced upon modification of the electrode, indicating that the flux of neutral species to the electrode was almost unaffected by the presence of the cellulose film.

Permeability of cellulose films

Using the voltammograms shown in Fig. 2, the permeability of the cellulose films to the redox-active species was determined using equation 1:²⁷

$$P = (i_{\text{film}}/i_{\text{bare}}) \times 100\% \quad (1)$$

where i_{film} and i_{bare} are the peak currents obtained at the cellulose-modified electrode and bare electrode, respectively. The permeability of the films to each probe molecule is shown in Table 1. The increased permeability of the films to the cationic $\text{Ru}(\text{NH}_3)_6^{3+}$ is shown by its large P value in Table 1. The negatively-charged mediator did not permeate the film significantly and the voltammetric peak current was reduced

Table 1 Permeability, diffusion coefficients in solution, apparent diffusion coefficients, diffusion coefficients in the film and partition coefficients for each redox mediator determined using cyclic voltammetry and RDE measurements. Error values are standard deviations based on three replicate measurements. $P = (i_{\text{film}}/i_{\text{bare}}) \times 100\%$. D_s and D_{app} were obtained from plots of i_L^{-1} versus $\omega^{-1/2}$. $\alpha = D_{\text{app}}/D_f$. α was obtained from equation 5.

	$\text{Ru}(\text{NH}_3)_6^{3+}$	FcOH	IrCl_6^{3-}
$P/\%$	216	81.0	33.9
$10^6 D_s/\text{cm}^2 \text{ s}^{-1}$	8.49 ± 1.61	2.07 ± 0.18	2.97 ± 1.28
$10^6 D_{\text{app}}/\text{cm}^2 \text{ s}^{-1}$	13.0 ± 3.36	3.71 ± 0.88	0.370 ± 0.01
$10^6 D_f/\text{cm}^2 \text{ s}^{-1}$	2.48 ± 0.64	4.59 ± 1.08	—
α	5.25	0.81	$\ll 1$

by almost 65% in the presence of the cellulose film. The fact that the permeability of the neutral mediator is close to 100% and the IrCl_6^{3-} and FcOH are of similar sizes indicates that the exclusion of IrCl_6^{3-} was based on charge and not size. Anionic ferrocene carboxylate (FcOO^-) was also used as a structurally-similar ferrocene analogue and its permeability was approximately 40%. The reduced permeability of FcOO^- within the film compared with the neutral FcOH indicates further that the reduced permeability of the film towards FcOO^- and IrCl_6^{3-} was based on electrostatic repulsion.

Charge transport within cellulose films

When an RDE is coated with a thin film, the limiting current is related to ω by equation 3:²⁸

$$\frac{1}{i_L} = \frac{d}{nFAD_{\text{app}}C_s} + \frac{1}{0.62nFAC_sD_s^{2/3}\nu^{-1/6}\omega^{1/2}} \quad (2)$$

where i_L is the limiting current (A), n is the number of electrons transferred in the redox reaction, F is the Faraday constant (96485 C mol^{-1}), A is the RDE area (cm^2), C_s is the bulk solution concentration of the redox species (mol cm^{-3}), D_s is the diffusion coefficient of the redox species in solution ($\text{cm}^2 \text{ s}^{-1}$), ν is the kinematic viscosity of the solution ($\text{cm}^2 \text{ s}^{-1}$) and ω is the RDE rotation rate (rad s^{-1}). D_{app} is the apparent diffusion coefficient of the redox species within the film and is equal to αD_f , where α is the partition coefficient and D_f is the diffusion coefficient in the film. α is the ratio of the concentration of the mediator in the film to that in the solution, C_f/C_s , and d is the film thickness. As shown in Fig. 3A, the limiting current for $\text{Ru}(\text{NH}_3)_6^{3+}$ reduction at a cellulose-modified RDE increased with ω . Equation 2 predicts that a graph of i_L^{-1} versus $\omega^{-1/2}$ (a Koutecky-Levich plot) should be linear for a film-modified electrode and that the intercept should be inversely proportional to C_s and directly proportional to d .

D_s may then be determined from the slope and D_{app} may be determined if the film thickness is known. Moreover, if D_{app} is known for a particular type of film, the intercept of the inverse Levich plot may be used to calculate the film thickness. Fig. 3B shows a graph of i_L^{-1} versus $\omega^{-1/2}$ for $\text{Ru}(\text{NH}_3)_6^{3+}$, which exhibited excellent linearity over the range of rotation rates studied (correlation coefficient = 0.996). Graphs of i_L^{-1} versus $\omega^{-1/2}$ were also linear for IrCl_6^{3-} and FcOH and the intercepts were inversely proportional to C_s and directly proportional to the film thickness. These observations justify our use of equation 2 in these calculations.²⁸ Using the intercepts and slopes from

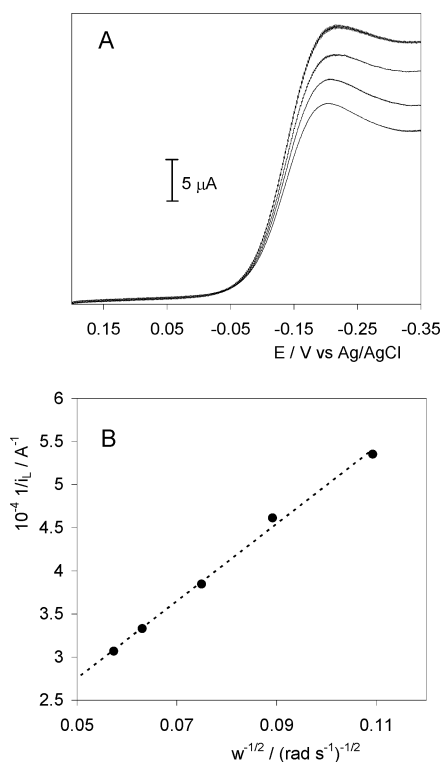


Fig. 3 (A) RDE linear sweep voltammograms obtained at a cellulose-modified 5 mm glassy carbon disk RDE in 0.25 mM Ru(NH₃)₆³⁺ at rotation rates of (from top to bottom) 2400, 1700, 1200 and 800 rpm, respectively. The voltammetric sweep rate was 0.1 V s⁻¹ and the potential sweep was from 0.2 to -0.35 V versus Ag/AgCl. (B) Graph of i_L^{-1} versus $\omega^{-1/2}$ for the data shown in (A).

these graphs, values of D_{app} and D_s were determined for each redox mediator and are shown in Table 1. The reported values for D_{app} must be considered a minimum as the dry thickness of the films was used in these calculations. However, it is likely that some swelling of the films occurred when in contact with water. The value for D_s obtained for each mediator using the cellulose-modified electrode agreed closely with that determined at a bare RDE. Significantly, the value of D_{app} was close to that of D_s for Ru(NH₃)₆³⁺ and FcOH, indicating that the diffusion of the cationic and neutral mediator was not significantly impeded by the cellulose film. However, the value of D_{app} for IrCl₆³⁻ was significantly smaller than that of D_s , indicating that the film hindered diffusion of IrCl₆³⁻. This observation agrees with the cyclic voltammetry data shown above indicating electrostatic blocking of the anionic mediator by the film.

Partition of redox species into cellulose films

Given the high permeability of Ru(NH₃)₆³⁺ within these films, we investigated the possibility of immobilising redox-active species within the cellulose films. To incorporate Ru(NH₃)₆³⁺ into the cellulose films, a glassy-carbon electrode that was coated with a freshly formed cellulose film was stored in a 1 mM Ru(NH₃)₆³⁺ solution overnight. The electrode was then rinsed thoroughly with de-ionized water and immersed in a 0.1 M KCl solution containing no Ru(NH₃)₆³⁺. Fig. 4 shows the first 100 cycles of a cyclic voltammetry experiment performed using such a film. A CV response, characteristic of that for Ru(NH₃)₆³⁺ in

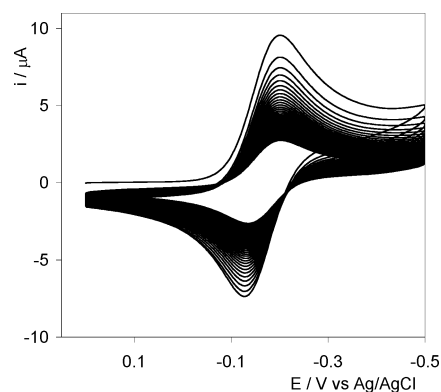


Fig. 4 The first 100 sweeps of a CV obtained using a cellulose-modified glassy-carbon electrode that had been stored overnight in 1 mM Ru(NH₃)₆³⁺. The electrolyte was blank 0.1 M KCl containing no Ru(NH₃)₆³⁺. The experimental sweep rate was 0.1 V s⁻¹ and the initial and switching potential were 0.2 V and -0.5 V versus Ag/AgCl, respectively.

solution was observed, which decayed to a constant value after approximately 40 cycles. After this time, the CVs did not change shape and were quite stable for periods up to 1 hour. This experiment was also carried out using IrCl₆³⁻ and FcOH.

A similar response was observed using FcOH, with the voltammogram exhibiting slightly lower peak currents. However, no voltammetric response for IrCl₆³⁻ was observed upon transferring the electrode to blank electrolyte from an IrCl₆³⁻ solution, indicating that IrCl₆³⁻ did not partition into the film to any significant extent. This was in agreement with our previous observation that IrCl₆³⁻ was blocked from the film electrostatically.

D_f was determined for Ru(NH₃)₆³⁺ and FcOH using a coulometric assay at a cellulose-modified electrode as follows:²⁷ A modified glassy carbon electrode was equilibrated with a 1 mM solution of Ru(NH₃)₆³⁺ or FcOH for approximately 6 hours and then transferred, after a set delay time, to a blank 0.1 M KCl solution containing none of the redox mediator. A linear sweep voltammogram was then recorded for the redox mediator at 0.1 V s⁻¹ and the peak current was integrated, yielding the charge for electrolysis. This was then repeated for a range of delay times and the data are shown for Ru(NH₃)₆³⁺ in Fig. 5. Clearly, the charge due to Ru(NH₃)₆³⁺ reduction decreased over time, indicating the gradual loss of Ru(NH₃)₆³⁺ from the film. This observation agrees with that obtained from Fig. 4, in which the peak current decreased during the first 40 cycles of a cyclic voltammogram. To account for this loss, the data shown in Fig. 5 was extrapolated to time zero in order to calculate the charge at time zero, Q_0 , which is correlated with the quantity of Ru(NH₃)₆³⁺ that partitioned into the film. Q_0 can then be related to α by equation 3:²⁷

$$\alpha = \frac{Q_0}{nFV_f C_s} \quad (3)$$

where V_f is the volume of the films (cm³). This procedure was repeated for FcOH, which displayed similar behaviour, and the partition coefficient was calculated for each mediator. These values are also shown in Table 1. As no detectable signal was observed for IrCl₆³⁻ using this assay, we must assume that the

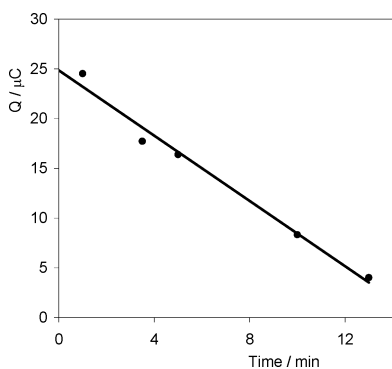


Fig. 5 Graph of the integrated peak current *versus* delay time for Ru(NH₃)₆³⁺ reduction. The modified electrodes were stored in 1 mM Ru(NH₃)₆³⁺ for 6 hours and then transferred to blank 0.1 M KCl before recording a linear sweep voltammogram for Ru(NH₃)₆³⁺ reduction. The delay time is the time between transferring the electrode into the blank electrolyte and recording the voltammogram.

partition coefficient for IrCl₆³⁻ is significantly less than 1. As described above, $\alpha = C_f/C_s$. Therefore, the data in Table 1 shows that the equilibrium concentrations of FcOH inside the film and in solution are approximately equal, while the equilibrium concentration of Ru(NH₃)₆³⁺ inside the film, C_f , is approximately 5 times the solution concentration (≈ 5.0 mM). These observations indicate that the neutral species diffused into the film down a concentration gradient until equilibrium was reached, clearly indicating that the presence of the film does not inhibit access of the neutral mediator to the underlying electrode. The increase in α for the cationic mediator compared to the neutral mediator clearly demonstrates the preferential partition of the cation into the film. Electrostatic interactions between the cationic redox probe and the anionic binding sites on the cellulose film result in preferential incorporation of the Ru(NH₃)₆³⁺ into the film. Incorporation of the Ru(NH₃)₆³⁺ ions occurs in competition with the K⁺ ions of the supporting electrolyte (KCl), which depends on the free energy of adsorption into the film and preferential incorporation of Ru(NH₃)₆³⁺ is most likely due to the electrostatic preference of the film for the more positively-charged ions. The relative stability of the Ru(NH₃)₆³⁺ within the film while redox cycling in the contact with blank electrolyte indicates a relatively large energy of interaction between the binding sites on the cellulose and the cationic redox mediator. In the following sections the rate of adsorption of Ru(NH₃)₆³⁺ into the film and the thermodynamics of adsorption of Ru(NH₃)₆³⁺ into the film are explored to obtain an insight into the magnitude of this interaction.

Effect of deposition time on cation partition into cellulose films

The response time of the cellulose films to the cationic mediator was measured by depositing a cellulose film onto a glassy carbon electrode and storing the electrode in a 5 mM Ru(NH₃)₆³⁺ solution for various time periods. The electrode was then rinsed thoroughly with deionized water and transferred to a cell containing blank 0.1 M KCl. Repetitive CVs were then recorded until the voltammetric current reached a constant value and the peak current was then recorded. Peak currents recorded using this approach at various deposition times are shown in Fig. 6. The peak currents reached a maximum value

at approximately 6 hours. This t_{\max} value was then used to determine thermodynamic information about the interaction between cellulose and Ru(NH₃)₆³⁺ as described in the following section.

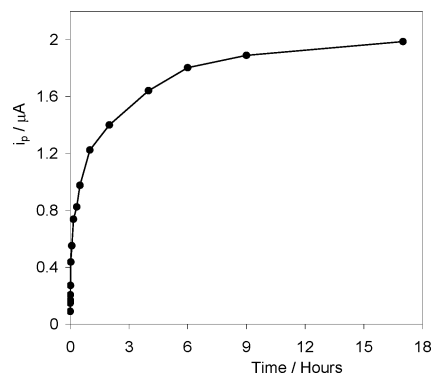


Fig. 6 Graph of the i_p *versus* time obtained after equilibrating a cellulose-modified electrode in 1 mM Ru(NH₃)₆³⁺ for various periods of time and transferring to blank electrolyte. i_p was recorded when the voltammetric current had reached a steady value upon redox cycling. The electrolyte was blank 0.1 M KCl.

Adsorption isotherms for the interaction between cellulose and Ru(NH₃)₆³⁺

The relationship between the equilibrium coverage, Γ , of an adsorbate and the bulk solution concentration, C_s , is described by an adsorption isotherm and the theory of adsorption isotherms is well established.²⁹

Therefore, we present here only a very brief description of the theory. The simplest isotherm is the Langmuir isotherm, which assumes that any interactions between adjacent adsorbates are due to size and no other attractive or repulsive interactions exist. The Langmuir isotherm can be expressed using equation 4 below.

$$KC = \frac{\theta}{1 - \theta} \quad (4)$$

where K is the binding constant, and θ is the fractional coverage, which is defined as Γ/Γ_s , where Γ_s is the saturation surface coverage. The Langmuir isotherm can be linearized, and we can replace θ with $i_{p,\max}/i_p$, yielding the following expression:³⁰

$$\frac{C}{i_p} = \frac{1}{K i_{p,\max}} + \frac{C}{i_{p,\max}} \quad (5)$$

where i_p is the voltammetric peak current (A) and $i_{p,\max}$ is the maximum experimental peak current (A). Therefore, the Langmuir isotherm can provide useful insights into the adsorption thermodynamics of a system if a plot of C/i_p *versus* C yields a straight line plot. In that case, $i_{p,\max}$ and K can be determined from the slope and the intercept, respectively. The Frumkin isotherm can provide a useful insight into whether lateral interactions do exist in a system and is expressed in equation 6.

$$KC = \frac{\theta}{1 - \theta} \exp(g\theta) \quad (6)$$

In the case of the Frumkin isotherm, attractive interactions are indicated by negative values of g , while positive values of g indicate repulsive interactions between adjacent adsorbates. In the case of no interactions (*i.e.*, as $g \rightarrow 0$), the Frumkin isotherm reduces to the Langmuir isotherm, as expected. Fig. 7A shows a plot of C/i_p versus C for a series of experiments in which voltammetric peak currents were recorded for $\text{Ru}(\text{NH}_3)_6^{3+}$ using cellulose-modified electrodes containing adsorbed $\text{Ru}(\text{NH}_3)_6^{3+}$ in blank 0.1 M KCl electrolyte. This data was obtained by depositing cellulose films at glassy carbon electrodes and storing the electrodes in solutions of $\text{Ru}(\text{NH}_3)_6^{3+}$ of varying concentrations for 6 hours. The electrodes were then rinsed thoroughly using deionized water and CVs were recorded in blank 0.1 M KCl immediately. The responses clearly show a linear dependence (correlation coefficient = 0.996). Using linear regression analysis (and equation 6), the maximum peak current was determined to be 1.86 μA , in excellent agreement with the experimental value (1.76 μA) and the binding constant was determined to be $1.57 \times 10^3 \text{ M}^{-1}$. Using these values, a theoretical Langmuir curve was constructed and is shown in Fig. 7B (solid line). As shown, an excellent fit was obtained between the calculated Langmuir curve and the experimental data (solid dots).

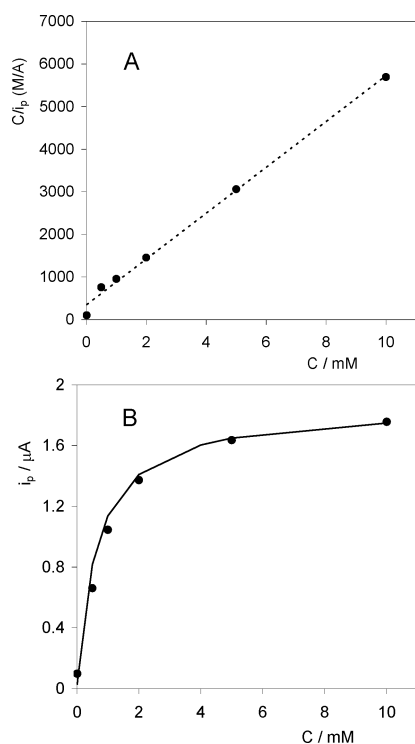


Fig. 7 (A) Langmuir plot of C/i_p versus C_s for $\text{Ru}(\text{NH}_3)_6^{3+}$. Peak currents were measured using cyclic voltammetry after storing the electrode for 6 hours in various deposition solutions, rinsing and transferring to blank 0.1 M KCl. (B) Graph of the experimental peak current versus deposition solution concentration. The solid dots show the experimental data and the solid line shows theoretical Langmuir curve using a binding constant of $1.57 \times 10^3 \text{ M}^{-1}$.

The free energy of binding from a dilute aqueous solution, ΔG° , can be obtained from the binding constant, in conjunction with equation 7:

$$\Delta G^\circ = -RT \ln bK \quad (7)$$

where R is the gas constant ($8.314 \text{ J K}^{-1} \text{ mol}^{-1}$), T is the temperature (K) and b is the solvent concentration (55.5 mol dm^{-3}), used to correct to a dimensionless binding constant.³⁰ ΔG° was thus determined to be $-28.2 \text{ kJ mol}^{-1}$. The binding between the cationic mediator and the anionic cellulose film, combined with the permselective properties indicate that these cellulose films may be extremely useful in the development of novel separation technologies or sensor devices. Furthermore, we are developing cellulose nanowhiskers with different surface groups that may allow us to tailor the permselective properties for particular sensing applications and permselective membranes. Varying the surface functionality will allow us to tailor the permselective properties and develop a new class of membranes based on renewable, biodegradable and biocompatible cellulose nanowhiskers.

Conclusions

The simple extraction of crystalline cellulose nanowhiskers from natural materials provides an extremely attractive route to the development of a valuable class of renewable nanomaterials. The propensity of these nanowhiskers to hydrogen bond extensively and form stable membranes that can adhere to surfaces or be handled as free-standing films, combined with their permselective properties, makes these materials attractive for numerous applications. For example, it may be possible to develop new membranes for separations that selectively transport species based on charge, as shown in this work. Furthermore, we have shown here that it may be possible to develop new membranes for sensor devices that selectively accumulate (preconcentrate) certain species while simultaneously excluding other interfering species. Modification of the surface chemistry of the cellulose nanowhiskers will also allow us to tailor the surface groups on the nanowhiskers to specific applications and we are currently exploring this area. Significantly, we have shown here the development of highly functional nanostructured materials constructed from building blocks that were extracted from natural, renewable sources using an environmentally-benign process. The development of application-specific devices using such renewable nanomaterials will be an important goal in our attempts to develop new technologies using natural resources.

Acknowledgements

We thank the EPSRC for funding through the DICE (Driving Innovation in Chemistry and Chemical Engineering) Project under the Science and Innovation Award (Grant Number EP/D501229/1).

References

- 1 M. Hehn, K. Ounadjela, J.-P. Bucher, F. Rousseaux, D. Decanini, B. Bartenlian and C. Chappert, *Science*, 1996, **272**, 1782–1785.
- 2 D. J. Maxwell, S. R. Emory and S. Nie, *Chem. Mater.*, 2001, **13**, 1082–1088.
- 3 S. H. Joo, S. J. Choi, I. Oh, J. Kwak, Z. Liu, O. Terasaki and R. Ryoo, *Nature*, 2001, **412**, 169–172.
- 4 C. C. Striemer, T. R. Gaborski, J. L. McGrath and P. M. Fauchet, *Nature*, 2007, **445**, 749–753.
- 5 M. S. Morsy and H. A. Aglan, *J. Mater. Sci.*, 2007, **42**, 10188–10195.
- 6 K.-B. Lee, E.-Y. Kim, C. A. Mirkin and S. M. Wolinsky, *Nano Lett.*, 2004, **4**, 1869–1872.

- 7 H. Zhao, J. H. Kwak, Z. C. Zhang, H. M. Brown, B. W. Arey and J. E. Holladay, *Carbohydr. Polym.*, 2007, **68**, 235–241.
- 8 E. Melzer, J. Kreuter and R. Daniels, *Eur. J. Pharm. Biopharm.*, 2003, **56**, 23–27.
- 9 K. Yonekura, K. Hayakawa, M. Kawaguchi and T. Kato, *Langmuir*, 1998, **14**, 3145–3148.
- 10 F. He and D. Zhao, *Environ. Sci. Technol.*, 2007, **41**, 6216–6221.
- 11 J. Cai and L. Zhang, *Biomacromolecules*, 2006, **7**, 183–189.
- 12 P. Wang, S. Jiang, D. Liu, H. Zhang and Z. Zhou, *J. Agric. Food Chem.*, 2006, **54**, 1577–1583.
- 13 M. N. Nadagouda and R. S. Varma, *Biomacromolecules*, 2007, **8**, 2762–2767.
- 14 H.-M. Park, X. Liang, A. K. Mohanty, M. Misra and L. T. Drzal, *Macromolecules*, 2004, **37**, 9076–9082.
- 15 I. Kvien, B. S. Tanem and K. Oksman, *Biomacromolecules*, 2005, **6**, 3160–3165.
- 16 M. A. S. Azizi Samir, F. Alloin and A. Dufresne, *Biomacromolecules*, 2005, **6**, 612–626.
- 17 J. C. Biffinger, R. Ray, B. Little and B. R. Ringeisen, *Environ. Sci. Technol.*, 2007, **41**, 1444–1449.
- 18 L. Wu, J. Chen, D. Du and H. Ju, *Electrochim. Acta*, 2006, **51**, 1208–1214.
- 19 K. Inoue, P. Ferrante, Y. Hirano, T. Yasukawa, H. Shiku and T. Matsue, *Talanta*, 2007, **73**, 886–892.
- 20 B. Wu, J. Li, H. Shi, J. Huang, J. Anzai, T. Oso and Q. Chen, *High Technol. Lett.*, 2006, **12**, 263.
- 21 M. J. Bonné, K. Edler, J. G. Buchanan, D. Wolverson, W. Thielemans, E. Psillakis, M. Helton and F. Marken, *J. Phys. Chem. C*, 2008, **112**, 2660–2666.
- 22 B. G. Ranby, *Acta Chem. Scand.*, 1949, **3**, 649–650.
- 23 J.-F. Revol, H. Bradford, J. Giasson, R. H. Marchessault and D. G. Gray, *Int. J. Biol. Macromol.*, 1992, **14**, 170–172.
- 24 W. Miao, Z. Ding and A. J. Bard, *J. Phys. Chem. B*, 2002, **106**, 1392–1398.
- 25 C. E. Jones, J. V. Macpherson, Z. H. Barber, R. E. Somekh and P. R. Unwin, *Electrochem. Commun.*, 1999, **1**, 55–60.
- 26 H. Olivia, B. V. Sarada, D. Shin, T. N. Rao and A. Fujishima, *Analyst*, 2002, **127**, 1572–1575.
- 27 J. Cruz, M. Kawaski and W. Gorski, *Anal. Chem.*, 2000, **72**, 680–686.
- 28 T. Ikeda, P. Schmehl, K. W. Denisevich and R. W. Murray, *J. Am. Chem. Soc.*, 1982, **104**, 2683–2691.
- 29 P. W. Atkins, J. de Paula, *Physical Chemistry*, 8th Edn.; Oxford University Press, 2006, pp. 917–920.
- 30 P. Pérez, C. Teijeiro and D. Marín, *Langmuir*, 2002, **18**, 1760–1763.

Long term continuous chemoenzymatic dynamic kinetic resolution of *rac*-1-phenylethanol using ionic liquids and supercritical carbon dioxide

Pedro Lozano,^{*a} Teresa De Diego,^a Corina Mira,^a Kimberley Montague,^a Michel Vaultier^b and José L. Iborra^{*a}

Received 2nd December 2008, Accepted 19th January 2009

First published as an Advance Article on the web 13th February 2009

DOI: 10.1039/b821623a

The long term continuous dynamic kinetic resolution (DKR) of *rac*-phenylethanol in IL/scCO₂ biphasic systems was carried out by simultaneously using immobilized lipase (Novozym 435) and acidic zeolite catalysts at 50 °C and 100 bar, providing good yields (up to 98.0%) for *R*-phenylethyl propionate with excellent enantioselectivity (up to 97.3% ee) and without any activity loss during 14 days of operation.

1. Introduction

The preparation of chiral drugs as single enantiomers is one of the most pressing goals in pharmaceutical science because of the different types of biological activity exhibited by each enantiomer. Kinetic resolution (KR) with enzymes is the most widely used method for separating the two enantiomers of a racemic mixture. However, the main drawback of this method is that the chemical yield is limited to 50% and, it is necessary to incorporate a further separation step (*e.g.* distillation, liquid–liquid extraction, membrane process, *etc.*) to isolate the desired enantiomer.¹ These limitations can be overcome by combining kinetic resolution with *in situ* racemisation of the undesired enantiomer, using so-called dynamic kinetic resolution (DKR). Classically, transition metal (*e.g.* Ru²⁺) complexes² and, more recently, solid acids³ (*e.g.* zeolites) have been described as suitable catalysts for the racemisation of *sec*-alcohols *via* hydrogen transfer processes. DKR based on lipases combined with metal catalysis has been assayed in anhydrous organic solvents (*e.g.* toluene) under argon atmosphere and in a discontinuous way, providing high yields (up to 99% and ee > 99.9%) of the enantiomerically pure ester product in 1–6 days. DKR approaches based on lipases combined with acidic zeolite catalysts have also been described using water/organic solvent biphasic media in a discontinuous way.^{3b,3c} The potential value of H-beta zeolites as heterogeneous alcohol-racemisation catalysts for benzylic alcohols in aqueous phase has been demonstrated, while the enzymatic KR step occurred in the organic phase, leading to a corresponding *R*-ester with 78% yield and 98% ee. The use of a perfluorous acyl donor (20,20,20-trifluoroethanol 1H,1H,2H, 2H-perfluoroundecanoate) in the Zr-

beta zeolite/Novozym-catalyzed DKR of benzylic alcohols in organic/fluorous biphasic system lead to no clear improvement in the process (95% yield, 75% ee).^{3d}

Water-immiscible ionic liquids (ILs) have recently emerged as exceptionally interesting green non-aqueous reaction media for biotransformations, because of the high level of activity,^{4a} stereoselectivity^{4b} and stability⁵ displayed by enzymes in chemical transformations. The use of ILs as suitable reaction media for the DKR of *sec*-alcohols catalyzed by lipase/ruthenium complex has been described, leading to good yields (up to 95%) after 2–6 days of reaction.⁶

Biphasic systems based on ILs and supercritical carbon dioxide (scCO₂) for enzyme catalysis have been put forward as the first approach to developing integral green bioprocesses in non-aqueous media, where both the biotransformations and extraction steps are coupled in efficient reaction/separation processes.⁷ In this context, DKR processes of *rac*-1-phenylethanol (**1**, see Fig. 1A) in IL/scCO₂ systems have been carried out combining immobilized *Candida antarctica* lipase B (CALB) with silica modified with benzenesulfonic acid groups as catalysts in a packed bed reactor at 50 °C and 100 bar.⁸ However, the use of both catalysts as a simple mixture resulted in a complete loss of activity, probably due to the acid environment around enzyme particles that could produce deactivation. Consequently, it was necessary to pack catalyst particles in three different layers (immobilized enzyme-acid catalyst-immobilized enzyme) physically separated by glass wool to obtain moderate results for the *R*-ester product (70% yield, 92% ee).

This paper describes for the first time the continuous DKR of **1** in IL/scCO₂ systems by using a combination of immobilized CALB (Novozym 435[®]) and acid zeolite catalysts packed as a heterogeneous particle mixture (Fig. 1). The reactor operated as a catalytic unit able to continuously transform *rac*-**1** in **R-2**, combining the advantages of ionic liquids to stabilize enzymes in supercritical fluids, as a non-aqueous “green” reaction/extraction system, with the advantages of a continuous flow process for easy product separation and catalyst reuse.

^aDepartamento de Bioquímica y Biología Molecular B e Inmunología, Facultad de Química, Universidad de Murcia, P.O. Box 4021, E-30100, Murcia, Spain. E-mail: plozanor@um.es, jliborra@um.es; Fax: 34.968.36.41.48; Tel: 34.968.36.73.92

^bLaboratoire de Chimie et Photonique Moléculaire, UMR CNRS 6510, Université de Rennes-1, Campus de Beaulieu, Av. Général Leclerc, F-35042, Rennes, France. E-mail: Michel.Vaultier@univ-rennes1.fr; Fax: 33.2.99.28.69.55; Tel: 33.2.99.28.62.74

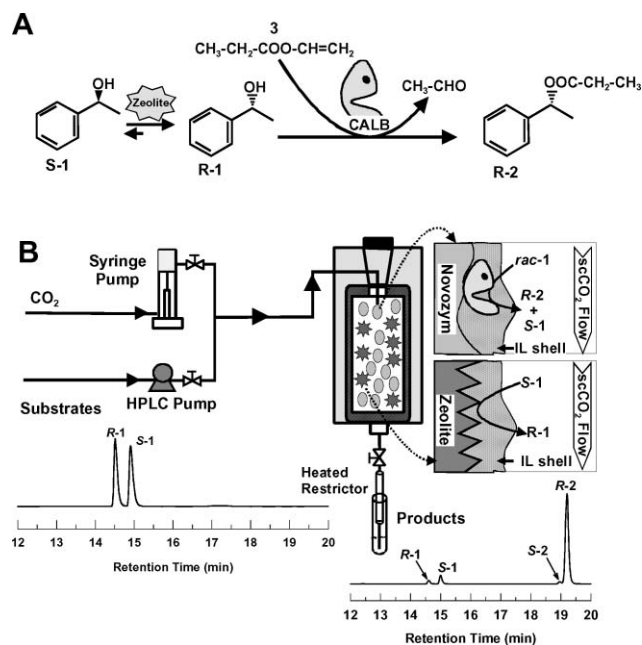


Fig. 1 A. DKR of *rac*-1-phenylethanol (*rac*-1) catalyzed by the combined action of zeolite and immobilized *Candida antarctica* lipase B (Novozym 435). B. Experimental set-up of the continuous packed bed reactor containing both Novozym 435 and zeolite coated with ILs, including GC chromatograms of the substrate inlet and product exit.

2. Experimental

Immobilized *Candida antarctica* lipase B (Novozym 435®, EC 3.1.1.3) was a gift from Novozymes S.A. (Spain). Zeolite Beta CP811E-150 (Si:Al molar ratio = 75), and, zeolites HY CBV400 (Si:Al = 2.5) and HY CBV720 (Si:Al = 15) were obtained from Zeolysts International (PA, USA). Substrates, solvents and other chemicals were purchased from Sigma-Aldrich-Fluka (Madrid, Spain), and were of the highest purity available. The ILs 1-butyl-3-methylimidazolium hexafluorophosphate ([Bmim][PF₆], 99% purity) and 1-butyl-2,3-dimethylimidazolium hexafluorophosphate ([Bdmim][PF₆], 99% purity) were from Solvent Innovation Inc. (Germany); 1-octadecyl-3-methylimidazolium bis((trifluoromethyl)sulfonyl)amide ([Odmim][NTf₂], 99% purity) was obtained from IoLiTec GmbH (Germany); trioctylmethylammonium bis((trifluoromethyl)sulfonyl)amide, [Toma][NTf₂], and butyltrimethylammonium bis((trifluoromethyl)sulfonyl)amide, [Btma][NTf₂], were synthesized as described previously.⁵

Adsorption of IL onto catalyst particles

In a 10-mL capacity test tube, 1 mL of IL ([Bmim][PF₆], [Bdmim][PF₆], [Odmim][NTf₂], [Toma][NTf₂], or [Btma][NTf₂]) were dissolved in 3 mL acetonitrile. Then, 1 g of catalyst (Novozym 435 or zeolite) was added, and the mixture was gently stirred for 30 min at room temperature. Finally, the acetonitrile was eliminated by continuous bubbling of N₂ for 30 min at room temperature. The resulting catalyst-IL particles were equilibrated to 0.11 water activity by over saturated LiCl solutions in closed containers at 25 °C for one week prior to use.⁹

Racemization reactions

Standard reactions were carried out in 1-mL screw-capped vials with teflon-lined septa, containing 0.6 M *S*-1 and 0.6 M **3** in hexane (0.5 mL overall volume). Reactions were started by adding zeolite catalyst previously coated with IL [Btma][NTf₂] (5 mg) and run at 50 °C in a glycerol bath for 3 h. At regular time intervals, 20 µL aliquots were taken and suspended in 480 µL hexane, and the biphasic mixture was strongly shaken for 3 min to extract all substrates and product into the hexane phase. Then, 400 µL of hexane phase were collected and mixed with 100 µL of 150 mM butyl butyrate (internal standard) solution in hexane, and finally analyzed by GC. All experiment were carried out in duplicate.

DKR of *rac*-1 in scCO₂

Both Novozym-IL (1 g) and zeolite-IL (0.5 g) catalysts were added to a 10-mL test tube, and the resulting mixture was strongly shaken for 5 min at room temperature to obtain an homogenous distribution of particles. The final mixture was placed in the cartridge of an ISCO 220SX (Teledyne Isco, Inc, Lincoln, NE, USA) high pressure extraction apparatus of 10 mL total capacity. The apparatus is equipped with a syringe pump (ISCO model 100DX, 100 mL overall volume), needle valves and devices for pressure, temperature and flow rate control. The ISCO system was started by the continuous pumping of scCO₂ at 100 bar and 50 °C, which automatically opens the exit valve, bubbling continuously the CO₂ through a calibrated heated restrictor (1 mL/min, 70 °C). Synthetic processes were carried out for 6 h by continuously pumping a **3**:*rac*-1 (2:1 mol:mol) mixture into the scCO₂ inlet flow at 6 µmol/min mass-flow rate, by using a HPLC pump (model LC-10AT, Shimadzu Europe, Duisburg, Germany) (see Fig. 1B). Substrates and products were transported by the scCO₂ flow through the catalytic cartridge, and then recovered by depressurizing through the calibrated heated restrictor by 30 minutes steps in a controlled amount of hexane placed on an ice-bath. Samples were analyzed by GC. In all cases, substrate and product mass-balances from the outlet were consistent with the substrate mass-flow inlet.

GC analysis

Analysis were performed with a Shimadzu GC-2010 (Shimadzu Europe, Duisburg, Germany) equipped with FID detector. Samples were analyzed on a Beta DEX-120 column (30 m × 0.25 mm × 0.25 µm, Supelco) and a FID detector in the following conditions: carrier gas (He) at 1 MPa (105 mL/min total flow); temperature programme: 60 °C, 10 °C/min, 130 °C; split ratio, 100:1; detector, 300 °C. The retention times of compounds were as follows: **2** (3.1 min); propionic acid (PrA, 5.6 min), butyl butyrate (internal standard, 7.1 min), *R*-1 (14.4 min), *S*-1 (14.9 min), *S*-2 (18.9 min) and *R*-2 (19.3 min).

3. Results and discussion

To know the activity of zeolites catalyzing racemization of *S*-1 in DKR conditions, these catalysts were tested in a hexane medium containing both *S*-1 and **3** substrates at the same concentration. As shown in Fig. 2, the H-Beta CP811E zeolite was a suitable

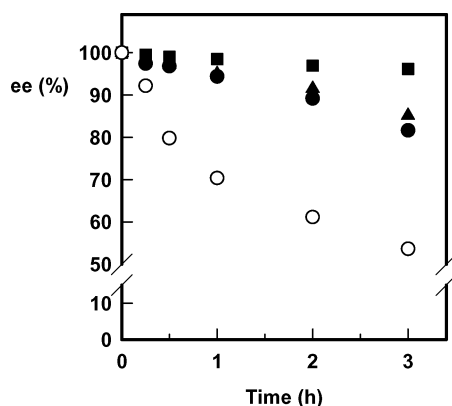


Fig. 2 Time-course profiles of ee for the racemisation of *S*-1 with H-Beta CP811E zeolite (○), and H-Beta CP811E (●), H-USY CBV720 (▲) H-USY CBV400 (■) zeolites coated with [Btma][NTf₂] in hexane at 50 °C.

catalyst for the proposed reaction in agreement with previous works, since it was able to reduce the ee_{s-1} from 100 to 53.6% in 3h. Note that no synthesis of 1-phenylethylpropionate was observed. However, the undesired hydrolysis of **3** catalyzed by the zeolite that produces propionic acid (PrA) was also detected (see Table 1). This fact was also observed when a silica gel modified with benzenesulfonic acid (SCX) was used as catalyst for the DKR of *rac*-1 in hexane or scCO₂, and is obviously a drawback for any continuous DKR process with an equilibrated mass-substrate concentration at the reactor inlet.⁸

The fact that the GC chromatograms did not show any production of acetophenone suggest that H-Beta zeolites catalyzed racemization as Brønsted acids.^{3c,12} Coating of this H-Beta zeolite with [Btma][NTf₂] lead to a clear decrease in the undesired hydrolysis of **3**, which was accompanied by a loss in the racemisation reaction rate. This fact could be related with the enhancement of mass-transfer limitations into the hexane media resulting from the IL-coating of zeolite particles.⁸ In this way, the coating of acid H-Beta zeolites by polyelectrolyte capsules to protect the pH-sensitive enzyme CALB has also been described as an interesting strategy that enables both catalysts to be used in a one-pot DKR of *sec*-alcohols.¹⁰ In our previous studies,⁸ a full enzyme deactivation was also observed when DKR processes were carried out by using a mixture of both immobilized lipase and SCX catalyst particles without IL coating, probably as a consequence of the acidification of the enzyme microenvironment.

Fajausite (H-USY) type zeolites (*i.e.* CBV720 and CBV400) coated with [Btma][NTf₂] were also able to catalyze the racemisation of *S*-1, but the observed racemisation reaction rate was clearly lower than the one obtained for the H-Beta zeolite case

Table 1 Zeolites coated with IL-catalyzed racemization of *S*-1 in hexane at 50 °C

Zeolite	Si/Al	IL	Rate (μmol min ⁻¹ g ⁻¹)	PrA at 3 h (%)
H-Beta CP811E	75	None	165.6	8.5
H-Beta CP811E	75	[Btma][NTf ₂]	37.3	1.4
H-USY CBV720	15	[Btma][NTf ₂]	24.7	1.2
H-USY CBV400	2.5	[Btma][NTf ₂]	6.9	0

(see Table 1). These results agreed with previous works,^{3b,3c,11,12} where de-aluminated zeolites resulted in fast racemization of **1**: the fastest reaction rates were always observed with H-Beta zeolites.

The ability of Novozym coated with IL to catalyze the KR of *rac*-1 in continuous operation with scCO₂ at 50 °C and 100 bar has been reported to increase the yield of *R*-2 product by only up to 50% with an excellent enantioselectivity ($ee > 99.9$).⁸

The suitability of acid zeolites combined with immobilized lipase catalyzing DKR of *rac*-1 in non-aqueous monophasic systems has been studied in discontinuous way.^{10,11} In spite of the different organic solvents assayed (*e.g.* toluene, hexane, 1,4-dioxane, *etc.*), as well as the reactions parameters (*e.g.* temperature, acyl donor, *etc.*), the best results were relatively poor (71% *R*-1-phenylethyl acetate yield and 87.5% ee after 6 h in toluene, improving to 82% yield and 83.1% ee after 48 h reaction time).¹¹ The encapsulation of H-Beta zeolite with polyelectrolytes did not improve these results (70% *R*-1 yield and 86% ee after 72 h in toluene).¹⁰

In this context, a (chemo)biocatalytic packed bed reactor, based on both immobilized lipase (Novozym 435) and zeolite particles coated with ILs, was developed to carry out the DKR of *rac*-1 in scCO₂ phase in continuous way (see Fig. 1B). The system operated as a biphasic reactor, the substrates being transported by the scCO₂ phase to each catalyst microenvironment across the IL shell, and the products returning to the supercritical phase. The stereoselective action of the enzyme permits the preferential conversion of *R*-1 to *R*-2, while the acidic catalysts provide *in situ* racemisation of the *S*-1 unreactive enantiomer. In this way, the product *R*-2 can theoretically be obtained optically pure with a 100% yield.¹³

Five different ILs, *i.e.* [Bmim][PF₆], [Bdmim][PF₆], [Odmim][NTf₂], [Toma][NTf₂] and [Btma][NTf₂], were assayed, and each Novozym-zeolite-IL system was tested for 6 h. The obtained *R*-2 yield, ee_{R-2} and PrA yield in the steady state are summarised in Table 2. As can be seen in entry 1, a low ee_{R-2} value (16.4%) was obtained when catalyst particles were assayed without IL coating, in spite of the reported⁴⁻⁷ excellent enantioselectivity of Novozym 435 for the kinetic resolution of *rac*-1, suggesting that the acidic zeolite was indeed interfering with the pH-sensitive enzyme. This fact was in agreement with previous works where uncoated acid catalysts (*e.g.* zeolites) combined with immobilized lipases were assayed in DKR reactions.^{8,10} Furthermore, the observed high content of PrA (58.7% of inlet acyl donor **3**) at the outlet of the reactor, corresponding to the hydrolysis of the excess of **3**, is worth noting. This fact could also be related with the loss of enzyme enantioselectivity. In this way, the use of catalyst particles coated with [Bmim][PF₆] (entry 2) greatly improved the efficiency of the system, because the racemizing activity of the H-Beta zeolite coupled with the enzyme catalysis was able to increase the *R*-2 yield up to 73.8%, while the enantioselectivity of the enzyme remained unchanged (99.5% ee_{R-2}). In this case, the undesired hydrolysis of **3** at the reactor outlet was reduced to 23.3% of its inlet concentration, suggesting that the transport of uncontrolled amounts of water from the CO₂ tank towards the catalytic environment was limited by the water-immiscible IL shell coating particles. The use of other water-immiscible ILs to cover both Novozym and H-Beta zeolite particles (entries 3

Table 2 Continuous DKR catalyzed by both Novozym (1 g) and zeolite catalysts coated with IL, by pumping a **3:1** (2:1 mol:mol) mixture at $6 \mu\text{mol min}^{-1}$ mass-flow rate into the scCO_2 inlet flow (1 mL min^{-1}) of the reactor at 50°C and 100 bar

Entry	Zeolite	IL	R-2 Yield (%)	ee_{R-2} (%)	PrA ⁱ (%)
1	CP811E ^a	None	48.0	16.4	58.7
2	CP811E ^a	[Bmim][PF ₆] ^d	73.8	99.5	23.3
3	CP811E ^a	[Toma][NTf ₂] ^e	75.5	82.1	11.3
4	CP811E ^b	[Odmim][NTf ₂] ^f	67.7	95.7	11.1
5	CP811E ^c	[Bdmim][PF ₆] ^g	59.5	96.2	10.4
6	CP811E ^c	[Btma][NTf ₂] ^h	72.3	>99.0	11.7
7	CBV720 ^c	[Btma][NTf ₂] ^h	72.0	90.4	11.9
8	CBV400 ^c	[Btma][NTf ₂] ^h	98.0	97.3	10.7

^a 200 mg, ^b 300 mg, ^c 500 mg, ^d Bmim: 1-butyl-3-methylimidazolium, ^e Toma: trioctylmethylammonium, ^f Odmim: 1-octadecyl-3-methylimidazolium, ^g Bdmim: 1-butyl-2,3-dimethylimidazolium, ^h Btma: butyltrimethylammonium. ⁱ With respect the mass inlet flow.

to 6) provided propionic acid concentrations lower than 12% of the inlet mass flow **3**, but did not achieve a clear improvement in either the *R-2* yield or ee_{R-2} , in spite of the increased amount of zeolite assayed (from 200 mg to 500 mg).

In spite of the low racemizing activity shown by fajaussite (Y-USY) type zeolites (see Table 1), both CBV720 and CBV400 chemical catalysts were seen to be suitable for the DKR process of *rac-1* in scCO_2 . The use of a Novozym/CBV720 mixture (2:1 w/w) coated with [Btma][NTf₂] allowed an interesting activity level (72% *R-2* yield and 90.4% ee_{R-2} , entry 7), which was similar to that observed for H-beta zeolite (entry 2). However, the best results (98% *R-2* yield and 97.3% ee_{R-2} , entry 8) were obtained for the Novozym/CBV400 catalysts mixture (2:1 w/w) coated with [Btma][NTf₂].

Fig. 3 shows the operational stability profile obtained for the continuous DKR process catalyzed by the Novozym 435/H-USY CBV400 catalyst mixture coated with [Btma][NTf₂] in scCO_2 under different conditions of pressure and temperature. As can be seen, both *R-2* yield and ee_{R-2} profiles remained practically unchanged for 6 days of operation. At 50°C , the increase in scCO_2 pressure to 120 bar involved a slight improvement in ee_{R-2} (up to 98.8%), while the *R-2* yield was reduced to 80%. At a pressure of 120 bar, the subsequent increase of temperature to 60°C improved the previous *R-2* yield (up to 90%) maintaining the same level of ee_{R-2} (up to 99.5%). A further decrease in pressure to 100 bar at the same temperature (60°C) allowed to improve the *R-2* yield (up to 97.5%), but

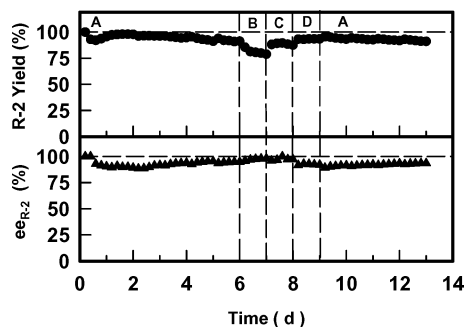


Fig. 3 Operational stability for continuous DKR catalyzed by both Novozym 435 (1 g) and zeolite CBV400 (0.5 g) coated with [Btma][NTf₂] (1 mL and 0.5 mL, respectively) in scCO_2 at $2 \mu\text{mol min}^{-1}$ mass-flow rate and (A) 50°C and 100 bar, (B) 50°C and 120 bar, (C) 60°C and 120 bar and (D) 60°C and 100 bar.

slightly reduced ee_{R-2} (up to 93.5). Finally, when the reactor was returned to the initial supercritical conditions (50°C and 100 bar) after 9 days of operation, both *R-2* yield and ee_{R-2} profiles returned to the activity levels shown at initial stages, remaining then unchanged for an additional four days of operation.

The excellences of IL-coating biocatalyst particles, as protective agents that improve both activity and stability of lipases in adverse processes (*e.g.* immobilization in sol-gel derived silica, KR in scCO_2 at 100 bar and 150°C , *etc.*), have been demonstrated.¹⁴ The effects of changes in pressure and temperature on enzyme-catalyzed reactions in scCO_2 have recently been reviewed.¹⁵ In the synthesis of butyl butyrate catalyzed by Novozym 435 in scCO_2 , it was observed that, within the range $40\text{--}60^\circ\text{C}$, an increase in temperature improves the enzyme activity at all the assayed pressures (80–150 bar). However, at a fixed temperature in the above range, an increase in pressure resulted in a decrease in the synthetic activity of the enzyme, and this effect was attributed to the increase in the density of scCO_2 .¹⁶ However, the effect of pressure on enantioselectivity is indeed noteworthy, although the reason for this is not clear. For example, Matsuda *et al.*¹⁷ reported how the enantioselectivity of Novozym 435-catalyzed acetylation of *rac-1*-(*p*-chlorophenyl)-2,2,2-trifluoroethanol with vinyl acetate in scCO_2 gradually decreased when the pressure increased from 80 to 190 bar, which was also related with changes in scCO_2 density. Conversely, for the same immobilized lipase-catalyzed continuous kinetic resolution of *rac-1*, it was reported that changes in pressure did not greatly affect conversion or enantioselectivity.¹⁸

Conclusions

The excellent suitability of the Novozym/H USY CBV400/[Btma][NTf₂] system for the continuous DKR of **1** in scCO_2 was clearly demonstrated. Once again, the excellent protective effect of ILs against enzyme deactivation by temperature, CO_2 and/or acidic pH was observed.⁵⁷ This work clearly demonstrates the exciting potential of multi-catalytic (enzymatic or chemo-enzymatic) systems in ILs/ scCO_2 for synthesizing optically active pharmaceutical drugs in green and clean non-aqueous continuous processes. In this way, the use of co-solvents or surfactants may aid to overcome the limitations of scCO_2 to only dissolve hydrophobic compounds, allowing to extend the proposed methodology to the hydrophilic cases.¹⁹ Fundamental studies on (bio)catalysis in IL/supercritical

fluid biphasic media should be carried out to establish clear criteria for specifically pairing the most appropriate IL and supercritical fluid with the corresponding (multi)catalytic system or bioprocess.

Acknowledgements

This work was partially supported by CICYT (CTQ2005-01571-PPQ and CTQ2008-00877), SENECA Foundation (02910/PI/05 and 08616/PI/08) and BIOCARM (BIO-BMC 06/01-0002) grants. Authors thank M. Ramiro Martinez (Novozymes, Spain) for the gift of enzymes.

Notes and references

- 1 A. Kamal, M. A. Azhar, T. Krishnaji, M. S. Malik and S. Azeza, *Coord. Chem. Rev.*, 2008, **252**, 568–592; R. Xie, L. Y. Chu and J. G. Deng, *Chem. Soc. Rev.*, 2008, **37**, 1243–1263.
- 2 (a) Y. Ahn, S. B. Ko, M. J. Kim and J. Park, *Coord. Chem. Rev.*, 2008, **252**, 647–658; O. Pamies and J. E. Backvall, *Trends Biotechnol.*, 2004, **22**, 130–135; S. B. Ko, B. Baburaj, M. J. Kim and J. Park, *J. Org. Chem.*, 2007, **72**, 6860–6864; S. Wuyts, J. Wahlen, P. A. Jacobs and D. E. De Vos, *Green Chem.*, 2007, **9**, 1104–1108.
- 3 (a) P. Ödman, L. A. Wessjohann and U. T. Bornscheuer, *J. Org. Chem.*, 2005, **70**, 9551–9555; (b) S. Wuyts, K. De Temmerman, D. E. De Vos and P. A. Jacobs, *Chem. Commun.*, 2003, 1928–1929; (c) S. Wuyts, K. De Temmerman, D. E. De Vos and P. A. Jacobs, *Chem.–Eur. J.*, 2005, **11**, 386–397; (d) E. L. Teo, G. K. Chuah, A. R. J. Huguët, S. Jaenicke, G. Pande and Y. Zhu, *Catal. Today*, 2004, **97**, 263–270.
- 4 (a) F. van Rantwijk and R. A. Sheldon, *Chem. Rev.*, 2007, **107**, 2757–2785; (b) J. Durand, E. Teuma and M. Gomez, *C. R. Chimie*, 2007, **10**, 152–157.
- 5 (a) P. Lozano, T. De Diego, D. Carrié, M. Vaultier and J. L. Iborra, *Biotechnol. Lett.*, 2001, **23**, 1529–1533; (b) M. Persson and U. T. Bornscheuer, *J. Mol. Catal. B: Enzym.*, 2003, **22**, 21–27; (c) T. De Diego, P. Lozano, S. Gmouh, M. Vaultier and J. L. Iborra, *Biomacromolecules*, 2005, **6**, 1457–1464; (d) E. Feher, B. Major, K. Belafi-Bako and L. Gubicza, *Biochem. Soc. Trans.*, 2007, **35**, 1624–1627.
- 6 M. J. Kim, H. M. Kim, D. Kim, Y. Ahn and J. Park, *Green Chem.*, 2004, **6**, 471–44.
- 7 (a) P. Lozano, T. De Diego, D. Carrié, M. Vaultier and J. L. Iborra, *Chem. Commun.*, 2002, 692–693; (b) M. T. Reetz, W. Wiesenhofer, G. Francio and W. Leitner, *Chem. Commun.*, 2002, 992–993; (c) P. Lozano, T. De Diego, S. Gmouh, M. Vaultier and J. L. Iborra, *Biotechnol. Prog.*, 2004, **20**, 661–669; (d) M. T. Reetz, W. Wiesenhofer, G. Francio and W. Leitner, *Adv. Synth. Catal.*, 2003, **345**, 1221–1228; (e) S. Garcia, N. M. T. Lourenco, D. Lousa, A. F. Sequeira, P. Mimoso, J. M. S. Cabral, C. A. M. Afonso and S. Barreiros, *Green Chem.*, 2004, **6**, 466–470; (f) S. Cantone, U. Hanefeld and A. Basso, *Green Chem.*, 2007, **9**, 954–971.
- 8 (a) P. Lozano, T. De Diego, M. Larnicol, M. Vaultier and J. L. Iborra, *Biotechnol. Lett.*, 2006, **28**, 1559–1565; (b) P. Lozano, T. De Diego, S. Gmouh, M. Vaultier and J. L. Iborra, *Int. J. Chem. React. Eng.*, 2007, **5**, A53.
- 9 P. Lozano, R. Piamtongkam, K. Kohns, T. De Diego, M. Vaultier and J. L. Iborra, *Green Chem.*, 2007, **9**, 780–784.
- 10 A. F. Fois, A. Yap, A. F. Masters and T. Maschmeyer, *Top. Catal.*, 2008, **48**, 153–157.
- 11 Y. Zhu, K. L. Fow, G. K. Chuah and S. Jaenicke, *Chem.–Eur. J.*, 2007, **13**, 541–547.
- 12 L. F. A. Costa, F. Lemos, F. R. Ribeiro and J. M. S. Cabral, *Catal. Today*, 2008, **133–135**, 625–631.
- 13 (a) O. Pamies and J. E. Backvall, *Chem. Rev.*, 2003, **103**, 3247–3261; (b) O. Pamies and J. E. Backvall, *Trends Biotechnol.*, 2004, **22**, 130–135.
- 14 (a) P. Lozano, T. De Diego, D. Carrié, M. Vaultier and J. L. Iborra, *Biotechnol. Prog.*, 2003, **19**, 380–382; (b) S. H. Lee, T. T. N. Doan, S. H. Ha and Y. M. Koo, *J. Mol. Catal. B: Enzym.*, 2007, **45**, 57–61.
- 15 (a) K. Rezaei, F. Temelli and E. Jenab, *Biotechnol. Adv.*, 2007, **25**, 272–280; (b) K. Rezaei, E. Jenab and F. Temelli, *Crit. Rev. Biotechnol.*, 2008, **27**, 183–195.
- 16 P. Lozano, G. Villora, D. Gomez, A. B. Gayo, J. A. Sanchez-Conesa, M. Rubio and J. L. Iborra, *J. Supercrit. Fluids*, 2004, **29**, 121–128.
- 17 T. Matsuda, T. Harada and K. Nakamura, *Curr. Org. Chem.*, 2005, **9**, 299–315.
- 18 T. Matsuda, K. Watanabe, T. Harada, K. Nakamura, Y. Arita, Y. Misumi, S. Ichikawa and T. Ikariya, *Chem. Commun.*, 2004, 2286–2287.
- 19 J. B. McClain, D. E. Betts, D. A. Canelas, E. T. Samulski, J. M. DeSimone, J. D. Londono, H. D. Cocharan, G. D. Wignall, D. Chillura Martino and R. Triolo, *Science*, 1996, **274**, 2049–2052.

Highly enantioselective L-thiaproline catalyzed α -aminoxylation of aldehydes in aqueous media†

Pei Juan Chua, Bin Tan and Guofu Zhong*

Received 15th October 2008, Accepted 28th January 2009

First published as an Advance Article on the web 13th February 2009

DOI: 10.1039/b817950f

Highly enantioselective L-thiaproline catalyzed α -aminoxylation of aldehydes in the presence of water and tetrabutylammonium bromide followed by *in situ* reduction to afford the respective α -aminoxy alcohols has been developed in good to high yields (74–88%) and excellent enantioselectivities (93–>99%).

Introduction

The presence of optically active α -hydroxycarbonyl moieties such as 1,2-diols in many biologically active natural products motivated research into finding new routes to provide better stereocontrol for these synthetically useful synthons.¹ Asymmetric α -hydroxylation of enolates² and the Sharpless asymmetric dihydroxylation of olefins³ are some methods to synthesize these compounds. The year 2000 saw a renaissance of organocatalysis, and since then organocatalysis has emerged as an extremely useful tool for the preparation of enantiomerically pure compounds.⁴ Operational simplicity, availability and the non-toxicity of the organic catalysts compared to the corresponding transition-metal species, as well as the high efficiencies and selectivities attained in many organocatalytic transformations made this methodology very attractive for the formation of enantiomerically pure compounds.

In 2003 Zhong,⁵ MacMillan⁶ and Hayashi⁷ and co-workers independently reported the direct proline-catalyzed α -aminoxylation of aldehydes with nitrosobenzene and the usefulness of this reaction was demonstrated in the synthesis of several biologically active compounds.⁸ Though the scope of the above-mentioned reaction has been quickly extended to that of ketones⁹ after the first report, there was little development in new organocatalysts¹⁰ or environmentally friendly reaction protocols.¹¹

Conventional chemical synthesis usually focused on improving yield and selectivity, with little regard to a chemical's impact on the environment. Recently, increasing demand for innovative and imaginative synthetic methodologies to improve efficiency and sustainability such as simplicity, atom economy, reduced chemical wastage and energy usage, safety, and environmental friendliness prompted much research in this area.¹² To date, α -aminoxylation is usually carried out in organic solvents such as acetonitrile,^{7,13} chloroform,⁶ dichloromethane,¹⁴

dimethylformamide¹⁵ and dimethylsulfoxide.^{5,16} The use of such solvents contributes to the organic waste and it is essential to develop more environmentally friendly protocols.

Water, no doubt, is the most inexpensive and environmentally benign solvent. Since Breslow reported that the use of water instead of organic solvents could significantly increase the rate of the Diels–Alder reaction¹⁷ considerable attention has been directed towards the development of organic reactions in water. To date, all of the most useful organic reactions have at least a reaction protocol that involves water as a solvent.¹⁸ Although Blackmond raised some doubts about the environmental friendliness and efficiency of water in organocatalysis,¹⁹ we cannot dismiss some of the advantages that accompanies the use of water as a solvent: acceleration of reaction rates and enhancement of reaction selectivities; elimination of tedious protection–deprotection processes for certain acidic-hydrogen containing functional groups and the recycling of water-soluble catalysts after separation from water-insoluble organic products.

Results and discussion

To probe the feasibility of the α -aminoxylation of aldehydes in aqueous media using a phase-transfer catalyst, we first performed α -aminoxylation of propanal to nitrosobenzene in the presence of L-proline **I**, tetrabutylammonium bromide and water at 0 °C and then warmed to room temperature. To our disappointment the yield obtained in this initial reaction was rather low, despite the high enantioselectivity achieved. This prompted us to screen more catalysts **II–VI** (Table 1, entries 2–6). Among all the catalysts investigated, only L-thiaproline **VI** gave a higher yield than **I**. Although **VI** needed a longer reaction time and gave a slightly lower enantioselectivity than **I**, we believed that higher enantioselectivity could be achieved with the optimization of reaction conditions. This is the first instance where L-thiaproline **VI** was used as a catalyst in an α -aminoxylation. The use of **VI** will potentially reduce much hassle for stereoselective reactions as it is commercially available.

For optimisation of the reaction conditions, we first investigated the effect of catalyst loading on the reaction (Table 2, entries 1–3). Highest yield and enantioselectivity were obtained when 20 mol% of catalyst was used. The results of the reaction

Division of Chemistry & Biological Chemistry, School of Physical & Mathematical Sciences, Nanyang Technological University, 21 Nanyang Link, Singapore, 637371, Singapore. E-mail: guofu@ntu.edu.sg; Fax: +65 6791 1961; Tel: +65 6316 8761

† Electronic supplementary information (ESI) available: General information, general experimental procedure, and experimental data and spectra for compounds **3a–k**. See DOI: 10.1039/b817950f

Table 1 Catalyst screening^a

Reaction scheme for Table 1: $\text{CH}_3\text{CH}_2\text{CHO} + \text{C}_6\text{H}_5\text{NO} \xrightarrow[2. \text{NaBH}_4, \text{EtOH}]{1. \text{Cat.}, \text{Bu}_4\text{NBr}, \text{H}_2\text{O}, 0^\circ\text{C to rt}}$ $\text{CH}_3\text{CH}_2\text{CH(OH)CH}_2\text{NHC}_6\text{H}_5$

Structures of catalysts I–VI:

- I**: L-proline
- II**: L-piperidine-2-carboxylic acid
- III**: L-proline derivative with a 1,2,4,5-tetrazole group
- IV**: L-proline derivative with an indole group
- V**: L-proline derivative with a hydroxyl group
- VI**: L-thiaproline

Entry	Catalyst	Time	Yield ^b (%)	ee ^c (%)
1	I	1 h	64	96
2	II	6 h	39	43
3	III	20 min	62	96
4	IV	30 min	14	23
5	V	30 min	65	82
6	VI	1 h 40 min	75	93

^a Conditions: Nitrosobenzene (0.3 mmol), propanal (3 equiv.), catalyst (30 mol%), tetrabutylammonium bromide (2 equiv.) and water (0.10 mL) was added at 0 °C and then warmed to rt (23 °C) unless otherwise stated.
^b Isolated yields. ^c Determined by chiral phase HPLC.

did not improve under neat conditions (Table 2, entry 4). Screenings of various organic solvents revealed that chloroform and dimethyl sulfoxide, preferred solvents for many α -aminoxylation reactions, were not the best solvents when **VI** was employed as catalyst (Table 2, entries 5–6). Although acetonitrile gave

comparable enantioselectivity, its lower yield and longer reaction time made water the preferred choice of solvent for this reaction (Table 2, entry 7). We discovered that 0.10 mL of water is the optimum amount of water added to the system to attain the highest yield and enantioselectivity (Table 2, entries 8–10). Both the yield and enantioselectivity dropped when the amount of phase transfer catalyst was reduced (Table 2, entries 11–12). A similar trend was also observed with decreasing amounts of propanal (Table 2, entries 13–14).

With the optimal reaction conditions established, we probed the scope of the reaction for a variety of aldehydes. The results are summarized in Table 3. In the cases investigated, the α -aminoxy alcohols were obtained in good to high yields (74–88%) and excellent enantioselectivities (93–99%). The L-thiaproline α -aminoxylation reaction between nitrosobenzene and propanal was completed in 2 h with good yield (84%) and excellent enantioselectivity (96%) (Table 3, entry 1). Not only propanal, but linear chain aldehydes such as *n*-butanal, *n*-pentanal and *n*-hexanal react with nitrosobenzene, affording α -aminoxy alcohols in good yield with excellent enantioselectivities (Table 3, entries 2–4). Branched aldehydes such as 3-methylbutanal are also suitable substrates as it was successfully converted to the α -aminoxy alcohols in good yield with excellent enantioselectivity (Table 3, entry 5). Aldehydes containing an aromatic moiety such as phenylacetaldehyde and 3-phenylpropanal were successfully employed in this reaction (Table 3, entries 6 and 7). It is interesting to note that the reaction time for phenylacetaldehyde was significantly reduced. This may be due to the activating effect of the benzene ring in the α -position of the phenylacetaldehyde. The introduction of a terminal double bond on the aldehyde did not drastically affect the yield and enantioselectivity of the reaction (Table 3, entry 8). The reaction also proceeded smoothly with protecting groups such as benzyl ethers and *tert*-butoxycarbonyl carbamates to

Table 2 Optimisation of reaction conditions^a

Reaction scheme for Table 2: $\text{CH}_3\text{CH}_2\text{CHO} + \text{C}_6\text{H}_5\text{NO} \xrightarrow[2. \text{NaBH}_4, \text{EtOH}]{1. \text{VI}, \text{Bu}_4\text{NBr}, \text{Solvent}, 0^\circ\text{C to rt}}$ $\text{CH}_3\text{CH}_2\text{CH(OH)CH}_2\text{NHC}_6\text{H}_5$

Entry	Solvent	Vol. of solvent	Time	Yield ^b (%)	ee ^c (%)
1 ^d	H ₂ O	0.10 mL	2 h 10 min	78	93
2	H ₂ O	0.10 mL	2 h	84	96
3 ^e	H ₂ O	0.10 mL	1 h 40 min	75	93
4	—	0.10 mL	1 h 15 min	62	94
5	CHCl ₃	0.10 mL	1 h 50 min	60	92
6	DMSO	0.10 mL	2 h 15 min	68	90
7	CH ₃ CN	0.10 mL	3 h 50 min	73	97
8	H ₂ O	0.05 mL	2 h 20 min	56	93
9	H ₂ O	0.20 mL	2 h 10 min	67	96
10	H ₂ O	0.30 mL	1 h 45 min	58	93
11 ^f	H ₂ O	0.10 mL	1 h 55 min	62	94
12 ^g	H ₂ O	0.10 mL	1 h 45 min	62	95
13 ^h	H ₂ O	0.10 mL	2 h 15 min	52	90
14 ⁱ	H ₂ O	0.10 mL	2 h 25 min	54	92

^a Conditions: Nitrosobenzene (0.3 mmol), propanal (3 equiv.), catalyst (20 mol%), tetrabutylammonium bromide (2 equiv.) and water (0.10 mL) was added at 0 °C and stirred at rt (23 °C) unless otherwise stated. ^b Isolated yields. ^c Determined by chiral phase HPLC. ^d 10 mol% of **VI**. ^e 30 mol% of **VI**. ^f No Bu₄NBr added. ^g 1 equiv. Bu₄NBr added. ^h 1 equiv. propanal added. ⁱ 2 equiv. propanal added.

Table 3 The generality of reaction of α -aminoxylation in the presence of water^a

Entry	R	3a-k	Time	Yield ^b (%)	ee ^c (%)
1	Me	3a	2 h	84	96
2	Et	3b	2 h 10 min	75	98
3	Pr	3c	2 h 20 min	79	97
4	Bu	3d	2 h 35 min	74	96
5	<i>i</i> -Pr	3e	2 h 10 min	76	97
6	Ph	3f	20 min	78	93
7	PhCH ₂	3g	2 h 30 min	77	> 99
8	CH ₂ =CHCH ₂	3h	1 h	88	96
9	BnOCH ₂ CH ₂	3i	2 h 20 min	86	97
10	BocNHCH ₂	3j	2 h 30 min	79	93
11 ^d	Me	3k	2 h 20 min	83	97

^a Conditions: Nitrosobenzene (0.3 mmol), propanal (3 equiv.), catalyst (20 mol%), tetrabutylammonium bromide (2 equiv.) and water (0.10 mL) was added at 0 °C and stirred at rt (23 °C) unless otherwise stated. ^b Isolated yields. ^c Determined by chiral phase HPLC. ^d Nitrosotoluene was used instead of nitrosobenzene.

afford the α -aminoxy alcohols in good yield with excellent enantioselectivities (Table 3, entries 9–10). The scope of nitroso compounds was briefly tested by replacing nitrosobenzene with nitrosotoluene. When nitrosotoluene was treated with propanal under the optimised conditions, the corresponding α -aminoxy alcohols were obtained in 83% yield with an enantioselectivity of 97%, which is consistent with the results of nitrosobenzene.

Conclusions

In conclusion, L-thiaproline was used to catalyze α -aminoxylation of aldehydes in aqueous media in the presence of a phase-transfer catalyst to afford the respective α -aminoxy alcohols in good to high yields (74–88%) and excellent enantioselectivities (93–>99%). This reaction protocol may find potential use for industrial-scale preparation due to its simple operation, wide scope, excellent enantioselectivities and environmental friendliness. Further investigation on the application of L-thiaproline in asymmetric catalysis is in progress.

Experimental

General experimental procedure for the α -aminoxylation of aldehydes to nitrosobenzene in aqueous media

Water (0.10 mL) and tetrabutylammonium bromide (193.4 mg, 0.6 mmol) was added to a 5 mL drum vial containing nitrosobenzene (**2**, 32.1 mg, 0.3 mmol), corresponding aldehydes (**1**, 0.9 mmol) and a magnetic stirring bar. After stirring for 5 min at 0 °C, L-thiaproline (8 mg, 0.06 mmol) was added. The reaction was first stirred at this temperature for about 10 min and then at room temperature until the green solution turned yellow which indicated complete consumption of the nitrosobenzene. As the α -aminoxy aldehyde product is rather labile, isolation and characterization was performed after conversion to the corresponding α -aminoxy alcohol **3** by treatment of the reaction mixture with NaBH₄. The excess NaBH₄ was quenched by the

addition of water. The reaction mixture was then extracted with CH₂Cl₂ (3 × 30 mL). The combined organic extracts were dried with Na₂SO₄ and concentrated *in vacuo*. The crude oil was purified by flash column chromatography (hexane/EtOAc = 9/1–7/3) yielding pure α -aminoxy alcohols **3**.

(R)-2-(N-Phenylaminoxy)propan-1-ol (3a). α -Aminoxy alcohol **3a** was prepared according to the general procedure from propanal (0.07 mL, 0.9 mmol) to provide the title compound as a pale yellow liquid (42.3 mg, 84% yield) after flash column chromatography on silica gel (hexane/EtOAc = 9/1–7/3). ¹H NMR (400 MHz, CDCl₃): δ 7.29–7.25 (2H, m), 7.04–6.96 (3H, m), 4.16–4.08 (1H, m), 3.80–3.70 (2H, m), 2.56 (1H, brs), 1.25 (3H, d, *J* = 6.4 Hz). ¹³C NMR (100 MHz, CDCl₃): δ 148.5, 129.0, 122.4, 114.7, 80.0, 66.5, 15.4. HPLC: Chiralpak AD-H (hexane/*i*-PrOH, 90/10, flow rate 1 mL min⁻¹, λ = 230 nm), *t*_R (minor) = 10.6 min, *t*_R (major) = 12.1 min; 96% ee. [α]_D²⁵ = +2.9 (*c* = 1.0, CHCl₃).

(R)-2-(N-Phenylaminoxy)butan-1-ol (3b). α -Aminoxy alcohol **3b** was prepared according to the general procedure from butanal (0.08 mL, 0.9 mmol) to provide the title compound as a pale yellow liquid (40.9 mg, 75% yield) after flash column chromatography on silica gel (hexane/EtOAc = 9/1–7/3). ¹H NMR (400 MHz, CDCl₃): δ 7.29–7.25 (2H, m), 7.07–6.96 (2H, m), 3.91–3.74 (3H, m), 2.67 (1H, brs), 1.78–1.53 (2H, m), 1.01 (3H, t, *J* = 7.5 Hz). ¹³C NMR (100 MHz, CDCl₃): δ 148.4, 129.0, 122.4, 114.8, 85.3, 64.9, 22.9, 10.1. HPLC: Chiralpak AD-H (hexane/*i*-PrOH, 90/10, flow rate 1 mL min⁻¹, λ = 230 nm), *t*_R (minor) = 10.2 min, *t*_R (major) = 11.6 min; 98% ee. [α]_D²⁵ = +36.0 (*c* = 1.0, CHCl₃).

(R)-2-(N-Phenylaminoxy)pentan-1-ol (3c). α -Aminoxy alcohol **3c** was prepared according to the general procedure from pentanal (0.10 mL, 0.9 mmol) to provide the title compound as a pale yellow liquid (46.0 mg, 79% yield) after flash column chromatography on silica gel (hexane/EtOAc = 9/1–7/3). ¹H NMR (400 MHz, CDCl₃): δ 7.28–7.15 (3H, m), 6.98–6.94 (2H, m),

3.94–3.91 (1H, m), 3.85–3.82 (1H, m), 3.75–3.71 (1H, m), 2.93 (1H, brs), 1.67–1.61 (1H, m), 1.54–1.33 (3H, m), 0.97–0.89 (3H, m). ^{13}C NMR (100 MHz, CDCl_3): δ 148.4, 129.0, 122.3, 114.7, 83.7, 65.1, 32.0, 19.0, 14.2. HPLC: Chiralpak AD-H (hexane/*i*-PrOH, 90/10, flow rate 1 mL min $^{-1}$, λ = 230 nm), t_{R} (minor) = 10.0 min, t_{R} (major) = 11.4 min; 97% ee. $[\alpha]_{\text{D}}^{25}$ = +28.6 (c = 1.0, CHCl_3).

(R)-2-(*N*-Phenylaminoxy)hexan-1-ol (3d). α -Aminoxy alcohol **3d** was prepared according to the general procedure from hexanal (0.11 mL, 0.9 mmol) to provide the title compound as a pale yellow liquid (46.4 mg, 74% yield) after flash column chromatography on silica gel (hexane/EtOAc = 9/1–7/3). ^1H NMR (400 MHz, CDCl_3): δ 7.29–7.26 (2H, m), 7.06–6.96 (3H, m), 5.93–5.82 (1H, m), 5.18–5.11 (2H, m), 4.05–4.00 (1H, m), 3.87–3.75 (2H, m), 2.54–2.32 (3H, m), 1.66 (1H, brs). ^{13}C NMR (100 MHz, CDCl_3): δ 148.3, 134.0, 129.0, 122.5, 117.8, 114.8, 83.3, 64.6, 34.6. HPLC: Chiralpak AD-H (hexane/*i*-PrOH, 90/10, flow rate 1 mL min $^{-1}$, λ = 230 nm), t_{R} (minor) = 9.5 min, t_{R} (major) = 11.4 min; 96% ee. $[\alpha]_{\text{D}}^{25}$ = +22.5 (c = 1.2, CHCl_3).

(R)-3-Methyl-2-(*N*-phenylaminoxy)butan-1-ol (3e). α -Aminoxy alcohol **3e** was prepared according to the general procedure from 3-methylbutanal (0.10 mL, 0.9 mmol) to provide the title compound as a pale yellow liquid (44.8 mg, 76% yield) after flash column chromatography on silica gel (hexane/EtOAc = 9/1–7/3). ^1H NMR (400 MHz, CDCl_3): δ 7.30–7.26 (2H, m), 7.03–6.99 (3H, m), 3.88–3.87 (2H, m), 3.76–3.74 (1H, m), 2.07–1.99 (1H, m), 1.05 (3H, d, J = 6.9 Hz), 1.01 (3H, d, J = 6.9 Hz). ^{13}C NMR (100 MHz, CDCl_3): δ 148.3, 129.0, 122.5, 115.0, 88.6, 63.6, 28.7, 18.7, 18.6. HPLC: Chiralpak AD-H (hexane/*i*-PrOH, 90/10, flow rate 1 mL min $^{-1}$, λ = 230 nm), t_{R} (minor) = 9.0 min, t_{R} (major) = 10.1 min; 97% ee. $[\alpha]_{\text{D}}^{22}$ = +33.4 (c = 1.0, CHCl_3).

(R)-2-Phenyl-2-(*N*-phenylaminoxy)ethanol (3f). α -Aminoxy alcohol **3f** was prepared according to the general procedure from 2-phenylacetaldehyde (0.11 mL, 0.9 mmol) to provide the title compound as a pale yellow liquid (53.5 mg, 78% yield) after flash column chromatography on silica gel (hexane/ether = 9/1–7/3). ^1H NMR (400 MHz, CDCl_3): δ 7.39–7.31 (5H, m), 7.28–7.20 (2H, m), 6.99–6.94 (3H, m), 5.00 (1H, dd, J = 3.5, 8.1 Hz), 3.99–3.92 (1H, m), 3.83–3.78 (1H, m), 2.58 (1H, brs). ^{13}C NMR (100 MHz, CDCl_3): δ 147.9, 137.7, 129.0, 128.7, 128.5, 127.0, 122.5, 115.0, 86.4, 66.4. HPLC: Chiralpak OD-H (hexane/*i*-PrOH, 95/5, flow rate 1 mL min $^{-1}$, λ = 230 nm), t_{R} (major) = 25.8 min, t_{R} (minor) = 30.2 min; 93% ee. $[\alpha]_{\text{D}}^{24}$ = –85.5 (c = 1.1, CHCl_3).

(R)-3-Phenyl-2-(*N*-phenylaminoxy)propan-1-ol (3g). α -Aminoxy alcohol **3g** was prepared according to the general procedure from 3-phenylpropanal (0.12 mL, 0.9 mmol) to provide the title compound as a pale yellow liquid (55.9 mg, 77% yield) after flash column chromatography on silica gel (hexane/ether = 9/1–7/3). ^1H NMR (400 MHz, CDCl_3): δ 7.32–7.18 (6H, m), 7.08 (1H, brs), 6.94 (1H, t, J = 7.3 Hz), 6.82 (2H, d, J = 8.0 Hz), 4.16–4.10 (1H, m), 3.85 (1H, d, J = 11.8 Hz), 3.04 (1H, dd, J = 6.8, 13.7 Hz), 2.84 (1H, dd, J = 7.0, 13.7 Hz), 2.62 (1H, brs). ^{13}C NMR (100 MHz, CDCl_3): δ 148.3, 137.8, 129.4, 128.9, 128.5, 126.4, 122.3, 114.6, 85.0, 64.1,

36.4. HPLC: Chiralpak OD-H (hexane/*i*-PrOH, 91/9, flow rate 1 mL min $^{-1}$, λ = 230 nm), t_{R} (major) = 57.9 min, t_{R} (minor) = 62.4 min; >99% ee. $[\alpha]_{\text{D}}^{22}$ = +55.2 (c = 1.3, CHCl_3).

(R)-2-(*N*-Phenylaminoxy)pent-4-en-1-ol (3h). α -Aminoxy alcohol **3h** was prepared according to the general procedure from 4-pentenal (0.09 mL, 0.9 mmol) to provide the title compound as a pale yellow liquid (51.0 mg, 88% yield) after flash column chromatography on silica gel (hexane/EtOAc = 9/1–7/3). ^1H NMR (400 MHz, CDCl_3): δ 7.29–7.26 (2H, m), 7.06–6.96 (3H, m), 5.93–5.82 (1H, m), 5.18–5.11 (2H, m), 4.05–4.00 (1H, m), 3.87–3.75 (2H, m), 2.54–2.32 (3H, m), 1.66 (1H, brs). ^{13}C NMR (100 MHz, CDCl_3): δ 148.3, 134.0, 129.0, 122.5, 117.8, 114.8, 83.3, 64.6, 34.6. HPLC: Chiralpak AD-H (hexane/*i*-PrOH, 90/10, flow rate 1 mL min $^{-1}$, λ = 230 nm), t_{R} (minor) = 10.5 min, t_{R} (major) = 12.5 min; 96% ee. $[\alpha]_{\text{D}}^{25}$ = –22.9 (c = 1.0, CHCl_3).

(R)-4-(Benzyloxy)-2-(*N*-phenylaminoxy)butan-1-ol (3i). α -Aminoxy alcohol **3i** was prepared according to the general procedure from 4-(benzyloxy)butanal (0.16 mL, 0.9 mmol) to provide the title compound as a pale yellow liquid (73.8 mg, 86% yield) after flash column chromatography on silica gel (hexane/EtOAc = 9/1–7/3). ^1H NMR (400 MHz, CDCl_3): δ 7.34–7.23 (6H, m), 7.05 (1H, brs), 6.98–6.94 (3H, m), 4.54–4.52 (2H, m), 4.14–4.11 (1H, m), 3.93–3.87 (1H, m), 3.81–3.77 (1H, m), 3.66 (2H, t, J = 5.7 Hz), 2.81 (1H, t, J = 5.9 Hz), 2.06–1.89 (2H, m). ^{13}C NMR (100 MHz, CDCl_3): δ 148.3, 138.0, 129.0, 128.5, 127.8, 122.4, 116.1, 114.8, 81.5, 73.2, 66.7, 64.8, 30.3. HPLC: Chiralpak AD-H (hexane/*i*-PrOH, 91/9, flow rate 1 mL min $^{-1}$, λ = 230 nm), t_{R} (minor) = 18.8 min, t_{R} (major) = 24.1 min; 97% ee. $[\alpha]_{\text{D}}^{22}$ = +15.5 (c = 1.1, CHCl_3). HRMS (ESI) calcd for $\text{C}_{17}\text{H}_{21}\text{NO}_3$, m/z 288.1600, found 288.1599.

(R)-tert-Butyl 3-hydroxy-2-(*N*-phenylaminoxy)propylcarbamate (3j). α -Aminoxy alcohol **3j** was prepared according to the general procedure from *tert*-butyl 3-oxopropylcarbamate (0.16 mL, 0.9 mmol) to provide the title compound as a pale yellow liquid (67.2 mg, 79% yield) after flash column chromatography on silica gel (hexane/EtOAc = 9/1–7/3). ^1H NMR (400 MHz, CDCl_3): δ 7.32–7.24 (3H, m), 6.98–6.94 (2H, m), 5.02 (1H, brs), 3.94–3.92 (1H, m), 3.80 (2H, s), 3.50–3.36 (2H, m), 1.45 (9H, s). ^{13}C NMR (100 MHz, CDCl_3): δ 157.1, 148.3, 129.0, 122.4, 114.6, 82.4, 80.0, 61.3, 39.6, 28.3. HPLC: Chiralpak OJ-H (hexane/*i*-PrOH, 95/5, flow rate 1 mL min $^{-1}$, λ = 230 nm), t_{R} (minor) = 24.8 min, t_{R} (major) = 26.6 min; 93% ee. $[\alpha]_{\text{D}}^{22}$ = –8.2 (c = 1.3, CHCl_3). HRMS (ESI) calcd for $\text{C}_{14}\text{H}_{23}\text{N}_2\text{O}_4$, m/z 282.1658, found 282.1659.

(R)-2-(*p*-Toluidinoxy)propan-1-ol (3k). α -Aminoxy alcohol **3k** was prepared according to the general procedure from propanal (0.07 mL, 0.9 mmol) and nitrosotoluene (36.3 mg, 0.3 mmol) to provide the title compound as a pale yellow liquid (45.0 mg, 83% yield) after flash column chromatography on silica gel (hexane/EtOAc = 9/1–7/3). ^1H NMR (400 MHz, CDCl_3): δ 7.07 (2H, d, J = 8.1 Hz), 6.99 (1H, brs), 6.88 (2H, d, J = 8.3 Hz), 4.13–4.07 (1H, m), 3.78–3.68 (2H, m), 2.28 (3H, s), 1.22 (3H, d, J = 6.5 Hz). ^{13}C NMR (100 MHz, CDCl_3): δ 145.8, 132.0, 129.5, 115.3, 79.8, 66.6, 20.6, 15.4. HPLC: Chiralpak AD-H (hexane/*i*-PrOH, 90/10, flow rate 1 mL min $^{-1}$, λ = 230 nm), t_{R} (minor) = 10.9 min, t_{R} (major) = 12.4 min; 97% ee. $[\alpha]_{\text{D}}^{25}$ =

+5.5 ($c = 1.5$, CHCl_3). HRMS (ESI) calcd for $\text{C}_{10}\text{H}_{16}\text{NO}_2$, m/z 182.1181, found 182.1181.

Acknowledgements

This work is financially supported by grants from the Ministry of Education, Singapore (ARC12/07, no. T206B3225) and the School of Physical and Mathematical Sciences, Nanyang Technological University (URC, RG53/07 and SEP, RG140/06).

Notes and references

- (a) F. A. Davis, and B. C. Chen, *Methods of Organic Chemistry (Houben-Weyl)*, Thieme, Stuttgart, 1995; (b) D. Enders and U. Reinhold, *Synlett*, 1994, 792.
- (a) F. A. Davis and B. C. Chen, *Chem. Rev.*, 1992, **92**, 919. and references herein; (b) B. B. Lohray and D. Enders, *Helv. Chim. Acta*, 1989, **72**, 980.
- H. C. Kolb, M. S. VanNieuwenhze and K. B. Sharpless, *Chem. Rev.*, 1994, **94**, 2483.
- (a) A. Dondoni and A. Massi, *Angew. Chem., Int. Ed.*, 2008, **47**, 4638; (b) S. J. Connon, *Chem. Commun.*, 2008, 2499; (c) J. M. M. Verkade, L. J. C. van Hemert, P. J. L. M. Quaedflieg and F. P. J. T. Rutjes, *Chem. Soc. Rev.*, 2008, **37**, 29; (d) J. Seayad and B. List, *Org. Biomol. Chem.*, 2005, **3**, 719; (e) P. I. Dalko and L. Moisan, *Angew. Chem., Int. Ed.*, 2004, **43**, 5138.
- (a) G. Zhong, *Angew. Chem., Int. Ed.*, 2003, **42**, 4247; (b) M. Lu, D. Zhu, Y. Lu, Y. Hou, B. Tan and G. Zhong, *Angew. Chem., Int. Ed.*, 2008, **47**, 10187; (c) D. Zhu, M. Lu, P. J. Chua, B. Tan, F. Wang, X. Yang and G. Zhong, *Org. Lett.*, 2008, **10**, 4585; (d) G. Zhong and Y. Yu, *Org. Lett.*, 2004, **6**, 1637; (e) G. Zhong, *Chem. Commun.*, 2004, 606; (f) X. Zhu, F. Tanaka, Y. Hu, A. Heine, R. Fuller, G. Zhong, A. J. Olson, R. A. Lerner, C. F. Barbas, III and I. A. Wilson, *J. Mol. Biol.*, 2004, **343**, 1269; (g) B. Tan, P. J. Chua, Y. Li and G. Zhong, *Org. Lett.*, 2008, **10**, 2437; (h) B. Tan, Z. Shi, P. J. Chua and G. Zhong, *Org. Lett.*, 2008, **10**, 3425.
- S. P. Brown, M. P. Brochu, C. J. Sinz and D. W. C. MacMillan, *J. Am. Chem. Soc.*, 2003, **125**, 10808.
- Y. Hayashi, J. Yamaguchi, K. Hibino and M. Shoji, *Tetrahedron Lett.*, 2003, **44**, 8293.
- (a) S. P. Kotkar, G. S. Suryavansh and A. Sudalai, *Tetrahedron: Asymmetry*, 2007, **18**, 1795; (b) S. P. Kotkar, G. S. Suryavanshi and A. Sudalai, *Tetrahedron: Asymmetry*, 2007, **18**, 1738; (c) S. P. Kotkar and A. Sudalai, *Tetrahedron Lett.*, 2006, **47**, 6813; (d) S. V. Narina and A. Sudalai, *Tetrahedron Lett.*, 2006, **47**, 6799; (e) S. G. Kim and T. H. Park, *Tetrahedron Lett.*, 2006, **47**, 6369; (f) Sousuke Hara, Kazuishi Makino and Yasumasa Hamada, *Tetrahedron Lett.*, 2006, **47**, 1081; (g) I. K. Mangion and D. W. C. MacMillan, *J. Am. Chem. Soc.*, 2005, **127**, 3696.
- (a) Y. Hayashi, J. Yamaguchi, T. Sumiya and M. Shoji, *Angew. Chem., Int. Ed.*, 2004, **43**, 1112; (b) A. Bøgevig, H. Sundén and H. A. Córdova, *Angew. Chem., Int. Ed.*, 2004, **43**, 1109.
- (a) T. Kano, A. Yamamoto, H. Mii, J. Takai, S. Shirakawa and K. Maruoka, *Chem. Lett.*, 2008, **37**, 250; (b) Y. Hayashi, J. Yamaguchi, K. Hibino, T. Sumiya, T. Urushima, M. Shoji, D. Hashizume and H. Koshino, *Adv. Synth. Catal.*, 2004, **346**, 1435; (c) H. Sundén, N. Dahlin, I. Ibrahim, H. Adolfsson and A. Córdova, *Tetrahedron Lett.*, 2005, **46**, 3385; (d) W. Wang, J. Wang, H. Li and L. Li, *Tetrahedron Lett.*, 2004, **45**, 7235; (e) N. Momiyama, H. Torii, S. Saito and H. Yamamoto, *Proc. Natl. Acad. Sci. U. S. A.*, 2004, **101**, 5374.
- (a) D. Font, A. Bastero, S. Sayalero, C. Jimeno and M. A. Pericàs, *Org. Lett.*, 2007, **9**, 1943; (b) H.-M. Guo, H.-Y. Niu, M.-X. Xue, Q.-X. Guo, L.-F. Cun, A.-Q. Mi, Y.-Z. Jiang and J.-J. Wang, *Green Chem.*, 2006, **8**, 682.
- (a) M.-K. Zhu, X.-Y. Xu and L.-Z. Gong, *Adv. Synth. Catal.*, 2008, **350**, 1390; (b) N. Mase, Y. Nakai, N. Ohara, H. Yoda, K. Takabe, F. Tanaka and C. F. Barbas, III, *J. Am. Chem. Soc.*, 2006, **128**, 734; (c) N. Mase, K. Watanabe, H. Yoda, K. Takabe, F. Tanaka and C. F. Barbas, III, *J. Am. Chem. Soc.*, 2006, **128**, 4966; (d) D. Gonzalez-Cruz, D. Tejedor, P. de Armas, E. Q. Morales and F. Garcia-Tellado, *Chem. Commun.*, 2006, 2798; (e) D. E. White and E. N. Jacobsen, *Tetrahedron: Asymmetry*, 2003, **14**, 3633; (f) S. E. Schaus, B. D. Brandes, J. F. Larrow, M. Tokunaga, K. B. Hansen, A. E. Gould, M. E. Furrow and E. N. Jacobsen, *J. Am. Chem. Soc.*, 2002, **124**, 1307; (g) A. G. Dossetter, T. F. Jamison and E. N. Jacobsen, *Angew. Chem., Int. Ed.*, 1999, **38**, 2398; (h) M. Tokunaga, J. F. Larrow, F. Kakuichi and E. N. Jacobsen, *Science*, 1997, **277**, 936.
- (a) A. Córdova, H. Sundén, A. Bøgevig, M. Johansson and F. Himo, *Chem.-Eur. J.*, 2004, **10**, 3673.
- D. B. Ramachary and I. C. F. Barbas, *Org. Lett.*, 2005, **7**, 1577.
- S.-G. Kim and T.-H. Park, *Tetrahedron Lett.*, 2006, **47**, 9067.
- (a) S. K. David, M. Shaw and S. V. Ley, *Chem. Commun.*, 2006, 3211; (b) H. Sundén, N. Dahlin, I. Ibrahim, H. Adolfsson and A. Córdova, *Tetrahedron Lett.*, 2005, **46**, 3385; (c) W. Wang, J. Wang, H. Li and L. Li, *Tetrahedron Lett.*, 2004, **45**, 7235.
- R. Breslow, *Acc. Chem. Res.*, 2004, **37**, 471.
- (a) C.-J. Li and L. Chen, *Chem. Soc. Rev.*, 2006, **35**, 68; (b) L. Chen and C.-J. Li, *Org. Lett.*, 2004, **6**, 3151; (c) C. J. Li, *Chem. Rev.*, 1993, **93**, 2023.
- D. G. Blackmond, A. Armstrong, V. Coombe and A. Wells, *Angew. Chem., Int. Ed.*, 2007, **46**, 3798.

Acute toxic effects of ionic liquids on zebra mussel (*Dreissena polymorpha*) survival and feeding

David M. Costello,^{*a} Loretta M. Brown^b and Gary A. Lamberti^a

Received 12th December 2008, Accepted 28th January 2009

First published as an Advance Article on the web 16th February 2009

DOI: 10.1039/b822347e

Ionic liquids (ILs) are being designed as green alternatives to volatile organic solvents that are currently used in a wide range of industrial processes. While knowledge about the toxicity of various ILs to aquatic organisms has expanded in recent years, toxicity data remains limited to a few animal taxa. Furthermore, few studies have examined the non-lethal effects of ILs on aquatic organisms. We investigated how ILs affect mortality and feeding of the zebra mussel (*Dreissena polymorpha*), a sessile bivalve that is invasive in North America and much of Europe. Lethal effects of six ILs (butyl-, hexyl-, or octyl-chains on either a methylpyridinium or methylimidazolium cationic base) were studied with 96 h acute bioassays. Filtering behavior was examined in 2 h feeding trials of individual mussels fed *Chlamydomonas reinhardtii* and exposed to sublethal concentrations of the three imidazolium-based ILs. The ILs tested caused acute mortality over a wide range of concentrations ($LC_{50} = 21.4$ to 1290 mg L⁻¹), ILs with longer alkyl chains were more toxic, and pyridinium- and imidazolium-based ILs had similar toxicities. When comparing toxicity to the same IL across organisms, zebra mussels exhibit some of the highest LC_{50} values and would be among the most resistant aquatic organisms in the event of an IL release. Short-term exposure to any IL reduced zebra mussel feeding. For butyl- and hexyl-chain ILs, feeding was significantly reduced at the acute LC_{50} , whereas the octyl-chain IL reduced feeding at the acute LC_5 . Reduced survival and feeding by zebra mussels in the presence of ILs could have substantial effects on other trophic levels, which could lead to changes to affected ecosystems that would not have been predicted solely from standard mortality bioassays. Based on our mortality data, ILs are no worse than currently used industrial solvents; however, results from our feeding experiments demonstrate the potential for significant effects at sublethal concentrations. Consequently, we suggest that more ecologically relevant endpoints should be incorporated into a thorough hazard assessment of ILs.

Introduction

Anthropogenic activities (e.g., agriculture, manufacturing) use an estimated one-third of the Earth's accessible freshwater, the majority of which produce some chemical pollution.¹ In response to this widespread pollution, government agencies and industry have moved to develop "greener" chemicals. The principles of green chemistry attempt to reduce contamination of natural ecosystems through multiple methods, including designing less toxic, more biodegradable compounds and using safer solvents.² Room-temperature ionic liquids (ILs) are being promoted as a "green" alternative to the currently used solvents that are responsible for two-thirds of all industrial emissions.³

Ionic liquids are organic salts that are liquid at room temperature, have a wide temperature stability, and are useful solvents in a number of chemical reactions.^{4,5} In general, ILs have a bulky, asymmetrical cation containing substitutable side groups (often alkyl groups) coupled with a smaller anion (Fig. 1).⁴ This simple framework can allow for a wide range

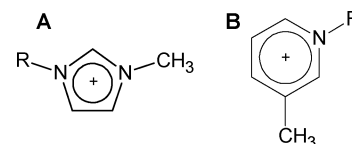


Fig. 1 Chemical structure of the ionic liquids used in this study: (A) 1-alkyl-3-methylimidazolium and (B) 1-alkyl-3-methylpyridinium. The imidazolium-based ILs are 1-butyl-, 1-hexyl-, and 1-octyl-3-methylimidazolium bromide (bmimBr, hmimBr, and omimBr, respectively). The pyridinium-based ILs are 1-butyl-, 1-hexyl-, and 1-octyl-3-methylpyridinium bromide (bmpyrBr, hmpyrBr, and ompyrBr, respectively).

of chemical characteristics by replacing the anion, changing the base cation entirely, or altering the cation side chains. The main environmental advantage of ILs over traditional solvents (e.g., benzene, toluene) is their non-volatility, which has the potential to greatly reduce atmospheric pollution.³ Although the physico-chemical properties of ILs could lead to reduced atmospheric pollution, these same properties (e.g., high solubility in water) increase the potential for contamination of aquatic ecosystems.^{3,6}

Because ILs have been promoted as green chemicals, some emphasis has been placed on determining their potential effects on aquatic ecosystems prior to intensive use in industrial

^aDepartment of Biological Sciences, University of Notre Dame, 107 Galvin Life Sciences, Notre Dame, IN 46556, USA.
E-mail: dcostel2@nd.edu; Tel: +1-574-631-0580

^bBiology Department, Saint Mary's College, Notre Dame, IN, USA

processes.^{3,7} The IL structure plays a major role in determining toxicity to many organisms,^{8,9} with the cation being more responsible for toxicity than the anion (but see ref. 10–12) and longer alkyl chains being more toxic than short alkyl chains (see reviews ref. 13 and 14). Conversely, ILs with longer alkyl chains are often more biodegradable than short alkyl chain ILs.^{15,16} In general, the suite of aquatic animals for which IL toxicity has been studied is relatively small, with the cladoceran *Daphnia magna* being the best studied.¹⁴ Furthermore, potential non-lethal effects of ILs on aquatic animals are very understudied (but see ref. 17 and 18). Our study expands knowledge of the lethal and non-lethal effects of ILs on aquatic animals with a detailed study of the sessile filter-feeding bivalve *Dreissena polymorpha* (zebra mussel).

In many freshwater ecosystems, bivalves represent the largest biomass of filter-feeding organisms, which makes them important components of aquatic food webs.¹⁹ Zebra mussels are invasive bivalves that have been suggested as a surrogate for freshwater bivalves that are often rare or endangered and not amenable to laboratory studies.^{19,20} Zebra mussels are widely distributed throughout North America and Europe and continue to spread,²¹ which makes them a readily available test organism. Filter feeding by zebra mussels can greatly reduce phytoplankton standing stocks in lakes²² and rivers,²³ and laboratory studies indicate that mussel filtration rate can be affected by exposure to contaminants.^{24,25} By studying the effects of ILs on zebra mussel survival and feeding in a series of acute bioassays, we sought to reveal how the population density and food web interactions of filter-feeding organisms may respond to environmental contaminants. We predicted that ILs would negatively affect zebra mussels, and that IL chemical structure would be a major determinant of zebra mussel mortality and filtering. Specifically, we predict that ILs with longer alkyl chains would reduce survival and filtering rates at lower concentrations than ILs with shorter alkyl chains.

Results

Zebra mussel survival

The IL ompyrBr was most toxic (the lethal concentration for 50% of the population (LC_{50}) = 21.4 mg L⁻¹) and bmimBr was least toxic (LC_{50} = 1290 mg L⁻¹) to zebra mussels (Table 1). Toxicity of the ILs tested increased with alkyl chain length (LC_{50} : octyl < hexyl < butyl) but was not affected by the heterocyclic base (LC_{50} : pyridinium = imidazolium) (Fig. 2). For each reduction in alkyl chain length by 2 carbons, we observed

Table 1 LC_{50} values for zebra mussels exposed to imidazolium- and pyridinium-based ILs

Base	IL	LC_{50} /mg L ⁻¹	95% confidence interval
Imidazolium	bmimBr	1290	952–2560
	hmimBr	106	nc ^a
	omimBr	21.8	6.75–61.0
Pyridinium	bmpyrBr	901	334–1450
	hmpyrBr	146	nc ^a
	ompyrBr	21.4	18.9–23.8

^a nc = not computable.

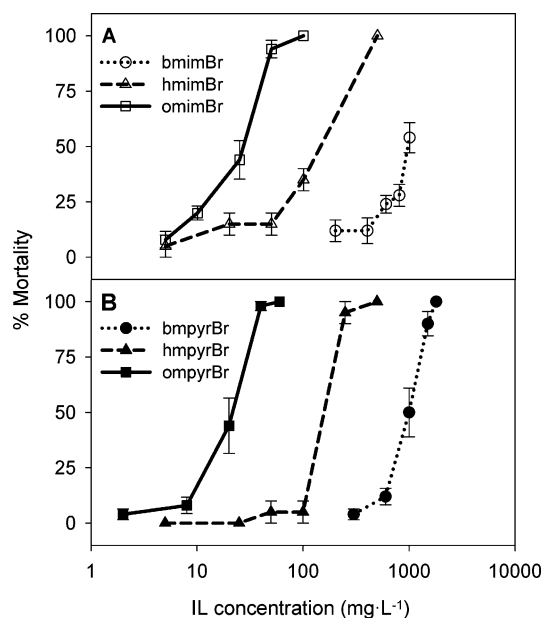


Fig. 2 Mean (± 1 SE) zebra mussel mortality in the presence of imidazolium- (A) and pyridinium-based (B) ILs with increasing alkyl chain length.

a lowering of toxicity (*i.e.*, increase in LC_{50}) of approximately an order of magnitude. Overlapping 95% confidence intervals suggest similarity between pyridinium- and imidazolium-based ILs with the same alkyl chains.

Zebra mussel filtering

Filtration rates for control mussels in test media (range = 26–43 mL h⁻¹ per capita) were similar to the 40 mL h⁻¹ reported by Berg *et al.*²⁶ for small zebra mussels (10–15 mm) also fed *Chlamydomonas reinhardtii*. When exposed to ILs, zebra mussel filtration rate either declined or did not differ from controls (Fig. 3). Exposure to bmimBr significantly reduced filtration rate ($F_{5,30}$ = 3.94, p = 0.007) and the two highest concentrations (1200 and 2000 mg L⁻¹) were significantly lower than controls (Tukey's HSD, p < 0.02) (Fig. 3A). Similarly, hmimBr reduced filtration rates ($F_{5,30}$ = 3.83, p = 0.008); zebra mussels exposed to the two highest concentrations of hmimBr (100 and 200 mg L⁻¹) filtered significantly less algae than controls (Tukey's HSD, p < 0.05) (Fig. 3B). Zebra mussels exposed to omimBr filtered significantly less algae ($F_{5,30}$ = 9.13, p < 0.001) at all concentrations when compared to control mussels (Tukey's HSD, p < 0.006) (Fig. 3C). For all imidazolium ILs, exposure at even the highest concentrations was not able to completely stop zebra mussel filtering activity. The lowest observed effect concentration (LOEC) values for bmimBr, hmimBr, and omimBr were 1200, 100, and 6 mg L⁻¹, respectively.

Discussion

In general, the toxicity of ILs to zebra mussels can be explained by structural properties, and trends in toxicity are similar to those seen for other organisms.^{6,9,13} The length of the alkyl chain has strong control over toxicity; ILs with octyl chains are more

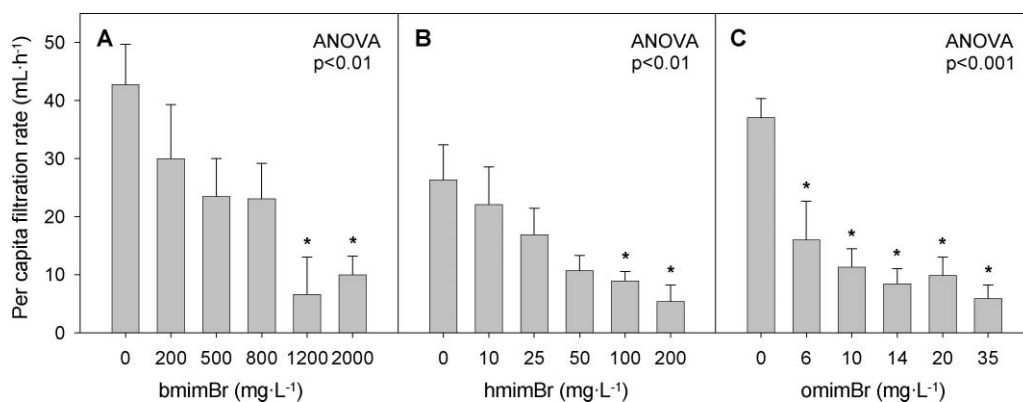


Fig. 3 Mean (\pm SE) per capita zebra mussel filtration rate when exposed to increasing concentrations of bmimBr (A), hmimBr (B), and omimBr (C). Asterisks represent treatments that are statistically different from no-IL controls (Tukey's HSD, $p < 0.05$).

toxic than those with hexyl chains, which are more toxic than butyl chains. Additionally, the heterocyclic base has a minimal contribution to toxicity, with pyridinium- and imidazolium-based ILs containing matching alkyl-chains having similar LC_{50} values. Comparable importance of IL alkyl chain length in determining toxicity has been seen for bacteria,^{9,11,34} algae,^{9,11,35–37} vascular plants,^{9,11,38} daphnids,³⁹ and snails.¹⁸ Furthermore, the similarity in toxicities seen in this study between pyridinium- and imidazolium-based ILs with identical alkyl chains supports evidence from other organisms.^{9,18,34,38}

The relationship between zebra mussel toxicity and alkyl chain length supports the proposed mechanism of IL toxicity of polar narcosis through membrane disruption.^{9,18} The structures of ILs are similar to cationic surfactants; cationic surfactants have bulky, positively charged head-groups with alkyl chains usually containing more than 10 carbons. Toxicity of cationic surfactants purportedly occurs when lipophilic alkyl chains integrate into and disrupt cellular membranes.^{40,41} Ionic liquids with longer alkyl chains are more lipophilic,⁴ and could therefore integrate more readily into cellular membranes. This mode-of-toxicity to zebra mussels is further supported by increased toxicity for cationic surfactants with alkyl chains longer than those of ILs (*i.e.*, benzethonium chloride and Clam-trol® CT 1) (Table 2).

Acute toxicity of ILs occurred at concentrations that were similar to some common industrial chemicals. The ILs with

butyl alkyl chains had similar toxicities to phenol, whereas octyl alkyl chain ILs were as toxic as hydrazine (Table 2). None of the ILs tested were as toxic as chemicals used to control zebra mussels or in wastewater treatment (*i.e.*, sodium hypochlorite, potassium permanganate, and chlorine dioxide) (Table 2). Our acute toxicity results for zebra mussels suggest that ILs with short alkyl chains represent a no-worse alternative to industrial solvents, whereas long alkyl chain ILs are comparable to some of the most toxic industrial solvents. However, these comparisons cannot be viewed as a complete assessment because a large proportion of industrial solvents have not been tested on zebra mussels.

Disruption of zebra mussel filtering was also influenced by the structure of ILs, with increasing alkyl chain corresponding to lower LOEC values. However, when compared across ILs, the sensitivity in zebra mussel filtering was not identical to those seen in mortality. The LOEC for reduced feeding occurred at the corresponding acute LC_{50} for bmimBr and hmimBr, whereas the LOEC for omimBr occurred at the acute LC_5 . This increased sensitivity to omimBr was also seen for egestion (a surrogate for feeding) by the snail *Physa acuta*.¹⁸ These results indicate that regulating IL concentrations based on mortality endpoints may not protect against non-lethal effects such as alterations to feeding.

The majority of studies that examine the effects of chemicals on zebra mussels measure a single endpoint (*e.g.*, mortality,

Table 2 Summary of zebra mussel acute toxicity values for ILs and some commonly used industrial chemicals

Chemical	Use	Endpoint	Test duration/d	Concentration/mg L ⁻¹	Reference
Phenol	Solvent, volatile	LC_{50}	2	1000	27
Butyl ionic liquids ^a	Solvent	LC_{50}	4	901–1290	p.w. ^d
1,1,2-Trichloroethane	Solvent, volatile	LC_{50}	4	320	28
Hexyl ionic liquids ^b	Solvent	LC_{50}	4	105.6–146.2	p.w. ^d
Octyl ionic liquids ^c	Solvent	LC_{50}	4	21.4–21.8	p.w. ^d
Hydrazine	Solvent	LC_{100}	1	>20	29
Benzethonium chloride	Surfactant	LC_{100}	1	10	30
Sodium hypochlorite	Disinfectant	LC_{50}	4.5	1.3	31
Potassium permanganate	Disinfectant	LC_{50}	7.2	1.1	31
Clam-trol® CT 1	Surfactant	LC_{50}	2	0.74	32
Chlorine dioxide	Disinfectant	LC_{50}	1	0.4	33

^a bmimBr and bmyrBr. ^b hmimBr and hmyrBr. ^c omimBr and omprBr. ^d p.w. = present work.

behavior), yet a single response variable does not allow for strong predictions of how a chemical will disrupt an organism in its natural environment. A review of the EPA ECOTOX database (<http://www.epa.gov/ecotox/>) shows that 47% of studies on zebra mussels measured mortality, 14% examined feeding, and only 7% (6 studies) quantified chemical effects on both filtering and mortality. The differential response in mortality and feeding (especially for omimBr) highlights the fact that a complete chemical hazard assessment cannot be determined by measuring a single endpoint.

Collectively, results from this study indicate that the release of ILs into an ecosystem may have direct effects on filter-feeding bivalves and potentially entire ecosystems. Zebra mussels can tolerate relatively high concentrations of ILs, and a comparison of bmimBr toxicity across multiple species indicates that zebra mussels have the highest LC₅₀ values of all animals tested to date.¹³ Although total freshwater bivalve biomass may not decline substantially when exposed to ILs, our results indicate that trophic interactions may be altered through behavioral changes. In the presence of ILs, filter feeding by freshwater bivalves could be reduced and phytoplankton would be released from that grazing. A reduction in algal consumption could allow increases in algal populations that are resistant to ILs (e.g., *C. reinhardtii*),³⁵ although species sensitive to ILs (e.g., *Scenedesmus quadricauda*)³⁵ might not benefit from reduced filter feeding. Such differential IL effects highlight the importance of testing a range of chemical structures, target species, and endpoints to fully assess the risk of these new chemicals. By understanding how contaminants alter species interactions we can begin to use ecological principles to model how potential pollutants may affect entire ecosystems.⁴²

Conclusions

This work adds to the growing body of knowledge on the potential effects of ILs on aquatic organisms and their ecosystems by stressing how IL chemical structure controls toxicity and demonstrating potential non-lethal effects. If acute toxicity is to be minimized, ILs with short alkyl chains should be promoted. Ionic liquids with longer alkyl chains also reduce the feeding rates of molluscs at a rate that is disproportionately greater than the concentrations that cause mortality, further stressing the need to develop ILs with short alkyl chains. Our study is unique in that it examines how ILs affect a trophic interaction, but we know little about how ILs may affect other ecological processes (e.g., competition, decomposition). If toxicologists, ecologists, and regulators wish to truly know how ILs may affect ecosystems, more studies must be done in ecologically realistic settings with multiple species and under different environmental conditions.

Experimental

Test chemicals

The ILs tested were chosen to represent six different cationic structures based on two nitrogen containing heterocycles (imidazolium and pyridinium) with three alkyl chain lengths (butyl, hexyl, and octyl) (Fig. 1). The imidazolium-based ILs tested

were bmimBr, hmimBr, and omimBr and the tested pyridinium-based ILs were bmpyrBr, hmpyrBr, and ompyrBr. The ILs were synthesized by the Department of Chemical and Biomolecular Engineering at the University of Notre Dame (Notre Dame, IN, USA) using established synthesis procedures.^{43–45} These specific IL cations were tested because previous data indicated that these and similar structures are the most promising candidates for future industrial application.^{8,15}

Zebra mussel collection

Rocks colonized by zebra mussels were collected from Juno Lake, MI, USA (41°48'2"N, 85°59'08"W) and transported to the laboratory in a cooler with water from Juno Lake. In the laboratory, zebra mussels were kept in aerated lake water and fed twice weekly with live algae (*C. reinhardtii* and *S. quadricauda*). Before conducting bioassays, zebra mussels were monitored for at least one week, but kept no longer than 6 weeks. At 24 hours prior to a trial, mussels were carefully removed from rocks with forceps, brushed clean, and placed in test media. Test media consisted of coarse-filtered, low-nutrient groundwater that was aerated to precipitate excess calcium carbonate.

Zebra mussel survival experiment

Zebra mussel survival in the presence of ILs was assessed using 96 h, static, acute toxicity tests similar to those completed by Bernot *et al.*¹⁸ for another mollusc, *Physa acuta*. For each test, 10 zebra mussels (5–12 mm shell length) were placed into each of 30 plastic tubs (250 mL) containing 200 mL of test solution and an ashed ceramic tile for zebra mussel attachment. Each test consisted of 5 IL concentrations and one groundwater control, each replicated 5 times ($n = 30$ per test). Concentrations used for definitive testing were based on preliminary range-finding tests. If a mussel did not begin filtering (determined visually) within 2 h of the start of the experiment, it was replaced. Mussels were examined daily for survival and dead mussels were removed. A zebra mussel was considered alive if it responded to probing with blunt forceps by closing its open shell. More than 90% of zebra mussels characterized as dead had their shells open with visible tissue degradation. Each test was conducted in the dark at room temperature (20 ± 2 °C). The LC₅₀ and 95% confidence intervals were calculated by fitting the final survival at 96 h to dose-response curves using the maximum likelihood method.⁴⁶

Zebra mussel filtering experiment

The effects of IL structure on zebra mussel filtering were examined in individual experiments. Due to similarities in survival between pyridinium- and imidazolium-based ILs, we tested just the three imidazolium-based ILs (bmimBr, hmimBr, and omimBr). For the filtering bioassays, we selected five IL concentrations relative to survival experiments (*i.e.*, LC₅, LC₁₅, LC₂₅, LC₅₀, and LC₇₅) and a groundwater-only control, each replicated 6 times ($n = 36$ per test). Individual mussels (10–15 mm shell length) were placed in a beaker with 130 mL of test media and given 10 mL of live *C. reinhardtii* stock (obtained from the University of Toronto Culture Collection; UTCC #243). We added algal cells at an initial concentration

of $\sim 100\,000$ cells mL^{-1} , which allows for maximum potential filtering activity.⁴⁷ If a zebra mussel did not open and begin filtering (determined visually) within 10 min it was replaced with another mussel. Control flasks of test media and *C. reinhardtii* without zebra mussels were established at each concentration to account for settling of algal cells. Zebra mussels were allowed to filter undisturbed at room temperature (20 ± 2 °C) in the dark for 2 hours.⁴⁷ Initial and final algal concentration was sampled by mixing with a syringe and removing 20 mL, which was filtered onto a GF/F filter and frozen until analysis (within 2 weeks). Algae samples were analyzed for chlorophyll *a* (chl *a*) on a fluorometer (TD-700, Turner Designs) after being extracted in methanol according to standard methods.⁴⁸

Zebra mussel filtration rate was calculated according to the formula in Berg *et al.*:²⁶

$$FR = \frac{(\ln C_0 - \ln C_{\text{treatment}}) - (\ln C_0 - \ln C_{\text{control}})V}{t}$$

where *FR* is the per capita filtration rate (mL h^{-1}), C_0 is the mean initial algal concentration ($\mu\text{g chl } a \text{ L}^{-1}$), $C_{\text{treatment}}$ is the final algal concentration of a beaker with a mussel present ($\mu\text{g chl } a \text{ L}^{-1}$), C_{control} is the mean final algal concentration of the no-zebra mussel controls ($\mu\text{g chl } a \text{ L}^{-1}$), *V* is the total experimental volume (mL), and *t* is the exposure time (h). Filtration rates were compared using one-way ANOVA followed by Tukey's HSD test ($\alpha = 0.05$) for multiple comparisons between treatments. The LOEC was determined to be the lowest concentration where a statistical difference was seen. Statistical analyses were completed using R 2.7.1.⁴⁹ Assumptions of statistical tests were verified using residual and normal Q-Q plots [plot(model) function in R]. Unless otherwise stated, values are reported as mean \pm 1 standard error.

Acknowledgements

We thank M. A. Brueseke, N. Kamat, and K. J. Kulacki for laboratory assistance. K. J. Kulacki provided useful comments on previous versions of this manuscript. This study was supported by grants from the US Department of Education's GAANN Program (Graduate Assistance in Areas of National Need) and the US National Oceanic and Atmospheric Administration (NOAA Awards No. NA04OAR4600076 and NA05OAR4601153). Additional funding to DMC was provided by a Bayer Predoctoral Fellowship.

References

- R. P. Schwarzenbach, B. I. Escher, K. Fenner, T. B. Hofstetter, C. A. Johnson, U. von Gunten and B. Wehrli, *Science*, 2006, **313**, 1072–1077.
- P. T. Anastas, and J. C. Warner, *Green Chemistry: Theory and Practice*, Oxford University Press, New York, 1998.
- J. F. Brennecke and E. J. Maginn, *AIChE J.*, 2001, **47**, 2384–2389.
- R. Sheldon, *Chem. Commun.*, 2001, **23**, 2399–2407.
- T. Welton, *Chem. Rev.*, 1999, **99**, 2071–2093.
- B. Jastorff, K. Mölter, P. Behrend, U. Bottin-Weber, J. Filser, A. Heimers, B. Ondruschka, J. Ranke, M. Schaefer, H. Schröder, A. Stark, P. Stepnowski, F. Stock, R. Störmann, S. Stolte, U. Welz-Biermann, S. Ziegert and J. Thöming, *Green Chem.*, 2005, **7**, 362–372.
- P. J. Scammells, J. L. Scott and R. D. Singer, *Aust. J. Chem.*, 2005, **58**, 155–169.
- D. J. Couling, R. J. Bernot, K. M. Docherty, J. K. Dixon and E. J. Maginn, *Green Chem.*, 2006, **8**, 82–90.
- S. Stolte, M. Matzke, J. Arning, A. Bösch, W.-R. Pitner, U. Welz-Biermann, B. Jastorff and J. Ranke, *Green Chem.*, 2007, **9**, 1170–1179.
- S. Stolte, J. Arning, U. Bottin-Weber, M. Matzke, F. Stock, K. Thiele, M. Uerdingen, U. Welz-Biermann, B. Jastorff and J. Ranke, *Green Chem.*, 2006, **8**, 621–629.
- M. Matzke, S. Stolte, K. Thiele, T. Juffernholz, J. Arning, J. Ranke, U. Welz-Biermann and B. Jastorff, *Green Chem.*, 2007, **9**, 1198–1207.
- C.-W. Cho, T. P. T. Pham, Y.-C. Jeon and Y.-S. Yun, *Green Chem.*, 2008, **10**, 67–72.
- K. J. Kulacki, D. T. Chaloner, D. M. Costello, K. M. Docherty, J. H. Larson, R. J. Bernot, M. A. Brueseke, C. F. Kulpa, Jr. and G. A. Lamberti, *Chim. Oggi*, 2007, **25**, 32–36.
- J. Ranke, R. Störmann, J. Arning and B. Jastorff, *Chem. Rev.*, 2007, **107**, 2183–2206.
- K. M. Docherty, J. K. Dixon and C. F. Kulpa, *Biodegradation*, 2006.
- M. Stasiewicz, E. Mulkiewicz, R. Tomczak-Wandzel, J. Kumirska, E. M. Siedlecka, M. Gołebowski, J. Gajdus, M. Czerwicka and P. Stepnowski, *Ecotoxicol. Environ. Saf.*, 2008, **71**, 157–165.
- M. A. Evans-White and G. A. Lamberti, *Environ. Toxicol. Chem.*, 2009, **28**, 418–426.
- R. J. Bernot, E. E. Kennedy and G. A. Lamberti, *Environ. Toxicol. Chem.*, 2005, **24**, 1759–1765.
- Freshwater Bivalve Ecotoxicology*, ed. J. L. Farris and J. H. Van Hassel, SETAC, Pensacola, FL, USA, 2006.
- R. Smolders, L. Bervoets, V. Wepener and R. Blust, *Hum. Ecol. Risk Assess.*, 2003, **9**, 741–760.
- J. M. Drake and J. M. Bossenbroek, *BioScience*, 2004, **54**, 931–941.
- J. H. Leach, in *Zebra mussels: biology, impacts, and control*, ed. T. F. Nalepa and D. W. Schloesser, CRC Press, Boca Raton, FL, 1993, pp. 381–397.
- H. A. Roditi, N. F. Curaco, J. J. Cole and D. L. Strayer, *Estuaries*, 1996, **19**, 824–832.
- M. H. S. Kraak, P. Wijnands, H. A. J. Govers, W. Admiraal and P. de Voogt, *Environ. Toxicol. Chem.*, 1997, **16**, 2158–2163.
- M. H. S. Kraak, C. Ainscough, A. Fernández, P. L. A. van Vlaardingen, P. De Voogt and W. A. Admiraal, *Aquat. Toxicol.*, 1997, **37**, 9–20.
- D. J. Berg, S. W. Fisher and P. F. Landrum, *J. Great Lakes Res.*, 1996, **22**, 779–788.
- M. M. Kamshilov, and B. A. Flerov, in *1st and 2nd USA-USSR Symposium on Effects of Pollutants upon Aquatic Ecosystems*, ed. D. I. Mount, W. R. Swain and N. K. Ivanikiw, Duluth, MN, 1976, pp. 181–192.
- D. M. M. Adema and G. J. Vink, *Chemosphere*, 1981, **10**, 533–554.
- D. W. Evans and L. M. Coughlin, *J. Shellfish Res.*, 1992, **11**, 224–225.
- D. L. Waller, J. J. Rach, W. G. Cope, L. L. Marking, S. W. Fisher and H. Dabrowska, *J. Great Lakes Res.*, 1993, **19**, 695–702.
- P. L. Klerks and P. C. Fraleigh, *J. Am. Water Works Assoc.*, 1991, **83**, 92–100.
- D. L. Waller, S. W. Fisher and H. Dabrowska, *Prog. Fish Cult.*, 1996, **58**, 77–84.
- G. Matisoff, A. Greenberg, G. Gubanich and J. Ciaccia, *J. Shellfish Res.*, 1992, **11**, 232–233.
- K. M. Docherty and C. F. Kulpa, *Green Chem.*, 2005, **7**, 185–189.
- K. J. Kulacki and G. A. Lamberti, *Green Chem.*, 2008, **10**, 104–110.
- A. Latafa, P. Stepnowski, M. Nędzi and W. Mroziak, *Aquat. Toxicol.*, 2005, **73**, 91–98.
- T. P. T. Pham, C.-W. Cho and Y.-S. Yun, *J. Biosci. Bioeng.*, 2008, **105**, 425–428.
- J. H. Larson, P. C. Frost and G. A. Lamberti, *Environ. Toxicol. Chem.*, 2008, **27**, 676–681.
- R. J. Bernot, M. A. Brueseke, M. A. Evans-White and G. A. Lamberti, *Environ. Toxicol. Chem.*, 2005, **24**, 87–92.
- D. W. Roberts and J. Costello, *QSAR Comb. Sci.*, 2003, **22**, 220–225.
- M. J. Rosen, F. Li, S. W. Morrall and D. J. Versteeg, *Environ. Sci. Technol.*, 2001, **35**, 954–959.

-
- 42 J. R. Rohr, J. L. Kerby and A. Sih, *Trends Ecol. Evol.*, 2006, **21**, 606–613.
- 43 C. P. Fredlake, J. M. Crosthwaite, D. G. Hert, S. N. V. K. Aki and J. F. Brennecke, *J. Chem. Eng. Data*, 2004, **49**, 954–964.
- 44 L. Cammarata, S. G. Kazarian, P. A. Salter and T. Welton, *Phys. Chem. Chem. Phys.*, 2001, **3**, 5192–5200.
- 45 P. Bonhote, A. P. Dias, N. Papageorgiou, K. Kalyanasundaram and M. Gratzel, *Inorg. Chem.*, 1996, **35**, 1168–1178.
- 46 M. C. Newman, *Quantitative Methods in Aquatic Ecotoxicology*, Lewis, Boca Raton, FL, 1995.
- 47 M. J. Horgan and E. L. Mills, *Can. J. Fish. Aquat. Sci.*, 1997, **54**, 249–255.
- 48 APHA, *Standard methods for the examination of water and wastewater*, Port City Press, Baltimore, MA, USA, 20th edn, 1999.
- 49 R. Core Development Team, *R Foundation for Statistical Computing*, Vienna, Austria, 2008.

Applications of a high performance platinum nanocatalyst for the oxidation of alcohols in water†

Prasenjit Maity,^a Chinnakonda S. Gopinath,^c Sumit Bhaduri^{*b} and Goutam Kumar Lahiri^{*a}

Received 11th September 2008, Accepted 12th January 2009

First published as an Advance Article on the web 17th February 2009

DOI: 10.1039/b815948c

Nanoparticles of platinum (NP-Pt), have been synthesized by supporting high nuclearity anionic carbonyl cluster (Chini cluster) on a water soluble anion exchanger, and the performance of this material, **1**, as an oxidation catalyst for alcohols in water has been studied. The E-factor for the synthesis of NP-Pt by this method has been calculated and compared with that of other NP-Pt recently reported in the literature. With **1** as a catalyst, oxidations of a variety of primary and secondary alcohols by dioxygen are achieved and high turnover numbers and selectivities are obtained. The performances of **1** in the oxidation of benzyl alcohol and 1-phenylethanol are compared with those of three other platinum catalysts. These are platinum nanoparticles **2** prepared by the hydrogen reduction of [PtCl₆]²⁻ supported on the same water soluble polymer, 5% Pt on carbon, and 5% Pt on alumina, designated as **3** and **4**, respectively. **1** has been found to be considerably more active than **2–4** and also other reported water soluble platinum nanocatalysts. After many turnovers (~1000 and ~165 for benzyl alcohol and 1-phenyl ethanol, respectively) partial deactivation (~40%) is observed, but the deactivated catalyst can be fully regenerated by treatment with dihydrogen. The TEM data of fresh, deactivated and regenerated **1** show a correlation between the particle size and activity. A mechanism consistent with this and other experimental observations including XPS data is proposed.

Introduction

Among many of the requirements of environmentally benign and economically viable chemical processes, the use of water rather than organic solvents is an important theme of current chemical research.^{1–7} Apart from being totally non-hazardous, water is cheap, and a number of gasses have good solubility in water thereby making it possible to develop manufacturing processes where such a gas is one of the reactants. From a green point of view equally important is the development of *catalytic* oxidation processes with dioxygen (O₂) as the oxidant, rather than heavy metal based stoichiometric oxidants such as CrO₃, KMnO₄.^{8–16} Besides obvious problems due to heavy metal toxicity, metal based oxidants have poor “atom utilisation” or “E-factor” indices as compared to the catalytic oxidation process.⁴ Thus, in recent years, water soluble complexes and nanoparticles (NP) of noble metals have come under increasing investigation as potential catalysts for oxidation reactions.

To the best of our knowledge the recent report of Sheldon and co-workers first time highlighted the advantages

of catalytic oxidation of alcohols in water, where a water-soluble palladium complex was used as a homogeneous catalyst for the oxidation of alcohol in water.^{8a} Subsequently other catalytic systems based on soluble ruthenium complexes and NP of gold, palladium and platinum have been reported, but the range of alcohols that could be oxidised with these catalytic systems with high turnovers and long life time are limited.^{17–20}

Notable improvements in catalytic performances have been reported recently where NP of platinum (NP-Pt) have been successfully used for the oxidation of a variety of alcohols in water by O₂.^{11–13} These catalytic systems give moderate to excellent turnover numbers for the oxidation of a range of alcohols and are fully selective towards the oxidation of the alcoholic functionalities. The differences in the catalytic activities that cover a wide range of turnover numbers (TON) resulting from the different matrices used for the stabilisation of NP-Pt, as well as the differences in the synthetic methods of generating NP-Pt from high valent platinum salts.

Thus Wang *et al.* report a platinum nanocatalyst (Pt-GLY) prepared by the reduction of H₂PtCl₆·6H₂O with glycol, stabilising it with poly (N-vinyl-2-pyrrolidone) (PVP), and then removing glycol *via* dialysis.¹³ The platinum nanocatalyst (ARP-Pt) reported by Yamada *et al.*¹¹ was prepared by supporting Zeise's salt on a functionalised amphiphilic resin and then reducing it with benzyl alcohol. The most active catalyst nPt@hC (hC = hollow carbon) recently reported by Ng *et al.*¹² was made in a three step process: reaction of phenol with H₂PtCl₆ using TiO₂ as a photocatalyst followed by carbonization at 973K, and finally removal of TiO₂ by HF.

^aDepartment of Chemistry, Indian Institute of Technology Bombay, Powai, Mumbai, 400076, India. E-mail: lahiri@chem.iitb.ac.in; Fax: (+91)-22-25723480; Tel: (+91)-22-2576-7159

^bReliance Industries Limited, Swastik Mills Compound, V. N. Purav Marg, Chembur, Mumbai, 400071, India. E-mail: sumit_bhaduri@ril.com; Fax: (+91)-22-67677381; Tel: (+91)-22-67677324

^cCatalysis Division, National Chemical Laboratory, Pune, 411008, India

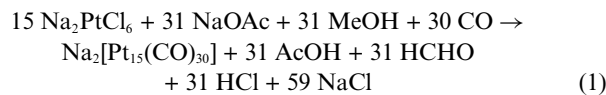
† Electronic supplementary information (ESI) available: E-factor calculations. See DOI: 10.1039/b815948c

The aforesaid recent reports clearly suggest that there is an urgent need for a high performance catalyst for the dioxygen assisted oxidation of alcohols in water. However, as has been pointed out recently for NP of gold, the “green” aspect of the synthetic method itself is an important consideration.²¹ The environmental friendliness of different synthetic methods for NP-Pt may be quantified in terms of the amounts of reagents used and waste generated *i.e.*, an approximate E-factor.⁴ Therefore an optimum balance between the E-factor of the synthetic method for NP-Pt and its performance as an oxidation catalyst is very important.

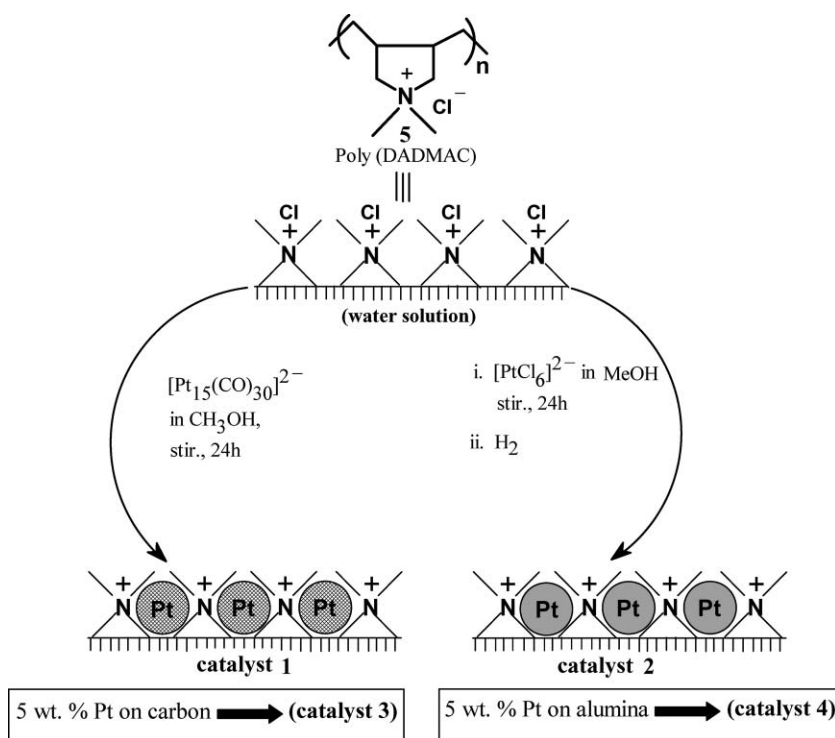
In addition to the above mentioned reports on the synthetic methodologies of NP-Pt, a few other preparative methods have also been reported.^{22–27} We have shown that nanostructured platinum hydrogenation catalysts could be prepared by supporting Chini clusters of the general formula $[\text{Pt}_3(\text{CO})_6]_n^{2-}$ on functionalised inorganic oxides as well as organic polymers.²⁸ Of special relevance in the present context is our recent finding, that a water soluble precursor for NP-Pt could easily be prepared by following the above general method using a water soluble polymer. Under hydrogenation conditions the CO ligands are lost and the resultant nanocatalyst has excellent activity and selectivity in hydrogenation reactions (Scheme 1). The recent reports on the remarkable performance of ARP-Pt,¹¹ Pt-GLY¹³ and $n\text{Pt}@h\text{C}$ ¹² as oxidation catalysts in water, prompted us to investigate the performance of **1** in oxidation reactions. Interestingly we find that for alcohol oxidation reactions in water, **1** is more active than ARP-Pt and Pt-GLY. Moreover, **1** is also found to be more active than **2**, a nanocatalyst prepared by the hydrogen reduction of $[\text{PtCl}_6]^{2-}$ supported on **5** (see Scheme 1 below), and two commercial platinum catalysts, **3** and **4** (5% Pt on carbon and alumina, respectively).

Results and discussion

Nanocatalyst **1** is prepared by adding an aqueous solution of poly (diallyldimethylammoniumchloride) **5**, a commercially available water soluble polymer, to a methanolic solution of the preformed cluster, $[\text{Pt}_{15}(\text{CO})_{30}]^{2-}$. The latter is prepared by reducing Na_2PtCl_6 under CO with methanol and sodium acetate according to the following equation.^{28a,b,29}

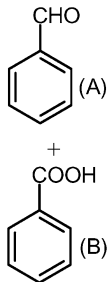
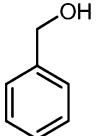
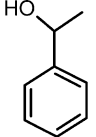
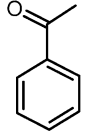


The amounts of the reagents used for the synthesis of **1** has been reported (see Experimental) and the E factor (amount of waste/amount of product) for the syntheses is 12.8 (see ESI†). As per convention, waste is defined as the amount of all reagents minus the weight of product, solvents are considered as reagents but water is not. On the basis of the reported synthetic details, the approximate E-factors for the other three nanocatalysts, $n\text{Pt}@h\text{C}$, Pt-GLY and ARP-Pt have also been calculated and for the first two the values are found to be 30.9 and 12.7, respectively. The E factor for ARP-Pt is 4.4 and this has been calculated by summing two E-factors, one for Zeise’s salt, $\text{K}[\text{Pt}(\text{C}_2\text{H}_4)\text{Cl}_3]$, and the other for the synthesis of the nanocatalyst. As shown in Scheme 1, the nanocatalyst **2** is synthesized by dihydrogen reduction of $[\text{PtCl}_6]^{2-}$ anchored on **5** in methanol with an E factor of 14.7. Studies on the catalytic performance of **2** in hydrogenation reactions have been reported by us and others.^{27,28a} The particularly high E-factor of $n\text{Pt}@h\text{C}$ arises because its synthesis involves the use of relatively large amounts of TiO_2 and hazardous HF as reactants. While



Scheme 1 Formulation of catalysts 1–4.

Table 1 Comparative activity of different catalysts used in this work for the oxidation of benzyl alcohol and 1-phenylethanol^a

Entries	Substrate	Product	Catalyst	Time (h)	% Conversion (A+B)	TON/TOF h ⁻¹
1 ^b			1	8	100 (2 (A) + 98 (B))	300/37.5
2 ^c			1	8	100 (4 (A) + 96 (B))	300/37.5
3 ^d			1	24	95 (5 (A) + 90 (B))	285/11.8
						
4 ^e			1	8	56 (54 (A) + 2 (B))	840/105
5 ^f			1	24	90 (12 (A) + 88 (B))	270/11.25
6 ^b			2	8	74 (4 (A) + 70 (B))	222/27.75
7 ^b			3	8	36 (4 (A) + 32 (B))	108/13.5
8 ^b			4	8	66 (6 (A) + 60 (B))	198/24.75
9 ^g			ARP-Pt	24	99 (0 (A) + 99 (B))	99/4.12
10 ^h			GLY-Pt	24	100 (0 (A) + 100 (B))	20/0.83
11 ^b			1	20	87	43.5/2.17
12 ^c			1	20	84	42/2.1
13 ^d			1	24	40	20/0.83
14 ^f			1	24	48	24/1
15 ^b			2	20	52	26/1.3
16 ^b			3	20	32	16/0.8
17 ^b			4	20	49	24.5/1.22
18 ^g			ARP-Pt	24	82	16.4/0.68
19 ^h			GLY-Pt	24	98.5	19.7/0.82
20 ⁱ			nPt@hc	24	81	405/16.8

^a Substrate/Catalyst molar ratio: for benzyl alcohol 300, for 1-phenyl ethanol 50, catalyst amount 100 mg, TON = mmole of product(s)/mmole of Pt; TOF = TON/Time, water 5 mL, temperature, 353 K. ^b O₂ as oxidant. ^c H₂O₂ as oxidant. ^d Air as oxidant. ^e Substrate/Catalyst molar ratio = 1500. ^f Reactions were carried out at 333 K temperature (under Uzomi's conditions, see reference 11 to compare the values). ^g From reference 11. ^h From reference 13. ⁱ From reference 12.

the calculated E factors are only indicative and not exact, it is clear that from an environmental point of view *nPt@hc* is less desirable, though among all the nanocatalysts it is the most active.

For comparative performance evaluation of catalysts **1–4**, ARP-Pt, Pt-GLY and *nPt@hc* the oxidation of benzyl alcohol and 1-phenylethanol have been studied in detail. As can be seen from Table 1, highest turnover numbers and turnover frequencies (TON and TOF) are consistently obtained with **1**. The TONs of **1** are also higher than that of ARP-Pt and Pt-GLY. For the oxidation of benzyl alcohol in terms of turnover frequencies (TOF, h⁻¹), **1** is almost an order of magnitude or more active than both the reported catalysts (Entries 1, 9, and 10), while for 1-phenylethanol, its activity is ≥ 2.5 times of the other two reported catalysts (ARP-Pt and Pt-GLY) (Entries 11,

18, 19). As the temperature used by Yamada *et al.* was 60 °C, the TOFs of **1** for benzyl alcohol and 1-phenyl ethanol have also been measured at this temperature (Entries 5, 14). At 60 °C for these two substrates **1** is ~2.5 and 1.5 times more active than ARP-Pt. As already mentioned, *nPt@hc* is the most active among all the catalysts and gives a TOF of 16.8 (h⁻¹) for 1-phenyl ethanol oxidation but has not been studied for benzyl alcohol oxidation. For both the substrates, benzyl alcohol and 1-phenyl ethanol, instead of dioxygen, 30% hydrogen peroxide may also be used with comparable results (Table 1, Entries 2, 12). Also if air is used as the oxidant, a lowering in TON is observed, presumably due to dilution of dioxygen by N₂ (Table 1, Entries 3, 13).

Benzyl alcohol oxidation to benzoic acid obviously proceeds through the intermediate formation of benzaldehyde as

confirmed by the time monitored concentration data of benzyl alcohol, benzaldehyde and benzoic acid (Fig. 1a). However, by increasing the substrate to catalyst concentration substantially (from 300:1 to 1500:1), benzaldehyde with TON > 800 and selectivity ~ 96% may be obtained (Table 1, Entry 4).

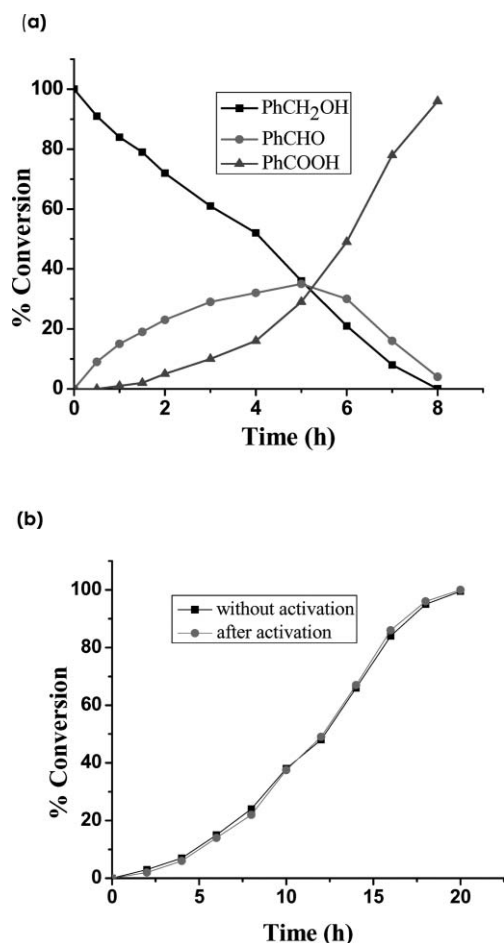


Fig. 1 (a) Time monitored conversion of benzyl alcohol to benzaldehyde and benzoic acid by **1** in water. **Reaction Conditions:** Catalyst (**1**) = 100 mg (5.4×10^{-3} mmol of Pt), benzyl alcohol = 175 mg (Substrate to platinum molar ratio: 300). Solvent (water) = 5 mL, temperature = 353 K, O₂ = 1 atm., stirring speed = 900 rpm. (b) Comparative time monitored conversion of 1-phenylethanol to acetophenone by **1** in water with and without activation. **Reaction Conditions:** Catalyst (**1**) = 100 mg (5.4×10^{-3} mmol of Pt), 1-phenylethanol = 33 mg, (Substrate to platinum molar ratio: 50). Solvent (water) = 5 mL, temperature = 353 K, O₂ = 1 atm., stirring speed = 900 rpm.

The time monitored concentration profiles of 1-phenylethanol oxidation by using freshly prepared **1**, and activated **1** (**1** fully decarbonylated by heating under vacuum) as catalysts have been recorded (Fig. 1b). The concentration vs. time plots are practically identical and both catalysts show induction periods ~5 h. As reported for hydrogenation reactions in water, in oxidation reactions also the CO ligands are quickly (< 5 min) lost. This has been confirmed by carrying out a separate experiment and monitoring the disappearance of ν_{CO} . These observations are significant from a mechanistic point of view, as they show that the long induction time is independent of the time required for CO loss.

The catalytic activity of **1** has been evaluated for the oxidation of other representative aliphatic and benzylic alcohols (Table 2). All primary alcohols are oxidized mainly to the acid while the secondary alcohols expectedly yield ketones. As mentioned earlier, in benzyl alcohol oxidation by increasing the substrate to catalyst concentration substantially, benzaldehyde with >95% selectivity may be obtained. Such a strategy may also work for the selective conversion of other primary alcohols to the corresponding aldehydes. Good TONs and TOFs are obtained in all the cases and no adverse effect due to olefinic functionalities are observed (Table 2, Entries 10, 12, 15). For substrates with such functionalities only the alcohol functionality is selectively oxidised. It may also be noted that as most of the reactions in Tables 1 and 2 were set to a fixed time, the TON and especially TOF given for the reactions that went to completion correspond to lower limits (Entries 1 and 2 in Table 1; entries 1 and 3 in Table 2).

The recycling and deactivation studies on **1** have been carried out under conditions where high turnovers are obtained per batch. As shown in Table 3, on recycling, partial deactivation of **1** is observed, from the first to the fifth batch the TONs drop from 300 to 183 and 44 to 26 for benzyl alcohol and 1-phenylethanol, respectively. The total turnovers over the five batches are 1150 and 165, respectively. This is to be contrasted with the reported data on recycling for ARP-Pt and Gly-Pt. For these two catalysts total turnovers ~80–90 over five batches were obtained but no deactivation was reported.

Interestingly and significantly, on treatment with dihydrogen (30 bar, 3 h, in water) the used **1** regains its original activity completely. This is evident from the conversion and TON data of the regenerated catalyst (Table 3, Entries 6, 12). The regenerated catalyst has been tested for more than one recycle for both the model substrates, benzyl alcohol and 1-phenyl ethanol. Its behaviour has been found to be identical to that of the fresh catalyst. As catalytic activity is very often found to be strongly correlated with the particle size, the TEM studies of the fresh, used and regenerated **1** have been performed (see Experimental). As reported in our earlier publications, freshly prepared **1** has CO-protected platinum nanoparticles within the size range of 2–8 nm with ca. 70% being within 3–5 nm.^{28a,b} After five catalytic runs no small (<6 nm) particles could be seen in the partially deactivated catalyst (Fig. 2a) which consists mainly of large particles (8–10 nm). However, the growth in particle size is reversible as the hydrogen treated regenerated catalyst shows a reduction in the particle size (Fig. 2b). The nanoparticle size measurements with the TEM facilities at our disposal are approximate. However, the overall trend, that of an increase in the particle size in the used catalyst and a reduction of particle size in the regenerated catalyst, is unambiguous.

The X-ray photoemission spectra (Fig. 3) of fresh and used **1** have also been recorded. Freshly prepared **1** shows signals for the Pt 4f core levels with the binding energy (BE) of Pt 4f_{7/2} ~71.0 eV being very close to the literature reported value of the free cluster.^{28a,d,30} The XPS signal of the five times used partially deactivated catalyst on deconvolution shows a strong peak at ~72.5 eV, and a much weaker one at ~71.0 eV. This indicates that the predominant oxidation state of platinum in the deactivated catalyst is +2.

Table 2 Aerobic oxidation of benzylic and aliphatic alcohols by catalyst 1^a

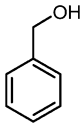
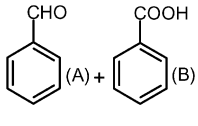
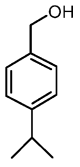
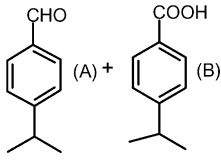
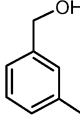
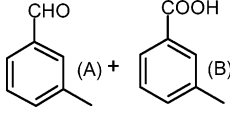
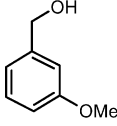
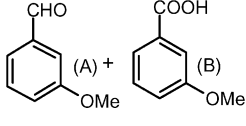
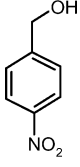
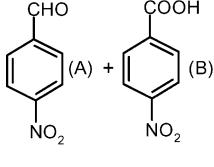
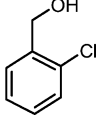
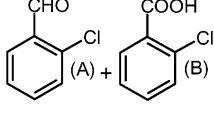
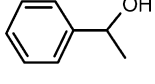
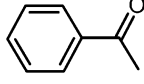
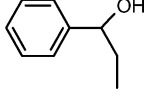
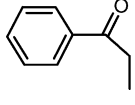
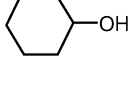
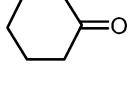
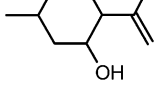
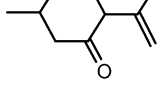
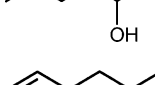
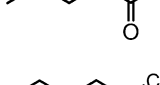
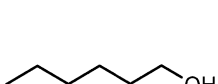
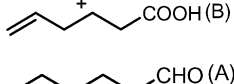

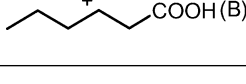
Entries	Substrate	Product	Time (h)	% Conversion (A + B)	TON (TOF ^{-h})
1			8	100 (2(A) + 98(B))	300 (37.5)
2			8	89 (2(A) + 87(B))	267 (33.3)
3			8	100 (5(A) + 95(B))	300 (37.5)
4			8	92 (12(A) + 80(B))	276 (34.5)
5			8	72 (7(A) + 65(B))	72 (9)
6			8	65 (8(A) + 57(B))	65 (8.1)
7			20	87 (100)	43.5 (2.17)
8			20	83 (100)	41.5 (2.07)
9			20	82 (100)	41 (2.05)
10			20	75 (100)	37.5 (1.87)
11			20	83 (100)	41.5 (2.07)
12			20	100 (2(A) + 98(B))	100 (5)
13			20	100 (4(A) + 96(B))	100 (5)

Table 2 (Contd.)

Entries	Substrate	Product	Time (h)	% Conversion (A + B)	TON (TOF ^b)
14		 CH ₃ (CH ₂) ₅ CHO (A) + CH ₃ (CH ₂) ₅ COOH (B)	20	95 (5(A) + 90(B))	95 (4.75)
15		 (A) + (B)	20	99 (90(A) + 9(B))	99 (4.95)

^a Substrate/Catalyst molar ratio: for benzyl alcohol 300, for 1-phenyl ethanol and 2° alcohols 50, for aliphatic primary alcohols 100, catalyst amount 100 mg (5.4×10^{-3} mmol of Pt), TON = mmole of product(s)/mmole of Pt; TOF = TON/Time, water 5 mL, temperature, 353 K. O₂ = 1 atm., stirring speed = 900 rpm. Entries 5, 6: solid substrates were dissolved in ethyl acetate and with a Substrate/Catalyst molar ratio of 100.

Table 3 Recycling data for the oxidation of benzyl alcohol and 1-phenylethanol by catalyst **1**^a

Entries	Substrate	Product	No. of cycle	% Conversion (TON)	TTON over five cycles
1		 (A) + (B)	1	100 (300)	1149
2			2	81 (243)	
3			3	73 (219)	
4			4	68 (204)	
5			5	61 (183)	
6 ^b			Regenerated	99 (297)	
7			1	87 (43.5)	165.5
8			2	74 (37)	
9			3	60 (30)	
10			4	59 (29.5)	
11			5	51 (25.5)	
12 ^b			Regenerated	91 (45.5)	

^a Catalyst (**1**) = 100 mg (5.4×10^{-3} mmol of Pt); Substrate to platinum molar ratio, 50 for 1-phenyl ethanol and 300 for benzyl alcohol; solvent (water) = 5 mL; temperature = 353 K; O₂ = 1 atm with vigorous stirring (900 rpm); reaction time, 20 h for 1-phenyl ethanol and 8 h for benzyl alcohol. (TTON = total turnover number). ^b Regeneration of used catalyst (5 runs) by keeping it under 30 bar of hydrogen pressure for 3 h in water.

The deactivation of **1** is clearly not due to metal leaching as estimation of Pt before and after the each batch shows no observable loss of metal. A likely mechanism that takes into account all the experimental observations is shown in Scheme 2.

The catalytic cycle that involves species of the type **1**, **6**, **7** and **8** is the generally accepted mechanism for the oxidation of alcohols with Pt-catalysts.³¹ As indicated in Scheme 2, the deactivation of the catalyst is due to over oxidation, *i.e.*, “Pt–O–Pt” bridge formation which leads to the growth of platinum oxide lattice and a concomitant increase in the size of the NPs. This is consistent with the TEM and XPS data. As the concentration of water is considerably more than that of the alcohol, the equilibrium between **6** and **9** is expected to lie more towards the latter. The induction period of ~5h mentioned earlier

probably results from the time taken for the build up of enough **6** under unfavorable equilibrium conditions.

Conclusion

In conclusion synthesis of NP-Pt through the anchoring high nuclearity platinum carbonyl cluster on a water soluble polymer has an approximate E-factor of 12.8. By using either dioxygen or hydrogen peroxide the NP-Pt obtained this way can selectively oxidise a wide variety of alcohols with high turnovers and selectivities. After many turnovers there is partial deactivation accompanied by an increase in the particle sizes, but the deactivated catalyst can be fully regenerated by treatment with dihydrogen and this is accompanied by a reduction in the particle

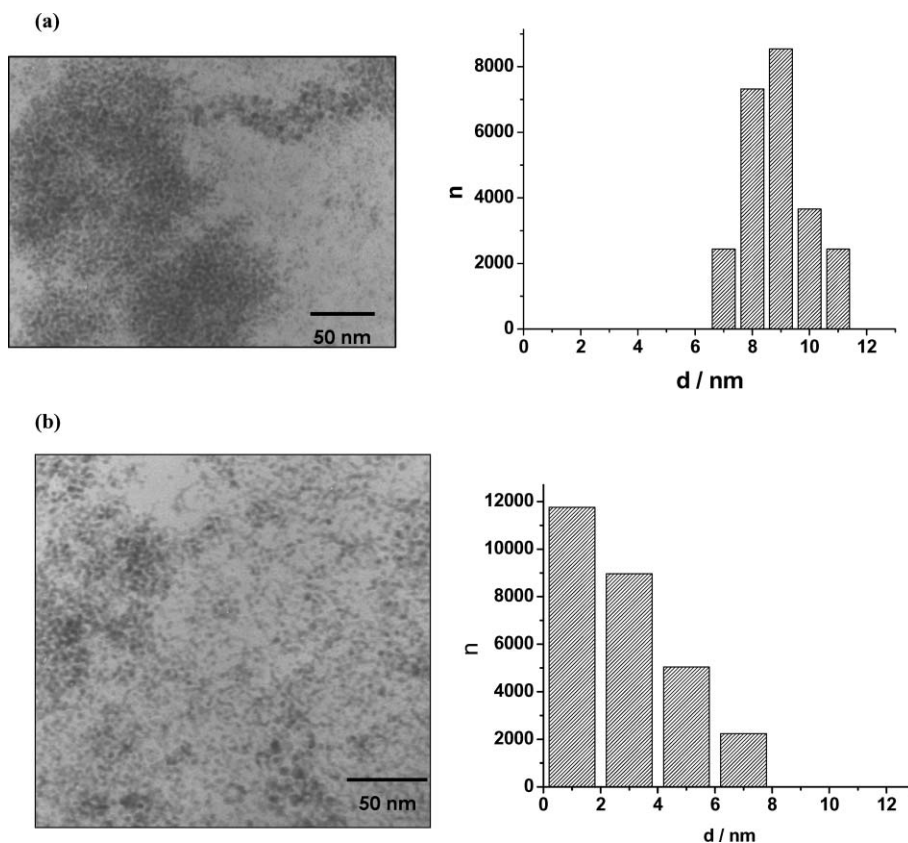


Fig. 2 (a) TEM picture and histogram of catalyst **1** after five runs. (b) TEM picture and histogram of used **1** from (a) after treatment with H₂ (30 bar) for 3 h.

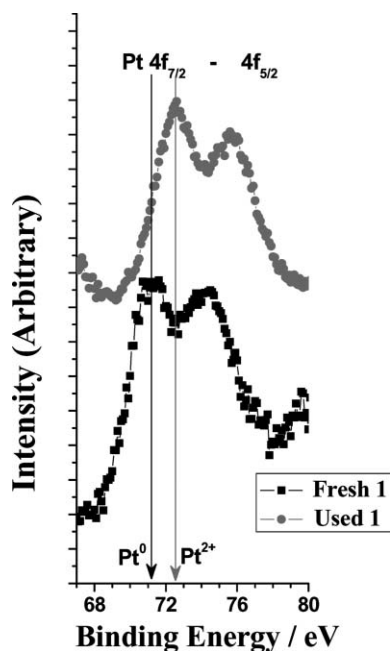
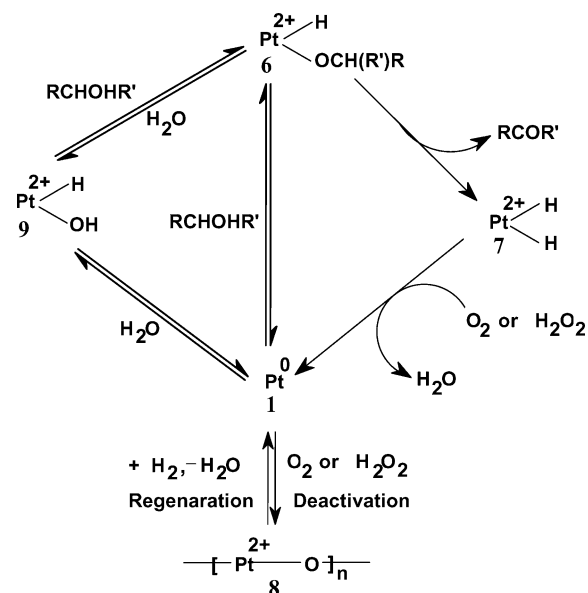


Fig. 3 XPS spectra of fresh and used catalyst **1**.

size. These and other experimental observations are consistent with the generally accepted mechanism for platinum catalysed oxidation of alcohols.



Scheme 2 Probable mechanistic pathway for the aerobic oxidation of alcohols by catalyst **1**.

Experimental

General methods

Methanol was dried over Mg-turnings/iodine and distilled under nitrogen prior to use. ¹H/¹³C NMR spectra were recorded

on a 400 MHz Varian spectrometer. TEM experiments were performed using a Philips 1200 EX at 120 kV. The histograms of TEM images were constructed manually from hard copies using the software ImageJ (<http://rsbweb.nih.gov/ij/>). The TEM pictures were scanned, saved as JPG files and opened by ImageJ program. After enlarging them substantially, sizes of fifty particles were measured manually for each picture and the histograms were obtained by using 'Origin' software.

UV-vis-NIR measurements were performed on a Perkin Elmer lamda-950 spectrophotometer. FT-IR spectra were taken on a Nicolet spectrophotometer with samples prepared as KBr pellets. All the samples were analysed by gas chromatographic technique with FID detector (Shimadzu GC-14A gas chromatograph) using a capillary column (CBP20 – M-25 – 025). The bulk platinum content of fresh and used **1** was determined using 8440 Plasma Lab ICP-AES instrument.

Poly(diallyldimethylammoniumchloride) (polyDADMAC, low molecular weight), 20 wt% solution in water, sodium hexachloroplatinate, and catalysts **3** and **4** were purchased from Aldrich, Germany and used as received. Carbon monoxide was supplied by BOC, India.

Synthesis of **1** and **2**

Syntheses of **1** and **2** were carried out according to the reported procedures^{28a} with the modification that methanol (10 gm) was used as the solvent.

Experimental protocol for the aerobic oxidation of alcohols in water using **1**

A mixture of **1** {100 mg, (5.4×10^{-3} mmol of effective platinum)} and respective alcohols (amount of alcohol varies as shown in Table 2) were taken in 3 mL of water. The mixture was stirred at 80 °C under a steady flow of oxygen gas at atmospheric pressure (The specific reaction time has been mentioned in Table 2). After cooling the reaction mixture was extracted with ethyl acetate (5×1 mL). The extract was dried over magnesium sulfate and analysed by GC or proton NMR. The aqueous catalyst solution was reused subsequently. Similar experimental procedures were followed for the catalysis using all other catalysts (**2–4**).

For the reactivation of the used catalyst, an aqueous solution of used **1** was kept under 30 bar of hydrogen pressure for 3 h and then used as the regenerated catalyst.

Acknowledgements

This work was financially supported by the Reliance Industries Limited, Mumbai and Council of Scientific and Industrial Research, New Delhi, India.

References

1 *Organic Synthesis in Water*, (Ed.: P. A. Grieco), Blackie, London, 1998.

- 2 (a) C.-J. Li, *Chem. Rev.*, 1993, **93**, 2023; (b) C.-J. Li, *Chem. Rev.*, 2005, **105**, 3095.
- 3 U. M. Lindstrom, *Chem. Rev.*, 2002, **102**, 2751.
- 4 (a) R. A. Sheldon, *Green Chem.*, 2007, **9**, 1273; (b) J. Auge, *Green Chem.*, 2008, **10**, 225.
- 5 H.-U. Blaser and M. Studer, *Green Chem.*, 2003, **5**, 112.
- 6 *Aqueous – phase Organometallic Catalysis: Concepts and Applications*, (Eds.: B. Cornils, W. A. Herrmann), Wiley-VCH, Weinheim, 1998.
- 7 F. Joo, *Aqueous Organometallic Catalysis*, Vol. 23, Kluwer Academic Pub., Dordrecht, 2001.
- 8 (a) G. ten Brink, I. W. C. E. Arends and R. A. Sheldon, *Science*, 2000, **287**, 1636; (b) G.-J. ten Brink, I. W. C. E. Arends, M. Hoogenraad, G. Verspui and R. A. Sheldon, *Adv. Synth. Catal.*, 2003, **345**, 1341; (c) G.-J. ten Brink, I. W. C. E. Arends, M. Hoogenraad, G. Verspui and R. A. Sheldon, *Adv. Synth. Catal.*, 2003, **345**, 497.
- 9 B. P. Buffin, J. P. Clarkson, N. L. Belitz and A. Kundu, *J. Mol. Catal. A: Chem.*, 2005, **225**, 111.
- 10 (a) Y. Uozumi and R. Nakao, *Angew. Chem. Int. Ed.*, 2003, **42**, 194; (b) R. Nakao, H. Rhee and Y. Uozumi, *Org. Lett.*, 2005, **7**, 163.
- 11 Y. M. A. Yamada, T. Arakawa, H. Hocke and Y. Uozumi, *Angew. Chem. Int. Ed.*, 2007, **46**, 704.
- 12 Y. H. Ng, S. Ikeda, T. Harada, Y. Morita and M. Matsumura, *Chem. Commun.*, 2008, 3181.
- 13 T. Wang, C. Xiao, L. Yan, L. Xu, J. Luo, H. Shou, Y. Kou and H. Liu, *Chem. Commun.*, 2007, 4375.
- 14 K. Mori, T. Hara, T. Mizugaki, K. Ebitani and K. Kaneda, *J. Am. Chem. Soc.*, 2004, **126**, 10657.
- 15 N. Jamwal, M. Gupta and S. Paul, *Green Chem.*, 2008, **10**, 999.
- 16 H. G. Manyar, G. S. Chaure and A. Kumar, *Green Chem.*, 2006, **8**, 344.
- 17 N. Komiya, T. Nakae, H. Sato and T. Naota, *Chem. Commun.*, 2006, 4829.
- 18 H. Tsunoyama, H. Sakurai, Y. Negishi and T. Tsukuda, *J. Am. Chem. Soc.*, 2005, **127**, 9374.
- 19 A. Biffis and L. Minati, *J. Catal.*, 2005, **236**, 405.
- 20 V. R. Choudhary, A. Dhar, P. Jana, R. Jha and B. S. Uphade, *Green Chem.*, 2005, **7**, 768.
- 21 Z. Wang, Q. Zhang, D. Kuehner, A. Ivask and L. Niu, *Green Chem.*, 2008, **10**, 907.
- 22 (a) A. M. Contreras, J. Grunes, X. -M. Yan, A. Liddle and G. A. Somorjai, *Catal. Lett.*, 2005, **100**, 115; (b) R. M. Rioux, H. Song, J. D. Hoefelmeyer, P. Yang and G. A. Somorjai, *J. Phys. Chem. B.*, 2005, **109**, 2192.
- 23 Y. Sakamoto, A. Fukuoka, T. Higuchi, N. Shimomura, S. Inagaki and M. Ichikawa, *J. Phys. Chem. B.*, 2004, **108**, 853.
- 24 V. Mevellec, C. Mattioda, J. Schulz, J. P. Rolland and A. Roucoux, *J. Catal.*, 2004, **225**, 1.
- 25 H. Lang, R. A. May, B. L. Iversen and B. D. Chandler, *J. Am. Chem. Soc.*, 2003, **125**, 14832.
- 26 M. Zhao and R. M. Crooks, *Angew. Chem. Int. Ed.*, 1999, **38**, 364.
- 27 A. B. R. Mayer and J. E. Mark, *J. Polym. Sci. A: Polym. Chem.*, 1997, **35**, 3151.
- 28 (a) P. Maity, S. Basu, S. Bhaduri and G. K. Lahiri, *Adv. Synth. Catal.*, 2007, **349**, 1955; (b) P. Maity, S. Basu, S. Bhaduri and G. K. Lahiri, *J. Mol. Catal. A: Chem.*, 2007, **270**, 117; (c) S. Basu, M. Mapa, C. S. Gopinath, M. Doble, S. Bhaduri and G. K. Lahiri, *J. Catal.*, 2006, **239**, 154; (d) S. Basu, H. Paul, C. S. Gopinath, S. Bhaduri and G. K. Lahiri, *J. Catal.*, 2005, **229**, 298; (e) S. Bhaduri, G. K. Lahiri, P. Munshi and D. Mukesh, *Catal. Lett.*, 2000, **65**, 61; (f) S. Bhaduri, V. S. Darshane, K. Sharma and D. Mukesh, *Chem. Commun.*, 1992, 1738; (g) S. Bhaduri and K. R. Sharma, *Dalton Trans.*, 1984, 2309.
- 29 G. Longoni and P. Chini, *J. Am. Chem. Soc.*, 1976, **98**, 7225.
- 30 G. Apai, S.-T. Lee, M. G. Mason, L. J. Gerenser and S. A. Gardner, *J. Am. Chem. Soc.*, 1979, **101**, 6880.
- 31 T. Mallat and A. Baiker, *Chem. Rev.*, 2004, **104**, 3037.

Base-free aqueous-phase oxidation of non-activated alcohols with molecular oxygen on soluble Pt nanoparticles

Tao Wang,^{a,b} Heng Shou,^a Yuan Kou^{*a} and Haichao Liu^{*a}

Received 29th October 2008, Accepted 12th January 2009

First published as an Advance Article on the web 17th February 2009

DOI: 10.1039/b818560c

Seven soluble metal nanoparticle catalysts including Pt, Ru, Rh, Pd, Ir, Ag and Au were synthesized and studied for the aqueous-phase selective oxidation of non-activated alcohols under atmospheric pressure of O₂. The effects of particle size were examined on the Pt catalysts with mean diameters of 1.5–4.9 nm. Pt nanoparticles efficiently catalyze the aerobic oxidation of alicyclic and aliphatic alcohols, in particular, primary aliphatic alcohols in the absence of any base. The particle sizes of the Pt catalysts strongly influence their activities, and the one of 1.5 nm exhibits much higher turnover frequencies. In comparison with the other metals examined in this work, it is concluded that Pt is the best metal of choice for the aerobic alcohol oxidation. Aliphatic primary alcohols reacts on the Pt catalysts more preferentially over their isomeric secondary alcohols with increasing their chain length or as they coexist. These steric effects, and the observed kinetic isotope effects with 1-C₄H₉OD and 1-C₄D₉OD are consistent with the general alcohol oxidation mechanism, which includes a sequence of elementary steps involving the formation of the alcoholate intermediates in quasi-equilibrated 1-C₄H₉OH dissociation on the Pt surfaces and the rate-determining hydrogen abstraction from the alcoholates. The inhibiting effects of hydroquinone, a typical radical scavenger, are indicative of the formation of radical intermediates in the H-abstraction step.

1. Introduction

Oxidation of alcohols to carbonyl or carboxyl compounds has been extensively studied, as a result of its ubiquitous importance in production of fine and specialty chemicals.^{1,2} Due to the ever-growing concerns over green chemistry and chemical processes, numerous efforts have been made to develop new catalytic protocols for the oxidation of alcohols particularly with O₂ as oxidant, in contrast to the traditional methods based on the use of stoichiometric amounts of noxious (inorganic or organic) oxidants.^{2–4} Among these studies, the progress in the aerobic oxidation of alcohols in water is considerably notable.^{5–9} However, very few catalysts are active for a wide range of alcohols in water, especially for non-activated alcohols, like alicyclic and aliphatic alcohols.^{5a,6,7,9b} Moreover, the oxidation of primary aliphatic alcohols in water frequently relies on the use of a strong base additive, such as KOH or K₂CO₃,^{5a,6,7,9b} which can cause the problems of corrosion and waste base disposal, *etc.*

Given these observed limitations, new catalysts more efficient for the green oxidation of alcohols with molecular

oxygen are in need of development, for which soluble metal nanoparticle catalysts are worthy candidates to be examined. Soluble nanoparticles exhibit superior catalytic properties relative to their counterparts of traditional supported metal catalysts in hydrogenation and hydrogenolysis reactions,^{10–13} such as low-temperature aqueous-phase Fisher-Tropsch synthesis on Ru nanoparticles,¹⁰ selective hydrogenation of o-chloronitrobenzene on Pt nanoparticles,¹¹ and selective hydrogenolysis of cellobiose (the simplest probe molecule for cellulose conversion) to C₆ polyols on Ru nanoparticles in water.¹² Soluble nanoparticles have also been found to be efficient catalysts for other reactions, such as green synthesis of methyl formate *via* carbonylation of methanol on Cu nanoparticles in the absence of base.¹⁴ These superior performances of the soluble nanoparticles most likely arise from their controllable sizes and morphologies as well as their unique accessibility to reactants.¹⁵

Recently, we have reported in a communication that a soluble Pt nanoparticle catalyst is efficient for the aerobic oxidation of a wide variety of activated and non-activated alcohols, in particular, non-activated aliphatic primary alcohols, in the absence of base.¹⁶ In this paper, we extend this preliminary study and present results on the effect of Pt nanoparticle size, the catalytic activities of other metal nanoparticles including noble metals of Ru, Rh, Ir, and Pd as well as Au and Ag, and the mechanistic examinations. These detailed studies are aimed at shedding light on the unique properties of Pt nanoparticles and the mechanism for the aerobic oxidation of nonactivated alcohols, specifically aliphatic alcohols, in water under base-free conditions.

^aPKU Green Chemistry Center, Beijing National Laboratory for Molecular Sciences, State Key Laboratory for Structural Chemistry of Stable and Unstable Species, College of Chemistry and Molecular Engineering, Peking University, Beijing, 100871, China.
E-mail: yuankou@pku.edu.cn, hcliu@pku.edu.cn;
Fax: 86-10-6275-1708; Tel: 86-10-6275-7792

^bCenter for Computational Science & Engineering, Peking University, Beijing, 100871, China

2. Experimental

2.1 Synthesis of various metal nanoparticle catalysts

Pt, Rh, Ru and Ir nanoparticles were synthesized in a similar way reported previously in the literature.¹⁷ Here, as an example, the synthesis of Pt nanoparticles is briefly described. 150 mg of NaOH (3.75 mmol) was added into a glycol solution of $\text{H}_2\text{PtCl}_6 \cdot 6\text{H}_2\text{O}$ (150 mg, 0.2895 mmol Pt in 15 mL glycol) with vigorous stirring to obtain a transparent yellow solution. Then, the solution was heated at 160 °C for 3 h with a N_2 (purity: 99.9995%) flow for taking away H_2O and some organic products formed during the preparation process. After the solution was cooled to room temperature, 1.288 g of poly(N-vinyl-2-pyrrolidone) (PVP; AR grade, MW = 30000; 11.6 mmol) was dissolved in it with vigorous stirring. Afterwards, the solution was dialyzed overnight (through a cellulose ester dialysis membrane with a cutoff molecular-weight of 12000) using deionized water to completely remove glycol, followed by dilution to 150 mL using deionized H_2O to form Pt nanoparticle solution. The pH value of the solution was measured to be ~7.

For the Pt nanoparticles, six samples with varying particle sizes were synthesized by a seeded-growth method. H_2 was used to reduce H_2PtCl_6 on seeds. For example, 2 ml aqueous solution of H_2PtCl_6 (3.86×10^{-2} mmol Pt) was added to 20 ml aqueous solution containing Pt nanoparticles of 1.5 nm in diameter (obtained following the procedure described above) as seeds (3.86×10^{-2} mmol Pt) with stirring. Then the solution was placed into a 60-ml stainless steel autoclave, and reduced by H_2 (3.0 MPa) at 25 °C for 1 h. Subsequently, the resulting black solution containing platinum nanoparticles of 2.0 nm in diameter was diluted to 40 ml, and used for preparing larger Pt particles. For all the solutions of Pt nanoparticles of 2.1, 3.0, 3.5, 4.3 and 4.9 nm prior to alcohol oxidation reactions, additional 0.171, 0.257, 0.300, 0.321 and 0.332 g PVP were added, respectively, to keep their PVP/Pt ratios at 40/1.

For the synthesis of Pd nanoparticles, PdCl_2 was first converted to H_2PdCl_4 in hydrochloric acid solution. The H_2PdCl_4 solution (0.03 mol/L, 6.42 ml, 0.1926 mmol) and PVP (0.855 g, 7.7 mmol) were then introduced to a mixture of water (8.58 ml) and methanol (15 ml), followed by changing the pH value of this solution to 9 using methanolic NaOH solution (0.1 mol/L). Then, the solution was stirred under reflux for 3 h, and turned black. Afterwards, the black solution was dialyzed overnight using deionized water, and then was diluted to 100 mL by deionized H_2O . The pH value of the solution was measured to be ~7.

The synthesis of Au and Ag nanoparticles was carried out in the same way. As an example, Au nanoparticles were synthesized as follows: $\text{HAuCl}_4 \cdot 4\text{H}_2\text{O}$ (49.9 mg, 0.0963 mmol) and PVP (0.427 g, 3.85 mmol) were added to 5 ml deionized water and stirred for 30 minutes in ice-water bath, to which a newly prepared aqueous solution of NaBH_4 (0.96 mmol, 5 ml) was then rapidly added under vigorous stirring. Immediately, the solution turned black. The resulting solution was then dialyzed overnight in deionized water. Afterwards, the black solution was diluted to 50 ml with deionized water to form Au nanoparticle solution (1.93×10^{-3} mol/L).

It was mentioned that the complete reduction of the metallic salts to metals, for the synthesis of the above metal nanopar-

ticles, was examined by UV spectroscopy before the dialysis procedure.

2.2 Characterization of metal nanoparticles

The metal nanoparticles were characterized by transmission electron microscope (TEM). The TEM micrographs were recorded on a Hitachi H-9000 high resolution transmission electron microscope (HRTEM) at 300 kV. Samples were prepared by dropping the metal nanoparticle solutions onto carbon-coated Cu grids. More than 200 particles for each sample were randomly counted to determine the particle size distributions.

2.3 Oxidation of alcohols

The typical procedure for the alcohol oxidation is described briefly. A mixture of 15 ml catalyst solution (1.93×10^{-3} mol/L, containing 2.895×10^{-2} mmol metal), and alcohol (e.g. 1-butanol, 1.45 mmol) was stirred in a flask at 80 °C for 1 h under atmospheric pressure of O_2 (1 atm, O_2 balloon). After cooling to room temperature, diethyl ether was used to extract the reaction system.

For examining the effect of a radical scavenger, varying amounts of hydroquinone (Sinapharm Chemical Reagent Co., Ltd, AR grade, >99.0%) in the range of 0.145 mmol and 1.45 mmol were introduced to a mixture of 15 ml catalyst solution (1.93×10^{-3} mol/L, containing 2.895×10^{-2} mmol Pt), and 1-butanol (1.45 mmol), and then reacted at 80 °C for 1 h under atmospheric pressure of O_2 (1 atm, O_2 balloon).

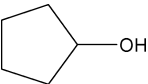
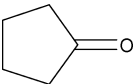
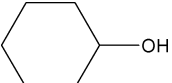
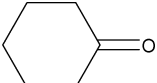
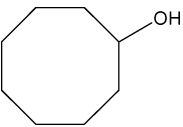
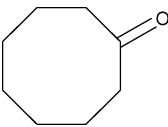

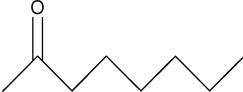


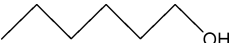
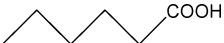


For measuring the kinetic isotope effect, deuterated 1-butanol, 1- $\text{C}_4\text{H}_9\text{OD}$ (Aldrich Chemical Company, 98 atom% D) and 1- $\text{C}_4\text{D}_9\text{OD}$ (Acros Organics, 99.5 atom% D), were used as reactants instead of 1- $\text{C}_4\text{H}_9\text{OH}$. The oxidation reactions were carried out with a mixture of 15 ml catalyst solution (1.93×10^{-3} mol/L, containing 2.895×10^{-3} mmol Pt), and 1-butanol (0.145 mmol) at 40 °C under atmospheric pressure of O_2 (1 atm, O_2 balloon).

The reactants and products were analyzed by a gas chromatograph (Agilent 6820) equipped with a FID detector and a HP innowax column (30 m \times 0.32 mm \times 0.5 μm), and by GC-MS (Agilent 6809/5973i). The metal contents in the organic phases were measured after the alcohol oxidation reactions by inductively coupled plasma-atomic emission spectroscopy (ICP-AES, PROFILE SPEC, LEEMAN LABS). The measured results showed that the metal contents for all the reactions with the metal nanoparticle catalysts in this work were below the detection limit (<1 μg -mg/ml), showing no leaching of the metals into the reaction media.

3. Results and discussion

As stated earlier, our recent communication reported the synthesis of a soluble Pt nanoparticle catalyst with a mean diameter of 1.5 nm, *via* reduction by glycol and stabilization by poly(N-vinyl-2-pyrrolidone) (PVP).¹⁶ The Pt catalyst is stable and exhibits high efficiencies in the absence of base for the selective oxidation of not only activated alcohols, e.g. benzyl alcohol, 1-phenylethanol and cinnamyl alcohol, but also non-activated alicyclic alcohols and aliphatic alcohols.¹⁶

Table 1 Aerobic oxidation of various non-activated alcohols on a soluble Pt nanoparticle catalyst with a mean diameter of 1.5 nm^a

Entry	Alcohol	Product	Conversion (%)	Yield (%)
1			100	97.1
2			88.4	78.4
3			99.1	88.8
4			95.2	94.2
5			100	99.7
6			100	99.3
7			96.0	94.5

^a Reaction conditions: 80 °C, 1.0 bar O₂, 24 h, 0.579 mmol alcohol, 2.895 × 10⁻² mmol Pt, 15 ml water, PVP:Pt = 40:1.

Table 1 shows the oxidation conversions and yields for representative non-activated alcohols on the Pt nanocluster (1.5 nm) catalyst in water under atmospheric pressure of O₂. Alicyclic alcohols, *i.e.* cyclopentanol, cyclohexanol and cyclooctanol, were oxidized to the corresponding cyclic ketones in good yields, being 97.1%, 78.4%, and 88.8%, respectively (Table 1, entries 1–3). This Pt catalyst also efficiently catalyzed the conversion of secondary aliphatic alcohols to ketones, for example, oxidation of 2-octanol gave a 94.2% yield to 2-octanone (Table 1, entry 4). For primary aliphatic alcohols, the most inactive alcohols, Pt was highly active under the identical conditions for their oxidation with O₂ in the absence of any bases (Table 1, entries 5–7). 1-butanol and 1-hexanol almost quantitatively converted to 1-butanolic acid and 1-hexanoic acid, respectively, achieving yields of as high as 99.7% and 99.3%, and 1-octanol to 1-octanoic acid with a yield of 94.5%, similar to that for the 2-octanol oxidation to 2-octanone. These results contrasted clearly with the previous findings that undesirable inorganic bases as co-catalysts are prerequisite for the aerobic oxidation of aliphatic primary alcohols.^{5a,6,7,9b} For example, Uozumi and coworkers reported that amphiphilic resin-supported Pt nanoparticles catalyzed oxidation of 1-octanol in the presence of equimolar K₂CO₃.⁷ These results demonstrate the efficiency of the Pt catalyst for the aqueous-phase oxidation of non-activated alcohols with O₂.

By referring to the previous studies on the alcohol oxidation by soluble metal nanoparticle catalysts in water, to our knowledge, only two kinds of catalysts have been reported to date, *i.e.*, Pd and Au nanoparticles stabilized by microgels and polymer, respectively.^{8,9} The Pd catalyst was only active

for 1-phenylethanol in the absence of a base additive,^{8a} and essentially not for non-activated alcohols such as 2-octanol and cyclohexanol.^{8b} The Au catalyst was active for a wide range of alcohols but K₂CO₃ or KOH is indispensable.^{9b} It is thus apparent that our Pt catalyst represents the first example that soluble metal nanoparticles are capable of catalyzing the aerobic oxidation of, in particular, non-activated primary alcohols with high efficiencies in the absence of any bases.

To further understand the activity of the Pt catalyst, we examined the effects of the Pt particle size and the activity of other metal nanoparticles for comparison. Six Pt samples were synthesized, and their TEM images (Fig. 1) show that the particles are roughly spherical and possess mean diameters of 1.5, 2.1, 3.0, 3.5, 4.3, and 4.9 nm respectively, with narrow size distributions. The activity of these Pt nanoparticles depends on their size. As shown in Fig. 2, the activity normalized by total Pt atoms in the aerobic 1-butanol oxidation increased gradually from 4.1 to 8.3 h⁻¹ with decreasing the particle size from 4.9 to 2.1 nm, and then sharply increased to 24.5 h⁻¹ at the particle size of 1.5 nm. The activity normalized by exposed surface Pt atoms (estimated by using the mean diameters of the Pt particles and by assuming that they are spherical) (Fig. 2), *i.e.* turnover frequency (TOF), was also much higher at 1.5 nm than the TOFs at other sizes. Such size effect was found prevalently with nanoparticle catalysts for many reactions, such as low-temperature CO oxidation on Au,¹⁸ low-temperature aqueous-phase Fisher-Tropsch synthesis on Ru,¹⁰ and aerobic oxidation of alcohols on Pd.¹⁹ Such effect has been generally ascribed to the existence of more coordinately unsaturated sites on smaller

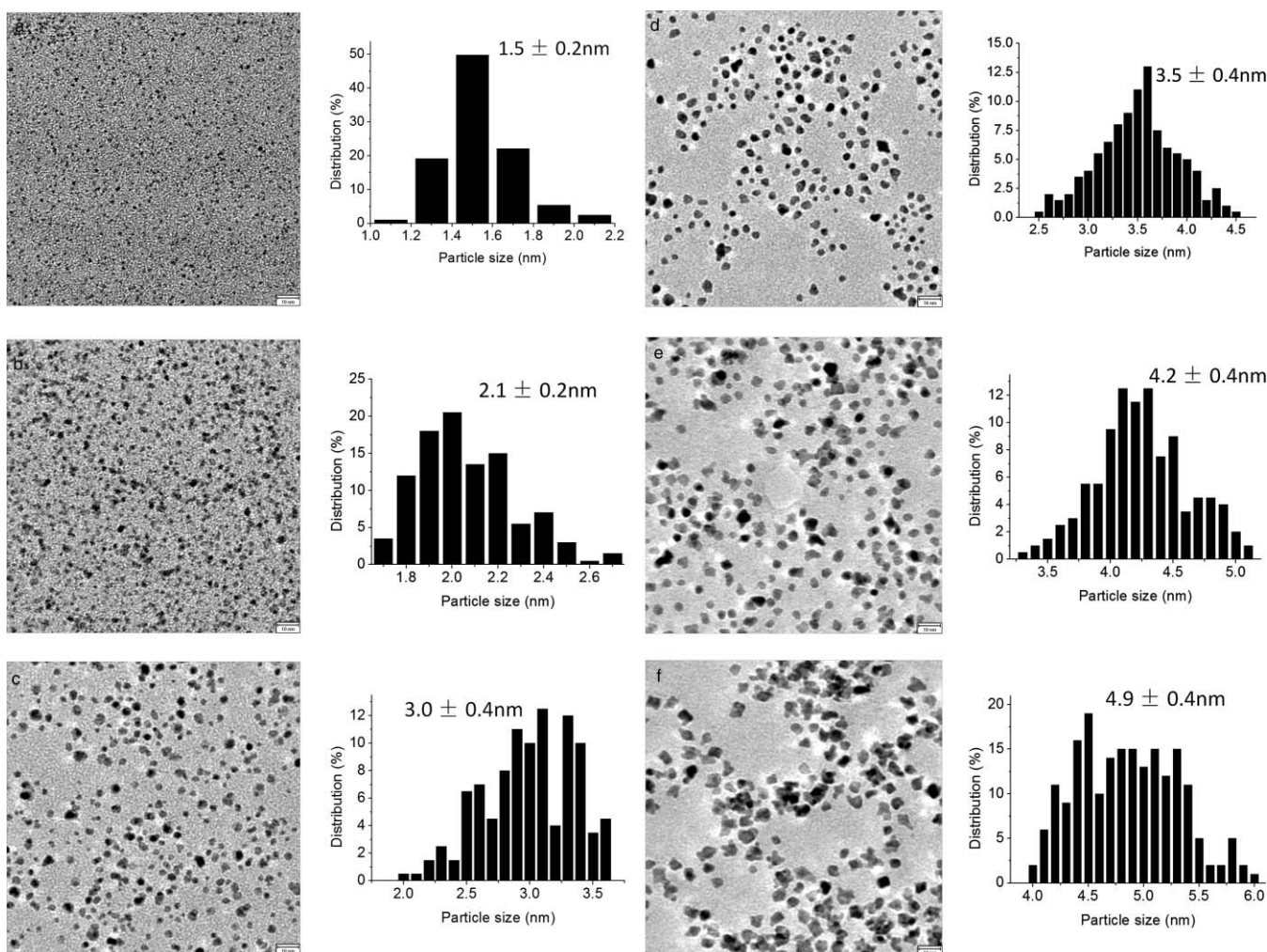


Fig. 1 TEM micrographs and size distributions of Pt nanoparticles with different diameters (scale bar = 10 nm). (a) 1.5 ± 0.2 nm. (b) 2.1 ± 0.2 nm. (c) 3.0 ± 0.4 nm. (d) 3.5 ± 0.4 nm. (e) 4.3 ± 0.4 nm. (f) 4.9 ± 0.4 nm.

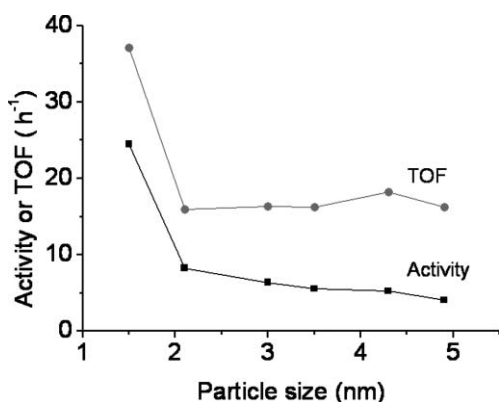


Fig. 2 The catalytic activity (normalized by total Pt atoms) and turnover frequency (TOF, normalized by exposed surface Pt atoms) as a function of Pt nanoparticle size. Reaction conditions: 80°C , 1.0 bar O_2 , 1 h, 1.45 mmol butanol, 2.895×10^{-2} mmol Pt, 15 ml water, PVP:Pt = 40:1.

particles and the changes in their electronic properties, however, the exact underlying reasons as well as the exact active sites (or structures and sizes of these particles) are still being discussed.

For example, Kiely and Hutchings, *et al.*²⁰ very recently found that the presence of 0.5 nm bilayer Au particles is correlated to the high catalytic activity for the extensively studied CO oxidation reaction on Au/ Fe_2O_3 , leading to deeper insights into the Au catalysts.

Table 2 shows the TOFs on Ru, Rh, Pd, Ir, Au and Ag nanoparticles for the aerobic 1-butanol oxidation. These catalysts were characterized by TEM, and possessed mean diameters of 1.1, 1.3, 2.4, 5.2, 3.2, and 4.0 nm respectively (Fig. 3). For comparison, the results of the Pt catalysts (presented in Fig. 2) were also listed in Table 2. Because of the known particle size effect, the comparison with the Pt catalysts was made for the different catalysts with similar sizes. Ru, Rh, and Ag were not active, and gave negligible or slight TOFs ($0.07\text{--}0.26 \text{ h}^{-1}$; Table 2, entries 1–3). Ir and Pd exhibited about 2.0 and 2.4 times lower TOFs than Pt at a comparable particle size of ~ 5 and 2.1 nm, respectively (Table 2, entries 4–5). As mentioned above, Au was active for the aliphatic alcohols only in the presence of strong bases, required presumably for H abstraction from the alcoholic OH groups.^{9b} Similarly, our Au nanoparticle catalyst (3.2 nm) is almost inactive (Table 2, entry 6), but its activity was dramatically increased upon addition of K_2CO_3 (Table 2,

Table 2 Aerobic oxidation of 1-butanol on various soluble metal nanoparticle catalyst^a

Entry	Catalyst	Particle size (nm)	TOF (h ⁻¹)
1	Ru	1.1 ± 0.2	0.26
2	Rh	1.3 ± 0.2	0.07
3	Ag	4.0 ± 2.6	0.1
4	Pd	2.4 ± 0.5	6.7
5	Ir	5.2 ± 1.1	8.1
6	Au	3.2 ± 0.7	0.62
7 ^b			76.0
8	Pt	1.5 ± 0.2	37.1
9 ^c			40.0
10	Pt	2.1 ± 0.2	16.0
11	Pt	3.0 ± 0.4	16.4
12	Pt	3.5 ± 0.4	16.3
13	Pt	4.2 ± 0.4	18.2
14	Pt	4.9 ± 0.4	16.3

^a Reaction conditions: 80 °C, 1.0 bar O₂, 1 h, 1.45 mmol 1-butanol, 2.895 × 10⁻² mmol metallic catalysis, 15 ml water, PVP: Metal = 40:1.

^b 300 mol% K₂CO₃ (K₂CO₃:1-butanol = 3:1) was added before the reaction. ^c 100 mol% K₂CO₃ (K₂CO₃:1-butanol = 1:1) was added before the reaction.

entry 7). In contrast, the activity of the Pt catalyst (1.5 nm) remained essentially unchanged in the presence of K₂CO₃ (Table 2, entry 9). Such a difference between the Au and Pt catalysts reflects their intrinsic difference in activating the alcoholic OH groups to form alcoholate intermediates. Taken together, these results clearly show the superiority of the Pt nanoparticles for catalyzing the oxidation of alcohols with O₂.

Concerning the reactivity of the aliphatic primary and secondary alcohols, although the primary alcohols are generally accepted as the most inactive ones, there are inconsistent results reported in the literature. Taking 1-octanol and 2-octanol as examples, Hutchings and coworkers²¹ found that 1-octanol oxidation readily proceeds on Au-Pd/TiO₂, whereas 2-octanol is completely inactive under identical conditions. However, Kaneda reported that 2-octanol is more reactive than 1-octanol with hydroxyapatite-supported Pd catalysts.⁴ In this regard, we systematically examined the oxidative reactivity of different aliphatic primary and secondary alcohols on the Pt catalyst (1.5 nm). As shown in Table 3, the TOFs were lower for 1-propanol and 1-butanol than 2-propanol and 2-butanol,

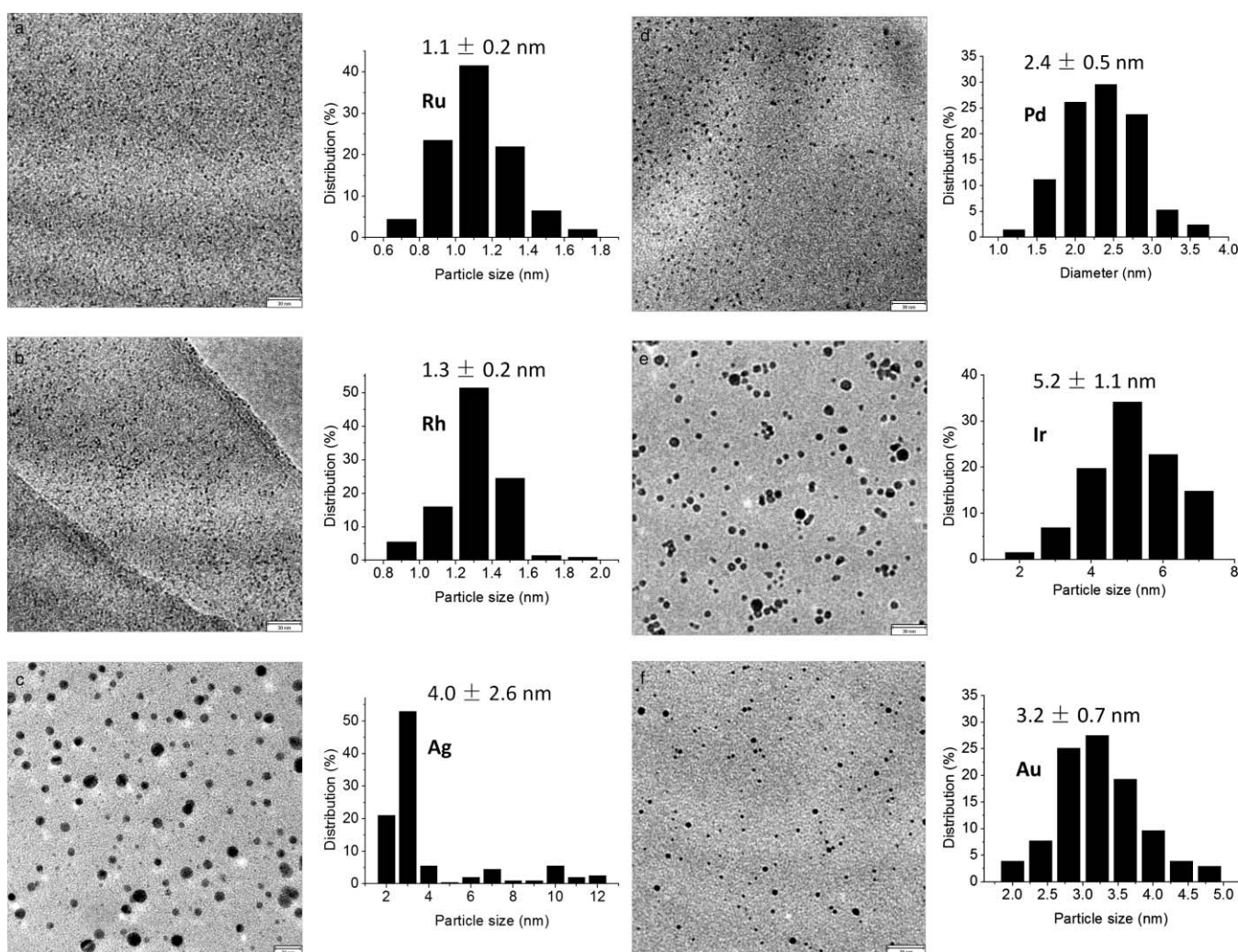


Fig. 3 TEM micrographs and size distributions of metal nanoparticles. (a) Ru, 1.1 ± 0.2 nm (scale bar = 30 nm). (b) Rh, 1.3 ± 0.2 nm (scale bar = 30 nm). (c) Ag, 4.0 ± 2.6 nm (scale bar = 20 nm). (d) Pd, 2.4 ± 0.5 nm (scale bar = 30 nm). (e) Ir, 5.2 ± 1.1 nm (scale bar = 30 nm). (f) Au, 3.2 ± 0.7 nm (scale bar = 30 nm).

Table 3 Turnover frequencies (TOF) for the aerobic oxidation of primary and secondary alcohols on Pt catalyst of 1.5 nm^a

Entry	Alcohol	TOF (h ⁻¹) (1-alcohol)	TOF (h ⁻¹) (2-alcohol)	TOF ratio (1-alcohol/2-alcohol)
1	1-propanol	40.7		0.88
2	2-propanol		46.2	
3	1-butanol	46.4		0.90
4	2-butanol		51.3	
5	1-hexanol	42.3		1.45
6	2-hexanol		29.1	
7	1-octanol	32.4		2.84
8	2-octanol		11.4	
9 ^b	1-propanol + 2-propanol	26.9	11.4	2.36
10 ^b	1-butanol + 2-butanol	29.3	10.8	2.71
11 ^b	1-hexanol + 2-hexanol	25.6	6.6	3.88
12 ^b	1-octanol + 2-octanol	20.4	5.5	3.71

^a Reaction conditions: 80 °C, 1.0 bar O₂, 1 h, 1.45 mmol alcohol, 2.895 × 10⁻² mmol Pt, PVP:Pt = 40:1, 15 ml water. ^b Equimolar mixture of 1-alcohol and 2-alcohol, *i.e.*, 7.24 × 10⁻⁴ mol for each alcohol.

respectively, whereas 1-hexanol and 1-octanol converted more rapidly than 2-hexanol and 2-octanol as these alcohols were individually used as reactants under identical conditions (Table 3, entries 1–8). Such a difference in the reactivity was noticed more clearly from the TOF ratios of the primary alcohols to secondary alcohols, which increased from 0.88 to 2.84 with increasing the carbon number of the alcohols from three (*i.e.* propanols) to eight (*i.e.* octanols). It is thus apparent that the reactivity of the primary and secondary alcohols depends on their chain length and steric hindrance; the primary alcohols with longer carbon chains tend to react more preferentially over the corresponding secondary alcohols. Such dependence was further confirmed by competitive oxidation of equimolar mixtures of the primary and secondary alcohols. As shown in Table 3 (entries 9–12), the coexistence of the primary and secondary alcohols led to more preferential reaction of the primary alcohols over the corresponding secondary alcohols, and accordingly an increase in their TOF ratios compared to the ratios obtained with the individual alcohols. This is exemplified by the oxidation of equimolar mixture of 1-propanol and 2-propanol, affording a 2.36 times greater reactivity of 1-propanol than 2-propanol, in contrast to the value of 0.88 obtained with individual reactants under identical conditions. Such steric effects of the alcohols are consistent with the alcohol oxidation mechanism, which is proposed to generally involve alcoholate intermediates derived from dissociative chemisorption of the alcohol molecules on the catalyst surfaces, and their subsequent conversion to carbonyl products in the presence of O₂.²

To probe the kinetic relevance of the elementary steps, as stated above, involving the alcoholate formation and hydride abstraction from the alcoholates, the oxidation of 1-butanols, fully deuterated (1-C₄D₉OD) and deuterated only at the hydroxyl group (1-C₄H₉OD), were examined. Kinetic relevance of the 1-butanol dissociation to form alcoholates would lead to normal kinetic isotope effects (KIE) for both 1-C₄H₉OD and 1-C₄D₉OD reactants, whereas normal KIE would be seen only for 1-C₄D₉OD rather than 1-C₄H₉OD if the reaction rate is limited by the hydride abstraction from the alcoholates. Table 4 shows the TOFs and kinetic isotope effects (KIE, denoted as *k_H*/*k_D*) measured at 40 °C on the Pt catalyst (1.5 nm) with similar conversions of ~5%. These conditions were chosen to fully keep the reactions in the kinetic region. Undeuterated 1-butanol

Table 4 Kinetic isotopic effects for aerobic 1-butanol oxidation on Pt catalyst of 1.5 nm^a

Entry	Alcohol	TOF (h ⁻¹)
1	1-C ₄ H ₉ OH	1.5
2	1-C ₄ H ₉ OD	1.6
3	1-C ₄ D ₉ OD	0.6
4	<i>k</i> _{1-C₄H₉OH} / <i>k</i> _{1-C₄H₉OD}	0.94
5	<i>k</i> _{1-C₄H₉OH} / <i>k</i> _{1-C₄D₉OD}	2.50

^a 40 °C, 1.0 bar O₂, 0.145 mmol alcohol, 15 ml water, 2.895 × 10⁻³ mmol Pt, PVP:Pt = 40:1, ~5% 1-butanol conversion.

(1-C₄H₉OH) and 1-C₄H₉OD showed similar TOFs, affording a KIE of 0.94. In contrast, much smaller TOF was obtained with 1-C₄D₉OD relative to 1-C₄H₉OH, and the corresponding KIE was as great as 2.50. It is thus apparent from these measured KIE values that the dissociative chemisorption to form the alcoholate intermediates is quasi-equilibrated, and the hydride abstraction from the alcoholates is the kinetically relevant step during the 1-butanol oxidation on Pt.

Further, the involvement of radical intermediates was suggested by the inhibiting effect of a radical scavenger on the TOFs in the aerobic 1-butanol oxidation on Pt. As shown in Fig. 4, upon addition of a slight amount of radical scavenger, 0.145 mmol hydroquinone (*i.e.* 1-butanol:hydroquinone = 10:1),

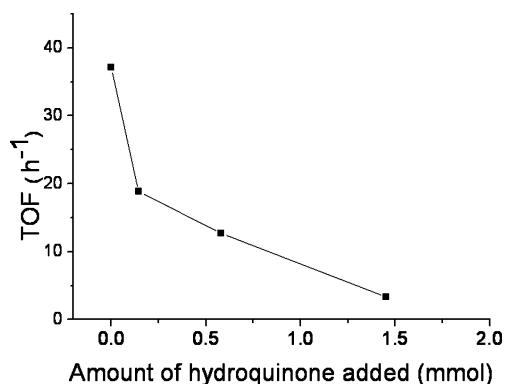


Fig. 4 Effect of radical scavenger, hydroquinone, on aerobic oxidation of 1-butanol catalyzed by soluble Pt nanoparticles (1.5 nm in diameter). Reaction conditions: 80 °C, 1.0 bar O₂, 1 h, 1.45 mmol butanol, 2.895 × 10⁻² mmol Pt, 15 ml water, PVP:Pt = 40:1.

the TOF decreased sharply from 37.1 to 18.9 h⁻¹, which then became negligible (3.3 h⁻¹) in the presence of an equivalent amount of the scavenger. Such a marked scavenger effect indicates that the kinetically relevant hydride abstraction from the alcoholates forms radical-type intermediates involving in the 1-butanol oxidation mechanism.

4. Conclusions

Soluble Pt nanoparticles efficiently catalyze the selective oxidation of non-activated alcohols, in particular, primary aliphatic alcohols with atmospheric O₂ in the absence of any base. Their activities depend on their particle size in the range of 1.5–4.9 nm, which reach the highest value on the catalyst with a mean diameter of 1.5 nm. At comparable particle sizes, the Pt catalysts are more active than other metal catalysts including Ru, Rh, Pd, Ir, Ag and Au, showing the superiority of Pt for the aerobic alcohol oxidation. The reactivity of isomeric aliphatic alcohols (primary and secondary alcohols) on Pt depends on their carbon-chain length. The primary alcohols are more reactive than the secondary alcohols with increasing their chain length; when they coexist, the primary alcohols always react preferentially over the secondary alcohols. Such steric effects are consistent with the documented reaction mechanism of the aerobic alcohol oxidation involving alcoholate intermediates derived from dissociative adsorption of the alcohol molecules on the catalyst surfaces. Normal and no kinetic isotope effects were observed for 1-C₄D₉OD and 1-C₄H₉OD, respectively, which suggest the quasi-equilibrated alcoholate formation and the rate-determining hydrogen abstraction from the alcoholate intermediates on the Pt catalysts.

Acknowledgements

This work was supported by the National Natural Science Foundation of China (Grant Nos. 20533010, 20673005, 20773005, 20825310).

References

- J. I. Kroschwitz, *Kirk Othmer Encyclopedia of Chemical Technology*, vol. 4, 4th edn., Wiley-Interscience Publication, New York, 1992.
- T. Mallat and A. Baiker, *Chem. Rev.*, 2004, **104**, 3037–3058.
- (a) W. J. Mijs and C. R. H. de Jonge, *Organic synthesis by Oxidation with Metal Compounds*, Plenum Press, New York, 1986; (b) H. Miyamura, R. Matsubara, Y. Miyazaki and S. Kobayashi, *Angew. Chem. Int. Ed.*, 2007, **46**, 4151–4154.
- K. Mori, T. Hara, T. Mizugaki, K. Ebitani and K. Kaneda, *J. Am. Chem. Soc.*, 2004, **126**, 10657–10666.
- (a) G. ten Brink, I. W. C. E. Arends and R. A. Sheldon, *Science*, 2000, **287**, 1636–1639; (b) G. ten Brink, I. W. C. E. Arends, M. Hoogenraad, G. Verspui and R. A. Sheldon, *Adv. Synth. Catal.*, 2003, **345**, 497–505; (c) G. ten Brink, I. W. C. E. Arends, M. Hoogenraad, G. Verspui and R. A. Sheldon, *Adv. Synth. Catal.*, 2003, **345**, 1341–1352; (d) N. Komiya, T. Nakae, H. Sato and T. Naota, *Chem. Commun.*, 2006, 4829–4831.
- A. Abad, P. Concepción, A. Corma and H. García, *Angew. Chem. Int. Ed.*, 2005, **44**, 4066–4069.
- (a) Y. Uozumi and R. Nakao, *Angew. Chem. Int. Ed.*, 2003, **42**, 194–197; (b) Y. M. A. Yamada, T. Arakawa, H. Hocke and Y. Uozumi, *Angew. Chem. Int. Ed.*, 2007, **46**, 704–706.
- (a) A. Biffis and L. Minati, *J. Catal.*, 2005, **236**, 405–409; (b) A. Biffis, S. Cunial, P. Spontoni and L. Prati, *J. Catal.*, 2007, **251**, 1–6.
- (a) H. Tsunoyama, H. Sakurai, Y. Negishi and T. Tsukuda, *J. Am. Chem. Soc.*, 2005, **127**, 9374–9375; (b) H. Tsunoyama, T. Tsukuda and H. Sakurai, *Chem. Lett.*, 2007, **36**, 212–213; (c) S. Kanaoka, N. Yagi, Y. Fukuyama, S. Aoshima, H. Tsunoyama, T. Tsukuda and H. Sakurai, *J. Am. Chem. Soc.*, 2007, **129**, 12060–12061.
- C.-X. Xiao, Z.-P. Cai, T. Wang, Y. Kou and N. Yan, *Angew. Chem. Int. Ed.*, 2008, **47**, 746–749.
- C. X. Xiao, H. Z. Wang, X. D. Mu and Y. Kou, *J. Catal.*, 2007, **250**, 25–32.
- N. Yan, C. Zhao, C. Luo, P. J. Dyson, H. Liu and Y. Kou, *J. Am. Chem. Soc.*, 2006, **128**, 8714–8715.
- (a) X. D. Mu, J. Q. Meng, Z. C. Li and Y. Kou, *J. Am. Chem. Soc.*, 2005, **127**, 9694–9695; (b) C. Zhao, H. Z. Wang, N. Yan, C. X. Xiao, X. D. Mu, P. J. Dyson and Y. Kou, *J. Catal.*, 2007, **250**, 33–40; (c) C. Zhao, W. Gan, X. Fan, Z. Cai, P. J. Dyson and Y. Kou, *J. Catal.*, 2008, **254**, 244–250.
- L. He, H. Liu, C.-X. Xiao and Y. Kou, *Green Chem.*, 2008, **10**, 619–622.
- D. B. Zhao, M. Wu, E. Z. Min and Y. Kou, *Catal. Today*, 2002, **74**, 157–189.
- T. Wang, C. X. Xiao, L. Yan, L. Xu, J. Luo, H. Shou, Y. Kou and H. Liu, *Chem. Commun.*, 2007, 4375–4377.
- Y. Wang, J. W. Ren, K. Deng, L. L. Gui and Y. Q. Tang, *Chem. Mater.*, 2000, **12**, 1622–1627.
- M. Haruta, S. Tsubota, T. Kobayashi, H. Kageyama, M. J. Genet and B. Delmon, *J. Catal.*, 1993, **144**, 175–192.
- J. Chen, Q. Zhang, Y. Wang and H. Wan, *Adv. Synth. Catal.*, 2008, **350**, 453–464.
- A. A. Herzing, C. J. Kiely, A. F. Carley, P. Landon and G. J. Hutchings, *Science*, 2008, **321**, 1331–1335.
- D. I. Enache, J. K. Edwards, P. Landon, B. Solsona-Espriu, A. F. Carley, A. A. Herzing, M. Watanabe, C. J. Kiely, D. W. Knight and G. J. Hutchings, *Science*, 2006, **311**, 362–365.

N-phosphorylation of amino acids by trimetaphosphate in aqueous solution—learning from prebiotic synthesis

Feng Ni,^a Shuting Sun,^a Chao Huang^a and Yufen Zhao^{*a,b}

Received 6th October 2008, Accepted 19th January 2009

First published as an Advance Article on the web 17th February 2009

DOI: 10.1039/b817013d

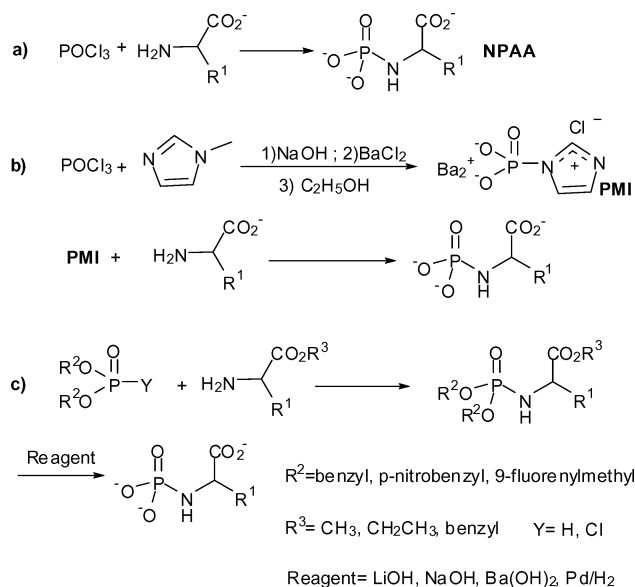
Inspired by a reactivity study between sodium trimetaphosphate (P₃m) and amino acids in prebiotic chemistry, a one-step reaction with efficient purification procedure in aqueous media has been developed for the synthesis of *N*-phosphono-amino acids (NPAA). P₃m was used to phosphorylate amino acids to NPAA with yields of 60–91%. The by-products, inorganic polyphosphates, were recycled to regenerate the phosphorylation reagent P₃m.

Introduction

Amino acid derivatives of phosphoramidates are an important class of compounds. *N*-Dialkyloxyphosphoryl amino acids showed the ability for both peptide and nucleic acid oligomerization and have been proposed as a coupling species in prebiotic chemistry.¹ *N*-Mononucleoside phosphoryl amino acids are multifunctional prodrugs of nucleotide analogues.² *N*-Phosphono-amino acids (NPAA) are non-esterified phosphoramidates. It has been found that they are potential inhibitors of some enzymes³ and phosphoryl donors to biomolecules.⁴ Additionally, NPAA are one of the suggested species existing in the prebiotic reaction of polyphosphates with amino acids.⁵ Elucidating the similarities and differences between NPAA and their counterparts, *N*-dialkyloxyphosphoryl amino acids, will be of great interest in aspects of peptide and nucleic acid oligomerization related to prebiotic chemistry.

Because of their acid-lability, syntheses of NPAAs have been limited to three categories, namely: use of highly-reactive POCl₃ as phosphorylation reagent followed by neutralization with strong base and repeated recrystallization for purification⁶ (Scheme 1a); a mild-reactive strategy using *N*-phosphoryl *N'*-methylimidazole (PMI) barium salts as phosphorylation reagents (prepared using POCl₃ and *N'*-methylimidazole⁷ (Scheme 1b); and a protection-deprotection strategy, the current prevailing method, whereby amino acid esters are phosphorylated by dialkyl phosphite/CCl₄ or dialkyl phosphorochloridate in organic solvent and deprotection by base or hydrogenolysis⁸ (Scheme 1c).

Trimetaphosphate (P₃m), known to exist in volcanic products,⁹ has been suggested as a probable phosphorylation reagent for bioorganic compounds and a coupling reagent for oligomerization of amino acids and nucleosides in prebiotic chemistry.^{5,10} It's worth noting that NPAA have been detected



Scheme 1 Literature methods for the synthesis of *N*-phosphono-amino acids.

in the reaction of P₃m with amino acids.⁵ In this paper, we would like to report the green chemistry-related direct synthesis of NPAA by amino acids and P₃m.

By optimizing the reaction of P₃m with amino acids in aqueous solution, a series of *N*-phosphono-amino acids were synthesized with yields of 60–91% and inorganic polyphosphate was recycled to regenerate P₃m.

Results and discussion

The general procedure is as follows: each amino acid was reacted with P₃m (1:1.2) in distilled water at 35–45 °C and at a fixed pH (Table 1), maintained by a real-time pH controller coupled to a sodium hydroxide solution dropping device. Taking serine as an example, in the ³¹P NMR spectra P₃m shows a distinct signal at –21.01 ppm, which will disappear as it is converted into other products, *N*-phosphono-serine (8.46 ppm), pyrophosphate (–5.18 ppm), and tripolyphosphate (–4.76 and –19.03 ppm). The ¹H-coupled ³¹P NMR spectra showed a

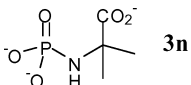
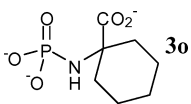
^aDepartment of Chemistry and Key Laboratory of Chemical Biology of Fujian Province, College of Chemistry and Chemical Engineering, Xiamen University, Xiamen, 361005, China.
 E-mail: yfzhao@xmu.edu.cn; Tel: +86 592 218 5610

^bKey Laboratory of Bioorganic Phosphorus Chemistry and Chemical Biology (Ministry of Education), Department of Chemistry, Tsinghua University, Beijing, 100084, P. R. China

Table 1 Synthesis of *N*-phosphono-amino acids, NPAA

2	3	Time (h)	Temp. (°C)	pH (±0.1)	Yield (%) ^a
Gly		16	45	11.4	60
Ala		24	45	11.3	63
Leu		20	40	11.2	84
Val		30	40	11.2	86
Ser		30	40	11.2	84 ^b
		15	35	10.7	90
Thr		16	35	11.8	75
Glu		20	35	11.3	91
Phe		35	40	10.8	64
Trp		40	45	11.0	89
Met		15	35	10.8	88
Pro		10	35	12.0	60
Arg		18	40	11.3	80
Homo serine		10	35	11.0	70

Table 2 Synthesis of *N*-phosphono-amino acids, NPAA

2	3	Time (h)	Temp. (°C)	pH (±0.1)	Yield (%) ^a
MeA	 3n			11.5	trace
cHex	 3o			11.5	no product

^a Calculation based on amino acids. ^b Recycled P₃m was used.

doublet signal at 8.46 ppm ($J_{\text{H,P}} = 7.7$ Hz) due to H_{α} -P coupling of *N*-phosphono-serine. ¹³C NMR spectra of the isolated *N*-phosphono-serine exhibited two doublet signals at 65.70 ppm (d, $^3J_{\text{C,P}} = 2.0$ Hz), 180.07 ppm (d, $^3J_{\text{C,P}} = 8.8$ Hz) attributed to C_β and the carbonyl carbon of *N*-phosphono-serine respectively.

Aliphatic amino acids (Gly, Ala, Leu, Val), aromatic amino acids (Phe, Trp), acidic amino acid (Glu), basic amino acid (Arg), hydroxy amino acids (Ser, Thr, Homoserine), sulfur-containing amino acid (Met), and Pro were each converted into the corresponding NPAA in reasonable yields by this method (Table 1). However, the amide amino acids (Gln, Asn) failed to give the expected products because of the instability of the amide side chain in alkali. Two sterically hindered, unnatural amino acids, 2-methylalanine (MeA) and 1-aminocyclohexanecarboxylic acid (cHex), also failed to give the expected products. To avoid peptide formation, phosphorylation of Gly and Ala was carried out at 0.1 M concentration.

Compared to the phosphorylation reagents in Scheme 1a–c, P₃m is a milder and more easily-handled reagent, being widely used as a food additive. In addition, this method is a one-step synthesis and is environmentally friendly, using water as the solvent. Consequently, it has many advantages over existing methods in the literature, especially for scale-up synthesis.

Recycling of polyphosphates

Due to the latent worldwide phosphate shortage, it is meaningful to recycle phosphates. In present work, the recycling of the by-products (pyrophosphate, triphosphate) was achieved by adjusting the mixture to pH to 4.18 and heating stepwise.¹¹ The regenerated P₃m with 96% purity was successfully put back into the synthesis of **3d**.

Purification and purity determination

In this paper, the isolation and purification of NPAA was tracked by ³¹P NMR. For example, serine was reacted with P₃m for 15 h and the reaction quenched with NaOH (A in Fig. 1). Then most of the pyrophosphate (−5.18 ppm) was precipitated by cooling the reaction mixture at 4 °C (B in Fig. 1).

For further purification, the reaction mixture was condensed and ethanol was added to the total solution (1:2 ratio) to remove the remaining triphosphate (−4.76 and −19.03 ppm) and pyrophosphate by cooling the H₂O/ethanol mixture at −10 °C¹² (C in Fig. 1). Finally, the pure *N*-phosphono-serine (8.46 ppm, D in Fig. 1) was precipitated as the sodium salt from the remaining solution by adding more ethanol, leaving unreacted amino acid in solution. The purity of the product was confirmed by ion-exchange chromatography.

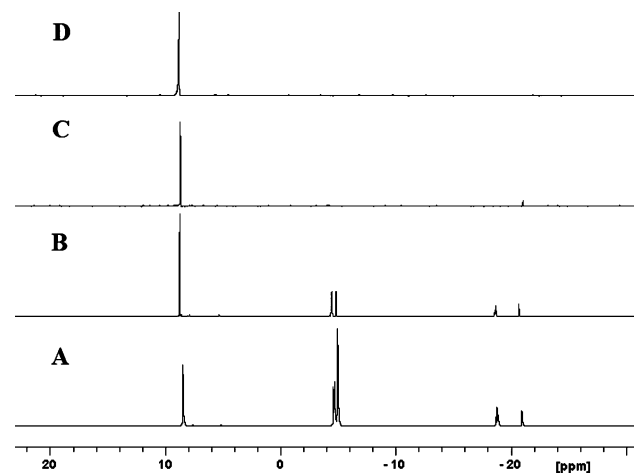
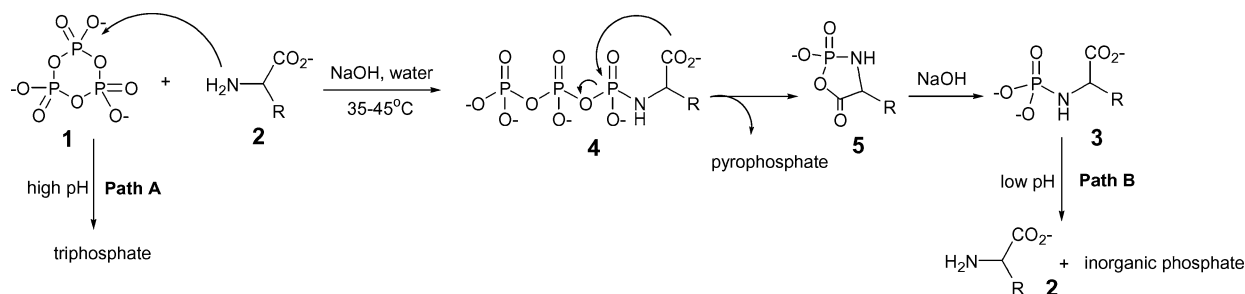


Fig. 1 ³¹P NMR monitoring the purification of *N*-phosphono-serine. **A**: Ser + P₃m (1:1.2), 35 °C, 15 h; **B**: Reaction mixture A concentrated and the precipitate removed; **C**: 1/2 volume of ethanol was added to reaction mixture B and the precipitate removed; **D**: the pure product *N*-phosphono-serine.

pH dependence of synthesis of NPAA

According to a reaction mechanism study of P₃m with amino acids,⁵ the reaction starts with deprotonation of the α-amino group of amino acid **2** in alkaline media followed by nucleophilic attack of NH₂ at phosphorus in P₃m. This leads to a P₃-AA intermediate **4** which fragments into a cyclic phosphoric-amino acid anhydride **5** and pyrophosphate. Intermediate **5** is converted



Scheme 2 Mechanism for *N*-phosphorylation of amino acids by P_3m .

into NPAA by ring-opening (Scheme 2). Control of pH is critical and delicate because higher pH results in hydrolysis of P_3m due to the high concentration of hydroxyl anion (**Path A**) while lower pH will cause NPAA to decompose into inorganic phosphate and amino acids (**Path B**).

Conclusions

In this paper, a one-step synthesis method for *N*-phosphono-amino acids in aqueous solution is described. A prebiotic phosphorylation reagent P_3m is used to phosphorylate thirteen amino acids. Compared with phosphorylation reagents in Scheme 1a–c, P_3m is cheaper, milder and a more easily-handled reagent and has significant advantages for scale-up synthesis. Moreover, the by-product pyrophosphate and triphosphate can be recycled to regenerate the reagent P_3m by filtration and heating. Finally, the critical prerequisite for successful synthesis is the accurate control of pH. The present work provides an example of learning from prebiotic synthesis and is within the scope of learning from nature.

Experimental

General procedure

Amino acid (15 mmol) and P_3m (18 mmol) were added to stirred distilled water (40 cm³) (for the synthesis of **3a** and **3b**, 150 cm³ 0.5 M pyrophosphate solution was used) at 35–45 °C. The pH was strictly maintained at the set pH (Table 1) by a real-time pH control coupled with a NaOH solution dropping device. After most of the P_3m had been consumed (monitored by ³¹P NMR), the reaction was quenched with 4 M NaOH solution (4 cm³). The reaction mixture was cooled to 4 °C and the precipitate (pyrophosphate) was filtered off and recovered. The filtrate was reduced to 20 cm³ volume under vacuum, then ethanol (10 cm³) was added and the solution stored at –10 °C for 10 h to precipitate excess triphosphate and residual pyrophosphate. According to the different properties of NPAA, one of the following two purification procedures was used. **a**) For the purification of **3a**, **3b**, **3e**, **3f**, **3g**, **3l** and **3m**, the filtrate comprised of two layers (underlayer was the oily crude NPAA), reduced to a volume of 10 cm³ and washed with ethanol (3 × 10 cm³). Finally, the oily NPAA was evaporated to dryness under reduced pressure to give the product as a white solid. **b**) For the purification of **3c**, **3d**, **3h**, **3i**, **3j** and **3k**, the homogeneous filtrate was reduced to a volume of 10 cm³ and mixed with methanol (20 cm³) to precipitate the NPAA which was filtered out and evaporated to

dryness under reduced pressure to give the product as a white solid. All the NPAAs are sensitive to moisture and should be kept in a dry environment. Their melting points are all above 300 °C.

¹H, ¹³C and ³¹P NMR spectra were recorded on a Bruker 400 MHz NMR spectrometer. ¹H NMR chemical shifts are relative to D₂O (δ = 4.70), ¹³C NMR chemical shifts are relative to CD₃OD (δ = 49.50 ppm), ³¹P NMR chemical shifts in D₂O were externally referenced to 85% H₃PO₄ (δ = 0.00 ppm).

Sodium salt of *N*-phosphono-glycine 3a. White solid; δ_H (400 MHz; D₂O; D₂O) 3.21(d, ³J_{P-H} = 6.4 Hz, 2H); δ_C(100 MHz; D₂O; CD₃OD) 46.27, 180.32(d, ³J_{C-P} = 11.8 Hz); δ_P(162 MHz; D₂O; 85% H₃PO₄) 8.29; ESI-MS *m/z* 221.8 [M + H].⁺

Sodium salt of *N*-phosphono-alanine 3b. White solid; δ_H (400 MHz; D₂O; D₂O) 1.15(d, ³J_{H-H} = 7.0 Hz, 3H), 3.38–3.46(m, 1H); δ_C(100 MHz; D₂O; CD₃OD) 20.74(d, ³J_{C-P} = 4.0 Hz), 52.06, 183.31(d, ³J_{C-P} = 8.4 Hz); δ_P(162 MHz; D₂O; 85% H₃PO₄) 8.13; ESI-MS *m/z* 235.8 [M + H].⁺

Sodium salt of *N*-phosphono-leucine 3c. White solid; δ_H (400 MHz; D₂O; D₂O) 0.79–0.82(m, 6H), 1.28–1.43(m, 2H), 1.45–1.55(m, 1H), 3.37–3.43(m, 1H); δ_C(100 MHz; D₂O; CD₃OD) 21.90, 22.80, 24.58, 45.22(d, ³J_{C-P} = 5.4 Hz), 56.47, 184.41(d, ³J_{C-P} = 5.2 Hz); δ_P(162 MHz; D₂O; 85% H₃PO₄) 7.77; ESI-MS *m/z* 277.9 [M + H].⁺

Sodium salt of *N*-phosphono-valine 3d. White solid; δ_H(400 MHz; D₂O; D₂O) 0.77–0.80(m, 6H), 1.71–1.80(m, 1H), 3.21(dd, ³J_{H-H} = 5.0 Hz, ³J_{H-P} = 10.71 Hz, 1H); δ_C(100 MHz; D₂O; CD₃OD) 18.17, 18.27, 32.53(d, ³J_{C-P} = 6.3 Hz), 62.66, 183.08(d, ³J_{C-P} = 3.7 Hz); δ_P(162 MHz; D₂O; 85% H₃PO₄) 8.35; ESI-MS *m/z* 263.9 [M + H].⁺

Sodium salt of *N*-phosphono-serine 3e. White solid; δ_H(400 MHz; D₂O; D₂O) 3.50–3.57(m, 2H), 3.66–3.71(m, 1H); δ_C(100 MHz; D₂O; CD₃OD) 58.99, 65.70(d, ³J_{C-P} = 2.0 Hz), 180.07(d, ³J_{C-P} = 8.8 Hz); δ_P(162 MHz; D₂O; 85% H₃PO₄) 7.93; ESI-MS *m/z* 251.8 [M + H].⁺

Sodium salt of *N*-phosphono-threonine 3f. White solid; δ_H(400 MHz; D₂O; D₂O) 1.01(d, ³J_{H-H} = 6.3 Hz, 3H), 3.20(dd, ³J_{H-H} = 7.2 Hz, ³J_{P-H} = 8.9 Hz, 1H), 3.57–3.64(m, 1H); δ_C(100 MHz; D₂O; CD₃OD) 18.61, 64.15, 71.40(d, ³J_{C-P} = 3.5 Hz), 180.61(d, ³J_{C-P} = 6.9 Hz); δ_P(162 MHz; D₂O; 85% H₃PO₄) 7.87; ESI-MS *m/z* 265.9 [M + H].⁺

Sodium salt of *N*-phosphono-glutamic acid 3g. White solid; δ_H(400 MHz; D₂O; D₂O) 1.62–1.80(m, 2H), 1.94–2.12(m, 2H),

3.34–3.39(m, 1H); δ_c (100 MHz; D₂O; CD₃OD) 32.13 (d, $^3J_{C-P}$ = 4.9 Hz), 33.81, 57.07, 182.89(d, $^3J_{C-P}$ = 5.3 Hz), 183.50; δ_p (162 MHz; D₂O; 85% H₃PO₄) 7.80; ESI-MS m/z 315.8 [M + H].⁺

Sodium salt of *N*-phosphono-phenylalanine 3h. White solid; δ_H (400 MHz; D₂O; D₂O) 2.71–2.76(m, 1H), 3.03–3.08(m, 1H), 3.66–3.71(m, 1H), 7.12–7.27(m, 5H); δ_c (100 MHz; D₂O; CD₃OD) 41.28(d, $^3J_{C-P}$ = 3.7 Hz), 59.07, 126.28, 128.31, 129.67, 138.73, 182.22(d, $^3J_{C-P}$ = 7.4 Hz); δ_p (162 MHz; D₂O; 85% H₃PO₄) 7.36; ESI-MS m/z 311.9 [M + H].⁺

Sodium salt of *N*-phosphono-tryptophan 3i. White solid; δ_H (400 MHz; D₂O; D₂O) 2.91–2.97(m, 1H), 3.16–3.20(m, 1H), 3.70–3.76(m, 1H), 7.00–7.68(m, 4H), 7.16(s, 1H); δ_c (100 MHz; D₂O; CD₃OD) 30.70(d, $^3J_{C-P}$ = 3.7 Hz), 58.00, 111.09, 111.47, 118.78, 119.26, 121.43, 124.11, 127.55, 135.86, 183.01(d, $^3J_{C-P}$ = 7.2 Hz); δ_p (162 MHz; D₂O; 85% H₃PO₄) 7.68; ESI-MS m/z 351 [M + H].⁺

Sodium salt of *N*-phosphono-methionine 3j. White solid; δ_H (400 MHz; D₂O; D₂O) 1.77–1.86(m, 2H), 2.01(s, 3H), 2.34–2.40(m, 1H), 2.43–2.49(m, 1H), 3.44–3.50(m, 1H); δ_c (100 MHz; D₂O; CD₃OD) 14.11, 29.24, 34.99 (d, $^2J_{C-P}$ = 3.7 Hz), 56.83, 182.44(d, $^3J_{C-P}$ = 6.4 Hz); δ_p (162 MHz; D₂O; 85% H₃PO₄) 7.78; ESI-MS m/z 295.9 [M + H].⁺

Sodium salt of *N*-phosphono-proline 3k. White solid; δ_H (400 MHz; D₂O; D₂O) 1.55–1.70(m, 3H), 1.94–2.02(m, 1H), 2.96–3.07(m, 2H), 3.78–3.83(m, 1H); δ_c (100 MHz; D₂O; CD₃OD) 25.24(d, $^3J_{C-P}$ = 5.6 Hz), 32.36(d, $^3J_{C-P}$ = 4.7 Hz), 48.54, 62.78(d, $^3J_{C-P}$ = 3.3 Hz), 185.82(d, $^3J_{C-P}$ = 4.9 Hz); δ_p (162 MHz; D₂O; 85% H₃PO₄) 10.738; ESI-MS m/z 261.9 [M + H].⁺

Sodium salt of *N*-phosphono-arginine 3l. White solid; δ_H (400 MHz; D₂O; D₂O) 1.31–1.62(m, 4H), 2.96–3.03(m, 2H), 3.37–3.42(m, 1H); δ_c (100 MHz; D₂O; CD₃OD) 23.69, 31.87(d, $^3J_{C-P}$ = 3.8 Hz), 41.07, 56.55, 156.98, 182.71(d, $^3J_{C-P}$ = 7.1 Hz); δ_p (162 MHz; D₂O; 85% H₃PO₄) 7.73 ESI-MS m/z 320.8 [M + H].⁺

Sodium salt of *N*-phosphono-homoserine 3m. White solid; δ_H (400 MHz; D₂O; D₂O) 1.53–1.61(m, 1H), 1.78–1.87(m, 1H), 3.45–3.55(m, 2H), 3.62–3.69(m, 1H); δ_c (100 MHz; D₂O; CD₃OD) 36.96(d, $^3J_{C-P}$ = 3.6 Hz), 54.74, 58.90, 183.07(d, $^3J_{C-P}$ = 5.2 Hz); δ_p (162 MHz; D₂O; 85% H₃PO₄) 8.11; ESI-MS m/z 265.8 [M + H].⁺

Acknowledgements

We acknowledge financial support from the Ministry of Science and Technology (2006DFA43030), and the Chinese National Natural Science Foundation (20572061 and 20732004).

References

- C. M. Cheng, X. H. Liu, Y. M. Li, Y. Ma, B. Tan, R. Wan and Y. F. Zhao, *Origins Life Evol. Biosphere*, 2004, **34**, 455–64.
- (a) D. P. Drontle and C. R. Wagner, *Mini-Rev. Med. Chem.*, 2004, **4**, 409–419; (b) S. J. Hecker and M. D. Erion, *J. Med. Chem.*, 2008, **51**, 2328–2345; (c) O. Adelfinskaya and P. Herdewijn, *Angew. Chem. Int. Ed.*, 2007, **46**, 4356–4358.
- (a) D. W. Christianson and W. N. Lipscomb, *J. Am. Chem. Soc.*, 1988, **110**, 5560–5565; (b) C. E. Rodriguez, H. Lu, A. R. Martinez, A. Brunelle and C. E. Berkman, *J. Enzym. Inhib.*, 2001, **16**, 359–365; (c) J. Maung, J. P. Mallari, T. A. Girtsman, L. Y. Wu, J. A. Rowley, N. M. Santiago, A. Brunelle and C. E. Berkman, *Bioorg. Med. Chem.*, 2004, **12**, 4969–4979.
- (a) H. L. Auleb, M. J. Dowler and H. I. Nakada, *Biochem. Biophys. Res. Commun.*, 1966, **23**, 280–286; (b) A. Fujimoto and R. A. Smith, *J. Biol. Chem.*, 1960, **235**, PC44–PC45.
- (a) N. M. Chung, R. Lohrmann, L. E. Orgel and J. Rabinowitz, *Tetrahedron*, 1971, **27**, 1205–1210; (b) H. Inoue, Y. Baba, T. Furukawa, Y. Maeda and M. Tsuhako, *Chem. Pharm. Bull.*, 1993, **41**, 1895–1899.
- T. Winnick and E. M. Scott, *Arch. Biochem.*, 1947, **12**, 201–208.
- (a) E. Jampel, M. Wakselman and M. Vilkas, *Tetrahedron Lett.*, 1968, **31**, 3533–3536; (b) S. Sheffer-Dee-Noor and T. Baasov, *Bioorg. Med. Chem. Lett.*, 1993, **3**, 1615–1618.
- (a) S. O. Li and R. E. Eakin, *J. Am. Chem. Soc.*, 1955, **77**, 1866–1870; (b) L. Zervas and P. G. Katsoyannis, *J. Am. Chem. Soc.*, 1955, **77**, 5351–5353; (c) L. Zervas and I. Dilaris, *J. Am. Chem. Soc.*, 1955, **77**, 5354–5357; (d) C. M. Kam, N. Nishino and J. C. Powers, *Biochemistry*, 1979, **18**, 3032–3038; (e) H. Y. Lu, R. J. Ng, C. C. Shieh, A. R. Martinez and C. E. Berkman, *Phosphorus, Sulfur Silicon Relat. Elem.*, 2003, **178**, 17–32; (f) L. Y. Wu and C. E. Berkman, *Tetrahedron Lett.*, 2005, **46**, 5301–5303.
- Y. Yamagata, H. Watanabe, M. Saitoh and T. Namba, *Nature*, 1991, **352**, 516–519.
- (a) J. Rabinowitz, J. Flores, R. Krebsbach and G. Rogers, *Nature*, 1969, **224**, 795–796; (b) A. W. Schwartz, *J. Chem. Soc. Chem. Commun.*, 1969, **23**, 1393; (c) R. Saffhill, *J. Org. Chem.*, 1970, **35**, 2881–2883; (d) M. Tsuhako, M. Fujimoto, S. Ohashi, H. Nariai and I. Motooka, *Bull. Chem. Soc. Jpn.*, 1984, **57**, 3274–3280; (e) J. Yamanaka, K. Inomata and Y. Yamagata, *Origins Life Evol. Biosphere*, 1988, **18**, 165–167; (f) Y. Yamagata, H. Inoue and K. Inomata, *Origins Life Evol. Biosphere*, 1995, **25**, 47–52.
- Dissolved the recovered polyphosphates in water and adjusted the pH to 4.18 by phosphoric acid, then the mixture was evaporated under vacuum to dryness and maintained at 105 °C for 1 h, then 553 °C for 5 h, cooling it slowly to rt.
- I. S. Kulaev, V. M. Vagabov, and T. V. Kulakovskaya, *The Biochemistry of Inorganic Polyphosphates*, John Wiley and sons, 2nd edn., 2004, ch. 1, pp. 10.

A recyclable triethylammonium ion-tagged diphenylphosphine palladium complex for the Suzuki–Miyaura reaction in ionic liquids†

Marco Lombardo,* Michel Chiarucci and Claudio Trombini

Received 5th September 2008, Accepted 19th January 2009

First published as an Advance Article on the web 17th February 2009

DOI: 10.1039/b815568b

Suzuki–Miyaura reactions of aryl bromides and arylboronic acids proceed in good to excellent yields in a pyrrolidinium ionic liquid by using a preformed air stable and easily handled triethylammonium-tagged diphenylphosphine palladium(II) complex (**2**). The reaction requires short reaction times and mild temperature conditions and does not show any tendency towards the formation of palladium black. After extraction of the product, the catalyst containing ionic liquid phase is easily recycled for 6 times, with no significant loss of catalytic activity.

Introduction

The use of the Suzuki–Miyaura (SM) reaction¹ in the challenging field of the synthesis of biaryls and of natural and bioactive products characterized by the presence of Csp²–Csp² single bonds, has recorded a huge growth over the last few years.² An attractive feature of the SM reaction is that a large number of forms of palladium can be used as precatalyst.^{3–7} A further element of flexibility of the SM reaction is the wide choice of solvent/base combinations available,^{3,5} including solvent-free protocols under microwave irradiation.⁸ Despite the tolerance of a broad range of functional groups and reaction conditions, the cost of palladium and environmental regulations urge to develop procedures which minimize metal loading and leaching.

Catalyst recyclability and metal leaching issues can be addressed in two ways. The first one involves metal immobilization on a solid support,^{5–7} a strategy that not only reduces product contamination but also allows the use of inherently less wasteful flow-through technologies.⁹

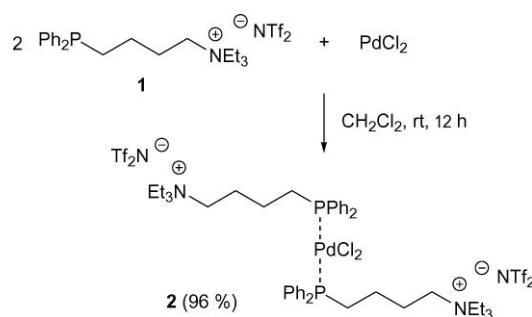
The second approach makes use of extremely low loadings of metal. The “active form of palladium” is considered to be a mononuclear Pd(0) entity which originates from the precatalyst. However, on heating, the mononuclear Pd(0) species tends to cluster and, eventually, to precipitate as inactive palladium black, unless highly diluted conditions are used.¹⁰ Active Pd nanoparticles can also be produced in environments capable of stabilizing them *via* coordination or electrostatic interactions that inhibit their aggregation.¹¹ Task-specific ionic liquids (TSILs), for example nitrile-functionalized imidazolium salts, have been proposed by Dyson *et al.* as excellent nanoparticles stabilizers.¹² TSIL-stabilized nanoparticles are supposed to act as a reservoir of catalytically active mononuclear Pd(0) species.¹³

As solvents for the SM reaction, ionic liquids (ILs) have been extensively used for Pd-catalyzed cross coupling reactions.¹⁴

In particular, enhanced reactivity and an increased catalyst stability were recorded in imidazolium based ILs, compared to conventional molecular solvents.¹⁵

Results and discussion

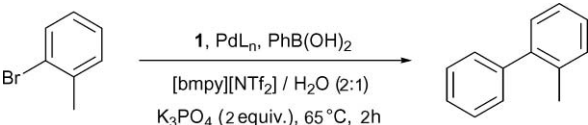
Within this field we committed ourselves to the design of a multiphase homogeneous catalytic system for the SM reaction, and focused the attention to the thermoregulated biphasic system consisting of 1-butyl-1-methyl-pyrrolidinium bis(trifluoromethylsulfonyl)imide ([bmpy][NTf₂]) and water. This system is heterogeneous at 25 °C, and when heated at 65 °C, it becomes a homogeneous phase where the SM reaction can be carried out. Eventually, upon cooling the mixture to rt, the system turns heterogeneous. In principle, the IL phase can be extracted, delivering the coupling product, for instance, in pentane. Then, it could be washed with water to remove the inorganic salts. If palladium is confined into the IL phase thanks to the ion-tagged ligand, an efficient multiphase homogeneous catalytic protocol will become available. The rational approach adopted was to incorporate a tetralkyl ammonium tag on a phosphine capable of binding the Pd catalyst and to confine it into the IL phase.¹⁶ After a preliminary screening of the carbon chain length, we chose ligand **1** to prepare the air stable Pd complex **2**, which could be directly used as the pre-catalyst of the SM reaction (Scheme 1).¹⁷



Scheme 1

Dipartimento di Chimica “G. Ciamician”, Università di Bologna, via Selmi 2, 40126, Bologna, Italy. E-mail: marco.lombardo@unibo.it; Fax: +39 051 2099456; Tel: +39 051 2099544

† Electronic supplementary information (ESI) available: ¹H-NMR, ¹³C-NMR and GC-MS spectra for all compounds reported. See DOI: 10.1039/b815568b

Table 1 Effect of palladium source and metal/ligand ratio


Entry	PdL _n , mol%	1 (mol%)	Yield (%) ^a
1	Pd ₂ (dba) ₃ , 1	2	—
2	Pd(OAc) ₂ , 1	2	79
3	PdCl ₂ , 1	2	92
4	PdCl ₂ , 1	1	60
5	PdCl ₂ , 1	3	—

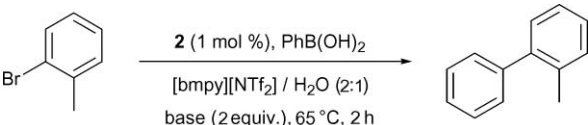
^a Isolated yields after purification by flash-chromatography on silica.

Using the cross-coupling of *o*-bromotoluene and phenyl boronic acid as the benchmark reaction, a preliminary optimization study was carried out. The effect of the palladium source and the palladium/ligand ratio on reactivity was evaluated using [bmpy][NTf₂] as the solvent (Table 1).

The catalytically active species is efficiently stabilized using a 1 : 2 palladium/ligand ratio, since the formation of Pd black, even after prolonged heating at 65 °C, is never observed. While Pd₂(dba)₃ failed to afford the desired product, PdCl₂ revealed itself as a better source of Pd than Pd(OAc)₂ (Table 1, Entries 1–3). By changing the metal/ligand ratio to 1 : 1, the formation of Pd black was rapidly observed and the yield dropped significantly (Entry 4). Using a 1 : 3 palladium/ligand ratio did not result in formation of Pd black, but the catalytic system became totally inactive (Entry 5). These results are in good agreement with the observation that the active catalyst in many palladium mediated transformations is a monoligated species derived from the initial loss of a phosphine ligand from the precatalyst.¹⁸

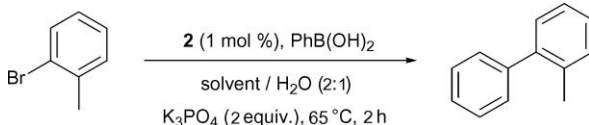
PdCl₂ and the ligand can be directly mixed in 1 : 2 ratio in the reaction flask. However, essentially the same results are obtained using the preformed L₂-PdCl₂ complex **2**. We continued the optimization study using the preformed complex **2**, since it is more practical to handle than the free ligand **1**.

In Table 2 the results obtained with different inorganic bases are reported. Yields strongly depended on the base used, K₃PO₄ being more effective as a base than K₂CO₃ and Na₂CO₃ (Table 2, Entries 1–3). This order of reactivity can be possibly ascribed to the greater solubility of K₃PO₄ in H₂O.

Table 2 Effect of the base


Entry	Base	Yield (%) ^a
1	Na ₂ CO ₃	57
2	K ₂ CO ₃	79
3	K ₃ PO ₄	94

^a Isolated yields after purification by flash-chromatography on silica.

Table 3 Effect of the solvent


Entry	Solvent	Yield (%) ^a
1	THF	—
2	CH ₃ CN	12
3	[mC ₁ CNpy][NTf ₂] ^b	—
4	[P(6,6,6,14)][Cl] ^c	—
5	[bmpy][OTf] ^d	39
6	[bmpy][NTf ₂] ^e	93
7	[bmim][NTf ₂] ^f	87

^a Isolated yields after purification by flash-chromatography on silica.

^b 1-Cyanomethyl-pyridinium bis(trifluoromethylsulfonyl) imide. ^c Trihexyl-tetradecyl-phosphonium chloride. ^d 1-Butyl-1-methyl-pyrrolidinium triflate. ^e 1-Butyl-1-methyl-pyrrolidinium bis(trifluoromethylsulfonyl) imide. ^f 1-Butyl-3-methyl-imidazolium bis(trifluoromethylsulfonyl) imide.

Using these preliminary optimized conditions, we tested several organic solvents and ionic liquids (Table 3). At 65 °C the reaction mixture is a single-phase homogeneous system, even in the case of ILs insoluble in water (Table 3, Entries 3,6,7).

THF and CH₃CN afforded disappointing results (Table 3, Entries 1,2). While the complex **2** is only sparingly soluble in THF, it dissolves completely in CH₃CN. In both cases, however, formation of Pd black is observed after heating the reaction mixture at 65 °C.

The reactivity of the catalytic system is completely suppressed if a nitrile-functionalized ionic liquid (Entry 3) or an ionic liquid with a coordinating counter anion (Entry 4) is used. Using 1-butyl-1-methyl-pyrrolidinium ionic liquids, the effect of the counter anion on the reactivity is apparent (Entries 5,6), with bis(trifluoromethylsulfonyl) imide giving much better results than triflate. When the 1-butyl-3-methyl-imidazolium cation is used (Entry 7), a slightly lower yield is obtained.

From these results, [bmpy][NTf₂] was selected as the solvent of choice, also considering that imidazolium-based ILs could produce mixed phosphine/*N*-heterocyclic carbene complexes (NHC).¹¹ Moreover, NTf₂⁻, chosen as the anion of both the catalyst and the IL, confers them the lowest solubility in H₂O and in pentane, a property necessary to separate biaryls and water soluble co-products from the catalyst-containing IL phase.

The effect of the temperature on the catalytic system under the conditions used in Entry 6 of Table 3 is reported in Fig. 1. To obtain good conversion in short reaction times a temperature above 40 °C is needed, while the product is formed only very slowly at room temperature (25 °C).

Finally, we tested different aryl electrophiles with boronic acids and, surprisingly, the order of reactivity was ArBr > ArI ≫ ArOTf, while ArCl are not reactive under the reaction conditions tested (Fig. 2).

Initial slopes in Fig. 2 suggest the presence of an induction effect, particularly for aryl triflates and iodides. Since the aromatic electrophile is added pure as the last reagent to the reaction mixture, the induction time observed reflects, in our

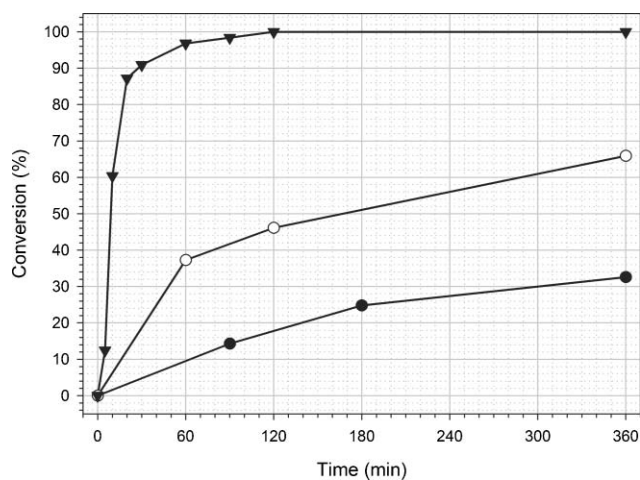


Fig. 1 Effect of temperature on conversion. ▼: 65 °C; ○: 40 °C; ●: 25 °C using reaction conditions reported in Table 3, Entry 6.

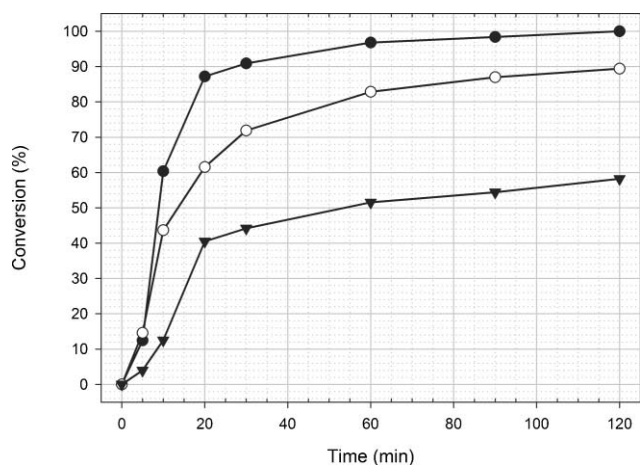


Fig. 2 Comparison of reactivity between aryl bromides (●), iodides (○) and triflates (▼) using reaction conditions reported in Table 3, Entry 6.

opinion, a slow mass transfer rate of the aryl triflate or halide in this viscous reaction medium.

In order to evaluate the possible effect of anion exchange with [bmpy][NTf₂] on reaction rates, we performed a series of experiments using the same conditions reported in Entry 6 of Table 3, but adding 1 equivalent of different potassium salts to the reaction mixtures. The results obtained are reported in Fig. 3.

The addition of 1 equivalent of KI considerably reduced the reaction rate, while a much smaller effect is observed in the case of KBr. Thus, the lower reactivity of aryl iodides with respect to bromides can be explained by considering that the corresponding potassium halide salts are formed during the course of the reaction. Conversely, the decrease of reaction rate due to the addition of 1 equivalent of KOTf cannot alone explain the much lower reactivity of triflates. Moreover, no trace of [bmpy][OTf] deriving from anion exchange was apparent by NMR analyses of the ionic liquid after the reaction work-up.

On the basis of these observations, a reference protocol was derived based on the use of 1 mol% of Pd in the form of L₂·PdCl₂ complex **2**, which was applied to a number of aryl bromide/aryl

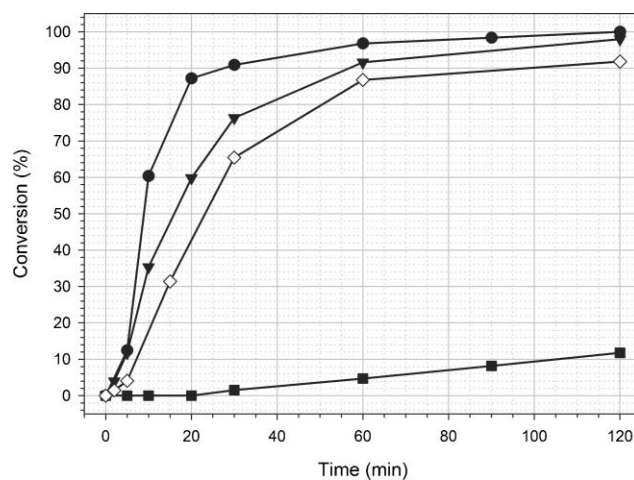


Fig. 3 Comparison of reaction rates without adding salts (●), by adding 1 equiv. of KBr (▼), 1 equiv. of KOTf (◇) and 1 equiv. of KI (■) using reaction conditions reported in Table 3, Entry 6.

boronic acid pairs in [bmpy][NTf₂] as the solvent at 65 °C for 2 h, as outlined in Table 4.

Good to excellent results were confirmed for aryl bromides and boronic acids containing electron-withdrawing or electron-donating groups. In particular, *o*-bromobenzonitrile and *p*-methyl phenylboronic acid (Table 4, Entry 6) afforded 97% of a coupled product which is a known intermediate for the synthesis of angiotensin II receptor antagonists.¹⁹ The time dependence study of the reaction conversions shows that the highest rates are recorded at the beginning of the reaction, in contrast to other catalytic Pd systems in ILs which present induction periods.²⁰ Irrespective of the true identity of the catalyst, a point of strength of this reaction protocol is the catalyst recyclability, which is ensured by the strong interaction between the ligand **1** and the IL, both being quaternary ammonium ions. Fig. 4 shows the results of six consecutive cycles carried out under identical conditions reported in Table 4, Entry 1, and no significant change in the catalytic activity and the reaction rates is observed.

Lowering the Pd loading is a further way to check catalyst activity. The reaction reported in Entry 1 of Table 4 was carried

Table 4 Suzuki coupling using ligand **2**

Entry	Ar ¹	Ar ²	Yield (%) ^a
1	Ph	2-Me-Ph	92
2	Ph	4-MeO-Ph	89
3	2-Me-Ph	2-Me-Ph	89
4	2-Me-Ph	1-Naphthyl	99
5	2-Me-Ph	4-Ph-Ph	99
6	4-Me-Ph	2-CN-Ph	97
7	3-NO ₂ -Ph	2-Me-Ph	86
8	4-MeO-Ph	1-Naphthyl	98
9	4-MeO-Ph	4-MeO-Ph	93
10	4-MeO-Ph	4-Ph-Ph	84
11	4-MeO-Ph	2-Me-Ph	89
12	4-MeO-Ph	2-CN-Ph	92

^a Isolated yields after purification by flash-chromatography on silica.

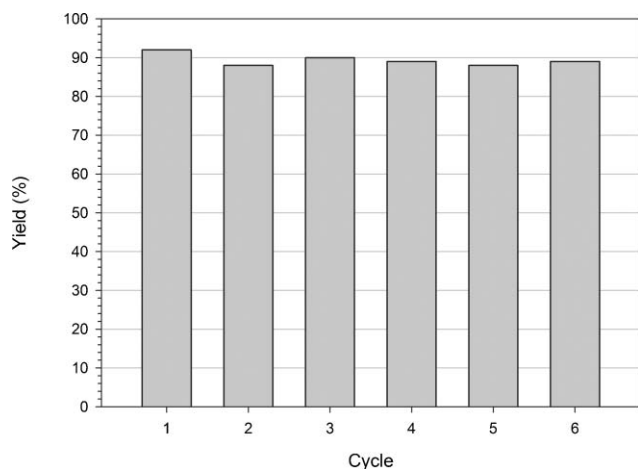


Fig. 4 Results of six consecutive cycles adopting conditions described in Table 4, Entry 1.

out using two different catalyst loadings, 0.1 and 0.01 mol% of Pd, respectively. The first reaction, run for 6 h at 65 °C, gave an 81% yield, with a TON of 810 and a TOF of 135 h⁻¹. In the second reaction, after 1.5 h at 95 °C, a 78% yield was recorded, corresponding to a TON of 7800 and a TOF of 5200 h⁻¹.

Finally, preliminary analyses of palladium contents in the organic phase extracts by atomic-absorption spectroscopy (AAS), showed that <10 ppb of the metal was released from the IL into the product during recycling. This value is very promising in terms of metal leaching and more detailed studies will be published in due course.

Conclusions

In conclusion, we showed that the triethylammonium tagged complex **2** provides a highly active catalyst for the SM reaction of aryl bromides in an IL. Formation of Pd black was never observed and the catalyst-containing IL phase could be recycled six times without substantial decrease of catalytic activity.

Experimental

Synthesis of the ionic liquids

All ionic liquids used were synthesized and purified according to known procedures.²¹

Synthesis of the catalyst

4-Bromobutyl-triethyl-ammonium bromide. Triethylamine (2.8 mL, 20 mmol) is added to 1,4-dibromobutane (7.1 mL, 60 mmol) and the solution is stirred for 2–3 h at 70–80 °C. The resulting suspension is cooled to 0 °C, the solid is collected by filtration and washed with EtOAc. 4-Bromobutyl-triethyl-ammonium bromide is obtained as an hygroscopic white solid (5.91 g, 18.7 mmol, 93%). ¹H-NMR (300 MHz, CDCl₃) δ = 1.40 (t, *J* = 7.2 Hz, 9 H), 1.86–1.99 (m, 2 H), 1.99–2.11 (m, 2 H), 3.43–3.60 (m, 10 H). ¹³C-NMR (75 MHz, CDCl₃) δ = 7.1, 19.4, 27.9, 32.0, 52.4, 55.4. Anal. Calcd for C₁₀H₂₃Br₂N (317.10): C, 37.88; H, 7.31; N, 4.42. Found: C, 37.76; H, 7.33; N, 4.41.

4-Diphenylphosphinobutyl-triethyl-ammonium bromide. *n*-BuLi (1 mL, 2.5 M in cyclohexane) is slowly added at 0 °C to a solution of Ph₂PH (350 μl, 2.48 mmol) in THF (1 mL). The orange solution is allowed to reach room temperature and further stirred for 30 min. The solution of Ph₂PLi is slowly added *via* syringe at 0 °C to a suspension of 4-bromobutyl-triethyl-ammonium bromide (0.66 g, 2.07 mmol) in THF (2 mL). The colorless suspension is allowed to reach room temperature and further stirred for 2 h. The reaction is quenched by adding water (2 mL), the organic solvent is evaporated the residue is extracted with CH₂Cl₂. The combined organic phases are washed with water, dried (Na₂SO₄) and evaporated under reduce pressure. The solid obtained is washed with Et₂O to afford the title compound as a white solid (0.753 g, 1.78 mmol, 86%). ¹H-NMR (300 MHz, CDCl₃) δ = 1.36 (t, *J* = 7.2 Hz, 9 H), 1.48–1.66 (m, 2 H), 1.78–1.94 (m, 2 H), 2.16 (t, *J* = 7.4 Hz, 2 H), 3.19–3.30 (m, 2 H), 3.49 (q, *J* = 7.2 Hz, 6 H), 7.24–7.57 (m, 10 H). ¹³C-NMR (75 MHz, CDCl₃) δ = 7.3, 22.2, 26.3, 26.5, 52.7, 56.2, 127.5, 127.6, 127.8, 127.8, 128.0, 129.8, 129.9, 130.0, 130.0, 130.9, 131.0, 131.7, 131.8, 132.0, 137.1, 137.3. Anal. Calcd for C₂₂H₃₃BrNP (422.38): C, 62.56; H, 7.87; N, 3.32. Found: C, 62.68; H, 7.85; N, 3.31.

4-Diphenylphosphinobutyl-triethyl-ammonium bis(trifluoromethylsulfonyl) imide (1). LiNTf₂ (0.474 g, 1.65 mmol) is added to a solution of 4-diphenylphosphinobutyl-triethyl-ammonium bromide (0.633 g, 1.5 mmol) in water (1 mL) and the reaction mixture is vigorously stirred at room temperature for 12 h. The solution is extracted with CH₂Cl₂ and the combined organic phases are washed with water until no bromide is detected by the AgNO₃ test. The combined organic phases are dried (Na₂SO₄) and CH₂Cl₂ is removed at reduced pressure to afford the title compound as a viscous liquid (0.793 g, 1.28 mmol, 85%). **1** can be further purified through a short pad of neutral alumina and of decolorizing charcoal, eluting with CH₂Cl₂. ¹H-NMR (300 MHz, CDCl₃) δ = 1.26 (t, *J* = 7.1 Hz, 9 H), 1.36–1.64 (m, 2 H), 1.64–1.92 (m, 2 H), 2.12 (t, *J* = 7.5 Hz, 2 H), 2.92–3.12 (m, 2 H), 3.21 (q, *J* = 7.1 Hz, 6 H), 7.28–7.86 (m, 10 H). ¹³C-NMR (75 MHz, CDCl₃) δ = 7.4, 22.7, 26.9, 27.1, 53.1, 56.8, 117.7, 122.0, 128.6, 128.6, 128.7, 128.8, 128.9, 129.0, 130.6, 130.8, 132.5, 132.6, 132.6, 132.8, 137.7, 137.9. Anal. Calcd for C₂₄H₃₃F₆N₂O₄PS₂ (622.62): C, 46.30; H, 5.34; N, 4.50. Found: C, 46.42; H, 5.35; N, 4.52.

Complex 2. PdCl₂ (0.044 g, 0.25 mmol) is added to a solution of ligand **1** (0.311 g, 0.5 mmol) in CH₂Cl₂ (1 mL) and the suspension is stirred at room temperature for 12 h, until a clear solution is obtained. The solution is filtered through a short pad of Celite[®] and the solvent is evaporated at reduced pressure to afford **2** as a yellow solid (0.338 g, 0.24 mmol, 95%). ¹H-NMR (300 MHz, CD₃CN) δ = 1.16 (t, *J* = 6.4 Hz, 18 H), 1.46–1.83 (m, 8 H), 2.43–2.54 (m, 4H), 2.88–3.04 (m, 4 H), 3.04–3.17 (m, 12 H), 7.29 (t, *J* = 7.0 Hz, 2 H), 7.39–7.59 (m, 12 H), 7.67–7.77 (m, 6 H). ¹³C-NMR (75 MHz, CD₃CN) δ = 7.8, 22.4, 23.3, 23.4, 23.4, 23.6, 23.7, 23.7, 24.9, 25.1, 25.3, 53.8, 57.2, 118.9, 123.1, 129.4, 129.5, 129.6, 129.7, 129.7, 129.9, 130.2, 130.3, 130.6, 130.9, 131.2, 131.5, 131.7, 132.0, 132.4, 132.8, 132.8, 134.2, 134.3, 134.4, 134.5, 134.6, 134.7. Anal. Calcd for C₅₀H₇₂Cl₂F₁₂N₄O₈P₂S₄ (1452.64): C, 41.34; H, 5.00; N, 3.86. Found: C, 41.37; H, 5.04; N, 3.88.

Optimized general procedure for the Suzuki coupling (Table 4, Entry 1)

Reactions have to be conducted under argon. In the presence of air, biphenyl, the homocoupling product of boronic acid, is formed up to ~15%, while in the absence of air it is limited to less than 2%.²² Complex **2** (14.5 mg, 0.01 mmol) is added to [bmpy][NTf₂] (1 mL) and the yellow solution is stirred at 65 °C for a few minutes. Phenylboronic acid (0.183 g, 1.5 mmol), K₃PO₄ (0.424 g, 2 mmol) and degassed water (0.5 mL) are added to the solution. After a few minutes, an orange homogeneous solution is formed. 2-Methyl-bromobenzene (0.12 mL, 1 mmol) is added to the reaction mixture and the solution is stirred at 65 °C for 2 h. After cooling to room temperature, the reaction mixture is directly charged onto a silica gel column and the desired product is isolated by elution with cyclohexane (0.155 g, 0.92 mmol, 92%).

2-Methylbiphenyl (Table 4, Entry 1). GC-MS (50 °C, 2 min → 280 °C, 10 °C min⁻¹ → 280 °C, 10 min): *t_R* = 14.1 min; *m/z* 168. ¹H-NMR (300 MHz, CDCl₃) δ = 2.32 (s, 3 H), 7.25–7.50 (m, 10 H). ¹³C-NMR (75 MHz, CDCl₃) δ = 20.4, 125.7, 126.7, 127.2, 128.0, 129.10, 129.13, 129.7, 130.3, 135.2, 141.89, 141.92. Anal. Calcd for C₁₃H₁₂ (168.23): C, 92.81; H, 7.19. Found: C, 92.55; H, 7.20.

4-Methoxybiphenyl (Table 4, Entry 2). m.p. = 85–86 °C. GC-MS (50 °C, 2 min → 280 °C, 10 °C min⁻¹ → 280 °C, 10 min): *t_R* = 17.6 min; *m/z* 184. ¹H-NMR (300 MHz, CDCl₃) δ = 3.87 (s, 3 H), 7.00 (d, *J* = 8.5 Hz, 2 H), 7.32 (t, *J* = 7.3 Hz, 1 H), 7.43 (t, *J* = 7.6 Hz, 2 H), 7.49–7.62 (m, 4 H). ¹³C-NMR (75 MHz, CDCl₃) δ = 55.3, 114.2, 126.6, 126.7, 128.1, 128.7, 133.7, 140.8, 159.1. Anal. Calcd for C₁₃H₁₂O (184.23): C, 84.75; H, 6.57. Found: C, 84.53; H, 6.58.

2,2'-Dimethylbiphenyl (Table 4, Entry 3). GC-MS (50 °C, 2 min → 280 °C, 10 °C min⁻¹ → 280 °C, 10 min): *t_R* = 14.4 min; *m/z* 182. ¹H-NMR (300 MHz, CDCl₃) δ = 2.07 (s, 6 H), 7.08–7.15 (m, 2 H), 7.18–7.33 (m, 6 H). ¹³C-NMR (50 MHz, CDCl₃) δ = 19.8, 125.5, 127.1, 129.2, 129.8, 135.8, 141.6. Anal. Calcd for C₁₄H₁₄ (182.26): C, 92.26; H, 7.74. Found: C, 92.43; H, 7.72.

1-*o*-Tolynaphthalene (Table 4, Entry 4). m.p. = 69–70 °C. GC-MS (50 °C, 2 min → 280 °C, 10 °C min⁻¹ → 280 °C, 10 min): *t_R* = 19.6 min; *m/z* 218. ¹H-NMR (300 MHz, CDCl₃) δ = 2.04 (s, 3 H), 7.17–7.57 (m, 9 H), 7.90 (dd, *J* = 8.1/11.5 Hz, 2 H). ¹³C-NMR (75 MHz, CDCl₃) δ = 20.0, 125.3, 125.6, 125.7, 126.0, 126.1, 126.6, 127.4, 127.5, 128.2, 129.8, 130.3, 132.0, 133.5, 136.8, 139.8, 140.2. Anal. Calcd for C₁₇H₁₄ (218.29): C, 93.54; H, 6.46. Found: C, 93.57; H, 6.44.

2-Methyl-4'-phenylbiphenyl (Table 4, Entry 5). m.p. = 88–89 °C. GC-MS (100 °C, 2 min → 280 °C, 10 °C min⁻¹ → 280 °C, 10 min): *t_R* = 17.2 min; *m/z* 244. ¹H-NMR (300 MHz, CDCl₃) δ = 2.32 (s, 3 H), 7.33–7.52 (m, 9 H), 7.56–7.71 (m, 4 H). ¹³C-NMR (75 MHz, CDCl₃) δ = 20.5, 125.8, 126.7, 127.0, 127.2, 127.3, 128.8, 129.6, 129.8, 130.4, 135.3, 139.6, 140.8, 140.9, 141.4. Anal. Calcd for C₁₉H₁₆ (244.33): C, 93.40; H, 6.60. Found: C, 93.31; H, 6.58.

4'-Methylbiphenyl-2-carbonitrile (Table 4, Entry 6). m.p. = 49–51 °C. GC-MS (50 °C, 2 min → 280 °C, 10 °C min⁻¹ →

280 °C, 10 min): *t_R* = 18.6 min; *m/z* 193. ¹H-NMR (200 MHz, CDCl₃) δ = 2.41 (s, 3 H), 7.26–7.34 (m, 2 H) 7.35–7.54 (m, 4 H) 7.56–7.68 (m, 1 H) 7.74 (dd, *J* = 1.5/7.7 Hz, 1 H). ¹³C-NMR (50 MHz, CDCl₃) δ = 21.1, 103.7, 111.0, 127.1, 128.4, 129.3, 129.8, 132.6, 133.5, 135.1, 138.5, 145.3. Anal. Calcd for C₁₄H₁₁N (193.24): C, 87.01; H, 5.74; N, 7.25. Found: C, 86.67; H, 5.75; N, 7.27.

2-Methyl-3'-nitrobiphenyl (Table 4, Entry 7). GC-MS (50 °C, 2 min → 280 °C, 10 °C min⁻¹ → 280 °C, 10 min): *t_R* = 19.2 min; *m/z* 213. ¹H-NMR (300 MHz, CDCl₃) δ = 2.29 (s, 3 H), 7.21–7.36 (m, 4 H), 7.55–7.70 (m, 2 H), 8.19–8.25 (m, 2 H). ¹³C-NMR (75 MHz, CDCl₃) δ = 20.1, 121.6, 123.8, 126.0, 128.2, 128.9, 129.4, 130.5, 135.0, 135.2, 139.1, 143.3, 147.9. Anal. Calcd for C₁₃H₁₁NO₂ (213.23): C, 73.23; H, 5.20; N, 6.57. Found: C, 73.16; H, 5.21; N, 6.55.

1-(4-Methoxyphenyl)naphthalene (Table 4, Entry 8). m.p. = 115–117 °C. GC-MS (50 °C, 2 min → 280 °C, 10 °C min⁻¹ → 280 °C, 10 min): *t_R* = 22.1 min; *m/z* 234. ¹H-NMR (300 MHz, CDCl₃) δ = 3.91 (s, 3 H), 7.02–7.08 (m, 2 H), 7.39–7.56 (m, 6 H), 7.79–7.97 (m, 3 H). ¹³C-NMR (50 MHz, CDCl₃) δ = 55.3, 113.7, 125.4, 125.7, 125.9, 126.0, 126.9, 127.3, 128.2, 131.1, 131.8, 133.1, 133.8, 139.9, 158.9. Anal. Calcd for C₁₇H₁₄O (234.29): C, 87.15; H, 6.02. Found: C, 87.35; H, 6.00.

4,4'-dimethoxybiphenyl (Table 4, Entry 9). m.p. = 178–179 °C. GC-MS (50 °C, 2 min → 280 °C, 10 °C min⁻¹ → 280 °C, 10 min): *t_R* = 20.1 min; *m/z* 214. ¹H-NMR (200 MHz, CDCl₃) δ = 3.86 (s, 6 H), 6.97 (d, *J* = 8.9 Hz, 4 H), 7.49 (d, *J* = 8.9 Hz, 4 H). ¹³C-NMR (50 MHz, CDCl₃) δ = 55.3, 114.1, 127.7, 133.4, 158.6. Anal. Calcd for C₁₄H₁₄O₂ (214.26): C, 78.48; H, 6.59. Found: C, 78.53; H, 6.58.

4-Methoxy-4'-phenylbiphenyl (Table 4, Entry 10). m.p. = 222–223 °C. GC-MS (100 °C, 2 min → 280 °C, 10 °C min⁻¹ → 280 °C, 10 min): *t_R* = 19.8 min; *m/z* 260. ¹H-NMR (300 MHz, CDCl₃) δ = 3.88 (s, 3 H), 7.01 (d, *J* = 8.8 Hz, 2 H), 7.32–7.42 (m, 1 H) 7.43–7.52 (m, 2 H) 7.55–7.71 (m, 8 H). ¹³C-NMR (75 MHz, CDCl₃) δ = 55.4, 114.3, 127.0, 127.0, 127.2, 127.5, 128.0, 128.8, 133.2, 139.5, 139.7, 140.8, 159.2. Anal. Calcd for C₁₉H₁₆O (260.33): C, 87.66; H, 6.19. Found: C, 87.54; H, 6.17.

4'-Methoxy-2-methylbiphenyl (Table 4, Entry 11). GC-MS (50 °C, 2 min → 280 °C, 10 °C min⁻¹ → 280 °C, 10 min): *t_R* = 17.3 min; *m/z* 198. ¹H-NMR (300 MHz, CDCl₃) δ = 2.31 (s, 3 H), 3.88 (s, 3 H), 6.98 (d, *J* = 8.8 Hz, 2 H), 7.22–7.33 (m, 6 H). ¹³C-NMR (75 MHz, CDCl₃) δ = 20.5, 55.2, 113.4, 125.7, 126.9, 129.8, 130.2, 130.2, 134.3, 135.4, 141.5, 158.5. Anal. Calcd for C₁₄H₁₄O (198.26): C, 84.81; H, 7.12. Found: C, 85.12; H, 7.15.

4'-Methoxybiphenyl-2-carbonitrile (Table 4, Entry 12). GC-MS (100 °C, 2 min → 280 °C, 10 °C min⁻¹ → 280 °C, 10 min): *t_R* = 20.3 min; *m/z* 209. ¹H-NMR (300 MHz, CDCl₃) δ = 3.88 (s, 3 H), 7.03 (d, *J* = 8.8 Hz, 2 H), 7.25–7.28 (m, 1 H), 7.41 (t, *J* = 7.6 Hz, 1 H), 7.47–7.56 (m, 2 H), 7.63 (t, *J* = 7.7 Hz, 1 H), 7.75 (d, *J* = 7.7 Hz, 1 H). ¹³C-NMR (75 MHz, CDCl₃) δ = 55.3, 111.0, 114.1, 118.9, 127.0, 129.8, 129.9, 130.5, 132.7, 133.7, 145.1, 160.0. Anal. Calcd for C₁₄H₁₁NO (209.24): C, 80.36; H, 5.30; N, 6.69. Found: C, 80.27; H, 5.28; N, 6.71.

Optimized procedure for catalyst recycling (Fig. 4)

Reactions were carried out as described in the general procedure. After cooling to room temperature, the product is extracted with pentane (5 × 4 mL) and further purified by flash-chromatography on SiO₂. The ionic liquid is washed with degassed water (2 × 2 mL), dried under vacuum (~1 mmHg) for 6–8 h and directly reused for the next cycle.

Acknowledgements

This work was supported by MIUR (Rome) PRIN project grant: “Sintesi e Stereocontrollo di Molecole Organiche per lo Sviluppo di Metodologie Innovative di Interesse Applicativo”.

Notes and references

- 1 N. Miyaura and A. Suzuki, *Chem. Rev.*, 1995, **95**, 2457; A. Suzuki, *Chem Commun.*, 2005, 4759.
- 2 J.-P. Corbet and G. Mignani, *Chem. Rev.*, 2006, **106**, 2651; V. M. Dembitsky, A. H. Abu and M. Srebnik, *Stud. Inorg. Chem.*, 2005, **22**, 119, (Contemporary Aspects of Boron: Chemistry and Biological Applications).
- 3 N. T. S. Phan, M. Van Der Sluys and C. W. Jones, *Adv. Synth. Catal.*, 2006, **348**, 609.
- 4 S. Yasushi and F. Tetsuaki, *Inorg. Chem.*, 2007, **46**, 1895.
- 5 L. Yin and J. Liebscher, *Chem. Rev.*, 2007, **107**, 133.
- 6 D. Astruc, *Inorg. Chem.*, 2007, **46**, 1884.
- 7 C. M. Crudden, K. McEleney, S. L. MacQuarrie, A. Blanc, M. Sateesh and J. D. Webb, *Pure Appl. Chem.*, 2007, **79**, 247.
- 8 G. W. Kabalka, R. M. Pagni and C. M. Hair, *Org. Lett.*, 1999, **1**, 1423; R. K. Arvela, N. E. Leadbeater, T. L. Mack and C. M. Kormos, *Tetrahedron Lett.*, 2006, **47**, 217.
- 9 G. M. Greenway, S. J. Haswell, D. O. Morgan, V. Skelton and P. Styring, *Sens. Actuators, B*, 2000, **B63**, 153; P. He, S. J. Haswell and P. D. I. Fletcher, *Lab Chip*, 2004, **4**, 38; B. P. Mason, K. E. Price, J. L. Steinbacher, A. R. Bogdan and D. T. McQuade, *Chem. Rev.*, 2007, **107**, 2300.
- 10 M. Reetz and J. G. de Vries, *Chem. Commun.*, 2004, 1559; A. Alimardanov, L. Schmieder-van de Vondervoort, A. H. M. de Vries and J. G. de Vries, *Adv. Synth. Catal.*, 2004, **346**, 1812; V. Farina, *Adv. Synth. Catal.*, 2004, **346**, 1553; W. Huang, J. Guo, Y. Xiao, M. Zhu, G. Zou and J. Tang, *Tetrahedron*, 2005, **61**, 9783; N. Jiang and A. J. Ragauskas, *Tetrahedron Lett.*, 2006, **47**, 197.
- 11 D. Astruc, F. Lu and J. R. Aranzas, *Angew. Chem., Int. Ed.*, 2005, **44**, 7852.
- 12 X. Yang, Z. Fei, D. Zhao, W. H. Ang, Y. Li and P. J. Dyson, *Inorg. Chem.*, 2008, **47**, 3292; Z. Fei, T. J. Geldbach, D. Zhao and P. J. Dyson, *Chem. Eur. J.*, 2006, **12**, 2122; C. Chiappe, D. Pieraccini, D. Zhao, Z. Fei and P. J. Dyson, *Adv. Synth. Catal.*, 2006, **348**, 68; D. Zhao, Z. Fei, T. J. Geldbach, R. Scopelliti and P. J. Dyson, *J. Am. Chem. Soc.*, 2004, **126**, 15876.
- 13 The role exerted by the anion in defining the structure of Pd complexed with TSILs has been investigated: see for example Z. Fei, D. Zhao, D. Pieraccini, W. H. Ang, T. J. Geldbach, R. Scopelliti, C. Chiappe and P. J. Dyson, *Organometallics*, 2007, **26**, 1588.
- 14 F. Fernández, B. Cordero, J. Durand, G. Muller, F. Malbosc, Y. Kihn, E. Teuma and M. Gómez, *Dalton Trans.*, 2007, 5572; S. Chowdhury, R. S. Mohan and J. L. Scott, *Tetrahedron*, 2007, **63**, 2363; V. I. Pârvulescu and C. Hardacre, *Chem. Rev.*, 2007, **107**, 2615.
- 15 P. Migowski and J. Dupont, *Chem.–Eur. J.*, 2007, **13**, 32; F. McLachlan, C. J. Mathews, P. J. Smith and T. Welton, *Organometallics*, 2003, **22**, 5350. For similar observations on the Heck reaction, see: S. A. Forsyth, H. Q. N. Gunaratne, C. Hardacre, A. McKeown, D. W. Rooney and K. R. Seddon, *J. Mol. Cat. A: Chem.*, 2005, **231**, 61.
- 16 Miao and Chan proposed the term ionic liquid-supported catalysts to define this strategy. See: W. Miao and T. H. Chan, *Acc. Chem. Res.*, 2006, **39**, 897. For a recent review on catalysts with ionic tags and their use in ionic liquids, see: R. Šebesta, I. Kmentová and Š. Toma, *Green Chem.*, 2008, **10**, 484.
- 17 A palladium catalyst derived from *N,N,N*-trimethyl-2-(di-*t*-butylphosphino)ethan ammonium chloride has been previously successfully used for an efficient room temperature Suzuki coupling of aryl bromides in CH₃CN/H₂O mixtures, see: K. H. Shaughnessy and R. S. Booth, *Org. Lett.*, 2001, **3**, 2757.
- 18 M. R. Biscoe, B. P. Fors and S. L. Buchwald, *J. Am. Chem. Soc.*, 2008, **130**, 6686; U. Christmann and R. Vilar, *Angew. Chem., Int. Ed.*, 2005, **44**, 366; M. W. Hooper, M. Utsunomiya and J. F. Hartwig, *J. Org. Chem.*, 2003, **68**, 2861.
- 19 M. A. H. Ismail, S. Barker, D. A. A. El Ella, K. A. M. Abouzid, R. A. Toubar and M. H. Todd, *J. Med. Chem.*, 2006, **49**, 1526.
- 20 N. A. Hamill, C. Hardacre and S. E. J. McMath, *Green Chem.*, 2002, **4**, 139.
- 21 M. J. Earle, C. M. Gordon, N. V. Plechkova, K. R. Seddon and T. Welton, *Anal. Chem.*, 2007, **79**, 758; J. H. Davis, Jr., C. M. Gordon, C. Hilgers, P. Wasserscheid, in *Ionic Liquids in Synthesis*, ed. P. Wasserscheid and T. Welton, Wiley-VCH, Weinheim, 2nd edn, 2002, vol. 1, ch. 2, pp. 7–56.
- 22 For the mechanism of oxygen promoted palladium-catalyzed homocoupling of arylboronic acids see: C. Adamo, C. Amatore, I. Ciofini, A. Jutand and H. Lakmini, *J. Am. Chem. Soc.*, 2006, **128**, 6829.

Toxicity of imidazolium and pyridinium based ionic liquids towards algae. *Chlorella vulgaris*, *Oocystis submarina* (green algae) and *Cyclotella meneghiniana*, *Skeletonema marinoi* (diatoms)

Adam Latała,^a Marcin Nędzi^a and Piotr Stepnowski^{*b}

Received 26th November 2008, Accepted 28th January 2009

First published as an Advance Article on the web 17th February 2009

DOI: 10.1039/b821140j

This paper reports on an investigation into the toxicity of 1-alkyl-3-methylimidazolium ionic liquids (ILs) towards two green algae (*Chlorella vulgaris* and *Oocystis submarina*) characteristic of freshwater and brackish environments, as well as two brackish and marine diatoms (*Cyclotella meneghiniana* and *Skeletonema marinoi*). The test kit of IL compounds consisted of five 1-alkyl-3-methylimidazolium chlorides (from -ethyl to -decyl) for evaluating the expected alkyl chain length effect, together with 1-butyl-3-methylimidazolium tetrafluoroborate, dicyanamide, trifluoromethanesulfonate, methyl sulfate and α -methyl[poly(oxy-1,2-ethanediyl)]sulfate for investigating the influence of the anion on IL toxicity towards various algal species. A pronounced alkyl chain effect was confirmed with all the organisms studied. EC₅₀ values were linearly very well correlated with the number of carbon atoms in the IL alkyl chains. The results indicate that diatoms are far more sensitive than green algae to ILs. Cell size also plays an important part in the intoxication process: a tenfold difference in cell size results in a 100% more sensitive reaction to ionic liquids in both the green algae and diatoms. No significant differences were observed between alkylimidazolium salts and an alkyipyridinium compound of similar lipophilicity. It was also found that the use of tetrafluoroborate and trifluoromethanesulfonate as counteranions in the IL structure gave rise to the most pronounced toxic effects in comparison with the other anions tested. In the case of tetrafluoroborate this is probably caused by the potential hydrolysis of this entity, which leads to the formation of fluoride and a further increase in toxicity. Whereas in the case of trifluoromethanesulfonate it is likely caused by relatively high lipophilicity of this anion, additionally known to be strongly associated with alkylimidazolium cations, that in turn may enhance cell wall penetration.

Introduction

Ionic liquids (ILs) are a new class of organic salts with melting points below 100 °C. They typically consist of nitrogen-containing organic cations such as 1-alkyl-3-methylimidazolium or *N*-alkylpyridinium together with an inorganic or organic anion commonly containing fluorine, for example, BF₄⁻, PF₆⁻, CF₃COO⁻, SbF₆⁻, or (CF₃SO₂)₂N⁻. Current research indicates that replacing conventional molecular solvents with these media can bring about remarkable improvements in well-known processes: ILs have already been applied in organic synthesis and catalysis, in the separation sciences, as electrolytes in batteries and solar cells, and as alternative lubricants.¹⁻²

ILs are often uncritically regarded as intrinsically environmentally friendly, since their vapour pressure is negligible, and hence are a good alternative to the emissions of toxic vapours from conventional molecular organic solvents. Merely reducing such gaseous discharges, however, does not automatically make

a process greener, and many other facts have to be taken into account before such a statement can be made.³

There are numerous reports covering the toxicity of ionic liquids. They evaluate this toxicity on the basis of test systems at different levels of biological complexity, starting with the Ames mutagenicity test⁴ and the inhibition of acetylcholinesterase⁵ or AMP deaminase⁶ enzymes, through growth inhibition tests performed on bacterial, algal and mammalian cell cultures⁷⁻¹¹ as well as developmental toxicity assessment in mice,¹² to ecotoxicological tests done on soil roundworms,¹³ freshwater crustaceans¹⁴ and freshwater snails.¹⁵ Most of these test systems indicate that the longer the *n*-alkyl chain in the ionic liquid cation, the greater the toxicity. The importance of side chain length (and hence lipophilicity) as a factor contributing to the overall observed biological effect has also been examined in detail.¹⁶⁻¹⁷ The potential persistence and toxicity of ionic liquids is also a function of their biodegradability: several investigations in this area have shown that the biodegradability of the most commonly used alkylimidazolium ionic liquids is poor to negligible.¹⁸⁻²¹ The most recent reports, however, indicate that the incorporation of oxygen functional groups in the cation and anion structures significantly enhances biodegradation and lowers toxicity.²²

^aFaculty of Oceanography and Geography, University of Gdańsk, Piłsudskiego 46, 81-378, Gdynia, Poland

^bFaculty of Chemistry, University of Gdańsk, Sobieskiego 18/19, 80-952, Gdańsk, Poland. E-mail: sox@chem.univ.gda.pl

In view of the chemical industry's great interest in these compounds, one has to anticipate a number of risk scenarios, including those in which certain amounts of ionic liquids are present in industrial effluents where, because of their great stability, they could become persistent pollutants and break through classical treatment systems into natural waters. Recent studies have demonstrated that only the most advanced techniques are effective in totally removing ionic liquids from such systems.^{23–25} Since these methods are not usually included in conventional wastewater treatment processes, there is a considerable risk of aquatic organisms becoming exposed to ILs. This is a problem that should be addressed as a matter of urgency.

There are many bioassay techniques using fish, invertebrates, phytoplankton and bacteria for detecting the toxic effects of chemicals in fresh and seawaters. Among these, algal assays have become widely used as biological tools in environmental impact studies. Current assessment procedures are based on the premise that algal tests can be used to predict the effects of chemical compounds in aquatic environments.²⁶ Growth-inhibition tests with freshwater algae²⁷ and seawater algae²⁸ are included in the base set of ecotoxicological tests recommended by the European Committee for Standardization (CEN), the International Organization for Standardization (ISO), and the Organization for Economic Cooperation and Development (OECD).

So far, the toxicity of ILs towards algae has only been tested to a preliminary extent in a few research projects. The first report published by our group indicated that the growth of two Baltic algae was effectively inhibited by even very low concentrations of alkylimidazolium ionic liquids.⁹ That study also demonstrated the evident influence of water salinity on toxicity towards algae; in general the higher the salinity, the lower the toxicological effects. Wells and Coombe²⁹ tested several imidazolium, phosphonium and ammonium ILs for their toxicity towards the green algae *Pseudokirchneriella subcapitata* and the invertebrate *Daphnia magna*. In general, the toxicity levels of a particular substance to algae and *Daphnia* were surprisingly similar, and toxicities of the most and least toxic ionic liquids were separated by more than four orders of magnitude for both trophic levels. In contrast, Kulacki and Lamberti,³⁰ in their study of the toxicity of imidazolium ionic liquids towards the freshwater algae *Scenedesmus quadricauda* ($EC_{50} = 0.005\text{--}13.23 \text{ mg L}^{-1}$) and *Chlamydomonas reinhardtii* ($EC_{50} = 4.07\text{--}2138 \text{ mg L}^{-1}$), demonstrated with clarity that ionic liquids can elicit a range of algal responses, suggesting that it is difficult to extrapolate the results of these bioassays across taxa. Stolte *et al.*³¹ examined the influence of different head groups, functionalised side chains and anions of ionic liquids on the freshwater green alga *Scenedesmus vacuolatus*. The set of 40 ILs these authors analysed confirmed the relation between the lipophilicity and toxicity of these compounds: the toxicity was clearly lower when short, functionalised compounds were used instead of long non-polar alkyl chains. The same group also investigated the toxic effects of mixtures of ILs on the same algae as well as on wheat.³² Green algae were approximately two orders of magnitude more sensitive to the mixture scenarios than wheat, thus proving to be a good reference test system for evaluating the measured effects. Recently, Pham *et al.*³³ found that the length of the alkyl chain in the cation of imidazolium

and pyridinium ionic liquids has a direct influence on the photosynthetic response of *P. subcapitata*. Apart from the alkyl chain effect, which was very distinct in all these studies, the type of anion was also found to influence the toxicity towards the alga *Selenastrum capricornutum*:³⁴ the most toxic anions were SbF_6^- and PF_6^- , which is probably due to them being hydrolysed to fluoride.

The cited results clearly demonstrate the wide diversity of responses of algae exposed to various ionic liquids. This is due not only to the different sensitivities of algal organisms, but also to the complexities of the chemical structures of ILs, where alkyl chain length, the various functional groups, cationic head groups and types of anions are active variables as far as the mode of toxic action is concerned. Moreover, since most of the studies undertaken so far have been done with freshwater algae, we possess only limited knowledge of the fate of ILs in the marine environment. It is important to know this fate if we wish to predict the full consequences of the release of these compounds into the environment.

The present study therefore addressed the problem of the toxicity of 1-alkyl-3-methylimidazolium ionic liquids towards two Baltic green algae—*Chlorella vulgaris* and *Oocystis submarina*—as well as two diatoms—*Cyclotella meneghiniana* and *Skeletonema marinoi*. Two of these species (*O. submarina* and *C. meneghiniana*) had previously been studied by our group in a very preliminary manner, so no EC_{50} values were obtained and only four ILs were tested on these species.⁹ In addition, *S. marinoi* was tested to see whether the previously observed higher sensitivity of diatoms to IL exposure was taxon-specific. The test kit of IL compounds consisted of five 1-alkyl-3-methylimidazolium chlorides (from ethyl to decyl) for evaluating the expected alkyl chain length effect, as well as of 1-butyl-3-methylimidazolium tetrafluoroborate, dicyanamide, trifluoromethanesulfonate, methyl sulfate and α -methyl[poly(oxy-1,2-ethanediyl)]sulfate in order to investigate the influence of the anion on IL toxicity towards various algal species (Fig. 1).

Results

Influence of alkyl chain length on toxicity of ionic liquids

In order to examine the well-known effect of IL alkyl chain length (lipophilicity) on toxicity towards the algal organisms under investigation, a test kit consisting of 1-alkyl-3-methylimidazolium chlorides, with alkyl varying from ethyl to decyl, was used. The influence of ILs on algal growth in relation to their toxicity was deduced from the ratio of the treated cells to the control sample. Fig. 2 exemplifies the dose response relationships obtained during this study, and Tables 1–4 set out the toxicities towards algae expressed as EC_{50} values. These data show that there is a distinct relationship between alkyl chain effect and toxicity: in nearly all cases, a two-carbon increase in chain length results in EC_{50} falling by nearly one order of magnitude. In the case of the green algae exposed to 1-ethyl-3-methylimidazolium chloride, the effective concentration of this compound remains in the millimolar range (6330.51–13 573.01 μM) but effectively inhibits the growth of both diatoms at levels from 59.24 to 112.36 μM . This trend is maintained

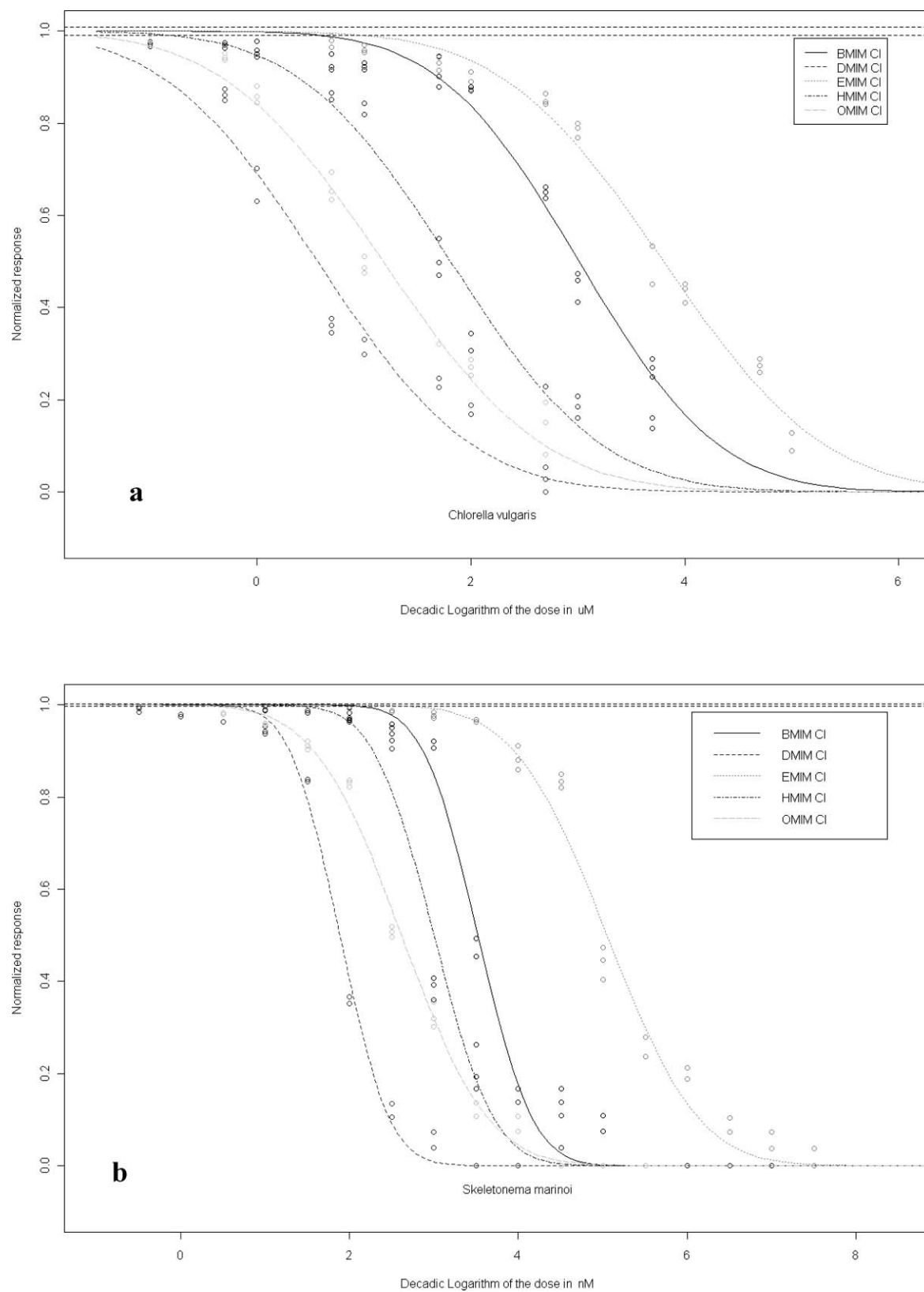


Fig. 2 Dose–response relationships plotted for (a) the green alga *Chlorella vulgaris* and (b) the diatom *Skeletonema marinoi* exposed to 1-alkyl-3-methylimidazolium chlorides with different alkyl chain lengths (EMIM Cl-1-ethyl-3-methylimidazolium chloride, BMIM Cl-1-butyl-3-methylimidazolium chloride, HMIM Cl-1-hexyl-3-methylimidazolium chloride, OMIM Cl-1-octyl-3-methylimidazolium chloride and DMIM Cl-1-decyl-3-methylimidazolium chloride).

Table 4 Influence of ionic liquids on the growth of *Cyclotella meneghiniana*, expressed as EC₅₀ ± standard deviation (μM)

Chemical name	Abbreviation	EC ₅₀ ± SD/μM	log EC ₅₀
1-R-3-methylimidazolium chloride			
R – Ethyl	EMIM Cl	59.24 ± 2.96	1.77
R – Butyl	BMIM Cl	7.21 ± 0.36	0.86
R – Hexyl	HMIM Cl	2.39 ± 0.12	0.38
R – Octyl	OMIM Cl	0.73 ± 0.04	-0.14
R – Decyl	DMIM Cl	0.27 ± 0.01	-0.57
1-Butyl-3-methyl imidazolium X			
X – tetrafluoroborate	BMIM BF ₄	2.75 ± 0.13	0.44
X – dicyanamide	BMIM DCNA	10.95 ± 0.54	1.04
X – trifluoromethanesulfonate	BMIM TFMS	5.72 ± 0.28	0.76
X – methylsulfate	BMIM MeSO ₄	11.64 ± 0.58	1.07
X – α-methyl[poly(oxy-1,2-ethanediyl)]sulfate	BMIM MPEGSO ₄	9.68 ± 0.48	0.99

Table 5 Linear correlation between the alkyl chain length of the imidazolium cation in the ionic liquid (expressed as the number of carbon atoms C_n) and log EC₅₀

Species	$C_n = a \log EC_{50} + b$		
	Slope (a)	Intercept (b)	Linear correlation R ²
<i>Chlorella vulgaris</i>	-0.414	4.561	0.9837
<i>Oocystis submarina</i>	-0.396	5.009	0.9839
<i>Skeletonema marinoi</i>	-0.362	2.379	0.9295
<i>Cyclotella meneghiniana</i>	-0.284	2.163	0.9766

with the other ILs, with the diatoms exhibiting a far higher sensitivity than the green algae. The toxicity of the next shortest alkyl chain compound (BMIM Cl) is still in the millimolar range as regards green algae and, as in the case of EMIM Cl, the effect can be treated as insignificant. In the case of the *C. meneghiniana* and *S. marinoi*, EC₅₀ dropped to 3.32 and 7.21 μM of EMIM Cl respectively; with 1-hexyl-3-methylimidazolium chloride, effective concentrations were still of the same order of magnitude (1.01–2.39 μM). This was not the case with *Chlorella vulgaris*, where the fall in effective concentration with HMIM Cl was more than one order of magnitude (64.52 μM). The other green alga (*O. submarina*) was relatively more resistant to the toxic effect of this IL, cultures of which were inhibited by 753.60 μM. The toxic effect of the longest alkyl chain compounds (OMIM Cl and DMIM Cl) in green algae was apparent already at very low concentrations (3.68–79.13 μM). In the diatoms, however, EC₅₀ values as low as 0.08–0.73 μM were recorded with these latter two compounds.

One alkyipyridinium salt—1-butyl-4-methylpyridinium chloride—was also tested for its toxicity towards *C. vulgaris* and *O. submarina*: in both cases the EC₅₀ values lay between those of EMIM Cl and BMIM Cl.

EC₅₀ values (expressed as log EC₅₀) were correlated linearly with the number of carbon atoms (C_n) in the IL alkyl chain. Table 5 presents the resultant intercepts (b), slopes (a) and linear correlation coefficients (R²) of the functions. The EC₅₀ values for both green algae were very well correlated with the length of the alkyl chain (R² ~ 0.984), and, in the case of *C. meneghiniana*, the resultant correlation coefficient was reasonably good (R² = 0.9766). The weakest relation was definitely that for *S. marinoi* (R² = 0.9295); this was probably due to the relatively high resistance of this species to the shorter-chain compounds and its greater sensitivity to the longest-chain IL being investigated.

The slopes obtained appear to be characteristic of particular taxa, at least as far as the green algae are concerned. The similar intercepts within the taxonomic groups (~ 0.5 for green algae, ~ 0.2 for diatoms) reflect the sensitivities of these organisms.

Influence of anions on ionic liquid toxicity

The effects of different anions in the IL structure on toxicity towards algae were also studied. To this end six 1-butyl-3-methylimidazolium salts containing tetrafluoroborate, dicyanamide, trifluoromethanesulfonate, methyl sulfate, chloride and α-methyl[poly(oxy-1,2-ethanediyl)]sulfate anions were compared. Tables 1–4 list the toxicities towards algae expressed as EC₅₀ values, and Fig. 3 shows examples of the dose-response relationships recorded for the series of ILs with different anions. Generally, both green algae were far less sensitive than the diatoms to the changes in anion. In the case of *C. vulgaris* and *O. submarina*, the toxicity levels were highest with 1-butyl-3-methylimidazolium tetrafluoroborate (EC₅₀ = 425.33 and 707.81 μM, respectively); fairly strong effects were also observed with ILs containing the α-methyl[poly(oxy-1,2-ethanediyl)]sulfate anion, a polymeric entity (EC₅₀ = 930.81 and 871.04 μM, respectively). The least toxic ILs in this test kit were 1-butyl-3-methylimidazolium dicyanamide (*C. vulgaris*) and 1-butyl-3-methylimidazolium methyl sulfate (*O. submarina*).

This study of the toxic effects of the 1-butyl-3-methylimidazolium cation with various anions on the two diatoms showed that the most effective growth inhibitor of *S. marinoi* was 1-butyl-3-methylimidazolium trifluoromethanesulfonate (EC₅₀ = 1.77 μM), while that of *C. meneghiniana* was 1-butyl-3-methylimidazolium tetrafluoroborate (EC₅₀ = 2.75 μM). Varying the anions when testing IL toxicity on diatoms also showed that *S. marinoi* was generally more sensitive than *C. meneghiniana*.

Discussion

The test kit of IL compounds was used to investigate the toxicity of 1-alkyl-3-methylimidazolium ionic liquids with different alkyl chain lengths. Moreover, the choice of algal species enabled the various effects of ILs on green algae (*Chlorella vulgaris* and *Oocystis submarina*) and diatoms (*Cyclotella meneghiniana* and *Skeletonema marinoi*) to be distinguished. The alkyl chain effect was pronounced in all four organisms. The length of the alkyl chain is the main structural feature of ILs determining

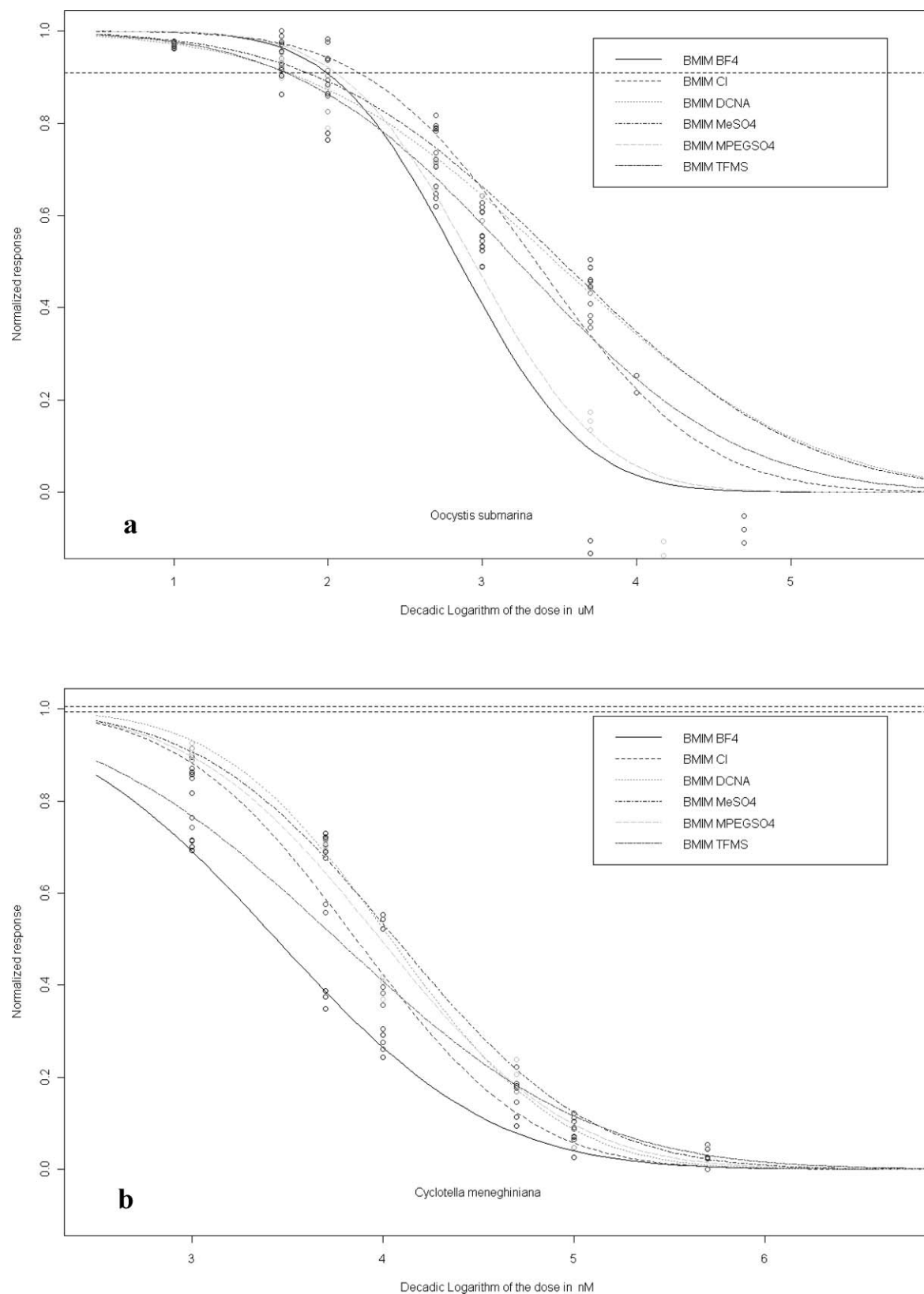


Fig. 3 Dose–response relationships plotted for (a) the green alga *Oocystis submarina* and (b) the diatom *Cyclotella meneghiniana* exposed to 1-butyl-3-methylimidazolium chloride (BMIM Cl), -tetrafluoroborate (BMIM BF₄), -dicyanamide (BMIM DCNA), -trifluoromethanesulfonate (BMIM TFMS), -methyl sulfate (BMIM MeSO₄) and - α -methyl[poly(oxy-1,2-ethanediyl)]sulfate (BMIM MPEGSO₄).

their lipophilicity.³⁵ The relation between a compound's toxicity towards aquatic organisms and its lipophilicity is known as the baseline toxicity: this causes a non-specific disturbance of the structure and functioning of the biological membranes.³⁶ Since ILs containing longer alkyl chains exhibit an adsorption potential through simultaneous hydrophobic and ionic interactions (in the same way as surfactants), they have a greater ability to accumulate at the algal membrane–water interface, which causes the disruption of the integral membrane.³⁷ The relation between the alkyl chain length and the toxicity of ILs towards freshwater algae has also been confirmed in other studies.^{29–32} In this report, however, we deliver, for the first time, systematic data on IL toxicity towards two marine diatom species. From this data it is clear that diatoms are far more sensitive to ILs than green algae. This concurs with the results of our preliminary study, where the greater sensitivity of diatoms exposed to ILs was postulated:⁹ on exposure to ILs, the *Cyclotella meneghiniana* culture, unlike the green algae population, did not acclimatise even to the low ionic liquid concentrations tested, and growth was inhibited throughout the experiment. Obtained results in this study may therefore suggest that the reason for the observed difference in sensitivity is to be found in the cell wall structure. Likely diatoms are much more sensitive to the toxic action of ILs because their cell walls are silica-based; in contrast, green algae, with their cellulose-based cell walls, are possibly more resistant to such action. Diatom cells have a range of features that make them highly divergent from the classical cellular structure of green algae and higher plants. As a consequence, one could almost consider diatoms as photosynthetic animals rather than unicellular plants.³⁸ The cell wall of diatoms is a composite of amorphous hydrated silica, the product of a partial condensation of orthosilicic acid, and various organic components mainly proteins. In the last decade, with the discovery of further classes of organic components involved in silicification and maintaining the integrity of the cell wall, three families of cell wall proteins were investigated: frustulins,³⁹ silaffins⁴⁰ and pleuralins.⁴¹ Analysis of these cell-surface protein sequences reveals stretches of amino acids highly enriched in acidic residues.^{38,42} These all make diatoms highly capable biosorbents for charged chemical entities including heavy metals and ionized organic substances. In comparison, the cell wall of green algae is a composite of indigestible cellulose, far stronger, insensitive and far less negatively charged than diatoms. It is known, for example, that the sorption capacity of copper is five times higher in the case of diatom *C. meneghiniana* than green algae *C. reinhardtii*.⁴³ If ionic liquid cations are of concern, it is highly possible that much more effective electrostatic biosorption on the diatom surface in comparison to green algae will be decisive in the further effectiveness of the toxic action in this taxonomic group.

Differences in the sensitivity of algae exposed to ILs were also observed by Kulacki and Lamberti:³⁰ they found that algae with cellulose-based cell walls (*S. quadricauda*) were more sensitive than *C. reinhardtii*, the cell wall of which is composed primarily of glycoproteins. In conjunction with our results, this provides ample demonstration of the baseline toxicity mode action of ionic liquids. Hence, the sensitivity of particular organisms will depend entirely on IL availability within the biological membrane structure; this availability, in turn, is governed by the membrane's surface chemistry.

Interestingly, the IL toxicity ranged widely not only between taxonomic groups but also between species from the same group. Among the green algae, *C. vulgaris* was twice as sensitive to ILs as *O. submarina*; likewise, among the diatoms, *S. marinoi* was twice as sensitive as *C. meneghiniana*. These differences in sensitivity within taxonomic groups correlate well with the size of the algal cells: those of *C. vulgaris* range between 15 and 20 μm^3 , whereas those of *O. submarina* are around ten times larger (170 μm^3). Among the diatoms, the more sensitive *S. marinoi* cells are from 100 to 150 μm^3 in size, and those of *C. meneghiniana* between 1350 and 2000 μm^3 .^{44–45} The relation between cell size and sensitivity again underscores the significance of the cell wall component in the toxic action of ionic liquids. Algal cultures consisting of smaller cells have a relatively larger cell wall surface area, which in turn enables toxins to be transported more efficiently into the cells. It is well known that intertropical oceanic waters, poor in nutrients and ions, are inhabited mainly by picoplanktonic species, which are able to absorb these deficient substances more efficiently as a result of the privileged ratio of cell wall surface to cell volume. In the present study, the tenfold difference in cell size resulted in a 100% more sensitive reaction to ionic liquids by both the green algae and the diatoms. This observation should be taken into consideration when further ecotoxicological risk assessment experiments with ionic liquids are designed.

Apart from the alkyl chain length, two other structural factors of ionic liquids may contribute to the toxic effects on algae: the type of cationic head group and the type of anion. In the case of the head group one alkylpyridinium salt (1-butyl-4-methylpyridinium chloride), the lipophilicity of which lies between that of BMIM Cl and HMIM Cl, was additionally tested. Its EC_{50} values towards both green algae species were in the same range as that of the four-six carbon alkyl chains of the imidazolium ILs. Stolte *et al.*³¹ likewise found that pyridinium and imidazolium ILs inhibited the growth of green algae in the same concentration range.

The effect of IL anions on their toxicity towards algae was also tested: in general, both diatoms turned out to be far more sensitive than the green algae to changes of IL anion. 1-butyl-3-methylimidazolium tetrafluoroborate and trifluoromethanesulfonate had the greatest toxic effect on *S. marinoi* and *C. meneghiniana*. In one of our first studies of IL toxicity, it was postulated that tetrafluoroborate could undergo hydrolysis, which would lead to the formation of fluoride and the consequent potentiation of the toxic effect.¹¹ This was confirmed by other authors, who reached the unequivocal conclusion that the elevated toxicity towards various species of algae was due to fluoride formation.^{30–33} In the case of trifluoromethanesulfonate elevated toxicity is likely to be caused by relatively high lipophilicity of this anion, additionally known to be strongly associated with alkyimidazolium cations, that in turn may enhance cell wall penetration.

1-butyl-3-methylimidazolium tetrafluoroborate most effectively inhibited the growth of both green algae, probably for the same reasons as in the case of diatoms. Relatively stronger effects with ILs containing α -methyl[poly(oxy-1,2-ethanediyl)]sulfate were also recorded. The main difference between this anion and the others tested lies in its polymeric nature. Therefore, the generally observed baseline toxicity of lipophilic cations may

well be potentiated by a polymeric anion, but this will have to be confirmed in further studies.

In the case of the green algae, the EC₅₀ value of none of the compounds used fell below the millimolar range, which further confirms that these organisms are less sensitive to the toxic effects of ionic liquids.

Conclusion

Two green algae (*Chlorella vulgaris* and *Oocystis submarina*) and two diatoms (*Cyclotella meneghiniana* and *Skeletonema marinoi*) were used to investigate the toxic effects of five 1-alkyl-3-methylimidazolium chlorides with different alkyl chain lengths and five 1-butyl-3-methylimidazolium salts with different counteranions. A pronounced alkyl chain effect was found with all the organisms. EC₅₀ values were very well correlated linearly with the number of carbon atoms in the IL alkyl chain, and diatoms used in this study were found to be far more sensitive to ILs than green algae. Cell size also played an important role in the intoxication of green algae and diatoms; the smaller the cell, the greater the sensitivity to ILs. There were no significant differences between the alkylimidazolium salts and an alkylpyridinium compound of a similar lipophilicity. The use of tetrafluoroborate and trifluoromethanesulfonate as counteranions in the IL structure gave rise to the most pronounced toxic effects in comparison with the other anions tested. In the case of tetrafluoroborate this was probably due to the hydrolysis of these entities, which leads to the formation of fluoride and consequently a rise in toxicity. Whereas in the case of trifluoromethanesulfonate it is likely caused by relatively high lipophilicity of this anion, additionally known to be strongly associated with alkylimidazolium cations, that in turn may enhance cell wall penetration.

Material and methods

Test organisms

Two taxonomically different planktonic algal species were used in this study: the green algae *Oocystis submarina* (BA-0001) and *Chlorella vulgaris* (BA-0002), and the diatoms *Cyclotella meneghiniana* (BA-0010) and *Skeletonema marinoi* (BA-0098). They were isolated from coastal waters of the Baltic Sea and maintained as unialgal cultures in the Culture Collection of Baltic Algae (CCBA), <http://ocean.univ.gda.pl/~ccba/>, at the Institute of Oceanography of the University of Gdańsk.^{46–47}

Ionic liquids

All ionic liquids were obtained from Merck (Darmstadt, Germany). They were: 1-ethyl-3-methylimidazolium chloride (EMIM Cl), 1-butyl-3-methylimidazolium chloride (BMIM Cl), 1-hexyl-3-methylimidazolium chloride (HMIM Cl), 1-octyl-3-methylimidazolium chloride (OMIM Cl) and 1-decyl-3-methylimidazolium chloride (DMIM Cl). Also used were 1-butyl-3-methylimidazolium tetrafluoroborate (BMIM BF₄), -dicyanamide (BMIM DCNA), -trifluoromethanesulfonate (BMIM TFMS), -methyl sulfate (BMIM MeSO₄) and - α -methyl[poly(oxy-1,2-ethanediyl)]sulfate (BMIM MPEGSO₄), as well as 1-butyl-4-methylpyridinium chloride (MBPy Cl).

Batch cultures and toxicity tests

The test algae were batch-cultured in f/2 medium⁴⁸ prepared in distilled water. The culture salinity of 8 PSU was similar to that in the southern Baltic Sea, the original environment of the test organisms. The salinity was made up using TropicMarin[®] sea salt (Tropic Marin, Wartenberg, Germany).

The stock cultures of test organisms were acclimatised for 10 days at 20 °C and illuminated with 25 $\mu\text{mol photons m}^{-2} \text{ s}^{-1}$ from daylight type fluorescent lamps (L : D photoperiod 16 : 8). The irradiance was measured with a LiCor (LI-189) quantum meter (LiCor, Lincoln, NE, USA).

The acute toxicity tests of ILs towards algae were carried out using modified versions of the methods recommended in the European Committee for Standardization's guidelines.^{25–26} The main modifications were the use of f/2 medium, the photoperiod and the choice of the test strains. The final batch cultures used in the experiments were obtained by mixing a known amount of cells in the log growth phase with sterile medium. The initial cell number was constant and was measured as optical density (OD) at two wavelengths (665 and 750 nm). The respective densities of green algae *C. vulgaris* and *O. submarina* were c. 0.022/665 nm and 0.019/750 nm; those of the diatoms *C. meneghiniana* and *S. marinoi* were 0.062/665 nm and 0.043/750 nm.

9.5 cm³ aliquots of algal suspension were transferred to glass conical flasks (25 ml), and to each of these 0.5 cm³ of different concentrations of an aqueous IL solution or distilled water (control cultures) was added. Final concentrations ranged from 50 mM to 0.000005 mM. All experiments were run in triplicate.

After 72 h incubation the number of cells in the cultures was determined by OD measurement. The variability of the results did not exceed 5% on the inhibition scale. The ILs were tested on a wide range of concentrations, which enabled the EC₅₀ values to be calculated.

Statistical analysis

To calculate the EC₅₀ values, dose–response curves were fitted with the non-linear least squares method using a linear logistic model.¹⁰ Calculations were carried out with the R-language in the statistical environment, version 2.7.2 (see: <http://www.r-project.org>). The data are the means of independent experiments conducted in triplicate for each compound.

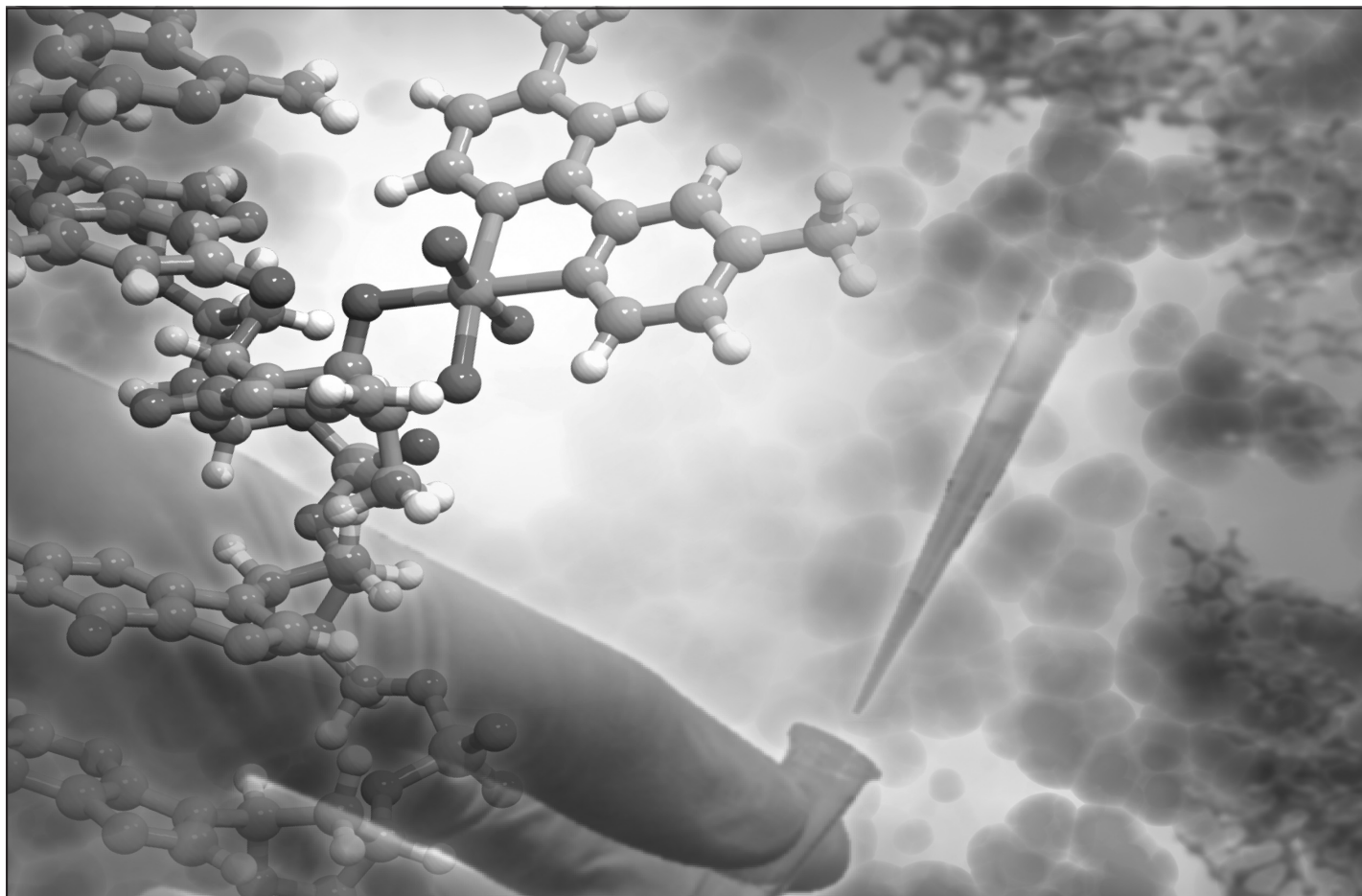
Acknowledgements

Financial support was provided by the Polish Ministry of Research and Higher Education under grants: 2P04G 118 29, 2P04F 036 30 and DS 8200–4–0085–8.

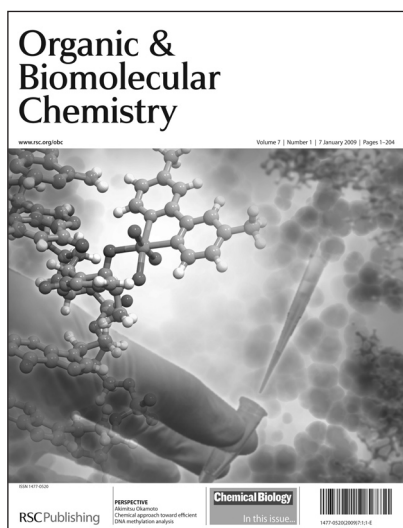
References

- 1 P. Wasserscheid and T. Welton, *Ionic liquids in synthesis*, Wiley VCH, Weinheim, 2nd ed., 2008.
- 2 N. V. Plechkova and K. R. Seddo, *Chem. Soc. Rev.*, 2008, **37**, 123–150.
- 3 D. Kralisch, A. Stark, S. Korsten, G. Kreisel and B. Ondruschka, *Green Chem.*, 2005, **7**, 301–309.
- 4 K. Docherty, S. Z. Hebbeler and C. F. Kulpa, Jr., *Green Chem.*, 2006, **8**, 560–567.

- 5 F. Stock, J. Hoffman, J. Ranke, R. Stormann, B. Ondruschka and B. Jastorff, *Green Chem.*, 2005, **6**, 286–290.
- 6 A. C. Składanowski, P. Stepnowski, K. Kleszczyński and B. Dmochowska, *Environ. Toxicol. Pharmacol.*, 2005, **19**, 291–296.
- 7 J. Pernak, J. Jędraszczuk and J. Krysiński, *Pharmazie*, 1987, **42**, 422–425.
- 8 J. Pernak, K. Sobaszekiewicz and I. Mirska, Anti-microbial activities of ionic liquids, *Green Chem.*, 2003, **5**, 52–56.
- 9 A. Latała, P. Stepnowski, M. Nędzi and W. Mroziak, *Aquatic Toxicol.*, 2005, **73**, 91–98.
- 10 J. Ranke, K. Mölter, F. Stock, U. Bottin-Weber, J. Poczobutt, J. Hoffmann, B. Ondruschka, J. Filser and B. Jastorff, *Ecotox. Environ. Saf.*, 2003, **28**, 396–404.
- 11 P. Stepnowski, A. C. Składanowski, A. Ludwiczak and E. Łączyńska, *Hum. Exp. Toxicol.*, 2004, **23**, 513–517.
- 12 M. M. Bailey, M. B. Townsend, P. L. Jernigan, J. Sturdivant, W. L. Hough-Troutman, J. F. Rasco, R. P. Swatloski, R. D. Rogers and R. D. Hood, *Green Chem.*, 2008, **10**, 1213–1217.
- 13 R. P. Swatloski, J. D. Holbrey, S. B. Memon, G. A. Caldwell, K. A. Caldwell and R. D. Rogers, *Chem. Commun.*, 2004, 668–669.
- 14 R. J. Bernot, M. A. Brueseke, M. A. Evans White and G. A. Lamberti, *Environ. Toxicol. Chem.*, 2005a, **24**, 87–92.
- 15 R. J. Bernot, E. E. Kennedy and G. A. Lamberti, *Environ. Toxicol. Chem.*, 2005, **24**, 1759–1765.
- 16 D. J. Couling, R. J. Bernot, K. M. Docherty, J. K. Dixon and E. J. Maggin, *Green Chem.*, 2006, **8**, 82–90.
- 17 P. Stepnowski and P. Storonik, *Environ. Sci. Poll. Res.*, 2005, **12**, 199–204.
- 18 M. T. Garcia, N. Gathergood and P. J. Scammells, *Green Chem.*, 2004, **7**, 9–14.
- 19 N. Gathergood, M. T. Garcia and P. J. Scammells, *Green Chem.*, 2004, **3**, 166–175.
- 20 N. Gathergood and P. J. Scammells, *Aust. J. Chem.*, 2002, **55**, 557–560.
- 21 N. Gathergood, P. J. Scammells and M. T. Garcia, *Green Chem.*, 2004, **2**, 156–160.
- 22 M. Stasiewicz, E. Mulkiewicz, R. Tomczak-Wandzel, J. Kumirska, E. M. Siedlecka, M. Gołębiowski, J. Gajdus, M. Czerwicka and P. Stepnowski, *Ecotox. Environ. Saf.*, 2008, **71**, 157–165.
- 23 P. Stepnowski and A. Zaleska, *J. Photochem. Photobiol., A*, 2005, **170**, 45–50.
- 24 E. M. Siedlecka, W. Mroziak, Z. Kaczyński and P. Stepnowski, *J. Hazard. Matter.*, 2008, **154**, 893–900.
- 25 E. Siedlecka and P. Stepnowski, *Environ. Sci. Poll. Res.*, DOI: 10.1007/s11356-008-0058-4.
- 26 O. M. Skulberg, in Use of algae for testing water quality, *Algae, environment and human affairs*, ed. W. Wiessner, E. Schnepf, R. C. Starr, Biopress Limited, Bristol, 1995, pp. 181–199.
- 27 EN, Water quality – Fresh water algal growth inhibition test with *Scenedesmus subspicatus* and *Selenastrum capricornutum* (ISO 8692:1993), European Committee for Standardization, Brussels, 1993.
- 28 EN ISO, Water quality – Marine algal growth inhibition test with *Skeletonema costatum* and *Phaeodactylum tricorutum* (ISO 10253:1995), European Committee for Standardization, Brussels, 1995.
- 29 A. S. Wells and V. T. Coombe, *Org. Process Res. Dev.*, 2006, **10**, 794–798.
- 30 K. J. Kulacki and G. A. Lamberti, *Green Chem.*, 2008, **10**, 104–110.
- 31 S. Stolte, M. Matzke, J. Arning, A. Boeshen, W. R. Pitner, U. Welz-Bierman, B. Jastorff and J. Ranke, *Green Chem.*, 2007, **9**, 1170–1179.
- 32 M. Matzke, S. Stolte, A. Böschchen and J. Filser, *Green Chem.*, 2008, **10**, 784.
- 33 T. P. T. Pham, C.-W. Cho, J. Min and Y.-S. Yun, *J. Biosci. Bioeng.*, 2008, **105**, 425–428.
- 34 C.-W. Cho, T. P. T. Pham, Y.-C. Jeon and Y.-S. Yun, *Green Chem.*, 2007, **10**, 67–72.
- 35 P. Stepnowski and P. Storonik, *Environ. Sci. Poll. Res.*, 2005, **12**, 199–204.
- 36 R. P. Schwarzenbach, B. I. Escher, K. Fenner, T. B. Hofstetter, C. A. Johnson, U. Gunten and B. Wehrli, *Science*, 2006, **5790**, 1072–1077.
- 37 W. Mroziak, C. Jungnickel, M. Skup, P. Urbaszek and P. Stepnowski, *Environ. Chem.*, 2008, **5**, 299–306.
- 38 C. Zurzolo and C. Bowler, *Plant Physiol.*, 2001, **127**, 1339–1345.
- 39 N. Kröger, C. Bergsdorf and M. Sumper, *EMBO J.*, 1994, **13**, 4676–4683.
- 40 N. Kröger, R. Deutzmann and M. Sumper, *Science*, 1999, **286**, 1129–1132.
- 41 N. Kröger and R. Wetherbee, *Protist*, 2000, **151**, 263–273.
- 42 A. K. Davis and B. Palenik, *Protist*, 2008, **159**, 195–207.
- 43 K. S. Button and H. P. Hostetter, *J. Phycol.*, **13**, 198–202.
- 44 I. Olenina, S. Hajdu, L. Edler, A. Andersson, N. Wasmund, S. Busch, J. Göbel, S. Gromisz, S. Huseby, M. Huttunen, A. Jaanus, P. Kokkonen, I. Ledaine and E. Niemkiewicz, Biovolumes and size-classes of phytoplankton in the Baltic Sea, HELCOM Balt. Sea Environ. proc. no. 106, 2006, p. 144.
- 45 M. Umorin and O. Lind, *Biotechnol. Lett.*, 2005, **27**, 347–354.
- 46 A. Latała, in *Biological Resource Centers and the Use of Microbes*, ed. N. Lima and D. Smith, Micoteca da Universidade do Minho, Braga, Portugal, 2003, pp. 323–345.
- 47 A. Latała, S. Jodłowska and F. Pniewski, *Algological Studies*, 2006, **122**, 137–154.
- 48 R. R. L. Guillard, in Culture of phytoplankton for feeding marine invertebrates, *Culture of marine invertebrate animals*, ed. W. L. Smith and M. N. Chanle, Plenum Press, New York, 1975, pp. 29–60.



Organic & Biomolecular Chemistry



OBC has achieved tremendous success since the first issue was published in January 2003. Can any other 'young' journal boast such highly cited papers, published quickly after independent peer review to such exacting standards?

- A leading journal in the field
- High impact factor 3.167*
- Short publication times
- World renowned editorial board

* 2007 Thomson Scientific (ISI) Journal Citation Reports®

... high quality - high impact!

RSC Publishing

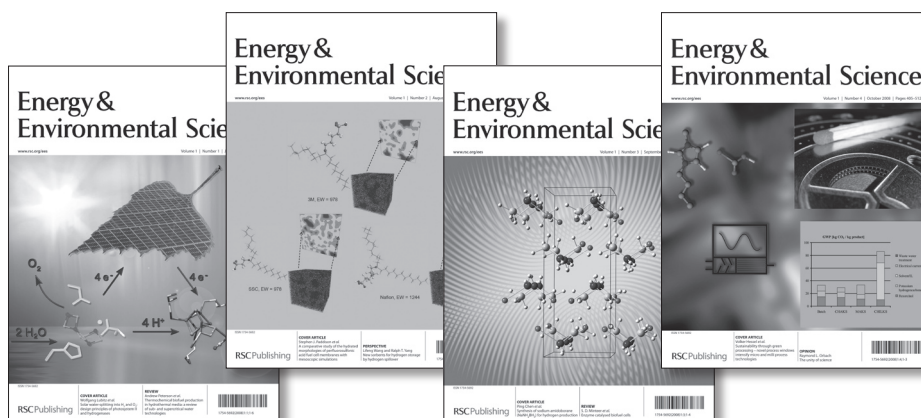
www.rsc.org/obc

Registered Charity Number 207890

Energy & Environmental Science

Linking all aspects of the chemical sciences relating to energy conversion and storage, alternative fuel technologies and environmental science

The choice of leading researchers...



"...I think the [journal's] focus ... will be of great value as it would be a major contribution to the creation of knowledge and the production of an area of literature where we still need an enormous amount of expansion and improvement..."

Rajendra Pachauri, *Chair of the Intergovernmental Panel on Climate Change (IPCC)*

"This journal provides the ideal forum for sharing ideas across a wide range of disciplines in the exciting fields of energy and environmental technology."

Peter J Dobson, *Advisory Board Member, Oxford University, UK*

"Energy and environment will provide the leading scientific problems of the next few decades and the RSC has once again shown its leadership by founding the first major journal in this area."

Robert H. Crabtree, *Yale University, USA*

"This new journal creates an excellent platform to advance the science and technology of energy production, conversion and storage, which is of significant importance to the sustainable growth of the human society."

Ping Chen, *Dalian Institute of Physical Chemistry, China*

Access the latest issue now!

RSC Publishing

www.rsc.org/ees

Registered Charity Number 207890



The must-have primary research journal for environmental issues

Comprehensive and high quality coverage of multidisciplinary, international research relating to the measurement, pathways, impact and management of contaminants in all environments.



- Highly visible and cited in MEDLINE
- Accelerated publication rates, typically around 80 days
- Dedicated to the measurement of natural and anthropogenic sources of pollution with a view to assessing environmental and human health effects

Submit your work to JEM today

RSC Publishing

www.rsc.org/jem

Registered Charity Number 207890



Energy Efficiency for Green Consumer Products

Plus pre-symposium Masterclass
and evening event

15-16 June 2009

The Green Chemistry and the Consumer annual symposia bring together a diverse audience of representatives from consumer product supply chains, academics, NGOs, government, trade associations, media and other stakeholders to learn about green chemistry solutions for sustainable product supply chains.

Who should attend?

These events are open to all and are aimed at organisations and individuals with an interest in green chemistry and sustainable chemical products. The event will provide an invaluable opportunity for mutual learning and technology transfer.

The Venue

The King's Manor in York is a group of medieval buildings that are one of historic York's most attractive sites and served the Tudors and Stuarts as a seat of government.

Registration

You can either register online or contact us:

Event Website -

<http://www.york.ac.uk/res/gcg/gogreen/index.htm>

Contact Us -

Miss Odette Murtland, GCN Assistant
Tel: 01904 434546
Email: om506@york.ac.uk

Programme of Activities

Masterclass (June 15th)

This pre-symposium event will provide training in establishing sustainable supply chains for greener products. It will introduce the principles and tools available to help in product development and will also highlight the opportunities for "greener" products. The event is targeted at representatives from the whole supply chain, and this year's theme is '**Reducing the Carbon Footprint across the Supply Chain**'.

Evening Event (June 15th, 5:30 - 7:30pm)

This will feature a plenary lecture given by **Roy Miller, Chemicals Advisor, B&Q Social Responsibility** as well as an exhibition and wine reception providing an opportunity for networking.

GC&C Symposium (June 16th)

The sixth symposium, '**Energy Efficiency for Green Consumer Products**', will explore recent advances in the field, including case studies on successful methods developed by industry and challenges in practice. The programme for the day will consist of a blend of both presentations and breakout sessions. Speakers will be announced shortly.

